DOCUMENT RESUME

ED 058 456   VT 014 597

TITLE   Exploring in Aeronautics. An Introduction to
                 Aeronautical Sciences.
INSTITUTION   National Aeronautics and Space Administration,
                 Cleveland, Ohio. Lewis Research Center.
REPORT NO   NASA-EP-89
PUB DATE   71
NOTE   398p.
AVAILABLE FROM   Superintendent of Documents, U.S. Governmer.t Printing
                 Office, Washington, D.C. 20402 (Stock No. 3300-0395;
                 NAS1.19:89, $3.50)

EDRS PRICE   MF-$0.65 HC-$13.16
DESCRIPTORS   Aerospace Industry; *Aerospace Technology;
                 *Curriculum Gvides; Illustrations; *Industrial
                 Education; Instructional Materials; *Occupational
                 Guidance; *Textbooks
IDENTIFIERS   *Aeronatics

ABSTRACT
        This curriculum guide is based on a year of lectures
and projects of a contemporary special-interest Explorer program
intended to provide career guidance and motivation for promising
students interested in aerospace engineering and scientific
professions. The adult-oriented program avoids technicality and
rigorous mathematics and stresses real life involvement through
project activity and teamwork. Teachers in high schools and colleges
will find this a useful curriculum resource, with many topics in
various disciplines which can supplement regular courses. Curriculum
committees, textbook writers and hobbyists will also find it
relevant. The materials may be used at college level for introductory
courses, or modified for use with vocationally oriented high school
student groups. Seventeen chapters are supplemented with photographs,
charts, and line drawings. A related document is available as VT 014
596. (CD)

EXPLORING

IN

AERONAUTICS

an Introduction to Aeronautical Sciences developed at

the NASA Lewis Research Center, Cleveland, Ohio.

National Aeronautics and Space Administration, Washington, D.C. 20546

1971

2

PREFACE

"Exploring in Aeronautics" is the second publication resulting from the NASA-Lewis Aerospace Explorer program; the first is titled "Exploring in Aerospace Rocketry" (NASA EP-88). Both publications are based on the lectures and projects of a contemporary, special-interest Explorer program sponsored by the NASA-Lewis Research Center. The principal objective of this program is to provide promising students from local schools with an opportunity for meaningful career guidance and motivation over a wide spectrum of aerospace engineering and scientific professions. Each year, candidates (ages 15 to 19 years) for the program are selected by school officials on the basis of their demonstrated interest and proficiency in mathematics and science.

In this adult-oriented program, we attempt to provide the young people with a meaningful career exposure through adult associations in a professional environment. Instead of merely lecturing to them, we try to involve the youths directly in the aerospace technology and to stress attendant project activity and teamwork. Fundamental scientific principles are explained through lectures and demonstrations. Technical sophistication and rigorous mathematical developments are generally avoided. The youths are committed to a realistic simulation of the "research-and-development" environment. Project activities are assigned, planned, implemented, analyzed, and reported on in significant detail. In effect, the youths are taken behind the scenes for a full view of the real engineering world.

Throughout the program, emphasis is placed on communication. The art of effective communication, of course, is vital to almost any career. To generate a high level of interest, to ensure clarity and understanding in the presentations, and to achieve a rapport with the lecturers, the participants are encouraged to raise questions. Explorer "project engineers" are periodically required to report to the membership on current project status and progress. Each year, the culmination of the program is a research symposium, in which the youths report the results of their researches to an audience of parents, teachers, and Lewis management officials.

NASA-Lewis employee participation in the program is considerable. Many employees enthusiastically and sincerely guide the young people in their scientific endeavors. Thus, the youths are exposed to a wide range of aerospace-oriented personnel - technicians, engineers, scientists, and administrators. The time donated to the program by these NASA employees is their personal contribution to the future well-being and success of our youth and our nation. In a very real sense, this effort goes hand in hand with the academic programs to focus and develop the interests and skills of our young men and women.

Lewis management believes that this work with young people is clearly in keeping with the spirit of the NASA Charter, wherein NASA is commissioned "to contribute materially to . . . the expansion of human knowledge of phenomena in the atmosphere and space." NASA is also charged with the "widest practicable . . . dissemination of information concerning its activities and the results thereof."

This publication is intended not only to provide a basic explanation of some of the fundamentals of aerodynamics but also to stimulate other government agencies, educational institutions, private industry, and business to establish career-motivation programs within their own special fields of knowledge.

The basis of this publication was just one year of the Lewis Explorer program. The various NASA-Lewis employees who lectured to the Explorers, and also served as associate advisers, during that year are identified as authors of the chapters of this publication. Other employees who donated their time and talents to the program included Dr. Abe Silverstein (Explorer Post sponsor); Billy R. Harrison, William J. Masica, Roy A. Maurer, Edward T. Meleason, Brent A. Miller, Larry E. Smith, and Calvin W. Weiss (all associate advisers for wind-tunnel projects); John F. Staggs and Michael C. Thompson (associate advisers for flight projects); Harold D. Wharton (institutional representative); Joseph F. Hobzek, Jr., (Chairman, Explorer Post Committee); William A. Brahms, Charles E. Kelsey, Donald A. Kelsey, Clair R. King, and Horace C. Moore, Jr., (all members of Explorer Post Committee); and Clifford W. Brooks (photographer for the program and associate adviser for flight projects).

James F. Connors
Director of Technical Services
(Adviser, Lewis Aerospace Explorer Post)

INTRODUCTION

The history of the airplane is much better known than the history of rockets and satellites. Aircraft flying overhead are a common sight in all technologically advanced countries. It is quite appropriate, therefore, that an educational publication on the principles of aeronautics should be made available by NASA.

An important use of this book could be as a curriculum resource for teachers in high schools and colleges. It might also be helpful to curriculum committees and textbook writers. It discusses many topics which teachers in various disciplines can use to supplement their regular courses. The comprehensive history of aviation given in the first chapter could enrich courses in general or physical science or the history of science. The chapter on weather safety and navigation in severe storms would be useful in Earth science courses. Many examples of applications of mathematics are found in the book. But the discipline which would find the most usefulness in the book is physics. Even a cursory glance through the book impresses one with the fact that the design and operation of aircraft would be impossible without an understanding of complex physical concepts.

A course in aeronautics for college-capable students in high school could be built around the book, especially if the teacher refers to related literature for problem material to reinforce the concepts presented. At the college level it could provide appropriate material for introductory courses in the science of aeronautics. With some modification, it could be used with vocationally oriented student groups in high school. Student and adult hobbyists in aeronautics will find much of the book relevant to their interests.

It is hoped that one outcome of the use of this book, and of the companion volume, "Exploring in Aerospace Rocketry" (NASA EP-88), will be to stimulate the interest and imagination of capable students so that many of them will be interested in following developments in the rapidly changing aerospace field.

CONTENTS

William H. Swann

Terrestrial grid system. Parallels of latitude. Meridians of longitude. Charts (maps). Desirable characteristics. Projections - Lambert, Mercator. Scale. Aeronautical charts. Plotting and measuring courses. Magnetic compass. Effect of wind on flight path. Vector diagrams. Navigation systems - radio compass, VOR, Tacan, Loran, Doppler, inertial.

I. Irving Pinkel

Storm hazards to flight - turbulence, hail, rain, icing, lightning. Characteristics of a thunderstorm. Development of a thundercell. Structure of a thundercell - areas of turbulence, precipitation, and icing. Navigation through storm areas.

James F. Connors

Lecture demonstrations. Aerodynamics experiments. Tours. Symposium on aeronautics. Design and construction of simple, low-speed, wind tunnels. Hand-launched, indoor glider project. Principles of aerodynamic stability in glider studies.

1. AERONAUTICS IN HISTORICAL PERSPECTIVE

James F. Connors*

The airplane has had a tremendous impact upon our society and our way of life. The world is smaller for it, people and nations are less isolated. Previous obstacles of distance have been virtually eradicated. In 1969 alone, there were 57 certified American airlines, which carried approximately 164 million originating passengers and some 20 billion revenue ton-miles of freight. Aso, the airplane is a vital element in our national defense.

How did all this come about? What can we learn from the dramatic accomplishments that have taken place in manned, powered flight?

With history going back many thousands of years, the extremely short time within which manned flight achievements have taken place is certainly impressive. For ages, man aspired to sustained flight. But, in terms of accomplishment, only one average life-span has elapsed between the first, manned, powered flight of the Wright brothers, in 1903, and the current era of supersonic flight. Man has even penetrated successfully the Earth's atmosphere and has ventured out into the vastness of space. Viewed on a time scale, these achievements are representative of the "technological explosion" that is popularly referred to in current writings.

Here, we will only briefly touch upon technical highlights in the evolution of the airplane and point out some of the major events in aviation history. Many excellent books and documentaries have been written on this subject. Some of them have been used as information sources for this chapter and are listed in the bibliography. For convenience, a brief aviation chronology is provided in appendix A. Some of the airplane terminology is defined in appendix B.

Over the years, truly prodigious numbers and kinds of aircraft have been designed and built. Some historical airplanes used by the United States Air Force are shown in figures 1-1 to 1-45 in more or less chronological order. The modern stable of USAF aircraft is illustrated in figures 1-46 to 1-70. These are but a small sampling. Many other configurations have been used by the Air Force and the other services, notably the Navy, and in the commercial, business, and sports-flying fields.

---

*Director of Technical Services.

The story of the airplane can be broken down logically into the following phases or time periods: before the Wright brothers; the era of the Wright brothers; World War I; the late '20's and the '30's; World War II; post-World War II; and the future.

Speed has always been the prime measuring stick for aircraft performance, especially to the military. The Wright Flyer flew at about 30 miles per hour (mph); World War I aircraft averaged about 100 mph. In the late 1930's, bombers operated at slightly above 200 mph, with fighters at 300 to 350 mph. By 1945, bombers traveled at approximately 350 mph, top fighters at 500 mph, and some jet-propelled fighters exceeded 550 mph. The Douglas D-558-II Skyrocket went 1238 mph in 1951, and the experimental, rocket-powered North American X-15 (fig. 1-60) reached a speed of 4104 mph in 1962, with Joseph Walker as pilot. Such tremendous increases in flight speed did not come easily. Many difficult technical problems, or "barriers," had to be overcome. These problems occurred in all areas: structures (e.g., vibration, flutter, compressibility, etc.), aerodynamics, propulsion, materials, navigation, and control. The so-called "sonic barrier" and "thermal barrier" were also overcome.

During the evolution of the airplane, progress in aeronautics has received its impetus largely from the urgency of military needs. Under the war influence, a great investment in resources was made in the research, design, and construction of progressively superior aircraft. Subsequently, the technology associated with advanced military airplanes was applied to new designs and adaptations for commercial purposes. Military design requirements were best indicated by the slogan "Higher, Faster, and Farther." No sooner was one requirement met than another, more stringent requirement was set, with primarily Government-sponsored research leading the way to continual improvements.

To attain its high levels of performance, aviation has required, perhaps most of all, a team of dedicated, creative, imaginative, and courageous people: scientists, researchers, inventors, designers, fabricators, experimental pilots, etc. Many people, with a great variety of specialized skills and technical disciplines, have contributed to the advancement of aeronautics. Whereas the Wright Flyer was largely the product of two minds, today's sophisticated airplane designs result from the contributions of many men.

Progress in aviation, from its very inception, has probably been best characterized as the product of research, or the application of the "scientific method." This method is the logic, or the examination and reasoning process, by which a particular problem or objective is approached. Stepwise, the process involves the collection of available pertinent knowledge, formulation of new hypotheses or theories, critical investigation and experimentation, and, finally, formulation of acceptable conclusions leading to new or revised laws. With sound engineering judgment, this approach translates into careful, systematic study, isolation of variables to evaluate their individual effects, and

2

extremely close attention to details. This is the fundamental research philosophy, or
method of inquiry, that is threaded through the story of aviation.

BEFORE THE WRIGHT BROTHERS

The first documented description of a practical device for manned flight is traceable
back to Leonardo da Vinci, around 1500. This remarkable Renaissance man, far ahead
of his time, produced detailed drawings of many flying machines, including a helicopter,
and a parachute as well. Unfortunately, these were lost to the world for over 300 years.
Leonardo and many who followed him were greatly fascinated by birds. As a result, they
expended much effort in the study of ornithopters, or flapping-wing devices. None of
these devices was ever successful.

In 1766, the English chemist Henry Cavendish found that hydrogen was lighter than
air, and the concept of the balloon was introduced. However, it was with a heated-air
system that the Montgolfier brothers made the first successful balloon flight, in France
in 1783. Interest in balloons led to the subsequent development of dirigibles. However,
with the disasters to the "Shenandoah," in 1925, and to the impressive "Hindenburg,"
in 1937, the death kenll virtually sounded for lighter-than-air ships.

The real prelude to manned powered flight came with the development of gliders.
The champion in this was Germany's Otto Lilienthal. With his gliders, Lilienthal made
more than 2000 flights over a 6-year period, traveling on some occasions more than
270 yards. His technique of shifting his body weight effected some measure of stability
and control. In 1896, he died in a glider crash, before he could complete previously laid
plans for a powered flight using a carbonic-acid-gas motor. A predecessor, Sir George
Cayley (1773-1857), was actually the first to assemble in theoretical form the many ele-
ments necessary for practical flight. His first model glider (1804) was accepted by some
as the original airplane. Cayley concentrated on the aerodynamics: the importance of
streamlining, movable tail surfaces, and the stabilizing effect of dihedral. Another
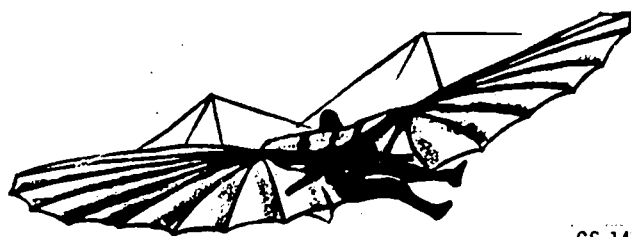
CS-14188

Otto Lilienthal (1894).

12

3
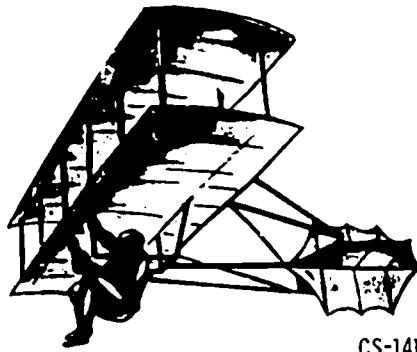
CS-14188

Octave Chanute (1896).

notable contributor among the glider enthusiasts was Octave Chanute, an American civil engineer. He introduced in a biplane glider a method of bracing the wings by struts and diagonal wires.

ERA OF THE WRIGHT BROTHERS

The story of powered flight must certainly include Samuel Pierpont Langley, architect, astronomer, physicist, mathematician, and, in later life, Secretary of the Smithsonian Institution. This esteemed scientist conducted many experiments in aerodynamics (e.g., using his "whirling table" to simulate airspeeds up to 70 mph). In 1896, he built and flew an unmanned, steam-powered model, which he called an "aerodrome," for a distance of 3200 feet. Based on this feat, Langley received a government subsidy to construct a full-size, man-carrying aerodrome. A most remarkable feature of this craft was the engine, built by Langley's assistant, Charles M. Manly. A five-cylinder, four-cycle, radial engine weighing only 125 pounds for 52.4 horsepower, it was far ahead of its time. An enormous publicity buildup preceded Langley's attempt at manned flight, but the aerodrome failed, in October 1903. As an aftermath, Professor Langley was thoroughly discredited in the eyes of the general public. He died heartbroken within a few years.
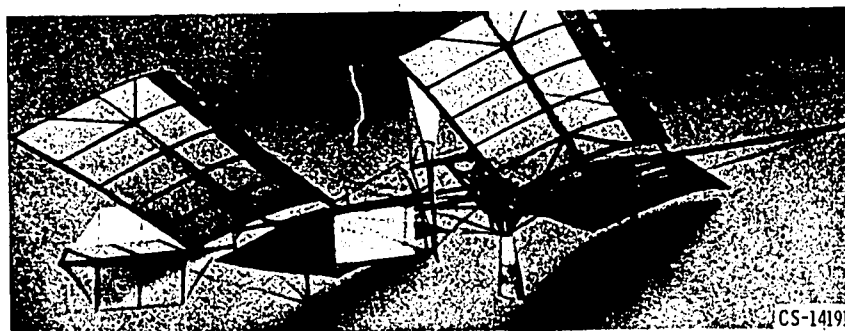
CS-14191

Professor Samuel P. Langley's aerodrome.

4

During these same several years, the Wright brothers - Orville and Wilbur - had dedicated themselves to the task of achieving manned powered flight. Their approach and concentration of energies differed from all others. They had recognized that the methods of construction for sustaining wings and for suitable powerplants were in such advanced stages that both would be worked out satisfactorily. Unlike other experimenters, however, they felt that the key to success was the development of a proper mechanism for achieving stability and control of the aircraft. Therefore, the Wrights focused their attention on this objective during their many glider and wind-tunnel tests. They had at an early point discovered the most important principle of control - the aileron principle.

The Wrights did not have formal engineering training. They owned and operated a bicycle shop in Dayton, Ohio. However, they were devoted experimentalists in their leisure and read extensively all publications relating to aerodynamics. In their experimentation, they found the existing gas-pressure tables in the literature to be in error and had to generate their own data. The Wrights built their own wind tunnel and studied a great variety of wing shapes in a detailed, systematic manner. They were true practitioners of the scientific method.

On the flat beach of Kitty Hawk, North Carolina, on December 17, 1903, a little more than 2 months after Langley's failure, the Wright brothers achieved the first manned, powered, sustained flight. On the last flight of the day, Wilbur remained aloft for 59 seconds and traveled 852 feet. Their Flyer (fig. 1-1) was a biplane with a wing span of 40 feet, 4 inches, and weighed 605 pounds. Its two propellers were driven by bicycle-type gears and chains connected to the engine shaft. They built their own engine, which produced 12 horsepower and weighed over 200 pounds. They also designed and built aerodynamically efficient propellers. The main feature of their airplane, however, was their system of control: elevator, warpable wings, and movable rudder. The ele-
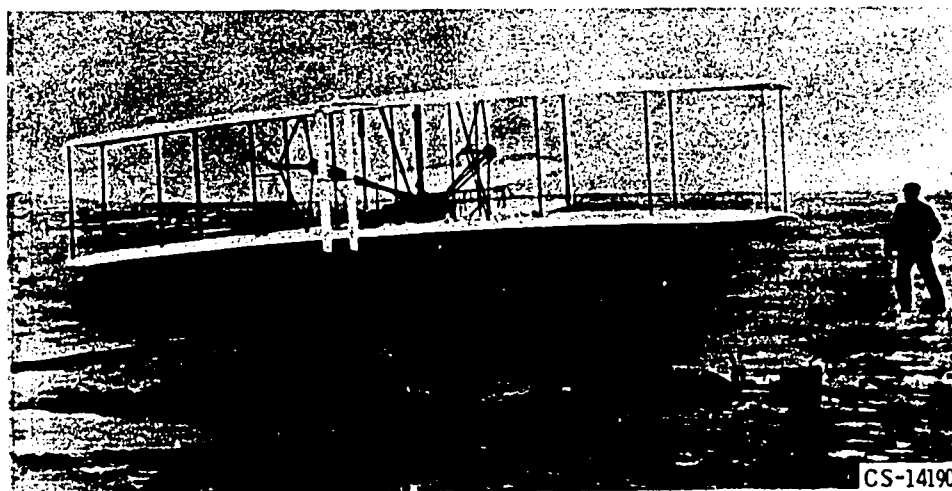
CS-14190

Wright brothers' airplane (1903).

vator, mounted at the front of the airplane, was lever-operated. Wing warping was achieved by means of cables attached to a cradle in which the operator lay. To bank the airplane to the left, for example, the operator swung his hips and the cradle to the left. This tightened the cable attached to the outer strut of the right wing and thereby warped the rear edge of that wing downward. The increased air pressure on the downward-warped wing caused it to rise. At the same time, an auxiliary cable gave the left wing an upward warp, which tended to lower that wing. The rudder was controlled by means of cables that were interconnected with the wing-warping cables, so that rudder movement and wing warping were synchronized. This overall scheme transferred control of the aircraft to the skill of the pilot. In later years, the Wrights' wing-warping method of control was supplanted by ailerons on the outboard portions of the wings.

Invention and achievement did not bring the Wright brothers the sweet taste of success. In the wake of Langley's fiasco, public interest in and reaction to flying were very low. The Wrights, of course, were pressing to capitalize on their invention. However, it was not until December 1907 that the U.S. Government (Army Signal Corps) first advertised for bids for an airplane. The Wrights' bid of $25,000 was accepted. For the remainder of their years, they were to be almost continually caught up in the stress of patent litigations. Glenn H. Curtiss emerged as the chief competitor of the Wrights. Meanwhile, through shows, competitions, and demonstrations, interest in flying caught on in Europe. Technical advancements were gradually incorporated into the airplane, particularly by Curtiss in his applications for the Navy. Elmer Sperry in this period also made significant contributions to aircraft instrumentation.

WORLD WAR I

At the onset of World War I in Europe (1914), France and Germany each had around 1500 aircraft. These initially were used only for reconnaissance. It was not long, however, until aerial dueling occurred with pilots using carbines, muskets, rifles, and even revolvers. Within 5 months of the start of hostilities, the French began mounting machineguns on the upper wings of their light Nieuports (fig. 1-8). By pulling on a lanyard, the pilot could fire the machinegun. Once the magazine was emptied, he had to land, reload, and take off again.

In February 1915, a Frenchman, Roland Garros, devised a way of firing a machinegun, mounted on the engine hood of his plane, straight ahead through the revolving propeller. The blades, fitted with metal plates, deflected about 7 percent of the bullets; the rest passed through unobstructed. This type of installation allowed the pilot to reload the gun in flight. This French technique took a heavy toll of German aircraft.

Before long, the Germans countered with a more lethal invention, by the Dutch air-

piane designer Anthony H. G. Fokker. He devised a forward-firing machinegun synchronized to fire through the propeller without striking the blades. With this invention, German airplanes for a time held mastery of the air. British pilots suffered so many casualties that they referred to themselves as "Fokker fodder." Eventually, of course, the Allies were able to reproduce the weapon for themselves and equalize the odds in combat.

Technological superiority in the design and arming of aircraft passed back and forth across the battlefronts of Europe. Whenever one side brought an improved airplane to the front, the other side strove to equal or surpass it. Fokker's airplanes made rate of climb and maneuverability requisites for combat. Dogfights approximated hand-to-hand combat in the air.

When the United States entered the war, in 1917, it did not have a single airplane fit for combat. The War Production Board was set up to administer the manufacture of aircraft. A patent pool was established to expedite the military program. In this arrangement, prime responsibility resided with the automotive industry. The Board's policy was to build only copies of foreign airplanes and to equip them with American designed motors. The principal airplane built was the DeHavilland 4, shown in figure 1-7. As a contribution to the war effort, the program was a rather dismal failure, with much gross inefficiency in evidence. This particular example of mass production had failed.

American fliers, on the other hand, gave an extremely good accounting of themselves in combat. At the end of the war, Rickenbacker's "Hat-in-the-Ring" squadron led all others, with 69 confirmed victories. Rickenbacker himself (fig. 1-6) had destroyed 26 German airplanes in combat. Many other U.S. heroes of the air emerged from battle.

The importance of the airplane in warfare was a subject of enormous controversy at the close of World War I. Brigadier General Billy Mitchell became the leading proponent and standard-bearer in a bitter campaign for the recognition and establishment of airpower. In 1921, plagued by sharp charges and demands by Mitchell, the military undertook, as an experiment, the aerial bombardment of captured German naval vessels off Chesapeake Bay. This undertaking was to evaluate the very basis of the controversy - the potency of the airplane as a weapon system. At the conclusion of the tests, Mitchell's bombers had sunk a submarine, a destroyer, a cruiser, and the dreadnought "Ostfriesland." His charges and demands became increasingly stronger and eventually forced his courtmartial in 1925 for insubordination. When convicted, Mitchell resigned from the Army. Public sentiment was in Mitchell's favor, but he had almost no support among the military.

LATE '20's AND THE '30's

Upon the close of war in Europe, many fliers returned to civilian life, only to find

7

generally widespread public apathy toward the airplane. Little opportunity was available to earn a livelihood by flying or to initiate commercial flight ventures. Many took to barnstorming: demonstration and stunt-flying at rural fairs all over the country. The Air Service, spurred by General Mitchell, took to establishing new transcontinental flight records and round-the-world exploits.

The Post Office was operating the airmail service, begun in 1918, with poor equipment and much hazard and hardship to the courageous men who flew. The passage of the Kelly Act by Congress in 1925 transferred the mail routes to private contractors. This provided fledgling air-transport companies the financial means to start expanding into the great airlines they have become today. In October 1925, Henry Ford was successful bidder for one of the first contract airmail routes (Cleveland-Detroit-Chicago) and was the first private operator to carry the mail. Ford put into service the Stout all-metal monoplane, powered by a single Liberty engine. Later, when Stout redesigned his monoplane to be powered by three Wright Whirlwind engines, Ford bought out the Stout organization, and this plane became the famous Ford Trimotor.
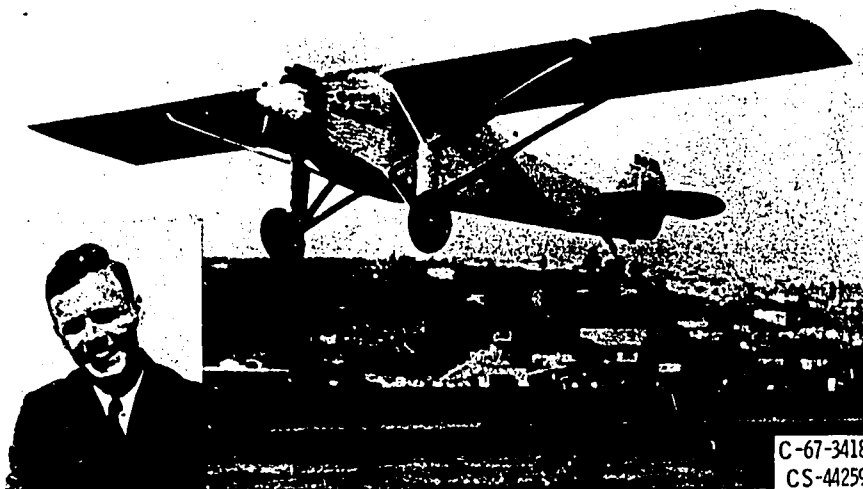
Charles A. Lindbergh and his Ryan monoplane, "Spirit of St. Louis," which he flew solo on a nonstop flight across the Atlantic from New York to Paris in 1927. (Courtesy of Smithsonian Institution.)

In 1927, Charles A. Lindbergh made the first nonstop solo flight across the Atlantic (New York to Paris). In his special Ryan monoplane "Spirit of St. Louis," he traveled 3610 miles in 33 hours, 32 minutes. As a result of his great personal achievement, "Lindy" became a national hero and the subject of public adulation. Aviation was on the upswing.

In 1933, Wiley Post established a record with his solo, round-the-world flight in a Lockheed Vega, the "Winnie Mae." The flight covered 15,596 miles in 7 days, 18 hours, 49.5 minutes. The "Winnie Mae" was powered by a Pratt & Whitney 9-cylinder, 425-

8
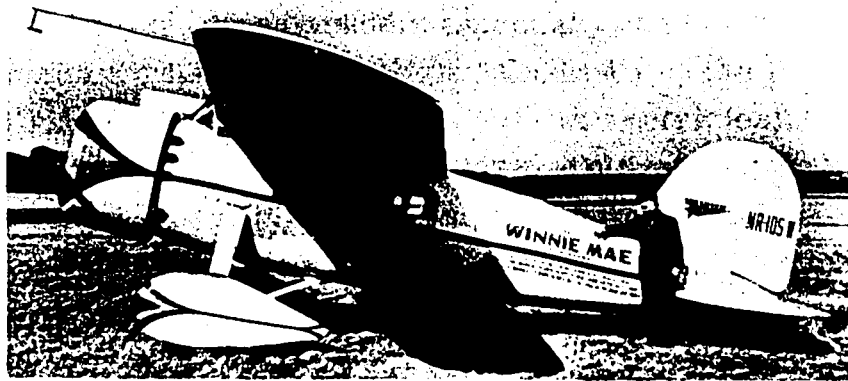
Wiley Post and his Lockheed Vega, "Winnie Mae," which he flew solo on a record-setting, around-the-world trip In 1933. (Photo from J. W. Caler collection.)

horsepower Wasp engine. On this flight, the plane was equipped with an improved version of the Sperry Gyroscope Company's automatic pilot and a radio-directional device that registered on a dial the direction of the station to which the radio was tuned. Post, in an impressive display of pilot stamina, made only 11 stops during the flight.

In 1936, an outstanding milestone in airplane technology was reached when the Douglas DC-3 (fig. 1-37) went into commercial service. This airplane had two 900-horsepower Wright Cyclone engines, weighed 24, 000 pounds, and had a useful payload of 9000 pounds - one-third greater than that of any preceding airplane. The DC-3's 185 mph represented a 50-percent increase in cruise speed over that of its predecessors. In retrospect, the DC-3 over the years has been outstandingly profitable and preeminently safe.

During the late 20's and the 30's, the National Air Races were firmly established. The best pilots, including James H. ("Jimmy") Doolittle, Roscoe Turner, Harold Neumann, Jacqueline Cochran, etc., competed annually for the most coveted prizes: the Thompson
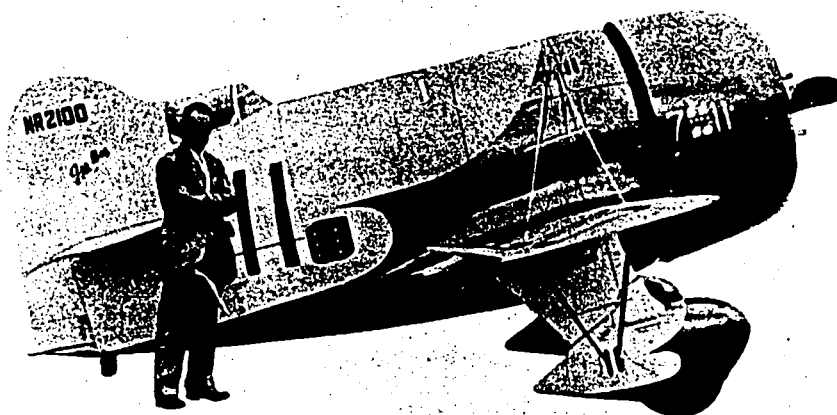
James H. Doolittle and the Granville Gue Bee racer which he flew to victory In the Thompson Trophy Race of 1932. (Photo from J. W. Caler collection.)

Trophy, for the fastest time in a closed-course pylon race, and the Bendix Trophy, for a transcontinental race. Speeds were increasing notably; for example, James H. ("Jimmy") Doolittle won the 10-lap, 100-mile Thompson Trophy Race in 1932 in a special Granville Gee Bee racer with an average speed of 252.68 mph. These races gave impetus to the development of the retractable landing gear, new fuels, and better engines.

During this period, the amazing technological advances of aviation resulted largely from the superb cooperation between the industry and the government research laboratories. The work of the National Advisory Committee for Aeronautics (NACA) was particularly noteworthy.

In aerodynamics, drag was significantly reduced as the monoplane with thick, internally braced, cantilever wings supplanted the biplane, with its interplane struts, and the externally braced monoplane. Between 1929 and 1934, more than 100 wing sections were tested in the wind tunnels of the NACA Langley laboratory. Of these, the famous NACA-23012 airfoil came to be widely used throughout the world. High wing loadings (i.e., high lift per unit area) were attained through the use of wing flaps and leading-edge slots. The guiding principle in increasing aerodynamic efficiency was the reduction of parasitic (or profile) drag. To reduce drag, therefore, NACA turned its attention to the powerplant and developed the NACA cowling in 1929. This device increased the economy of the airplane by more than 10 percent, simply by covering the knobby engine parts to streamline the nacelle and by providing an ingenious ducting system for handling the required cooling air for the enclosed engine.

There were other important developments, such as standardization on the all-metal monocoque, or stressed-skin, construction, which is a single-shell fuselage wherein the skin and stiffeners bear most of the flight loads; improvements in the use of the supercharger to permit higher altitude capabilities; developments in radio for instrument flying and blind landings; and the introduction of the variable-pitch propeller. In the late 30's, aeronautical research facilities in England, France, Germany, and Italy were expanding rapidly, for Europe was getting ready for war.

WORLD WAR II

In September 1938, President Franklin D. Roosevelt set dramatic new U.S. goals for airpower and aircraft production: 10,000 combat airplanes per year. Brigadier General Henry H. ("Hap") Arnold was made Chief of the Army Air Corps. Mass production of military aircraft was to be America's first step against the threat of Fascist aggression. To avoid the costly technological errors of World War I, the U.S. Government selected aircraft manufacturers as the prime contractors, and the automotive industry was drawn into production schemes as subcontractors. This plan resulted in industrial miracles. The annual rate of aircraft production increased steadily and reached its peak in 1944,

19

when, in that single year, 96,318 military aircraft were produced.

When World War II began, it fast became obvious that this was to be a war of air-power. For Americans, the Japanese attack on Pearl Harbor was a stunning demonstration of this fact. Thus, the tremendous U.S. production rate of military aircraft became a major factor in deciding the war in favor of the Allies. Throughout the war, many U.S. aircraft were to carry the brunt of battle - among them, notably, the B-17 Flying Fortress (fig. 1-28), B-29 Superfortress (fig. 1-43), P-47 Thunderbolt (fig. 1-35), P-38 Lightning (fig. 1-42), P-39 Airacobra, P-40 Warhawk (fig. 1-27), P-51 Mustang (fig. 1-38), B-24 Liberator (fig. 1-33), B-25 Mitchell (fig. 1-34), and the B-26 Marauder (fig. 1-41).

In its pursuit of the war effort, America took the view that the principal function of the airplane was bombardment. The Boeing B-17 Flying Fortress was first produced in 1939 and established international records for distance and weight carrying. It was not only fast, but was astonishingly sturdy and had a featherlike maneuverability. After a mission, it was not at all unusual to find a B-17 badly shot up but limping safely back to base. In Europe, the results of high-altitude, precision and saturation bombing proved to be the real turning point of the war. The remarkable Norden bombsight ensured success in daylight bombing from altitudes above the flak of antiaircraft fire.

Round-the-clock air attack on Germany was the prime objective of the air war in Europe. The bombing missions needed the support of a long-range fighter escort. But not until July 1943 did the P-47 Thunderbolts attain an escort range of 340 miles, which was inadequate. The P-38 Lightnings in 1944 had an escort range of 585 miles. About the same time, the P-51 Mustangs were delivered. These airplanes were able to speed ahead of the bombers and clear the skies of German aircraft for a distance of 850 miles.

The P-51 Mustang (fig. 1-38), an outstanding combat performer during World War II, was largely a product of NACA research. Early tests in the Langley low-turbulence wind tunnel showed that considerable drag reductions were possible by controlling the pressure distribution over the wing. In 1940, the NACA's Annual Report to President Roosevelt included this one brief paragraph:

Discovery during the past year of a new principle in airplane-wing design may prove to be of great importance. The transition from laminar to turbulent flow over a wing was so delayed as to reduce the profile drag, or basic air resistance, by approximately two-thirds. It is too early to appraise adequately the significance of this achievement. So far, its application is limited to small airplanes, but there are indications of its ultimate applicability to larger airplanes through continued research. It should increase the range and greatly improve the economy of airplane operation.

This new principle was applied to the wing design of the Mustang airplane. The P-51 was also subjected to other aerodynamic cleanup studies and remedies by NACA. The results are now history. In both speed and range, the P-51 was the foremost propeller-driven fighter of this period.

In the bomber class, the successor to the B-17 was the famous Boeing B-29 Super-fortress. First flowin in July 1943, this airplane brought about the defeat of Japan. The

B-29's four engines produced 2200 horsepower each, compared with 1200 in the B-17. Takeoff weight was 140,000 pounds, compared with the 55,000 pounds of the B-17. With a wing span of more than 140 feet and a pressurized cabin, the B-29 could be flown with comfort at 35,000 feet. It had an operational radius of 2300 miles with a 10,000-pound payload. In 1945, of course, it was the B-29 that carried the atomic bomb to Hiroshima and brought about the end of the war.

During the latter stages of the war, the jet airplane began to emerge. Bell Aircraft in 1943 produced the YP-59 Airacomet, the first jet fighter in America. This airplane utilized the turbojet engine researched and developed by Frank Whittle in England. Actually, the Germans had been busy, too, and had put into operation in the preceding year the Messerschmitt-262 jet fighter. For a given thrust level, the turbojet engine is smaller, lighter, and simpler in design than the reciprocating engine. However, it also has a higher fuel consumption. Propulsive efficiency of the jet engine increases with speed, whereas with a propeller, compressibility losses (associated with high-speed airflow over a lifting surface) cause performance to fall off drastically. Introduction of the jet engine thus opened up still higher ranges of aircraft speed.

POST-WORLD WAR II

One of the successors to the B-29 bomber was the Strategic Air Command's B-36, built by Convair (fig. 1-40). This was the largest airplane to enter the Air Force inventory. It had a wing span of 230 feet and a length of 162 feet. Its gross weight on takeoff was 370,000 pounds, compared with 140,000 pounds for the B-29, and its nominal range was 10,000 miles. Early versions of the B-36 were powered by six propeller engines.
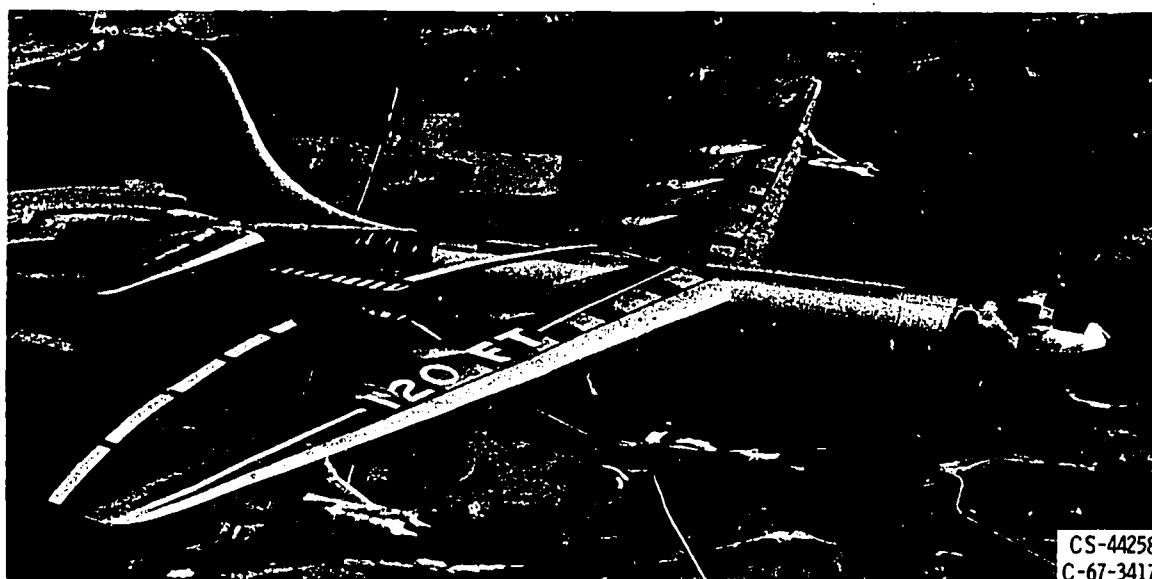
CS-44258
C-67-3417

Convair B-36 long-range strategic bomber in contrast to Wright Flyer.

On later versions, four turbojet engines were added. The B-36 was expensive: $3,500,000, compared with $640,000 for the B-29. Its top speed was about 435 mph. For further size comparison, the original Wright Flyer is sketched on the photograph, illustrating again the dramatic evolution of the airplane.

Currently, the primary heavy bomber of the Strategic Air Command is the B-52 Stratofortress (fig. 1-47). The Boeing B-52 is powered by eight jet engines, each with a thrust rating of 17,000 pounds. In 1957, with in-flight refueling, the B-52 flew 24,325 miles in 45 hours, an average of 540 mph. The role of the long-range, high-speed bomber is now being challenged by the application of rocket-powered, guided missiles, such as ICBM's.

The Century series jet fighters are illustrated in figures 1-49 to 1-54. These airplanes are highly sophisticated aerodynamically and are electronically complicated. All generally have transonic or supersonic dash capability. In contrast with World War I fliers, today's combat pilots must be highly trained and are more dependent on systems performance than on individual flying skills. This change is obviously a consequence of the tremendous flight speeds, which preclude human observations and determinations in flight. Electronic systems for navigation, control, weapons firing, etc., must necessarily predominate. One look into the pilot's compartment of a modern jet will quickly corroborate this.

In 1960, Russia announced that a U.S. aircraft had been shot down over Soviet territory as it was attempting a photoreconnaissance mission. The airplane was the Lockheed U-2. This airplane is of interest here because it was designed for a very special and specific purpose. Originally, the U-2 was to be used by NASA for weather research and high-altitude radiation sampling. The design objective was to achieve maximum possible altitude performance within the state of the art. This performance was obtained by using a sailplane-type wing, keeping structural weight and strength low, and using a specially designed high-altitude version of the Pratt & Whitney J-57 engine with low-volatility fuel.
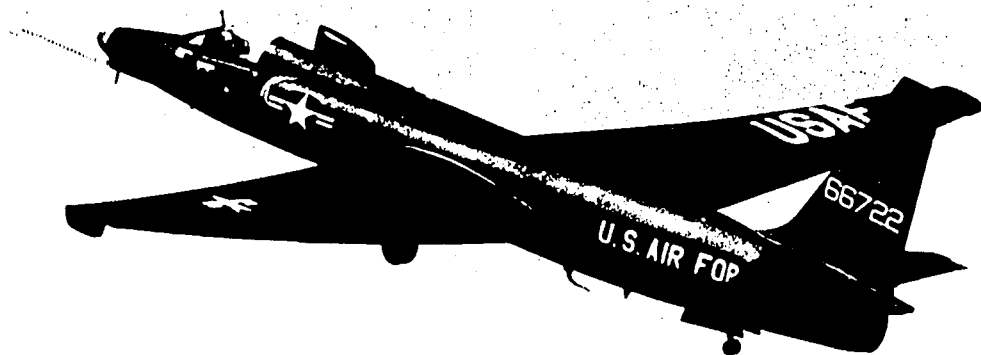
C-67-3414

Lockheed U-2 high-altitude jet aircraft for weather and radiation research and photoreconnaissance missions. (Courtesy of Smithsonian Institution.)

13

An example of U-2 weight savings is the single main landing gear. Small jettisonable wheels keep wings level during takeoff roll. The U-2 is able to maintain level flight at altitudes above 70,000 feet, with a range of 3000 miles or more. This aircraft illustrates the practical trade-offs and compromises available to the designer to meet particular specifications. Speed, for example, was the uppermost consideration in the Gee Bee racer, shown previously. Therefore, that airplane was practically all engine, and everything else was minimized. In World War II, speed of American airplanes was sacrificed for the weight requirements of electronic navigation packages and personnel armor protection. The aircraft designer must balance all requirements as he searches for an optimum.

The F-111A (fig. 1-59) exemplifies another novel approach. With its variable-geometry wings that can be extended in flight for takeoff, landing, and subsonic speeds and then swept back sharply for supersonic operations, the F-111 is designed as a multi-purpose aircraft. It can be used for counter-air missions, interdiction, close air support of ground forces, and reconnaissance. Its design Mach number is about 2.5 (i.e., a speed 2.5 times the speed of sound).

The XB-70 Valkyrie was a large, tail-first (canard), delta-wing aircraft, which was designed as a strategic bomber. This airplane was intended to replace the B-52 Strato-fortress in service with the Air Force in the mid-1960's. The original B-70 was designed to travel the entire distance to the target and back (a maximum of about 7600 miles) un-refueled, at Mach 3. In March 1963, the decision was made to build two XB-70A aero-dynamic research aircraft. The first flight was made in 1964. Thereafter, the XB-70A was used in a joint research program conducted by NASA and the Air Force. At takeoff,
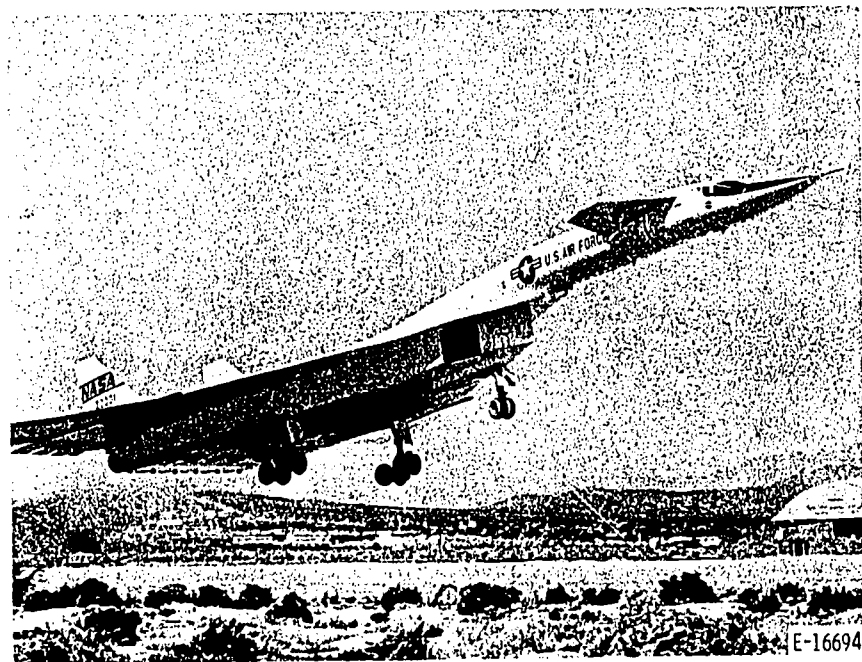
XB-70A research aircraft (Mach 3).

23

14

this airplane weighed over 500,000 pounds. The design cruising speed of Mach 3 (approximately 2000 mph) was first attained during the 17th flight, in October 1965. During routine test flights, altitudes of around 70,000 feet were reached. The XB-70A was powered by six General Electric YJ-93-3 turbojet engines (each producing 31,000 pounds of thrust with afterburning) clustered side by side in the rear of the powerplant duct, under the wing trailing edge. The wing span with the tips spread was 105 feet. The length, including the nose probe, was 196 feet. The wings were cantilevered delta wings of very thin cross section. A large, canard foreplane, also with very thin wings was adjustable for trim purposes and was fitted with trailing-edge flaps. North American Aviation was the prime contractor. The XB-70A research program is now finished. Although the B-70 never got into production, results of this research program are expected to feed directly into the planning, design, and operational characteristics of this country's commercial supersonic transport program.

To meet its responsibility - ''to supervise and direct the scientific study of the problems of flight, with a view of their practical solution'' - NACA/NASA also joined with the Air Force, Navy, and aerospace industry in building and flying a number of advanced, high-speed, research airplanes, including the X-15 (fig. 1-60). The program has been
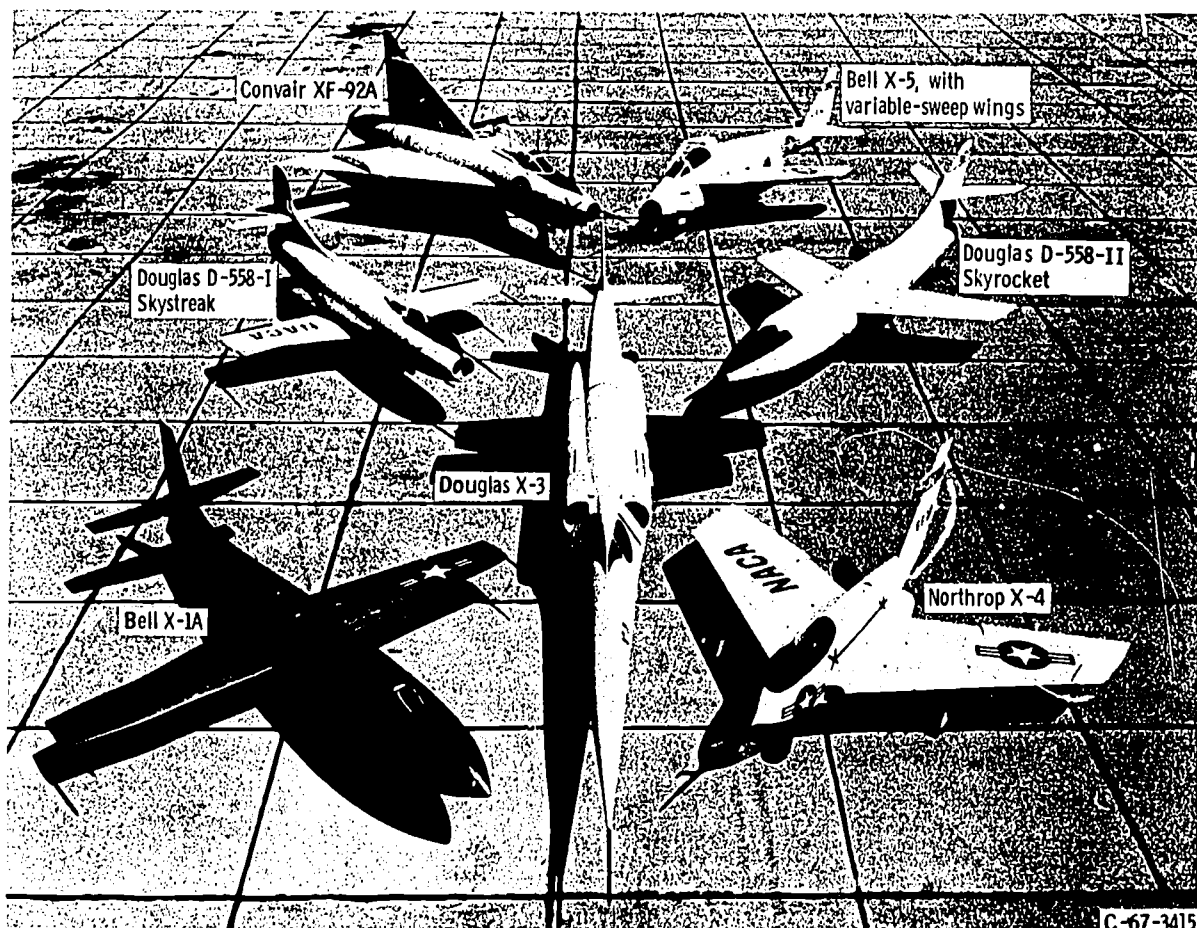
Research airplanes (1956). (Photo courtesy of Smithsonian Institution.)

essentially completed, with tremendous success. The first supersonic flight was achieved by Charles Yeager on October 14, 1947, in the Bell X-1. In 1951, William Bridgeman flew the Douglas D-558-II at Mach 1.89. In 1953, Yeager took the Bell X-1A to Mach 2.5 - 1650 mph. Airplanes flown by service and civilian pilots pushed both speed and altitude records steadily higher. By 1962, test flights of the North American X-15 rocket plane had taken the heat-resistant craft to an altitude of 314,750 feet and a speed of 4104 mph. Each X-15 flight has furnished important design data for high-altitude, hypersonic operational aircraft. The practicability of pilot-controlled reentry into the atmosphere from space has been demonstrated, and a great amount of data on physiological and psychological reactions of man to space flight has been provided.

THE FUTURE

As we look to the future, we can see only further rapid expansion in the field of aeronautics, particularly in the civilian commercial sector. In the immediate offing are the large, subsonic, jumbo jets and the supersonic transports. Both are presently in various stages of research and development.

In the large subsonic airplane category, Boeing has developed its 747 version, already in commercial use, and Lockheed (Marietta, Georgia) is working on the C-5A. By way of illustration, the latter airplane will have a gross takeoff weight of 728,000 pounds, a wing span of 223 feet, and a 65-foot-high tail. The C-5A is being designed to move 110 tons (or up to 900 passengers, on three decks) 3000 miles in 7 hours.
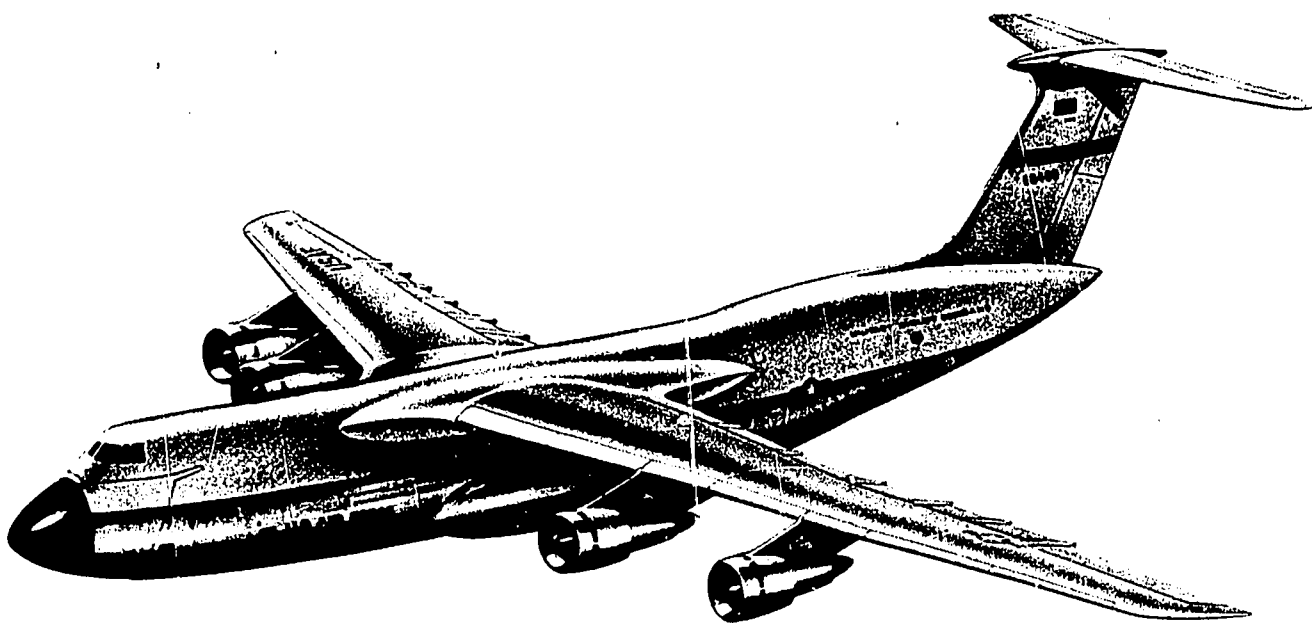
CD-10635-02

Lockheed C-5A subsonic jumbo jet.

25

Power for this job will be supplied by four TF-39 turbofan jet engines, built by the General Electric Company, each developing 41,000 pounds of thrust. This fan engine is expected to have a specific fuel consumption one-quarter less than that of a standard turbojet. This type of airplane will offer large-scale, economic transportation in both the passenger and cargo markets.

The commercial supersonic transport (SST) also has been an international technological challenge, with the British and the French cooperating to develop the 128-passenger,
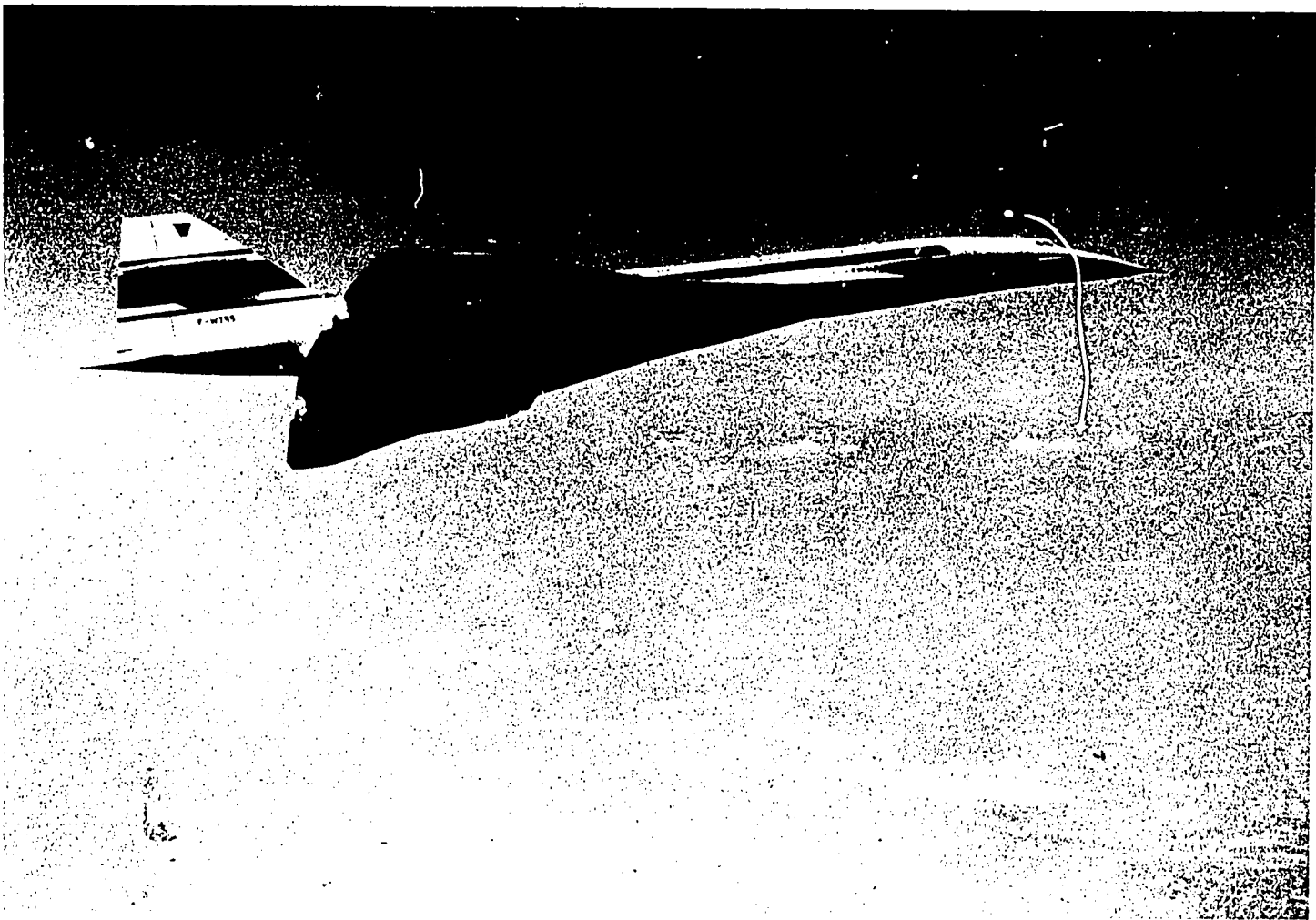
First prototype Concorde 001, a cooperative British-French project.

Mach 2.2 Concorde; the Soviet Union developing a comparable aircraft, the TU-144; and the United States working with the Boeing Company on a larger and faster SST prototype. These various efforts began in the mid-1960's. When commercial supersonic transports become operational, the sonic-boom problem is expected to restrict their use mainly to transoceanic and transpolar flights.

The original Boeing SST design had pivoted, variable-sweep wings. But because pivoted wings, for this type of aircraft, imposed unacceptable weight penalties, the design
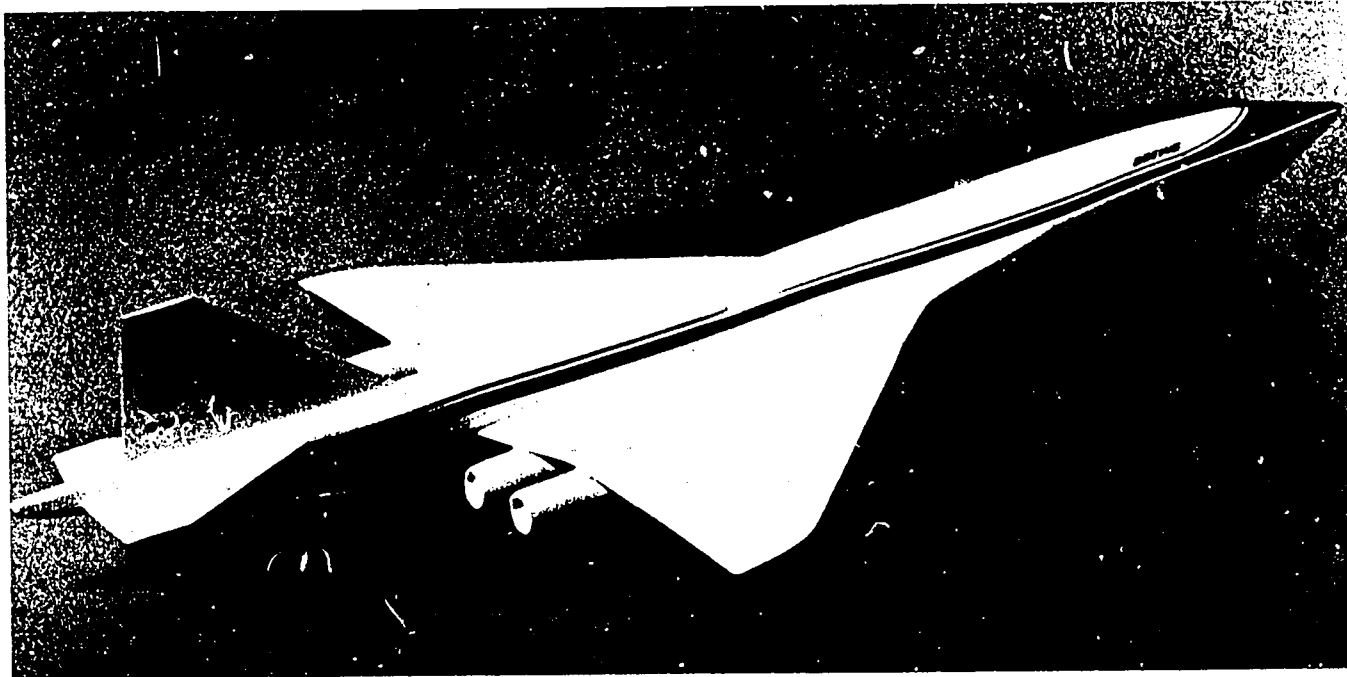
Model of proposed Boeing fixed-wing supersonic transport. (Reprinted from Interavia, January 1969, with their permission.)

was modified to a fixed-wing configuration. This aircraft was designed to carry 250 to 350 passengers at a speed of Mach 2.7 (1800 mph) and at a cruising altitude of 64,000 feet. The estimated range, with 313 passengers, was over 4000 miles. Plans called for building most of the Boeing SST of an alloy of 90 percent titanium, 6 percent aluminum, and 4 percent vanadium. Maximum takeoff weight was set at 750,000 pounds, with propulsion provided by four 67,000-pound-thrust General Electric GE4/J5P turbojet engines mounted under the rear of the wing.

Another general area of special interest to the aeronautics program is V/STOL (Vertical and Short TakeOff and Landing) aircraft. The utility of the helicopter, particularly in the military situation (Vietnam), is unquestionable. Some helicopters are illustrated in figures 1-68 to 1-70. A great variety of other V/STOL configurations are under active study. With tomorrow's mushrooming populations, the megalopolitan areas will have an acute need for short-distance, high-speed transportation. V/STOL aircraft may pose an attractive and practical solution. However, much research and development work remains.

It is appropriate here to quote the late Dr. Hugh L. Dryden:

Aeronautical technology ... has exploited the power of organized effort, learning to draw on all the resources of science, and to synthesize and integrate the effort of men of many disciplines and skills.

The future looks to be even more promising.

18

APPENDIX A

AN AVIATION CHRONOLOGY IN BRIEF

1903   Langley's aerodrome, with Charles Manly as pilot, fails in its second attempt to fly and plunges into the Potomac River. Six days later, on December 14, Wilbur Wright travels about 40 feet in 3.5 seconds. On December 17, the Wright Flyer goes 852 feet in 59 seconds at Kitty Hawk, North Carolina. This is the first, manned, powered, airplane flight.

1906   Santos-Dumont (France) makes first airplane flight in Europe. Flight duration, 8 seconds.

1908   Lt. Thomas E. Selfridge is first U.S. military man to fly "heavier-than-air" machine. Glenn Curtiss pilots "June Bug" 1 kilometer before official witnesses. First airplane owned by U.S. Army is Wright biplane. In France, Henri Farman goes up with a passenger (Delagrange) for 150-foot hop - the first passenger-carrying flight.

1909   Herrig-Curtiss Co., the Wright Co., and the Glenn L. Martin Co. are established. The first airplane flight across the English Channel is made by L. Bleriot in his "Number XI."

1910   A Curtiss biplane, piloted by Eugene Ely, takes off from land and flies out to a platform on the cruiser "Pennsylvania." This act forms basis for concept of a naval aircraft carrier. Shortly afterward, Captain I. Chambers, USN, develops compressed-air catapult for launch from shipboard.

1911   Curtiss is recognized for his invention and successful demonstration of the hydroplane - the Triad - a seaplane equipped with retractable wheels for ground landing. First airplane is delivered to the American Navy. First airmail in U.S. is carried aloft by Earle Ovington on Long Island.

1912   The first fighter plane is single-seat Farnborough B.S. 1, designed by de Havilland.

1913   Elmer A. Sperry demonstrates his gyroscopic stabilizer to the Navy. Sikorsky designs first multiengined airplane, the four-engined biplane "Bolshe."

1914   Elmer A. Sperry develops optical-type drift indicator and gyroscopic compass. Lawrence Sperry develops automatic pilot.

1915   The NACA is established by act of Congress. The first fighter is equipped with a fixed, forward-firing machinegun; this is Anthony Fokker's Eindecker Scout. The gun is synchronized to fire through the whirling propeller. Junkers designs

first cantilever-wing, low-wing, all-metal airplane - the J-1 monoplane.

1916   World altitude record of 16,500 feet is set by V. Carlstrom in a twin-engined JN Curtiss.

1917   U.S. declares war on Germany. McCook Field, Dayton, Ohio, is established as the Air Service Experimental Base.

1918   Army begins regular airmail service between Washington, D.C., and New York City. First Navy Curtiss-1 (NC-1) flying boat is successfully flown.

1919   Leak-proof tanks, free parachute back-pack, reversible- and variable-pitch propellers, syphon gasoline pump, and fins and floats for emergency water landings are developed. The turbocompressor, or supercharger, is developed by Dr. Sanford Moss of General Electric. Lieutenant Commander A. C. Read and five-man crew fly a Curtiss NC-4 Navy flying boat in the first airplane crossing of the Atlantic (New York to Lisbon via Newfoundland and the Azores). First nonstop crossing by Captain Alcock and Lieutenant Whitten-Brown in a Vickers Vimy from Newfoundland to Ireland in approximately 16 hours.

1921   As an outgrowth of charges by Brigadier General William ("Billy") Mitchell, the military undertakes experimental aerial bombardment of captured German vessels in Chesapeake Bay. Submarine, destroyer, cruiser, and dreadnought "Ostfriesland" are sunk in these tests.

1922   Wing-type radiator is developed by Curtiss. World speed record of 222.96 mph is set by Billy Mitchell in Curtiss racer. Berliner helicopter rises vertically to 12 feet and hovers successfully. DeBothezat helicopter is successfully test-flown for 1 minute, 42 seconds.

1923   First refueling in midair between two airplanes. World speed record is set at 266.6 mph in Curtiss racer.

1924   First aerial circumnavigation of the globe - four Army Douglas biplanes leave Seattle, and two return after covering 26,345 miles in an elapsed time of 175 days.

1925   Oleo landing gear is tested for Navy on NB-1 airplane. Ford Motor Company takes over the Stout Metal Airplane Company and begins producing the Ford Tri-motor, an all-metal monoplane designed by William A. Stout. Billy Mitchell is court-martialed and found guilty of insubordination. Cleveland opens its $1,000,000 municipal airport, which covers 1000 acres.

1926   Pratt & Whitney Aircraft Company produces its first engine, a nine-cylinder, radial, air-cooled engine, developing 400 horsepower at 1800 revolutions per minute. Lieutenant Commander Richard E. Byrd and Floyd Bennett fly over the North Pole in a trimotored Fokker.

1927   Lindbergh makes first, nonstop, solo flight across Atlantic (New York to Paris) in Ryan monoplane "Spirit of St. Louis" - 3610 miles in 33 hours, 32 minutes.

1928   Frank Whittle, a young, English air cadet, publishes a paper predicting application of jet propulsion to high-speed aircraft.

1929   James H. Doolittle makes first, public demonstration of instrument flying. Major Spaatz, with a crew of four, sets refueling endurance record in Fokker Army transport "Question Mark" - 150 hours, 40 minutes, 15 seconds. NACA cowling is developed.

1932   Doolittle wins the 100-mile Thompson Trophy Race in a Gee Bee racer with an average speed of 252.68 mph. New developments are a mechanism for controlling pitch of propeller and a liquidometer for displaying the condition of all fuel tanks on the airplane.

1933   Westbound transcontinental record of 11 hours, 30 minutes, established by Colonel Roscoe Turner in Wasp-powered, Wedell-Williams monoplane (Bendix Trophy Race, New York to Los Angeles). Wiley Post in a Lockheed Vega, the "Winnie Mae," sets record for solo round-the-world flight (15,596 miles in 7 days, 18 hours, 49.5 minutes). James R. Wedell breaks speed record for landplanes with 305.33 mph. Boeing builds 75 Model 247-D, all-metal transports for airlines and a fleet of P-26-A pursuit planes for Army. Retractable landing gears and a new radio compass are introduced.

1935   Howard Hughes sets new landplane speed record of 352.388 mph in his "Special." Douglas Aircraft produces first of famous DC-3 transports. Device for elimination of propeller ice is introduced.

1936   Pratt & Whitney develops new 1160-horsepower, 14-cylinder, twin-row, Wasp engine. Whittle begins experiments on gas-turbine engine.

1937   Hughes flies from Los Angeles to New York in 7 hours, 28 minutes, 25 seconds for average of 327.5 mph. Dirigible "Hindenburg," filled with hydrogen, crashes and burns, marking the beginning of the end for rigid-airship transportation.

1938   First production Supermarine Spitfire fighter (low-wing, single-seater) is completed in England.

1939   B-17 Flying Fortress goes into production.   Bell Aircraft builds P-39 Airacobra for Army.   Heinkel He 178 (first jet plane) is flown successfully in Germany.

1940   Puncture-proof gasoline tanks are tested at Wright Field.   Boeing 307-B Stratoliner, first supercharged, pressurized-cabin airplane, is introduced.

1941   First successful true "flying wing," developed by Northrop, is announced by the Army.   Jet-powered Gloster plane, powered by a Whittle-I jet engine, is built and flown on May 14.   The 650-pound Whittle engine produces more thrust than a comparable Rolls-Royce reciprocating engine that weighs 1650 pounds.

1942   Doolittle leads his B-25 Mitchell bombers in raid against Japanese mainland after taking off from carrier "Hornet."   First operational military jet, the Messerschmitt-262, is tested in Germany.   First flight of Bell YP-59 Airacomet, first jet fighter in America.

1943   Water injection is used for power augmentation in fighters.

1944   U.S. Army Air Force peaks at 2,383,000 men and 64,591 planes.   Germany puts first rocket-propelled airplane into operation, the Messerschmitt-163 Komet.

1945   B-29 drops atomic bomb on Hiroshima, Japan.

1947   Mantz wins Bendix classic (2045 miles in P-51 Mustang at average speed of 460.4 mph).   Allison announces production of its new liquid-cooled, V-1710-G6 engine rated at 2250 horsepower.   Allison also introduces new jet engine rated at 7500 horsepower at 600 mph.   Lockheed P-80R sets speed mark at 623.3 mph.   Douglas D-558-I Skystreak flies 650.6 mph.   First, manned, supersonic flight (Mach 1.06, or approx 670 mph) is achieved by Charles Yeager in rocket-powered Bell X-1.   A separate Air Force is established as a coequal partner with the Army and Navy - the realization of Billy Mitchell's dream.

1948   Wright Aeronautical announces new 18-cylinder, air-cooled engine (R3350-26-W Cyclone), rated at 2700 horsepower.   F-86 Sabrejet flown at 674 mph by Major R. L. Johnson.   Vickers Viscount (with turboprop engines) enters airline service.

1949   Douglas D-558-II Skyrocket hits speed of 710 mph at 26,000 feet.

1951   D-558-II Skyrocket flown 1238 mph at 79,494 feet.

1952   Convair XF2Y-1 Sea Dart, first combat-type airplane equipped with hydroskis, makes its debut in San Diego.   With the Air Force and NACA, Bell investigates variable-sweep wings on the X-5.
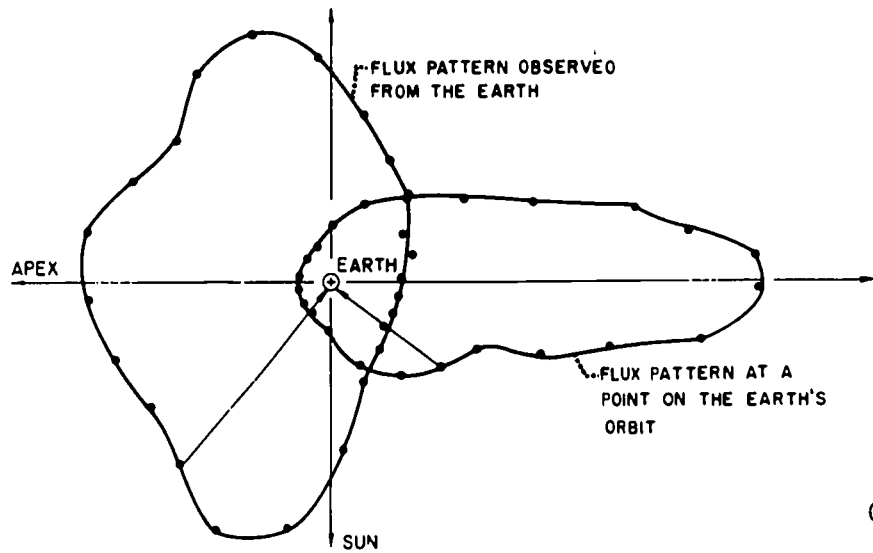
Figure 1-18. - Meteoroid flux distribution relative to Earth and to point on plane of ecliptic.
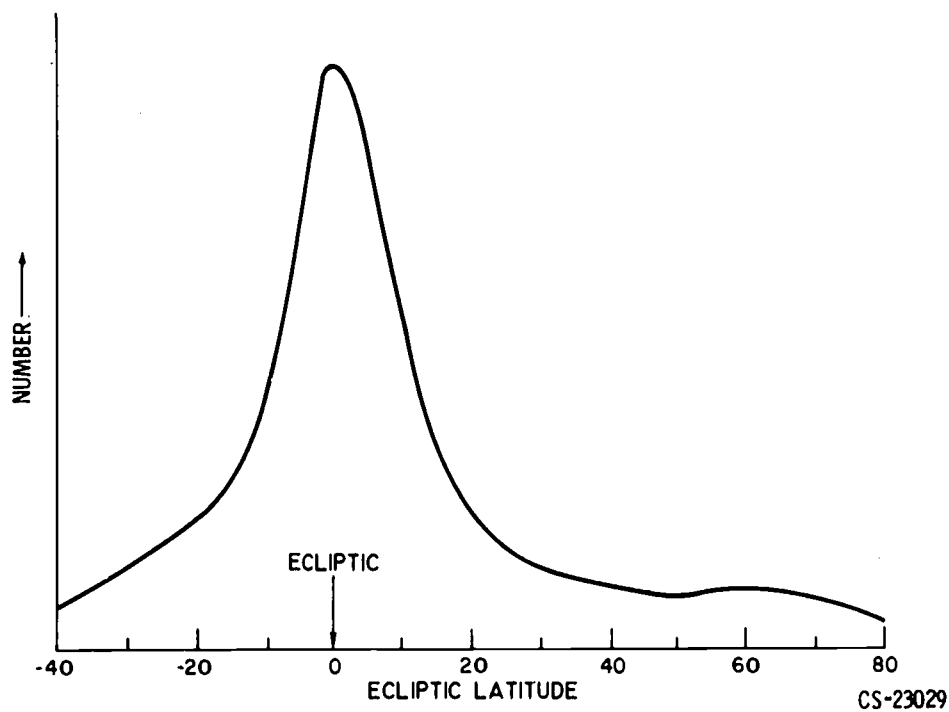
Figure 1-19. - Meteoroid distribution relative to plane of ecliptic.

general direction as the Earth.

The distribution of the meteoroids relative to the plane of the ecliptic (the orbital plane of the Earth about the Sun) is shown in figure 1-19. It is obvious that most of the particles are distributed within approximately 20° on each side of the plane of the ecliptic. The majority of the meteoroids are orbiting around the Sun, but some of them may also be trapped in orbits around our Earth-Moon system. The paths of some meteoroids form very large angles to the plane of the ecliptic, and these particles are probably of cometary origin. Scientists now assume that these meteoroids of cometary

23

origin have very low densities of less than 0.5 gram per cubic centimeter.

Scientific speculation has led to several theories regarding the origin of meteoric material. If meteoroids originate outside the solar system, they probably follow hyper-bolic paths and make just one pass through the system. However, such meteoroids can become trapped in the solar system if they undergo gravity turns near one of the planets.

The following sketches show how a gravity turn can change the speed and direction of a meteoroid as it makes a near approach to a planet. Relative to the planet, the path of the meteoroid is a hyperbola and its speed is constant, but its direction is different after the near encounter. Relative to a fixed point in space, however, the speed of the meteoroid is also different after the near encounter with the planet.

Planet adds energy to meteoroid   Planet subtracts energy from meteoroid
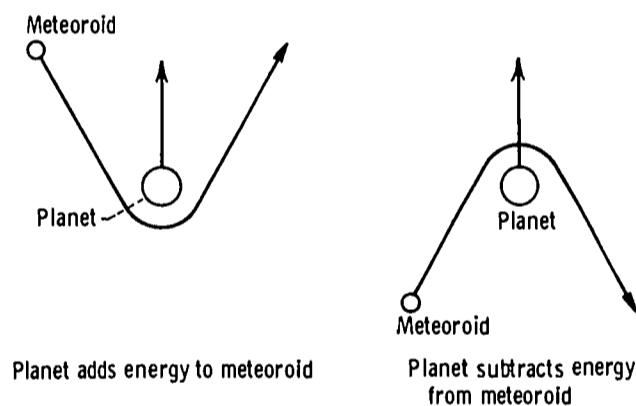
The meteoroids might come from the asteroid belt between Mars and Jupiter. Particles can diffuse out of this belt by a combination of gravity turns. The orbits of the individual particles can be altered upon close approach to another mass center. If this explains meteoroids, then the meteoroid population near Mars must be larger than near Earth. The meteoroids near Earth might actually come from the Moon. A meteoroid impact on the surface of the Moon may carry so much energy that four or five times as much mass as that of the impinging meteoroid might be knocked off the Moon's surface and propelled to an escape velocity. Some eminent scientists believe that the tektites (small glassy bodies of probably meteoric origin and of rounded but indefinite shapes) found on the Earth came from the Moon. Some people hold the theory that meteoroids originate in the tails of comets. This is an interesting theory, but it does not explain the origin of the comets themselves.

The principal reason for the great interest in meteoroids is that there is a finite probability that a space vehicle might be damaged or destroyed by meteoroid puncture. Therefore, the various components of a spacecraft must be made strong enough to prevent penetrations or destructive damage by meteoroids. Without sufficient and accurate meteoroid damage data, spacecraft would likely be underdesigned or overdesigned;

underdesign could result in early loss of mission, while overdesign could result in over-weight craft, sluggish performance, or compromised payload.

Manned exploration of the planets depends to a great extent on the planetary environments. This is why the interest in manned flights to Venus waned suddenly when data obtained from the Mariner II satellite indicated that Venus has a surface temperature of 800° F. Since more recent spectra showing the presence of water vapor on Venus have cast some doubt on the validity of the Mariner II data, some interest in the manned exploration of this planet is being revived. However, more instrumented-probe data are needed prior to any decision on the feasibility of manned landings on Venus.

Mars has also been considered as the object of manned exploration. However, a careful study of the environment on the Martian surface reveals that it is not at all attractive. For example, the atmospheric pressure at the surface is less than 10 millibars, which corresponds to the pressure at an altitude of approximately 100 000 feet above the Earth. The oxygen content is less than 1 percent, which is equivalent to the oxygen content at an altitude of approximately 160 000 feet above the Earth. The water-vapor content on Mars is perhaps only 1/2000th of the moisture on Earth; therefore, rivers, lakes, and oceans are probably nonexistent. What little water there is on Mars may be salty. Also, the surface of Mars is probably bombarded with asteroids and meteoroids from the asteroidal belt. This condition may be much more serious than it is on Earth because of the greater meteoroid population near Mars and because of the thin atmosphere. On Earth, meteors penetrate to perhaps 50 000 feet altitude; a similar particle on Mars would strike the surface. Also, the theory of planet formation suggests that Mars has a solid core and no mountains of the folded type. With a solid core, there probably is no appreciable magnetic field, and hence, no trapped radiation belts of the Van Allen type. On the surface of Mars, severe radiation intensities can be expected during giant solar flares because of both the rarefied atmosphere and the lack of magnetic-field trapping of ionized particles. Thus, strong shielding would be required on the Martian surface during giant solar flares. To survive, man would have to take his Earth environment with him. Conditions are so hostile that colonization is probably out of the question in our times. Nevertheless, manned exploration of Mars will take place and can be justified solely on its scientific merits.

GLOSSARY

apogee. That point in the orbit of a satellite of the Earth that is farthest from the center of the Earth.

astronomical unit. The mean distance of the Earth from the Sun, amounting to approximately 93 million miles; used as the principal measure of distance within the solar system.

galaxy. A vast assemblage of stars, nebulae, star clusters, globular clusters, and interstellar matter, composing an island universe separated from other such assemblages by great distances.

ionization. The process by which neutral atoms or groups of atoms become electrically charged, either positively or negatively, by the loss or gain of electrons.

ionosphere. A layer of the Earth's atmosphere characterized by a high ion density. Its base is at an altitude of approximately 40 miles, and it extends to an indefinite height.

nebula. An immense body of highly rarefied gas or dust in the interstellar space of a galaxy. It is seen as a faint luminous patch among the stars.

perigee. That point in the orbit of a satellite of the Earth that is nearest to the center of the Earth.

refraction. The deflection from a straight path undergone by a light ray or a wave of energy in passing obliquely from one medium into another in which its velocity is different.

solar corona. The tenuous outermost part of the atmosphere of the Sun extending for millions of miles from its surface. It contains very highly ionized atoms of iron, nickel, and other gases that indicate a temperature of millions of degrees. It appears to the naked eye as a pearly gray halo around the Moon's black disk during a total eclipse of the Sun, but it is observable at other times with a coronagraph.

solar prominence. A tongue of glowing gas standing out from the Sun's disk, sometimes to a height of many thousands of miles, and displaying a great variety of form and motion. Prominences are especially numerous above sunspots.

sunspot. A disturbance of the solar surface which appears as a relatively dark center (umbra), surrouned by a less dark area (penumbra). Sunspots occur generally in groups, are relatively short lived, and are found mostly in regions between 30° North and 30° South latitudes. Their frequency shows a marked period of approximately 11 years. They have intense magnetic fields and are sometimes associated with magnetic storms on the Earth.

troposphere. That part of the Earth's atmosphere in which temperature generally decreases with altitude, clouds form, and there is considerable vertical wind motion. The troposphere extends from the Earth's surface to an altitude of approximately 12 miles.

REFERENCES

1. Russell, H. N.: Minimum Radiation Visually Perceptible. Astrophys. J., vol. 45, Jan. 1917, pp. 60-64.

2. Farley, T. A.: Space Sciences. Vol. 6 of Space Technology. NASA SP-114, 1966, pp. 19-36.

3. Malitson, Harriet H.: Predicting Large Solar Cosmic Ray Events. Astron. Aerospace Eng., vol. 1, no. 2, Mar. 1963, pp. 70-73.

2. PROPULSION FUNDAMENTALS

James F. Connors*

Having considered the nature and the scope of the aerospace environment, let us direct our attention to the means by which man ventures out into space. Obviously, propulsion is the key which opens the door to all pioneering achievements in space. The "muscle" of the space program is the rocket engine. In it resides man's basic capability to hurl instrumented unmanned and manned payloads out beyond the restricting influences of the Earth's atmosphere and gravitational field.

Before we can intelligently examine any hardware details of the propulsion system and the vehicles, it is essential that we have some insight into what actually is a rocket engine. What are the fundamental design criteria? What factors influence performance? What is thrust? How is it derived from the hot jet issuing from the engine? The following discussion is centered on these questions.

Man's interest in exploring the "heavens" dates back to the earliest recorded civilizations. But a rational basis for modern rocketry was first established by Sir Isaac Newton in 1687; in that year, Newton published his book "Principia", in which he presented his principles of motion. Those principles, or laws, are examined in this chapter. (Symbols are defined in the appendix.)

THRUST

Newton's Second Law of Motion

Newton's Second Law of Motion (fig. 2-1) states simply that if a 1-pound force, or push, is applied to a body of unit mass (that is, 1 slug, defined as 32.2 lb), that body will accelerate 1 foot per second each second. In the illustration it is presumed that the body rides on frictionless wheels. Momentum is a term that describes a body in motion and may be defined as the product of mass and velocity. (Mass is related to weight by the equation $m = W/g$.) Newton's Second Law of Motion can be stated mathematically by the

---

*Director of Technical Services.

~~23~~/29
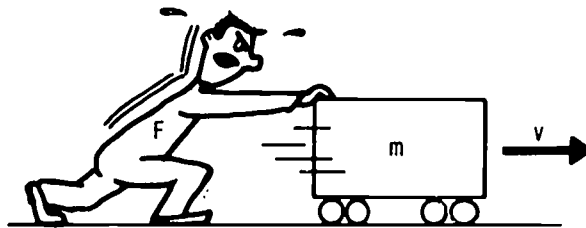
Momentum = mv

Figure 2-1. – Newton's Second Law of Motion: Acceleration – The change in a body's motion is proportional to the magnitude of any force acting upon it and in the exact direction of the applied force.

equation

$$F = ma = m \frac{\Delta v}{\Delta t} \qquad (1)$$

or

$$F = \frac{\Delta mv}{\Delta t} = \frac{\text{Change in momentum}}{\text{Change in time}}$$

Simply, thrust is equal to the rate of change in momentum.

Newton's Third Law of Motion

Newton's Third Law of Motion (fig. 2-2) states that for every action there is an equal and opposite reaction. If we picture our little character here standing on frictionless

Skater (reaction)

Ball (action)

Figure 2-2. – Newton's Third Law of Motion. Reaction – For every acting force there is always an equal and opposite reacting force.

38

roller skates and holding a bowling ball, we will find that upon the action of throwing the ball there is a reaction force pushing him back in the opposite direction. The same situation exists with a high-pressure water hose. With a jet of water issuing from the nozzle, there is a force pushing back on the hose in the opposite direction. These are examples of the principle of action and reaction.

Probably, the simplest form of rocket with which we all are acquainted is a toy balloon. The balloon rocket (fig. 2-3) uses the principles of both laws of motion. When the
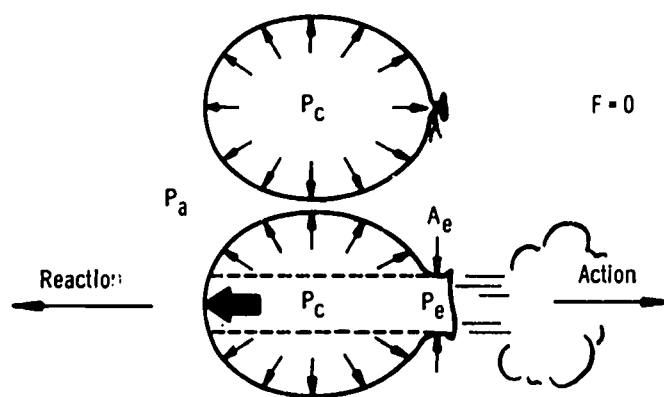
Figure 2-3. - Balloon rocket.

balloon is inflated and the outlet is tied off, the internal pressures acting in all directions against the wall of the balloon are in balance. Since no gas issues from the balloon, there is no thrust. When the outlet is opened, however, gas discharges through the opening (action), and the balloon moves in the opposite direction (reaction). The internal pressures are no longer balanced, and there is a reaction force equal to the open exit area times the difference between the internal and ambient pressures.

$$F = (P_c - P_a)A_e$$

This reaction is equal to the action force which is created by the exiting gas stream and which consists of a momentum term of mass flow rate $\dot{m}$ times the exit gas velocity v_e plus a pressure term $(P_e - P_a)A_e$.

$$F = \dot{m}v_e + (P_e - P_a)A_e \qquad (2)$$

(Note: A dot over a symbol indicates a rate flow or means "per unit time.") In both the action and reaction forces, the effect of the surrounding environment has been taken into account by referring to P_a. Obviously, in a vacuum ($P_a = 0$) the thrust of a balloon rocket is larger than it is in the atmosphere (at sea level, for example, $P_a = 14.7$ psia).

Figure 2-4. - Actual rocket engine.

In principle, there is no difference between a balloon rocket (fig. 2-3) and an actual rocket engine (fig. 2-4). In actuality, however, a rocket engine must have many practical refinements which a balloon rocket does not have. For example, a strong, high-temperature structure with intricate cooling provisions must be used to stably contain the high-pressure, hot gases. A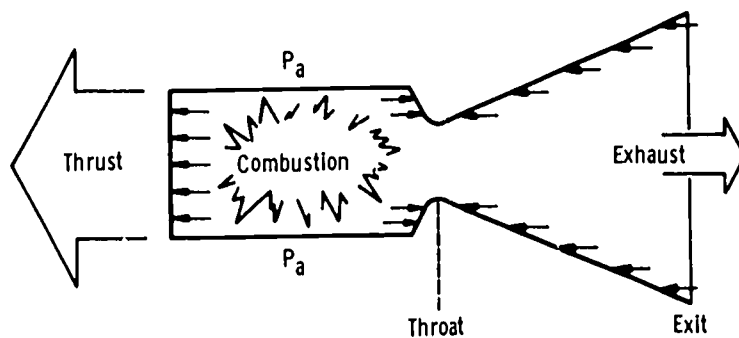 combustion process (involving a fuel and an oxidizer at some particular mixture ratio, or o/f) is utilized to generate the hot, high-pressure gases. These gases are then expanded and exhausted finally through a nozzle at high velocity to the ambient environment. The purpose of the nozzle is to convert efficiently the random thermal energy of combustion into a high-velocity, directed kinetic energy in the jet. As with the balloon, thrust is determined by the momentum of the exit gas (eq. (2)). Thrust, of course, could also be obtained by integrating or summing up the incremental component pressures acting on all the internal surfaces of the combustion chamber and the nozzle. For an ideal nozzle, the gases are expanded such that the final exit pressure P_e is equal to the ambient pressure P_a. In this case, then, the pressure term is zero and

$$F = \dot{m}v_e = \left(\frac{\dot{W}}{g}\right)v_e \tag{3}$$

Equation (3) also generally holds in vacuum, or out in space, where the pressure term can be considered to be negligibly small. In space and in the absence of any external force fields, a spacecraft's motion can only be affected by thrust resulting from mass ejection.

Newton's Second Law of Motion can also be stated as

$$a = \frac{F}{m} = g\left(\frac{F}{W}\right)$$

32   40

In vertical flight, the net upward thrust equals the total thrust minus the vehicle weight, or F - W. Therefore,

$$a = g \frac{F - W}{W}$$

or

$$a = g \left(\frac{F}{W} - 1 \right) \tag{4}$$

For lift-off, of course, F/W must be greater than 1; usually, it is approximately 1.3 to 1.5 for conventional rocket boosters.

ROCKET-ENGINE PARAMETERS

Specific Impulse

Specific impulse is a measure of rocket engine efficiency, just as "miles per gallon" is a measure of automobile economy performance, and is defined as follows:

$$I_{sp} = \frac{F}{\dot{m}g} = \frac{\text{Pounds force}}{\text{Pounds mass per second} \times g}$$

or

$$I_{sp} = \frac{F}{\dot{W}}$$ (usually specified in seconds; here, $\dot{W}$ is the propellant utilization rate in pounds per second.)

Rewriting equation (3) yields

$$\frac{F}{\dot{W}} = \frac{v_e}{g} = I_{sp} \tag{5}$$

Total Impulse

Total impulse is given by the following equation:

$$I_t = Ft \tag{6}$$

33

41

where t is the firing duration.

Some of the many factors which must be considered in the design of the rocket nozzle are chamber pressure P_c, ambient pressure P_a, ratio of specific heats for the particular gas γ, and nozzle area ratio ϵ. In thermodynamics, specific heat is a property of the gas that describes a work process involving changes in states (such as pressure, temperature, and volume). In practice, the effects of these factors are included in the ideal thrust equation:

$$F = C_F P_c A_t \tag{7}$$

where the thrust coefficient C_F varies from about 0.9 to approximately 1.8, depending on the nozzle pressure ratio. For an ideal nozzle (isentropic expansion to P_e, i.e., no energy losses), a rather complicated expression exists for C_F:

$$C_F = \sqrt{\frac{2\gamma^2}{\gamma-1}\left(\frac{2}{\gamma-1}\right)^{(\gamma+1)/(\gamma-1)}\left[1 - \left(\frac{P_e}{P_c}\right)^{(\gamma+1)/\gamma}\right]} + \frac{P_a - P_e}{P_c}\epsilon \tag{8}$$

Using equations (3) and (7) yields

$$F = C_F P_c A_t = \frac{\dot{W} v_e}{g}$$

$$v_e = \frac{g C_F P_c A_t}{\dot{W}} \tag{9}$$

Characteristic Exhaust Velocity

For the special case where C_F equals 1, v_e is designated as the characteristic exhaust velocity c^* (pronounced "see-star"). This quantity depends only on the combustion gases and is unaffected by what happens in the nozzle. As such, it is of value in comparing the potential of various propellants and is readily determined from experimentally measured parameters as follows:

$$c^* = \frac{g P_c A_t}{\dot{W}} \tag{10}$$

34

42

$$\text{Theoretical } c^* = \frac{\sqrt{\gamma g R T_c}}{\gamma \left(\frac{2}{\gamma + 1}\right)^{(\gamma+1)/2(\gamma-1)}}$$

This theoretical value is determined from the properties of the hot combustion gas and thus is a function of the particular propellant combination. The ratio of experimental to theoretical c^* is generally used as an indicator of combustion efficiency.

From the preceding relation it can be shown that

$$c^* = \text{(a constant)} \sqrt{\frac{T_c}{m}}$$

Stated another way, c^* is directly proportional to the square root of the combustion temperature and inversely proportional to the square root of the molecular weight of the propellant. From equations (9) and (10),

$$c^* = \frac{v_e}{C_F}$$

Then

$$F = \frac{\dot{W}}{g} (c^* C_F)$$

From equations (5) and (7),

$$I_{sp} = \frac{C_F P_c A_t}{\dot{W}} \tag{11}$$

Substituting with equation (10) yields

$$I_{sp} = \frac{c^* C_F}{g} \tag{12}$$

The interrelations of all the foregoing rocket-engine parameters are shown in detail in table 2-I. Review them for familiarity. All that is required are a few definitions and a little algebra.

TABLE 2-I. - PROPULSION FUNDAMENTALS

[Interrelation of rocket-engine parameters.]

Parameter	In terms of -							
	A_t	v_e	c^*	C_F	F	I_{sp}	P_c	$\dot{W}$
Nozzle throat area A_t		$\dfrac{v_e \dot{W}}{g P_c C_F}$	$\dfrac{c^* \dot{W}}{g P_c}$	$\dfrac{F}{C_F P_c}$	$\dfrac{F}{C_F P_c}$	$\dfrac{I_{sp}\dot{W}}{C_F P_c}$	$\dfrac{F}{C_F P_c}$	$\dfrac{\dot{W} c^*}{g P_c}$
Exhaust gas velocity v_e	$\dfrac{g A_t P_c C_F}{\dot{W}}$		$c^* C_F$	$c^* C_F$	$\dfrac{gF}{\dot{W}}$	$g I_{sp}$	$\dfrac{g P_c C_F A_t}{\dot{W}}$	$\dfrac{gF}{\dot{W}}$
Characteristic exhaust velocity c^*	$\dfrac{g A_t P_c}{\dot{W}}$	$\dfrac{v_e}{C_F}$		$\dfrac{v_e}{C_F}$	$\dfrac{gF}{C_F \dot{W}}$	$\dfrac{g I_{sp}}{C_F}$	$\dfrac{g P_c A_t}{\dot{W}}$	$\dfrac{gF}{\dot{W} C_F}$
Nozzle thrust coefficient C_F	$\dfrac{F}{P_c A_t}$	$\dfrac{v_e}{c^*}$	$\dfrac{v_e}{c^*}$		$\dfrac{F}{P_c A_t}$	$\dfrac{g I_{sp}}{c^*}$	$\dfrac{F}{P_c A_t}$	$\dfrac{gF}{\dot{W} c^*}$
Thrust F	$A_t P_c C_F$	$\dfrac{v_e \dot{W}}{g}$	$\dfrac{c^* C_F \dot{W}}{g}$	$C_F P_c A_t$		$I_{sp}\dot{W}$	$C_F P_c A_t$	$I_{sp}\dot{W}$
Specific impulse I_{sp}	$\dfrac{A_t C_F P_c}{\dot{W}}$	$\dfrac{v_e}{g}$	$\dfrac{c^* C_F}{g}$	$\dfrac{C_F c^*}{g}$	$\dfrac{F}{\dot{W}}$		$\dfrac{C_F P_c A_t}{\dot{W}}$	$\dfrac{F}{\dot{W}}$
Combustion-chamber pressure P_c	$\dfrac{F}{C_F A_t}$	$\dfrac{v_e \dot{W}}{g C_F A_t}$	$\dfrac{c^* \dot{W}}{g A_t}$	$\dfrac{F}{C_F A_t}$	$\dfrac{F}{C_F A_t}$	$\dfrac{I_{sp}\dot{W}}{C_F A_t}$		$\dfrac{c^* \dot{W}}{g A_t}$
Weight-flow rate $\dot{W}$	$\dfrac{g A_t P_c}{c^*}$	$\dfrac{gF}{v_e}$	$\dfrac{gF}{c^* C_F}$	$\dfrac{gF}{c^* C_F}$	$\dfrac{F}{I_{sp}}$	$\dfrac{F}{I_{sp}}$	$\dfrac{g P_c A_t}{c^*}$	

NOZZLE FLOW AND PERFORMANCE

Let us now turn our attention to the exhaust nozzle and examine some of the pertinent flow mechanisms. Figure 2-5 shows how a small disturbance propagates. Probably all of us have observed an action at some distance away and have noted the passage of a finite time before the sound reached our ears. A sharp noise generates a spherical sound wave which travels outward from the source at the speed of sound c. At sea level and room temperatures, c is about 1100 feet per second.

The effect of stream velocity on the propagation of small disturbances is shown in figure 2-6. In the subsequent discussion, Mach number M is simply the ratio of flow
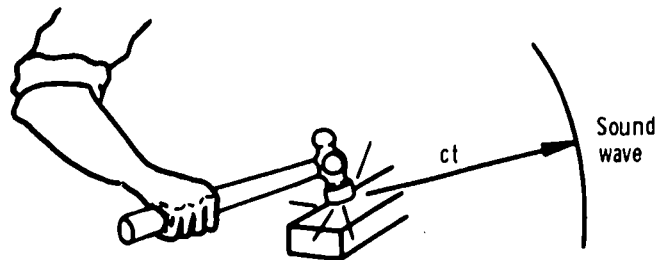
Figure 2-5. - Propagation of small disturbances in air. Instantaneous distance of sound wave from source = ct where c is speed of sound in air (at sea level, ≈ 1100 ft/sec) and t is time in seconds.

$$\alpha_M = \sin^{-1} \frac{1}{M}$$
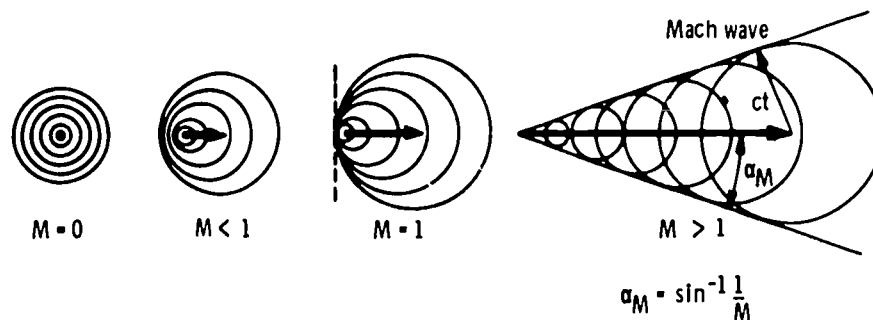
Figure 2-6. - Effect of velocity on sound-wave propagation.

velocity to the local speed of sound. If it is assumed that disturbances are generated in discrete increments of time, then for quiescent air conditions (M = 0) the waves are arrayed in concentric circles at any instant of time and are moving out uniformly in all directions. At subsonic speeds (M < 1), the waves are eccentric and are moving out in both directions, but they are moving faster in the downstream direction than in the upstream drection. At sonic flows (M = 1), there is no upstream propagation because the relative velocity is zero. At supersonic velocities, the envelope of small disturbances forms a Mach cone, the half-angle of which is equal to the Mach angle.

$$\alpha_M = \sin^{-1} \frac{1}{M} \tag{13}$$

At supersonic conditions, small disturbances can only propagate downstream within a volume defined by the Mach cone. A Mach wave thus defines the so-called region of influence.

Convergent-Divergent Nozzle

The flow conditions for a typical rocket nozzle are shown in figure 2-7. This figure shows the pressure distribution along the walls of a DeLaval convergent-divergent nozzle
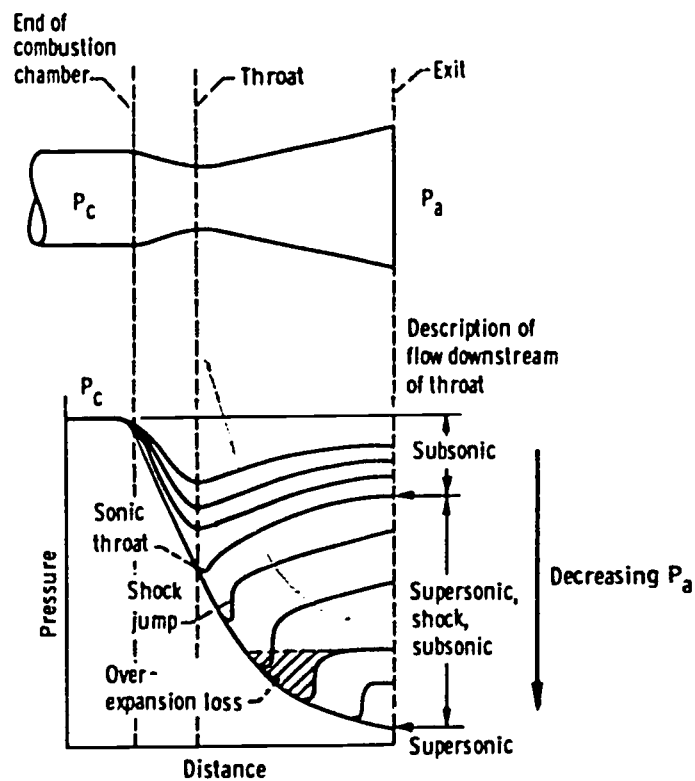

Figure 2-7. - Pressure distribution in DeLaval convergent-divergent nozzle.

for various pressure ratios. The pressure ratio is changed by varying the ambient pressure P_a and holding the chamber pressure P_c constant. At low pressure ratios, where P_a is relatively high, subsonic flow exists throughout the convergent and divergent portions of the nozzle. A small decrease in P_a causes the pressures to fall off all the way back to the combustion chamber. As was shown in figure 2-6, disturbances propagate upstream in the subsonic flow. This process continues with decreasing P_a until the pressure ratio in the throat corresponds to "choking" or sonic velocity. With further decreases in P_a, the flow upstream of the throat remains unaffected (remember: small disturbances cannot propagate upstream against a sonic or supersonic flow) while the flow downstream expands supersonically to a point where a normal shock is located. This normal shock is evidenced by a sharp rise in pressure (the so-called shock jump) and provides an abrupt transition of the flow back to the subsonic condition again. Further decreases in P_a cause the shock to move rearward in the nozzle and to occur at pro-

38

gressively higher Mach numbers. Eventually, the flow separates from the walls behind the shock wave. This is indicated here by the flatness in the distributions existing downstream of the shock jumps which are located well down in the nozzle. Note again that slight decreases in P_a can affect the location of the shock jump but cannot propagate any effects upstream thereof in the supersonic flow. When P_a is decreased to the point where supersonic flow is first established throughout the nozzle, and there is no shock jump, the nozzle is at design pressure ratio. Any further decreases in P_a will not affect the nozzle pressures, and the flow will continue to expand outside the nozzle.

At less than design pressure ratio, overexpansion losses occur. These are indicated for one such representative condition by the crosshatched area in figure 2-7. Overexpansion losses result from local pressures in the nozzle being less than ambient pressure. Pressures less than P_a constitute a loss in thrust or a drag on the propulsion system. For the particular P_a, the nozzle area ratio ϵ (equal to A_e/A_t) is simply too large and the flow overexpands with attendant energy losses.

At any point within the nozzle, the flow velocity, or Mach number, depends on the ratio of the local cross-sectional area to the throat area A/A_t as shown in figure 2-8. There is an evident need for a convergent channel to accelerate the gas subsonically and for a divergent channel to accelerate the gas supersonically. Theoretical considerations based on the conservation of mass, momentum, and energy across the nozzle yield the following expression to describe the variation in area:

$$\frac{A}{A_t} = \frac{1}{M}\left[\frac{2}{\gamma+1}\left(1 + \frac{\gamma-1}{2}M^2\right)\right]^{(\gamma+1)/2(\gamma-1)}$$
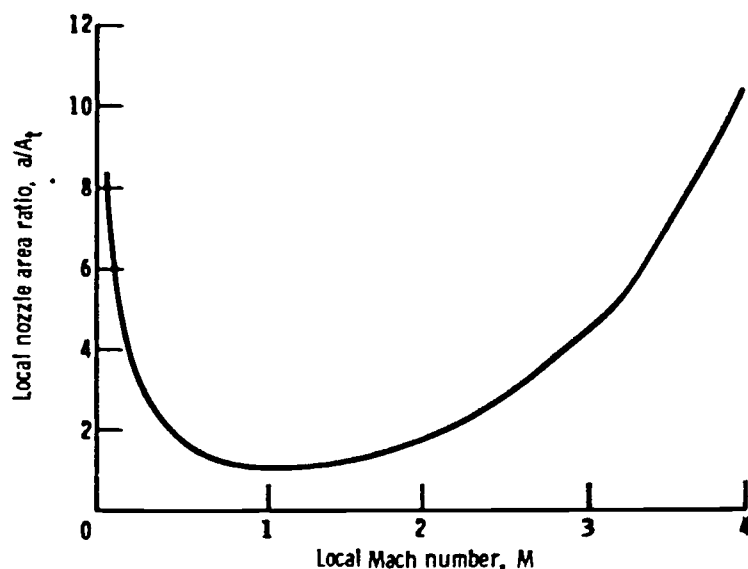

Figure 2-8. – Nozzle-area variation with flow Mach number.

It should be understood that for larger nozzle pressure ratios P_c/P_a the gases can be expanded to higher exit Mach numbers M_e. Higher exit Mach numbers require larger nozzle area ratios A_e/A_t.

Variable-Area Nozzle

During an actual rocket boost phase through the atmosphere, the ambient pressure P_a decreases rapidly with altitude (as described in chapter 1). With a constant chamber pressure P_c, this changing ambient pressure causes a wide variation in the nozzle pressure ratio. For an ideal nozzle to match every point on the trajectory would require a variable-area nozzle and a concomitant variation in exit Mach number M_e to correspond to the variations in pressure ratio. Such a variable-area-ratio nozzle could possibly be accomplished mechanically. However, it would involve much structural complexity and added weight that would probably offset any gains in performance over a fixed-geometry nozzle. It would be especially difficult with a three-dimensional axisymmetric arrangement.

Free-Expansion Nozzle

Another possibility in achieving this adjustment in expansion ratio is to do it aerodynamically as suggested in figure 2-9. The Prandtl-Meyer flow-expansion theory permits
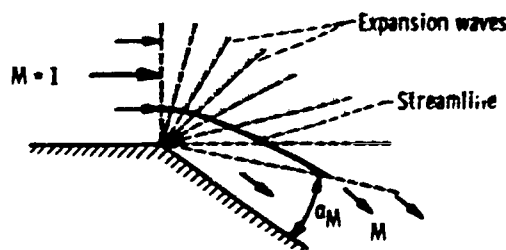
(a) Prandtl-Meyer flow turning around a corner.
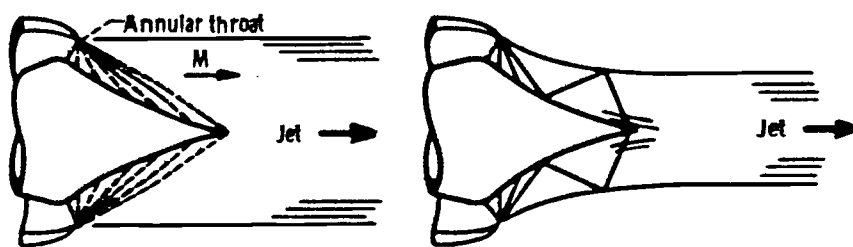
(b) Plug nozzle (on design).

(c) Plug nozzle (off design).

Figure 2-9. - Altitude compensation by means of free-expansion nozzles.

calculation of supersonic flow turning about a point as illustrated in figure 2-9(a).
Streamlines can be readily calculated through this expansion field at any specified radius.
These theoretical streamlines can be used as surface contours for plug-type nozzles as
shown in figures 2-9(b) and (c). Note the similarity in expansion fields. Operation of the
plug nozzle is shown for both on- and off-design conditions. Also, note the variation in
the size of the two exiting jets for on and off design. This aerodynamic adjustment of the
flow is referred to as "altitude compensation." In this free-expansion process, no over-
expansion losses are incurred as in the contrasting case for the convergent-divergent
nozzles at off-design conditions. In some advanced engine concepts for the 20- to
30-million-pound-thrust category, modular combustors or clusters of small high-
pressure engines are envisioned as feeding combustion gases onto a common plug nozzle
for further expansion externally.

ROCKET-ENGINE PERFORMANCE

Let us now briefly consider the thrusting phase of a rocket flight. Because of the ap-
plication of continuous thrust by the engine, the speed of the vehicle increases steadily
and reaches a maximum when the propellant is finally consumed. At this point the veloc-
ity is referred to as the "burnout velocity" and is designated v_b. In determining this ve-
locity increment, we will neglect for now the gravitational effec's and aerodynamic drag.
Now we will concern ourselves only with the thrust of the rocket engine. By using
Newton's Second Law of Motion $(F = \Delta mv/\Delta t)$ and integrating over the burning period,
a logarithmic expression can be derived for v_b:

$$v_b = v_e \ln \frac{m_i}{m_f} = 2.3 \, v_e \log \frac{m_i}{m_f} \qquad (14)$$

where m_i is the initial total mass of the vehicle (at lift off), and m_f is the final mass at
burnout. By using equation (5) the expression for v_b can be rewritten as follows:

$$v_b = gI_{sp} \ln \frac{m_i}{m_f}$$

But, by definition

$$MR = \frac{m_f}{m_i} = \frac{m_f}{m_f + m_p}$$

Therefore, by substitution,

$$v_b = gI_{sp} \ln \frac{1}{MR} = 2.3 \, gI_{sp} \log \frac{1}{MR} \tag{15}$$

This is the basic rocket equation. It shows the direct role of specific impulse in the attainment of high vehicle velocity. Burnout velocity is the parameter that best reflects rocket engine performance for either analyzing or accomplishing specific boost or space missions. It must be remembered, however, that in equation (15) we have neglected an additional gravity term. This gravity term will be taken into account in the next chapter, where we consider actual flight trajectories.

50

APPENDIX - SYMBOLS

A area, in.^{2}

A_e nozzle exit area, in.^{2}

A_t nozzle throat area, in.^{2}

a acceleration, (ft/sec)/sec

C_F nozzle thrust coefficient

c velocity of sound, ft/sec

c_p specific heat at constant pressure (for air, approx. 0.241), Btu/(lb)(^{O}F)

c_v specific heat at constant velocity (for air, approx. 0.17), Btu/(lb)(^{O}F)

c^* characteristic exhaust velocity, ft/sec

F thrust or force, lb

g acceleration due to gravity, 32.2 (ft/sec)/sec

I_{sp} specific impulse, sec

I_t total impulse, lb-sec

M Mach number

M_e Mach number at nozzle exit

MR mass ratio, m_f/m_i

m mass, slugs

m_f final mass of vehicle at burnout, slugs

m_i initial total mass of vehicle, slugs

m_p mass of propellant, slugs

$\dot{m}$ mass-flow rate, slugs/sec

m molecular weight (for hydrogen, 2; for oxygen, 32), lb/mole

o/f oxidizer to fuel (mixture) ratio

P_a ambient pressure, lb/in.^{2}

P_c combustion-chamber pressure, lb/in.^{2}

P_e nozzle exit pressure, lb/in.^{2}

R gas constant (universal gas constant, 1544 ft-lb/(^{O}R)(mole); specific gas constant for air, 53.3 ft-lb/(lb)(^{O}R))

T_c combustion temperature, ^{O}R

t time, sec

v velocity, ft/sec

v_b burnout velocity, ft/sec

v_e exhaust gas velocity

W weight, lb

$\dot{W}$ weight-flow rate, lb/sec

α_M Mach angle, deg

γ ratio of specific heats, c_p/c_v

Δ change in quantity or magnitude

ϵ nozzle area ratio, A_e/A_t

BIBLIOGRAPHY

Glasstone, Samuel: Sourcebook on the Space Sciences. D. Van Nostrand Co., Inc., 1965.

Sutton, George P.: Rocket Propulsion Elements. Third ed., John Wiley and Sons, Inc., 1963.

Wiech, Raymond E., Jr.; and Strauss, Robert F.: Fundamentals of Rocket Propulsion. Reinhold Publishing Corp., 1960.

44

3. CALCULATION OF ROCKET VERTICAL-FLIGHT PERFORMANCE

John C. Evvard[*]

In calculating the altitude potential of a rocket, one must take into account the forces produced by both the thrust of the engine and the gravitational pull of the Earth. A simplified approach can be developed for estimating peak altitude performance of model rocket vehicles. The principles involved, however, are basic and are applicable to all rocket-powered vehicles. The method of calculating vertical-flight performance is to use Newton's law to compute acceleration. Then, velocity and vertical distance, or altitude, are computed from acceleration. (Symbols used in these calculations are defined in the appendix.)

CALCULATIONS

According to Newton's law of motion, a mass M exerts a force (in weight units) of value M on its support. If the support is removed, this mass will fall freely with an acceleration of 32.2 feet per second per second. That is, the vertical speed will increase by 32.2 feet per second for each second of free fall. Imagine that this mass M is resting on a frictionless table top. A force of M (weight units) in a horizontal direction will produce an acceleration g of 32.2 feet per second per second in the horizontal direction. If the force is increased or decreased, the acceleration will be correspondingly increased or decreased. If the force in weight units is designated W and the acceleration is a, then this proportionality is expressed as

$$\frac{W}{a} = \frac{M}{g} \tag{1}$$

or

$$Wg = Ma$$

Physicists do not like to keep writing g in the equation. They distinguish between force and weight. Hence, they define the force F as Wg.

---

[*]Associate Director for Research.

$$F = Wg = Ma$$

Hence,

$$F = Ma \tag{2}$$

This is the equation we will use. Because this equation is independent of Earth's gravity, it is equally valid everywhere in the universe.

A thrusting rocket has at least two forces acting on it: (1) the force F_R due to the motor, and (2) the force $F_W = -Mg$ due to the weight of the rocket. The force F is the sum of F_R and F_W

$$F = F_R + F_W$$

or

$$F = F_R - Mg \tag{3}$$

Acceleration

From equations (2) and (3) the acceleration is given as

$$a = \frac{F_R}{M} - g$$

For convenience, the subscript on the symbol for the force due to the rocket motor will now be dropped so that

$$a = \frac{F}{M} - g \tag{4}$$

The acceleration is thus made up of two acceleration terms. The first, F/M, is due to the thrust-to-mass ratio. This would be the acceleration if there were no gravity. The second acceleration is that of gravity. This term reflects the so-called gravity loss. Equation (4) is general for vertical flight if instantaneous values of thrust and mass are inserted.

Velocity

If the acceleration is constant, then the velocity is clearly the acceleration multiplied by the time. This quantity is the area under the acceleration-time curve. If the
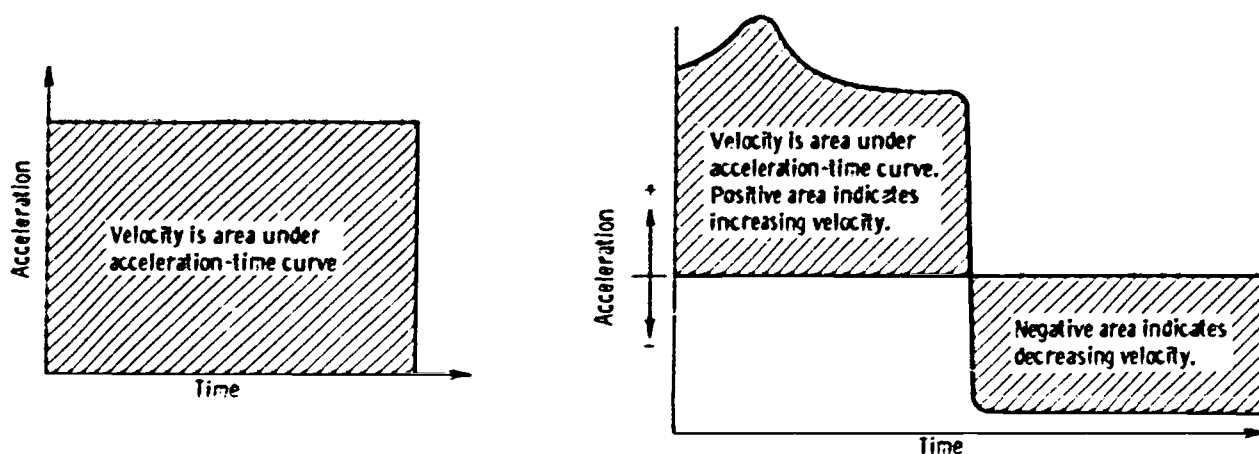
acceleration is not constant, then each increment in velocity is the local average acceleration multiplied by the time increment. The total velocity is the sum of the incremental velocity changes. This is, in fact, the area under the acceleration-time curve. Note that the areas generated by the curve can be positive or negative. A positive area denotes increasing velocity. A negative area denotes decreasing velocity. The velocity is zero initially and also when the positive and negative areas are equal. The velocity at any time is the area generated by the acceleration up to that time. Positive velocity means that the rocket is rising. Negative velocity means that the rocket is falling.

Flight Altitude

In a similar manner, each increment of vertical distance traveled Y by the rocket (flight altitude) is the local average velocity multiplied by the time increment. Thus, distance or altitude is the area under the velocity-time curve. The maximum altitude occurs when the velocity is zero (when the positive and negative areas under the acceleration-time curve are equal).

Note that the equations and graphical solution are general if instantaneous thrust and mass are employed in calculating the acceleration as a function of time. For example, the second-stage motor thrust and the combined weight of all remaining stages would be
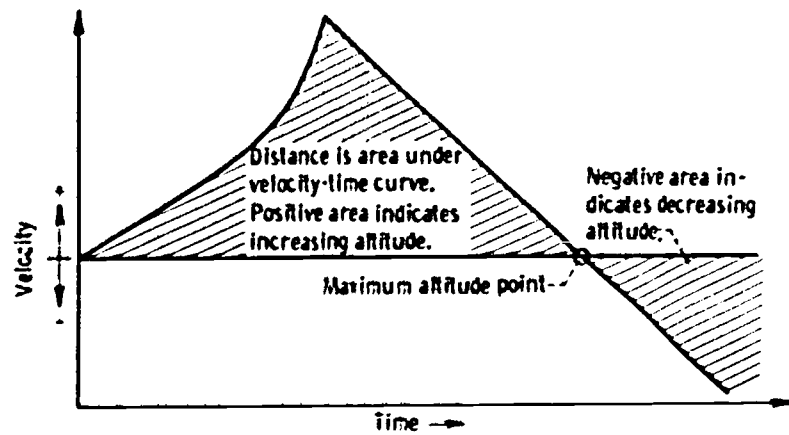
used just after first-stage burnout. The thrust and duration of thrust are given in model rocket catalogs. Remember to use consistent units. If thrust is in pounds, multiply by 32.2 to get F. Use M in pounds, time in seconds. The value of g is 32.2 feet per second per second. If thrust is in ounces, the mass should be in ounces, but 32.2 is still the multiplication factor to obtain F. Note that maximum thrust and average thrust are quite different for most model rocket motors.

APPROXIMATE ANALYTIC SOLUTIONS

The propellant weight for model rockets will likely be small compared to the launch weight. Hence, the mass can be nearly constant. Also, an average thrust might be employed instead of instantaneous thrust. Hence, acceleration is constant. The following equations result for a single-stage rocket. These equations can be obtained from the area plots already discussed.

During powered flight

$$a = \left(\frac{F}{M} - g\right) \tag{5}$$

$$V_a = \left(\frac{F}{M} - g\right)t_a \tag{6}$$

$$y_a = \left(\frac{F}{M} - g\right)\frac{t_a^2}{2} \tag{7}$$

The time t_a is limited to the thrust duration of powered flight. The initial velocity was taken as zero. For coasting flight, time t_c is measured from burnout. The height increase during coasting flight is y_c.

For coasting flight

$$a = -g \tag{8}$$

$$V = -gt_c + V_a \tag{9}$$

But at peak altitude $V = 0$, so

$$t_c = \frac{V_a}{g} \tag{10}$$

$$y_c = -\frac{gt_c^2}{2} + V_a t_c \tag{11}$$

Inserting t_c from equation (10) into equation (11) gives

$$y_c = \frac{V_a^2}{2g} \tag{12}$$

The total height is then

$$Y = y_a + y_c$$

or

$$Y = \left(\frac{F}{M} - g\right)\frac{t_a^2}{2} + \left(\frac{F}{M} - g\right)^2 \frac{t_a^2}{2g}$$

This then reduces to

$$Y = \frac{F^2}{M^2}\frac{t_a^2}{2g} - \frac{F}{M}\frac{t_a^2}{2} \tag{13}$$

Let T be the total impulse as given in rocket motor tables. This is force in pounds multiplied by time in seconds. Then

$$F \approx \frac{T}{t_a} g \qquad (14)$$

Substituting into equation (13),

$$Y = \frac{Tg}{2M} \left(\frac{T}{M} - t_a \right) \qquad (15)$$

The t_a term in equation (15) results from the gravity loss. This subtraction from the flight altitude can be minimized by (a) choosing motors with high total impulse T, (b) designing rockets with low mass M, and (c) choosing motors with very short burning time (minimizing t_a).

Tabulated values of motor characteristics are now required. The model rocket catalogs generally list such motors. These have been found to have an average specific impulse of about 82.8 seconds. That is, the motors generate 82.8 pounds of thrust for each pound per second of propellant flow rate. The jet velocity of these motors is then $82.8 \times g = 82.8 \times 32.2 = 2666$ feet per second. Other useful motor characteristics are listed in table 3-I. The quantities T and t are the total impulse and burning time included in equation (15). The quantity m is the propellant weight. This should be small compared to the rocket weight if the assumptions of equation (15) are to hold. Division of propellant weight by burning time gives the average propellant flow rate, or burning rate, $\dot{m}$. The term gt_a is the velocity loss during powered flight due to gravity,

TABLE 3-I. - MODEL ROCKET MOTOR CHARACTERISTICS

Motor	Total impulse, T, lb-sec	Burning time, t_a, sec	Propellant weight, m, lb	Average propellant burning rate, $\dot{m}$, lb/sec	Velocity loss, gt_a, ft/sec	Distance loss, $gt_a^2/2$, ft
$\frac{1}{4}$A.8	0.17	0.17	0.00211	0.0124	5.49	0.466
$\frac{1}{2}$A.8	.35	.40	.00422	.01055	12.89	2.58
A.8	.70	.90	.00844	.00938	29.0	13.04
B.8	1.15	1.40	.0139	.00992	45.1	31.50
B3	1.15	.35	.0139	.0397	11.27	1.97
C.8	1.50	2.00	.0181	.00905	64.4	64.4

while $gt_a^2/2$ is the altitude loss due to gravity during powered flight (see eqs. (6) and (7)). The velocity loss during powered flight, of course, leads to an additional altitude loss during coasting flight.

Sample problem:

Each of three different rockets is to be fired with three separate motors. The loaded weights, or masses, M of the rockets are 0.15, 0.25, and 0.5 pound, respectively. The three motors to be used are the A.8, the B3, and the C.8. Use equation (15) to calculate the expected altitude for each of the rockets. (The values of T and t_a for each of the motors are given in table 3-I.) Note that the B3 engine outperforms the C.8 engine on the heavy rocket in spite of the smaller total impulse. This is due to the gravity-loss term.

Motor	T/M	t_a	T/M - t_a	Y, ft
0.15-Pound rocket				
A.8	4.67	0.9	3.77	283.2
B3	7.67	.35	7.32	903.5
C.8	10.00	2.00	8.00	1288
0.25-Pound rocket				
A.8	2.80	0.9	1.9	85.6
B3	4.60	.35	4.25	314.7
C.8	6.00	2.00	4.00	386.4
0.5-Pound rocket				
A.8	1.40	0.9	0.5	11.2
B3	2.30	.35	1.95	72.2
C.8	3.00	2.00	1.00	48.3

SIMPLE THEORY FOR MULTISTAGE ROCKETS

Let subscripts 1, 2, 3, . . . , and n refer to conditions of the first, second, third, . . . , and n^{th} stages during thrusting flight. For example, t_2 is the time increment during second stage firing, y_2 is the distance, or altitude, increase during second-stage firing, V_2 is the velocity increase due to the second stage, etc. The general equations (constant mass) for the nth stage are

$$a_n = \left(\frac{F_n}{M_n} - g\right) \tag{16}$$

$$V_n = \left(\frac{F_n}{M_n} - g\right)t_n \tag{17}$$

Hence, the total velocity of the rocket after n stages have fired is

$$V = V_1 + V_2 + V_3 + \dots V_n \tag{18}$$

Hence,

$$V = \left(\frac{F_1}{M_1} - g\right)t_1 + \left(\frac{F_2}{M_2} - g\right)t_2 + \dots \left(\frac{F_n}{M_n} - g\right)t_n \tag{19}$$

$$y_n = \left(\frac{F_n}{M_n} - g\right)\frac{t_n^2}{2} + t_n\left[\left(\frac{F_1}{M_1} - g\right)t_1 + \left(\frac{F_2}{M_2} - g\right)t_2 + \dots \cdot \left(\frac{F_{n-1}}{M_{n-1}} - g\right)t_{n-1}\right] \tag{20}$$

The second term of equation (20) is the velocity of the rocket just prior to n^{th} stage firing multiplied by the nth stage firing time, and y_n is the altitude increase during n^{th} stage firing. The total altitude will then be

$$Y = y_1 + y_2 + y_3 \dots y_n + y_c \tag{21}$$

or

$$Y = \left(\frac{F_1}{M_1} - g\right)\frac{t_1^2}{2} + \left[\left(\frac{F_2}{M_2} - g\right)\frac{t_2^2}{2} + \left(\frac{F_1}{M_1} - g\right)t_1 t_2\right]$$

$$+ \left[\left(\frac{F_3}{M_3} - g\right)\frac{t_3^2}{2} + \left(\frac{F_2}{M_2} - g\right)t_2 t_3 + \left(\frac{F_1}{M_1} - g\right)t_1 t_3\right] + \dots + \frac{v^2}{2g} \tag{22}$$

In equation (22) it is assumed that there is no time delay between stage firings. Note from equation (14) that

60

$$F_n = \frac{T_n g}{t_n}$$

Hence

$$V_n = \left(\frac{T_n}{M_n} - t_n\right)g \tag{17a}$$

$$V = \left(\frac{T_1}{M_1} - t_1\right)g + \left(\frac{T_2}{M_2} - t_2\right)g + \ldots \left(\frac{T_n}{M_n} - t_n\right)g \tag{18a}$$

$$y_n = \left(\frac{T_n}{M_n} - t_n\right)\frac{gt_n}{2} + t_n g\left[\left(\frac{T_1}{M_1} - t_1\right) + \left(\frac{T_2}{M_2} - t_2\right) + \ldots \left(\frac{T_{n-1}}{M_{n-1}} - t_{n-1}\right)\right] \tag{20a}$$

or

$$y_n = \frac{V_n t_n}{2} + t_n(V_1 + V_2 + V_3 + \ldots V_{n-1}) \tag{20b}$$

$$Y = y_1 + y_2 + \ldots + y_n + \frac{V^2}{2g} \tag{22a}$$

or

$$Y = \left(\frac{T_1}{M_1} - t_1\right)\frac{gt_1}{2} + \left[\left(\frac{T_2}{M_2} - t_2\right)\frac{gt_2}{2} + \left(\frac{T_1}{M_1} - t_1\right)gt_2\right]$$

$$+ \left[\left(\frac{T_3}{M_3} - t_3\right)\frac{gt_3}{2} + \left(\frac{T_2}{M_2} - t_2\right)gt_3 + \left(\frac{T_1}{M_1} - t_1\right)gt_3\right] + \ldots + \frac{V^2}{2g} \tag{22b}$$

or

$$Y = \frac{V_1 t_1}{2} + \left(\frac{V_2}{2} + V_1\right)t_2 + \left(\frac{V_3}{2} + V_2 + V_1\right)t_3 + \ldots + \frac{V^2}{2g} \tag{22c}$$

53

62

These mathematical derivations may be confusing. The final results, however, are almost self-evident from sketches of acceleration and velocity against time. Acceleration is constant for each stage and for coasting flight. The area under the acceleration-time curve gives the velocity. The velocity increase for each stage is then the area of the rectangle given by the product of acceleration and time. For example, the second-stage velocity increase from the sketch is $a_2 t_2$ or $V_2 = \left[(T_2/M_2) - t_2\right] g t_2$. In a similar manner the terms of equation (22c) may be recognized as the various shaded areas of
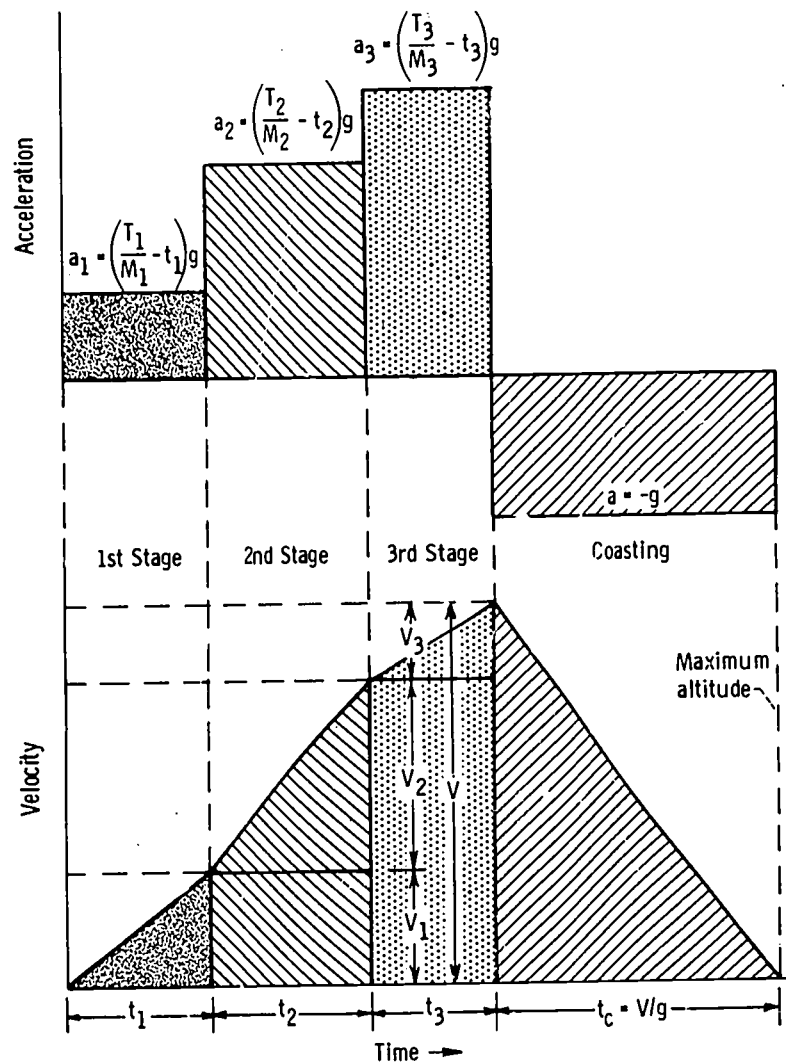
the lower part of the sketch. For example, the term $V_1 t_1/2$ of equation (22c) is the first triangular area of the velocity-time curve. The second term is the area of the rectangle plus the triangle over the time interval t_2, etc.

Sample problem:

A rocket is to be fired with a B3 motor for its first stage and an A.8 motor for its second stage. The launch weight of the rocket is 0.3 pound, and the second-stage weight is 0.15 pound. What altitude is the rocket expected to attain? (In the following calculations the subscript number denotes the stage.)

From the problem:

$$M_1 = 0.3 \text{ lb} \qquad M_2 = 0.15 \text{ lb}$$

From table 3-I:

$$T_1 = 1.15 \text{ lb-sec} \qquad T_2 = 0.7 \text{ lb-sec}$$

$$t_1 = 0.35 \text{ sec} \qquad t_2 = 0.9 \text{ sec}$$

From equation (17a):

$$V_1 = \left(\frac{1.15}{0.3} - 0.35\right)32.2 \qquad V_2 = \left(\frac{0.7}{0.15} - 0.9\right)32.2$$

$$V_1 = 112.1 \text{ ft/sec} \qquad V_2 = 121.4 \text{ ft/sec}$$

From equation (18):

$$V = 112.1 + 121.4$$

$$V = 233.5 \text{ ft/sec}$$

From equation (20b):

$$y_1 = \frac{112.1 \times 0.35}{2} \qquad y_2 = \frac{121.4 \times 0.9}{2} + (0.9 \times 112.1)$$

$$y_1 = 19.6 \text{ ft} \qquad y_2 = 155.5 \text{ ft}$$

Finally, from equation (22a):

$$Y = 19.6 + 155.5 + \frac{(233.5)^2}{64.4}$$

$$Y = 1021.7 \text{ ft}$$

These equations have neglected the change in mass associated with propellant ejection. Hence, the actual performance would be higher than the calculated value. On the other hand, wind resistance, which would decrease performance, has also been neglected. The actual performance would also change if the thrust were not constant with time. Most model rocket motors give a peak in thrust soon after ignition. High initial thrust leads to improved performance.

EXACT EQUATIONS FOR CONSTANT-THRUST ROCKET VEHICLES

At any point in time, neglecting drag,

$$a = \frac{F}{M} - g = \frac{I_{sp} g \dot{m}}{M} - g \qquad (23)$$

where I_{sp} is the specific impulse (≈ 82.8 sec for the model rocket motors that we have examined), $\dot{m}$ is the average propellant burning rate in pounds per second, and M is the instantaneous weight of the vehicle in pounds. Over the period of acceleration or motor thrust duration, this equation yields the following expression for velocity at burnout:

$$V = 2.3 \, I_{sp} g \, \log \frac{M_i}{M_f} - gt \qquad (24)$$

where M_i is the initial total mass of the vehicle, M_f is the final mass of the vehicle at burnout, and t is the burning time of the rocket motor. This is the same as equation (16) of the previous chapter except for the second (or gravity-loss) term. The powered-flight altitude is then given by the equation

$$y = I_{sp} g \, \frac{M_i}{\dot{m}} \left(1 - \frac{M_f}{M_i} - 2.3 \frac{M_f}{M_i} \log \frac{M_i}{M_f} \right) - \frac{gt^2}{2} \qquad (25)$$

The maximum altitude (or altitude after coasting) is then

$$Y = y + y_c$$

or

$$Y = y + \frac{V^2}{2g} \tag{26}$$

Aerodynamic drag has been ignored in the relations presented herein. This drag force, which would be included in equation (3), generally has the form

$$F_D = \frac{1}{2} \rho V^2 C_D A$$

where ρ is the air density, and V is the instantaneous speed of the rocket. The drag coefficient C_D is related to the geometry of the rocket and the quality of flow (laminar, turbulent, etc.) over the surface of the rocket. The quantity A is a reference area to indicate rocket size. The theory and prediction charts for rocket performance with aerodynamic drag are presented in reference 1.

APPENDIX - SYMBOLS

A	area
a	acceleration
C_D	aerodynamic drag coefficient
F	force
F_D	force due to aerodynamic drag
F_R	force due to rocket motor
F_W	force due to weight of rocket
g	acceleration due to Earth's gravity
I_{sp}	specific impulse
M	mass of rocket
M_f	final mass of rocket
M_i	initial mass of rocket
$M_1, M_2, M_3, \ldots, M_n$	mass of rocket during respective firing of first, second, third, . . ., n^{th} stage
m	weight of propellant
$\dot{m}$	average burning rate of propellant
T	total impulse (force multiplied by time)
$T_1, T_2, T_3, \ldots, T_n$	total-impulse increase associated with firing of first, second, third, . . ., n^{th} stage, respectively
t	time
t_a	time duration of acceleration (for single-stage rocket)
t_c	time duration of coasting flight ($V > 0$)
$t_1, t_2, t_3, \ldots, t_n$	incremental time increase during firing of first, second, third, . . ., n^{th} stage
V	velocity of rocket
$V_1, V_2, V_3, \ldots, V_n$	incremental velocity increase associated with firing of first, second, third, . . ., n^{th} stage
W	force in weight units
Y	flight altitude ($V \geq 0$)

58

y	incremental altitude increase
y_c	altitude increase associated with coasting flight
$y_1, y_2, y_3, \ldots, y_n$	incremental altitude increase during firing of first, second, third, . . ., n^{th} stage
ρ	air density

REFERENCE

1. Malewicki, Douglas J.: Model Rocket Altitude Prediction Charts Including Aero-
dynamic Drag. Tech. Rep. No. TR-10, Estes Industries, Inc., Penrose, Colo.,
1967.

4. THERMODYNAMICS

Marshall C. Burrows*

By using the equations which were presented in chapter 2, it can be shown that specific impulse, or the pounds of force exerted by the rocket per pound of propellant flowing each second, is dependent on the composition and temperature of the combustion products. Therefore, studying the various kinds of propellants and noting what happens when they react or burn is important. Observing how fast heat is produced by each pound of propellant that enters the combustion chamber is also important, since this determines the size and weight of the chamber.

The study of propellants, their reactions, and the energy changes needed to perform work is called thermodynamics. This practical subject gives engineers many tools they need to improve systems that interchange energy and work. Some such systems are rocket engines, automotive engines, and even refrigerators. We will not concern ourselves with the details of this subject but will only examine several rules or laws of thermodynamics that are important to remember. The first rule concerns temperature, a term which we hear applied to the weather every day. The point to remember is that a group of bodies (or molecules) all at the same temperature are said to be in "thermal equilibrium" with each other. The second rule to remember is that we cannot get more useful energy out of a system than we put into it. In other words, we cannot get more useful thrust out of a rocket engine than we put into it in the form of energy-containing propellants. This is analogous to the adage which states that "you can't get something for nothing." The final rule that we will consider is that heat flows only from hotter to cooler bodies. Many novel methods of propelling a rocket engine have failed because the inventor forgot one of these basic rules. Even the refrigerator in your home obeys these rules. The fluid that absorbs heat from the inside of the box is compressed and pumped to the bottom or back of the refrigerator where heat is rejected to the room.

Now that we have discussed some rules which govern the operation of a rocket engine, we shall examine in greater detail the characteristics and combustion processes of some available propellants.

The first genuine rocket propellant was probably made by the Chinese for their "arrows of flying fire" in the 13th century. Ingredients may have included tow, pitch,
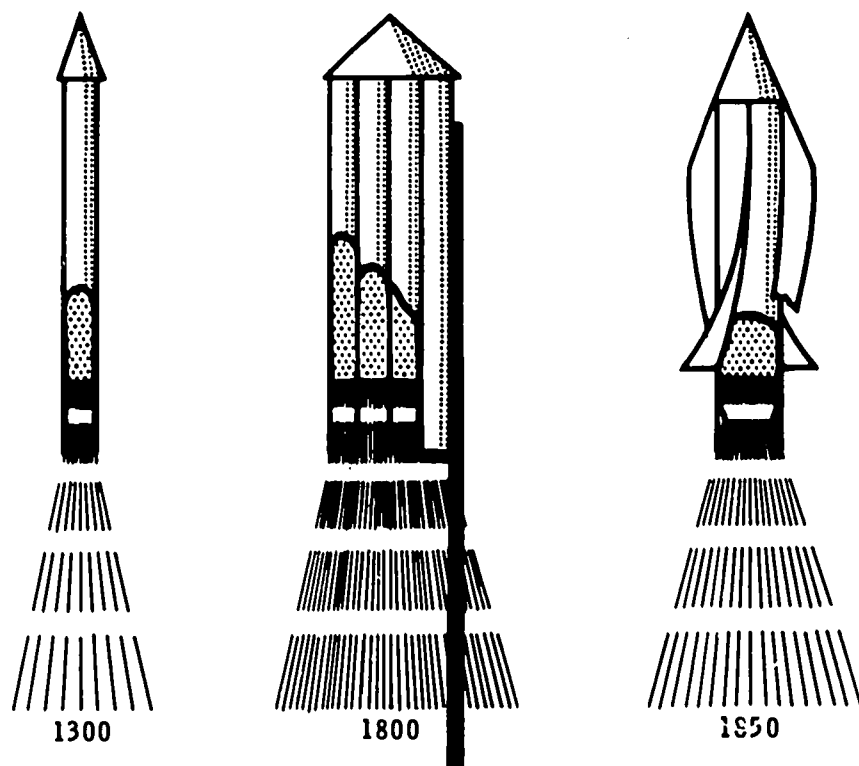
---

*Aerospace Scientist, Rocket Combustion Section.

Figure 4-1. - Early solid-propellant rockets.

turpentine, sulfur, charcoal, naphtha, petroleum, incense, and saltpeter. Eventually, gunpowder (or black powder) became the standard propellant, first in powder form, and later in granular form. In all the early solid-propellant rockets, burning proceeded upstream from the nozzle in a rather uncontrolled manner. Figure 4-1 shows how these early rocket configurations progressed from simple "fire arrows" to spin-stabilized missiles. Late in the 19th century it was found that combustion could be controlled more reliably if the powder was pressed into pellets or "grains." This latter term is still used today to define a propellant charge.

Near the end of the 19th century, a double-base (nitrocellulose-nitroglycerine) propellant was introduced, and it partly replaced the traditional gunpowder. The smokeless exhaust of this new propellant was a significant advantage for military uses.

The first use of liquid propellants in rockets was claimed by Pedro E. Paulet, in Peru in 1895, when he operated a small rocket on gasoline and nitrogen peroxide. Robert H. Goddard, an American, demonstrated a gasoline - liquid-oxygen rocket in 1926, and he has been considered the pioneer in this field. Work on the improvement of the liquid-propellant rocket continued throughout the 1930's. This work enabled the Germans to build a workable missile in the form of the V-2 rocket during World War II. The variation among these early liquid-propellant rockets is shown in figure 4-2.

Work on both liquid and solid propellants has been accelerated since that time until we now have a variety of liquids and solids from which to choose. The most common liquid propellants are listed in table 4-I. Liquid oxygen and alcohol powered the V-2
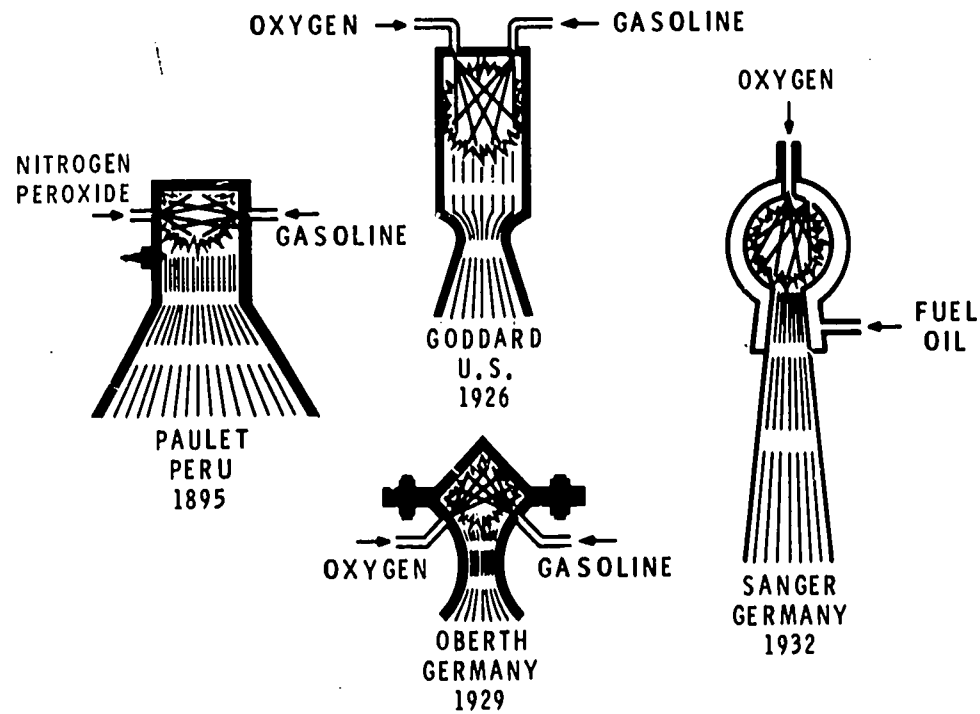
OXYGEN → ← GASOLINE

OXYGEN

NITROGEN
PEROXIDE
← GASOLINE

GODDARD
U.S.
1926

FUEL
OIL

PAULET
PERU
1895

OXYGEN → ← GASOLINE

OBERTH
GERMANY
1929

SANGER
GERMANY
1932

Figure 4-2. - Early liquid-propellant rockets.

TABLE 4-I. - COMMON CHEMICAL-ROCKET-PROPELLANT COMBINATIONS

Oxidizer			Fuel			Typical oxidant-fuel weight ratio, O/F	Specific impulse, (lb)(sec) lb (a)
Name	Formula	Storage temperature, ^oF	Name	Formula	Storage temperature, ^oF		
Liquid							
Oxygen	O_2	-297	Ethyl alcohol	C_2H_5OH	60	2.00	287
Nitrogen tetroxide	N_2O_4	60	Hydrazine	N_2H_4	60	1.30	291
Oxygen	O_2	-297	RP-1 (kerosene)	-------	60	2.60	301
Oxygen	O_2	-297	Hydrogen	H_2	-423	4.00	391
Solid							
Potassium perchlorate	K_4ClO_4	60	Asphalt resin	$(CH_2)_x$	60	High	220
Ammonium perchlorate	NH_4ClO_4	60	Rubber or plastic resin	------	---	High	250
Double-base type propellant (nitrocellulose-nitroglycerine); boiling point, 60° F						----	250

[a]Maximum theoretical impulse for products expanding from a combustion-chamber pressure of 1000 lb/in.^{2} to atmospheric pressure.
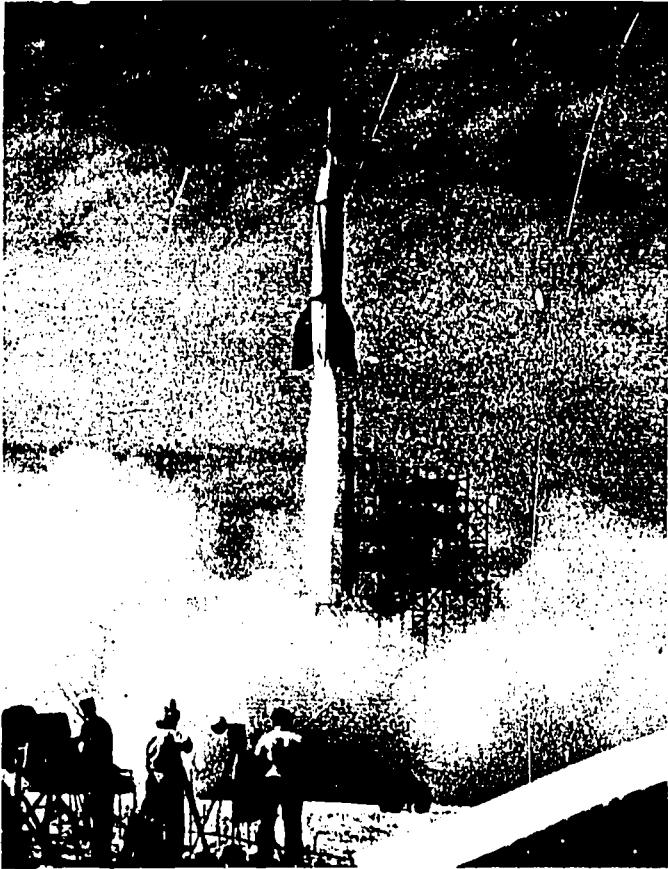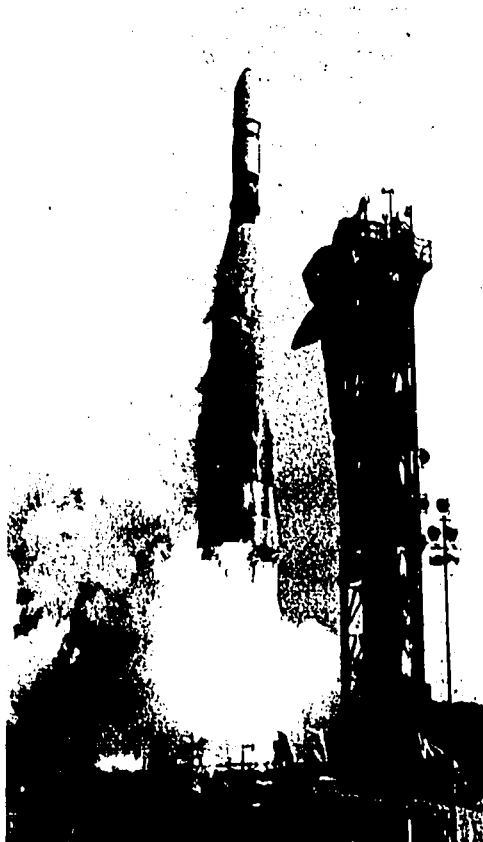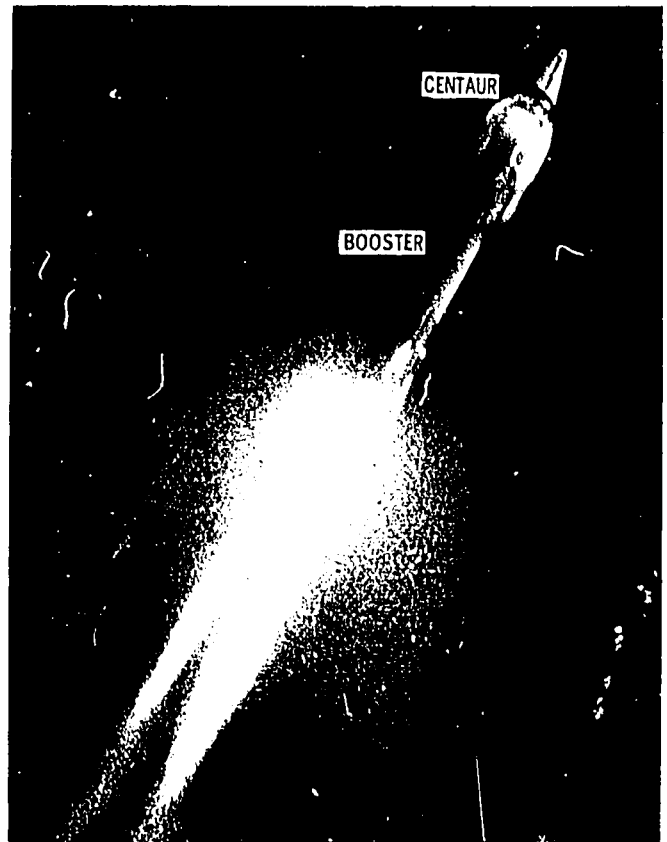
(a) Modified V-2 booster. Propellant, liquid-oxygen - ethyl alcohol.
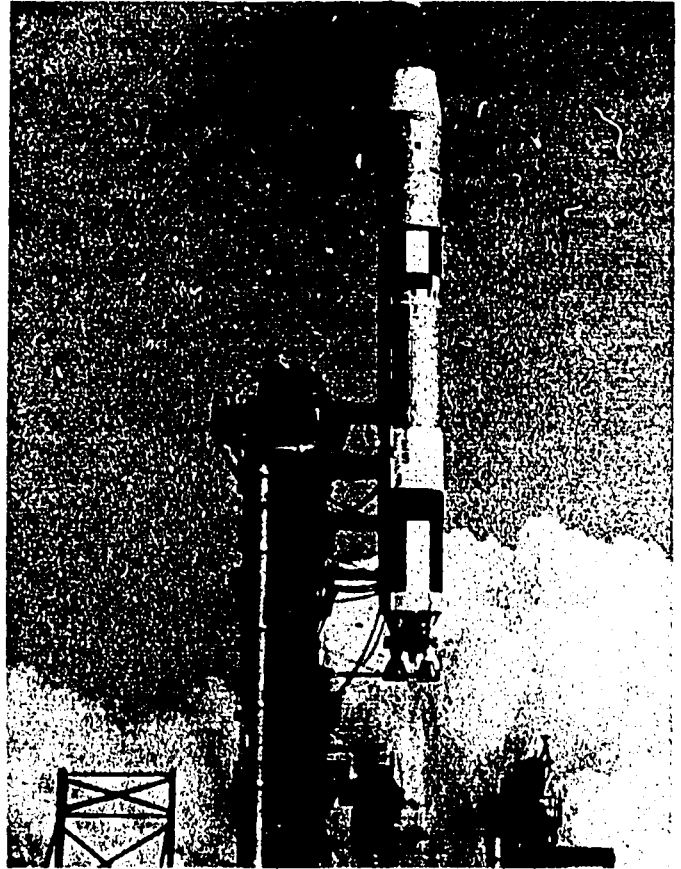
(b) Titan II booster. Propellant, nitrogen tetroxide - Aerozine.

(c) Atlas booster. Propellant, liquid oxygen - RP-1.

(d) Centaur upper stage. Propellant, liquid oxygen - liquid hydrogen.

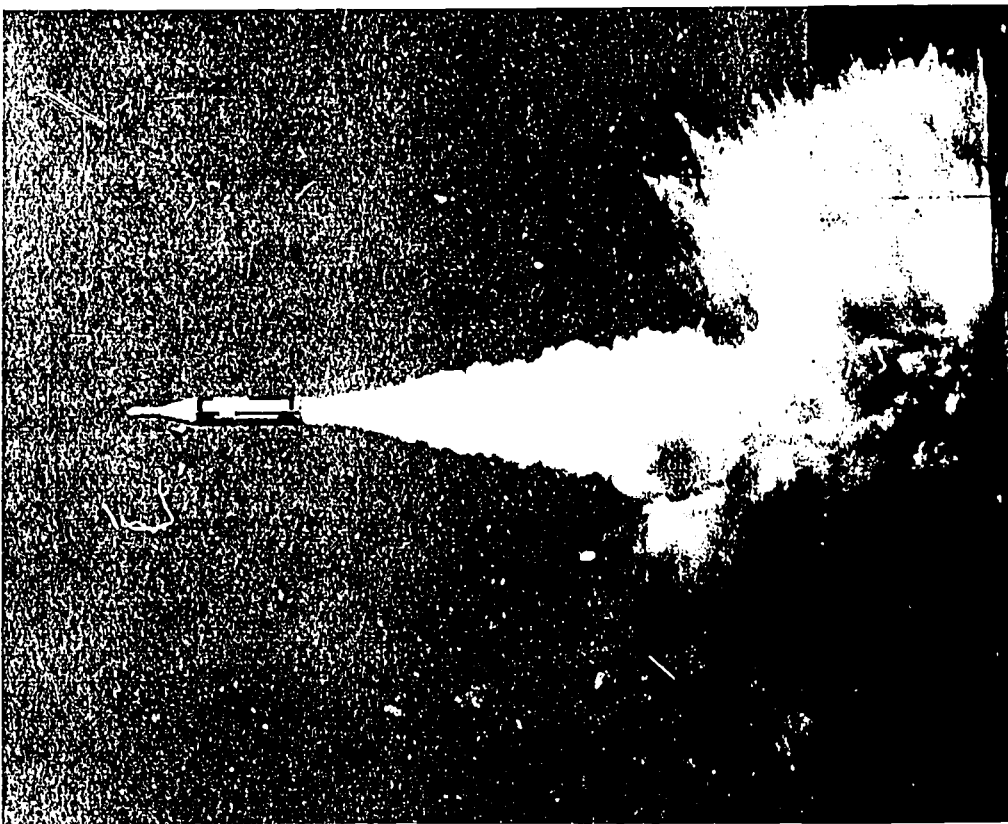Figure 4-3. - Liquid-propellant applications.

rocket (fig. 4-3(a)) that we mentioned earlier. Oxygen is liquid only at very low temperatures, so it must be refrigerated or stored in well-insulated tanks. From the standpoint of storage, the second set of propellants is attractive. Nitrogen tetroxide is the oxidizer, and hydrazine is the fuel. Both of these propellants are liquid in the temperature range of 40° to 70° F. Both propellants are very toxic, and hydrazine can burn alone, or act as a "monopropellant." This property of hydrazine can cause it to be dangerous to handle or use when it is heated excessively. However, when hydrazine is mixed with an equal amount of another liquid fuel called UDMH (unsymmetrical dimethyl hydrazine), the resulting mixture (Aerozine) is reasonably safe to use. Nitrogen tetroxide and Aerozine were used in the Titan II boosters (fig. 4-3(b)) which launched the Gemini series of manned satellites. Liquid oxygen has been used with RP-1 and hydrogen to power several important rocket vehicles. RP-1 is a type of kerosene, and, with liquid oxygen, powers the Atlas booster (fig. 4-3(c)). Hydrogen is liquid at a much lower temperature than oxygen. It is much more energetic than the other fuels, but it is very light as a liquid, just as it is very light as a gas. Hence the tank that holds the hydrogen must be large in volume and very well insulated. The Centaur (fig. 4-3(d)), which operates in a space environment, uses liquid hydrogen and liquid oxygen as propellants.

Other oxidizers that are used in liquid propellant systems are fluorine, fluorine compounds, nitric acid, and hydrogen peroxide. Other liquid fuels include ammonia, metallic hydrides, various hydrocarbons, and amines.

Despite the poor performance and bad physical properties of gunpowder, it is still used as a solid propellant. For example, Model Missiles, Inc., uses sporting black powder in its Type A motors for missile model propulsion. However, new composite propellants are replacing it because their performance is much higher, and their physical properties are much improved.

In table 4-I the most common solid propellants are listed. The first new composite that resulted from research work early in World War II consisted of a mixture of potassium perchlorate oxidizer and asphalt resin fuel. This combination was used in the initial JATO (Jet Assisted Take-Off) units. Ammonium perchlorate was soon substituted as the oxidizer, and plastics or synthetic rubbers replaced asphalt resins as the fuel. These combinations yielded considerably less smoke in the exhaust, produced higher impulse, and presented fewer handling problems than previous composite propellants. The Polaris and Blue Scout boosters (fig. 4-4) use improved types of composite propellants.

The double-base propellant has been used for various military rocket applications since Robert Goddard first experimented with it during World War I. The three major materials used are nitrocellulose, nitroglycerin, and diethylene glycol dinitrate (DEGN). Unfortunately, each of these materials is about as hazardous as the mixed composite pro-

(a) Polaris missile. Composite propellant grain.
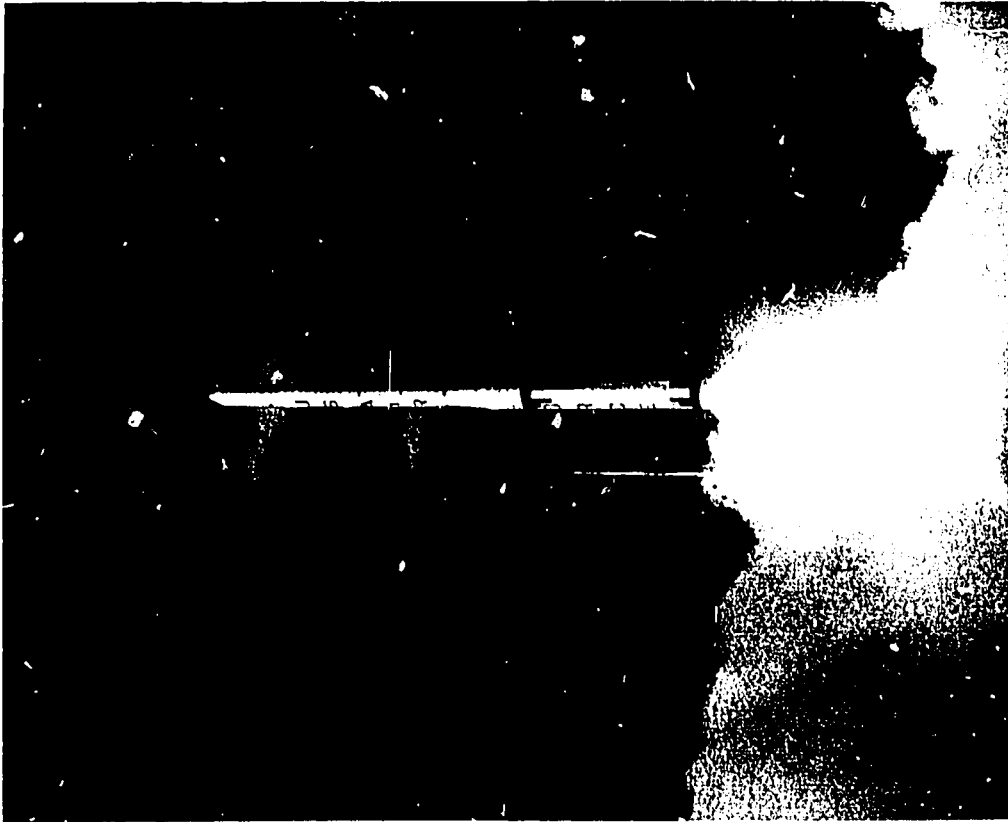
(b) Blue Scout booster, composite propellant grain; third stage, double-base propellant grain.

Figure 4-4. – Solid-propellant applications.

74

<table>
<tr><td>1. INJECTION</td><td></td></tr>
</table>

SHOWERHEAD   LIKE-ON-LIKE IMPINGING   UNLIKE IMPINGING   CONCENTRIC TUBE

2. MIXING

GAS-LIQUID   LIQUID PHASE   GAS PHASE

3. COMBUSTION

4. ACCELERATION

5. HEAT TRANSFER: FILM COOLING, REGENERATIVE COOLING, ABLATION

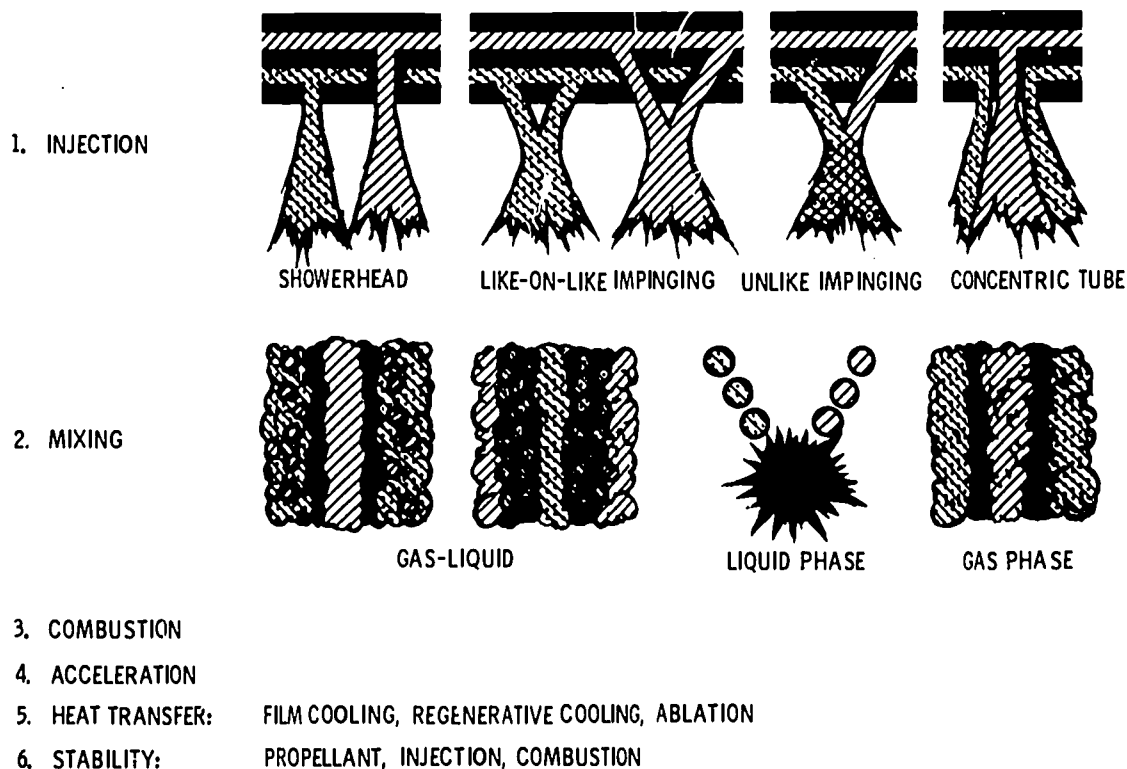6. STABILITY: PROPELLANT, INJECTION, COMBUSTION

Figure 4-5. - Liquid-propellant combustion.

pellant. Dry nitrocellulose, nitroglycerin, and DEGN are all high explosives and sensitive to shock. Mixing and forming are always done remotely, and numerous materials are added to increase the safety and reliability of the propellant. The Nike booster and the final stage of the Blue Scout utilize homogeneous propellants.

Now that the common types of propellants have been described, let us consider the manner in which the two basic types of propellant, liquid and solid, burn to produce hot, gaseous products.

Figure 4-5 shows various means of injecting liquid propellants into the combustion chamber. These means of injection include showerhead jets, impinging streams of several types, and concentric tubes in various sizes and arrangements. Injection of the propellant is followed by the mixing process. There are four processes by which liquid propellants may mix. Cold liquids such as cxygen and hydrogen may be near their boiling temperatures when they enter the combustion chamber. On the other hand, liquids such as RP-1 (kerosene) must be heated up to their boiling temperatures by the combustion gases themselves. Hence, one mixing process is that of slowly heating fuel droplets and streams surrounded by vaporized oxidizer. Oxygen-alcohol and oxygen - RP-1 propellants mix by this process because the oxygen vaporizes before the alcohol or the RP-1. In a second mixing process oxidizer droplets are surrounded by vaporized fuel. Oxygen-hydrogen propellants mix by this process because the vaporization of hydrogen exceeds that of the oxygen. Liquids that react spontaneously (hypergolic pro-
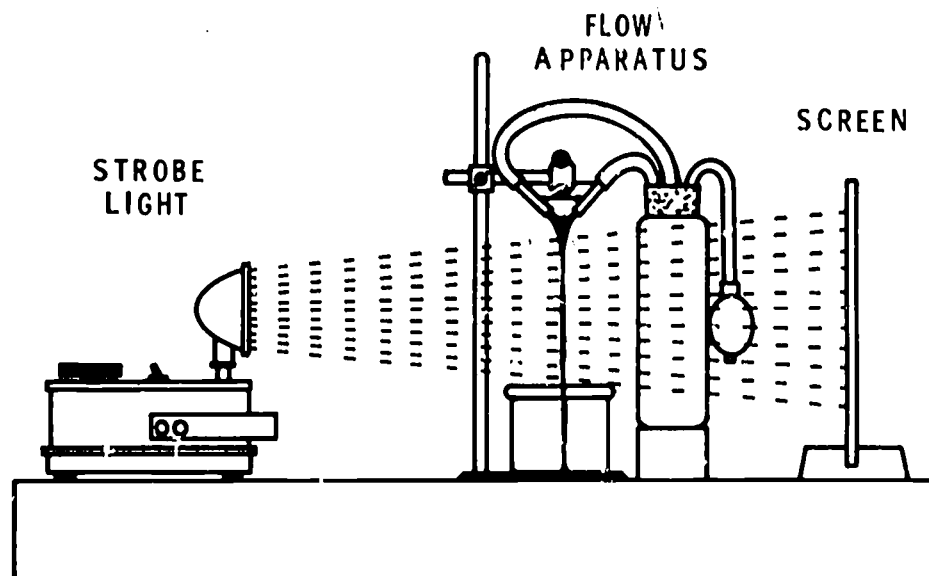
Figure 4-6. - Cold-flow injection apparatus.

pellants) mix by a third process. In this process, neither of the ingredients is boiling, but they mix as liquids. The liquids then react at their interfaces or from within to break up the liquid streams into droplets and vaporized gases. A fourth process is the mixing of gases. This process occurs in gaseous-propellant rockets or where liquids have been heated so that they enter the combustion chamber as gases.

The injection and mixing processes can be observed in cold flow tests with an apparatus like that shown in figure 4-6. When water or one ingredient of the propellant mixture is flowed through the injector, the spray pattern shows the extent of propellant mixing and the size of the droplets produced in the mixing process. The injection behavior of nonboiling propellants can be observed by flowing water through the tubes and illuminating the stream with a strobe light. If liquid nitrogen is substituted for the water and the impinging streams are again illuminated, the behavior of a boiling liquid can be observed. These observations can also be made with an actual combustor if it is equipped with special windows. Such a combustor has been used at Lewis Research Center for studies of alcohol burning in vaporized oxygen, oxygen streams burning in vaporized oxygen, oxygen streams burning in hydrogen, and impinging streams of hypergolic propellants, all at a combustion-chamber pressure of approximately 20 atmospheres. Photographs obtained in these studies are presented in figure 4-7. The results of such tests are used to determine what mathematical model is to be used to describe the behavior of a particular propellant combination.

Combustion follows very rapidly after mixing has taken place. The gaseous products increase in velocity toward the nozzle and mix with the unburned propellants as they go. Ideally all the unburned propellants mix, react, and mix again as products before they reach the nozzle. Incomplete mixing and incomplete reaction result in reduced rocket efficiency, which in turn, reduces the payload.
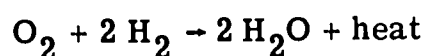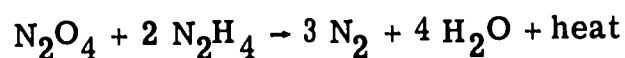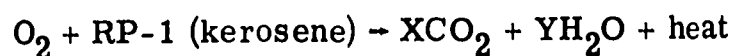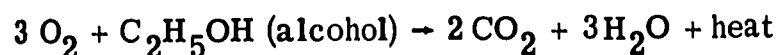
68

(a) Ethyl alcohol drops in vaporized oxygen.
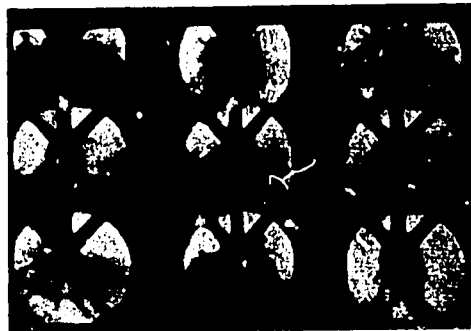
(b) Nitrogen tetroxide and hydrazine jets.
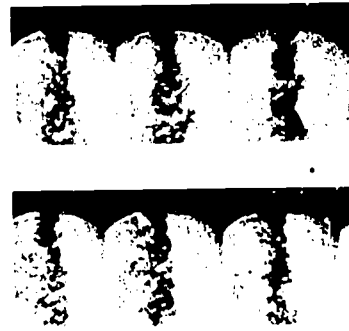
(c) Liquid-oxygen jets in gaseous hydrogen.

Figure 4-7. - Liquid-propellant vaporization and combustion. Combustion-chamber pressure, 20 atmospheres.

The simplest way to state the combustion reaction of a liquid propellant combination is to write the equation that describes it. The following equations describe the combustion reactions of the liquid propellants which have been discussed previously:

$$3\,O_2 + C_2H_5OH \text{ (alcohol)} \to 2\,CO_2 + 3\,H_2O + \text{heat}$$

$$O_2 + RP\text{-}1 \text{ (kerosene)} \to X\,CO_2 + Y\,H_2O + \text{heat}$$

$$N_2O_4 + 2\,N_2H_4 \to 3\,N_2 + 4\,H_2O + \text{heat}$$

$$O_2 + 2\,H_2 \to 2\,H_2O + \text{heat}$$

The actual reaction for each of these propellant combinations is not as simple as shown in these equations. One reason for this is that there are more products than shown here. Another reason is that the oxidant-fuel weight ratio O/F for highest impulse is fuel rich (that is, there is not enough oxidant to react with all the fuel). Hence, the actual reaction of oxygen and hydrogen can be described more accurately by the following equation:

$$O_2 + 4\,H_2 \to 1.98\,H_2O + 1.97\,H_2 + 0.06\,H + 0.03\,OH + \text{heat}$$
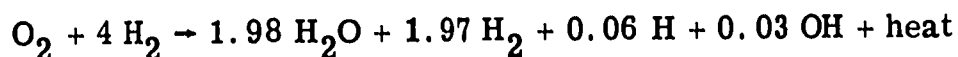
The combustion of composite solid propellants (fig. 4-8) is somewhat analogous to that of liquid-propellant mixtures. Solid-propellant surface heating takes the place of the injection process. Solid or liquid fuel and oxidizer particles decompose to form gases which subsequently react. Since the solid propellant is an excellent insulator, the solid is heated at or very near the surface until the oxidizer and fuel start decomposing at their common boundaries. Soon the oxidizer particles are no longer held in place by the fuel

69

1. BURNING RATE

2. MIXING

3. COMBUSTION

4. ACCELERATION

5. HEAT TRANSFER: PROPELLANT, ADDITIVES, INHIBITOR

6. STABILITY: PROPELLANT, CONFIGURATION, COMBUSTION

Figure 4-8. - Composite-propellant combustion.

binder, and they break loose to be carried along in the gas stream with the decomposing binder. Other materials such as metallic particles of aluminum are sometimes added to the composite propellant for better combustion and higher impulse. Also, the burning aluminum is a great aid in the observation of the burning of the propellant (fig. 4-9).

The reaction of a double-base propellant is different from that of a composite because the oxidizer and fuel of the double-base propellant are chemically mixed rather than just in physical proximity to each other. In order to describe the burning of a double-base propellant it is necessary to consider three zones called the foam, fizz, and flame zones. Heating very close to the surface melts some of the propellant and causes some low-
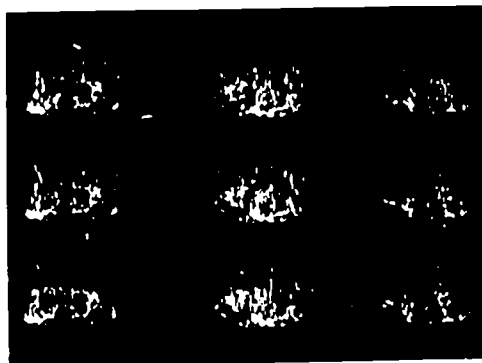

Figure 4-9. - Burning composite propellant with added aluminum. Pressure, 1 atmosphere.

70

temperature reactions. Bubbles of gas are released (foam zone) which rise and enter the fizz zone, where the remaining propellant decomposes. Final reactions and flame temperature occur in the flame zone.

Thus far the discussion has centered on the characteristics and the behavior of the propellants. The following discussion pertains to the combustion chamber. At the end of the chamber opposite the nozzle, there is an injector in the liquid-propellant engine, and there is usually a layer of solid propellant and inhibitor in the solid-propellant engine. In the liquid-propellant engine there is sufficient liquid entering the combustion chamber from the propellant manifold to prevent melting or burning of the injector face. However, care must be taken to prevent very hot, oxidizer gases from hitting the surface of the chamber wall at high velocity, because these gases can act just like a cutting torch. In the solid-propellant engine, a layer of propellant and inhibitor prevents overheating of the combustion-chamber walls, so the walls need only be strong enough to withstand the chamber pressure. As the solid propellant is burned away, the inhibitor acts as a heat shield and as a very slow burning fuel (fig. 4-10). Latex paint is a good example of an inhibitor.
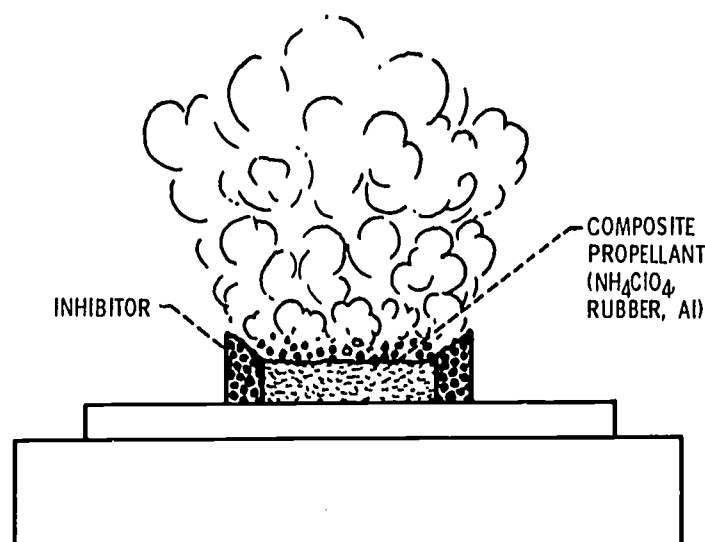

Figure 4-10. - Burning strand of solid propellant.

The combustion-chamber walls of a liquid-propellant engine are more complex than those of a solid-propellant engine. One of the liquid propellants, usually the fuel, passes at high velocities through thin tubes on its way to the injector. The tubes form part of the outside chamber walls. This procedure is called regenerative cooling and helps to prevent overheating of the chamber walls. Sometimes regenerative cooling is not sufficient to ensure cool walls. Then part of the liquid fuel is sprayed on the inner surfaces of the walls to act as a liquid or vapor shield against the heat from the combustion

71

79

gases. This procedure is known as film cooling. Of course, the walls must be strong enough to contain the chamber pressure.

The nozzle of a liquid-propellant engine is cooled the same way as the chamber walls (regenerative and film cooling). But the nozzle of a solid-propellant engine is necessarily uncooled. Therefore, it is made of a strong heat-resistant material such as tungsten, graphite, or a metal-ceramic combination.

Normally, there are low-velocity, cool gases close to the inside surfaces of the chamber walls. These cool gases help to shield the walls from the high-velocity, hot gases in the center of the chamber. If the cool gases are removed, the wall surfaces may burn out in the liquid-propellant engine, or they may erode in the solid-propellant engine. Pressure oscillations within the chamber can have the same effects, and they can even rupture the chamber walls themselves. These pressure oscillations are known as combustion instability. One form of combustion instability is called chugging and is characterized by severe oscillations in pressure at low frequencies (<100 cps). Another form of combustion instability is characterized by severe, high-frequency oscillations in pressure and is called screaming.

Chugging can be compared to a surging in which the propellants flow alternately at low and high velocities. The chamber pressure then responds to this flow behavior. Chugging may not be destructive to the engine itself, but it can result in violent shaking of the whole rocket structure.

Screaming can be compared to the pressure vibrations in pipe-organ tubes. Pressure waves can travel at sonic velocities up and down the chamber length, around it, across it, or radially in and out (fig. 4-11). All these high-frequency oscillations have been measured in research engines. Waves around the chamber have recently been produced in a specially built engine which can burn liquid propellants (O_2 and H_2) or solid composite propellants. Figure 4-12 shows stable and unstable combustion with both types of propellant.
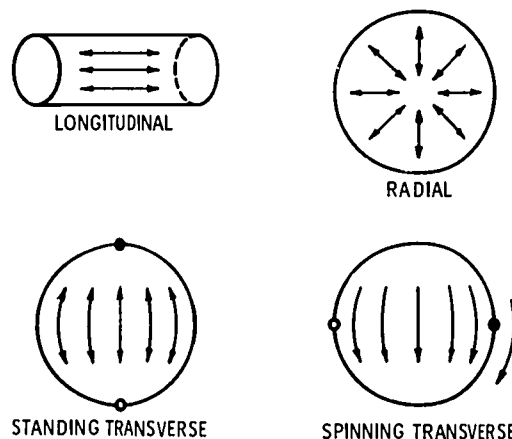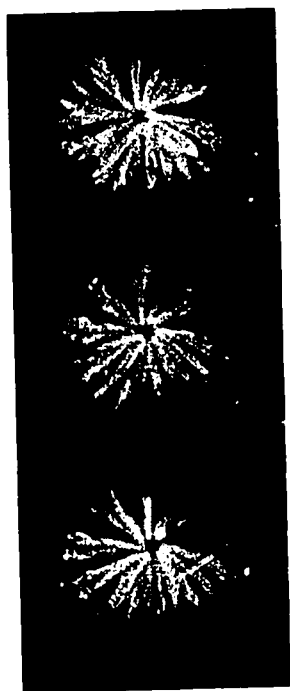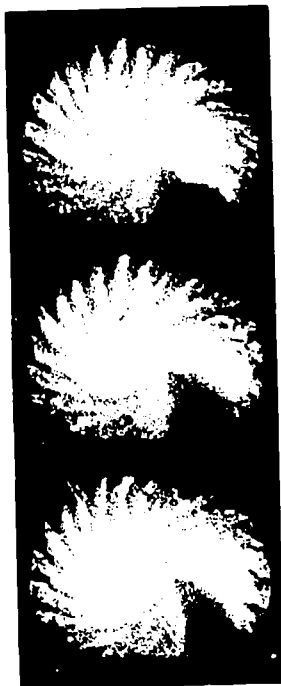

Figure 4-11. – Fundamental modes of acoustic combustion instability.

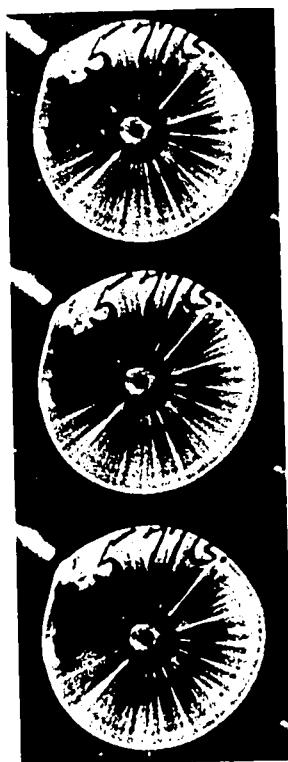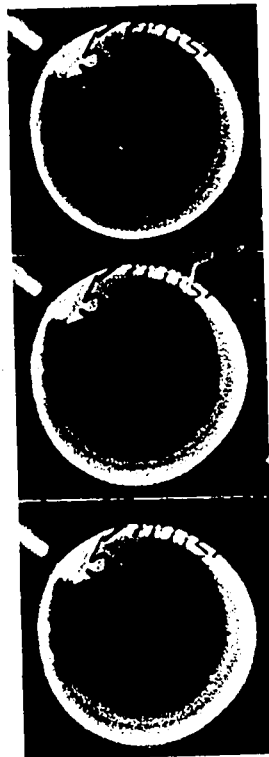STABLE   TRANSITION   UNSTABLE

(a) Combustion of liquid-oxygen - liquid-hydrogen propellant.

STABLE   TRANSITION   UNSTABLE

(b) Combustion of composite propellant.

Figure 4-12. - Screaming in liquid- and solid-rocket combustors.

In this chapter, a general discussion of the development, uses, burning processes, and problems of propellants has been presented. However, no attempt has been made to select the "best" propellant, injection method, or combustion-chamber shape. There really is no absolute best in these things, because no one propellant has all the desirable characteristics, and because the combustion-system hardware must be optimized for each propellant combination. The principal desirable features of propellants and of combustion systems are presented in the following lists.

Propellants:
    (1) High chemical energy (high impulse, high temperature)
    (2) Low molecular weight of combustion products
    (3) Chemical stability during storage
    (4) Small variation of physical properties with temperature
    (5) No change in state at storage temperature
    (6) High propellant density
    (7) Predictable physical and combustion characteristics
    (8) Easily ignitable, but safe and nontoxic during storage
    (9) Stable, efficient burning behavior
    (10) Nonluminous, smokeless, nontoxic exhaust

Combustion systems:
    (1) Injector or grain optimized for most stable, efficient combustion
    (2) Use of minimum chamber volume necessary for maximum system efficiency
    (3) Nozzle shape optimized for propellants and mission

GLOSSARY

ablation. Removal of surface material from a body by sublimation, vaporization, or melting due to heating resulting from a fluid moving past it at high speed. This phenomenon is often used to protect a structure from overheating by providing an expendable ablation surface, such as the heat shield on a reentry vehicle, or a protective coating in a combustion chamber.

additive. A substance added to a base to achieve some purpose such as a more even rate of combustion in a propellant or improved lubrication properties of working fluids such as RP-1, etc.

airbreathing engine. An engine which requires the intake of air for combustion of the fuel, as a ramjet or turbojet. This is contrasted with the rocket engine, which carries its own oxidizer and can operate beyond the atmosphere.

alcohol. See ethyl alcohol.

ammonium perchlorate (NH_4ClO_4). Solid compound used as an oxidizer in composite propellants. Available oxygen content is low, so high percentages are required for high performance. Exhaust contains very little smoke.

chemical fuel. A fuel depending on an oxidizer for combustion or for development of thrust, such as liquid- or solid-rocket fuel, jet fuel, or internal-combustion engine fuel; distinguished from nuclear fuel.

chemical rocket. A rocket using chemical fuel.

chugging. A form of combustion instability in a rocket engine, characterized by a pulsing operation at a fairly low frequency, sometimes defined as occurring between particular frequency limits.

combustion. A chemical process characterized by the evolution of heat; commonly, the chemical reaction of fuel and oxidizer; but, by extension, the term includes the decomposition of monopropellants and the burning of solid propellants.

combustion instability. Unfavorable, unsteady, or abnormal combustion of fuel, especially in a rocket engine. Unfavorable combustion oscillation such as chugging or screaming.

combustion chamber. See thrust chamber.

composite propellant. A solid rocket propellant consisting of an elastomeric fuel binder, a finely ground oxidizer, and various additives.

cryogenic propellant. A rocket fuel, oxidizer, or propulsion fluid which is liquid only at very low temperatures.

ethyl alcohol (C_2H_5OH). Colorless liquid used extensively in the chemical and liquor industries. Used with water as the fuel in the German V-2 rocket. (25 percent H_2O, 75 percent C_2H_5OH).

film cooling. The cooling of a body or surface, such as the inner surface of a rocket combustion chamber, by maintaining a thin fluid layer over the affected area.

hybrid motor. A rocket-propulsion unit that burns a combination of propellants of different composition and characteristics (as a liquid oxidizer and a solid fuel) to produce a propulsive force.

hydrazine (N_2H_4). Toxic, colorless liquid with high freezing point (34° F); soluble in water and alcohol; very flammable and burns by itself (monopropellant).

hydrogen. Lightest chemical element; flammable, colorless, tasteless, odorless gas in its uncombined state; used in liquid state as a rocket fuel; boiling point of -423° F.

hydrogen-fluorine. High-energy liquid propellant for rocket engines. Hydrogen is the fuel and fluorine is the oxidizer.

hypergolic fuel. Rocket fuel, such as hydrazine, that ignites spontaneously upon contact with the oxidizer and thereby eliminates the need for an ignition system.

inhibitor. A substance bonded, taped, or dip-dried onto a solid propellant to restrict the burning surface and to give direction to the burning.

initiator. A unit which receives electrical or detonation energy and produces a chemical deflagration reaction.

liquid hydrogen. Supercooled hydrogen gas, usually used as a rocket fuel; boiling point is -423° F; low density requires bulky, well insulated tanks and lines; very flammable.

liquid oxygen (LOX). Supercooled oxygen used as the oxidizer in many liquid-fuel engines; boiling point is -297° F; burns with fuels, metals, and organic materials.

liquid propellant. A liquid ingredient used in the combustion chamber of a rocket engine.

multipropellant. A rocket propellant consisting of two or more substances fed separately to the combustion chamber.

nitrogen tetroxide (N_2O_4). Yellow-red, toxic oxidizer used in storable-liquid-propellant systems. Reacts spontaneously with fuel and many other materials; very corrosive; boiling point is 70° F; stable at room temperature.

nozzle. The part of a rocket thrust-chamber assembly in which the gases produced in the chamber are accelerated to high velocities.

oxidizer. A substance that supports the combustion reaction of a fuel.

oxygen. See liquid oxygen.

oxygen-hydrocarbon engine. A rocket engine that operates on propellant of liquid oxygen as oxidizer and a hydrocarbon fuel such as a petroleum derivative.

propellant. A liquid or solid substance or substances which either separately or mixed can be changed into a large volume of hot gases at a rate which is suitable for propelling projectiles or air vehicles.

rocket engine. A reaction engine that contains all the substances necessary for its operation or for the consumption or combustion of its fuel. Does not require intake of any outside substance, and is capable of operation in outer space. Also called rocket motor.

rocket propulsion. A type of reaction propulsion in which the propulsive force is generated by accelerating and discharging matter contained in the vehicle. To be distinguished particularly from jet propulsion.

RP-1. Rocket propellant, type 1, is a nearly colorless liquid fuel resembling kerosene in its characteristics; contains a variety of hydrocarbon chemicals; boils at temperatures from 220° to 570° F; easily storable at normal temperatures.

screaming. A form of combustion instability, especially in a liquid-propellant rocket engine, of relatively high frequency and characterized by a high-pitched noise.

solid propellant. Specifically, a rocket propellant in solid form, usually containing both fuel and oxidizer combined or mixed and formed into a monolithic (not powdered or granulated) grain.

stoichiometric. Of a combustible mixture, having the exact proportions required for complete combustion.

subsonic. Of or pertaining to speeds less than the speed of sound.

supersonic. Of or pertaining to speeds greater than the speed of sound.

thermodynamics. The study of the relations between heat and mechanical energy.

thrust. The pushing force developed by an aircraft engine or a rocket engine. Specifically, the product of propellant mass flow rate and exhaust velocity relative to the vehicle.

thrust chamber. The chamber of a jet or rocket motor in which volume is increased through the combustion process to obtain high velocity gases through the nozzle.

UDMH. Unsymmetrical dimethyl hydrazine, a clear, colorless liquid with low freezing point, -71° F; boils at $+146^\circ$ F; soluble in water, ethyl alcohol, and most hydrocarbon fuels; one of a group of fuels known as the amines; mixed equally with hydrazine to form Aerozine; used in numerous current engines.

vaporization rate. The unit mass of a solid or liquid that is changed to a vapor or gas in a unit of time.

BIBLIOGRAPHY

Hill, Philip G.; and Peterson, Carl R.: Mechanics and Thermodynamics of Propulsion. Addison-Wesley Publ. Co., 1965.

Siegel, Bernard; and Schieler, Leroy: Energetics of Propellant Chemistry. John Wiley and Sons, Inc., 1964.

Sutton, George P.: Rocket Propulsion Elements. Third ed., John Wiley and Sons, 1963.

5. MATERIALS

William D. Klopp*

In the space program, materials can make the difference between success and
failure. Some of the most important materials problems are associated with uncooled
nozzles for both solid- and liquid-propellant rockets. Problems of crack propagation in
large welded structures are also interesting, as is the development of lightweight, tough
tank materials for containment of cryogenic fuels.

TYPES OF ROCKET ENGINES

In the liquid-propellant engine (fig. 5-1), liquid fuel, such as kerosene, is pumped
by a turbine-driven pump directly into the combustion chamber. At the same time the
liquid oxidizer, typically liquid oxygen at -297° F, is pumped through hollow passages
in the walls around the engine before entering the combustion chamber. Injector nozzles
spray fuel and oxidizer into the chamber where they are mixed and burned. The hot gas-
eous products are expelled through the nozzle to provide the propulsive thrust. The
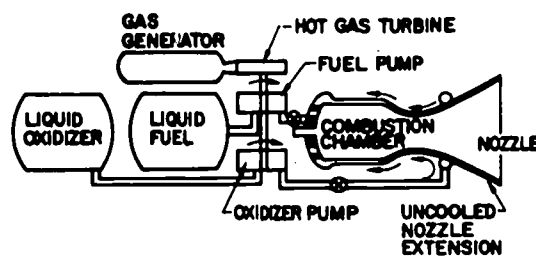
(a) Liquid-propellant rocket motor.
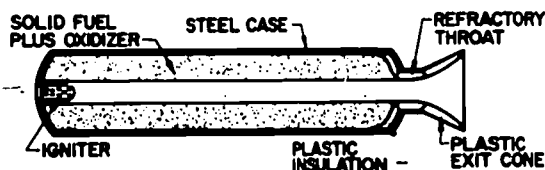
(b) Solid-propellant rocket motor.

Figure 5-1. - Basic types of rocket motors.

---

*Head, Refractory Metals Section.

process of pumping the liquid oxygen through the lining of the nozzle and combustion chamber is called regenerative cooling. This is necessary because the materials, such as stainless steel, which are strong enough to be used safely have melting points significantly below the temperature of the combustion gases.

The liquid-propellant engine has a number of problems caused by clogged injectors or improper burning, such as screech (harmonic acoustic waves) and burn-through of the walls. However, these problems have been solved by improved design rather than through the use of advanced materials.

One version of the liquid rocket motor, which is planned for use on the Apollo mission, uses liquid fuels which are storable at room temperature. This type of fuel is unsuitable for regenerative cooling, and thus the engine must use heat-resistant materials in the combustion chamber and in the critical throat region of the nozzle. These pose a serious materials problem.

The solid-propellant rocket motor (fig. 5-1) employs a solid fuel-oxidizer combination rather than the more conventional liquids. Normally, the fuel, the oxidizer, and a bonding agent are mixed together in the liquid state, then cast to shape, and finally cured to a solid, rubbery mass. When heated to ignition temperature, the fuel and oxidizer combine at the surface to produce hot combustion gases which are expelled through the nozzle to provide thrust. Since in this motor no cryogenic liquids are available, regenerative cooling of the hot combustion chamber and nozzle is impossible. The ability of heat-resistant materials to withstand the extreme erosion and corrosion conditions in these hot regions is a limiting factor in the design and operation of solid-propellant motors.

HEAT-RESISTANT MATERIALS

Several types of material are potentially suitable for use in the critical throat region of uncooled nozzles. Many tests are employed to determine the best materials for a particular motor and a particular set of operating conditions.

The potentially suitable materials can be divided into two general classes, the refractories and the ablatives. The refractories, characterized by high melting points in the range 4000° to 6000° F, include such materials as tungsten, molybdenum, graphite, and certain oxides and carbides. These materials maintain their strength at high temperatures so that they are sufficiently tough to withstand the erosive effects of the hot gas stream. During engine operation, the internal surfaces of throats and nozzles of these materials are heated to close to the temperature of the gas stream. This heat is absorbed by the material and dissipated by normal thermal radiation and convective cooling by the atmosphere on the outside.

In contrast to the refractories, the ablative materials are not high melting and tough. Instead, they absorb heat from the gas stream by chemical reactions as well as by melting and vaporizing. A typical ablative material is a composite called phenolic-refrasil. This material consists of a tape woven from silica glass fibers and impregnated with a plasticlike phenolic resin. The tape is wound on a mandrel to form the nozzle, which is heated under pressure to bond the tapes together with the phenolic resin. During use, the resin decomposes to form graphite and organic compounds which melt and vaporize (ablate). The silica tape also melts, absorbing heat in the process, and reacts with the graphite to form silicon carbide. The compound is fairly high melting and tough and imparts a certain degree of resistance to mechanical erosion to the nozzle. The ablative nozzles are cheap and easily fabricated and can be used in engines where the operating conditions are not so severe as to require the use of a tougher, refractory material.

MATERIALS EVALUATION

The selection of a material for the nozzle of a given motor designed to produce a predetermined thrust generally requires an experimental program to evaluate the candidate materials under the given conditions. The two major parameters measured during test firings are the temperature distribution in the nozzle and the gas pressure in the combustion chamber.

Figure 5-2 shows the temperature distribution profile in a refractory throat insert as a function of firing time. In the first few seconds of firing, the temperature of the
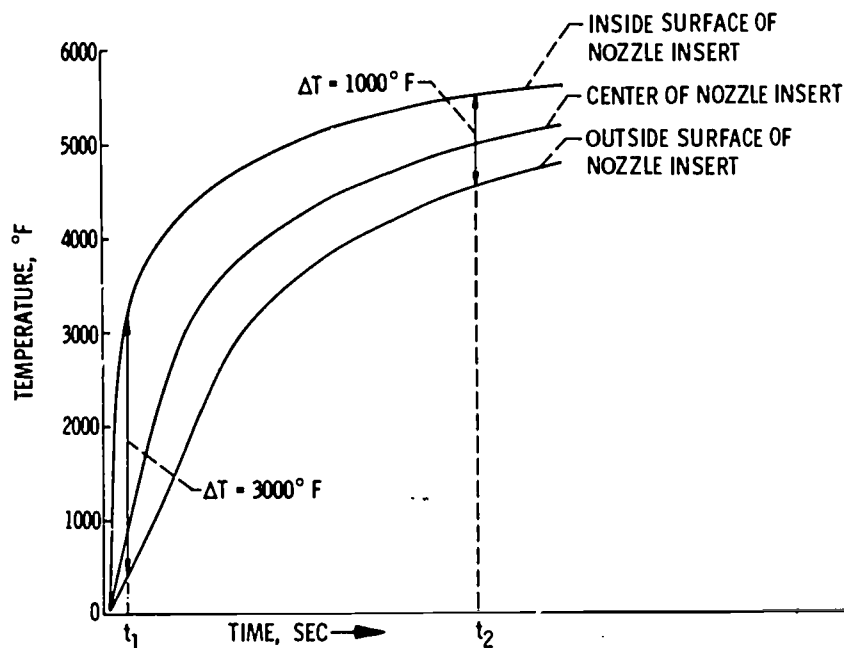

Figure 5-2. - Typical temperature distribution profiles in nozzle insert.

81

inside surface of the nozzle insert rises very quickly; it then begins to level off and approaches the flame temperature asymptotically. At the outside surface of the insert, the heat is supplied by conduction and the temperature rise is slower. This condition leads to a temperature difference of 3000° F between the inside and the outside surfaces at the start of firing, as indicated at time t_1. The difference decreases as firing proceeds, as at time t_2.

The large temperature differential between the inside and the outside surfaces just after ignition is a real problem with refractory inserts which are brittle when cold, such as tungsten, molybdenum, and the refractory oxides and carbides. The inside surface material tends to expand as it heats up, putting the outside surface in tension. Cracking of the nozzle can result if the material cannot deform plastically to relieve these stresses.

Typical pressure-time traces are shown in figure 5-3. These traces indicate the amount of material removed from the throat area by mechanical erosion and chemical
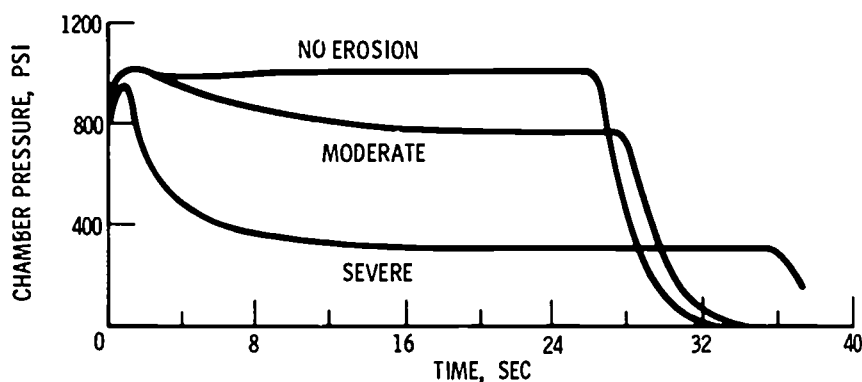

Figure 5-3. - Typical pressure-time traces for varying degrees of nozzle throat erosion.

corrosion during firing. As the throat becomes larger, the gaseous combustion products escape more rapidly and the pressure within the combustion chamber decreases. Thus, an erosion resistant nozzle material shows a relatively constant chamber pressure during the entire firing cycle, while a large pressure drop indicates severe erosion in the critical throat region.

The results of two experimental programs recently conducted at the Lewis Research Center offer an insight into the behavior of several nozzle materials in two different uncooled motors.

The first program used a small solid-propellant engine test facility to study the behavior of various types of throat insert materials under carefully controlled test conditions. The important characteristics of the engine were as follows:

Propellant . . . . Arcite 368, a solid combination of fuel and oxidizer which burns to give entirely gaseous products

Flame temperature . . . . Calculated to be 4700° F, an intermediate temperature for solid propellants

Chamber pressure, psi . . . . 1000, typical for solid-propellant engines

Burn time, sec 30

Nozzle throat diameter, in. 0.289

The appearance of several refractory and ablative nozzles after firing under these conditions is shown in figure 5-4.

The tungsten nozzle (fig. 5-4(a)) demonstrated excellent erosion and corrosion resistance. A pressure drop of about 10 percent indicated that slight erosion had occurred, probably by oxidation of the tungsten to form volatile tungsten trioxide. Although it is a brittle material at low temperatures, the tungsten did not crack because the walls were relatively thin and thus thermal stresses were relatively low.

In contrast to tungsten, the graphite nozzle shown in figure 5-4(b) suffered considerable erosion and corrosion. The combustion chamber pressure decreased from 1000 to about 500 psi; this decrease indicated an unacceptably high loss of material from the throat area.

Figure 5-4(c) shows a nozzle of LT2, a cermet (ceramic-metal) material consisting of aluminum oxide (Al_2O_3) in a metallic tungsten-chromium matrix. Figure 5-4(d) shows a nozzle made of a ceramic compound, silicon nitride. Both of these materials showed good strength and corrosion resistance. There was no throat erosion, and chamber pressure during firing remained constant. Both of these materials, however, are quite sensitive to thermal shock and cracked severely on cooling after firing. Neither material is adequate under these conditions.

Two ablative nozzles are shown in figures 5-4(e) and (f). The darkened regions near the inside surfaces of these two nozzles indicate the depth of resin decomposition during firing. Both nozzles suffered high, though uniform, erosion. The 40-percent resin material in figure 5-4(e) showed a pressure drop from 1000 to 500 psi, while the 20-percent resin material showed a pressure drop from 1000 to 400 psi during firing. Both, of course, are unacceptably high pressure losses and indicate that these materials are unsuitable for this type of engine.

The results of this small-scale program indicated that for high-pressure solid-fueled engines, tungsten is preferable to the other materials tested, provided that thermal shock can be avoided when the engine is made larger.

A second study at Lewis illustrates how different engine conditions dictate the use of materials other than tungsten. The object of this study, the engines for the service module of the Apollo moon mission, uses liquid fuel which is storable at room temperatures. The nozzle material is ablative phenolic-refrasil for both the large main thrust
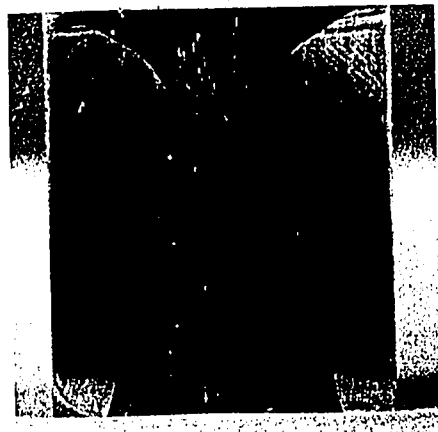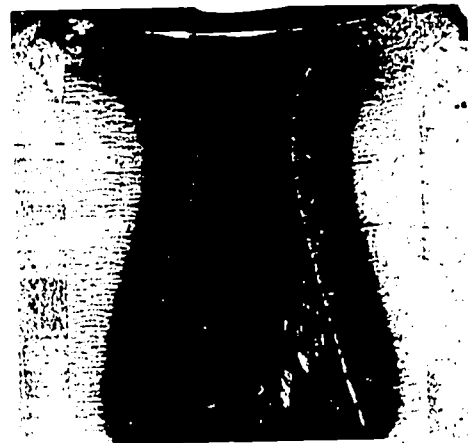
(a) Tungsten.
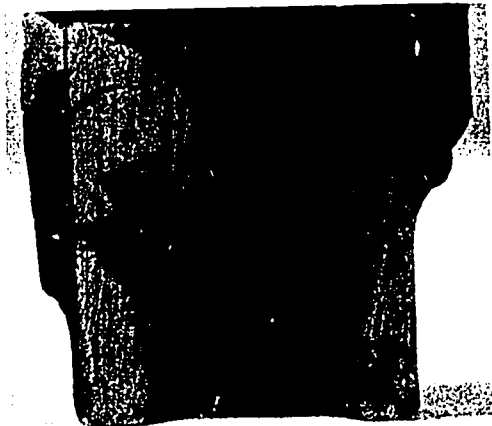
(b) Graphite.   CS-26529

(c) LT 2.

(d) Silicon nitride.

(e) Phenolic-refrasil (40 percent resin).

(f) Phenolic-refrasil (20 percent resin).

Figure 5-4. - Nozzles of various materials after firing in small solid-propellant motor.

engine, which has an 8-inch throat diameter, and the smaller vector control engines, which have a 1-inch throat diameter. The operating conditions are moderate because the engine will be functioning only in a low-density atmosphere. The chamber pressure is expected to be less than 100 psi, flame temperature, 4000° to 4500° F, and total burn time, 700 seconds with several restarts.

For these operating conditions, the ablative material appears adequate. However, possibly more thrust may be required of the engine, necessitating a higher chamber pressure or a higher flame temperature. Under these conditions, the adequacy of the ablative nozzle is marginal, and thus various alternative nozzle materials for both the 1- and the 8-inch-throat-diameter engines are being studied. The alternatives include other refractory metals and compounds, various types of reinforced refractory combination, and other ablatives.

Figure 5-5 shows several large- and small-diameter nozzles after being test-fired with the storable liquid fuel. Figure 5-5(a) shows an 8-inch-diameter nozzle of phenolic-refrasil ablative material after a 160-second firing. The nozzle has suffered relatively severe charring, and too much melting and running of the silica tape has occurred. A large-diameter nozzle such as this can tolerate more erosion from the throat region than a small-diameter nozzle.
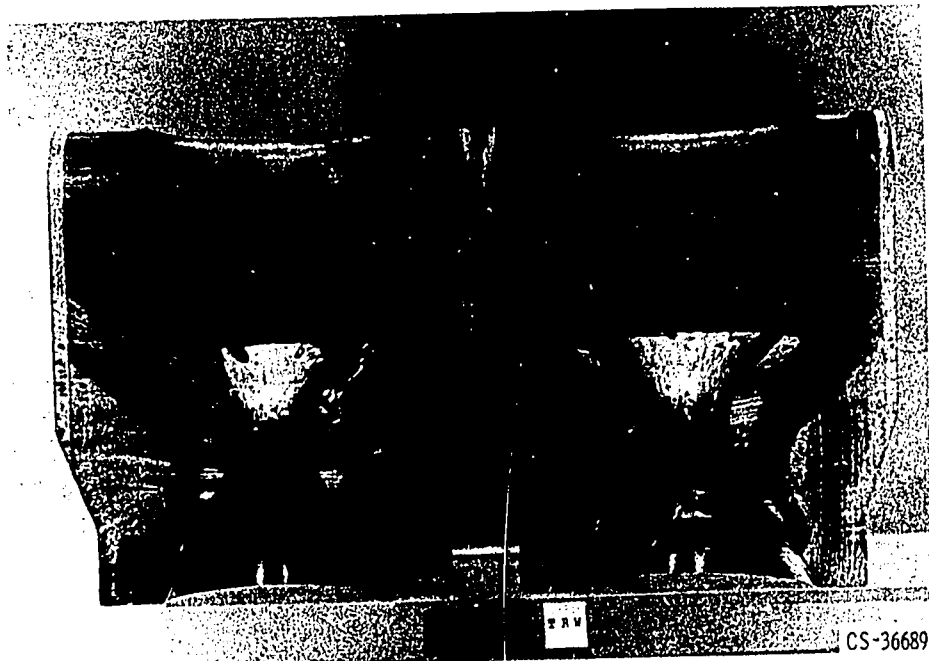
Figure 5-5(b) shows a molybdenum nozzle after firing for 47 seconds. This 1-inch-diameter nozzle has suffered severe erosion at the throat because of the highly oxidizing flame. Although molybdenum behaves similarly to tungsten, which was suitable for the less oxidizing flame of the solid-propellant engine described previously, molybdenum is a poor material for the liquid-fueled engine.

The throat insert which performed best is pictured in figure 5-5(c). This insert is made from sintered zirconia (ZrO_2) reinforced with tungsten-rhenium alloy wire. After a 734-second firing, the nozzle is still intact although beginning to deteriorate. It shows some erosion and cracking but appears adequate for at least 700 seconds of firing. Also visible in figure 5-5(c) are the graphite heat sink to reduce heat transfer from the throat insert to the ablative nozzle holder and a portion of the exit cone, which is also constructed of ablative material. Tests are continuing on this and similar materials.
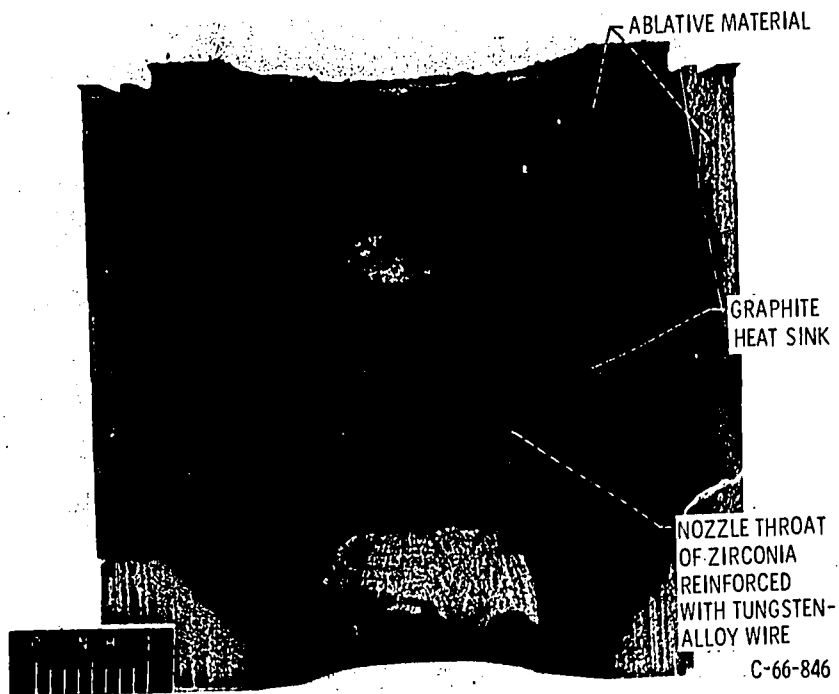
For a small solid-propellant rocket engine, a ceramic nozzle may be adequate. An example is the engine used by the Lewis Aerospace Explorers. It is designated type B-8-4 and has a short firing time of 1.4 seconds. After firing (fig. 5-6) the inside surface of the nozzle shows some erosion and also had a fused layer about 5 mils thick. Since silica melts at 3200° F, this suggests a flame temperature of approximately 4000° to 4500° F. The extent of throat erosion indicates a moderate pressure drop in the engine during the firing cycle.

(a) Ablative nozzle after firing for 160 seconds. Diameter, 8 inches.

(b) Molybdenum nozzle after firing for 47 seconds. Diameter, 1 inch.

ABLATIVE MATERIAL

GRAPHITE HEAT SINK

NOZZLE THROAT OF ZIRCONIA REINFORCED WITH TUNGSTEN-ALLOY WIRE

C-66-846

(c) Composite tungsten alloy-reinforced-zirconia nozzle after firing for 734 seconds. Diameter, 1 inch.

Figure 5-5. - Nozzles of various materials after firing in storable-liquid-propellant motor.

Figure 5-6. - Ceramic nozzle after firing for 1.4 seconds in solid-propellant model rocket engine, type B-8-4.

COMBINATION METHODS

Some rocket engines use a combination of refractory and ablative principles to achieve good heat-resistance in the nozzle. An example is the Polaris Missile, which is capable of being fired from a submerged submarine. This is a two-stage missile, with both stages being powered by solid-fueled engines. The first-stage engine burns for approximately 90 seconds with a combustion chamber pressure of 800 psi. The nozzle material for this engine is a refractory-ablative combination of a porous tungsten skeleton infiltrated with silver. The tungsten provides strength at high temperatures while the silver absorbs heat by melting and boiling. The drawing in figure 5-7 shows the extent of silver loss at various regions in the nozzle after firing. The silver loss reaches 100 percent near the hot inside surface and is 40 to 50 percent in the cooler areas near the external surface.

The second stage of the Polaris operates at a higher altitude and less total thrust is required. The chamber pressure for this engine is 200 to 300 psi, and because of the less erosive nature of the gas stream, graphite is a satisfactory nozzle material.
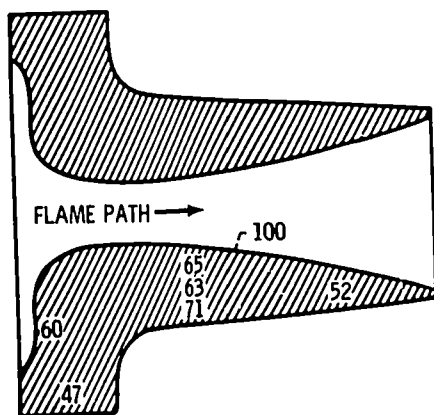
(a) Cross section showing percentage of silver loss at various locations during firing.

Inside surface   Center section   Outside surface
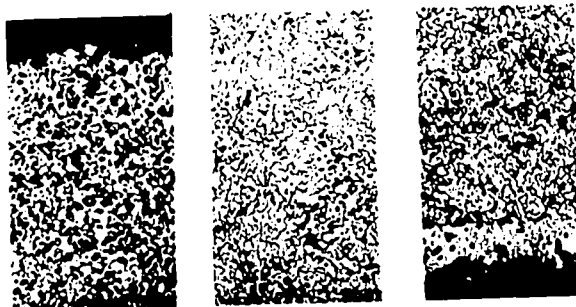
(b) Microstructure of silver-infiltrated tungsten after firing.

Figure 5-7. - Silver-infiltrated tungsten nozzle of type used in Polaris Stage I.

SUMMARY OF VARIABLES

Each of the important variables for engines requiring uncooled nozzles can range extensively as shown by the following summary:

Combustion chamber pressure, psi . . . . <100 to about 1000

Temperature, ^{O}F. . . . . About 4000 to 6500

Firing times, sec . . . . About 60 to 700

Chemical nature . . . . Combustion products may be reducing or oxidizing

Erosive nature . . . . Solid-propellant combustion products may contain erosive solid particles, such as alumina

Fuel . . . . Typical storable liquid fuel is NTO (nitrogen tetroxide) - Aerozine 50; typical solid fuel is polyvinyl chloride - ammonium perchlorate

The choice of material suitable for the various classes of engine is generally based on the extent of throat erosion during firing under simulated engine operating conditions:

Tungsten: Good erosion resistance but poor corrosion resistance; can he used as ablative by infiltrating with silver or copper

Molybdenum: Similar but slightly inferior to tungsten

Graphite: Fair erosion and corrosion resistance; usable in low-pressure engines

Ceramics and cermets: Good erosion and corrosion resistance, but subject to severe thermal cracking

Plastic ablative: Poor erosion resistance; light weight and low cost make it attractive for large, low-pressure nozzles where erosion is tolerable

ROCKET CASINGS

Other parts of rocket engines that new materials have improved are the casings for holding solid propellants and the tanks for liquid propellants. An example is the large steel casing for the 260-inch-diameter solid-propellant rocket which has been under development for several years as a low-cost backup vehicle for the more expensive and complicated liquid-fueled rockets that have powered all of our important space missions to date.

The rocket casing is constructed by welding together 3/4-inch-thick segments of high-strength steel. Structures such as this, however, are notoriously subject to premature brittle fracture, as demonstrated by costly losses of welded Liberty ships during World War II.

Such a failure occurred during proof testing of the first casing. This failure occurred at 56 percent of the intended proof pressure and, according to accelerometer measurements made during the test, originated at two welding flaws at the area indicated in figure 5-8. This figure shows the pieces from the casing laid out in a hangar where the cause of failure was under study. Once initiated, the cracks propagated rapidly and catastrophically through the entire structure.

In order to determine the influence of welding techniques on the structural integrity of the casing, the susceptibility of two types of welds to crack propagation was studied. The two types of weld investigated, a two-pass arc-weld and a multipass arc-weld, are shown diagramatically in figure 5-9. Steel specimens welded by the two techniques were then notched and fatigue-cracked to a predetermined depth by alternately stretching a small distance and releasing in order to simulate a weld flaw. The specimens were then pulled in tension to failure. These tests showed that the welds produced by the multipass welding technique were approximately three times stronger than those produced by the two-pass technique.
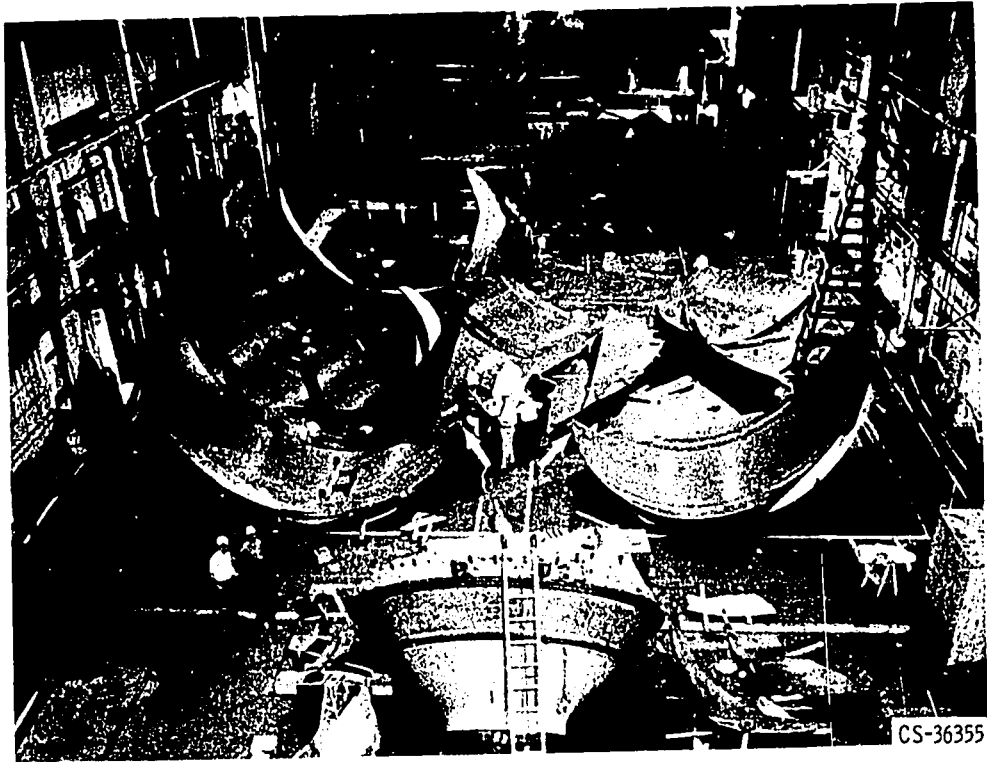
37

Figure 5-8. - 260-Inch-diameter rocket casing after failure during hydraulic proof testing. Arrows indicate weld flaw which caused failure.

FRACTURE STRENGTH, LB/SQ IN.

62 000

190 000

TWO-PASS SUBMERGED ARC WELD

ARTIFICIAL CRACKS
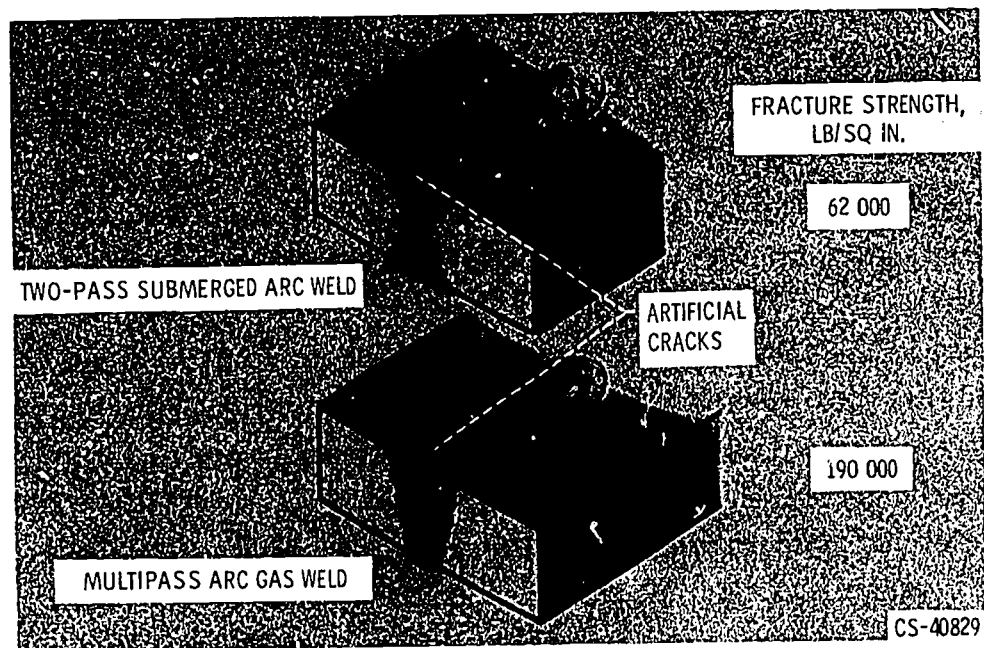
MULTIPASS ARC GAS WELD

CS-40829

Figure 5-9. - Types of weld used In manufacturing 260-inch-diameter solid propellant rocket casings.
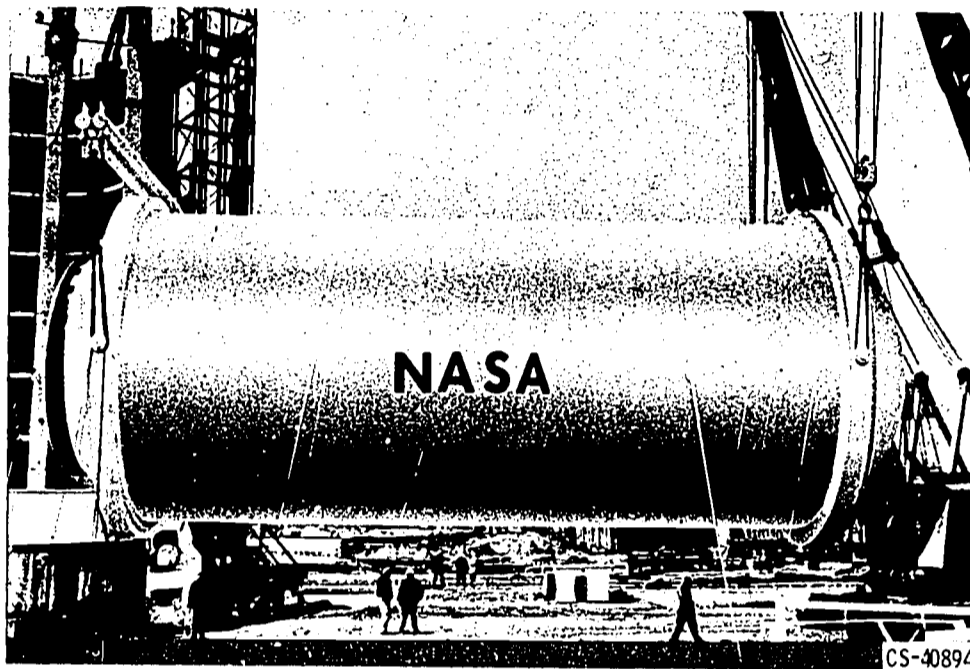
Figure 5-10. - 260-Inch-diameter casing manufactured with the use of multiple-pass tungsten-inert gas welding technique.

Figure 5-10 shows a second 260-inch-diameter casing which was welded by the multi-pass technique. This casing passed the hydraulic proof test and subsequently was success-fully ground test-fired. This engine, incidentally, uses an ablative nozzle with an 89-inch-diameter throat. The chamber pressure is 600 psi and the flame temperature 5500° F with a 2-minute firing time.

The determination of the proper welding technique for the casing is an excellent example of the successful application of a modern laboratory technology, in this case the study of crack initiation and propagation, to the solution of an important manufacturing problem.

FUEL TANKS

The storage of cryogenic fuels is important to the success of post-Apollo missions. These trips will need large quantities of liquid oxygen and liquid hydrogen for long periods of time. This means not only adequate insulation to prevent excessive fuel losses through vaporization but also protection from damage by high-velocity micrometeoroids. Since much of the vehicle structure will consist of tankage, it must be as light weight as possi-ble.

Although micrometeoroids are less common in space than was estimated several years ago, there are enough to constitute a potentially serious hazard. Most have very low masses, but, because of their high velocities (of the order of 17 000 miles per hour), their momentums are quite large.

(a) Before impact.


POINT OF
PENETRATION

C-59294
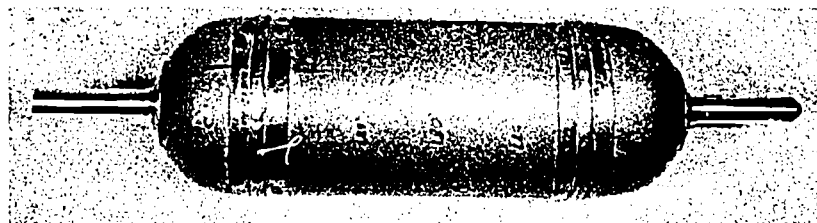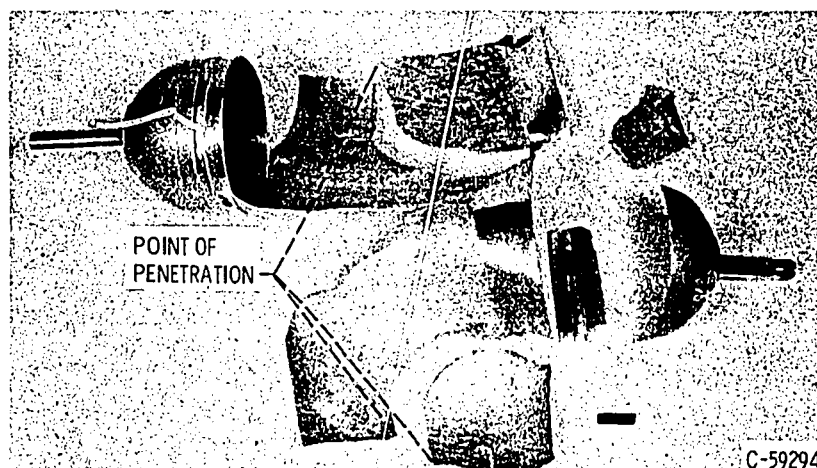
(b) After impact.

Figure 5-11. – Damage to water-filled aluminum tank resulting from impact by high-
velocity projectile.

The damage resulting from impact of a high-velocity particle with a liquid-filled
tank can be catastrophic. Figure 5-11 shows a metal tank which was filled with water and
then hit with a high-velocity projectile. The extensive damage resulted not from the
immediate shock of impact but from the high-energy shock wave created in the liquid as
a result of the projectile passing through. The shock wave, on hitting the tank, literally
tore the tank apart. Even more extensive damage occurs when the tank is filled with a
cryogenic fluid such as liquid oxygen or liquid nitrogen since the toughness of the metal
tank is reduced at low temperatures. Obviously, micrometeoroid impact into a metal
tank containing a cryogenic fuel during a space flight could seriously damage or destroy
the entire vehicle.

Several possible solutions to this potentially serious problem have been studied in
the laboratory. For example, the tanks could be covered with a lightweight armor such
as beryllium, which would reduce the probability of penetration by an impacting particle.
Alternatively, the metal tanks could be protected by a "bumper," that is, a thin sheet
of metal positioned a fraction of an inch outside of the tank. This would cause an impact-
ing particle to fragment. Although the total momentum of the fragments would be the
same as that of the original particle, the individual momentums would be lower; further-
more, the area of impact would be much larger and the probability of penetration would

be significantly decreased. Both of these possible solutions have merit, but at the same time, both involve a significant weight penalty which can be measured directly in terms of reduced payload.

One attractive solution is to construct the tanks from plastic-bonded glass fiber material, which is both lightweight and shatter-proof. This is done by winding glass fibers into layers that are alternately oriented at 90° from each other and then impregnating and bonding them with an epoxy resin binder. Since the composite is permeable by the small hydrogen molecule, the inside must be lined with a layer of aluminum foil. The cylinder shown in figure 5-12 was filled with liquid nitrogen and hit with a high-velocity projectile. The cylinder contains a small hole where the projectile entered and another hole in the back where the projectile exited. However, the elasticity of the tank enables it to withstand the secondary, high-energy, shock wave in the liquid nitrogen. During space flight, the fuel in this tank would, of course, be lost, but damage to adjacent tanks and to the vehicle itself would be avoided. Thus, it appears that this material will be highly useful in our extended post-Apollo space missions.

PROJECTILE
ENTRANCE
HOLE
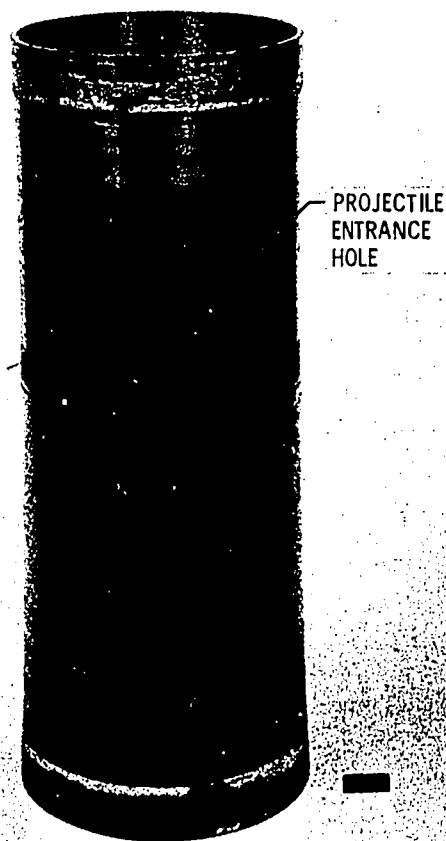
C-66-4375

Figure 5-12. - Damage to liquid-nitrogen-filled, plastic-bonded
glass fiber cylinder resulting from impact by high-velocity projectile.

101

CONCLUDING REMARKS

In this chapter a few of the materials problems which directly affect and limit our space propulsion systems have been described. Of necessity, the discussion has emphasized the applied aspects of these problems and their solutions. It was impossible to cover the scientific and often more interesting aspects of the problems, such as the details of the oxidation behavior of refractory metals or the basic mechanisms of crack propagation. Furthermore, it avoided many other areas where materials properties are also limiting factors, such as the loops and radiators of self-contained systems for generating electric power in space. Development and selection of materials for these applications tax the ingenuity of the materials scientists.

6. SOLID-PROPELLANT ROCKET SYSTEMS

Joseph F. McBride*

HISTORY OF SOLID ROCKETS

The first use of rockets was historically recorded about the year 1232, when Chinese writers told of "arrows of flying fire" with propulsive power furnished by an incendiary powder. Rockets using mixtures of sulfur, charcoal, saltpeter, petroleum, and turpentine were used as weapons by the Arabs, Greeks, Italians, and Germans from 1280 to 1800.

A great variety of rockets propelled by gunpowder and similar solid-fuel combinations have been used in fireworks demonstrations and as missiles in battle for the past several centuries. The British attacked Copenhagen with 30 000 rockets in 1807, and in 1814 Francis Scott Key wrote his famous poem under "the rockets red glare" as the British bombarded Fort McHenry near Baltimore.

Interest in solid rockets of much larger size and increased performance came at the beginning or World War II, when the first jet-assisted takeoff units for aircraft were developed and used (1940-41 at Jet Propulsion Laboratory, Pasadena).

Since World War II, solid-rocket propulsion devices have been further improved in performance and greatly increased in size for use as air-to-air missiles (Sidewinder, Genie), ground-to-air missiles (Nike, Hawk), intercontinental ballistic missiles (Minuteman, Polaris), ground-to-ground tactical weapons (Sergeant, Honest John, Shillelagh), air-to-ground delivery systems (Skybolt), sounding rockets (Argo, Astrobee), space launch vehicles (Scout), and space boosters (Titan III, 156-inch and 260-inch boosters).

DESCRIPTION OF SOLID ROCKET

A solid-fueled rocket propulsion system (motor) consists of a propellant fuel-and-oxidizer charge (grain) of a certain configuration, with the following associated hardware (fig. 6-1):

(a) A case, the high-pressure gas container which encloses the grain

(b) A nozzle, the gas-expansion device through which the rocket exhaust flows
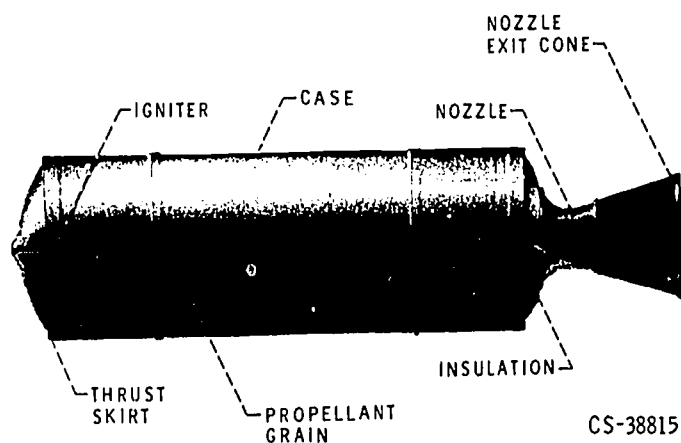
---

*Aerospace Engineer, Solid Rocket Technology Branch.

Figure 6-1. - Solid-fueled rocket motor.

(c) An igniter, the device which starts combustion of the propellant grain in a controlled manner

(d) Insulation, a temperature-resistant, low-conductivity material protecting case and nozzle from exposure to hot gases

SOLID-PROPELLANT GRAIN

A solid propellant is basically a mixture of fuel and oxidizer which burn together, with no other outside substance injected into the combustion chamber, to produce very hot gases at high pressure. Various additives may be mixed into the fuel-oxidizer combination for purposes of:

(a) Controlling the rate of burning

(b) Giving hotter-burning, more energetic, chemical mixtures

(c) Optimizing propellant grain physical properties (tensile and shear strengths, modulus of elasticity, ductility)

Grain Mixture

Most modern solid-propellant grains belong to one of two classes, double-base or composite.

The double-base propellant is a mixture of two very energetic compounds, either one of which alone would make a rocket propellant. Usually the two constituents are nitroglycerin $[C_3H_5(ONO_2)_3]$ and nitrocellulose $[C_6H_7O_2(ONO_2)_3]$. As the chemical formulas

indicate, both the fuel (carbon and hydrogen) and the oxidizer (oxygen) atoms are contained in each of these molecules; both substances are monopropellants which burn without any added oxidizer. The nitrocellulose provides physical strength to the grain, while nitroglycerin is a high-performance and fast-burning propellant. Double-base grains are generally formed by mixing the two constituents and additives, then pressing or extruding the puttylike mixture into the proper shape to fit the motor case.

A composite grain is so named because it is formed of a mixture of two or more unlike compounds into a composite material with the burning properties and strength characteristics desired. None of these constituent compounds would make a good propellant by itself; instead, one is usually the fuel component, another the oxidizer.

The most modern of the composite propellants use a rubbery polymer (in fact, a synthetic rubber such as polybutadiene or polysulfide) which acts as the fuel and as a binder for the crumbly oxidizer powder. The oxidizer is generally a finely ground nitrate or perchlorate crystal, as, for example, potassium nitrate (KNO_3) or ammonium perchlorate (NH_4ClO_4). The composite mixture can be mixed and poured like cake batter, cast into molds or into the motor case itself, and made to set (cure) like hard rubber or concrete. The cured propellant is rubbery and grainy with a texture similar to that of a typewriter eraser.

Composite propellants often contain an additional fuel constituent in the form of a light-metal powder. Ten to twenty percent by weight of aluminum or beryllium powder added to a polymer-based grain has the effect of smoothing the burning (combustion) process and increasing the energy release of the propellant. This added energy in the hot gases produced in combustion appears as added specific impulse I_{sp} of the rocket propulsion system.

Grain Design

Solid grains are also classed by the shapes of their exposed burning surfaces and the manner in which the propellants are burned out of the case. A great deal of engineering is devoted to the shape of the grain, the configuration of the combustion chamber, and the sizes of the parts of the grain to control stresses and the burning of the propellant.

A solid-propellant grain will burn at any point on its surface which is:

(a) Exposed to heat or hot gases of a high enough temperature to ignite the propellant mixture

(b) Far enough separated from the other case or propellant surfaces to allow gas flow past the point

Grains are classified as end-burning or internal-burning; this classification describes the propellant surface on which burning is allowed to take place. An unlimited
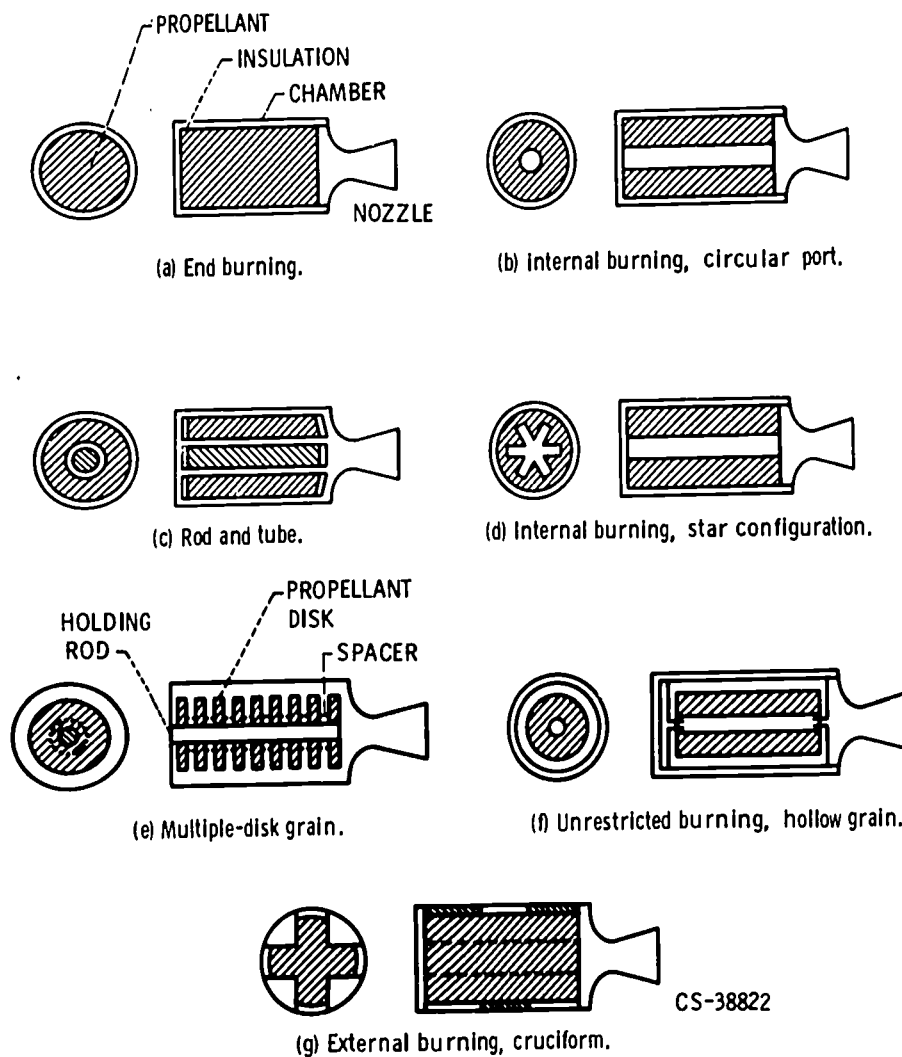
(a) End burning.

(b) Internal burning, circular port.

(c) Rod and tube.

(d) Internal burning, star configuration.

(e) Multiple-disk grain.

(f) Unrestricted burning, hollow grain.

(g) External burning, cruciform.

Figure 6-2. – Typical solid-propellant grain configurations. (Patterned after illustrations appearing in Rocket Propulsion Elements by George P. Sutton.)

number of combinations and variations of the basic end-burning or internal-burning grain are possible (fig. 6-2).

BURNING PROCESS

As was stated previously, a correct chemical mixture of fuel and oxidizer will support combustion when exposed to high temperature and gas flow; it will continue to burn as long as the gaseous products of combustion are allowed to escape from the burning surface.

The rate at which hot gases are produced by the burning propellant depends on the total area over which burning is occurring A_b; the rate at which burning is progressing into the propellant $\dot{r}$; and the density of the propellant being transformed into gas ρ.

(Symbols are defined in the appendix.) The flow of combustion gases off the burning surface is described by the rate equation

$$\dot{W} = A_b \dot{r} \rho \tag{1}$$

It is a characteristic of any solid propellant that its burning rate at any point on the grain surface is determined by:

(a) The composition of the propellant at that point

(b) The pressure of the gases surrounding the point

(c) The temperature of the grain at that point just as the "burning zone" approaches

These characteristics at each point on the grain are averaged for the entire grain in the general, solid-propellant, burning-rate equation

$$\dot{r} = a_B P_c^n \tag{2}$$

where $\dot{r}$ is the instantaneous burn rate (in./sec), a_B is the burn-rate constant (which varies slightly with the overall temperature of the grain), P_c is the instantaneous motor chamber pressure (psi), and n is the burn-rate exponent for the particular propellant (typical values range from 0. 4 to almost 1. 0).

Combining the burning-rate equation (2) with the weight-flow-of-gas-produced equation (1) yields

$$\dot{W} = A_b \left(a_B P_c^n \right) \rho \tag{3}$$

Now, for any rocket device, the thrust produced by expansion of exhaust gases through a nozzle can be expressed as

$$F = C_F A_t P_c \tag{4}$$

where F is the thrust (lb), C_F is the nozzle thrust coefficient (a constant which is a measure of the expansion efficiency of the nozzle and the properties of the propelling gases), A_t is the nozzle throat area (in.^{2}), and P_c is the rocket chamber pressure (psi).

But, thrust is also given by the equation

$$F = \dot{W} I_{sp} \tag{5}$$

where $\dot{W}$ is the gas weight flow through the nozzle (lb/sec) and I_{sp} is the engine specific impulse (a measure of propellant energy release and efficiency of gas expansion through the nozzle).

Combining equations (4) and (5) gives

$$\dot{W} = \frac{F}{I_{sp}} = \frac{C_F A_t P_c}{I_{sp}} \tag{6}$$

In the rocket, a steady-state condition is reached when the rate of gas produced equals the rate of gas flow out of the chamber

$$\dot{W}_{produced} = \dot{W}_{out}$$

or, from equations (3) and (6),

$$A_b \left(a_B P_c^n \right) \rho = \frac{C_F A_t P_c}{I_{sp}} \tag{7}$$

At any instant during the firing, everything in equation (7) is invariable except the chamber pressure. Thus, the pressure in the rocket chamber stabilizes at the instantaneous value found by solving equation (7):

$$P_c = \left(\frac{A_t C_F}{A_b I_{sp} a_B \rho} \right)^{1-n} \tag{8}$$

And so, the motor designer can control the pressure at which the rocket will operate by:

(a) Selecting the propellant, thereby fixing I_{sp}, a_B, ρ, and n

(b) Designing a nozzle size and configuration, thereby fixing A_t and C_F

(c) Designing the grain burning surface to make A_b vary as desired during the firing

THRUST-TIME HISTORY

Since the thrust of the rocket can be expressed as

$$F = C_F P_c A_t$$

We find, using equation (8), that

$$F = (C_F A_t)^{2-n}(A_b I_{sp} a_B \rho)^{n-1} \qquad (9)$$

So the thrust, like the chamber pressure, is controlled primarily by the amount of burning surface A_b exposed at each moment during the firing.

The thrust-time curve is the most important performance characteristic of a rocket motor. In space, acceleration of the vehicle propelled by this motor follows Newton's Second Law of Motion

$$a = \frac{F_{motor}}{m_{vehicle}}$$

at any instant. Therefore, the entire velocity history (mission profile) of the vehicle depends on the thrust-mass-time relationship it experiences.

Solid-motor grain design concentrates on the problem of tailoring the thrust curve by configuring the burning surface area to give the desired thrust with time (see fig. 6-3).

Thrust curves are typically progressive, regressive, neutral, or a combination of these, as shown in figure 6-4. Also noted are some of the grain port shapes which will produce these thrust variations by the manner in which their burning surfaces vary in area as burning proceeds.
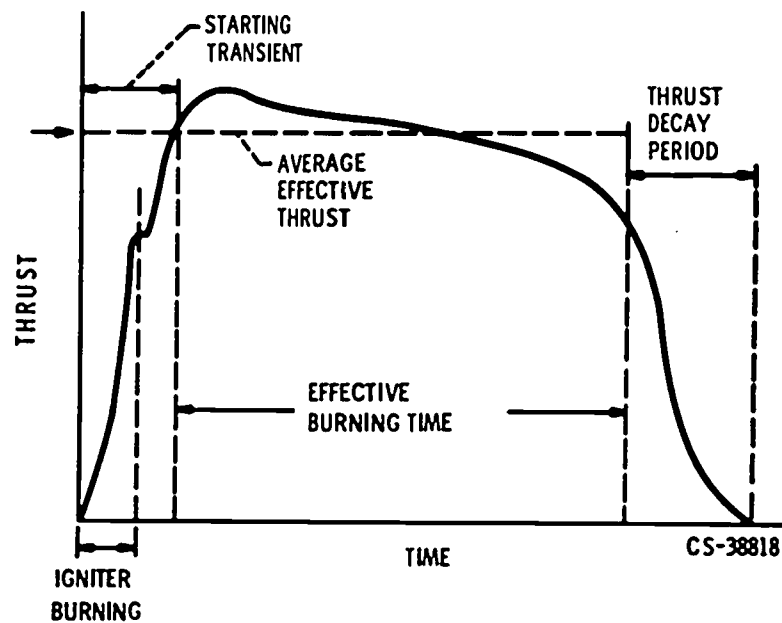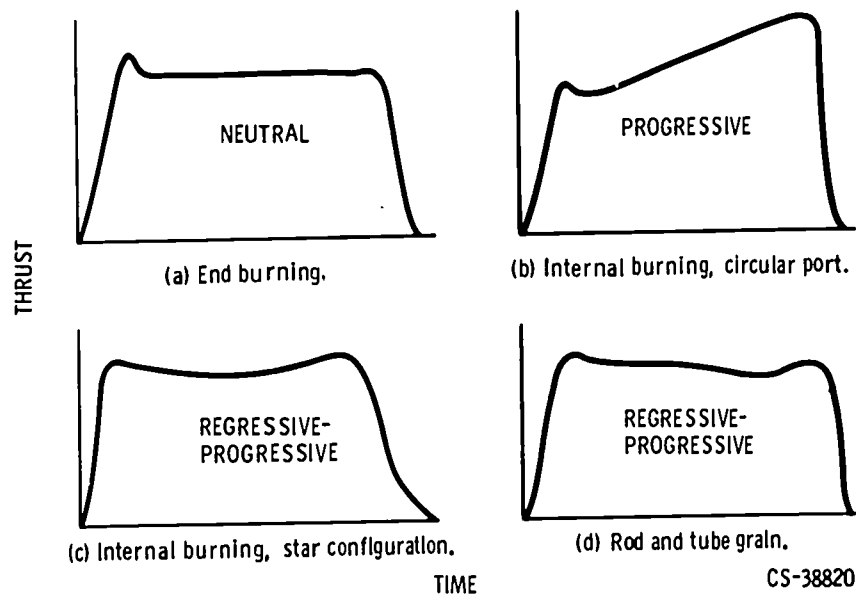

Figure 6-3. - Typical thrust-time diagram.

101

Figure 6-4. – Thrust-time histories.

Another major design problem comes in the elimination of long thrust tailoff, or decay period, at the end of rocket firing. Long tailoff time wastes propellant by burning it inefficiently at low pressure for a relatively long time. Long tailoff also endangers the motor case by exposing it to hot gases while it is no longer protected by propellant. Short, abrupt tailoff is desirable but difficult to achieve, particularly in complex star grain designs. In such grains, the nature of the burning-surface shape gives decreased burning area near the end of the firing because of residual propellant slivers.

CONTROLLABLE SOLID MOTORS

Rocket propulsion developers have done much within the past five years to correct the two great drawbacks of the solid rocket motor:

(a) Inability to shut down on command once ignited and before propellant burns out
(b) Inability to throttle chamber pressure and thrust

Developmental solid rockets have been successfully stopped by using rapid pressure decay (opening the throat or venting the case), by quenching with water or CO_2, or by using bi-grain motors (one grain fuel-rich, one grain oxidizer-rich) with the two chambers connected by a throttle valve.

Throttling has been achieved in bi-grain rockets and, of course, in liquid-solid hybrid rocket engines.

INERT COMPONENTS OF MOTOR

The propellant grain is the "live" part of the solid motor. The other parts provide no propulsive gases and do not burn, so they are "inert." The major inert components of the motor are case, nozzle, igniter, and insulation.

Case

The motor case is the pressure- and load-carrying structure enclosing the propellant grain. Cases are usually cylindrical with curved, nearly hemispherical end closures. Some motors are made with completely spherical cases.

Highest motor performance demands the lightest possible inert weight, so case design becomes a problem of obtaining the thinnest, lightest structure to contain the chamber pressure (typically 400 to 1000 psi in modern solid rockets) and to withstand the loads the vehicle encounters during its flight.

In a cylindrical pressure vessel, which most solid motor cases are, the principal stress in the wall material is given by the equation

$$S = \frac{P_c R_c}{t_w} \tag{10}$$

where S is the hoop stress (psi), R_c is the radius of the cylinder, and t_w is the thickness of the wall.

From this equation we see that the wall thickness

$$t_w = \frac{P_c R_c}{S} \tag{11}$$

can be minimized by using the highest allowable stress S, or the strongest case material, for the given chamber pressure and case size. A good case material is one with a high strength-to-weight ratio. Among today's best materials are high-strength titanium alloys, fiber-glass-and-plastic composite materials, and high-toughness steel alloys. The following examples show the uses of these materials:

(a) Steel alloys: 260-inch booster, 120-inch booster, Minuteman first stage

(b) Titanium: Minuteman second stage

(c) Filament-wound fiber-glass composite: Minuteman third stage, Polaris

Nozzle

The nozzle is the only portion of the solid motor which must withstand exposure to high-temperature, high-velocity propellant gases for the full duration of the rocket firing. The most critical location is in the nozzle throat (smallest area) section, where gas flows at Mach 1 velocity with relatively high pressure and density. In the throat, heat transfer to the nozzle wall is highest.

The greatest nozzle problem is one of finding materials suitable for high-temperature, long-duration application. A solid-rocket nozzle, of course, cannot be cooled by running fuel through its wall as in regenerative cooling of liquid rocket chambers and nozzles. Instead, the nozzle must be lined with one of the following types of material, which will withstand high temperature for long duration:

(a) A refractory substance (tungsten, graphite, etc.) which will not melt, crack, or crumble when heated to temperatures over 3000° F

(b) An ablative composite substance (plastic or rubber reinforced with refractory-type fibers or crystals) which gives off decomposition gases and erodes during firing

Ablatives are used in those applications (e.g., very large rockets) where rocket performance is not seriously degraded by change of nozzle contour or increase in throat area during firing. Refractories are mandatory in applications which cannot tolerate nozzle configuration changes.

The nozzle, too, is a pressure vessel and must be structurally designed to contain the internal pressure and aerodynamic flight loads acting upon it. The pressure within the nozzle decreases rapidly downstream of the throat, and wall thickness can be decreased sharply for a saving of inert weight.

Igniter

The solid-propellant grain burning surface must be bathed in hot gas before it will ignite and support its own combustion. The rocket igniter is a gas producer which can be started easily and dependably by a signal from the firing switch.

The most-used igniter today (fig. 6-5) is a small rocket motor itself, and it exhausts hot gas into the grain cavity of the main rocket. This igniter can be mounted at the head end or the aft end of the main rocket motor, or even outside with its hot gases directed into the main nozzle.

The igniter itself is started by yet another small charge of very fast-burning solid propellant in the form of pellets or powder. This igniter booster is started by the primary initiator, which is a hot-wire resistor or an exploding bridgewire connected to the firing switch through the ignition circuit.
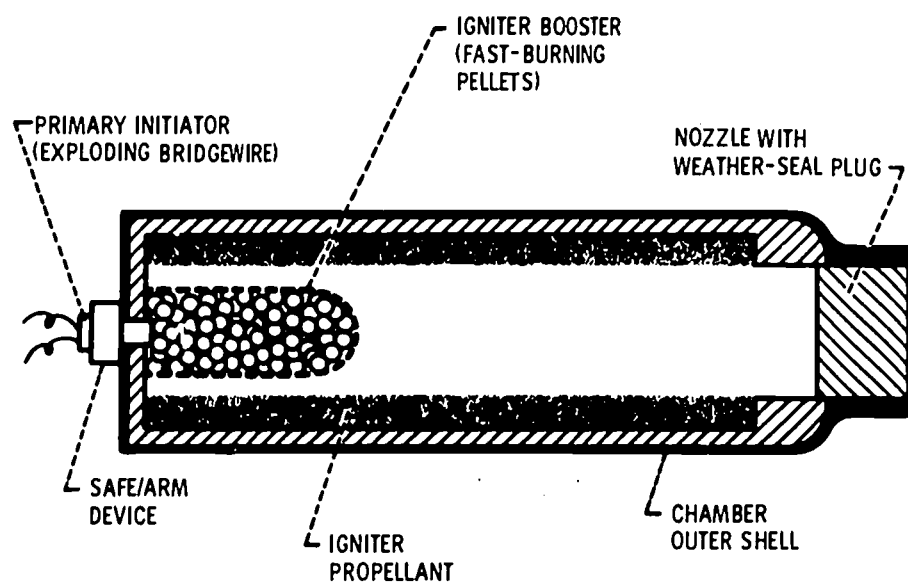
Figure 6-5. - Typical igniter.

Most of the accidents involving solid rockets have resulted from premature igniter firing, either by inadvertent application of voltage to the exploding bridgewire or by igni- tion of the highly sensitive igniter pellets by impact shock, stray currents, static dis- charge, or even radio transmissions too close to the rocket. Great effort in safety pro- cedures has made these premature ignitions quite rare. Igniter circuits are locked open until just before firing, shunting circuits are placed across igniter input leads to elimi- nate stray currents, and personnel working around solid motors are required to wear conductive shoes (to prevent static electricity buildup) and use nonsparking tools.

Insulation

Unless it is protected by insulation, the motor case will quickly lose strength and burst or will burn through whenever hot combustion gases reach the case wall. This burning through of the case could occur near the end of the burning time in the internal- burning grain or throughout the firing time at the aft end of an end-burning grain.

Every solid motor contains a certain thickness of insulation between the propellant grain and the motor case to protect the chamber walls until all propellant has burned out and chamber pressure goes to zero. This insulation is usually an asbestos-filled rubber compound which is bonded with temperature-resistant adhesives to the case wall on one side and to the propellant grain on the other.

113

STEERING CONTROL

A missile or space vehicle requires a significant amount of steering control as it flies through atmospheric winds and performs the pitch, yaw, and roll maneuvers necessary in the performance of its mission. Most liquid-propelled vehicles are steered by engine gimbaling; that is, the entire chamber and nozzle assembly is moved relative to the rest of the vehicle so that the direction of thrusting is changed.

Moving a solid-rocket chamber relative to the vehicle is a large task because the chamber is a major portion of the vehicle and contains all of the rocket's propellant. The combustion chamber is not separate from the propellant tankage as it is in a liquid or nuclear rocket system. Solid rockets are therefore steered by moving the nozzle alone,

(a) Movable nozzle.
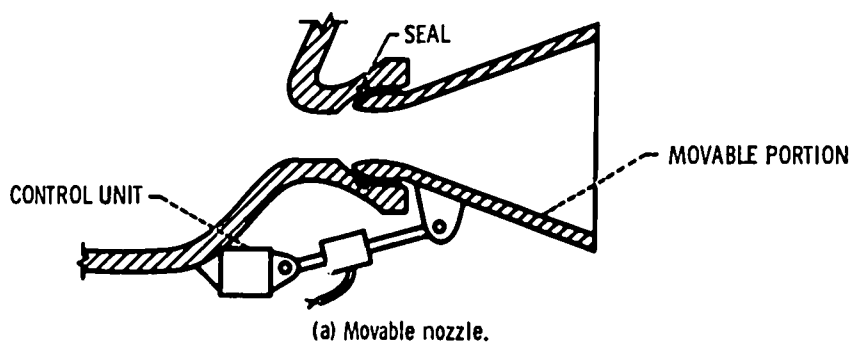
(b) Jet tabs on a rocket developed by Lockheed for the U.S. Air Force.

CS-38817
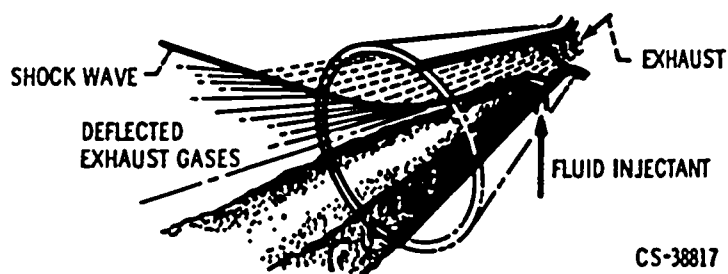
(c) Secondary injection.

Figure 6-6. – Thrust vector control.

114

by moving the exit cone of the nozzle alone, or by changing the direction of the exhaust jet coming from the nozzle. Any method of controlling the direction of thrusting in relation to the engine or the vehicle is termed "thrust vector control" or TVC.

Moving the entire nozzle or the exit cone (fig. 6-6(a)) has been done successfully in many missiles (Minuteman, Skybolt, air-to-air missiles). Deflection of the exhaust-gas jet alone has also been accomplished by placing obstacles such as vanes or tabs in the nozzle to disturb the exhaust flow pattern (fig. 6-6(b)), or by injecting a fluid (gas or liquid) through the nozzle wall at right angles to the main gas stream (fig. 6-6(c)). In this way, the jet and the thrust direction are deflected a few degrees off the vehicle centerline. This method of steering is used in such operational rocket vehicles as Minuteman II, Polaris, and the 120-inch boosters for the Titan III C.

Another method of steering for rocket vehicles involves the use of aerodynamic surfaces (vanes, fins, or canards) which give steering-control forces through lift, like an airplane wing (fig. 6-7). A vehicle with this kind of control needs no thrust vector control in

Figure 6-7. - Aerodynamic control.
Nike missile with fin stabilizers
and canard steering.

the propulsion system (e.g., most air-to-air and ground-to-air missiles). However, aerodynamic control can occur only in the atmosphere and while the vehicle has sufficient velocity through the air. Aerodynamic steering may be combined with TVC; the TVC provides steering control near the ground before the vehicle has built up velocity, and on the edge of the atmosphere or in space where a wing becomes useless.

115

SOLID-ROCKET PERFORMANCE

There are two major indicators of rocket system performance, specific impulse I_{sp} and mass fraction M. F.:

$$I_{sp} = \frac{Thrust}{Rate\ of\ propellant\ usage}$$

$$M.\ F.\ = \frac{(Initial\ mass) - (Burnout\ mass)}{Initial\ mass}$$

$$= \frac{Weight\ of\ propellant}{Weight\ of\ total\ propulsion\ system}$$

Solid propellants are typically less energetic than the better liquid-propellant combinations. Modern solids have sea-level I_{sp} values in the range of 220 to 250 seconds, compared with over 350 seconds for the liquid-oxygen/liquid-hydrogen combination.

On the other hand, solid-rocket mass fractions can be quite high because there are no valves, piping, or pumps to add to the inert weight. High-performance upper-stage solid motors typically attain mass fractions nearing 0.95 through the use of filament-wound glass cases and refractory-lined nozzles. Even the large solid boosters have mass fractions exceeding 0.90, a value which liquid-fueled missiles with very thin tank walls (e. g., Atlas) can barely achieve.

The solid rocket's real advantages are its strength, since the propellant grain has considerable strength of its own and also acts as a stiffener and shock dampener, and its instant readiness, since there are no fuel tanks to be filled just prior to firing and launch.

SAFETY PRECAUTIONS

Because a solid grain consists of fuel and oxidizer in a mixture all ready for burning upon the application of heat, a solid motor can be a serious fire and explosion hazard. Double-base propellants are explosive by nature and much more hazardous than the castable composites, which are merely fire hazards. For this reason, double-base propellants are not used in large-sized motors, only in air-to-air and antiaircraft missiles and in final-stage space vehicles for which the propellant grain does not exceed several hundred pounds in weight. A high-energy double-base grain has a potential explosive yield higher than a like amount of TNT. These explosive grains can be detonated by the shock of dropping, being struck by a rifle bullet, or overheating in a fire.

The danger with a nonexplosive composite grain is that it may ignite prematurely in a fire, and the motor will become propulsive at a time and place hazardous to personnel and property.

Solid motors are processed, loaded, and stored in facilities well away from dwellings. They are surrounded by blast walls and heavy earthen bunkers to stop shrapnel and pieces of burning propellant. Motors are transported with care and with a minimum number of personnel present to reduce the chance of injury in case an accident does occur.

The same kind of care for safety is taken during the mixing of propellants, when fuel and oxidizer are first brought together in large containers and stirred by intermeshing paddles. Serious fires and explosions have occurred during mixing operations at several propellant plants. However, because of the use of remote controls, fire-control systems, and proper isolation and protection of the mixing facilities, there have been relatively few injuries and deaths in these accidents.

APPENDIX - SYMBOLS

A_b exposed grain burning area, in.^{2}

A_t nozzle throat area, in.^{2}

a acceleration, ft/sec^2

a_B propellant burn rate constant

C_F nozzle thrust coefficient

F thrust, lb

I_{sp} specific impulse, sec

M. F.   rocket mass fraction

m mass, slugs

n propellant burn rate exponent

P_c combustion-chamber pressure, lb/in.^{2}

R_c radius of cylinder, in.

$\dot{r}$ propellant burning rate, in./sec

S stress, lb/in.^{2}

t_w thickness of wall, in.

$\dot{W}$ weight-flow rate, lb/sec

ρ density, lb/in.^{3} or lb/ft^3

7. LIQUID-PROPELLANT ROCKET SYSTEMS

E. William Conrad*

Liquid-propellant rockets may be classified as monopropellant, bipropellant, or tri-propellant. In a monopropellant rocket, a propellant, such as hydrazine, is passed through a catalyst to promote a reaction which produces heat from the decomposition of the propellant. A bipropellant rocket burns two chemical materials, a fuel and an oxi-dizer, together. In a tripropellant rocket, three different chemical species, such as hy-drogen, oxygen, and beryllium, are mixed in the combustion chamber and are burned to-gether. These tripropellant rockets have great potential, but they are not yet in actual use because they present many developmental problems. The following discussion will be restricted to bipropellant rockets because this type is used for the bulk of our present space activities.

ROCKET ENGINE

A simple, liquid-propellant rocket engine is shown in figure 7-1. The principal com-ponents of this engine are the injector, the combustion chamber, and the exhaust nozzle.
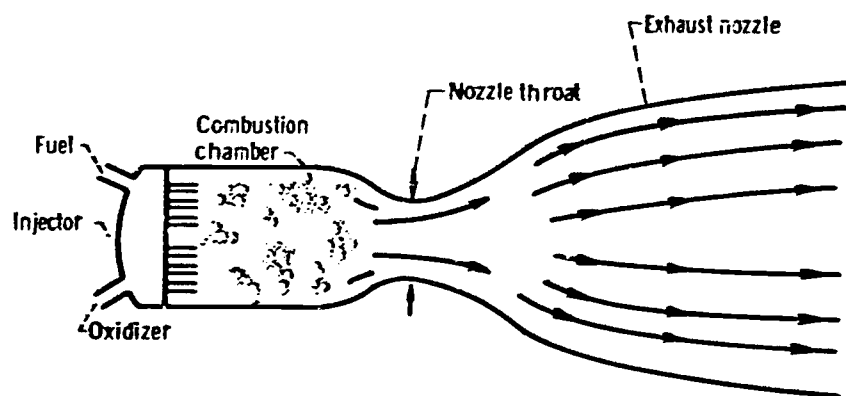

Figure 7-1. - Bipropellant liquid rocket engine.

---

*Chief, Chemical Rocket Evaluation Branch.

The propellants enter the combustion chamber through the injector. In the combustion chamber the propellants mix and are ignited. Some propellants, such as the oxygen-kerosene combinations used in the Atlas launch vehicle, are ignited by means of a spark plug. Other propellants, such as the nitrogen tetroxide - hydrazine combination used in the advanced Titan launch vehicle, are hypergolic; that is, when the two propellants are mixed, they ignite spontaneously. When the propellants burn, they produce very hot gases. The high temperature, in turn, raises the pressure of these gases in the combustion chamber. The increased pressure causes the gases to be discharged through the exhaust nozzle. As these gases pass through the exhaust nozzle, they are accelerated and expanded. The area reduction at the nozzle accelerates the gas to sonic velocity at the throat. Then, in the diverging portion of the nozzle, the gases are expanded and accelerated to supersonic velocities. (This flow process is discussed in chapter 2.)

Fuel Injector

The design of the injector is of great importance because the propellants must be introduced into the combustion chamber in such a way that they will mix properly. The objectives of the mixing process are to attain fine atomization of the propellants, rapid evaporation and reaction of the propellants as close as possible to the injector face, and a uniform mixture ratio throughout the combustion chamber. The ultimate goal is to have each molecule of fuel meet an appropriate number of oxidizer molecules and be completely consumed in the combustion process. A detailed discussion of the fundamental processes of combustion is presented in chapter 4.

Injectors of many types are used to accomplish the desired mixing of the propellants. Some of the most commonly used injectors are shown in figure 7-2. The double impinging stream injector, shown in figure 7-2(a), is a relatively common design. Fuel and oxidizer are supplied to the combustion chamber through alternate manifolds, so that each fuel stream impinges on an oxidizer stream. This impingement shatters the streams into ligaments, which, in turn, break up into droplets. Finally, the droplets evaporate and burn. The triple impinging stream injector (fig. 7-2(b)) is also very common and highly efficient. With this design, two streams of one propellant impinge on a stream of the other propellant at a common point. Figure 7-2(c) shows the self-impinging pattern, in which two streams of the same propellant impinge on each other and shatter to produce a fine, fan-shaped, misty spray. Alternate manifolds in the injector produce fans of fuel mist and of oxidizer mist. These fans mix and burn along their intersections. The shower-head stream injector, shown in figure 7-2(d), was very common in the early days of rocketry. With this design, streams of each propellant are simply injected parallel to one another. The efficiency of this system is, in general, relatively poor. Too much of

(a) Double impinging stream.

(b) Triple impinging stream.

(c) Self-impinging stream.

(d) Shower-head stream.

(e) Spray injection.

(f) Splash plate.

(g) Nonimpinging stream.
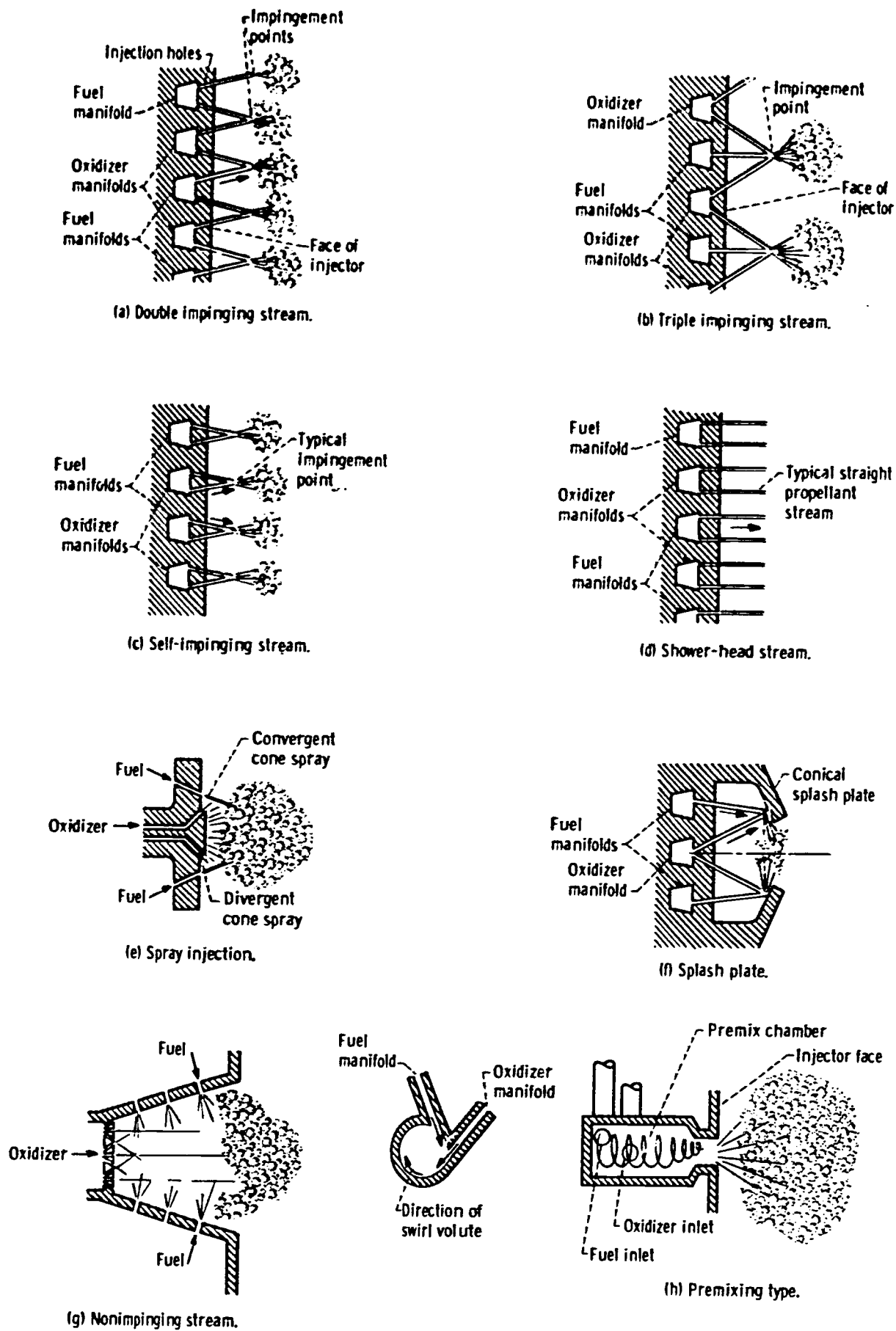
(h) Premixing type.

Figure 7-2. - Several injector types.

each propellant goes out the exhaust nozzle without mixing and reacting with the other propellant. Because of this low efficiency, very few current engines use shower-head injectors.

Also shown in figure 7-2 are some rather unusual injector designs. The spray injector (fig. 7-2(e)) produces a cone of oxidizer and impinging streams of fuel. Figure 7-2(f) shows a splash-plate injector, in which streams of fuel and oxidizer impinge at a point on the splash plate. This impingement produces sprays that eddy around the splash plate and promote further mixing of the propellants. The nonimpinging stream injector, shown in figure 7-2(g), has a precombustion chamber in the form of a cup sunk into the injector face. Many streams of both propellants are injected into this precombustion chamber to produce a rather violent mixing. The premixing injector (fig. 7-2(h)) has a premixing chamber into which the two propellants are injected tangentially to produce a swirling mixing action. There is a new and relatively efficient injector which uses a quadruple impinging stream pattern. With this design, two streams of each propellant impinge at a common point. This injector is particularly effective for use with storable propellants.

The concentric tube injector, shown in figure 7-3, is probably the optimum design for hydrogen-oxygen propellant combinations. The oxidizer enters the oxidizer cavity through the center pipe, then flows outward throughout this cavity, and enters the combustion chamber through the hollow oxidizer tubes. The fuel enters the fuel cavity, which is just under the injector face, and thence it flows into the combustion chamber through the annuli which surround the oxidizer tubes.
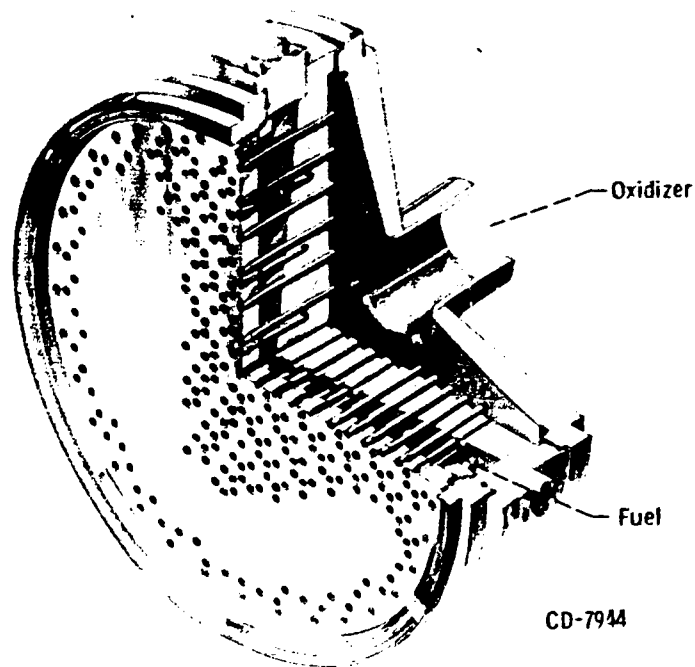

Figure 7-3. – Cross section of concentric-tube injector.

Combustion Instability

All these injection techniques create a combustion zone which has a great deal of energy contained in it; this concentration of energy can cause severe problems. One great difficulty in developing new rocket engines is combustion instability, particularly the variety at high frequency which we call "screech" or "screaming." This phenomenon has plagued propulsion people since afterburners were developed in the late 1940's and has continued through ramjets and into the rocket field. Screech can increase heat transfer by a factor of as much as 10 and thus is extremely destructive. As an example, in figure 7-4 is shown an injector face which experienced screech for only 0.4 second. Why screech happens is not yet fully understood, but there has been, and there still is, a great effort aimed at trying to solve the combustion instability problem. What apparently happens in the engine is that pressure waves are set up which have various possible modes of oscillation as acoustic systems. The waves may oscillate, or pulse, from the injector face down to the exhaust nozzle throat where there is a sonic plane, and bounce back to the injector face - the longitudinal mode. They do this at the speed of sound,

C-66-932
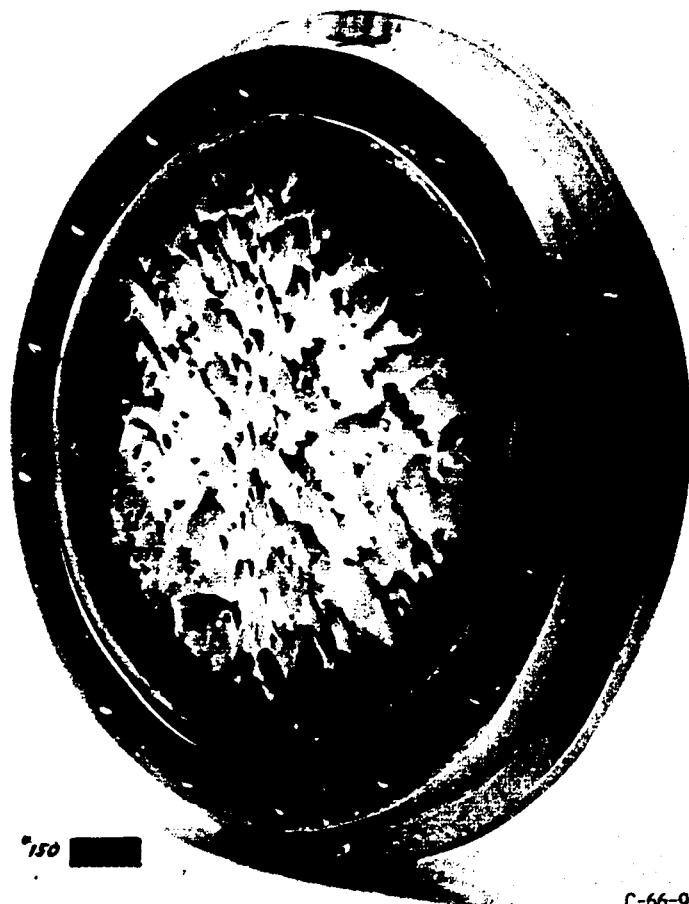
Figure 7-4. - Injector after operation with screech for 0.4 second.

115

which in that medium is very high so that the frequencies in a large engine would be of the order of 2500 to 3000 cycles per second. It is also possible for the pressure wave to travel from the center of the engine or injector area out radially to the walls of the chamber and back into the center in an expanding-contracting fashion - the radial mode. There is another mode, the transverse, or tangential, where the pressure waves start at the top point and travel around and bump into one another at the bottom and reflect back around to the top. This tangential mode of screech is particularly destructive.

Acoustic liners. - There are numerous ways of combating high frequency instability; one of the most promising techniques is the use of an acoustic liner which works much like the acoustic tile used on ceilings. The liner presents a perforated surface to the combustion zone and although part of each wave hits the solid part of the surface, bounces back, and is not dissipated efficiently, other parts pass through the liner into an acoustic resonator, an example of which is shown in figure 7-5. Helmholtz resonator theory is used to determine the size of the cavity behind the holes so that the sound energy, or pressure wave energy, that passes through the hole is broken up and dissipated. These liners have been quite effective, but they are not a cure-all. They are a very valuable tool, but we have not yet learned how to fully optimize the design of these devices to achieve maximum effectiveness.

Baffles. - Another way of eliminating this instability which is usually successful is by the use of baffles on the injector face. Shown in figure 7-6 is an injector with such baffles from the Air Force Transtage engine. Four baffles are used that extend down into
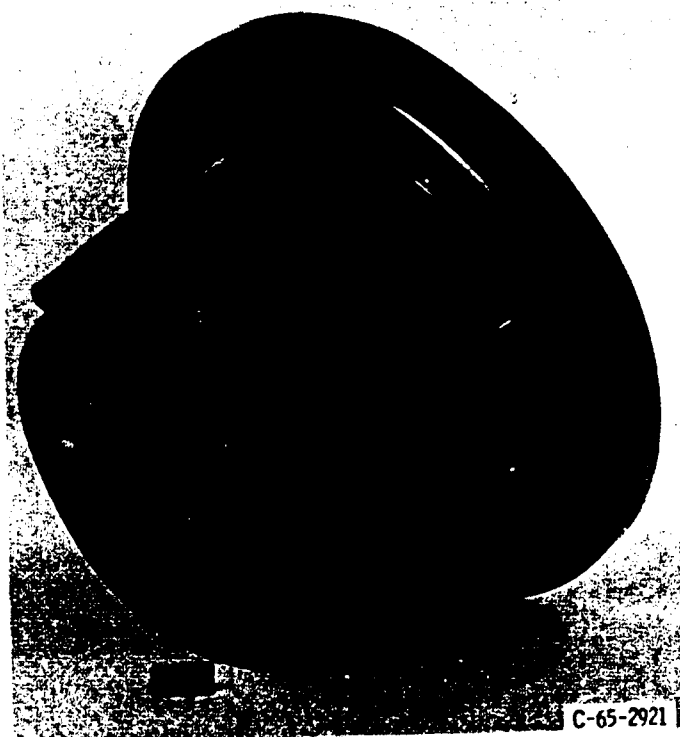

C-65-2921

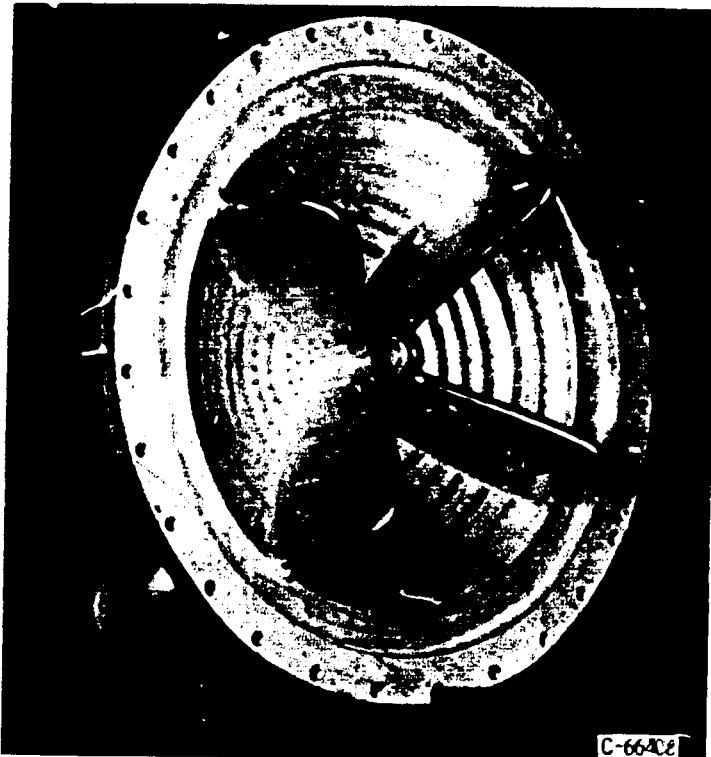Figure 7-5. - Flight weight acoustic liner for screech suppression.

Figure 7-6. - Baffles attached to injector face for screech prevention.

the combustion zone to interrupt the progress and reinforcement of these tangential pressure waves. This method is based on the hypothesis that screech originates much like a detonation wave; once the disturbance is created in the combustion zone, the waves accelerate the combustion process locally, which, in turn, provides energy to reinforce the wave. These waves will propagate and grow as they feed on the chemical energy that is present. The baffles represent an attempt to interrupt the waves and reflect them back into a zone where there is no unburned propellant to supply energy for their continuation. Other hypotheses have been advanced, however, and no theory is yet confirmed.

Cooling

Having created an inferno, the designer is next faced with the problem of how to contain it. The gas temperatures vary between about 4000° and 7000° F, depending upon the particular propellant combination. However, most of the structural materials in common use melt at much lower temperatures. For example, stainless steel or Inconel melt at about 2200° or 2400° F, much below the combustion gas temperature. There are refractory alloys such as molybdenum which melts at around 4700° F. However, the use of molybdenum poses some problems because it oxidizes extremely rapidly; in fact, it will simply sublimate, going directly from the solid phase into the gas phase unless it is pro-

tected from oxygen attack. Coated molybdenum is, therefore, one of the materials that are being carefully considered in advanced engines.

Regenerative method. - Since no known material will work unassisted, the designer must employ active cooling techniques. There are many ways to cool engines, none of which are optimum for all propellant combinations or all types of engine. Therefore, several different techniques are used. Regenerative cooling, perhaps the most common system, is used in the Atlas engines, in the F-1, and the J-2 engines used in the Saturn booster stages. Figure 7-7 shows a cross section of a regeneratively cooled eng .ne
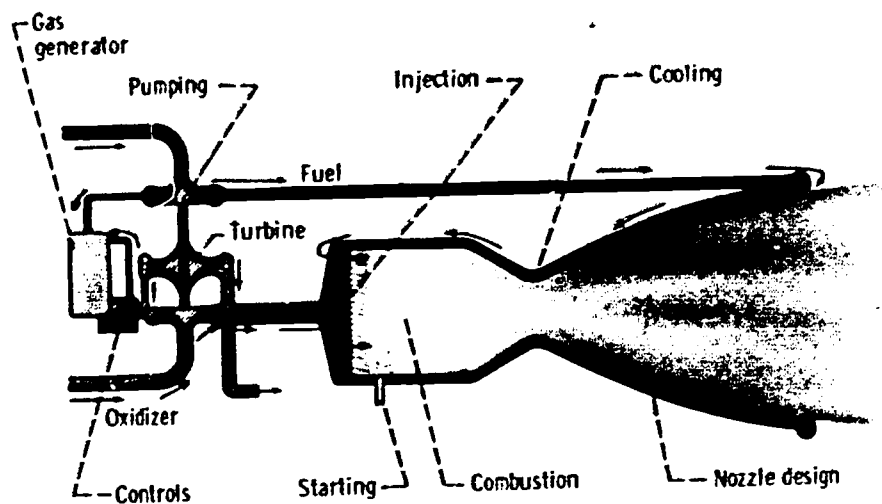
CS-36188

Figure 7-7.- Regeneratively cooled rocket engine.

where one of the two propellants is used as a coolant. The propellant used for cooling is piped into the engine at the downstream end of the exhaust nozzle. There it is divided among as many as perhaps 100 small tubes which extend the entire length of the engine and are orazed together to form the walls of the engine. Each of these tubes is specially formed and tapered to change the local velocity of the coolant as it passes forward to the injector. The lc al coolant velocity is calculated to match the expected heat distribution from the combustion process. In the case of the hydrogen burning engines, hydrogen is used as the coolant because it is excellent in this regard. It can be heated to almost any temperature and will continue to absorb heat so that the hydrogen itself does not pose a limitation. If, on the other hand, hydrazine is used to cool an engine, like those in the Titan, local velocity must be very high because the hydrazine will detonate if it gets above 210° or 220° F.

126

Ablative cooling. - There are some cases where the regeneratively cooled engine cannot be made to cool properly. One of these cases is where there is a need to throttle the engine to produce a lower thrust. When the engine is throttled, propellant flow is reduced and the velocity of the coolant in each of the coolant tubes is reduced. Accordingly, the heat-transfer capability of the coolant in the tube decreases. Consequently, the metal begins to overheat and burnout will occur. The engines for the Apollo landing vehicle, which require a 10:1 throttling, use ablative cooling. These thrust chambers are made essentially of glass fibers and a plastic. The problem of reduced propellant velocity is avoided because the ablative engine is not adversely affected by operation at reduced thrust. In figure 7-8 is shown an example of an ablative engine after firing.
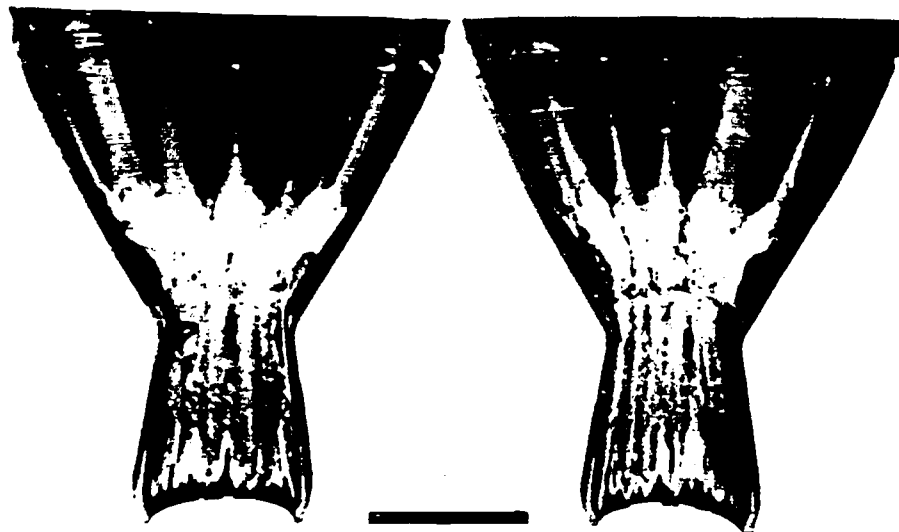
C-66-290

Figure 7-8. - Sectioned ablative combustion chamber after 151 seconds of operation.

This engine is almost the same size as the engine to be used in making the lunar landings with Apollo. The Apollo engine is made of quartz fibers which are more or less perpendicular to the engine centerline; these are imbedded in a phenolic resin. The principle of operation here is this: the heat vaporizes the resin, each pound of resin absorbing between 2000 and 5000 British thermal units of heat in the process. The gases that evaporate from the resin flow over the hot inside surface of the combustion chamber and nozzle, cooling these surfaces by evaporation. Furthermore, the gases act as a barrier to prevent more heat from entering the ablative wall from the hot combustion gases. Eventually, however, the quartz fibers melt and beaded runoff of quartz occurs. This principle was used on the heat shield of the first reentry body returned from space. It is also the principle that is used on the Mercury capsule heat shield and on the Apollo heat shield as well as the engines.
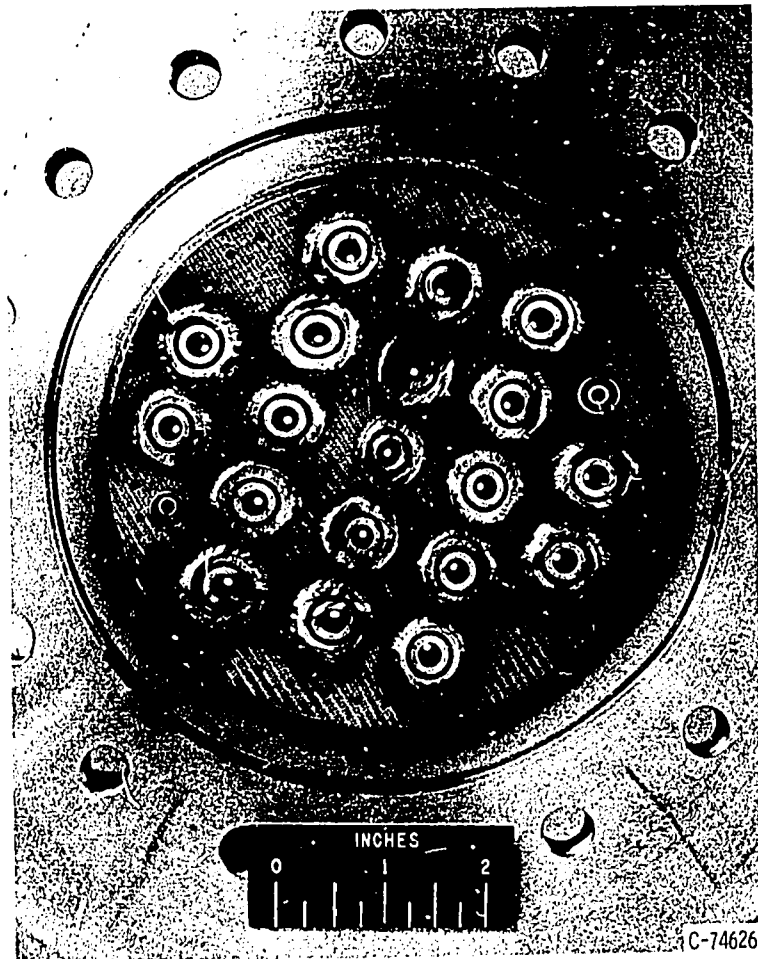
Figure 7-9. - Injector with porous faceplate for transpiration cooling.

Transpiration cooling. - Another technique for cooling rocket engines is transpiration cooling. Transpiration cooling simply consists of using a porous material to fabricate the chamber wall, and forcing through the porous wall a small quantity of one of the propellants. This is practical, particularly with a propellant such as hydrogen which is gaseous by the time it emerges on the hot side of the wall. Figure 7-9 is a view of an injector with a porous faceplate for transpiration cooling. One common way of making a porous wall consists simply of layers of stainless screen that are then pressed and sintered to make a rather rigid structure. The merit of the transpiration cooling system is that it probably can be made to work under the most severe heat-transfer conditions we can imagine. It will probably allow higher chamber pressure (with its consequent higher heat transfer) than will either the regenerative system or the ablation system. There is a penalty, however, in performance in using transpiration cooling, particularly if extremely severe heat-transfer conditions require high coolant flows. Much of the propellant used as a coolant flows through as a boundary layer and does not become fully involved in the combustion process. This means that more propellant is needed with this cooling system than with either of the others, propellant which adds weight but little

120

thrust. Therefore, by comparison, a transpiration cooled engine is slightly less effi-
cient than either a regenerative or an ablative cooled one.

Dump cooling. - An experimental engine using the dump cooling technique is shown
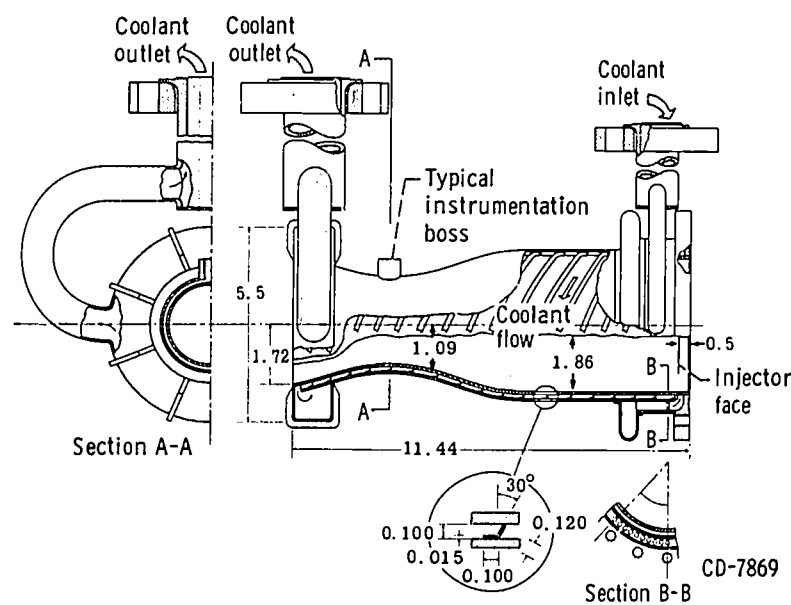in figure 7-10. The dump coolant, hydrogen in this case, enters a concentric shell

Figure 7-10. - Sketch of experimental engine with "dump" cooling.

around the combustion chamber at the injector end and flows around the chamber through
helical passages to the aft end, thus cooling the chamber wall. In a flight engine, the
warm hydrogen resulting would flow through an exhaust nozzle independent of the main
stream and would produce an impulse almost as high as the main propellant stream.
This technique is probably most applicable to engines operating at low chamber pressure.

Radiation cooling. - A final method, which has been used on small engines in partic-
ular, is radiation cooling. With this technique, the combustion chamber is made from a
coated refractory alloy such as columbium, molybdenum, or tantalum-tungsten which can
operate at metal temperatures of the order of 3000^C F; such a chamber operates white
hot. The inside of the chamber receives heat from the combustion gases which are of
the order of 5000° F, while the outside of the chamber radiates the heat so received into
space. The heat transfer due to radiation is in accordance with the Stefan-Boltzmann
Law, which states mathematically:

$$Q = \epsilon\left(T_m^4 - T_o^4\right)$$

129

where

Q   quantity of heat transferred/unit time

ϵ emissivity (usually about 0.9), the ratio of radiation emitted by a surface to that emitted by a perfect radiator

T_m thrust chamber temperature, $^\circ R$

T_0 temperature of matter surrounding engine, $^\circ R$

Inasmuch as the temperature T_0 in space is almost absolute zero, the equation becomes

$$Q = \epsilon T_m^4$$

When a radiation-cooled engine is started, the chamber will quickly heat to some very high temperature at which the heat rejected by radiation is exactly equal to the heat received from the combustion in the chamber. In practice, such engines must be carefully located to avoid overheating any portion of the spacecraft which can "see" the hot chamber and, therefore, can receive radiation from it.

PROPELLANT SUPPLY

Since the combustion chamber and its operation have been examined, it is appropriate to examine next the systems which deliver the propellants to the combustion chamber. Basically, only two system types are used: pressure-fed or pump-fed, although many variations are possible with either system.

Pressure-fed system. - A typical pressure-fed system is shown schematically in figure 7-11. An inert gas, usually helium or nitrogen, is stored under high pressure in the bottle labeled "gas supply." Prior to engine start, the gas is allowed to enter the fuel and oxidant tanks through check valves (one way) and a pressure regulator which will maintain the pressure in the tanks at some preset value higher than the desired thrust chamber pressure. The engine is started by opening the fire valves in a carefully controlled sequence (with the use of an electronic timer) to allow the gas pressure to force the propellants into the thrust chamber. As the propellants are consumed, additional gas is supplied to the tanks by the pressure regulator to maintain constant pressure until the tanks are empty or shutdown is commanded. More sophisticated systems include various methods of heating the pressurant gas to reduce the quantity required. It should be noted that with pressure-fed systems, the propellant tanks must operate at high pressure and must, therefore, be strong and heavy. As a result, this system is competitive with pump fed systems only for fairly small missile stages.
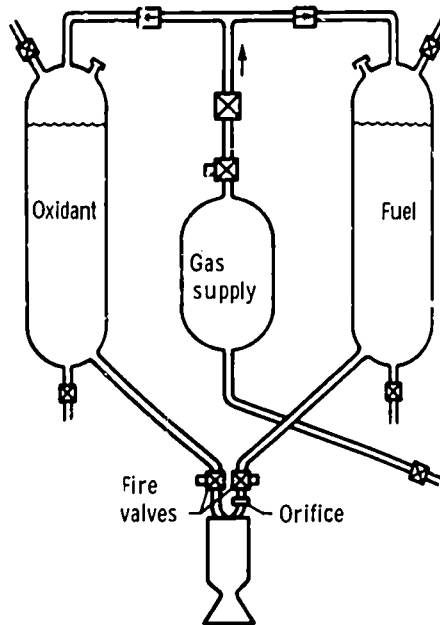
Figure 7-11. - Typical pressure-fed propellant system.

Pump-fed system. - One version of a pump-fed system, used for the RL-10 engines in the Centaur vehicle, is shown schematically in figure 7-12. Boost pumps at each propellant tank, not shown, are driven by catalytic decomposition of hydrogen peroxide in a gas generator to supply propellants at relatively low pressures to the inlet of the pumps shown in the figure. The oxygen is pumped to a pressure of about 500 psi and then passes through the mixture ratio control valve to the injector, which sprays it into the combustion chamber. Hydrogen, on the other hand, is pressurized by a two-stage pump; from there,
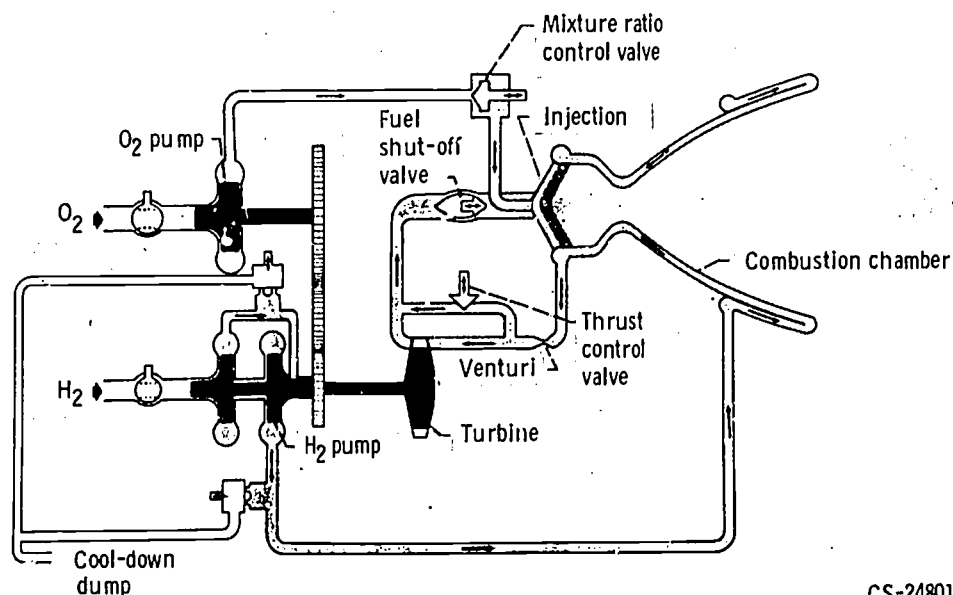
CS-24801

Figure 7-12. - Standard RL-10 engine and propellant supply system.

it enters the engine cooling jacket wh re, in cooling the chamber its temperature is increased from about 40° to 300° R. The warm gaseous hydrogen leaving the front end of the cooling jacket is then used to drive a turbine which powers both the hydrogen and oxygen pumps. After leaving the turbine, the hydrogen passes through the injector into the combustion chamber. Pump speed is regulated by a controlled bypass of some of the hydrogen around the turbine. The system just described is referred to as a "bootstrap" system. Another common system simply employs a separate combustion chamber or gas generator using engine propellants tapped off the main supply lines to drive the turbine which drives the pumps. The exhaust gas from the turbine is ducted overboard through a separate nozzle.

Propellants

To round out this brief description of chemical rocket propulsion, it is appropriate to consider the propellants - and the reasons for their selection. In figure 7-13, specific impulse is plotted as a function of the bulk density of the propellant combination for a number of combinations. It should be recalled from a preceding chapter that specific impulse is a figure of merit much like gas mileage of an automobile. It is equal to the pound-seconds of thrust produced for each pound-per-second of propellant flow. It will be
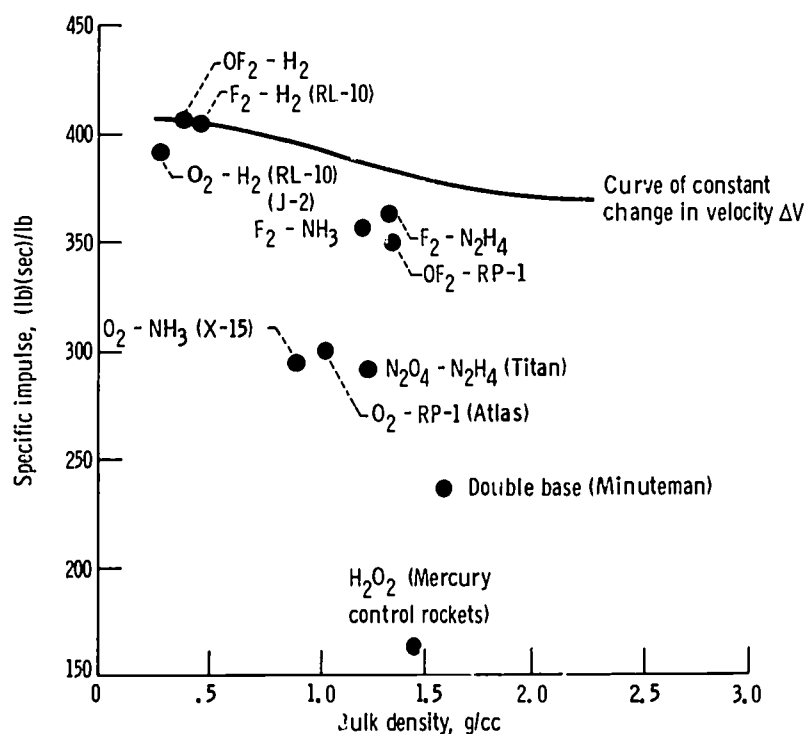
Figure 7-13. - Performance characteristics of typical propellant combinations.

132

seen that the maximum values of specific impulse are achieved with OF_2-H_2 and F_2-H_2, followed by O_2-H_2. These propellant combinations are, of course, of considerable interest since they give significantly higher values of impulse than the O_2-RP-1 used in Atlas or the N_2O_4-N_2H_4 used currently in Titan.

By itself, however, specific impulse is not a singular criterion of merit – other factors must be considered, such as the bulk density shown by the abscissa. The overall objective of a missile stage is to impart a maximum change in velocity to the stage and its payload. As given in chapter 2, the equation relating these factors in space is:

$$V_f - V_i = \Delta V = I_{sp}g \ln\left(\frac{W_f}{W_e}\right)$$

where

V_f final velocity

V_i initial velocity

I_{sp} specific impulse

g   universal gravitational constant (32.217 ft/sec^2)

W_f weight of stage loaded with propellant

W_e empty weight (at burnout)

Inspection of this equation shows that the velocity change can be increased by increasing specific impulse, but also, it can be increased by decreasing the vehicle empty weight or structural weight. In this regard then, the use of higher density propellants will result in smaller propellant tanks and, hence, a lower structural weight. The trade-off between specific impulse and bulk density is indicated in figure 7-13 by the curve of constant ΔV. From this, it may be seen that F_2-H_2 will produce a greater velocity change than will OF_2-RP-1 (for an equal velocity change, OF_2-RP-1 would have to show a specific impulse of 380 seconds instead of 350). Thus, the ΔV produced is not simply given by the ratio of the specific impulse values, but is also affected by the bulk density.

Miscellaneous Considerations

There are other factors that are important in the propellant selection; one of them is hypergolicity. This ability of some propellant combinations to burn spontaneously is a desirable characteristic because it eliminates spark plugs or other ignition devices and thereby improves reliability. Another important consideration is the temperature at which the fuel and the oxidizer are liquid. Ideally, this temperature should be the same

for both; otherwise, the colder propellant will freeze the warmer one solid. For example, although hydrogen and nitrogen tetroxide make a good propellant combination, their liquid temperature ranges are so different as to require heavy insulation between the storage tanks. This means extra weight with its consequent interference with performance unless the storage tanks are placed far apart - a design difficult to achieve in most rockets, and one which frequently adds weight in the form of extra piping and bracing. Toxicity is another factor. Fluorine is extremely toxic; nitrogen tetroxide is somewhat more toxic than phosgene. These toxic propellants have to be treated with respect and involve costly safety equipment and procedures which the user would like to avoid. The designer must consider propellants with an adequate supply and reasonable cost. These have generally not been factors in the programs to date; however, they are important in selecting propellants for advance missions, inasmuch as it is possible to specify something that is beyond our ability to supply. For example, if the tripropellant combination involving finely powdered beryllium were suddenly the only way of meeting a very energetic mission requirement, there would be enormous problems of finding supplies and suppliers. Storage and insulation are important; for example, if the mission were to fly close to the Sun, say within 1/10 astronomical unit, and return, the mission time would be about 220 days. To contain liquid hydrogen for long time periods such as this without excessive boiloff requires exceptional insulation, and the designer must pay the penalty in terms of weight. Other propellant combinations then, in this particular type of mission, are competitive, because, even though their impulse may be lower, the designer can avoid all this insulation weight. Finally, there is the consideration of the cooling capacity of the propellant; for example, hydrazine detonates at about 210° F and, therefore, is limited in the amount of heat it can absorb, but hydrogen can absorb any quantity of heat without limitations except those imposed by the materials to contain the hot hydrogen.

This discussion has covered the more important factors of the many that govern the behavior of liquid propellant rockets and which the designer must consider. A detailed treatment of the subject is contained in Rocket Propulsion Elements by George P. Sutton, Third ed., John Wiley and Sons, Inc., 1963.

134

8. ZERO-GRAVITY EFFECTS

William J. Masica*

Gravity is as familiar to us as breathing and probably just as much taken for granted. We expect water to be at the bottom of a glass, warm air to rise, a football pass to be completed, and, when we sit, to have a certain part of ourselves in firm contact with an object on the ground. We view balls that roll uphill and Indian rope tricks with suspicion, for experience tells us that we cannot defy gravity.

Isaac Newton, at the early age of 23, was the first to really define the operations of gravity. Using the idea of accelerated motion discovered by Galileo and the planetary data supplied by Brahe and Kepler, Sir Isaac, with brilliant insight, arrived at the universal rule of gravity:

The gravitational force or the force of attraction between two bodies is directly proportional to the product of the masses of the two bodies and inversely proportional to the square of the distance between them.

Expressed mathematically,

$$F = G \frac{m_1 m_2}{r^2}$$

where G is a constant. To be precise, this equation applies only to very, very small volumes of mass. Given a little more time (needed to develop calculus!), Newton was able to show that his equation also applied to any spherical mass of constant density material. The gravity force acts as if all the mass were at the center of the sphere, and the r in the equation is the distance between the centers of the spheres.

The amazing part about this rule is that it is universal. Provided that we do not ask too many questions, Newton's equation works 99.44 percent of the time. The gravitational force between masses of any shape can be calculated by breaking a large body into many small mass volumes, using Newton's equation to find the force caused by each of these small masses, and then adding all the forces together. Only the arithmetic becomes more difficult.

*Head, Fluid Dynamics and Heat Transfer Section.

Newton's gravity equation is an experimental rule; that is, it describes most ob-
served facts of gravity. It cannot be derived, and it avoids explaining why or how one
mass body attracts another. Einstein pretty well completed the remaining 0.56 percent
of the problem when he developed his theory of general relativity. Despite numerous
challenges, general relativity has remained virtually unchanged since its formulation
over 40 years ago - a truly remarkable fact (and testimonial) in view of the sweeping
changes in every other area of science. Today, Einstein's theory of gravity is generally
accepted because it appears to agree with experimental observations. There remains,
however, considerable disagreement as to just how good is the agreement. Recent
measurements of the shape of the Sun by Dr. R. H. Dicke and his colleagues at
Princeton University seem to suggest that Einstein's theory needs some modification.
Professor Dicke's challenge is being taken seriously. The debates continue in the
scientific periodicals, and apparently it will be some time before the question is resolved.
(For a readable text on gravity, including some of the original relativistic aspects,
see ref. 1.)

ZERO GRAVITY

What would a world without gravity be like? In a classical world (one with reasonably
large objects, times of the order of minutes and hours, and speeds well below the speed
of light - in brief, the kind of world we live in), Newton's gravity equation works very
well. According to Newton's equation, a gravity-free world would then be effectively a
massless world. For example, if the only mass system in our world were a glass of
water, the glass of water would experience no gravitational force. But, the mass of the
water alone would still cause some small gravity force on the glass. The gravity forces
due to the mass of water in a glass are extremely small, so small that they can be re-
garded as zero, simply because the masses themselves are small. For all practical
cases, then, a gravity-free world could mean a world of small mass volumes, where
very massive objects, such as planets, are absent. Actually this is only one way of pic-
turing a gravity-free world. If the glass of water could be magically placed at a spot be-
tween the Earth and the Moon where the gravity caused by the mass of the Earth exactly
cancels the Moon's gravity, the glass of water is in a gravity-free environment. The
gravity force caused by the other planets is negligible because of their remoteness.

A third way of describing a gravity-free world is a very practical one that can
actually be obtained. Imagine that you are on an elevator, initially resting at the top
floor. In one hand you are holding a ball, in the other, a glass of water. You feel grav-
ity acting on your body because the elevator floor is in contact with your feet, pushing up

with a force exactly equal to your weight. If you drop the ball, it falls, accelerating at a rate of about 32 feet per second per second. Just as you pick the ball up, the elevator cables break, and the elevator begins to fall. Because of a streamlined elevator floor, there is no air drag, and you and the elevator begin to accelerate freely. While pondering your fate, you notice that the familiar tug of gravity on your body has vanished - to over-simplify, your feet cannot quite catch up to the elevator floor. If you gently release the ball, it will just stay there, floating in the elevator. As far as you are concerned, your short-lived world is gravity-free. Of course, the panic-stricken fellow standing on the ground sees all sorts of gravity forces: you, the elevator, and the ball all accelerating downward because of the Earth's gravity force.

A gravity-free world, or zero gravity, or weightlessness is, therefore, a relative thing. In general, zero gravity means more than the effective absence of gravitational force in a world of small masses or at certain select places in space between planets. As long as a body, a rocket ship, or a glass of water is accelerating freely under gravity-type forces only, with no friction, air drag, or other forces acting, it will be in a zero-gravity environment to an observer moving along with it. Thus, the contents of a rocket with its engine shut off, coasting freely towards the Moon, are in zero-g. Objects on a platform falling freely on Earth in a vertical tower, evacuated to eliminate air drag, are in zero-g. The contents of a Gemini capsule that is moving freely in a stable orbit around the Earth are in zero-g. (Contrary to some popular statements, the net force acting on an orbiting spacecraft is not zero, nor could it possibly be zero - remember Newton's first law of motion?) Since friction-type forces are almost always present, a practical definition of zero-g, preferably in mathematical form, is still required. Later in this chapter, such a definition of zero-g for a fluid system is given.

Your quick thinking has saved you in that ill-fated elevator ride. While calmly awaiting rescue from the crushed elevator, your thoughts return to what happened during your brief moments in zero-g to the water in that glass you are still holding.

SPACE FLIGHT IN ZERO GRAVITY

The requirements of space flight have stimulated zero-g research. How will man, his life-support equipment, space vehicles, and all the various systems used in space flight perform in zero-g? The problems, which are many, range from the subtle bio-physical ones to the very practical problem of just turning a wrench. Since systems such as liquid propellants and life support are vital, much attention has been given to finding out what happens to a liquid-vapor or fluid system in zero gravity. A few of the problems and questions which have to be answered are shown in figure 8-1. This figure shows a

ACCELERATION
DISTURBANCES

GAS
VENT

HEAT GAINS

PAYLOAD
SUPPORTS

CREW
MOVEMENTS

SOLAR AND
PLANETARY
RADIANT
HEAT

DRAG
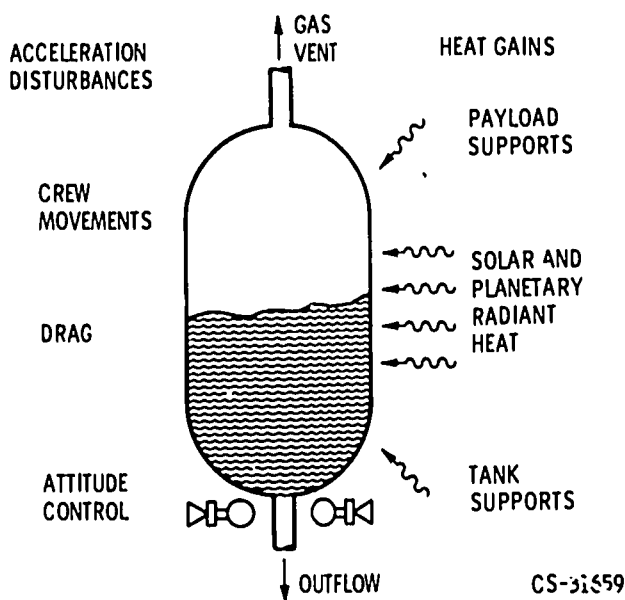
ATTITUDE
CONTROL

TANK
SUPPORTS

OUTFLOW

CS-3i559

Figure 8-1. - Fluid management problems.

propellant tank holding a cryogenic fluid (liquid hydrogen, liquid oxygen, etc.). On Earth
under normal gravity, or 1-g conditions, the liquid is exactly where it should be: like
water in a glass, the liquid is at the bottom. If liquid must be removed to start our en-
gines on the pad, all that is needed is an outlet located somewhere at the bottom of the
tank. Since cryogenics evaporate very easily and build up pressure in the tank, a vent
located at the top of the tank can be opened to prevent a pressure explosion. If the vent
is opened while the rocket is on the ground or during launch, only gas or vapor will be
lost and not the precious liquid fuel supply.

In zero-g while the vehicle is coasting, the requirements are much the same. The
liquid should be at the tank outlet in order to be able to restart the engines; because of
the heat from the Sun and the like, the tank must be vented. Consequently, the liquid and
vapor must be in a proper position in the tank. The problems have, however, been in-
creased in zero-g. Now an attitude control maneuver, for example, could easily cause
the liquid and vapor to move around in the tank. In zero-g, the liquid will not necessarily
return to the bottom or pump outlet part of the tank as it would in 1-g; gone is the reli-
able restoring force of gravity.

CAPILLARITY AND SURFACE ENERGY

The first question is obviously what is the shape of the liquid surface in zero-g? The
glass of water in 1-g has a fairly flat liquid surface or (to sound scientific) liquid-vapor
interface, except near the walls of the glass, where the liquid curves up slightly. This

138

curvature near the walls is due to very short-range, molecular forces that act something like electric forces. Another force, which acts along the entire liquid surface, is the surface tension force. Usually, we forget all about these forces in 1-g because they are very small; but in zero-g these are the only forces present and, therefore, these capillary forces are, relatively speaking, very large.

Surface tension, or the fact that a liquid surface acts like a thin elastic film, is not quite a force. It might act like a force, but surface tension is really an energy-type quantity. Energy is a defined quantity used in physics and is very handy and easy to work with; it is a scalar, that is, a number. Numbers can easily be added, multiplied, or otherwise handled. A force is a vector and not quite so simple to work with. For example, as in chapter 9, if you want to add forces, you must consider both the magnitude and the direction of each force. In one form, energy is the amount of work or effort required to move something somewhere. An arbitrary numbering system is given to energy to indicate that it takes more work to push a car 50 feet than to push it 5 feet. Closely related to the definition of energy is the principle that all physical systems, when left alone, take the path (or shape or form) that requires the least amount of energy. Although this is given without proof, the principle is very familiar to all of us: we do the least amount of work to get a job done. Nature happens to work the same way.

The idea of energy and the principle of minimum energy are powerful tools in physics. Together they can be used to solve many problems. They are especially useful in capillarity. It takes work to remove a molecule from a liquid or solid surface; the larger the area between the molecule and its neighbors, the easier it is to pull out that molecule. For liquids, this amount of work, or energy, divided by the available area is called the surface tension. Generally, a large group of molecules over any unit area (an area of 1 mm^2, 1 cm^2, etc.) is usually considered. Surface tension is then an energy per unit area. Solids also have surface energies, and, as one might suspect, these are usually larger than those of liquids. It takes more work to pull out a tightly held metal surface molecule than a rather loosely held liquid surface molecule. Most liquids have surface energies in the range from 2 to 80 energy units per unit area, while solids cover the wider range from about 15 to over 800 energy units per unit area.

Surface energy and the principle of minimum energy explain many everyday facts of capillarity. Water has a surface tension of 70 energy units per unit area. Wax has a surface energy of about 40 energy units per unit area. Water on a newly waxed car beads because the solid wax surface has the lower energy. The water tries to cover as small an area of the lower energy wax surface as possible. This is the same principle behind the nonstick frying pans. These solid surfaces have very low energies, much lower than most food products. Thus, by the minimum energy principle, food will not stick to form new surfaces of higher energy. Of course, things also happen in reverse - a drop of oil with a surface tension of 30 will spread on wax to try to keep the new surface energy at

a minimum. Detergents, another example, lower the surface tension of water and, among other things, let the water spread more easily over fabrics to aid in washing.

It is essential when using minimum-energy principles that all the energies be considered. In the last paragraph, we have quite incorrectly neglected one of the energies. All solid-liquid-vapor systems (a glass of water, for example) have three surface energies: the liquid-to-vapor, the solid-to-vapor, and the solid-to-liquid surface energies. If gravity is present, there is also the gravitational energy, for it takes extra work to move something against the gravity force. When each surface energy per unit area is multiplied by the area that particular surface covers, the product is an energy term, or simply a number. For example, if σ_{lv} represents the surface energy per unit area of the liquid-vapor surface and A_{lv} is the area of that surface, then

$$\sigma_{lv} \times A_{lv} = \frac{Energy}{Area} \times Area = Energy$$

All the energy terms are added to give the total energy, and according to the principle of minimum energy, this total energy will be as small as possible. The only way the energy can change is if the areas of the surfaces change. Since all the areas cannot be made as small as possible (the glass of water is a fixed size), those that multiply the largest surface energies will be changed more. Thus, the liquid shape will be that shape where the surface areas become as small as possible, with the largest area changes being for those terms that affect the energy the most.

CONTACT ANGLE

Finally, the boundary conditions have to be considered. One obvious boundary condition is that the liquid is in the glass; another condition is the contact angle. For many combinations of liquids and solids, the spreading of the liquid is not perfect. The liquid meets the solid at some definite angle. This angle is called the contact angle (θ in fig. 8-2) and its value may range from 0° to well above 90°. Water on a very clean glass surface has a 0° contact angle; on wax, about 90°. Mercury on glass has about a 130° contact angle. Obviously, the contact angle is related to the surface energies. For example, a high contact angle means that the surface tension of the liquid is probably greater than the solid surface energy. The contact angle has been shown both theoretically and experimentally to be independent of gravity. Its value remains constant whether at 1-g or zero-g.

(a) Wetting liquid, $0° < \theta < 90°$.   (b) Nonwetting liquid, $90° < \theta < 180°$.
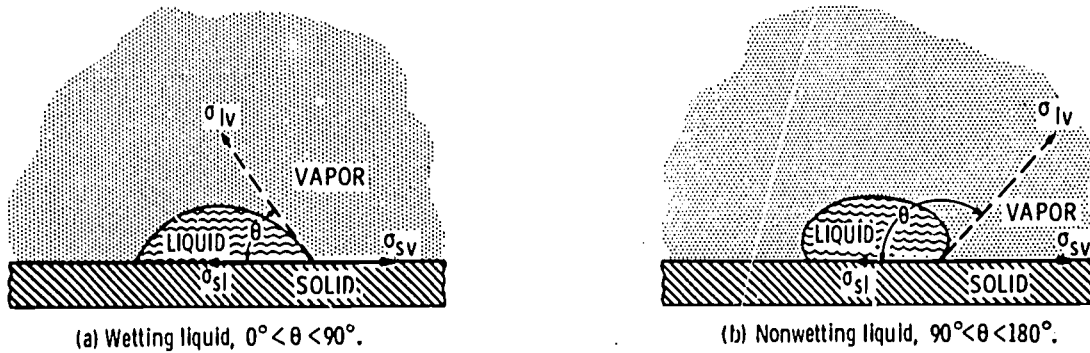
Figure 8-2. – Contact angle definition.

LIQUID SURFACES IN ZERO GRAVITY

With this information we can now explain what happened in that glass of water during the elevator ride. In zero-g the only forces present are capillary forces. According to the principle of minimum energy, the zero-g shape will be that shape where the sum of the surface energies is the smallest. This sum is made small by changing the areas of the liquid, vapor, and solid surface, while keeping the contact angle the same. Figure 8-3 shows the zero-g shapes in various tanks for liquids with a $0°$ contact angle. The zero-g interface shape in a spherical tank is a vapor bubble, completely surrounded by liquid. In a partly filled cylindrical tank the liquid forms a hemispherical surface. Notice that in each case, the area of solid (to vapor) is "minimized" to keep that relatively

(a) Spherical tank.   (b) Cylindrical tank.   (c) Conical tank.
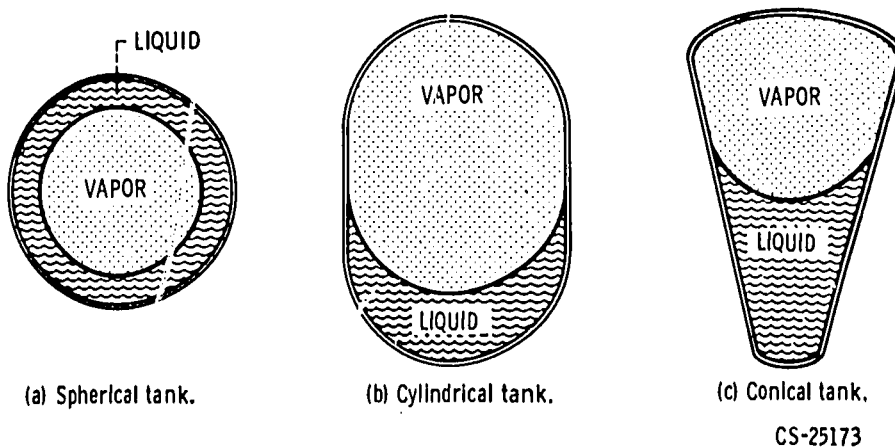
CS-25173

Figure 8-3. – Zero-g interface configurations for 0° contact angle liquids.
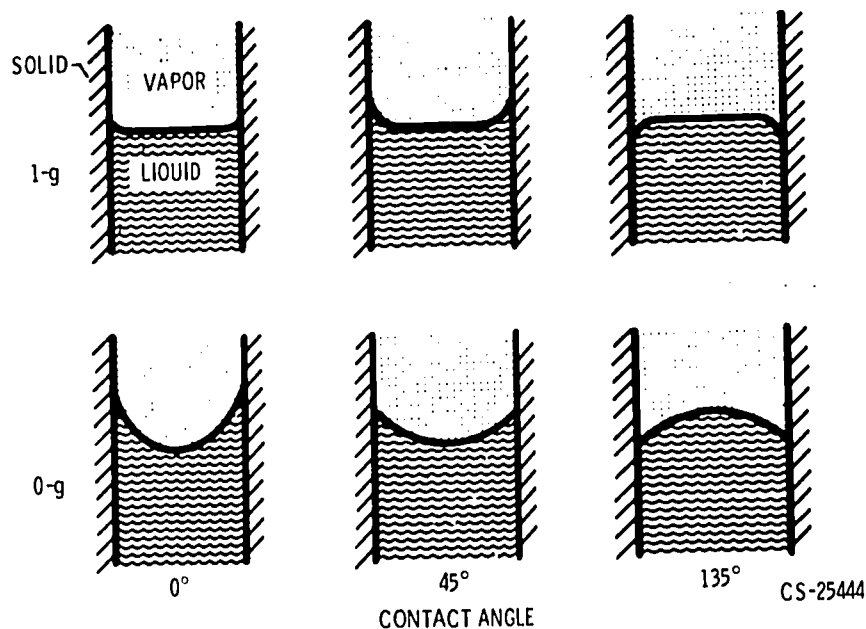
Figure 8-4. – One-g and zero-g interface configurations.

large energy term as small as possible. Figure 8-4 compares surface shapes in a cylinder for different values of contact angle. In summary, the zero-g interface shape depends on three things: the fluid properties including the contact angle, the shape of the container, and the percentage of liquid in the tank. Given these, the zero-g shape can be defined by use of the idea of minimum total energy.

ZERO-GRAVITY BAFFLES

It is apparent from figure 8-3 that the zero-g location of the liquid and vapor could cause problems in rocket engine restart and venting operations. In a spherical tank, for example, the vent may be covered by liquid. Some method of positioning the liquid in zero-g is necessary. Since liquid surface shape in zero-g depends on tank shape, the position of the liquid can be controlled by changing the interior shape of the tank, for example, by adding baffles. A simple baffle is shown in figure 8-5. It is merely a tube mounted over the tank outlet with holes provided to allow the liquid to flow freely between the tank and the tube. For this baffled tank, a 0° contact angle liquid fills the tube over the tank outlet while the remaining liquid is distributed around the tube. Note that the tube also positions the vapor at the vent part of the tank. Another type of baffle is shown in figure 8-6. It consists of a sphere mounted off-center in the direction of the tank outlet within the main spherical tank. It can be shown, to use the familiar textbook words (which usually means, as it does here, with a lot of work), that these zero-g shapes do result in minimum total surface energy.
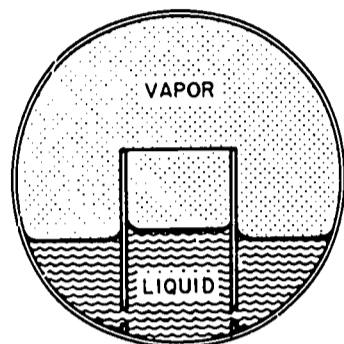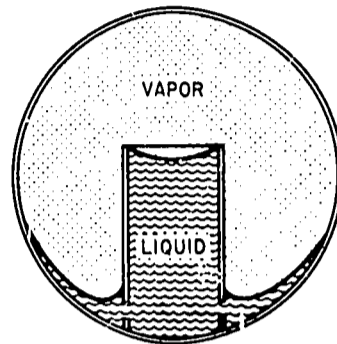
(a) One-g configuration.　　　　(b) Zero-g configuration.

CS-25176

Figure 8-5. - Capillary standpipe baffle.
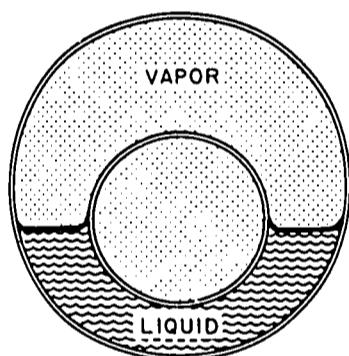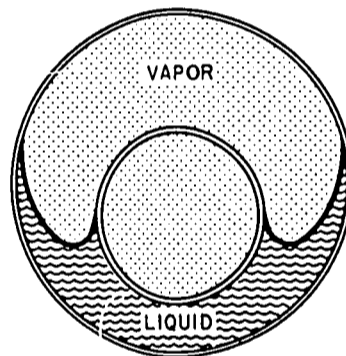
(a) One-g configuration.　　　　(b) Zero-g configuration.

CS-25175

Figure 8-6. - Spherical baffle.

Baffles like these work fine in zero-g, where surface energies are dominant, but they usually cannot position the liquid under conditions of acceleration disturbances, such as those from space vehicle attitude control or docking maneuvers. However, they are able to move the liquid back to the desired location once the disturbance is removed. Figure 8-7 shows a baffled tank with the liquid away from the desired position, as if displaced by some acceleration. Once the disturbance is removed, and a zero-g condition is restored, the liquid will return to the desired position over the tank outlet. All that is needed is that the liquid initially reach the baffle, so that it "knows" its minimum-energy shape.

There are many other kinds of baffles, as well as other methods (a piston, spinning the tank, screens, use of electric forces acting on the liquids, and acoustics are just a few) which can be used to control liquid in zero-g. All have their advantages and disadvantages (weight, sizes, reliability, etc.). One major advantage of passive baffles is that they have no moving parts, but one big disadvantage is that they generally cannot

LIQUID POSITION
DURING ACCELERATION
DISTURBANCE

LIQUID BEHAVIOR
AFTER ACCELERATION
IS CUT OFF

FINAL ZERO-GRAVITY
LIQUID-VAPOR POSITION

g

g

g

LIQUID
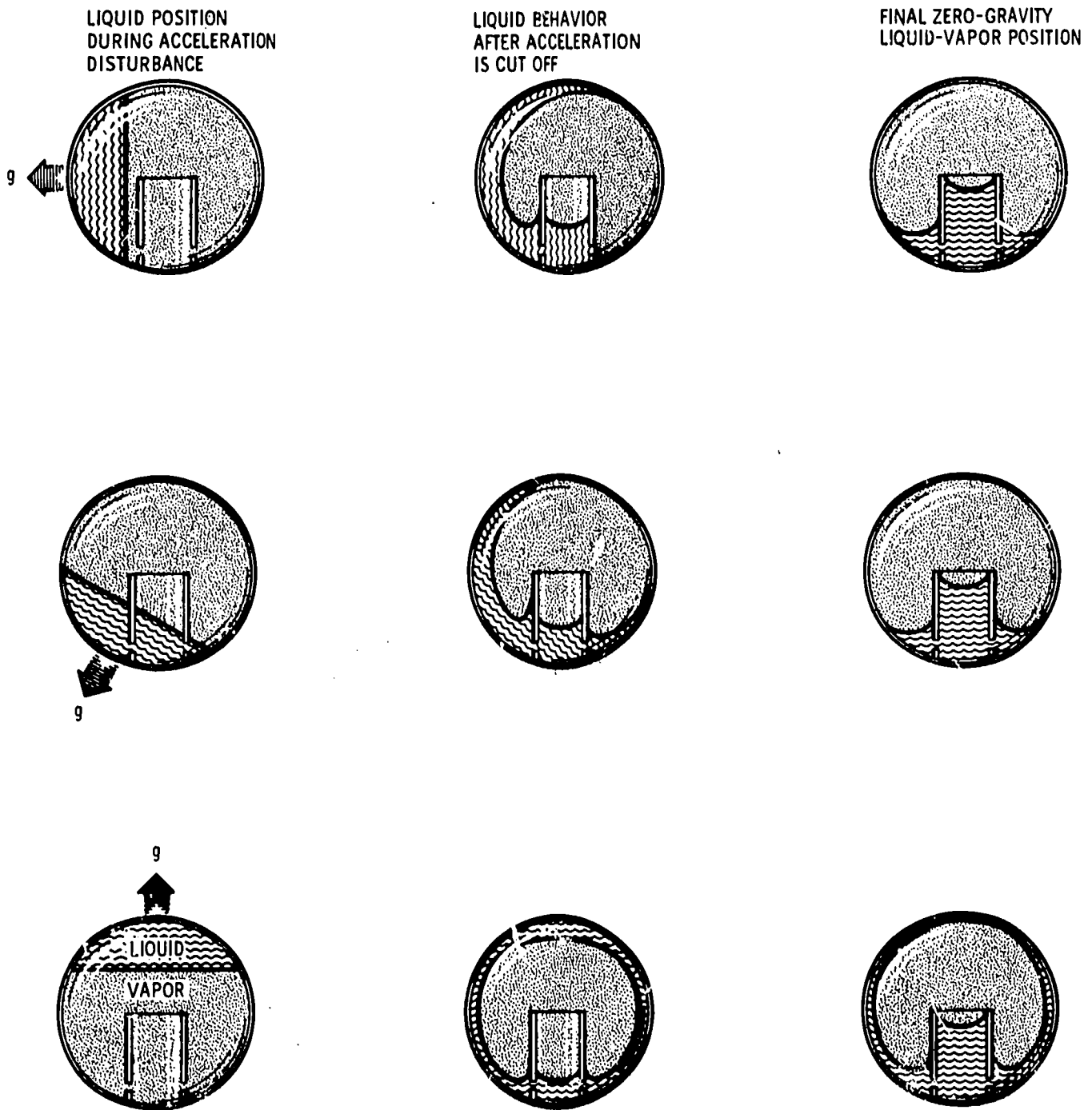
VAPOR

CD-9637

Figure 8-7. - Fluid behavior in baffled tanks.

guarantee that the vapor will be at the vent, especially under very low-g rather than zero-g conditions.

BOND NUMBER

At this stage in the discussion, it is very disheartening to admit that true zero-g does not exist. The streamlined elevator floor of the earlier example will produce some drag because the elevator shaft cannot be evacuated completely. Even a rocket ship in space will have solar wind and light pressure causing small but measurable forces. In brief, "accelerating freely" is really impossible. When the Agena-Centaur or Saturn coast in low Earth orbits, they all will be in a low-g field as a result of atmospheric drag. Although the effective accelerations due to the air drag at these altitudes may be small, say less than 0.00001-g (10^{-5}-g), they are significant.

A quantity called the Bond number indicates how large the acceleration forces are in comparison with the capillary forces. For a cylinder, the Bond number is

$$Bo = \frac{aR^2 \, \Delta\rho}{\sigma_{lv}}$$

where a is the effective acceleration, R is the cylinder radius, $\Delta\rho$ is the difference in density of liquid and vapor, and σ_{lv} is the surface tension. The Bond number appears in all mathematical solutions of low-g fluid problems. For our purposes, the Bond number may be regarded as an experimentally defined quantity. The Bond number has no dimensions. For Bond numbers much less than 1, surface tension is dominant; for Bond numbers greater than 1, gravity dominates. A glass of water in 1-g has a Bond number of about 200 - gravity is important. For liquids, zero-g really means that the Bond number of about 200 - gravity is important. For liquid, zero-g really means that the Bond number is very small, say less than 0.01. In a fluid system, gravity or acceleration-type forces can be neglected below Bond numbers of 0.01.

If a cylinder is small enough, the Bond number will be small, even in normal gravity conditions. The liquid surface in a soda straw looks like the zero-g shape in figure 8-4, even though the straw is not accelerating freely, but is motionless in 1-g. This is so because zero-g is a relative thing and to a fluid system of small size, gravity effects may be very small when compared with others. On the other hand, in a tank of large radius, a very small acceleration could result in a significant gravity effect. In general, a large Bond number (greater than about 100) means a flat liquid surface and that gravity or acceleration effects are important. A low Bond number (say less than 10) means that capillary effects predominate and, if the contact angle is small, a highly curved liquid
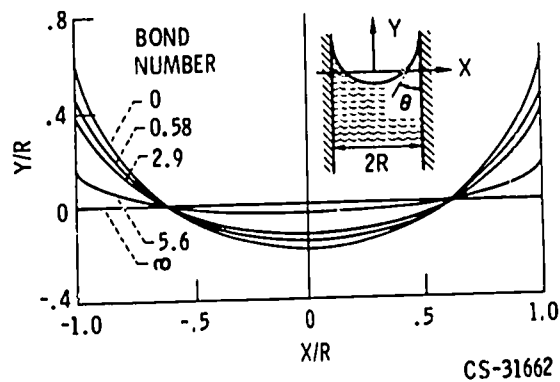
Figure 8-8. – Calculated interface configurations at various Bond numbers when θ = 10°.

surface results. A set of interface shapes for different Bond numbers is shown in figure 8-8.

In the real case of low Earth orbits, the Bond number is particularly useful. Air drag will act in a direction to cause the liquid to move. A liquid surface is not capable of resisting very much acceleration before it starts to move. For instance, although water will run out of an inverted glass, it will remain in the straw as long as the top end stays closed. How large an acceleration can be applied (or, in 1-g, how large can the straw's radius be) before liquid will move? Surface tension prevents the liquid from flowing in a straw, and the overall criterion of liquid flow is given by the Bond number. If the Bond number is less than about 1, no liquid will flow; if the Bond number is greater than 1, liquid will flow. Some of the data which provided this information are shown in figure 8-9.
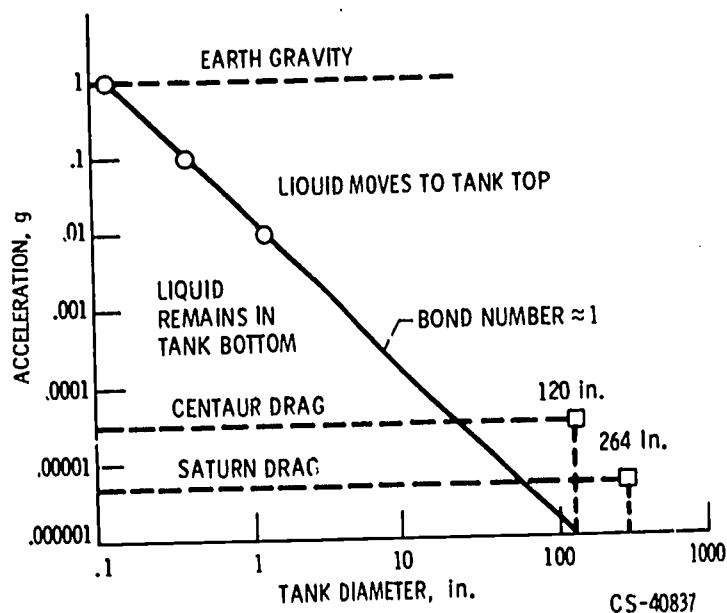
Figure 8-9. – Criterion for liquid stability.

For vehicles like Centaur in low Earth orbits, the Bond number is greater than 1 because of the large radius of the vehicle's tank. Thus, under the action of very small drag forces alone, the liquid propellants will move to the front of the tank. While baffles could trap some liquid at the pump inlet of the tanks, no baffle of reasonable weight can positively prevent liquid from covering the vent. For Centaur and Saturn, a positive method of locating the propellant was required. The chosen systems are similar and are summarized in figure 8-10. Each system positions the propellants during the entire coast period by applying a small acceleration sufficient to overcome the drag. The Bond numbers created by the accelerations are greater than the Bond number caused by drag. In the case of Centaur, this acceleration is produced by small rocket engines which burn for the entire 25-minute coast period. The Saturn system obtains thrust by properly directing the vented gas from propellant boiloff.

Residual air drag and its effect on propellant location is only one of the many problems. When the vehicle shuts off its engines to enter the coast period, other types of disturbances act on the propellant. The tank walls may give a little and then spring back, propellant slosh or the back-and-forth movement of the liquid in the tank may build up, and various return lines leading from the engine pumps to the tank may create liquid streams into the tank. If nothing were done to prevent these disturbances, the propellant would indeed be in a chaotic state. Eventually, the propellant would settle, but venting might be required in the meantime. A large part of zero-g development goes into finding simple and reliable ways of preventing or damping out liquid disturbances. The settling thrusts are increased in size to handle large liquid flow velocities, and various baffles are used to keep propellant sloshing below some reasonable level.

For long-duration space missions, the continuous application of even a small thrust
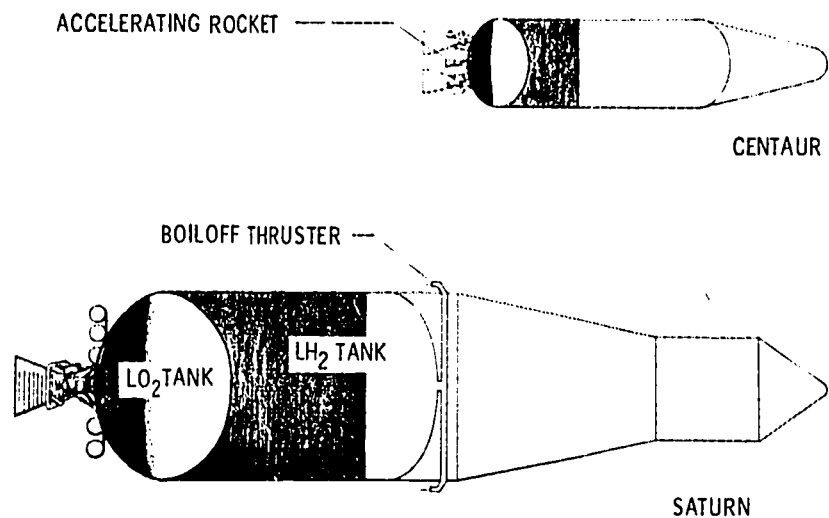
Figure 8-10. - Cryogenic propellant management systems.

139

to maintain liquid-vapor control would result in an important weight penalty. The subject of heat transfer - how the heat inputs build up the tank pressure - requires additional study. Heat transfer depends in part on free convection (for example, warm air rising) and buoyancy effects (an air bubble rising in a liquid to the surface). Both of these rely on density differences and gravity, and, therefore, free convection and buoyancy are reduced or entirely absent in zero-g.

A large part of the research investigating these and other similar zero-g problems is conducted at the Lewis Research Center. Lewis has two drop-tower facilities to produce short-time-duration, zero-g and low-g environments. The drop tower is identical to the freely falling elevator. One tower uses a drag shield around the experiment to reduce air

INTERNAL PACKAGE CONTAINS EXPERIMENT, CAMERA, TAPE RECORDER

SUSPENSION WIRE RUNS THROUGH TO INSIDE PACKAGE; DROP IS STARTED BY CUTTING WIRE

DRAG SHIELD
SPIKES

6 ft

86 ft

SANDBOX   C S-25229
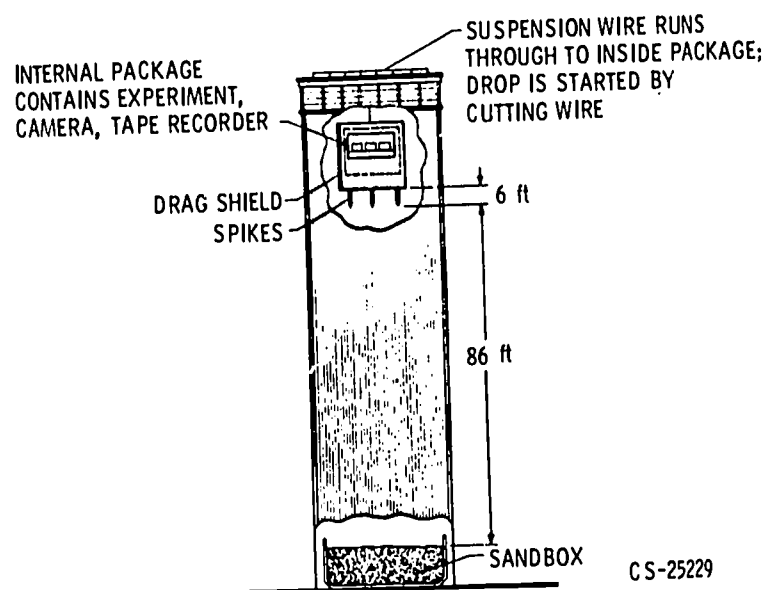
Figure 8-11. - Drop tower zero-gravity facility. Maximum payload, 500 pounds; 2.25 seconds of gravity less than 10^{-5}-g.

drag (fig. 8-11), while the newest zero-g facility (fig. 8-12) uses an evacuated chamber. In both facilities, the drag acceleration is less than 10^{-5}-g, so that if our experiments are reasonably sized, very low Bond numbers (or zero-g) can be obtained. Zero-g times range from about 2 to 10 seconds. To obtain the 10 seconds, the experiment is shot upwards by an accelerator or cannon-like piston. As soon as the experiment leaves the accelerator, it is moving freely under the influence of gravity only. Both the up and the down flight of the experiment will result in a zero-g condition. While 10 seconds does not seem to be a long time, and it is not, things happen relatively faster in small model tanks. Drop-tower results can be scaled up to larger sizes and longer times by using scaling-type parameters (numbers) like the Bond number.
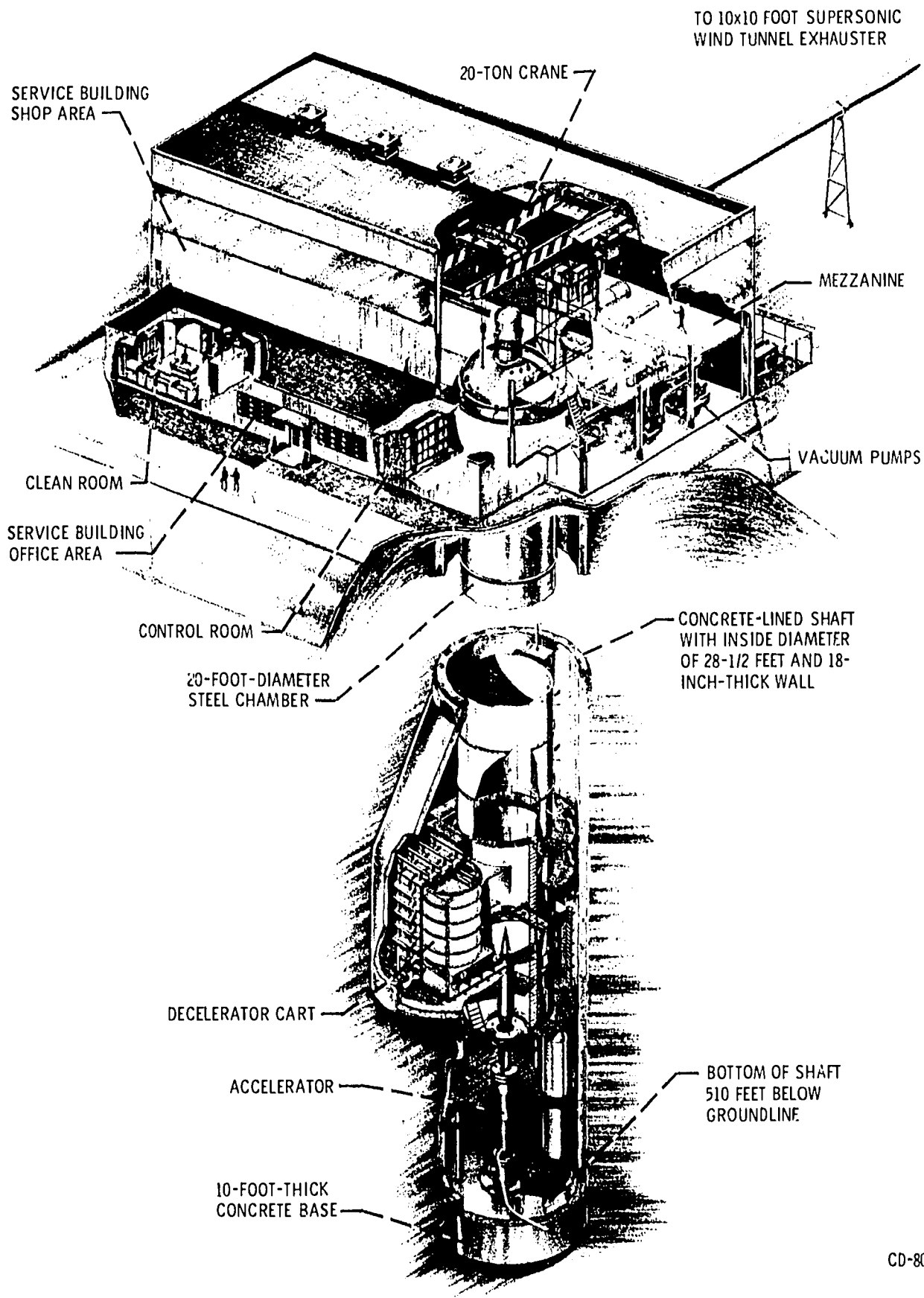
Figure 8-12. - Cutaway view of 10-second zero-gravity research facility.

Labels in figure:

TO 10x10 FOOT SUPERSONIC WIND TUNNEL EXHAUSTER

20-TON CRANE

SERVICE BUILDING SHOP AREA

MEZZANINE

VACUUM PUMPS

CLEAN ROOM

SERVICE BUILDING OFFICE AREA

CONTROL ROOM

20-FOOT-DIAMETER STEEL CHAMBER

CONCRETE-LINED SHAFT WITH INSIDE DIAMETER OF 28-1/2 FEET AND 18-INCH-THICK WALL

DECELERATOR CART

ACCELERATOR

BOTTOM OF SHAFT 510 FEET BELOW GROUNDLINE

10-FOOT-THICK CONCRETE BASE

CD-8069

In conclusion, we have examined the meanings of zero gravity, the importance of capillarity and surface energy, the powerful physical tools of energy and the principle of minimum energy, and the behavior of fluids in zero-g. The subject is fascinating, covering the full range from the implications of relativity to the practical areas of manned space flight in a world free of gravity.

REFERENCE

1. Gamow, George: Gravity. Doubleday & Co., Inc., 1962.

9. ROCKET TRAJECTORIES, DRAG, AND STABILITY

Roger W. Luidens*

TRAJECTORIES

The three phases of a typical model rocket flight are powered flight, coasting, and parachute descent. These phases, shown in figure 9-1, are analyzed in the following discussion. (Vertical flight has already been discussed in chapter 3. However, the current
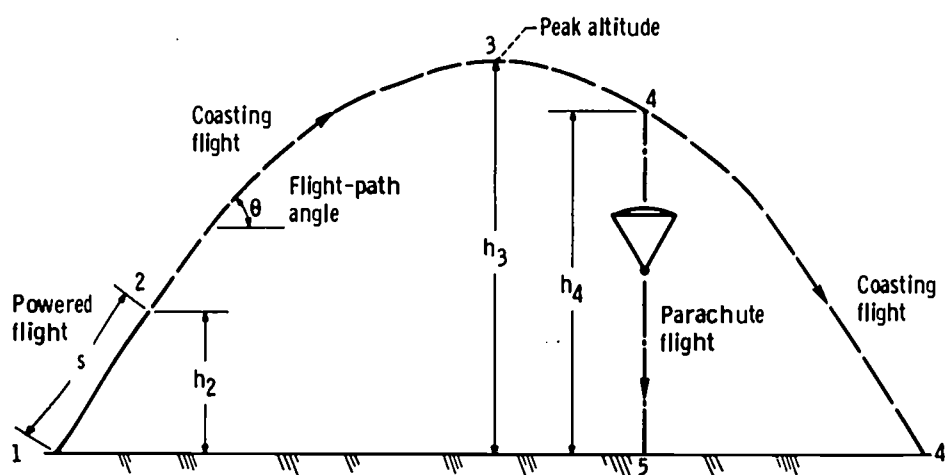
Figure 9-1. - Typical model rocket flight.

discussion concerns the more general, oblique trajectory.) The analysis depends primarily on the use of Newton's law, which states that the net force, or the unbalanced force, F applied to a body is equal to the mass m of the body multiplied by its acceleration A.

$$F = mA \tag{1}$$

where F is in pounds, m is in slugs ($m \equiv W/g$, where W is the weight of the object in lb, and g is the acceleration due to gravity in ft/sec^2), and A is in feet per second per second ($A \equiv \Delta V/\Delta t$, or time rate of change of velocity).

---

*Head, Flight Systems Section.

According to Newton's law, if there are no unbalanced forces, then there is no acceleration; and, conversely, if the acceleration is zero, then the forces are balanced. A zero acceleration means that the mass m is moving at a constant velocity which may or may not be zero.

Powered Flight

In order to simplify the analysis, it is assumed that the entire powered flight is accomplished with a single stage. However, the equations can be applied to multistage rockets, as will be explained at the end of this section. Also for the sake of simplicity, the effects of drag are not considered.

For those who are unfamiliar with trigonometry, some simple definitions will be useful here. The functions (sine, cosine, and tangent) are defined as ratios of sides of a right-angled triangle, as shown in figure 9-2.
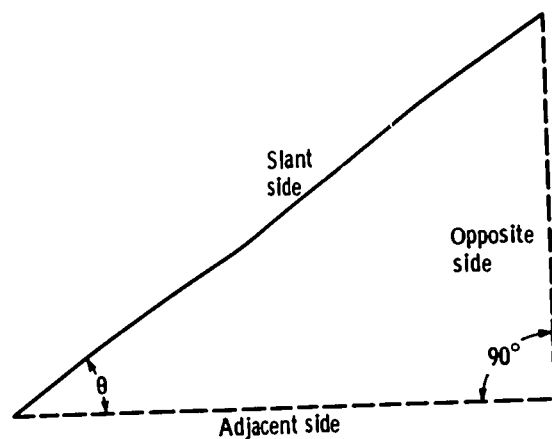
Figure 9-2. - Right-angled triangle as it applies to definitions of trigonometric functions.

Thus,

$$\sin \theta = \frac{\text{Side opposite } \theta}{\text{Slant side}}$$

$$\cos \theta = \frac{\text{Side adjacent to } \theta}{\text{Slant side}}$$

$$\tan \theta = \frac{\text{Side opposite } \theta}{\text{Side adjacent to } \theta}$$

These functions depend only on the angle θ, provided that the angle opposite the slant

144
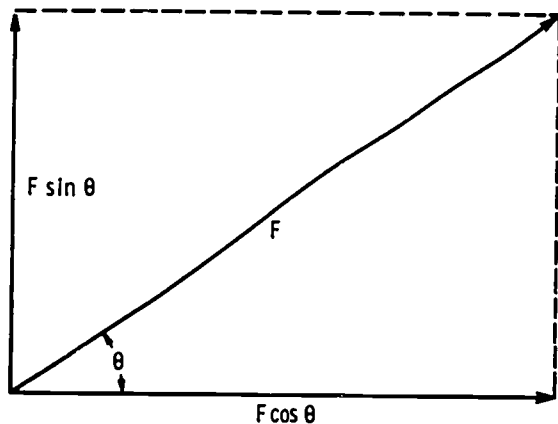
Figure 9-3. - Vector relations.
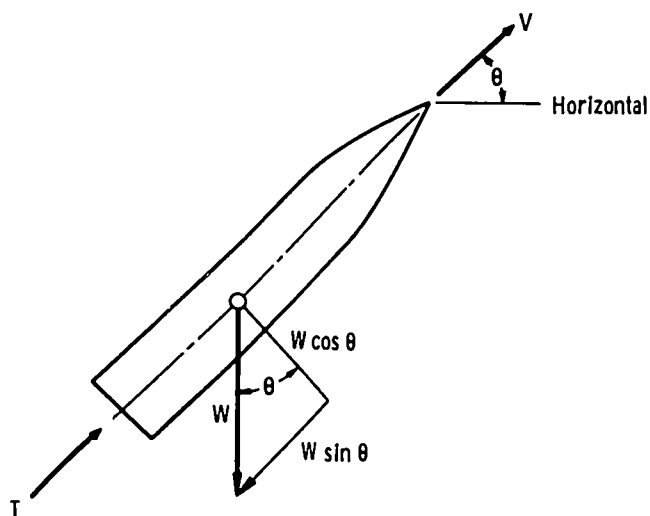
Figure 9-4. - Forces on a rocket during powered flight.

side (hypotenuse) is 90°.

Trigonometric functions are useful in vector considerations. (A vector is any quantity or characteristic that has both magnitude and direction, such as an applied force or the velocity of an object.) For example, a force F applied along the slant side at an angle θ is equivalent to, or can be replaced by, a force along the adjacent side $F \cos \theta$ and a force parallel and equal to the opposite side $F \sin \theta$. This relation is illustrated in figure 9-3. Usually, but not necessarily, the adjacent side is considered horizontal, and the opposite side is considered vertical; in all cases, however, the two components are perpendicular to each other.

As shown in figure 9-4, the net force F applied to the rocket in the line of flight is the rocket thrust T minus (because it is the direction opposite to the thrust) the component of the rocket weight in the line of flight, $W \sin \theta$. The flight-path angle θ is measured from the horizontal. So, in the line of flight

$$F = T - (W \sin \theta) \tag{2}$$

The mass m of the rocket is

$$m = \frac{W}{g} \tag{3}$$

By substitution of equations (2) and (3) into equation (1), the acceleration A of the rocket along the line of flight is found to be

$$A = \left(\frac{T}{W} - \sin \theta\right)g \tag{4}$$

The weight, and therefore the mass, of the rocket varies during the powered flight because of the "burning" and exhausting of the propellant. Thus, the acceleration varies. The acceleration at the beginning of the powered flight (point 1 of fig. 9-1) is

$$A_1 = \left(\frac{T_1}{W_1} - \sin \theta_1 \right) g \tag{5}$$

The acceleration at the end of the powered flight (point 2, fig. 9-1) is

$$A_2 = \left(\frac{T_2}{W_2} - \sin \theta_2 \right) g \tag{6}$$

where

$$W_2 = W_1 \text{ minus weight of propellant burned}$$

The average acceleration A_{av} is

$$A_{av} = \frac{A_1 + A_2}{2} \tag{7}$$

From the definition of acceleration, the change in velocity ΔV is

$$\Delta V \equiv V_2 - V_1 = A_{av}(t_2 - t_1) \tag{8}$$

where $t_2 - t_1 \equiv t_b$ is the rocket burning time, and V_1 for a one-stage rocket is zero. The average velocity V_{av} during powered flight is

$$V_{av} = \frac{V_1 + V_2}{2} = V_1 + \frac{\Delta V}{2} \tag{9}$$

The distance travelled Δs during powered flight is then

$$\Delta s = V_{av} t_b \tag{10}$$

and the altitude reached by the end of powered flight is

155

$$\Delta h = h_2 - h_1 = \Delta s \, \sin\left(\frac{\theta_1 + \theta_2}{2}\right) \tag{11}$$

The velocity increase due to rocket thrust (eq. (8)) can be written in other forms. If a rocket engine is test fired, the thrust can be plotted as a function of time, as shown in figure 9-5. This is known as the thrust-against-time history, or simply thrust-time
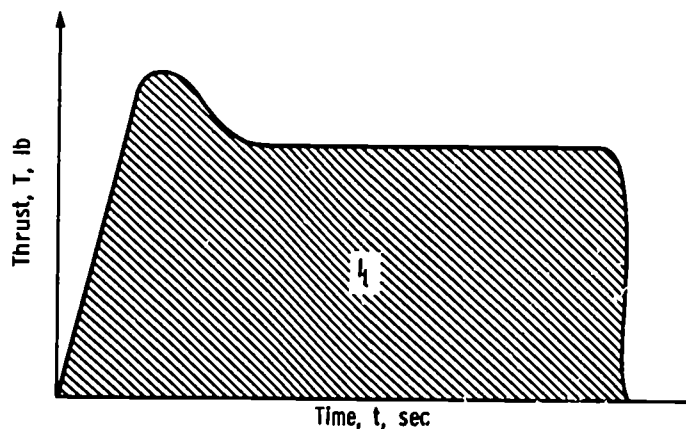
Figure 9-5. - Thrust-time history of rocket engine.

history (discussed in chapter 6). The area under the thrust-time curve represents the total impulse I_t of the rocket (discussed in chapters 2 and 15). The change of velocity can be stated in terms of I_t as follows:

$$\Delta V = V_2 - V_1 = \frac{I_t}{\dfrac{W_1 + W_2}{2}} - gt_b \, \sin\frac{\theta_1 + \theta_2}{2} \tag{12a}$$

If in figure 9-5 the thrust is constant during the burning time, then ΔV can be written in the commonly seen form

$$\Delta V = I_{sp} g \, \ln\frac{W_1}{W_2} - gt_b \, \sin\frac{\theta_1 + \theta_2}{2} \tag{12b}$$

where ln means "natural logarithm of" and I_{sp} is the specific impulse (discussed in chapters 2, 6, 11, and 15). The altitude may then be calculated as before, starting with equation (9).

The preceding equations and discussion have been based on the assumption that the powered flight was accomplished with only a single stage. However, these same equa-

tions also can be applied in the analysis of the powered flight of a multistage rocket.

Consider a rocket consisting of a first stage designated by the subscript a and a second stage designated by the subscript b. Apply equations (5) to (12) to the first stage. The resulting values at the end of the first stage of powered flight are V_{2_a}, from equation (8), and h_{2_a}, from equation (11). For efficient staging (i.e., to achieve maximum velocity after the two stages have burned), the second stage should ignite immediately after the burnout of the first stage. Thus, the conditions at the end of the first stage (conditions designated by subscript 2_a) become the conditions for the beginning of the second stage (conditions designated by the subscript 1_b); that is, $V_{1_b} = V_{2_a}$, and $h_{1_b} = h_{2_a}$. Now, equations (5) to (12) may be applied a second time. Coasting flight then begins at burnout of the second stage.

Coasting Flight

The coasting trajectory of a rocket (point 2 to point 4' in fig. 9-1) may be analyzed by considering separately the vertical and horizontal components of the velocity. For the sake of simplicity, the effects of drag are ignored in this analysis.

<u>Vertical component of velocity</u>. - This part of the flight is most easily understood by first considering the rocket at peak altitude (point 3 in fig. 9-1 and fig. 9-6). Here, the vertical velocity V_v is zero, the vertical distance, or altitude, is h_3, and the time is t_3. The only force acting on the rocket is that due to gravitation, and the acceleration of the rocket is thus the acceleration due to gravity.

$$A = g = 32.2 \ (ft/sec)/sec \tag{13}$$
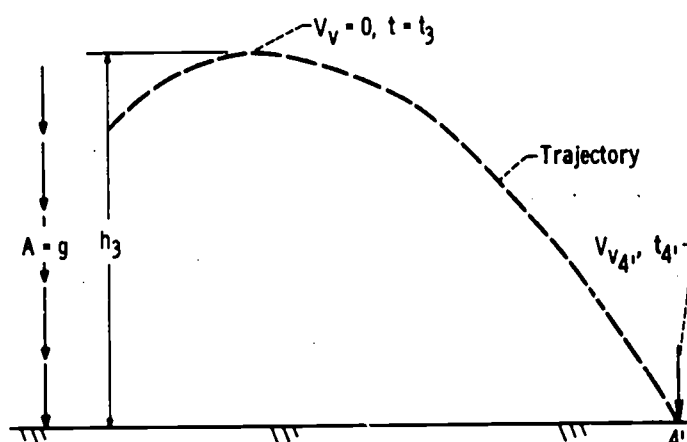
Figure 9-6. - Vertical components of acceleration, velocity, and altitude during coasting part of rocket trajectory.

The velocity of the rocket when it reaches the ground at the end of coasting (point 4' in fig. 9-6) is the acceleration g multiplied by the coasting time from peak altitude $t_{c'}$ (where $t_{c'} = t_{4'} - t_3$):

$$V_{v_{4'}} = gt_{c'} \qquad (14)$$

The distance traveled h_3 is

$$h_3 = V_{v_{av}} t_{c'} = \frac{V_{v_{4'}} + 0}{2} t_{c'} \qquad (15)$$

or, by use of equation (14) in equation (15)

$$h_3 = \frac{1}{2} gt_{c'}^2 \qquad (16)$$

A more useful equation for the vertical velocity at the end of coasting may be obtained by another combination of equations (14) and (15). If the altitude h_3 is known, then

$$V_{v_{4'}} = \sqrt{2gh_3} \qquad (17)$$

The ascending leg of the coasting trajectory is similar to the descending leg; that is, one leg is a mirror image of the other leg in a vertical plane through the peak altitude. The vertical velocity V_{v_2} at the end of powered flight (at burnout) can be determined by calculations which will be discussed in the section Relating the vertical and horizontal velocity components. Equation (17) can be rearranged to give the altitude increase above the burnout altitude. So, the peak altitude is

$$h_3 = h_2 + \frac{v_{v_2}^2}{2g} \qquad (18)$$

Horizontal component of velocity. - The horizontal component of velocity is shown in figure 9-7. Because there is no force acting in the horizontal direction during coasting flight (gravity acts only in the vertical direction), the horizontal component of velocity V_h remains constant even though the vertical component of velocity changes. Therefore,

$$V_{h_2} = V_{h_3} = V_{h_{4'}} = V_h \qquad (19)$$
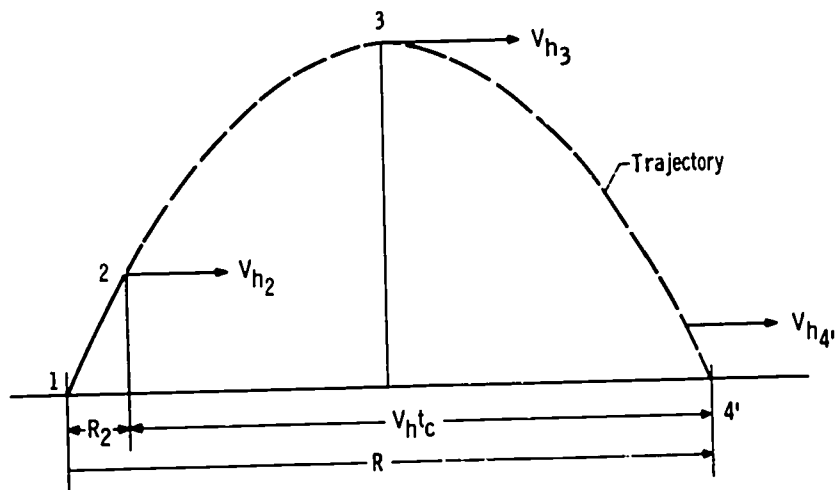
Figure 9-7. - Horizontal components of velocity and distance during coasting part of rocket trajectory.
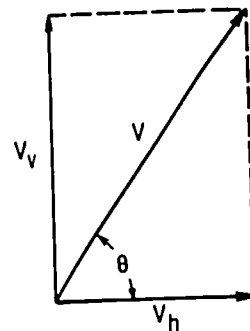
Figure 9-8. - Relation between vertical component, horizontal component, and total rocket velocities.

The horizontal distance, or range, during coasting is

$$R_c = V_h t_c \tag{20}$$

where t_c is the time in coasting flight from the end of burnout either to the point of parachute deployment ($t_c = t_4 - t_2$) or to the ground, if no parachute is used, ($t_c = t_{c'} = t_{4'} - t_2$). The total range from launch is $R = R_2 + R_c$.

Relating the vertical and horizontal velocity components. - In general, the vertical and horizontal components of velocity are related as shown in figure 9-8. In this figure, V is the velocity of the rocket along its flight path, and θ is the flight-path angle measured from the horizontal. The velocities shown in figure 9-8 are related as follows:

$$\tan \theta = \frac{V_v}{V_h} \tag{21}$$

and

$$V_v^2 + V_h^2 = V^2 \tag{22}$$

Sometimes it is convenient to write these relations in other forms. For example,

$$V_{v_2} = V_2 \sin \theta_2 \tag{23}$$

and

$$V_{h_2} = V_2 \cos \theta_2 \tag{24}$$

150

158

When these equations are applied at burnout (point 2 in fig. 9-1), as is indicated in equations (23) and (24), then equation (23) gives the value required in equation (18), and equation (24) gives the value required in equation (20).

The coasting flight path described by the preceding equations (zero drag assumed) is a parabola.

Parachute Flight

When a parachute is deployed (point 4 in fig. 9-1), the vehicle quickly reaches its terminal velocity, which is a condition of no acceleration (constant velocity). As is shown in figure 9-9, there are now only two forces acting on the vehicle, and they are in equi-
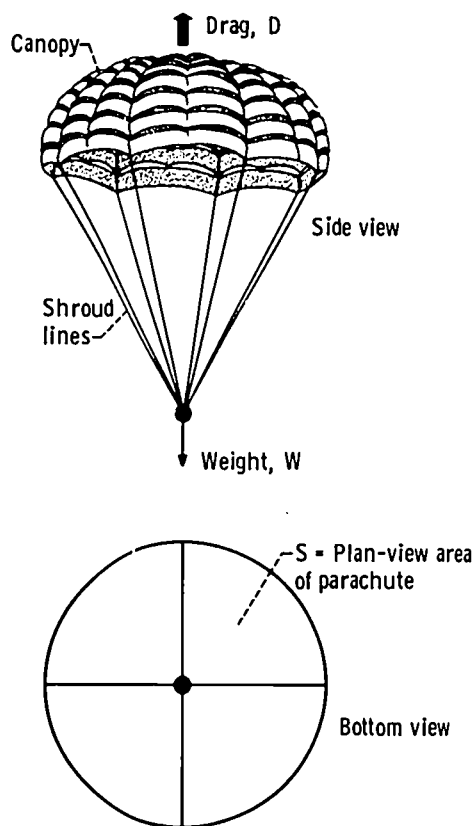
Figure 9-9. - Forces on a rocket during parachute descent.

librium (equal and opposite). These forces are the aerodynamic drag D_p of the parachute and the weight W of the vehicle. It should be recalled that Newton's law states that when the forces are in equilibrium, the acceleration is zero; this law does not state that the velocity is zero. Since the drag increases with velocity, there is just one velocity at which the drag equals the weight, and that is the terminal velocity. The aerodynamic drag of the parachute, in pounds, can be expressed as

151

$$D_p = C_{D_p} \frac{\rho V_p^2}{2} S_p \tag{25}$$

where C_{D_p} is the aerodynamic drag coefficient of the parachute approximate value of 1.3), ρ is the air density in slugs per cubic foot (mass in slugs is weight in pounds divided by acceleration due to gravity in feet per second per second), V_p is the terminal velocity in feet per second of the parachute along its flight path, and S_p is the reference area for the drag coefficient of the parachute (plan-view area of parachute in square feet). By equating the drag to the vehicle weight, equation (25) may be solved for the terminal velocity V_p, which is a vertical velocity:

$$V_p = \sqrt{\frac{2W}{S_p \rho C_{D_p}}} \tag{26}$$

The time for the parachute to reach the ground t_p is

$$t_p = t_5 - t_4 = \frac{h_4}{V_p} \tag{27}$$

General Equations of Motion

The previous equations have been generated for special parts of the flight path. Equations of motion which are completely general and applicable to all phases of the flight may be found as follows:

If the forces in the direction of flight in figure 9-10, including the drag that was previously omitted, are summed, the general vehicle acceleration can be determined to be

$$A = \left(\frac{T - C_D \frac{\rho V^2}{2} S}{W} - \sin \theta \right) g \tag{28}$$

where in equation (26) S is the reference area for the drag coefficient.

The change in velocity ΔV in an increment of time Δt is

$$\Delta V = A \, \Delta t \tag{29}$$
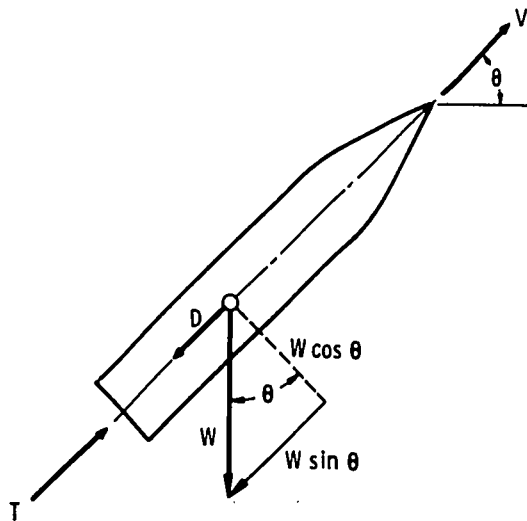
Figure 9-10. – Forces acting on a rocket.

and the velocity at the end of Δt is

$$V_{t+\Delta t} = V_t + \Delta V \tag{30}$$

The increment of distance traveled is

$$\Delta s = \left(V_t + \frac{1}{2}\Delta V\right)\Delta t \tag{31}$$

The rocket weight at the end of Δt is

$$W_{t+\Delta t} = W_t - \dot{W}\,\Delta t \tag{32}$$

where $\dot{W}$ is the weight flow rate of the propellant and

$$\dot{W} = \frac{T}{I_{sp}} \tag{33}$$

where I_{sp} is the rocket specific impulse. (Weight flow rate and specific impulse are discussed in chapter 2.)

From the summation of forces normal (perpendicular) to the flight path, the change in path angle $\Delta\theta$ is

$$\Delta\theta = \frac{g \cos \theta \, \Delta t}{V} \tag{34}$$

and the path angle at the end of Δt is

$$\theta_{t+\Delta t} = \theta_t + \Delta\theta \tag{35}$$

These equations may be integrated (i.e., used repeatedly) over successive steps in time to determine the rocket flight path. This is usually done by an electronic computer, but it may also be done by hand calculations. For near-vertical flight, $\sin\theta$ in equation (28) is 1.0, and equations (34) and (35) are not required.

Orbital Flight

The terminal velocity of the parachute was found by equating the vehicle weight to its drag. The two forces were in equilibrium. Orbital flight is an equilibrium between the centrifugal force and gravity, as shown in figure 9-11.

The centrifugal force F_c is given by the equation

$$F_c = \frac{mV^2}{r} \tag{36}$$
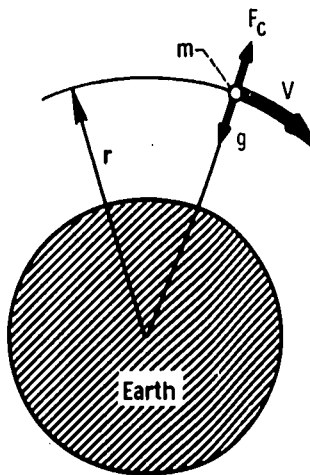
Figure 9-11. - Balance of forces in orbital flight.

162

where r is the radius of curvature of the orbital path and is only slightly larger than the radius of curvature of the Earth's surface. (In the equations of the preceding sections the curvature of the Earth's surface has been ignored because the effect of this curvature on the trajectory of a model rocket is negligible.). For orbital flight, the centrifugal force F_c must be equal to the pull of gravity mg, so that

$$\frac{mV^2}{r} = mg \qquad (37)$$

The velocity of a circular orbit about the Earth V_c is then found by rearranging equation (37)

$$V_c = \sqrt{gr} \qquad (38)$$

The gravity of the Earth is about 32.2 feet per second per second, and the radius is about 4000 miles. Therefore, the velocity for a low circular orbit is

$$V_c = \sqrt{32.2 \times 4000 \times 5280} \approx 26\ 000 \text{ ft/sec}$$

or 17 800 miles per hour. These numbers are only approximate. The circular velocity V_c is the velocity that must be provided by a rocket to achieve orbital flight.

To escape from the Earth's gravity, an additional 41 percent in velocity is required. With this velocity, the rocket will occupy essentially the same orbit about the Sun as does the Earth. To go to another planet, a still higher velocity is required. To go to the Moon, a slightly lower velocity is sufficient because the Moon is in orbit about the Earth.

Orbital flight may be viewed in another way to relate it to more familiar ideas of trajectories. Consider an imaginary cannon on top of an imaginary mountain that extends out of the Earth's atmosphere, as shown in figure 9-12. The cannon points horizontally. A small powder charge will send the cannon ball a short distance before it falls to the Earth's surface (trajectory 1). A larger charge of powder will send it a greater distance before it falls to the Earth's surface (trajectory 2). With a sufficiently large charge, the cannon ball will never fall to the Earth's surface, because the Earth's surface curves away at the same rate the cannon ball is "falling." The cannon ball is then in orbit (trajectory 3).
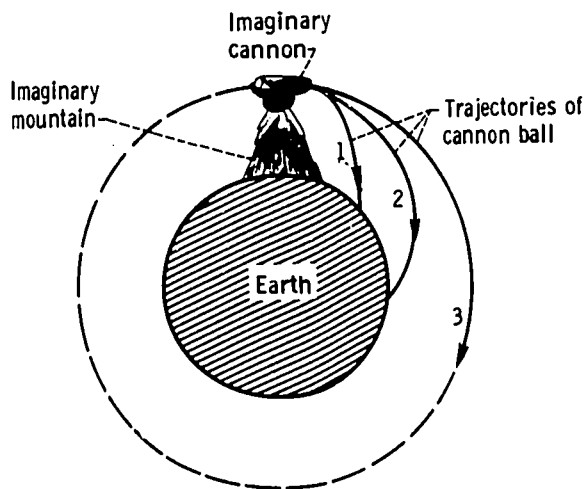
Figure 9-12. - Another view of orbital flight.

DRAG

The rocket drag affects the rocket flight path and maximum altitude. The rocket drag consists of friction drag and form drag (fig. 9-13). The friction drag is the molasseslike effect of the air on the vehicle as it passes through the air. This friction drag D_f may be estimated by the equation

$$D_f = C_f \frac{\rho V^2}{2} \times \text{Surface area of rocket} \tag{39}$$

where C_f is the friction-drag coefficient. For a typical model rocket, C_f is 0.0045 for turbulent skin friction (for rough body surface), and it is 0.0015 for laminar flow (for smooth body surface).

The form drag is the result of low pressures acting on the rear or base areas of the rocket because of poor streamlining which leads to flow separation and turbulent air. The form drag can be determined by measuring the base pressure in a wind tunnel.
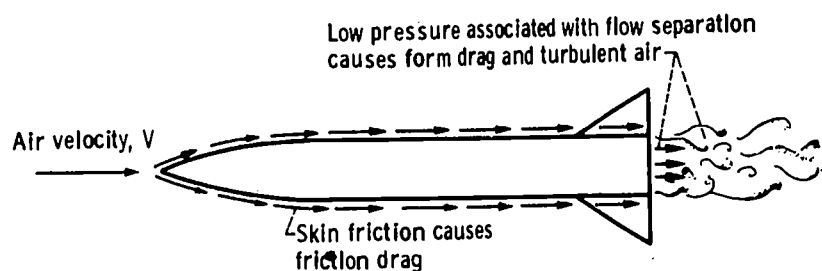
Figure 9-13. - Drag forces on a rocket.
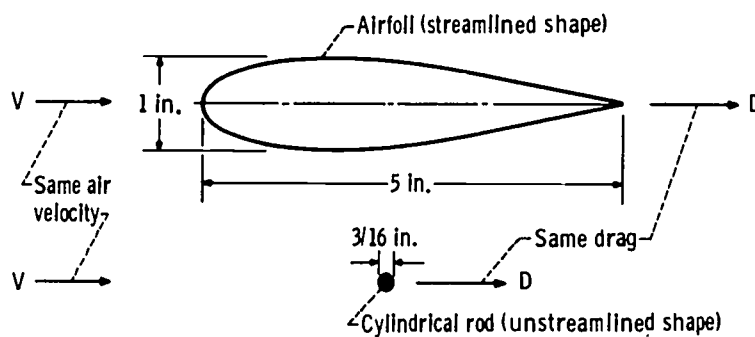
Figure 9-14. - Streamlining minimizes drag.

The importance of good streamlining is illustrated in figure 9-14. The two shapes shown in the figure have the same drag. Obviously, a cylinder with its axis normal to the flow direction is a high-drag shape.

STABILITY

Basic Concepts

Center of gravity. - The center of gravity, C. G., is the point on a body where all its mass (or weight) can be considered to be concentrated. A spinning or rotating body which is not under the influence of aerodynamic forces or mechanical constraints (e. g., a body thrown into the air so that it is spinning freely) will rotate about its center of gravity. Under static conditions, a body balances about its center of gravity.

The C. G. of a model rocket can be determined by finding its center of balance. The center of balance can be found by either of the methods shown in figure 9-15. In figure 9-15(a), the C. G. lies at the intersection of the longitudinal axis of the rocket and a vertical line through the pivot point at which balance is achieved. In figure 9-15(b), the C. G. lies at the intersection of the longitudinal axis of the rocket and the extension of the line of the string. (The rocket should be built to be symmetrical about its longitudinal axis in weight, thrust, and aerodynamics.)

Center of pressure. - The aerodynamic forces act on all the external surfaces of the rocket to yield lift, side force, and drag. The point on the body where all these forces can be considered to be acting (concentrated) is the center of pressure, C. P.

The most accurate way to determine the C. P. is in a wind tunnel or any airstream, as shown in figure 9-16. First, the rocket model is mounted on a pivot and is alined so that its longitudinal axis is parallel to the direction of the airstream and its nose is pointing upstream. In this position the model has zero angle of attack. (The angle of attack is formed by the longitudinal axis of the rocket and a line in the direction of the air-
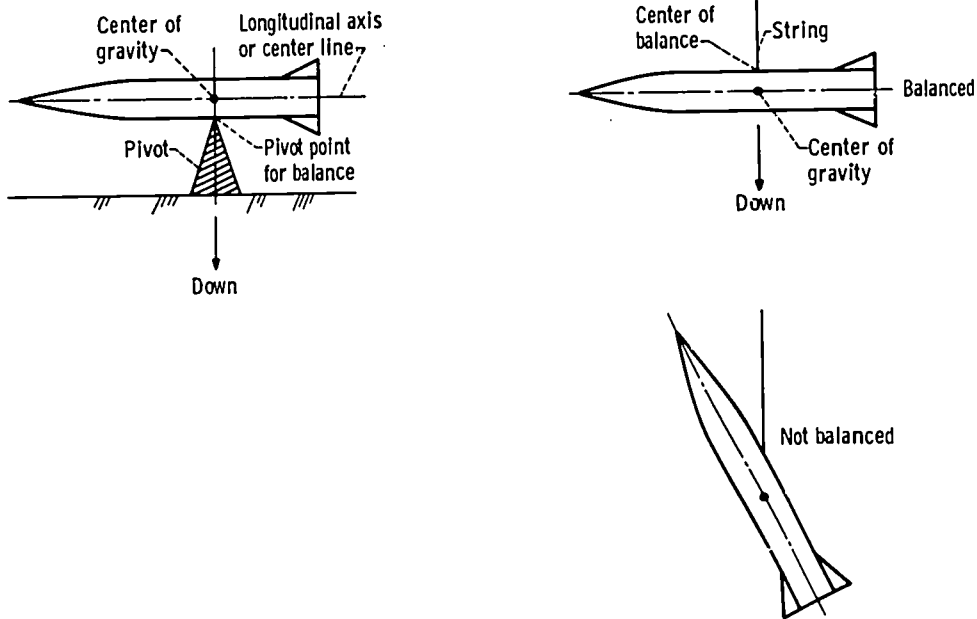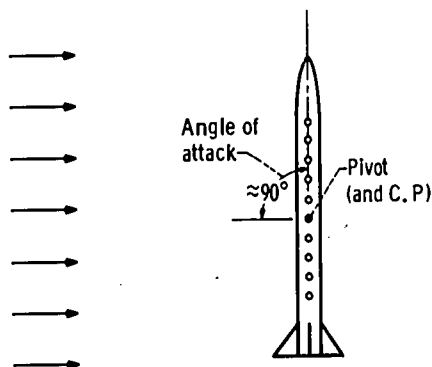
(a) By resting model on pivot.

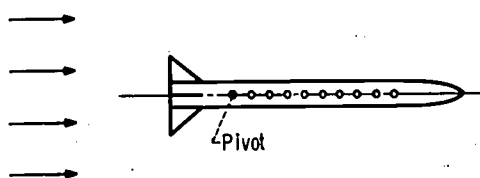(b) By suspending model on string.

Figure 9-15. - Methods of determining center of balance (and center of gravity) of model rocket.
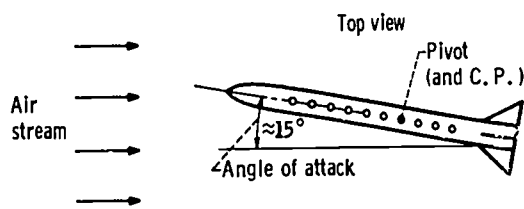
(a) Low-angle-of-attack center of pressure.

(b) High-angle-of-attack center of pressure.

(c) Pivot behind both high- and low-angle-of-attack
centers of pressure.

Figure 9-16. - Centers of pressure of model rocket.

stream.) Next, the tail of the rocket is displaced to one side so that the rocket has a small angle of attack of approximately 15° (fig. 9-16(a)). If the airstream causes the model to return to zero angle of attack, then the pivot point is ahead of the C. P. Several more rearward pivot locations are tried until one is found at which the model rocket no longer has the tendency to return to zero angle of attack. This pivot point, then, is the low-angle-of-attack C. P.

A similar procedure may be followed to obtain the high-angle-of-attack C. P. In this case the rocket model is displaced to a high angle of attack of almost 90° (fig. 9-16(b)). The pivot point at which the model maintains the high angle of attack to which it is displaced is the high-angle-of-attack C. P. The high-angle-of-attack C. P. is generally ahead of the low-angle-of-attack C. P.

If the pivot point were moved to the rear of the low-angle-of-attack C. P., then a displacement of the model from zero angle of attack to any other angle of attack would result in the rocket pointing downstream (fig. 9-16(c)).

A method of estimating the location of the C. P. of a model rocket without a wind-tunnel test is to locate its center of lateral area. The high-angle-of-attack C. P. is very close to the center of lateral area. The procedure for finding the center of lateral area is to cut from a piece of cardboard the side outline (or shadow) of the model rocket. The center of lateral area of this cardboard outline is also its center of gravity. The center of gravity can be determined by the method already described in the section Center of gravity.

Positive Static Stability

Positive static stability is a property of a rocket such that when the rocket is disturbed from zero angle of attack, it tends to return to zero angle of attack. Since the rocket rotates about its C. G. and the aerodynamic restoring forces act at the C. P., the relative positions of these two points determine the stability of the rocket. If the C. P. is behind the C. G., the rocket has positive static stability. If the C. P. and C. G. are at the same point, the rocket has neutral stability. If the C. P. is ahead of the C. G., the rocket has negative stability (i. e., the rocket is unstable).

For a stable rocket, the relative locations of the C. G., the center of lateral area, the high-angle-of-attack C. P., and the low-angle-of-attack C. P. are shown in figure 9-17. Positive stability is essential for a predictable flight path. An unstable rocket can be a hazard to the persons launching or observing the rocket because its flight path cannot be predicted and it will not fly in the direction in which it is aimed. To ensure positive stability for all angles of attack, a model rocket should be designed so that the C. G. is located ahead of the high-angle-of-attack C. P. by a distance of 1 caliber (di-
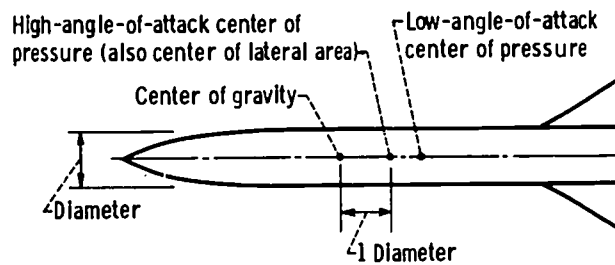
159

High-angle-of-attack center of
pressure (also center of lateral area)

Low-angle-of-attack
center of pressure

Center of gravity

Diameter

1 Diameter

Figure 9-17. – Designing a rocket for positive static stability.

ameter of rocket), as shown in figure 9-17. The locations of the C.G. and the C.P.
can be controlled by varying the size of the tail fins and/or the weight distribution of the
model. Using the center of lateral area as the C.P. and locating the C.G. a distance
of 1 diameter ahead of the C.P. generally results in a conservative and stable design.

10. SPACE MISSIONS

Richard J. Weber*

FLIGHT PATHS

To serve as a foundation for the understanding of space missions, it is helpful first to consider the characteristic flight paths of spacecraft. It has already been explained in chapter 9 that if an object is given a sufficiently high horizontal velocity, it will not fall back to Earth. Instead it will continue to "fall" around the Earth in a circular path (provided that the altitude is high enough so that atmospheric drag does not cause it to lose energy and descend). When the object is thus in a circular orbit (path A in fig. 10-1), its
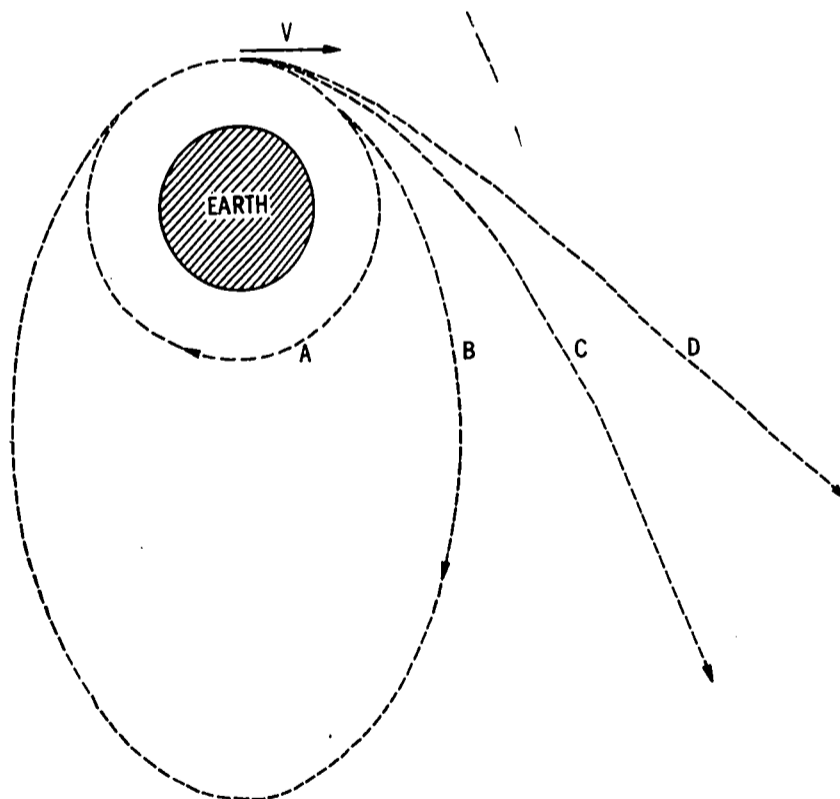
Figure 10-1. - Changes in flight path caused by changes in initial velocity.

---

*Chief, Mission Analysis Branch.

velocity is such that the centrifugal force just equals the gravitational attraction:

$$\frac{V_c^2}{R} = g_0 \frac{R_0^2}{R^2}$$

$$V_c = \sqrt{\frac{g_0 R_0^2}{R}} \approx \sqrt{32.2 \times 4000 \times 5280} \approx 26\ 000\ \text{ft/sec}$$

where V_c is the circular-orbit velocity, R is the radius of the orbit, R_0 is the radius of the Earth, and g_0 is the acceleration due to gravity at the Earth's surface.

If the initial velocity of the object is greater than V_c, the orbital path is an ellipse (path B in fig. 10-1). With further increases in initial velocity, the apogee of this elliptic orbit is moved farther away from the Earth. In the limit, the distance of the apogee from the Earth is infinity, the ellipse changes into a parabola (path C in fig. 10-1), and the object travels so far away from the Earth that it "escapes" from the Earth's gravitational attraction and does not return. The initial velocity required for the object to just barely escape in this fashion can be determined by using calculus. The approximate value of this escape velocity V_{esc} is

$$V_{esc} = \sqrt{2}\ V_c \approx 36\ 000\ \text{ft/sec}$$

An object with this initial velocity will coast away from Earth at gradually decreasing speed until it finally reaches a very great distance from Earth at zero speed. The zero speed is relative to the Earth; since the Earth itself is moving around the Sun, the object will also be moving around the Sun in a circular orbit, just like a planet.

If the initial velocity of the object is greater than the escape velocity, then the trajectory of the object relative to Earth is a hyperbola (path D in fig. 10-1). After the object has coasted a great distance away from Earth, it still has some excess velocity. Hence, instead of going into a circular orbit around the Sun, the object enters an elliptic orbit, as shown in figure 10-2. With each additional increase in initial velocity, the apogee of this elliptic orbit is displaced farther from the Sun, and the orbit may intersect the orbits of other planets (fig. 10-3). An interplanetary transfer mission can be accomplished by aiming the trajectory and timing the launch so that the object and the other planet arrive simultaneously at the point of intersection of their orbits.

Note that all the space trajectories discussed herein are simple conic sections (circles, ellipses, parabolas, hyperbolas) and that the flights consist primarily of coast paths only. Rockets are needed only to give the necessary velocity at the beginning of
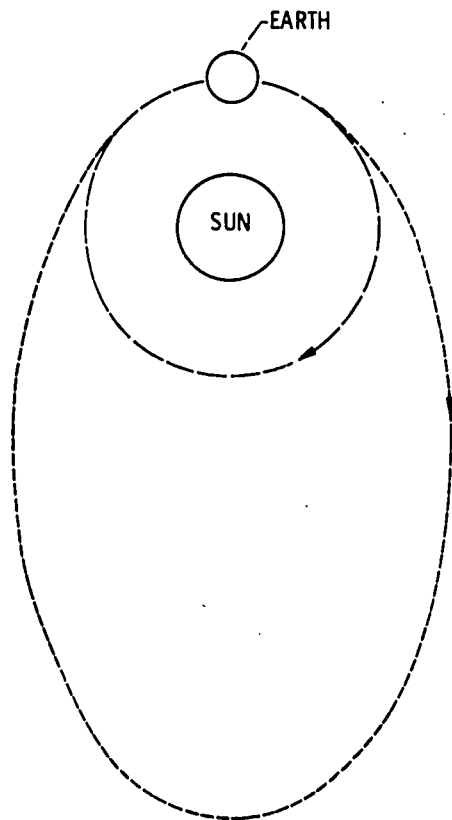
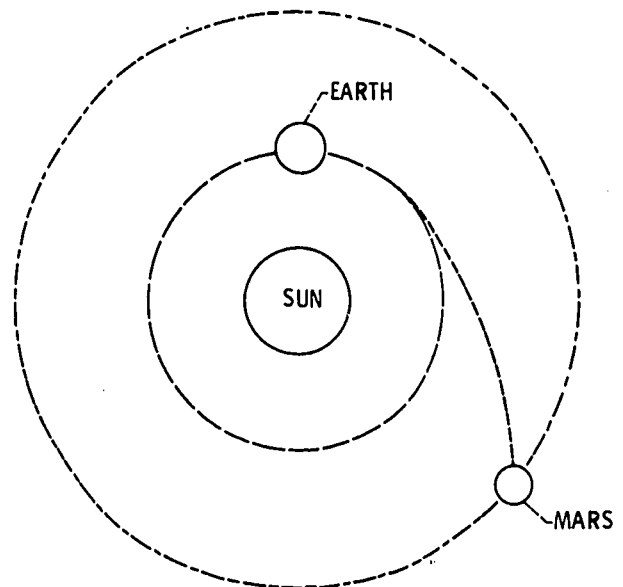Figure 10-2. - Excess energy yields elliptic orbit about the Sun.

Figure 10-3. - Proper elliptic path intercepts planet.

the flight (or at the end if we wish to slow down). (An exception to this simple condition is discussed in chapter 20, which concerns the use of electric propulsion.)

For real missions, of course, the analyses of trajectories are complicated by such factors as the orbits and orbital planes of other planets, the timing of the launch, the direction of the launch, the duration of the mission, etc. However, the basic concepts used in these analyses are the simple ones which have been described herein.

MISSION OBJECTIVES

A space mission essentially consists of a spacecraft traveling along a trajectory and carrying equipment to accomplish a particular job. A mission normally has one "direct" objective, and it may also have one or more "indirect" objectives. Some of the most common mission objectives are presented in the following list:

(1) Direct

(a) Application (weather study, communication, navigation)

(b) Science (measurement of environmental conditions)

(c) Engineering (development and testing of equipment)

(d) Exploration

(2) Indirect

    (a) Prestige

    (b) Military value

    (c) Technological advancement

    (d) Stimulation of national economy

    (e) Alternative to war

The mission objective determines the destination of the spacecraft and the mission profile (the general way the mission is to be carried out). Destination and profile constitute the mission type. The following are the various mission types:

(1) Destination

    (a) Near-Earth

    (b) Lunar

    (c) Planetary

    (d) Other (solar, extra-ecliptic, asteroidal, solar escape)

(2) Profile

    (a) Unmanned; manned

    (b) One-way; round trip

    (c) Flyby; gravitational capture (orbit); landing

    (d) Direct departure from Earth's surface; departure from Earth's surface by way of Earth parking orbit

SOUNDING ROCKETS

Sounding rockets are of particular interest because model rockets are more similar to them than to other full-size rockets. "Sounding" is the measurement of atmospheric conditions at various altitudes. A sounding rocket is relatively small. It is fired vertically, and without sufficient energy to place it into orbit or to cause it to escape Earth's gravitational attraction. For the purpose of obtaining atmospheric data, a sounding rocket has the following advantages over other devices:

(1) A rocket can obtain data at altitudes higher than that of a balloon (30 km) but lower than that of a satellite (200 km). Many important phenomena occur in this altitude region. Most of the radiation approaching Earth (X-rays, ultraviolet rays, energetic particles) is absorbed here, airglow and aurorae occur, meteoroids burn up, transition occurs between nonionized and ionized regions, etc.

(2) Even at high altitudes, a rocket is superior to a satellite for determining vertical variations and for reaching a preselected point at a particular instant.

(3) In general, a rocket is more flexible than a satellite in terms of operation and payload. Also, the rocket has a much lower initial cost.

The major disadvantage of a sounding rocket is its very limited lifetime; it is there-fore expensive in terms of cost per unit of information obtained. Nevertheless, sounding rockets have been used extensively in the past and will, no doubt, continue to be used in the future.

MISSION PAYLOADS

Once the mission objective is specified, the payload (equipment, power supply, etc.) necessary to accomplish the mission must be selected. In many cases the payload must be made smaller than is really desired, just because the available rocket launcher is limited in its capability. The following are two examples of typical mission payloads.

Mariner IV

The Mariner IV spacecraft (fig. 10-4) was designed to make scientific measurements about the planet Mars. It was launched by an Atlas-Agena booster on November 28, 1964 and passed Mars on a flyby trajectory on July 14, 1965. During this time it traveled 325 million miles on an elliptical path that missed Mars by only 6118 miles. Figure 10-5 shows one of the pictures of Mars it took. The true payload of the spaceccraft consisted of the scientific instruments listed in table 10-I. The combined weight of these instruments was only 35 pounds. But other items which had to be added to this payload included
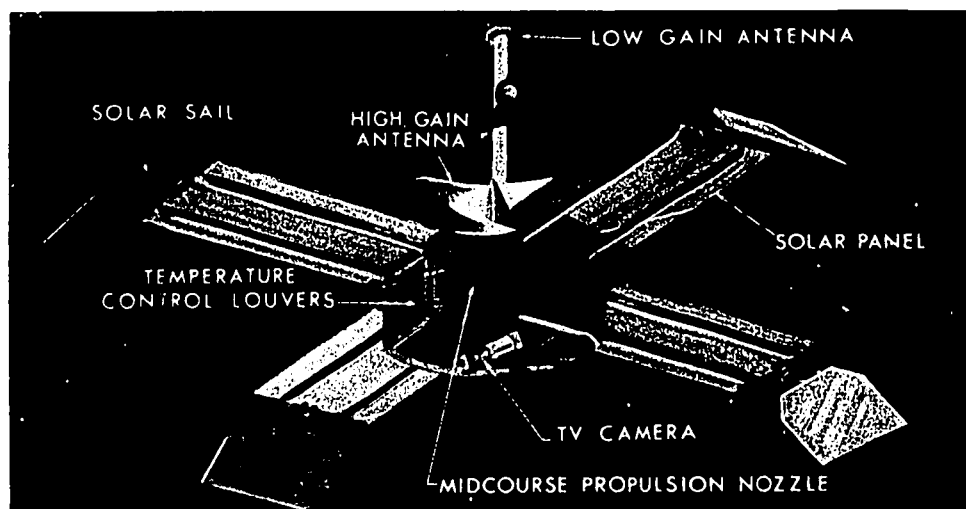
Figure 10-4. - Mariner IV spacecraft. Mission, Mars flyby; weight, about 570 pounds; launch vehicle, Atlas Agena.

Figure 10-5. — Photograph of planet Mars taken by Mariner IV spacecraft.

TABLE 10-I. - MARINER IV SCIENTIFIC

INSTRUMENTS

Description	Weight, lb	Power requirement, W
Cosmic-ray telescope	2.58	0.60
Cosmic-dust detector	2.10	.20
Trapped-radiation detector	2.20	.35
Ionization chamber	2.71	.46
Plasma probe	6.41	2.90
Helium magnetometer	7.50	7.30
Television	11.28	8.00

a radio to receive commands from Earth and to send back data, solar panels to provide electrical power for the instruments and radio, louvers for thermal control, propulsion for attitude control and midcourse guidance, structure to hold all the pieces together, etc. The weight of all this additional equipment was 535 pounds. Thus, although the true payload was only 35 pounds, the actual total payload which had to be launched into space was 570 pounds. This Mariner payload is typical of current unmanned, scientific flyby probes.

Manned Mars Vehicle

As an example of a very different type of vehicle payload, let us examine what might be required for a manned Mars landing mission. The true payload in this case will be the crew of perhaps seven men plus whatever samples of Mars they try to bring back. The weight of the men and the samples would only be about 2000 pounds. But as far as the spaceship is concerned, this basic payload must be increased by all the equipment and supplies necessary to keep the crew alive during their journey. As shown in figure 10-6, it is convenient to divide this total payload into two parts. One part will be carried all the way to Mars and back again to Earth, whereas the other part is no longer needed after Mars is reached and so can be discarded there in order to lighten the spaceship.
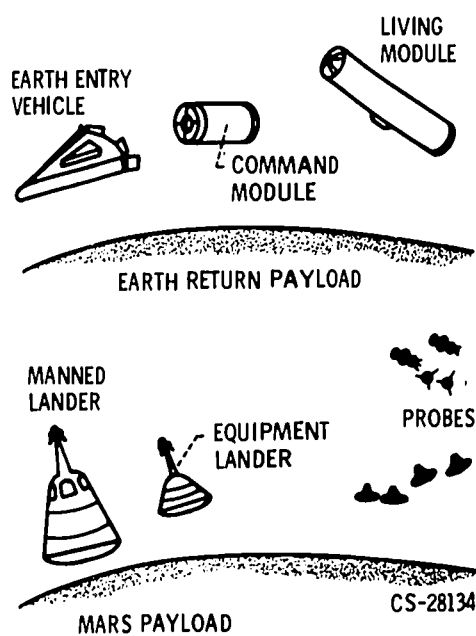
166

174

Figure 10-6. - Payloads for interplanetary vehicle.

In the particular study quoted here, the round-trip payload consists of a command module, a living module, and a lifting reentry vehicle to return the crew to the surface of the Earth; the total weight of this payload is estimated to be 80 000 pounds. Additional equipment to be expended at Mars includes Apollo-type landing capsules and assorted orbital probes; the weight of this additional equipment is also approximately 80 000 pounds.

ANALYSIS OF TYPICAL MISSION

Even a brief analysis of a manned interplanetary mission reveals the great complexity of such a mission and the vast amount of planning required. As a typical example, let us consider a mission with the specific objective of landing men on the surface of Mars for 40 days of exploration and then returning them to Earth. Theoretically, there are many ways of accomplishing this mission. The following is a breakdown of one reasonable method:

(1) Various components of the interplanetary spacecraft are launched individually by Saturn V boosters into a parking orbit around the Earth. Then, from these components, the spacecraft is assembled in orbit.

(2) The assembled spacecraft is injected into an elliptic trajectory toward Mars. Nuclear rocket engines and hydrogen fuel are used for this phase of the mission.

(3) After the spacecraft has coasted for 260 days, it is decelerated by nuclear rockets into a parking orbit around Mars.

167

(4) From this parking orbit, some of the crew members descend to the surface of the planet by means of Apollo-type landing capsules.

(5) After the men have completed their 40 days of exploration, they return to the orbiting spacecraft by means of the landing capsules. Chemical rocket propulsion is used for this part of the mission.

(6) Nuclear rockets are used again to inject the spacecraft into an elliptic path toward Earth.

(7) After the spacecraft has coasted for 200 days, the crew transfers to an atmospheric entry vehicle. Chemical rockets are used to slow down this vehicle to a velocity of 50 000 feet per second. As the vehicle enters the Earth's atmosphere, it is slowed further by air drag. Finally, the vehicle glides to a landing on Earth. The trip has lasted a total of 500 days.

The preceding example is just one, arbitrarily chosen method out of many, theoretically possible ways of accomplishing the Mars mission. Many alternative methods will have to be analyzed thoroughly before the best one can be selected for the actual mission.

Many of the factors that must be studied and analyzed are related to the trajectory of the spacecraft. For instance, the flight duration is very important. Fast trips require more fuel, while slow trips require more life-support supplies and equipment. Also, slow trips are more harmful to the crew because the men are exposed to more cosmic rays and solar flares, their muscles deteriorate from zero gravity, they become homesick, etc. If the flight path approaches too close to the Sun, the effect of solar-flare radiation is intensified. If the velocity in returning to Earth is too high, the entry vehicle may burn up like a meteor.

In picking the propulsion system there are also many alternatives. Chemical rockets are very light but use up much fuel. Nuclear rockets are much more efficient but are heavier and produce dangerous radiation. Hydrogen fuel is light but boils away unless the temperature is less than -423° F.

With so many alternatives (of which these have been but a few examples), it is not surprising that there is great controversy about the best way to carry out the mission. Many engineers and scientists are now studying the problem so that a logical choice may be made in the future. One possible design for the spaceship is shown in figure 10-7. The weight of this ship in Earth orbit would be about 2 million pounds. A booster rocket large enough to launch this spaceship directly from the ground would weigh about 40 million pounds (more than six times the weight of the Saturn V rocket). Special maneuvers and/or design techniques which may make it possible to reduce these weights include (1) using fuel for radiation shielding of the crew, (2) atmospheric braking at Mars, (3) midcourse thrusting, (4) Venus swingby, and (5) dividing the payload into manned and unmanned parts that are transported by separate vehicles traveling on dissimilar trajectories.
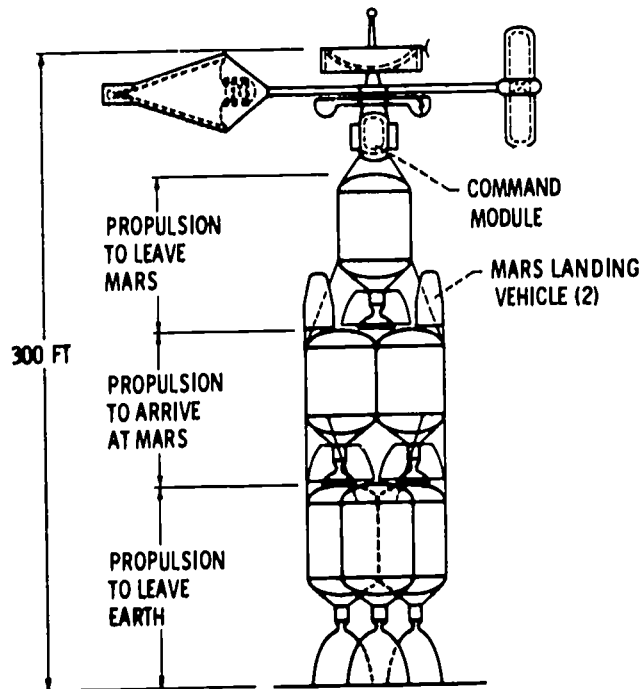
168

Figure 10-7. - Assembled Mars space vehicle in Earth orbit. Earth return mission payloads shown deployed for space flight.

Obviously, the planning and execution of a space mission, particularly a manned mission, require the work of experts from almost every branch of engineering. Some examples of these branches are trajectory analysis, life support systems, radiation shielding, structural design, heat transfer, aerodynamics and fluid flow, instruments and radio, and propulsion systems.

.177

11. LAUNCH VEHICLES

Arthur V. Zimmerman*

INTRODUCTION

Investigation or exploration of space involves placing an instrument package or astronauts and their life support and return capsule into space. Placing these payloads into space is the job of the launch vehicle. Although this chapter discusses only the problems and characteristics of launch vehicles for placing a payload into an orbit about the Earth (fig. 11-1(a)), there are two other general classes of launch vehicle missions: sounding probes, and missions beyond the Earth to other bodies or regions of the Solar System. Sounding probes (fig. 11-1(b)) are generally lofted by relatively small launch vehicles (usually multistage solid rockets) to a high altitude above the Earth. Here, the space data are obtained quickly and the probe falls directly back to Earth. The other class of

```
------ Coasting flight
_____ Powered flight
```


(a) Earth orbit.   (b) Sounding probes.   (c) Beyond Earth.

CS-39352
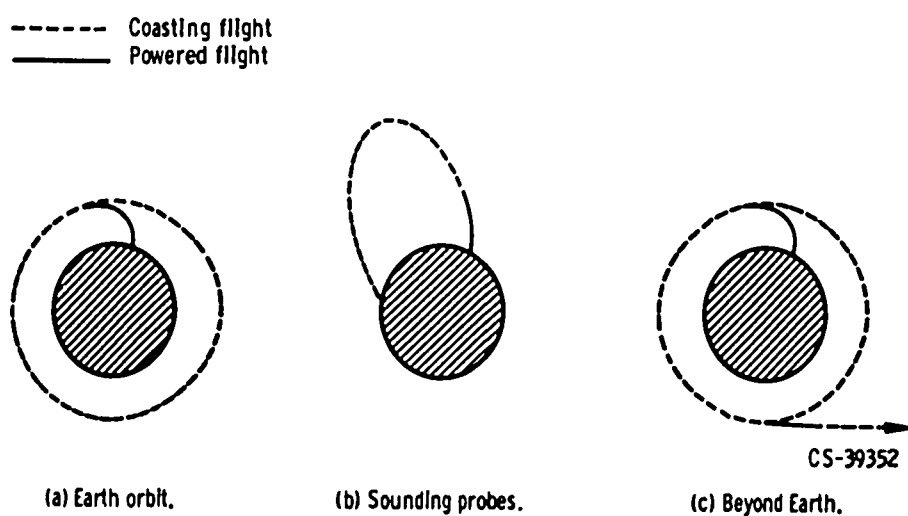
Figure 11-1. - Launch vehicle missions.

*Chief, Launch Vehicle Analysis Branch.

missions, that is missions beyond the Earth (fig. 11-1(c)), is really an extension of Earth orbit missions. The first step in going beyond the Earth is usually to place the payload and one or more propulsion stages into an Earth orbit. Then, this assembly coasts in Earth orbit until the proper position in space is achieved and the remaining stage or stages of the launch vehicle are fired. This firing accelerates the payload to the proper velocity and direction for ultimately reaching the target body.

Later, we will describe the NASA family of launch vehicles and give facts about the main vehicles. However, an appreciation of specific features of these launch vehicles requires an understanding of their general characteristics and some of the factors that determine their performance.

TYPICAL TWO-STAGE LAUNCH VEHICLE

Most launch vehicles designed to establish an orbit around the Earth have more than one stage, usually two. The main reason for this is that an immense fuel weight is required to launch a payload into orbit, and the fuel containers or tanks are a large part of the hardware weight of a launch vehicle. Late in the flight, most of these tanks are empty and represent dead weight that has to be carried along. To be efficient, as the vehicle flies into orbit, it throws away or jettisons stages consisting of empty tanks and other no longer useful weight. A mathematical explanation of this will be presented later.

A sketch of a two-stage launch vehicle is shown in figure 11-2. Note that each stage is basically a complete vehicle in itself. Each stage has an engine system, fuel tank, and oxidant tank, all united by a structure. An interstage adapter is used to connect the second stage to the first. When the propellants of the first stage are consumed, the second stage is released from the forward end of the interstage adapter, and the second stage engine is started. The second stage and payload continue to accelerate to orbit, while the empty first stage falls back to Earth. The instrument compartment contains all of the electronic systems of the launch vehicle. This includes such things as the guidance and control systems, tracking and telemetry systems, electrical systems, batteries, etc. In figure 11-2, all these systems are neatly packaged into an instrument compartment. In practice, some or all of these systems are often scattered throughout the vehicle, alongside the tanks, on top of the tanks, between tanks, etc.

The payload is attached to the launch vehicle through a structure called a payload adapter. Upon reaching orbit, the payload is usually released from the payload adapter and separated from the launch vehicle. Since the payload usually consists of relatively delicate instruments and equipment, it must be protected from aerodynamic heating and
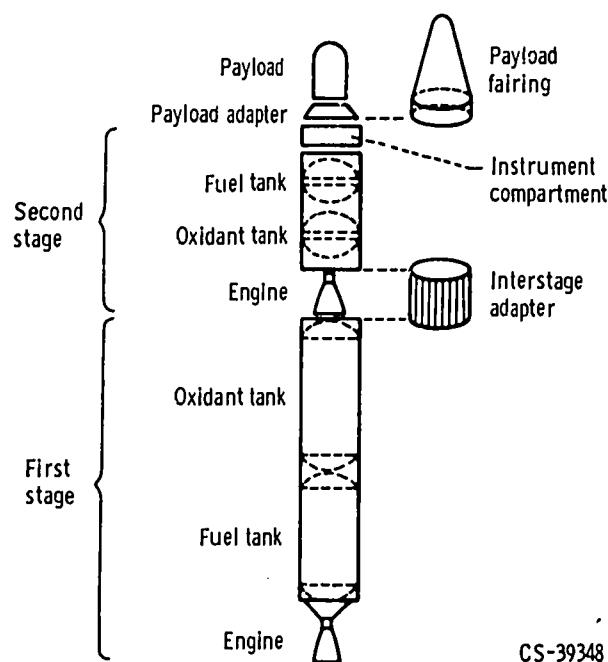
179

Figure 11-2. – Typical two-stage launch vehicle.

loads during the high velocity flight through the atmosphere. This is done by covering the payload with a large conical payload fairing. The payload fairing usually encloses the entire payload and is attached to the forward end of the second stage or instrument compartment. After the vehicle passes through the Earth's atmosphere on its way to orbit, the payload fairing is no longer required, and often, then, it is jettisoned by splitting it in two halves and allowing it to fall away while the vehicle continues to accelerate to orbit.

Launch Vehicle Systems

Many of the systems in a two-stage launch vehicle are the subjects of other chapters in this book, and so they will only be discussed briefly here.

The weights of the major systems of the second stage of a typical launch vehicle are listed in table 11-I. This stage uses liquid propellants. Notice that the total empty or jettison weight for the stage shown is 4100 pounds. Since the stage has a propellant capacity of 30 000 pounds, the ratio of hardware weight to propellant weight is 0.1366. For high performance, stages must have as low a hardware weight as possible. Typical stage hardware weights range from 10 to 20 percent of the stage propellant weight.

Structure and tankage. - For many stages the propellant tanks also serve as part of the stage structure, and their respective weights cannot be readily separated. The stage structure and tanks are commonly fabricated from thin aluminum or stainless steel

TABLE 11-I. - SYSTEM WEIGHTS

FOR A TYPICAL LIQUID PRO-

PELLANT SECOND STAGE

$$\left[\frac{\text{Hardware weight}}{\text{Propellant weight}} = \frac{4100}{30\ 000} = 0.1366. \right]$$

System	Weight, lb
Structure and tankage	1 000
Propulsion and plumbing	1 250
Guidance	350
Control	150
Pressurization	200
Electrical	250
Flight instrumentation	250
Payload adapter	150
Residuals	500
Total hardware	4 100
Usable propellant	30 000
Total stage	34 100

sheets. The sheets are formed and welded into cylindrical sections. The cylindrical sections of the vehicle are often strengthened by using a series of circumferential rings and longitudinal stringers.

Propulsion and plumbing. - Both liquid propellant and solid propellant rocket systems have been discussed in previous chapters, and most of the discussion here assumes the use of liquid propellant rockets. The most common liquid fuels used currently in NASA vehicles are RP-1 (essentially kerosene), liquid hydrogen (LH_2), and unsymmetrical dimethyl hydrazine (UDMH, a derivative of hydrazine N_2H_4). The most common oxidizers are liquid oxygen (LOX), used with RP-1 and hydrogen, and nitrogen tetroxide (N_2O_4) and inhibited red fuming nitric acid (IRFNA), both used with UDMH.

Guidance. - The purpose of the guidance system is to keep track of the vehicle position and velocity throughout the flight and to command the maneuvers required to reach the desired target or burnout conditions. In radio guidance, most of the tracking and computations are done on the ground, and the maneuvers are commanded through a radio link with the moving vehicle. In a full inertial system, all the position and velocity determinations and computations are done on board the vehicle itself. The guidance system consists of accelerometers to determine vehicle acceleration, gyroscopes to determine

the vehicle orientation in space, and an on-board computer to perform the necessary calculations. Guidance and control systems will be the subject of chapter 12.

Control. - The control system is the on-board equipment that actually maneuvers and stabilizes the vehicle in response to the commands given by the guidance system. In many cases the attitude of the vehicle is controlled during main engine firing by gimbaling the engine. During coasting, when the main engine is not firing, the control system consists of a series of small, low thrust rockets which are turned on and off to maintain and stabilize the vehicle attitude.

Pressurization. - The pressurization system provides pressurizing gas to the propellant tanks. This is required to force the propellants to the engine pumps or combustion chamber. Helium, a common pressurizing gas, is stored under high pressure in small, separate tanks on board the vehicle. During flight, a series of valves, regulators, and pipes are used to properly meter the gas to the propellant tanks.

Flight instrumentation. - The flight instrumentation system consists of on-board vehicle and engine instrumentation, radio-telemetry systems, range safety systems, and tracking systems. These on-board systems transmit vehicle data back to ground stations for range safety, tracking, and systems performance evaluation purposes.

Electrical. - The electrical system provides electrical power to the on-board guidance, control, and flight instrumentation systems. It consists of batteries, power conditioning equipment, wiring harnesses, etc.

Residuals. - The residuals consist of trapped liquid propellants and gases remaining in the tanks and feed lines after the main propellants have been consumed.

Payload adapter. - The payload adapter is the structure that unites the payload and the launch vehicle. Its weight and configuration depend, of course, on the size and shape of the payload.

Launch Sites

Extensive ground facilities are required to prepare and launch a multistage vehicle to orbit. The Eastern Test Range (ETR) is used for launches that are predominantly eastward, and the launch sites are located at Cape Kennedy, Florida. The eastward launches are desirable, when feasible, since they take advantage of the rotation of the Earth to add velocity to that generated by the vehicle. The Earth's velocity at the latitude of Cape Kennedy is approximately 1350 feet per second eastward. The Western Test Range (WTR), with launch sites located near Vandenberg Air Force Base, California, are used for westerly and southerly launches. Southerly launches are desired for obtaining polar or near-polar Earth orbits.

The direction of launches from both ETR and WTR are limited by range safety con-
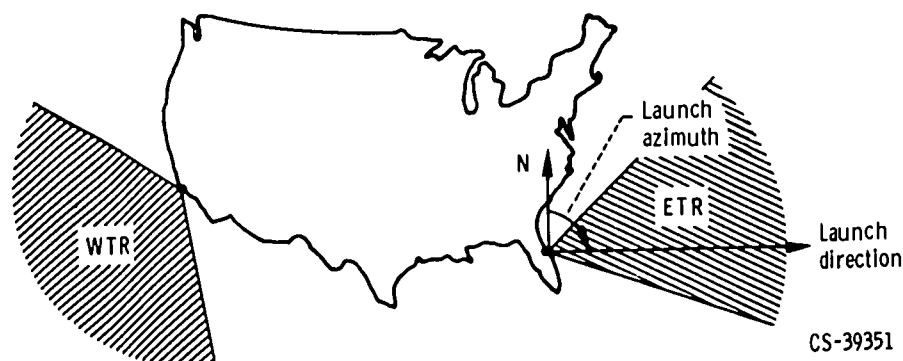
Figure 11-3. - Typical launch site restrictions.

siderations. That is, the vehicles are not generally allowed to fly over populated land areas. The direction of the launch is given by an angle called the launch azimuth. The azimuth angle is the angle measured clockwise from the geographical north around to the direction of launch (fig. 11-3). Launches from the ETR are generally limited to azimuth angles between 45° and 110° and launches at WTR from 170° to 300°.

Launch Vehicle Performance

The computation of a launch vehicle trajectory and performance is a complicated procedure requiring the use of large electronic computers to obtain accurate solutions. However, some simplifying assumptions allow an approximate answer to be easily obtained. Assume that the launch vehicle will fly a 100-mile circular orbit. Actually, a wide variety of Earth orbits are required to accomplish the various NASA missions. However, almost all of these missions require minimum orbit altitudes near or above 100 miles. Below 100 miles, the Earth's atmosphere, although very thin, is sufficiently dense that, in combination with the high orbital velocities, it exerts a measurable drag on the payload. This may result in undesirable payload heating and, also, rapid decay of the orbit back to Earth. The problem, then, is to accelerate the vehicle from zero velocity and altitude at the launch site to orbital velocity at 100 miles. Assume that the Earth is not turning; this permits the initial velocity due to the Earth's rotation to be neglected and simplifies the calculations.

A sketch of a typical launch trajectory is shown in figure 11-4. Notice that the vehicle launches vertically and gradually turns over as it accelerates. For a circular final orbit, the orientation of the vehicle at burnout must be horizontal, or parallel to the Earth's surface. The required orbital velocity was determined in chapter 9 to be about 26 000 feet per second. Recall that in circular orbital flight the vehicle is in balance

120 ┌
100 ├
80 ├
60 ├
40 ├
20 ├

Altitude, miles

Injection
velocity,
25 750 ft/sec

0   250   500   750   1000   1250   1500
Range, miles

CS-39350
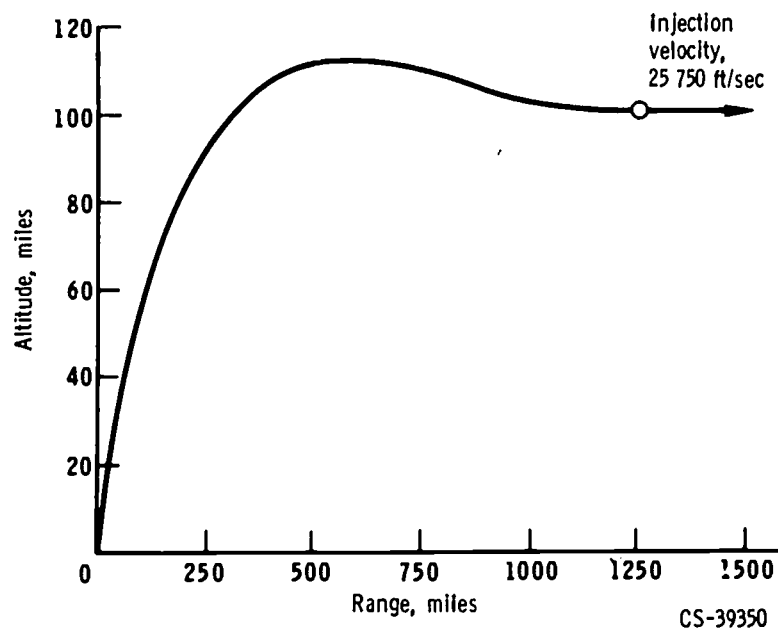
Figure 11-4. - Typical launch trajectory.

between the outward centrifugal force and the inward pull of gravity. The centrifugal force is given by

$$F_c = \frac{mv_c^2}{r_o} \tag{1}$$

and this is equal to the pull of gravity mg_o, so that

$$\frac{mv_c^2}{r_o} = mg_o \tag{2}$$

(All symbols are defined in the appendix.) The velocity in a circular orbit above the Earth v_c is then found by rearranging equation (2) to give

$$v_c = \sqrt{g_o r_o} \tag{3}$$

The acceleration due to gravity at the surface of the Earth g_e is 32.2 feet per second per second. Actually, g_o gets smaller away from Earth (inversely proportional to the radius squared), and the g_o at altitude is given by

$$g_o = g_e \frac{r_e^2}{r_o^2} \tag{4}$$

177

Substituting this into equation (3) gives

$$v_c = \sqrt{\frac{g_e(r_e)^2}{r_o}} \qquad (5)$$

Using 4000 miles as the radius of the Earth and introducing the proper numbers into equation (5) give the circular velocity in a 100-mile orbit as

$$v_c = \sqrt{32.2 \ \frac{4000^2}{4100} \ \frac{5280^2}{5280}} = 25\ 750 \text{ ft/sec}$$

The problem, then, is to accelerate the vehicle from zero velocity at launch to a horizontal burnout velocity of 25 750 feet per second at an altitude of 100 miles.

The performance of the launch vehicle will be computed by using the ideal or basic rocket equation discussed in chapter 2. This equation gives the burnout velocity of a vehicle as

$$v_b = g_e I_{sp} \ \ln \frac{W_i}{W_f} \qquad (6)$$

It is called the ideal equation because it gives the maximum velocity that a vehicle can achieve flying in a vacuum in gravity-free space. It does not account for losses such as gravity losses and aerodynamic drag losses which will be discussed later. Nonetheless, equation (6) is of great use in determining launch vehicle performance, and it bears some detailed discussion. First, g_e is the standard value of 32.2 feet per second per second. The specific impulse, I_{sp}, is a measure of the performance of the rocket engines as defined and discussed in previous chapters. The specific impulse of engines used today on NASA launch vehicles range from a little over 200 seconds to as high as 440 seconds, depending on the propellants used. The initial weight of the vehicle is W_i; the final weight is W_f. The weight of the propellant used can be determined from

$$W_p = W_i - W_f \qquad (7)$$

Given the initial weight of a launch vehicle, the amount of propellant on board, and the specific impulse of its engines, the vehicle's burnout velocity can be determined by using equations (6) and (7). Conversely, if given a required burnout velocity, the final weight can be determined. These computations, however, require the logarithm of the initial- to

178
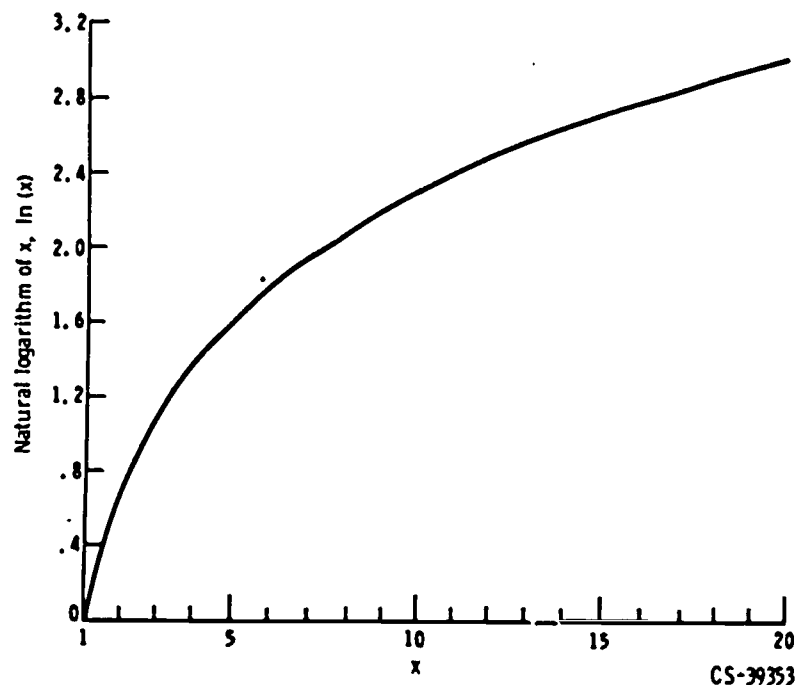
Figure 11-5. - Natural logarithm curve.

final-weight ratio. The logarithm used here is the natural logarithm (to the base e, where $e = 2.7183$), and the relation between a number and its natural logarithm is shown in figure 11-5. As an example, assume a launch vehicle whose burnout weight is one-fifth its initial weight. Then, $W_i/W_f = 5$, and from figure 11-5 the natural logarithm of 5 is 1.61. If the specific impulse of the vehicle engine is 350 seconds, the vehicle burn-out velocity from equation (6) is

$$v_b = (32.2)(350) \ln 5 = (32.2)(350)(1.61) = 18\ 150 \text{ ft/sec}$$

Before equation (6) will apply to a vehicle flying to orbit, the losses encountered in flying a real trajectory must be considered. There are three fundamental losses. First, some of the thrust of the engines will be lost in overcoming the aerodynamic drag im-posed on the vehicle in flying through the atmosphere. This was discussed in chapter 9. Secondly, not only must the vehicle obtain a horizontal velocity of 25 750 feet per second, but it must also increase altitude from 0 to 100 nautical miles; this means that early in the flight (see fig. 11-4) all thrust is directed upward to gain altitude, and this thrust does not contribute directly into acquiring horizontal velocity. Finally, there are losses due to the gravitational pull of the Earth which are referred to as gravity losses. These exist because part of the engine thrust is used to overcome the Earth's gravitational pull on the vehicle, and only part of the thrust is then left to accelerate the vehicle. Con-sider the example shown in figure 11-6 which indicates the status of a vehicle that has

Weight = 100 000 lb

Thrust = 125 000 lb

CS-39349
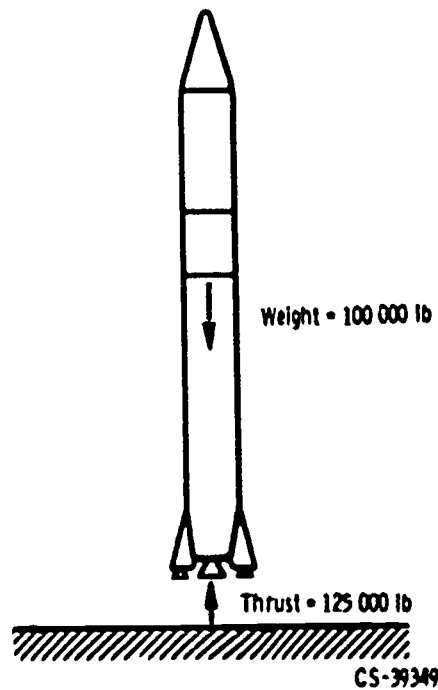
Figure 11-6. - Gravity loss early in the trajectory.

just left the launch pad. This vehicle weighs 100 000 pounds and has a thrust of 125 000 pounds. This initial thrust-to-weight ratio of 1.25 is typical of liquid propellant vehicles we are flying today. Notice that 100 000 pounds of thrust is used to support the vehicle (against the Earth's gravitational pull), and only 25 000 pounds is left to accelerate the vehicle. Thus, initially, 80 percent of the thrust is lost in overcoming gravity. Fortunately, this loss decreases rapidly as the vehicle continues along the trajectory since it is getting lighter as it consumes propellants. Also, as the trajectory begins to curve over (fig. 11-4), part of the gravitational pull of the Earth is counterbalanced by the centrifugal force of the vehicle. Indeed, when it reaches orbit, the entire gravitational pull of the Earth is balanced by the centrifugal force.

Exact determination of the three losses is a complicated calculation requiring solution on an electronic computer. Experience indicates, however, that for a typical launch to orbit, these losses total about 4000 feet per second. Thus, the hypothetical launch vehicle whose performance is being calculated must have an ideal velocity capability of 30 000 feet per second: 25 750 feet per second to acquire orbital velocity and 4250 feet per second to account for the losses in an actual trajectory.

Now, the performance of a launch vehicle to orbit can be finally calculated. Assume that the initial weight of the vehicle is 110 000 pounds, its specific impulse is 390 seconds, and its hardware weight is equal to 10 percent of the propellant weight. Equation (6) will now appear as

$$30\ 000 = (32.2)(390) \ln \frac{W_i}{W_f}$$

or

$$\ln \frac{W_i}{W_f} = \frac{30\ 000}{(32.2)(390)} = 2.40$$

Using figure 11-5 to evaluate the logarithmic function gives

$$\frac{W_i}{W_f} = 11.0$$

and for the initial weight of 110 000 pounds,

$$W_f = \frac{110\ 000}{11.0} = 10\ 000\ \text{lb}$$

From equation (7), the propellant weight now becomes

$$W_p = 110\ 000 - 10\ 000 = 100\ 000\ \text{lb}$$

Thus, the vehicle has a burnout weight of 10 000 pounds in orbit and used 100 000 pounds of propellant getting there. To obtain payload we need to subtract the hardware or jettison weight of the stage from the burnout weight. Since the hardware weight was assumed to be 10 percent of the propellant weight, the hardware weight is 10 000 pounds which when subtracted from the burnout weight leaves no weight for payload. This example demonstrates that it is very difficult to deliver payloads to Earth orbit with a single-stage vehicle. In practice, then, most payloads are delivered to orbit by using more than one stage. To demonstrate the advantage of staging we will repeat the problem using two stages to reach orbit. The payload and burnout velocity of the first stage are the initial weight and velocity of the second stage. Again, the total vehicle weight is taken as 110 000 pounds, and each stage has a specific impulse of 390 seconds and a hardware percentage equal to 10 percent of the propellant weight. Finally, we assume that the 30 000-foot-per-second ideal velocity is divided equally between the two stages, that is, 15 000 feet per second each. For the first stage (using eq. (6)),

$$15\ 000 = (32.2)(390) \ln \frac{W_i}{W_f}$$

or

$$\ln \frac{W_i}{W_f} = \frac{15\ 000}{(32.2)(390)} = 1.194$$

Using figure 11-5 gives

$$\frac{W_i}{W_f} = 3.30$$

and the burnout weight of the first stage is

$$W_f = \frac{110\ 000}{3.30} = 33\ 300 \text{ lb}$$

The propellant weight is

$$W_p = 110\ 000 - 33\ 300 = 76\ 700 \text{ lb}$$

and thus the hardware or jettison weight of the first stage is

$$W_{hw} = (0.10)(76\ 700) = 7670 \text{ lb}$$

Subtracting this from the burnout weight of the first stage gives a payload equal to 33 300 - 7670 or 25 630 pounds. The initial weight of the second stage then is 25 630 pounds, and the second stage has to provide another 15 000 feet per second to reach orbit. For the second stage (using eq. (6)),

$$15\ 000 = (32.2)(390) \ln \frac{W_i}{W_f}$$

or

$$\ln \frac{W_i}{W_f} = \frac{15\ 000}{(32.2)(390)} = 1.194$$

and

$$\frac{W_i}{W_f} = 3.30$$

The final weight in orbit is, then, given by

$$W_f = \frac{25\ 630}{3.30} = 7770\ \text{lb}$$

and the second-stage propellant load is

$$W_p = 25\ 630 - 7770 = 17\ 860\ \text{lb}$$

The hardware weight of the second stage is, then, 1786 pounds which when subtracted from the burnout weight gives us a payload in orbit of 7770 - 1786 = 5984 pounds. Thus, whereas the single-stage vehicle can deliver essentially no payload to orbit, the two-stage vehicle can deliver over 5 percent of its initial weight to orbit.

NASA LAUNCH VEHICLES

It is impractical to use a large vehicle such as the Saturn V to launch a small instrument package that can be launched by a smaller, less expensive vehicle such as the Scout. On the other hand, to develop a new vehicle for each mission is expensive. Consequently, NASA has developed a family or "stable" of vehicles of various sizes, and tries to use each member for a range of missions within its capability. Moreover, the more experience we have with a few vehicles, the more reliable we can make them. With this in mind, NASA's aim is to develop the smallest number of vehicles consistent with the full scope of space missions now foreseen.

At present, NASA is actively using seven launch vehicles. They are the Scout, Delta, Thor-Agena, Atlas-Agena, Atlas-Centaur, Uprated Saturn I, and Saturn V. The Thor-Agena and Atlas-Agena were developed by the U. S. Air Force and are used jointly by NASA and the Air Force. The remaining vehicles were or are being developed by NASA. The Uprated Saturn I and Saturn V are man-rated vehicles and will be used for manned missions. The other vehicles are all used for unmanned missions. The characteristics of all the vehicles are summarized in table 11-II.

TABLE 11-II. - LAUNCH VEHICLE CHARACTERISTICS

Vehicle (a)	Height, ft	Weight, lb	Payload to orbit Weight, lb	Payload to orbit Altitude, n mi	Launch site	Program application	First stage Designation	First stage Propellant	First stage Thrust, lb	Second stage Designation	Second stage Propellant	Second stage Thrust, lb	Third stage Designation	Third stage Propellant	Third stage Thrust, lb	Fourth stage Designation	Fourth stage Propellant	Fourth stage Thrust, lb
Scout	68	38 900	240	300	Wallops, WTR	Explorer, reentry probes, ESRO, others	Algol	Solid	88 000	Castor	Solid	61 000	Antares	Solid	23 000	Altair	Solid	5 800
Delta[b]	90	114 000	880	300	ETR, WTR	Explorer, OSO, Tiros, Relay, ESSA, others	DM-21	RP-1/LOX	170 000	-------	UDMH/IRFNA	7 500	Altair	Solid	5 800	------	-----	-----
Thor-Agena[b]	76	----------	1 600	300	WTR	Nimbus, Echo II, Alouette, others	DM-21	RP-1/LOX	170 000	Agena	UDMH/IRFNA	16 000	--------	---------	---------	------	-----	-----
Atlas-Agena	91	----------	5 950	300	ETR, WTR	OAO, OGO, Mariner, Ranger, others	Atlas	RP-1/LOX	388 000	Agena	UDMH/IRFNA	16 000	--------	---------	---------	------	-----	-----
Atlas-Centaur	100	300 000	8 500	300	ETR	Surveyor, Mariner	Atlas	RP-1/LOX	388 000	Centaur	LH2/LOX	30 000	--------	---------	---------	------	-----	-----
Uprated Saturn I	225	1 300 000	40 000	100	ETR	Apollo	S-IB	RP-1/LOX	1 600 000	S-IVB	LH2/LOX	200 000	--------	---------	---------	------	-----	-----
Saturn V	365	6 100 000	285 000	100	ETR	Apollo	S-IC	RP-1/LOX	7 500 000	S-II	LH2/LOX	1 000 000	S-IVB	LH2/LOX	200 000	------	-----	-----

[a] All the vehicles are operational except the Saturn V, which is still under development.
[b] Currently being launched with three solid motors strapped to the first stage for increased launch thrust and payload capability (and increased vehicle weight). The thrust-augmented Delta is called TAD, and the thrust-augmented Thor-Agena is called TAT.

APPENDIX - SYMBOLS

F_c	centrifugal force, lb		v_b	burnout velocity, ft/sec
g_o	acceleration due to gravity at orbital altitude, ft/sec^2		v_c	circular orbital velocity, ft/sec
g_e	acceleration due to gravity at Earth's surface, ft/sec^2		W_f	final weight, lb
			W_{hw}	hardware or jettison weight, lb
I_{sp}	specific impulse, sec		W_i	initial weight, lb
m	mass, slugs		W_p	propellant weight, lb
r_o	orbit radius, ft			
r_e	radius of the Earth, ft			

12. INERTIAL GUIDANCE SYSTEMS
Daniel J. Shramo[*]

NAVIGATION

The ancient navigation problem is one of determining the position of a moving vehicle. This problem can be extended into knowing the position of the destination, which also may be moving, and then comparing the present position of the vehicle with that of the destination to provide steering signal informaticn. But the heart of the problem is the constant knowledge of the present position of the vehicle. Inertial navigation is one of the most recent solutions. Pilotage and celestial navigation are classic methods still very much in use. Pilotage is simply looking for familiar landmarks or features that can be identified on charts. Celestial navigation is based on the fact that at a given instant of time, the observed positions of the stars are unique for any point on Earth. Recently, various electronic aids have been developed to simplify the navigation problem. Some electronic aids, such as loran and shoran, are based on phase relations between signals received from two or more ground stations; others, like omnirange or VOR, are based on the unique phase relation of two signals from one station. Radar on the vehicle itself can reproduce an image of the terrain which can be interpreted as in pilotage.

All navigation systems, except the inertial navigation systems, have one feature in common: that is, the vehicle must collect external information - visual or electronic - to determine its present position. The uniqueness of inertial navigation is that it is self-contained and needs no external information. Once it has been given an initial orientation, the inertial system senses only the motion of the vehicle and navigates by calculating the change in position. This independence is increasingly important in vehicles that must operate in all kinds of weather or away from ground radio transmitters and at speeds which may ionize the surrounding air and interfere with radio transmission. Because of inertial navigation, ballistic missiles, satellites, and spacecraft can now be designed to operate anywhere.

---

[*]Chief, Guidance and Flight Control Branch, Centaur Project Office.
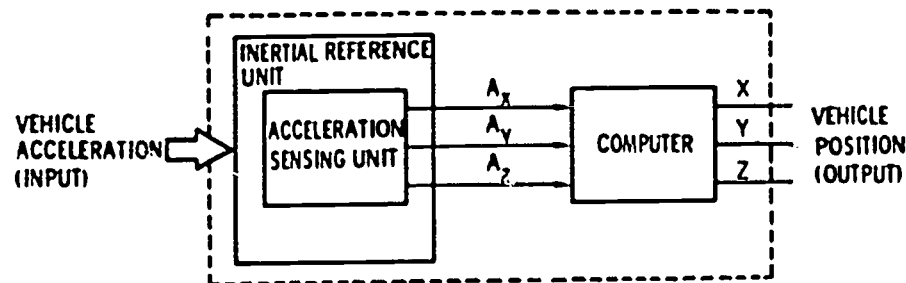
Figure 12-1. - Basic inertial navigation system.

INERTIAL NAVIGATION SYSTEM

The basic inertial navigation system can be thought of as a system whose orientation is fixed, whose input is a physical acceleration (i. e., a rate of change of velocity), and whose output is the vehicle's present position (fig. 12-1). This process of converting acceleration to position requires three major components: the inertial reference unit, the acceleration sensing unit, and the computing unit.

INERTIAL REFERENCE UNIT

The function of the inertial reference unit is always to maintain a fixed orientation regardless of the direction in which the carrier vehicle is moving. Like a compass needle, the inertial reference unit always "points north," but it differs from a compass in that it does not need a lump of magnetic material to tell it where "north" is. Moreover, unlike a compass needle, the inertial reference unit must remain fixed in three directions - "north-south, east-west, and up-down." These directions are seldom those of the compass, so they may be called the x, y, and z axes of the reference system. However, since the inertial reference unit can maintain orientation in any reference system, it is generally desirable to select a system that has at least one visible reference point, such as a star.

No matter what is happening to the vehicle, the inertial reference unit must always maintain its fixed orientation. This is achieved first by mounting a platform so that it is completely free to move, and second, by adding gyroscopes to keep the platform orientation constant.

Gimbals

Gimbals are simply a series of rings of diminishing sizes which are mounted one

188   134
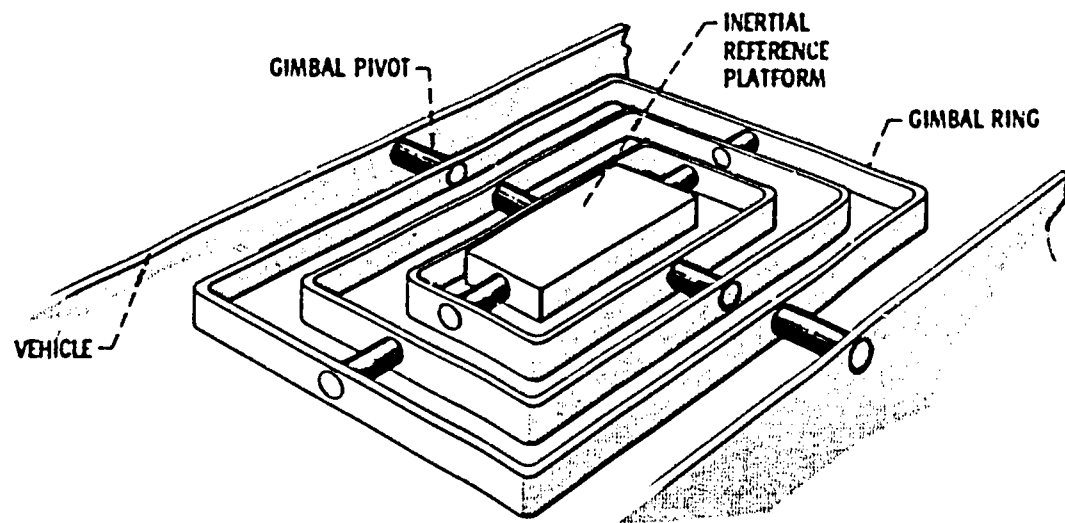
Figure 12-2. – Inertial reference platform mounted on gimbals in vehicle.

inside the other on pivots. The pivots, located 90° apart, allow each ring to rotate independently. The most freedom of motion is achieved with four rings that can move freely about their pivots. Mounted on the last, inside ring, or replacing it, is the inertial platform, which must maintain the fixed orientation (fig. 12-2).

Gyroscope

Gyroscopes keep the inertial platform oriented independently of the motion of the vehicle. They provide the stable reference axes for the rest of the system. Since there are three, mutually perpendicular axes (x, y, and z), there must be one gyroscope mounted along each of them. However, since all gyroscopes operate in the same way, only one needs to be discussed here.

Any discussion of the behavior of a gyroscope necessitates the use of certain terms which must be clearly understood. These terms are torque, moment of inertia, couple, and input turning rate. These terms are illustrated in figure 12-3.

Torque. - Torque T is the common measure of the effectiveness of a twisting force acting on a body. This effectiveness is measured by the product of the force F and the perpendicular distance d from the line of action of the force to the axis of rotation.

Moment of inertia. - This is a measure of the resistance offered by a body to angular acceleration. The moment of inertia I of a body about a turning axis is the product of the mass M of the body and the square of the distance r from the mass to the axis of rotation.

Couple. - A couple consists of two parallel forces (F_1 and F_2) that are equal in

189
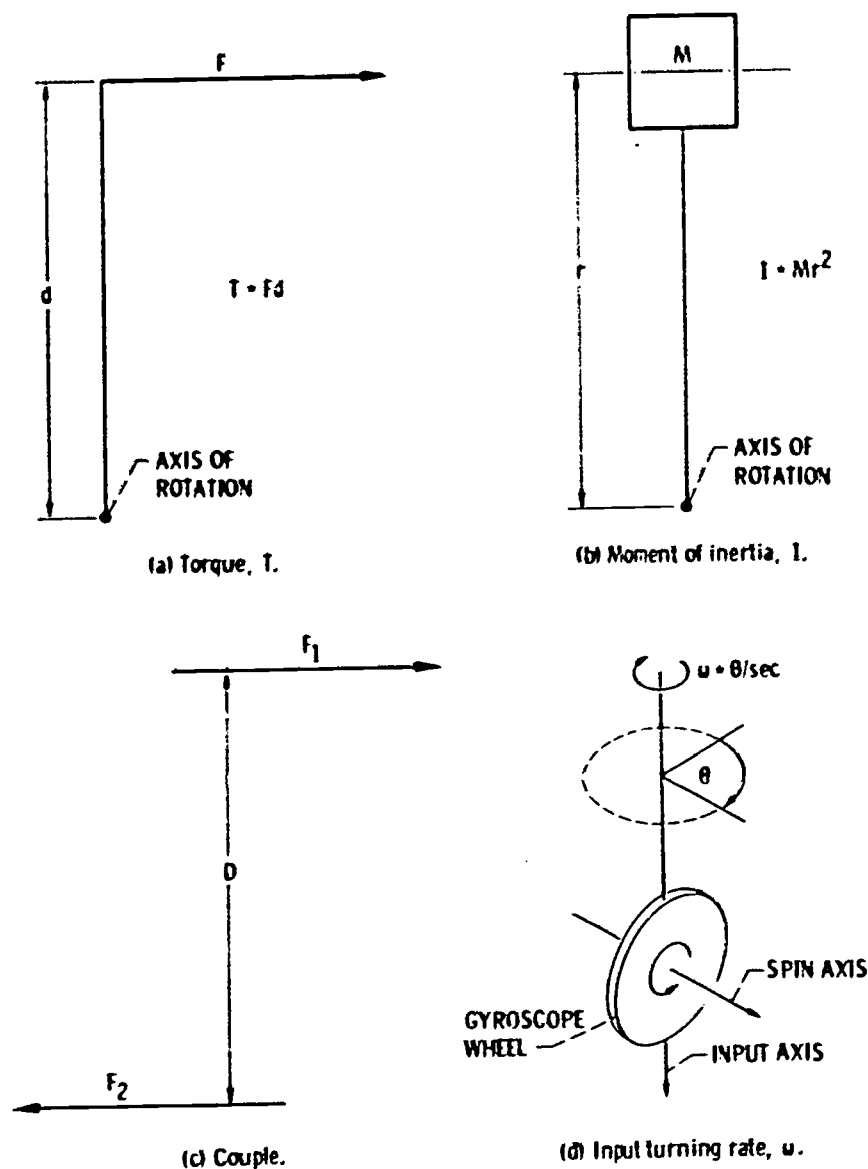
Figure 12-3. - Basic terms and concepts.

magnitude but opposite in direction and whose lines of action do not coincide. The sole effect of a couple is to produce rotation. The resultant torque produced by a couple is equal to the product of either of the forces constituting the couple and the perpendicular distance D between their lines of action. This product is called the moment of the couple. The moment of a couple is the same about all axes perpendicular to the plane of the forces constituting the couple.

Input turning rate. - Input turning rate ω is a measure of the response of a point or body to a torque. To allow a comparison of the effects of the same torque on bodies of different sizes, the turning rate is often expressed in angular degrees per second, or radians per second (1 radian = 57. 3°).

A useful characteristic of a gyroscope is that a turning rate about its input axis causes a torque about its output axis (these two axes are perpendicular to each other).
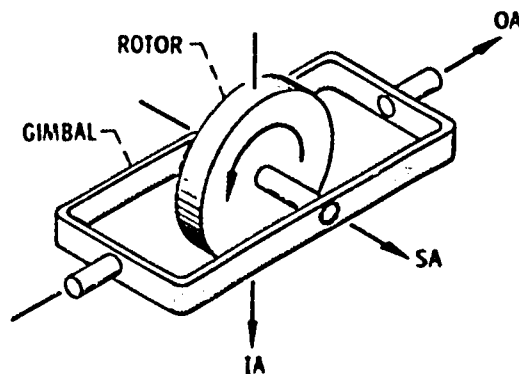
Figure 12-4. - Gyroscope reference axes.

The three axes of a gyroscope are shown in figure 12-4, where SA is the spin axis, IA is the angular turning rate input axis, and OA is the gyroscope gimbal torque output axis. (Note that these gyroscope axes are not the same as the orientation axes.) The interrelation of the three axes is such that if the positive end of SA is rotated towards the positive end of IA, the positive direction of OA is determined by the "right-hand rule." This rule is a common method of designating a sign convention (either positive or negative) for the direction of rotation about an axis and for the relative directions of the three mutually perpendicular axes of a gyroscope.

One form of the right-hand rule is used to determine the direction of rotation about an axis relative to the direction of that axis (fig. 12-5(a)). For example, assume that the thumb of the right hand lies along the spin axis of the gyroscope wheel and that the thumb is pointing in the positive direction along this axis. Then, the positive direction of rotation about this spin axis is the direction in which the fingers of the right hand point as they curl around the line (or axis) formed by the thumb. Obviously, this rule can also be used in reverse; that is, if the positive direction of rotation about an axis is known, then this rule can be used to determine the positive direction of the axis.

Another form of the right-hand rule can be used to determine the relative directions of three mutually perpendicular axes (fig. 12-5(b)). In this application, assume that the right thumb pointing upward indicates the positive direction of a single axis. Then, the positive direction of a second axis can be indicated by the index finger pointing forward so that it is perpendicular to, and in the same plane as, the thumb. The positive direction of a third axis can be indicated by the middle finger pointing in such a way that it is perpendicular to the plane of the thumb and index finger. Thus, if the thumb, the index finger, and the middle finger of the right hand are used to represent the three axes of a gyroscope, the relative positive (or negative) directions of these axes are the directions in which the fingers are pointing.

The right-hand rule can be used to describe the behavior of a gyroscope. Assume that the spin axis is the thumb, the input axis is the index finger, and the output axis is
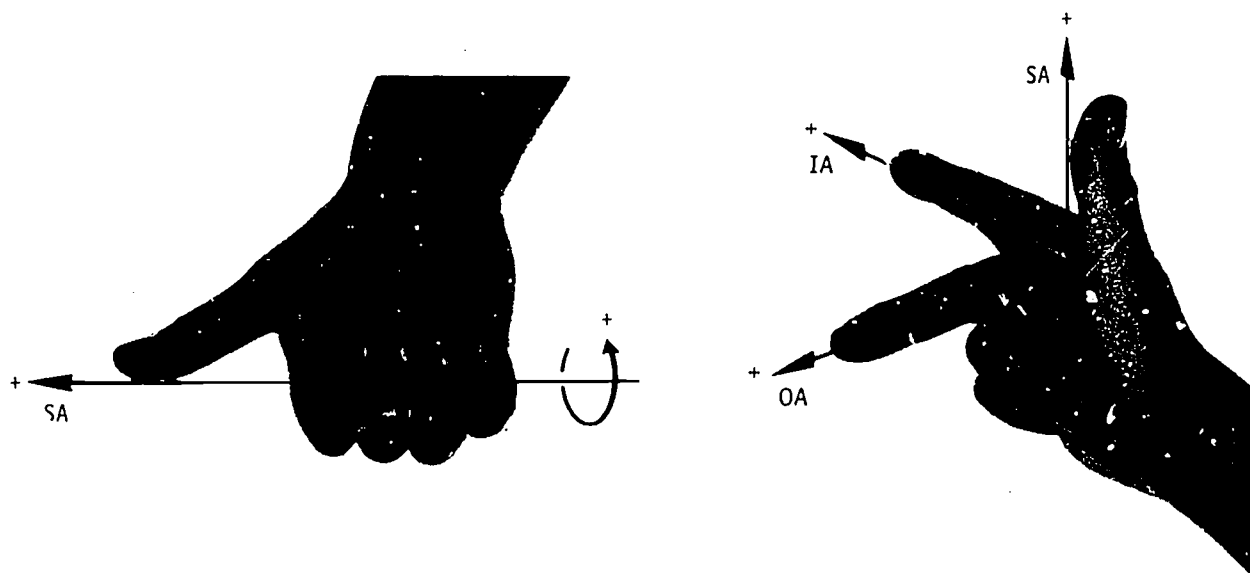
(a) Determining direction of rotation relative to direction of axis.

(b) Determining relative directions of three mutually perpendicular axes.

Figure 12-5. - Applications of right-hand rule.

the middle finger. Also assume that the gyroscope wheel is spinning about the spin axis (thumb) in the positive direction according to the right-hand rule. Now, if positive rotation (according to the right-hand rule) is initiated about the input axis (index finger), the gyroscope will rotate about the output axis (middle finger) in the positive direction according to the right-hand rule.

Some practice with the right-hand rule can be of considerable help in the understanding of the sign conventions and of the operation of a gyroscope.

The gyroscopic torque or precession phenomenon should be understood before gyro performance characteristics are considered. In a nonspinning disk which is turning about an axis that lies along a diameter of the disk, as shown in figure 12-6(a), the masses at points A and C lying along the input axis have no velocity; however, the masses at points B and D at 90° to the input axis have maximum velocity and are opposite in direction.

Now if the disk is set in rotation about the spin axis normal to the surface of the disk (fig. 12-6(b)), the input turning rate ω causes no rim velocity to the mass at point A. But since this mass is moving towards point B, it must accelerate to maximum velocity by the time it reaches there, and then it must decelerate to zero velocity again at point C. At point C, the mass must reverse direction and begin to accelerate. At point D, the mass has attained maximum opposite velocity and must begin to decelerate again.

A force is required to change the direction or the velocity of any mass $(F = ma)$. Therefore, a force is required to accelerate the mass from the instant it leaves point D,

192

(a) Nonspinning disk.   (b) Spinning disk.
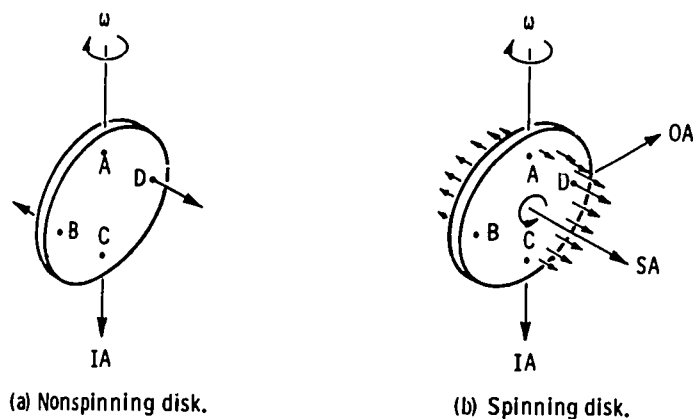
Figure 12-6. - Particle on disk that is turning about axis that lies along
its diameter.

passing through A, until it reaches point B. An opposite force acts on the mass as it leaves point B, passes through C, and reaches point D. These two forces form a couple which produces a torque about the BD axis. Thus, any attempt to rotate a gyro about an axis at right angles to a spin axis causes a torque about an axis at right angles to both the input axis and the spin axis. This torque T at 90° to the input axis is proportional to the spin rate Ω, the moment of inertia of the disk about its spin axis I, and the input turning rate ω; so that $T = I\Omega\omega$. Since most gyros are designed for a constant spin rate, the moment of inertia and the spin rate are more often combined into a constant angular momentum H, where $H = I\Omega$, and the torque equation becomes $T = H\omega$. The input can be either a torque or a turning rate causing either a turning rate or torque output.

To convert a spinning wheel into a useful device, the wheel is mounted in a single gimbal so that the output axis is perpendicular to the wheel spin axis. This is a single-degree-of-freedom gyro, shown in figure 12-7. The remaining axis, which is perpendicular to both the output and spin axes, is the input or sensitive axis. This is the axis that must be parallel to one of the orientation axes. For the right-hand rule, the axes go in alphabetical order: input, output, and spin. The input axis is the axis around which the turning rate or angle is measured and is the stable reference axis that the gyro provides for the inertial navigation system. The signal which gives information is obtained from the resulting motion of the gimbal about the output axis relative to the frame.

When a simple gyro is mechanized for use in an inertial guidance system, several additional elements are added to the basic gyro (fig. 12-8). One of the elements is a damper around the output axis. The second element is a signal generator which senses the rotation of the gyro output axis. The third element is a torque generator which supplies torque to the output axis of the gyro. A simple gyro with these additional elements is shown incorporated into a single-axis platform stabilization scheme in
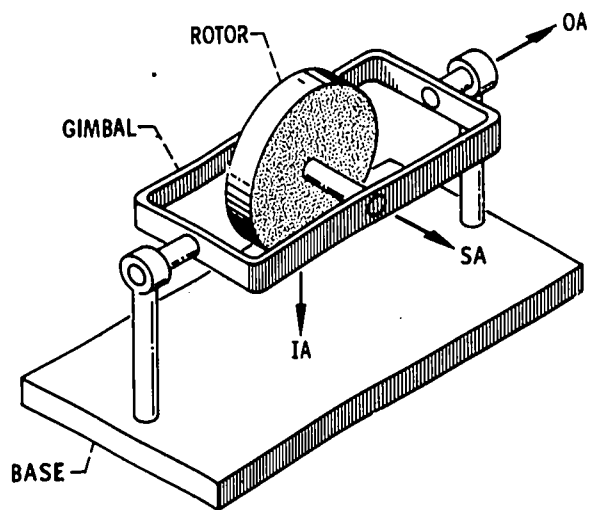
Figure 12-7. – Gyroscope with single degree of freedom.
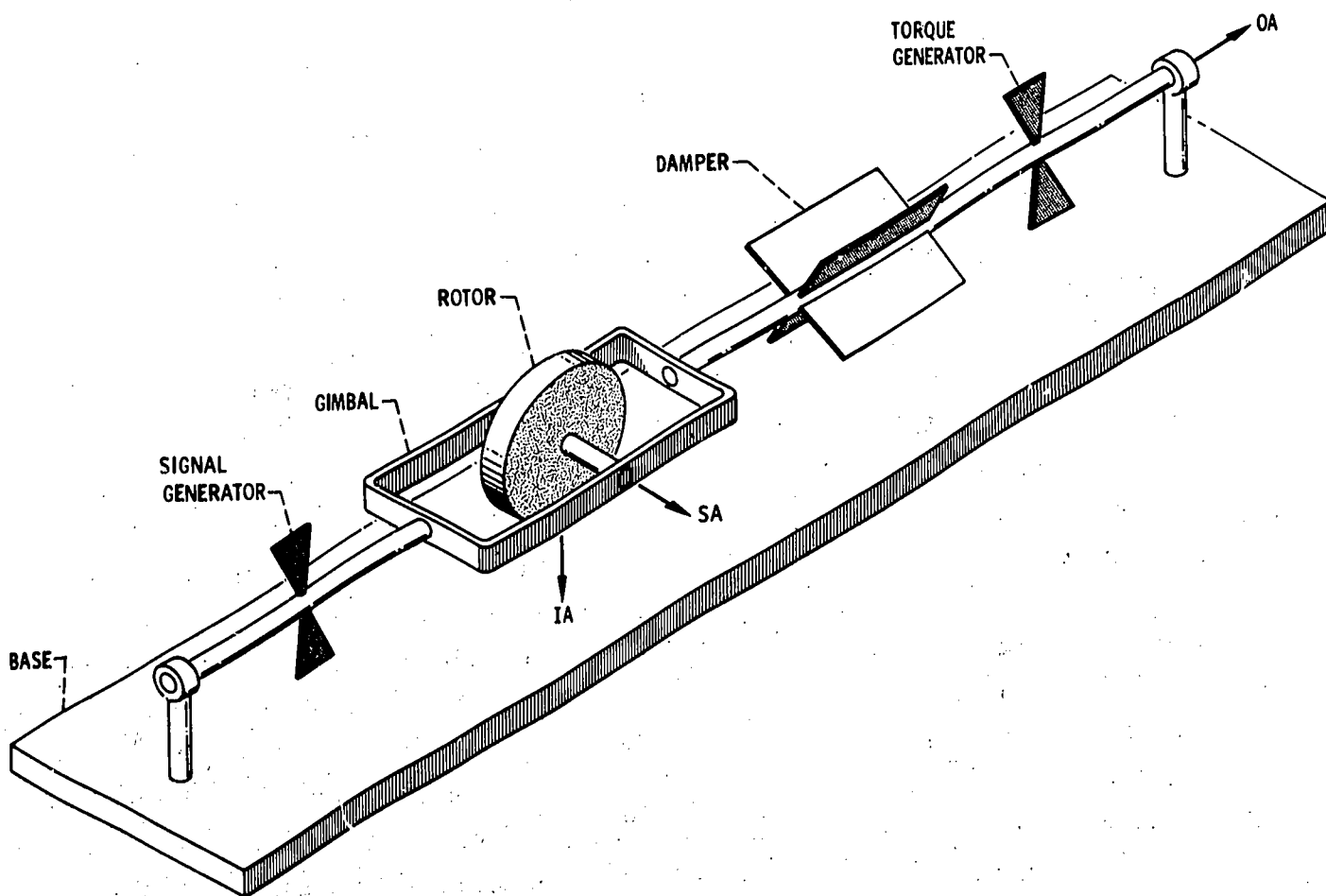
Figure 12-8. – Inertial gyroscope mechanization.
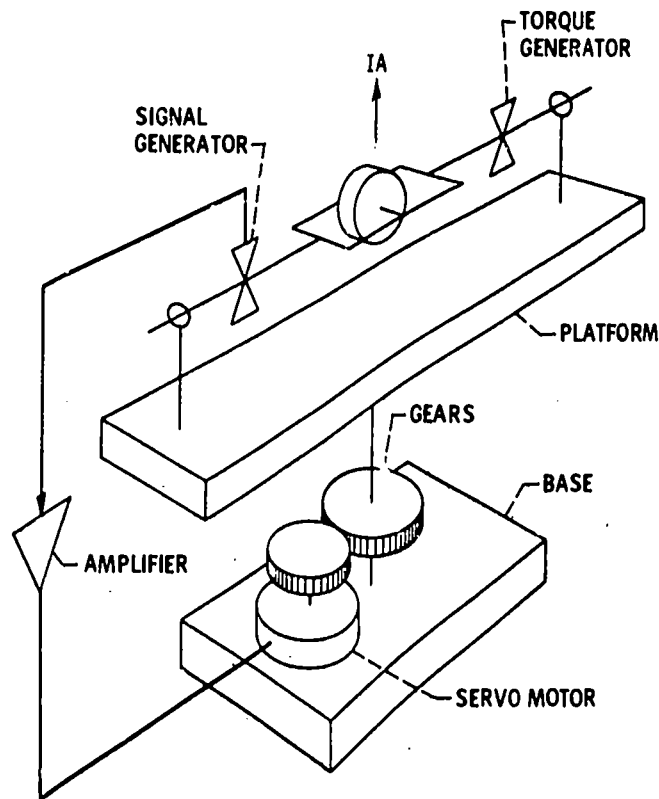
Figure 12-9. - Single-axis platform stabilization.

figure 12-9. Information from the signal generator is used by the servomotor to keep the platform oriented, while the torque generator is used to correct errors in the gyro and to calibrate it (to be discussed later). In the single-axis representation of the platform-mounted gyro shown in figure 12-9, any rotation of the platform about the gyro input axis will be sensed by the signal generator, amplified, and then used to drive the servomotor to return the platform to the initial orientation.

Examples of gyroscopic behavior are common in everyday life. For instance, an ordinary hand power drill is much more awkward to wave around at random when it is running than when it is not. More scientifically, an ordinary power drill can be used to observe the responses of a gyroscope. If the electric motor is considered the spinning mass of the gyro, its axis is the spin axis SA; the pistol-grip handle of the drill is then the input axis. Now, hold the drill by its grip and switch it on (note: do not use a bit in the drill). While it is running, point the drill at a spot on the wall. By using only wrist action, swing the drill 90° to the right; then repeat the procedure to the left. Notice that the drill is easier to swing in one direction than in the other; furthermore, in the more difficult direction the handle of the drill is gently pushing against your palm. It is this pushing force that is called precession and is used to maintain the orientation of a gyroscope.

Gyroscopic Drift

The preceding explanation of the behavior of a gyroscope assumed that the gyroscope was functioning ideally. Unfortunately, this assumption seldom holds true. A gyroscope seldom maintains an exact orientation for long because many small forces that are present due to magnetism, friction, mass unbalance, etc. cannot be eliminated and because the gyroscope is so sensitive. The shifting of a gyroscope away from its assigned orientation is called drift.

The two categories of drift are (1) constant drift, and (2) drifts that are proportional to acceleration forces. Constant drift is caused by small forces that are constantly present and are of fixed magnitude. The drifts that are proportional to acceleration are caused by net mass unbalances along the spin axis and along the input axis. When these unbalanced masses are subjected to acceleration forces, they cause a rotation about the output axis (fig. 12-10). This rotation is an equivalent gyroscopic drift.

Within each of the two categories of drift there is a portion that is predictable and a portion that is random. There are two methods of correcting for predictable drift. One method is to apply an electrical signal to the torque generator to cause a rotation about the output axis that will counteract the effects of the predictable drifts. The other method is to allow the gyroscope to drift and to add (or subtract) a correction factor to (or from) the information supplied by the gyroscope. Predictable drift in an inertial gyroscope is only about 2° per hour. Random drift is more difficult to control. Since the exact magnitude and direction of this drift are unknown, no mechanical or mathematical correction is possible. About the only effective approach to this problem is to seek and to reduce its causes. This has already been done to such an extent that for a typical inertial-grade gyroscope the error due to random drift is only about 0.05^{o} per hour (or approximately $1\frac{1}{4}^{o}$ per day).
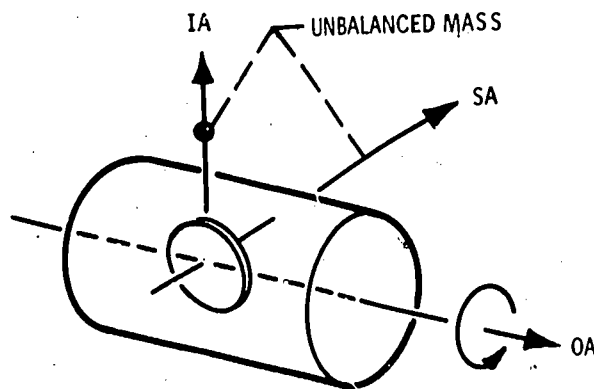
Figure 12-10.- Gyroscope mass unbalance. (Accelerations along either IA or SA will cause torque about OA due to mass unbalance.)

ACCELERATION SENSING UNIT

The acceleration sensing unit is mounted on the inertial reference unit. Its function is to sense change in the velocity of the vehicle. It is important to understand that the sensing unit cannot measure velocity alone; that is, it cannot sense that the vehicle is moving so many miles per hour. All that it can sense is the change in velocity--if the vehicle's velocity changes from 0 to 20 feet per second, that rate of change, the acceleration, is all that is sensed. If the change in velocity took place in 1 second, then the sensor would note an acceleration of 20 feet per second per second. Just as the inertial reference unit must remain oriented in the x, y, and z directions, the acceleration sensing unit must respond to changes in velocity in all three directions; it follows that the acceleration sensing unit can then also respond to changes that occur between the axes, such as in an xy direction.

If it is mounted on the constantly oriented inertial reference unit, the acceleration sensing unit is constantly oriented too. The job of the acceleration sensing unit is more complex than that of the inertial reference unit because the three axes represent six directions. The acceleration sensing unit must indicate not only the existence of an acceleration along a particular axis, but also the direction of that acceleration. Moreover, the acceleration sensing unit must also be able to indicate the amount of the acceleration. Fortunately, there is a device which can measure both the direction and magnitude of a force; this device is an accelerometer. Three accelerometers are needed, one for each axis. But since the three accelerometers are similar in operation and differ only in orientation, only one needs explaining.

The function of the accelerometer is simply to sense linear physical accelerations and to provide a proportional electrical output signal. The term accelerometer is also in common use for certain types of vibration pickups, but the linear accelerometer is the one of principal interest in inertial navigation. The basic accelerometer may be thought of as a damped, spring-restrained mass whose displacement is proportional to acceleration. However, for various design reasons the rotation equivalent of a damped spring-restrained pendulum is more commonly used. Figure 12-11 is a diagram of this type of accelerometer. The axis about which the pendulum rotates is called the output axis OA. The pendulous axis PA is the arbitrary neutral position of the pendulum. The input axis IA is the sensitive axis of the accelerometer and is perpendicular to both the output axis and the pendulous axis. The determination of a positive direction of acceleration is such that OA rotated into IA by the right-hand rule equals PA. The pendulous accelerometer may be thought of as a torque-summing device. The steady-state torque equation is

$$pa = K\varphi + F$$
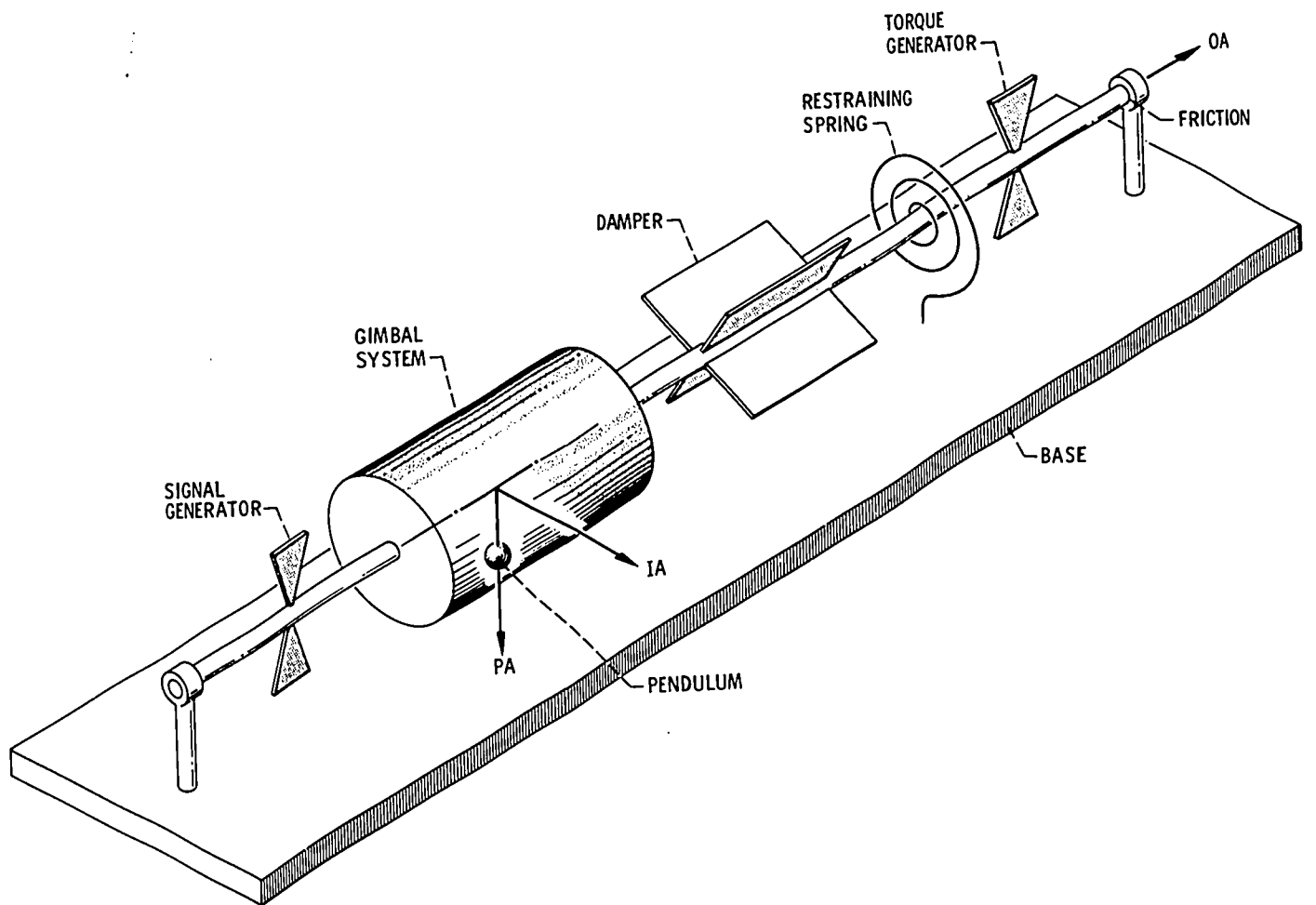
Figure 12-11. - Functional diagram of basic pendulous accelerometer.

where

p   pendulosity (the pendulum mass multiplied by its distance from the point of rotation)

a   linear acceleration acting perpendicular to the output axis and the pendulous axis

K   constant (the spring rate of the restraining springs)

φ angular displacement of the pendulum

F   friction in the system

If **K** and **p** are constant and **F** is negligible, the equation resolves to

$$a = \varphi\left(\frac{K}{p}\right)$$

and the displacement of the pendulum is then directly proportional to the acceleration measured.

198

Generally, the pendulous accelerometer does not have a mechanical spring but derives its spring restraint from closed loop operation of an electrical circuit. In most applications the output motion φ resulting from an input acceleration is sensed by a moving coil signal generator. This signal is sent to an electronic circuit which determines the magnitude and the direction (+ or -) of the motion (i.e., if the +y direction were designated as north, then the -y direction would be south). The accelerometer also contains two opposing torquing coils through which an electrical signal can be used to force the pendulum in one direction or the other. The electrical signal derived from the signal generator output is channeled to the proper torquing coil and the accelerometer pendulum is moved in a direction to match exactly the input acceleration, thereby keeping the pendulum at the center position. The electrical rebalance signal is a direct measure of the input acceleration and is used by the computing unit.

The accelerometer has a number of significant parameters whose stabilities determine the accuracy of its performance in an inertial guidance system. These parameters are scale factor, threshold, null uncertainty, and bias. The current in the torquer is proportional to the measured acceleration. Accelerometer scale factor is the current required to balance out a given acceleration input divided by that input acceleration. The smallest acceleration input which causes a detectable output is the threshold. In inertial applications, a threshold of less than 1×10^{-6} g is common. When the acceleration input to an accelerometer is changed from a positive to a negative number of the same value, the exact location of the output null or zero reading should be repeatable to within 5×10^{-5} g. The nonrepeatability is called the null uncertainty. The bias of an accelerometer is the output reading that the accelerometer gives when it is sensing zero gravity. Zero gravity can be simulated on the Earth's surface by orienting the accelerometer so that the input axis is at right angles to the Earth's gravity field. With the input axis of the accelerometer perpendicular to the Earth's gravity field, the accelerometer should indicate a zero output. The actual reading is the accelerometer bias. In addition to the accelerometer parameters discussed here, a number of secondary parameters that influence accelerometer performance are also present. Among these are cross-coupling effects and vibration effects. These are discussed in the references 1 and 2, and an understanding of them is not required for a basic discussion of inertial navigation systems.

Because accelerometer parameters are variable, they cannot be measured exactly, and so these parameters become the primary sources of error when such an accelerometer is used in an inertial navigation system. However, the combined error or uncertainty of all the parameters is extremely small. The method of calibration of an accelerometer is relatively simple and is discussed in reference 2. Inertial accelerometers are designed so that bias and scale factor are the predominant sources of error; therefore, only these parameters need to be measured to ensure accurate system operation.

Typical values for the limits of stability for short durations (approximately 12 hr) are 20 parts per million for the accelerometer scale factor and 40 parts per million for the accelerometer bias.

COMPUTING UNIT

Signals from the acceleration sensing unit are sent on to the computing unit where the accelerations are converted to the distance and direction information that is needed to determine the vehicle position. The computing unit converts accelerations to distance by integrating the electrical acceleration signals. Direction of travel is determined from the relative activity of each sensor. For example, if the only acceleration signal the computer receives is from the north end of the "north-south" sensor, then the vehicle is moving north. If the acceleration signals from the north end of the "north-south" sensor and from the west end of the "east-west" sensor are equal in strength, then the vehicle is traveling northwest.

Distance traveled is more difficult to compute since it depends not only on which sensor is responding and the strength of that response but also on the time during which that response takes place. Time is usually measured by sampling the response of the sensors at fixed intervals, perhaps every 1/100 second. For example, let us assume that the first sample indicates an acceleration of 0 feet per second per second from all sensors, that during the next 100 samples the x and y sensors continue to indicate zero acceleration while the z sensor indicates a velocity change of 100 feet per second, and that a final sample indicates that all sensors are again at 0. From this information, the computer can calculate that during the elapsed second the vehicle has increased its velocity by 100 feet per second. The computer adds this velocity increase to the previous velocity calculation. If the sample above was taken during the first second after a launch, the computer would then show that the vehicle had moved 100 feet in the z direction. Since the final indication from the sensors was 0, and if it remains 0, the computer will continue to add 100 feet to the distance traveled for every additional second of flight. Actually, the computer performs these calculations each time it samples the responses of the sensors instead of each second; therefore, its answers are more precise. The information from the computer is used to generate guidance signals to control the vehicle.

CENTAUR GUIDANCE SYSTEM

The Centaur launch vehicle is guided by an inertial navigation system which uses three gyros to orient an inertial platform in a known inertial reference frame, three

accelerometers to measure the accelerations along the axes of that frame, and a guidance computer to determine the precise position of the spacecraft and thus generate steering signals so that the vehicle will inject its payload into the proper trajectory. Figure 12-12 shows the Centaur guidance system, which comprises five individual units - a miniature inertial platform, its associated platform electronics, a coupler, the digital computer, and the signal generator. Figure 12-13 shows the miniature inertial platform and its relation to the platform electronics and to the coupler. The primary purpose of the Centaur inertial platform is to maintain a fixed reference point in space and to measure the acceleration of the Centaur vehicle. Figure 12-14 shows the platform electronics unit, which receives output signals from the gyros and, in turn, sends electrical signals which cause the platform gimbal motors to counteract any disturbing forces on the gyros. Thus, the platform is maintained in a fixed position with respect to inertial space. Figure 12-15 shows the guidance-system coupler, or accelerometer rebalance electronics and power-supply system. The accelerometer signal-generator output is sent to the coupler where the direction of the disturbance is detected and a new rebalance signal is sent back to the accelerometer such as to bring the accelerometer pendulum to zero or null. These rebalance forces are proportional to the input acceleration, and the electronics are mechanized in such a fashion that positive and negative pulses are sent to the accelerometer to keep it at its balance point. The algebraic sum of the rebalance pulses in any given time period is a measure of the velocity change, or acceleration, during that time period. Figure 12-16 shows the Centaur digital computer. The computer counts the net rebalance pulses sent to each accelerometer. Each pulse represents a change in velocity, or acceleration. The computer mathematically processes the number of pulses per unit of time and determines the direction of flight and speed of the rocket vehicle. This information is compared to similar information permanently stored in the computer memory. The computer generates steering signals for the rocket autopilot to reduce the difference between information stored in the computer and the actual speed and direction of the vehicle in flight. The final item in the Centaur inertial guidance system is the signal conditioner (fig. 12-17). Although the signal conditioner is not required to perform an inertial navigation task, it is important on scientific flights. The signal conditioner receives samples of important guidance-system electrical signals. When necessary, it converts these to radio signals which are transmitted through the rocket vehicle telemetry system to ground receiving stations. With this flight information received from the signal conditioner, the in-flight performance of the inertial navigation system can be reconstructed by using mathematical formulas and ground computers. Figure 12-18 shows schematically the interrelation of the five components of the total Centaur guidance system.

COUPLER

DIGITAL COMPUTER
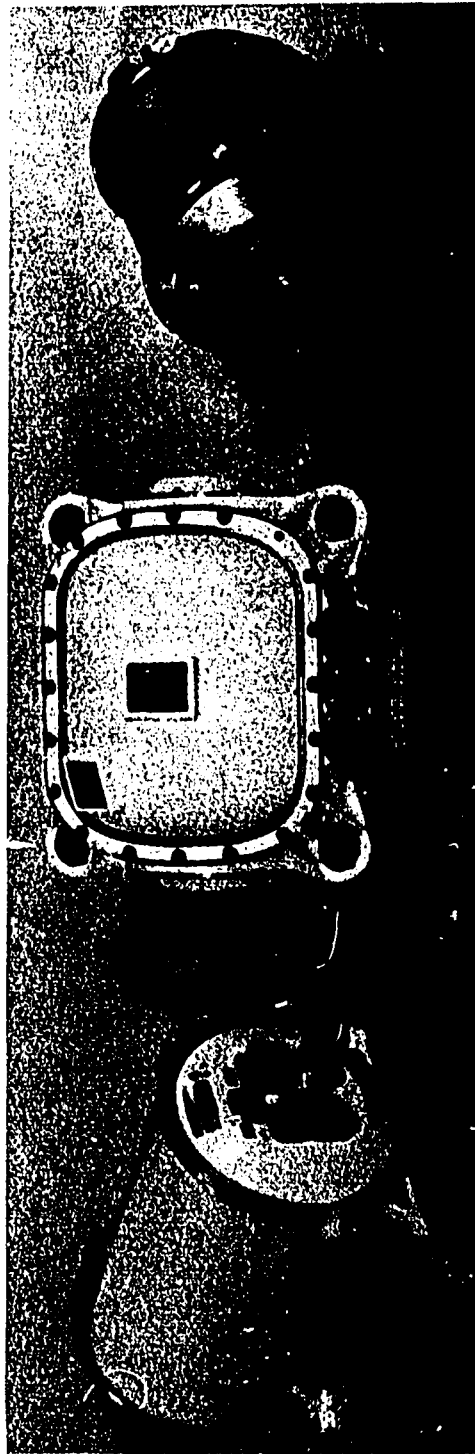
MINIATURE INERTIAL PLATFORM

SIGNAL CONDITIONER

PLATFORM ELECTRONICS

Figure 12-12. – Centaur guidance system.
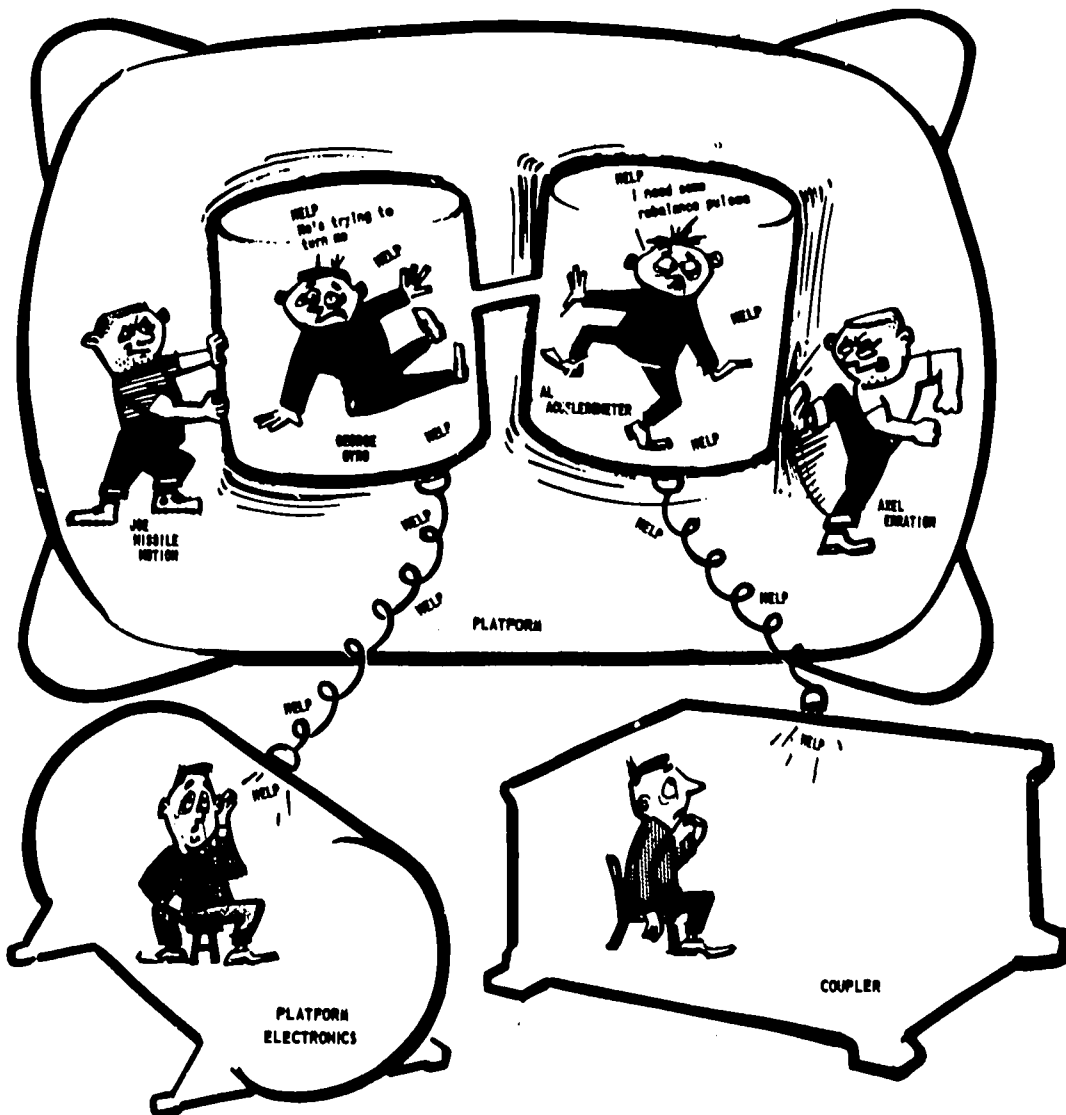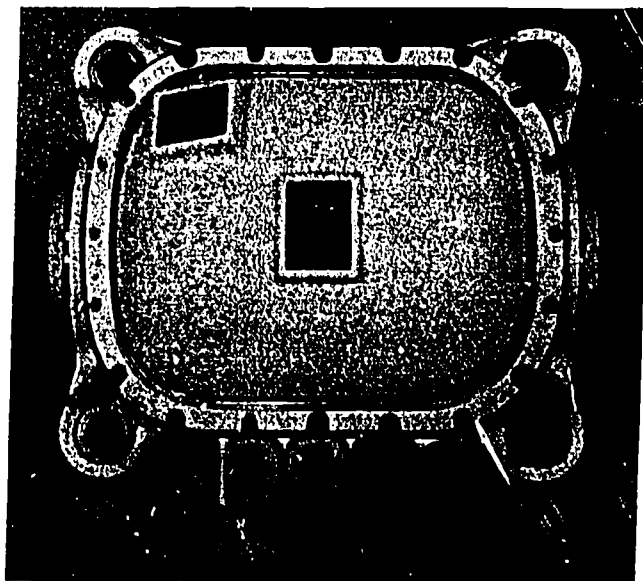
Figure 12-13. - Miniature inertial platform (four-gimbal, all-attitude). Weight, 32 pounds; volume, 0.99 cubic foot.
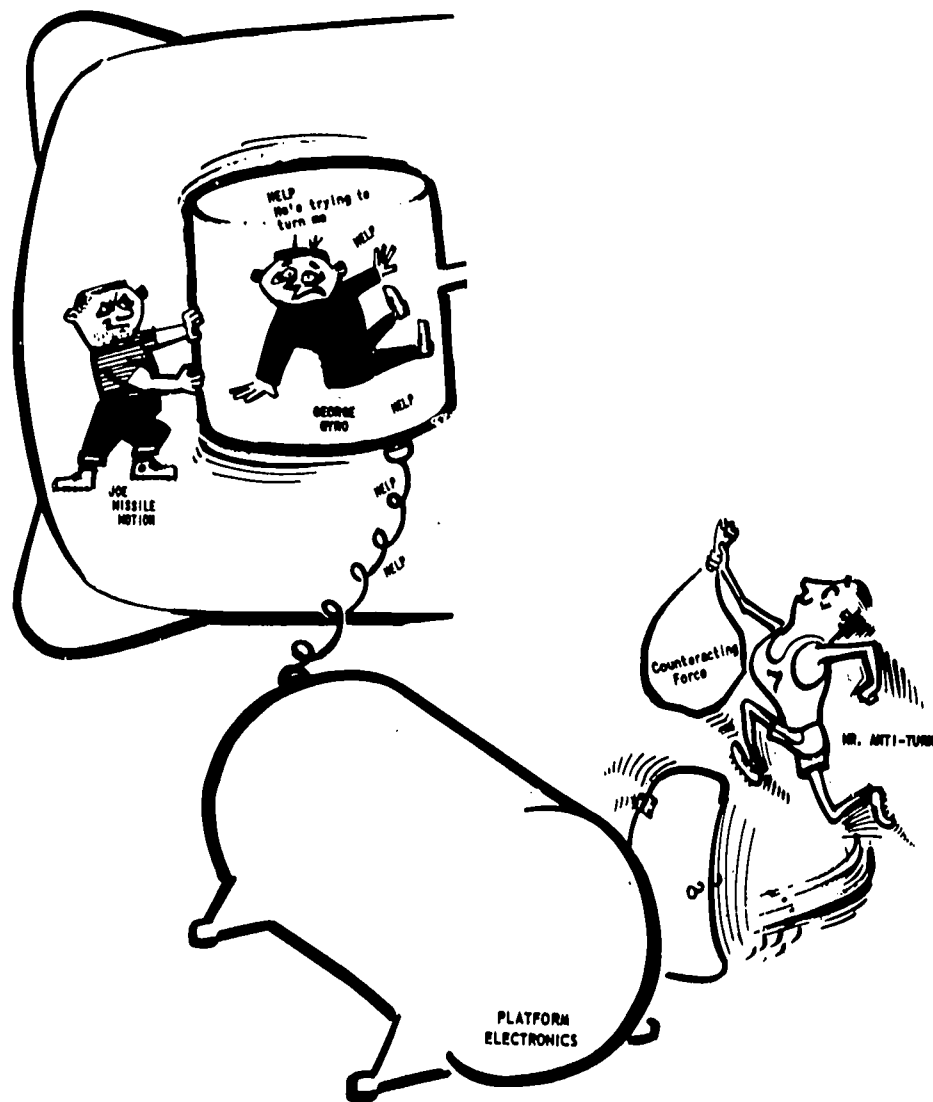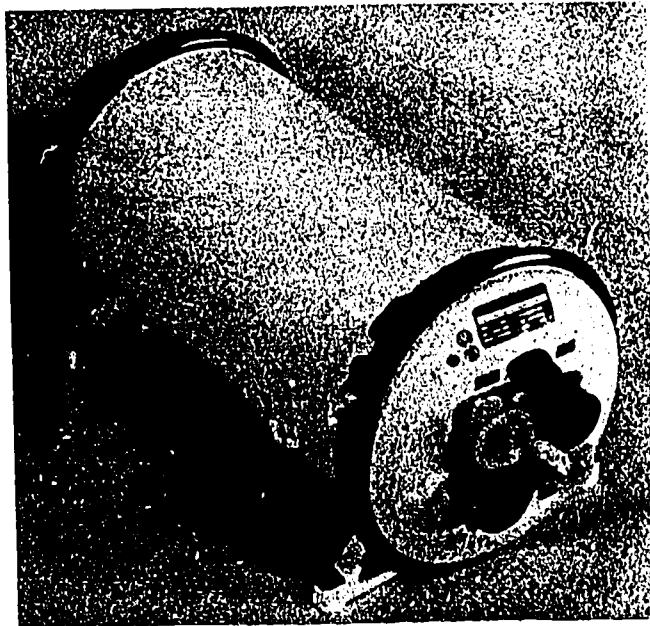
Figure 12-14. – Platform electronics unit. Weight, 18.5 pounds; volume, 0.61 cubic foot.
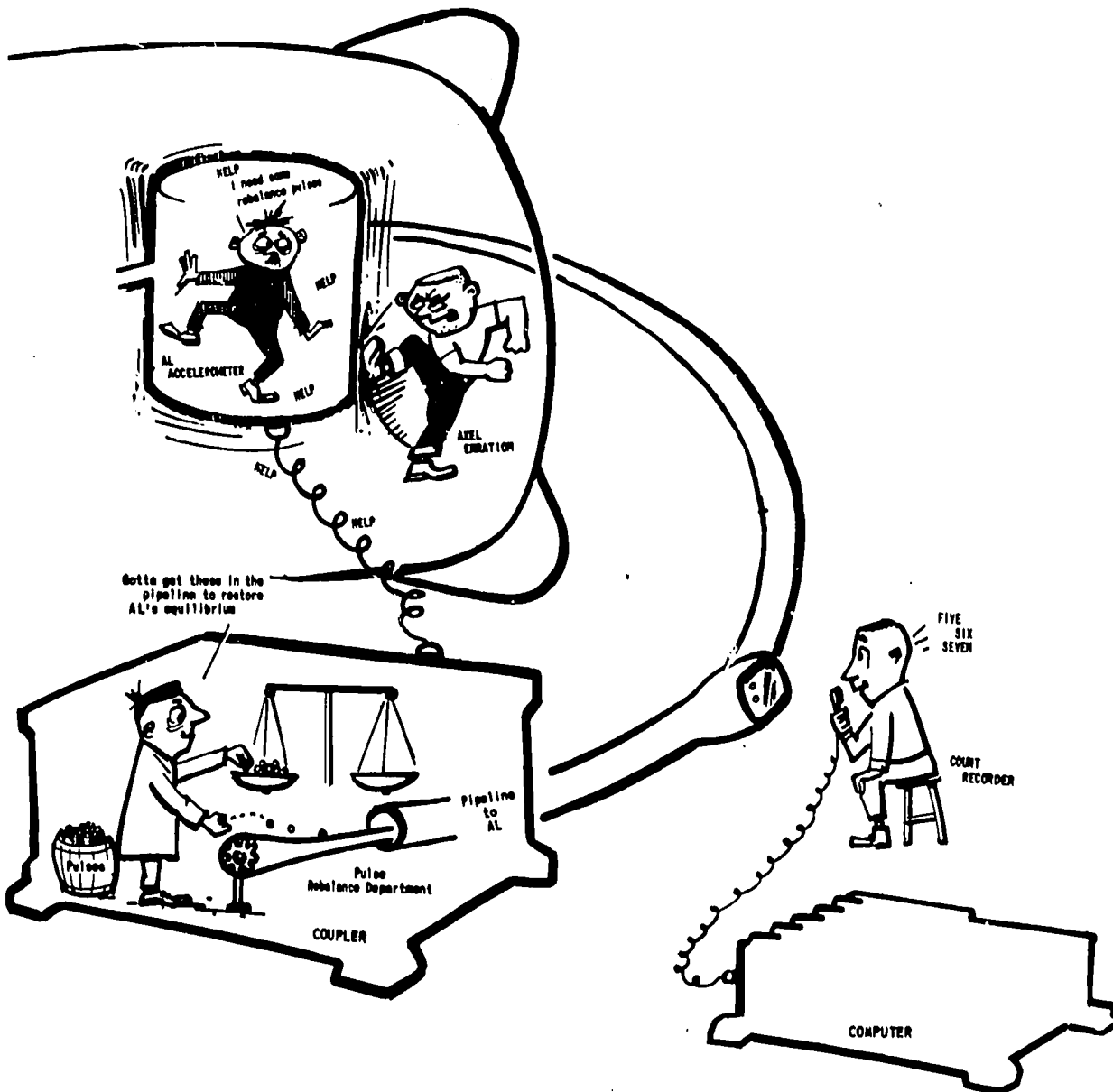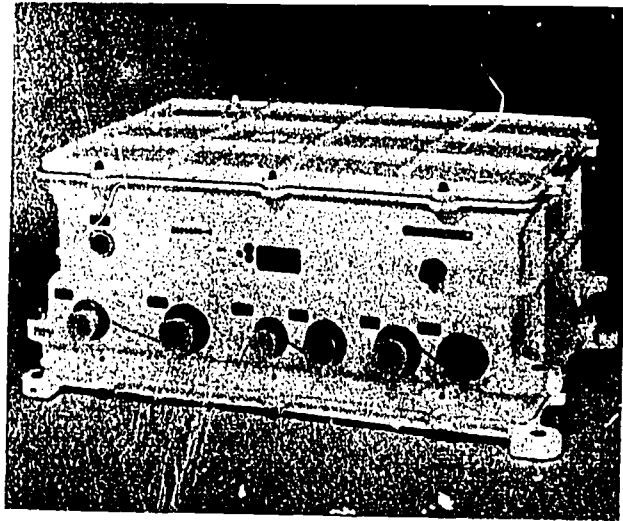
Figure 12-15. - Guidance-system coupler (accelerometer rebalance electronics and system power supplies). Weight, 60 pounds; volume, 1.58 cubic feet.

AL ACCELEROMETER reports 5 pulses to the right
Steer left 3 degrees
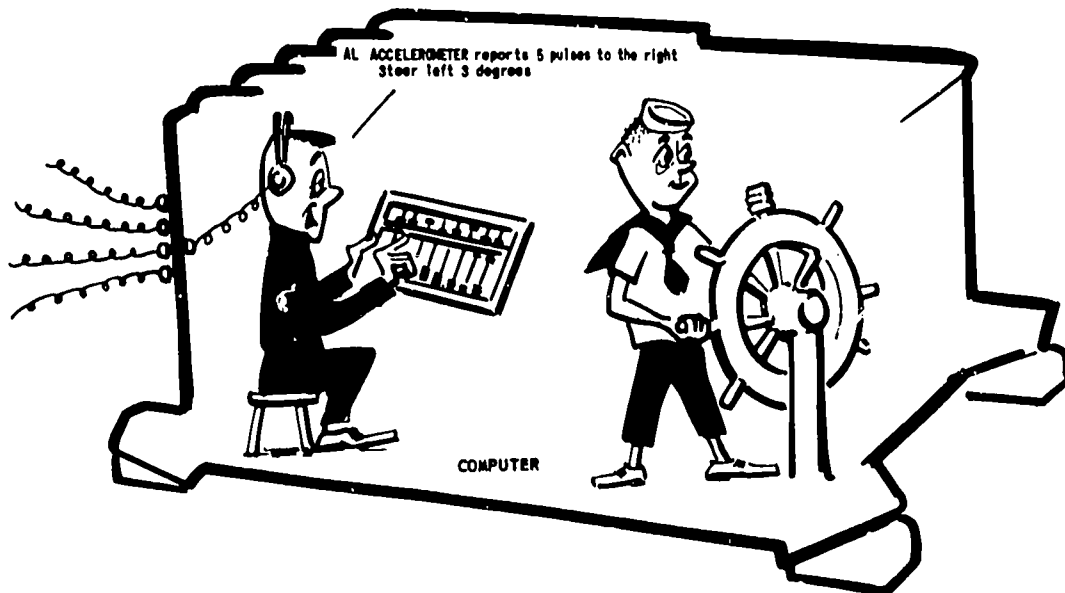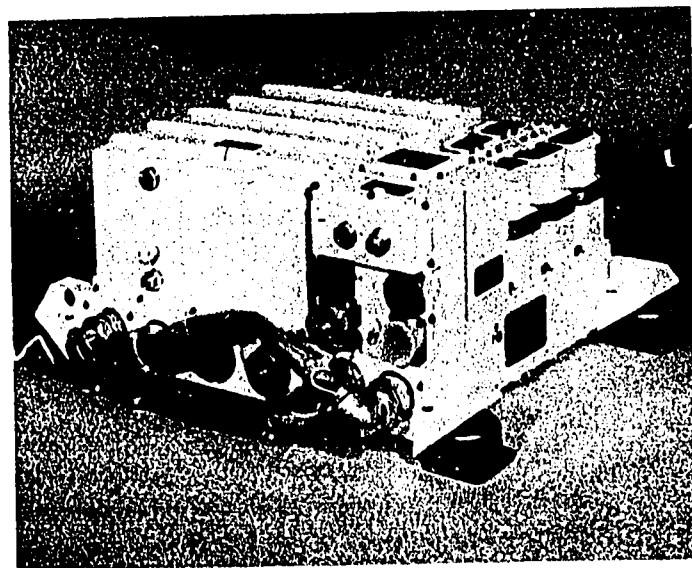
COMPUTER

Figure 12-16. - Digital computer (memory unit plus input-output unit). Weight, 65 pounds; volume, 1.46 cubic feet.
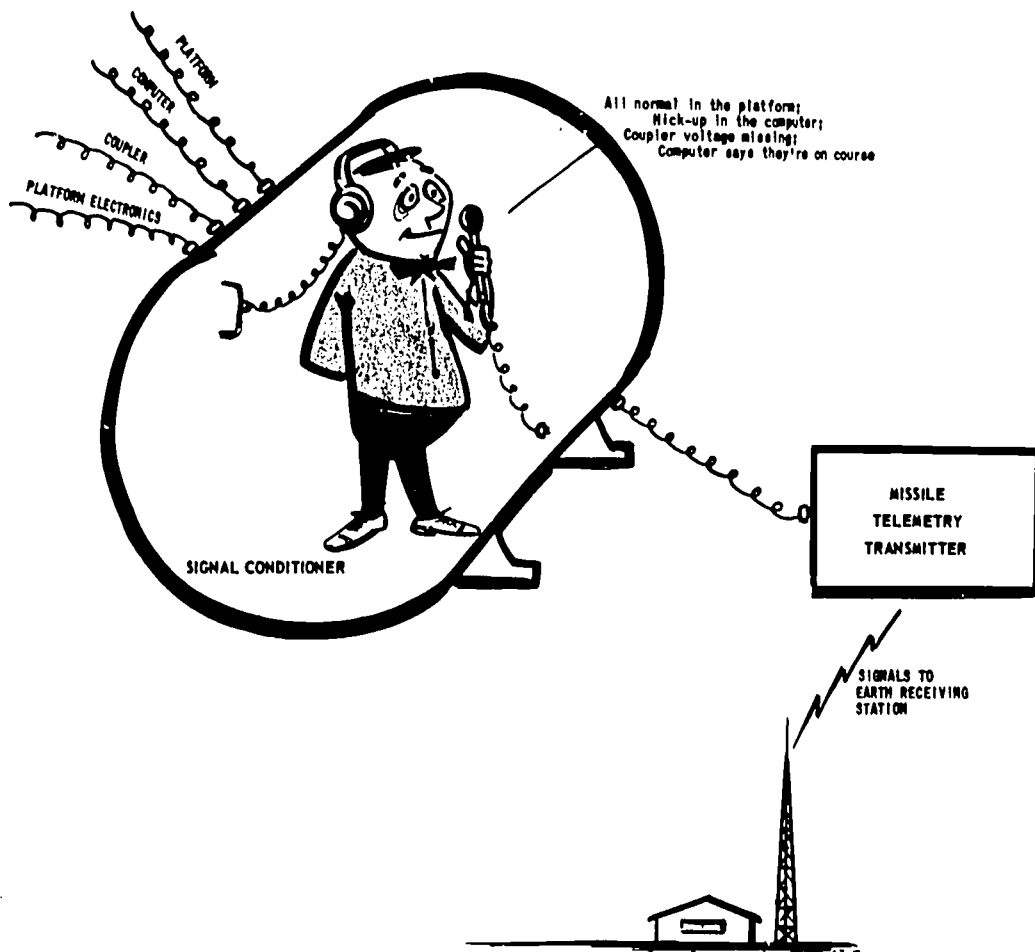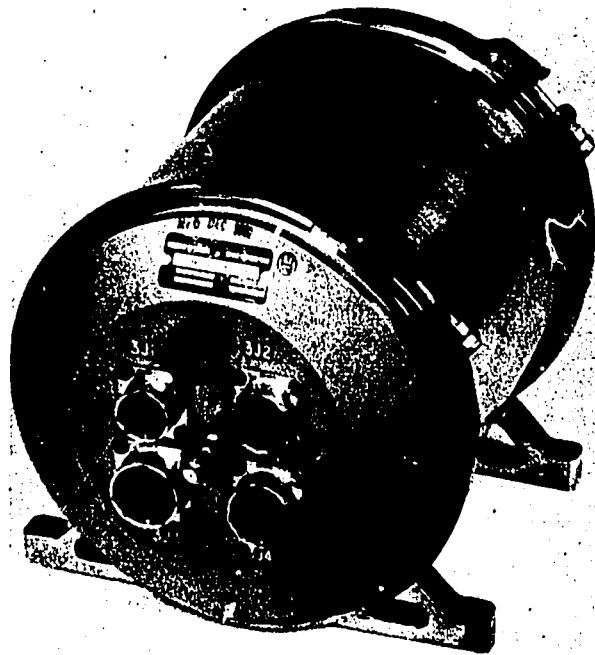
Figure 12-17. - Signal conditioner. Weight, 10 pounds; volume, 0.4 cubic foot.
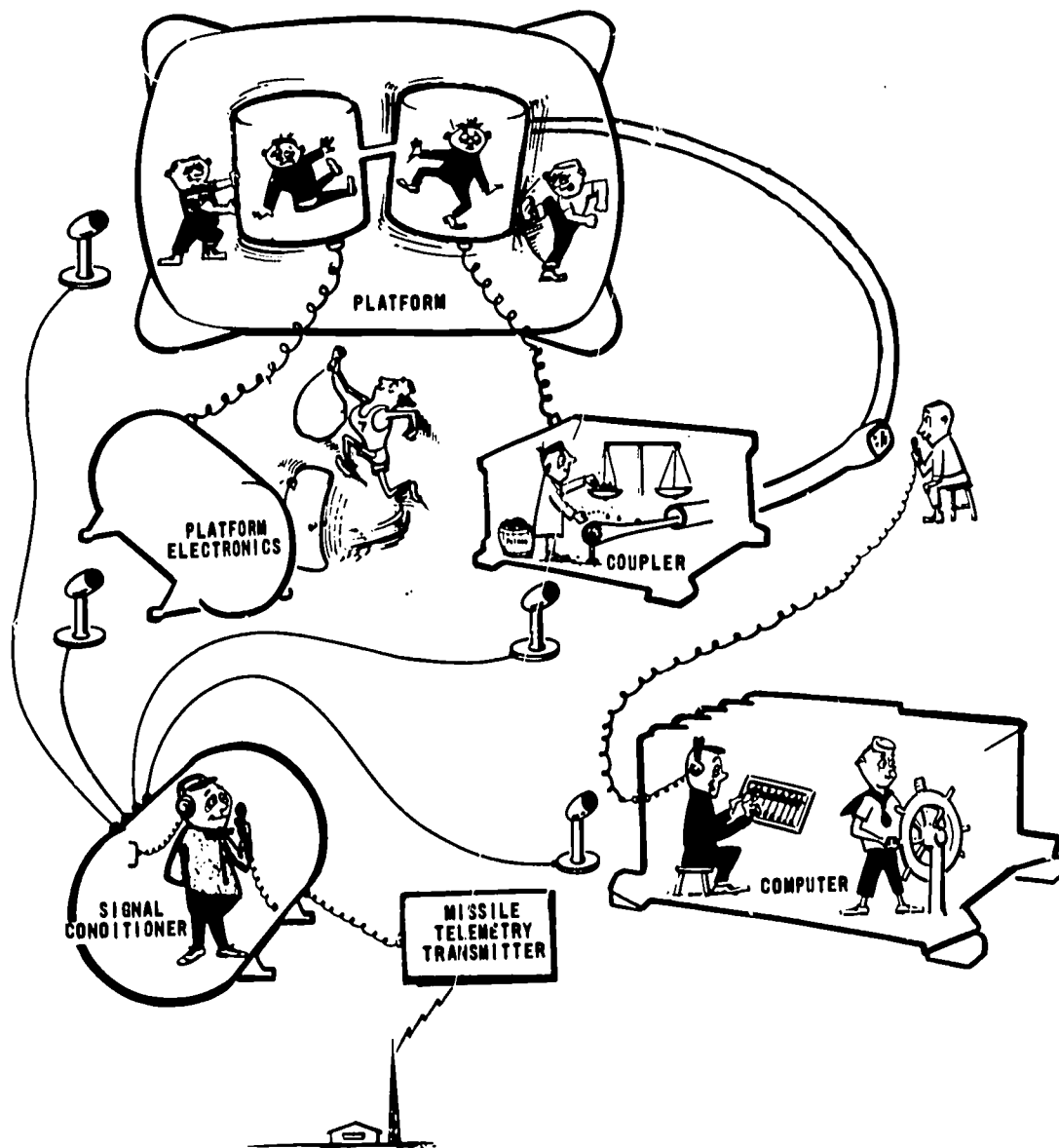
Figure 12-18. - Interrelation of components of Centaur guidance system.

As long-distance air travel increases and as space travel becomes more common, inertial navigation systems will be relied upon more heavily to perform the guidance and navigation functions for these modes of transportation. Since no external information about the route of travel is necessary to perform inertial navigation, the use of inertial navigation systems will be valuable for space exploration and for long-distance flights over remote areas of the Earth where navigation aids are not available.

REFERENCES

1. Pitman, George R., ed.: Inertial Guidance. John Wiley & Sons, Inc., 1962.

2. Parvin, Richard H.: Inertial Navigation. D. Van Nostrand Co., Inc., 1962.

13. TRACKING

John L. Pollack*

The purpose of tracking is to establish the position-time history of a vehicle for observation, guidance, or navigation. The techniques employed are essentially the same for these various purposes. The required positional information consists of angular deviations from the line of sight between the tracker and the target and possibly angular rate deviations. From these data the position, range (distance from the tracker), altitude, velocity, and acceleration of the vehicle can be calculated. Extrapolation of the data can be used to predict the path of the vehicle and to provide guidance and control information to alter its flight. In the case of unknown satellites, successive observations can be used to determine the actual size, shape, and surface area of an orbiting vehicle. By using known orbital data it is possible to follow the satellite's path in reverse order and determine its actual launching point on the Earth.

Many tracking systems employ the technique of locating two or more trackers on well-established baselines and applying the principles of intersection and triangulation to obtain positional data. This method of tracking is most applicable to model rocketry and is explained in the excerpt from reference 1 given in the section TECHNIQUE OF TRACKING MODEL ROCKETS.

The two principal types of tracking systems employed by NASA at its launch sites at Cape Kennedy and Vandenberg Air Force Base are radar and radio systems and optical systems.

RADAR AND RADIO TRACKING SYSTEMS

These systems employ radio frequencies from 100 kilocycles to 30 000 megacycles. Below this frequency range, antennas with adequate directivity become unpractically large, and ionospheric propagation difficulties become severe. Above this frequency range there are practical limitations on the power that can be generated. There are also regions near the upper end of this frequency range that must be avoided because of water vapor absorption and attenuation due to scattering by rain. In tracking against a background of cosmic noise certain frequencies must also be avoided.

---

*Head, Optics Section.

Radar systems are classified into active and passive systems. An active system requires transmitting equipment in the vehicle, and this equipment is generally referred to as a beacon or transponder. Passive systems depend on the reflective properties of the vehicle to return the incident radio waves. These reflective properties may be enhanced by the use of special reflectors, or they may be degraded by special surface treatment. Active systems are generally superior to passive systems with respect to range capability and tracking accuracy, but their requirement of special equipment on board the vehicle is a disadvantage.

Depending on the method of measuring range, radar tracking systems are also categorized as continuous-wave systems or pulsed systems. Angle measurements are sometimes accomplished by a scanning technique in which the antenna position is moved either by mechanical or electronic means about the direction of maximum signal return. This method is employed by the more conventional types of radar and by some of the radio telescopes used in radio astronomy. Another method of measuring angles uses the principle of the interferometer to compare the phases of signals received in separate antennas on well established base lines. The frequency of the return signal from a vehicle being tracked depends not only on the transmitted frequency but also on the relative motion of the vehicle and the tracker. This change in frequency due to the relative motion of the vehicle and the tracker is known as the Doppler effect and necessitates designing the tracker to follow automatically the changing frequency. This frequency change, or Doppler effect, can be used to measure the relative velocities of the vehicle and the tracker. (Ref. 2 presents an excellent exercise on the use of the Doppler effect in satellite tracking.)

OPTICAL TRACKING SYSTEMS

Optical systems make use of the visible light portion of the electromagnetic spectrum. (Usually, ultraviolet and infrared systems are also included in this category.) All optical trackers consist essentially of a telescope mounted on gimbals to permit rotation about two axes. One type of tracker, the cinetheodolite, produces a photographic record of the position of the target image with respect to cross hairs on a telescope; it also provides azimuths, elevation angles, and timing indications on the film. With two or more such instruments on an accurately surveyed base line, the position of a target in space is obtained by triangulation. Tracking is usually manual or partially manual. Another type of optical tracking instrument is the ballistic camera, which determines angular position by photographing the vehicle against a star background. This instrument

90 000 ft

IGOR, ROTI, TELEMETRY,
RADAR, CW RADAR TO
END OF SYSTEM RANGE

CINE-THEODOLITE

6000 ft

CZR
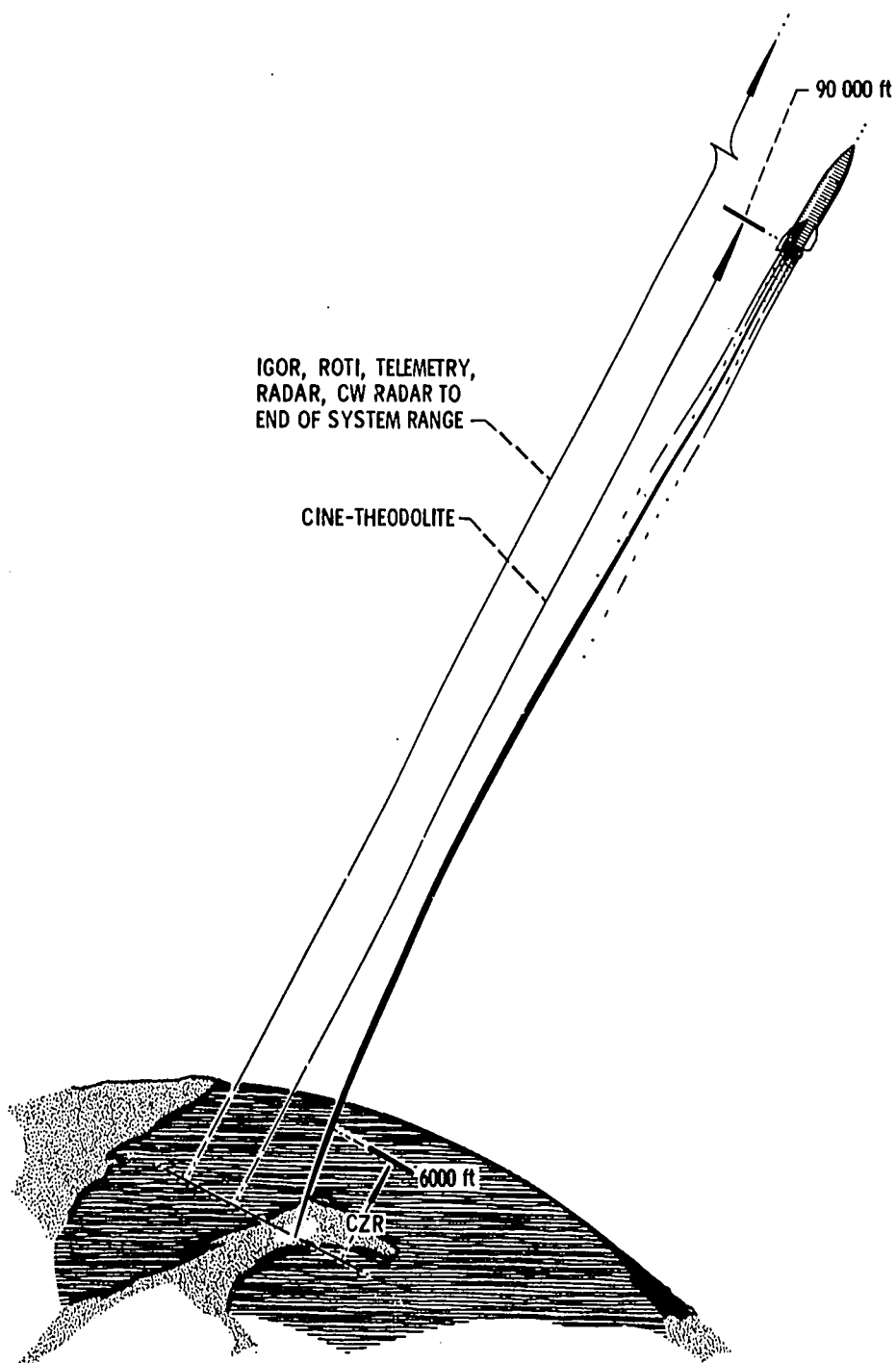
Figure 13-1. – Typical tracking coverage of missile launch. (CW, continuous wave; CZR, camera, special ribbon frame; IGOR, intercept ground optical recorder; ROTI, recording optical tracking instrument.)
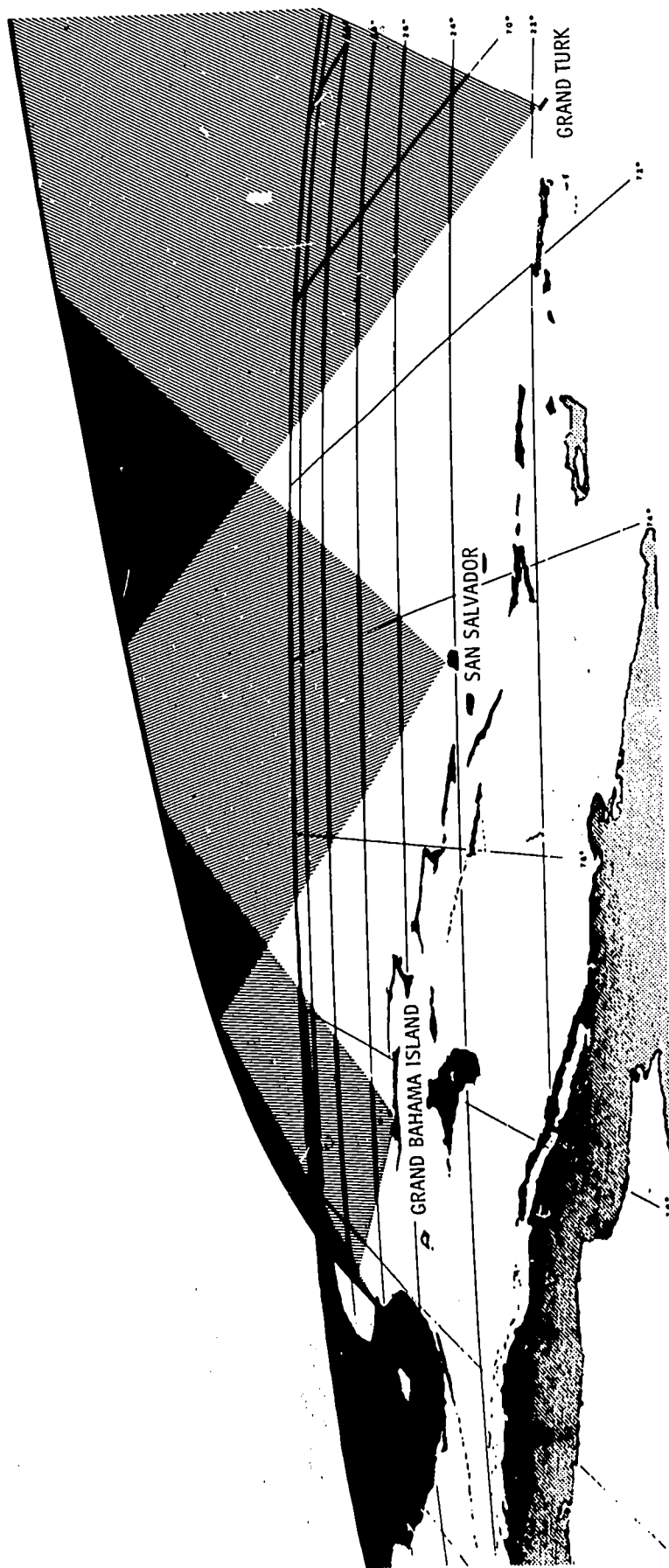
Figure 13-2. – Typical pulse-radar tracking coverage during midcourse phase of flight. (Midcourse phase extends from end of launch phase to some arbitrary point in space or time when terminal phase begins.)

GRAND TURK

SAN SALVADOR

GRAND BAHAMA ISLAND
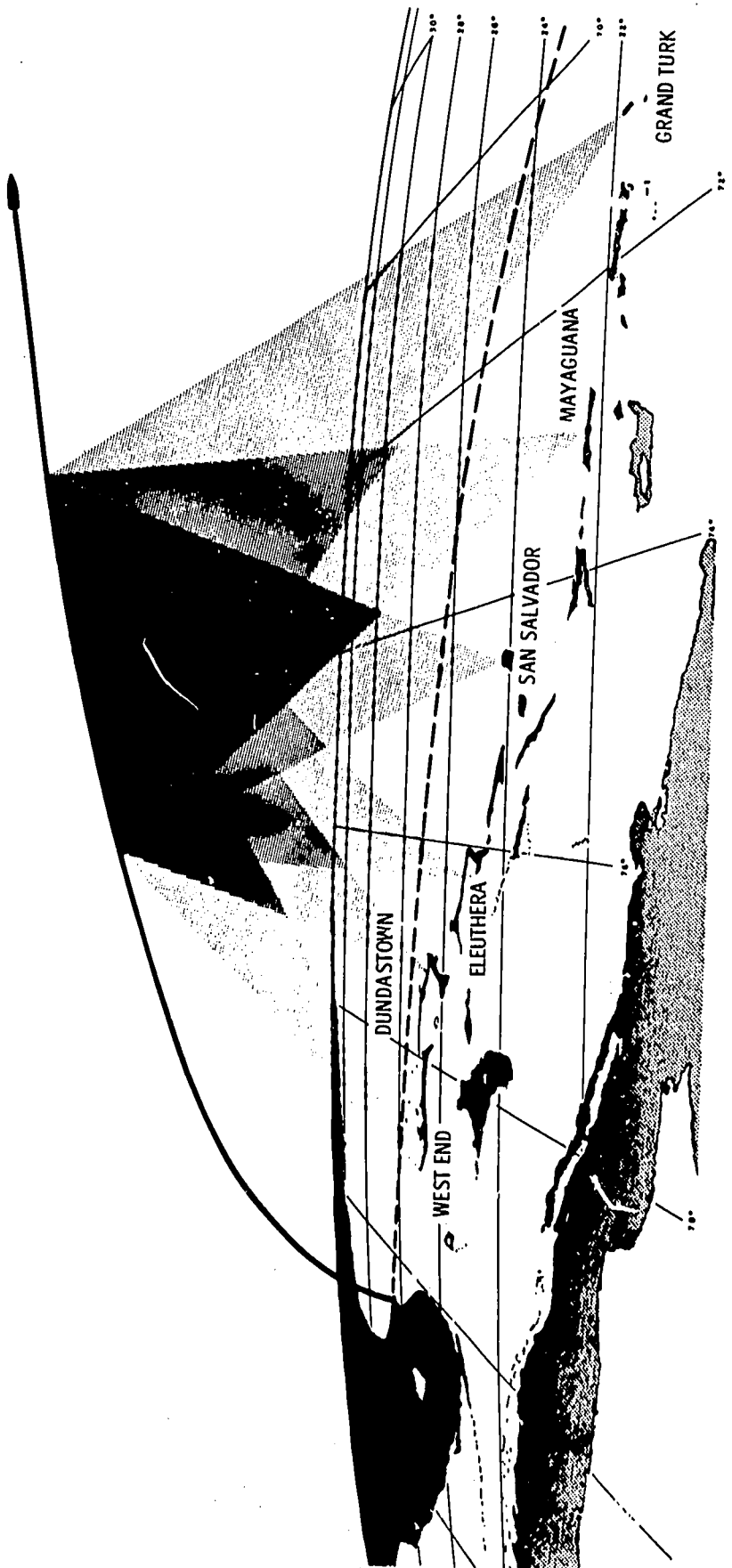
Figure 13-3. – Typical ballistic-camera tracking coverage during postburnout phase of flight.

GRAND TURK

MAYAGUANA

SAN SALVADOR

ELEUTHERA

DUNDASTOWN

WEST END

213

is capable of a very high order of accuracy, but the data require special processing by skilled personnel, and the time delay involved is sometimes a disadvantage. Schemes for making some or all of the procedures automatic are under development.

Angle tracking with optical equipment can be accomplished with much greater precision than with radio equipment, but darkness, clouds, and haze limit the usefulness of optical equipment. Another important limitation of optical trackers is the fact that data reduction often delays the output beyond the period of usefulness. Automating procedures are under development.

For tracking certain objects some advantages may be gained by using ultraviolet or infrared radiation. Ultraviolet radiation in certain rocket exhausts and the infrared radiation from rocket engines may provide better contrast with the background radiation. Infrared radiation also penetrates fog, clouds, and haze more readily. Newer developments include the use of photoelectric detection and scanning techniques to permit automatic readout of angular position information. Television techniques to improve sensitivity, selectivity, and rapid readout are also in use. Laser trackers are being developed. An up-to-date review of optical tracking techniques and new developments is presented in reference 3.

Radar and optical techniques complement one another at NASA launch sites. In general, optical techniques are used primarily in the launch phases of flight and for exact permanent records, while the radar systems encompass the globe and are used for in-flight guidance corrections. Figures 13-1 to 13-3 show typical tracking coverage in the vicinity of Cape Kennedy. There are about eight different radar systems and 30 large tracking cameras capable of being deployed on this range. These systems are identified by their acronyms in the figures.

TECHNIQUE OF TRACKING MODEL ROCKETS

Tracking of model rockets utilizes the same principles of intersection and triangulation as those used by NASA. Because of cost and complexity, radar tracking methods are not used in model rocketry; instead, optical techniques with manual readout of data are employed. The main goal of tracking a model rocket is to obtain the maximum altitude of the rocket. Using two visual pointers - with or without optical aids - and employing trigonometry is the most practical way of obtaining this information.

Before choosing a measurement technique or a particular measuring instrument one must determine the accuracy required to fulfill the goal; judgment is the key factor here. If too high an accuracy is demanded, costs and complexity rise sharply. We have chosen to follow the guidelines of the National Association of Rocketry (NAR) in the adoption of

220

the 10-Percent Rule. This rule and its application are described in the excerpt from the Handbook of Model Rocketry (ref. 1, copyright 1965, 1967), reprinted by permission of the Follett Publishing Company. The application of trigonometry to the determination of maximum altitude, the use of the NAR flight sheet, and the use of the NAR "Quickie Board" are also described in this excerpt. (The basic trigonometric functions - sine, cosine, and tangent - have already been defined in chapter 9.)

The excerpt from reference 1 is as follows:

The tracking situation is shown diagrammatically in Figure [13-4].

The theodolites are set up and leveled so that their azimuth dials are horizontal. They are zeroed in by sighting at each other along the base line. While zeroed in, their azimuth and elevation dials are set at zero.

When the model is launched, both station operators follow it up in flight until it reaches maximum altitude. Tracking then ceases, and the scopes are locked in final position or left undisturbed. Azimuth and elevation angles on each theodolite are read. On some ranges, this data is communicated to the launch area by means of a telephone system. On other ranges, data is recorded at each tracking station and later taken to the launch area for final reduction.

We now have a tracking situation with a known distance between two stations, plus an elevation and an azimuth angle from each station. To understand how altitude is computed from this data, let's derive the equations to be used. Refer to Figure [13-4].

Given: Distance b
Angle $\angle A$
Angle $\angle D$
Angle $\angle C$
Angle $\angle E$
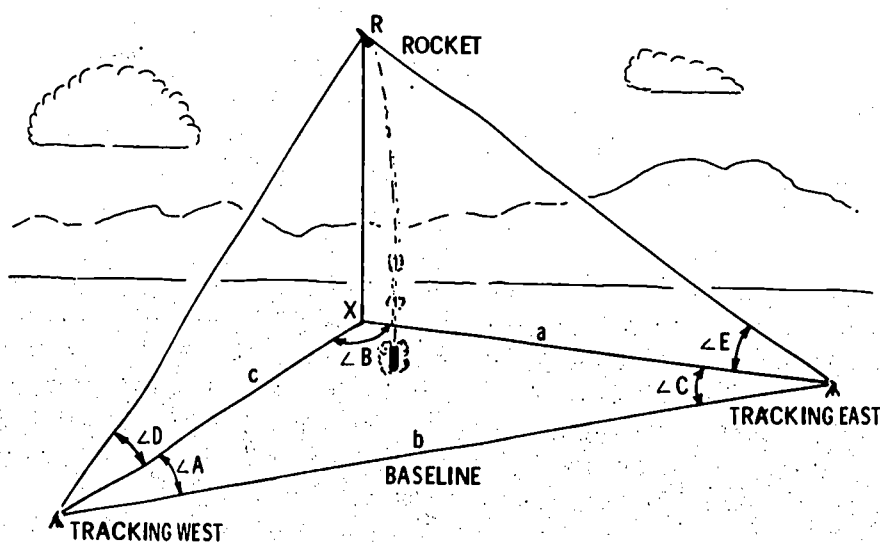
Figure 13-4. - Geometry of two-station tracking system. (From ref. 1.)

Point X is directly under the model R, and the distance RX is the altitude of the model. When we find distance a or c, we can then locate point X on the ground under the model and solve the triangles in the vertical plane to find RX.

There are two right vertical triangles (R-X-West and R-X-East). We can compute both separately and average the value RX obtained from both, thus giving a more accurate altitude reading.

The Law of Sines in trigonometry states:

$$\frac{c}{\sin \angle C} = \frac{b}{\sin \angle B} = \frac{a}{\sin \angle A}$$

Therefore:

$$c = \sin \angle C \frac{b}{\sin \angle B} = \sin \angle C \frac{b}{\sin[180^0 - (A + C)]}$$

Since R is directly above X by definition, the angle R-X-West is a right angle. We can therefore compute the western triangle as follows:

$$\tan \angle D = \frac{RX}{c}$$

$$RX = c \tan \angle D$$

Substituting for c:

$$RX = \sin \angle C \tan \angle D \frac{b}{\sin[180^0 - (A + C)]}$$

The other right vertical triangle is solved in a similar manner to give:

$$RX = \sin \angle A \tan \angle E \frac{b}{\sin[180^0 - (A + C)]}$$

The two values of RX are then compared. If they are off by more than about 10 per cent, somebody goofed on tracking. If they are close, it means that "the triangles closed." By adding the two values together and dividing by two, or averaging them, the resultant altitude is very close to that actually achieved by the model.

However, since tracking is usually carried out to the nearest degree of arc, there are errors in the system, and the NAR has adopted a "roundoff" procedure to compensate for these. If the last digit of the average altitude is 1 to 4, it is dropped to zero. If it is 6 to 9, it is raised to the next 10-foot interval. In the case of the digit 5, the rule is: Keep it even. If the 5 is preceded by an even number, the 5 is dropped to zero. If preceded by an odd number, it is raised to the next 10-foot interval.

222

In addition to the "roundoff," NAR has also adopted the 10 Per Cent Rule for acceptable tracking data. According to the rule, there has been good tracking if the altitude readings from the two triangles are within 10 per cent of the rounded-off average.

To see how all of this works, let's take an example and work it through.

Given a 1,000-foot base line:
Tracking East azimuth: 23° ($\angle C$)
Tracking East elevation: 36° ($\angle E$)
Tracking West azimuth: 45° ($\angle A$)
Tracking West elevation: 53° ($\angle D$)

For one triangle:

$$RX = \sin \angle C \, \tan \angle D \, \frac{b}{\sin[180^O - (A + C)]}$$

$$= \sin 23^O \times \tan 53^O \, \frac{1,000}{\sin[180^O - (45^O + 23^O)]}$$

$$= .391 \times 1.33 \times \frac{1,000}{\sin 68^O}$$

$$= .391 \times 1.33 \times 1,079$$

$$= 561 \text{ feet}$$

Solving for the other triangle by the same means, we get $RX = 555$ feet.

Averaging, the altitude is 558 feet. Rounding off, this is 560 feet. Ten per cent of 560 feet is 56 feet. Both 561 and 555 are within 56 feet of the average. The track is good.

Since the complex term on the far right of the equation is the same when solving either triangle, it can be precomputed as a table of $1,000/\sin \angle B$.

A rapid method of this data reduction has been developed by John Roe, of Colorado Springs, Colorado, and used in the NAR for many years. Each model flown has a flight sheet on which is recorded the angles from both stations. Also printed on the sheet are the sine and tangent tables, plus the table for $1,000/\sin \angle B$. This flight sheet is shown in Figure [13-5], filled out for the flight we just reduced above. This fast method requires only some multiplication with the use of a slide rule. So it's a good idea to learn how to use a slide rule if you want to compute altitudes fast.

To provide even quicker data reduction, John and Jim Bonine, of Denver, Colorado, worked out their "Quickie Board" analog computer in 1960. This is shown in modified form in Figure [13-6]. It is set up for both 1,000-foot and 2,000-foot base lines. Although it is a graphical method, it is very accurate, even in small size. First, the azimuth angles from both stations are drawn out

Figure 13-5. - NAR flight-sheet method of data reduction. (From ref. 1.)

Name Tom TRUE NAR # 50 Date 9-12-62

Model name GARGOYLE Motor type 2 A.8-4

National Association of Rocketry

RANGE FLIGHT SHEET

Tracking East: Azimuth (∠A) 23° sin .391 (1) Elevation (∠D) 36° tan .727 (2)

Tracking West: Azimuth (∠C) 45° sin .707 (3) Elevation (∠E) 53° tan .33 (4)

6B = ∠B. Table value 1079 (5)

V = 1000' ÷ sin ∠B

b=1000'

SAFETY APPROVAL

Recorder _____ Track lost ☐

Launcher R-5 _____ Misfire ☐

Launcher _____ Misfire ☐

Launcher _____ Misfire ☐

(5) x (2) x (3) = 551

(5) x (4) x (1) = 561

÷2 538

= average altitude

Figure 13-6. – NAR "Quickie Board" altitude computer. (From ref. 1.)

to an intersection. To compute the triangle for Tracking West, swing the intersection point down to the base of the graph with the Tracking West point as the center of swing. Draw a vertical line upwards from this intersection. Set up the elevation angle from Tracking West; where this line intersects the vertical line, read over to the edge for the length of base line, and read altitude directly. For Tracking East, carry out the same operations around the Tracking East point.

RANGE LAYOUT

The final layout of the firing range takes into consideration the various topographical features of the site, such as woods, hills, streams, roads, buildings, etc.; meteorological factors, such as wind direction and the position of the Sun, must also be considered. In addition to these considerations, the ideal elevation angles and azimuths are also determining factors in the positioning of the trackers.

Elevation Angle

Visual sightings, even with the use of aids such as telescopes, are only approximate, and the elevation angle read by an observer should be in the range which will be most conducive to the most accurate reading possible. Too small elevation angles (less than 25°) or too large angles (greater than 60°) increase the likelihood of a greater margin of error in determining elevation. Generally speaking, if the tracking stations are too close to the launch site, the elevation angles will be relatively large (approaching 90°) and, therefore, unreliable; if the trackers are too far from the launch site, the elevation angles will be small (approaching 0°) and equally unreliable. The sketch below shows that elevation angles taken from point W are approximately 64°, which is too large for accuracy. (When you look straight up, it is difficult to estimate how high in the air an object is.) For large elevation angles, a large difference in altitude is reflected as only a small

Distance of tracker from launch site, ft
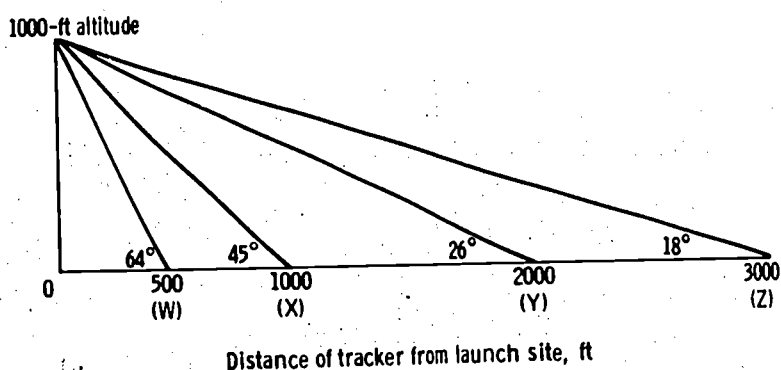
difference in the angle, because the angle is calculated from the tangent function, which increases to infinity as the angle approaches 90°. Also, readings taken from point Z are relatively inaccurate, because when the tracker is too far from the launch site and the elevation angle is small, even a substantial change in altitude does not cause a large enough difference in the elevation angle.

A rule of thumb is that the distance of the tracking station from the launch site should be at least equal to, but not more than twice, the expected altitude of the rocket. Positioning the tracking stations according to this rule will provide ideal elevation angles of 25° to 60°. Obviously, if rockets of greatly varied altitude capabilities are to be launched from the same site, several sets of tracking positions must be established.

Azimuth

The ideal intersection angle between the azimuths from any two tracking stations is 90°. If the intersection angle is too small (approaching 0°) or too large (approaching 180°), it is difficult to determine accurately the point of intersection. For full-scale launch sites, such as Cape Kennedy, where the missile range is basically a chain of islands, it is often impossible to set up tracking stations in the ideal locations. For model rocket launches, however, a site can usually be found which has the desirable topographical features and meteorological conditions, and the range can be laid out to approximate the ideal configuration from the standpoints of elevation angle and azimuth.

The importance of proper tracking-station positions and base-line layout is shown in figure 13-7. Figure 13-7(a) shows tracking-station locations which provide relatively

(a) Properly located tracking stations.

(b) Improperly located tracking stations.
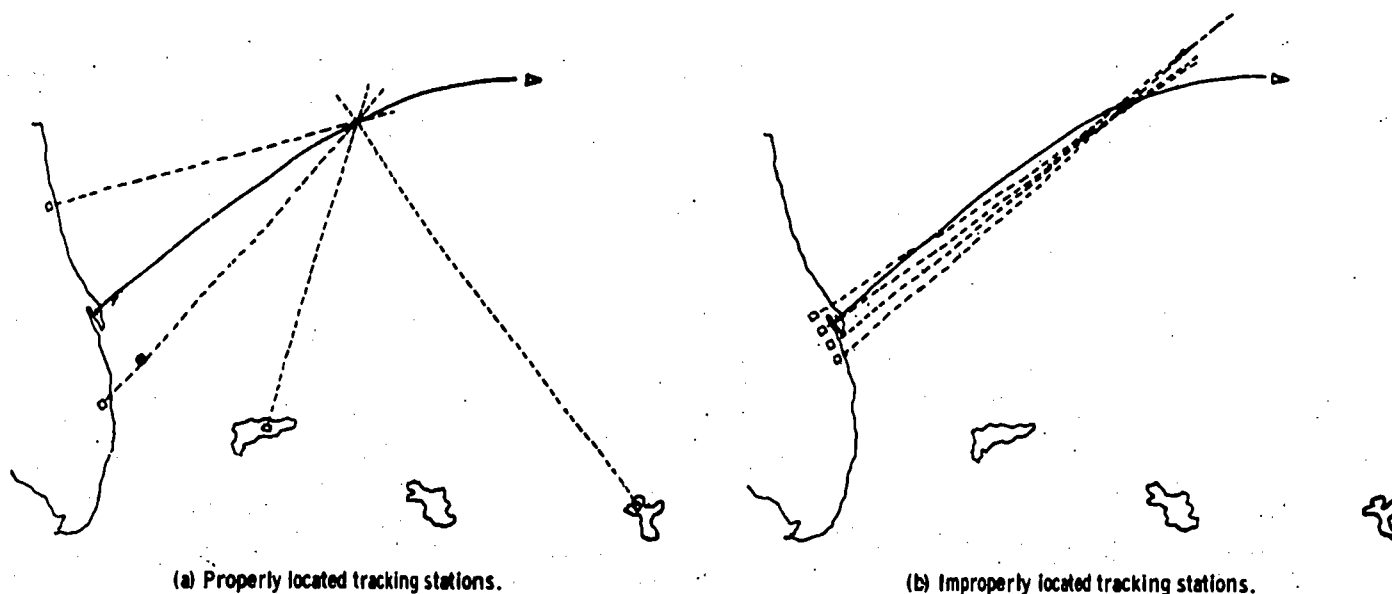
Figure 13-7. – Azimuthal location of tracking stations. (From ref. 4.)

good azimuth intersection angles. Here, the range layout cannot provide the completely ideal intersection angles of 90° because the range is a chain of islands and the trackers have to be located on these islands. However, the intersection angles are large enough to show clearly the point of intersection of the various azimuths. Four improperly located tracking stations are shown in figure 13-7(b). With such small intersection angles the azimuths are almost parallel, and their exact point of intersection is very difficult to determine.

Sometimes, imprecise intersections of azimuths may be obtained even from well-situated tracking stations. The azimuth from one tracking station may fail to pass through the common point of intersection of the azimuths from the other stations (fig. 13-8(a)). In such a situation, the azimuth which failed to pass through the common point of intersection would be disregarded, and a thorough investigation would be made to determine the cause of this stray azimuth. Figure 13-8(b) shows azimuths from various tracking stations intersecting at random. (For a postburnout, ICBM trajectory, typical separation of the various intersection points would be about 15 to 25 ft.) In this case, the most probable common point of intersection would be obtained by averaging.
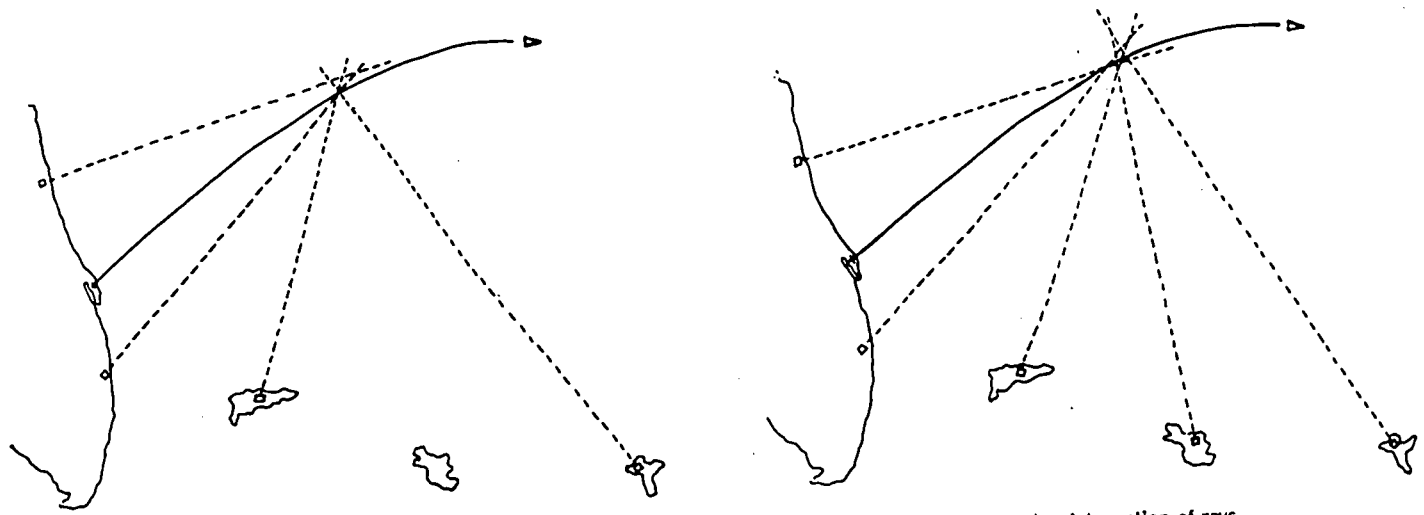
(a) Failure of one ray to pass through common intersection point of other rays.

(b) Random intersection of rays.

Figure 13-8. - Typical tracking intersections. (From ref. 4.)

222

REFERENCES

1. Stine, G. Harry: Handbook of Model Rocketry. Follett Publishing Co. , 1965, pp. 230-237.

2. Thompson, Robert A.: Using High School Algebra and Geometry in Doppler Satellite Tracking. The Mathematics Teacher, vol. 58, no. 4, Apr. 1965, pp. 290-294.

3. Marquis, D. C.: Optical Tracking; a Brief Survey of the Field. Appl. Optics, vol. 5, no. 4, Apr. 1966, pp. 481-487.

4. Glei, A. E.: The Design and Operational Philosophy of the Ballistic Camera Systems at the Atlantic Missile Range. J. Soc. Motion Picture Television Eng. , vol. 71, no. 11, Nov. 1962, pp. 823-827.

14. ROCKET LAUNCH PHOTOGRAPHY

William A. Bowles*

Ever since May 5, 1961, when astronaut Alan B. Shepard rode America's first manned spacecraft 302 miles down the Atlantic Missile Range, we have become accustomed to seeing dramatic photographs of space vehicles thrust spaceward by powerful rocket engines. These documentary pictures, however, represent only a minute part of the total role of photography in aerospace technology. Photography has long been recognized as a valuable and indispensable scientific tool. The human eye cannot review or recall the image of an object which it has previously seen, and neither can it prolong into minutes the split-second timing of an event. Conclusions drawn from the visual observation of a malfunction could be erroneous. On the other hand, photographic instrumentation enables engineers and scientists to make detailed and accurate analyses of problems, and it can show the reasons for the success or failure of a project.

The cameras used by aerospace scientists and engineers are highly specialized and unlike those used for home movies, snapshots, or news photography. Their capability of recording at high speed permits time to be frozen or to be extended to many times normal. This extension of time is accomplished by filming at rates of up to several thousand frames per second and then projecting (viewing) the film in single frames or at low frame rates. For example, if an occurrence is filmed at 24 frames per second and the film is projected at the same rate, the filmed sequence takes the same length of time as the actual occurrence. However, if the occurrence is filmed at 400 frames per second and the film is projected at 24 frames per second, the duration of the filmed sequence is $16\frac{2}{3}$ times as long as the duration of the actual occurrence. Filming at 5000 frames per second and projecting at 24 frames per second extends the duration of the filmed sequence to $208\frac{1}{3}$ times that of the actual occurrence.

Various types of cameras are used to record the trajectory, velocity, roll, pitch, and yaw of vehicles and to furnish statistical data at altitudes up to 40 or 50 miles. However, long before the vehicle is ready for flight, the testing of countless items, such as the umbilical-cord release, cooling-blanket removal, launcher release, nose-fairing separation for spacecraft ejection, etc., has benefited from photography.

Camera operating speed is not the only consideration in choosing photographic equipment to meet a particular requirement. Film sizes of 16, 35, or 70 millimeters may be

---

*Assistant Chief, Photographic Branch.

used. The 16-millimeter film can be used at higher camera speeds than can the 35- and 70-millimeter films, but the latter two sizes provide better image quality. Therefore, the larger sizes are used when the need for superior image quality exceeds the demand for high frame rate (camera speed).

Telescopic lenses of extremely long focal lengths (up to 500 in.) are used to provide data on missiles at high altitudes. Such lenses have effective ranges up to 100 000 feet and are located approximately this same distance from the launch pad. This location provides a good elevation angle, if the lens is used for tracking, and a good overall view of the missile, if the lens is used for general observation. (The principles of good camera positioning are discussed in chapter 13.) The image size factor must also be considered in the selection of a camera location. For any given lens, the image completely fills the frame when the subject is at some specific distance from the camera. Therefore, if the camera is located too close to the subject, the image size becomes excessive.

In addition to photographing missiles at high altitudes, it is also necessary to film small areas of action on or near the vehicle during the critical lift-off period. For these requirements, lenses with much shorter focal lengths are used, and the cameras are mounted at the base of the vehicle and on the service and umbilical towers. Some requirements may involve the study of an area only 6 inches square, and the camera which is used to fulfill such a requirment may encounter temperatures in excess of 2500° F. The camera must be protected against these high temperatures by means of a special housing cooled by an inert gas (usually nitrogen). The gas is fed into the protective housing, and then, by means of exhaust ports, it is routed across the cover glass to minimize fogging or condensation. The inert-gas purge acts as a safety factor in preventing the ignition of the rocket-fuel vapors by the electrical system of the camera. The engineering value of photography can be increased considerably by using precise timing marks along the edge of the film. These marks enable the viewer to determine the exact timing of some particular occurrence.

The installation of 60 cameras is not an unusual requirement for a major launch. Each instrument is programmed to perform a special function. Some photographic requirements cannot be fulfilled by ground-based equipment. For example, studies of zero-gravity effects inside the fuel tanks or observation of the staging of the spacecraft necessitate the installation of photographic or television equipment within the vehicle.

The possibilities of optical and photographic instrumentation are practically unlimited. With its constant technological advances, space age photography should continue to be a valuable scientific tool.

Figures 14-1 to 14-12 were selected to illustrate the significant role of photography in rocket launch operations. The depth of detailed information to be derived from photography is obvious.
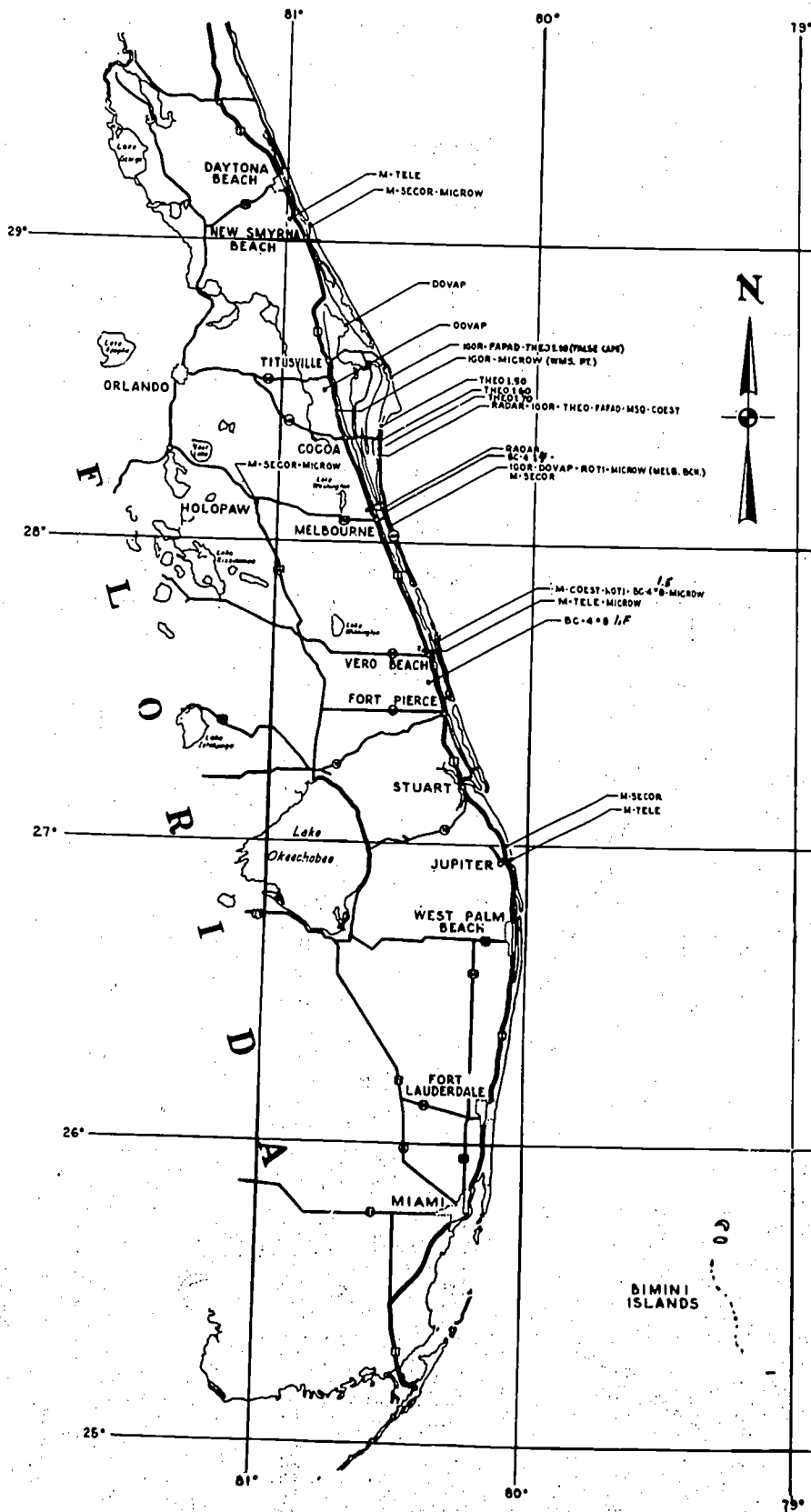
Figure 14-1. - Map of east coast of Florida showing locations of long-range cine-theodolite, Roti, and Igor tracking cameras. Extreme distances from launch sites required for triangulation and for image ratios with 350- to 500-inch lenses are also apparent.
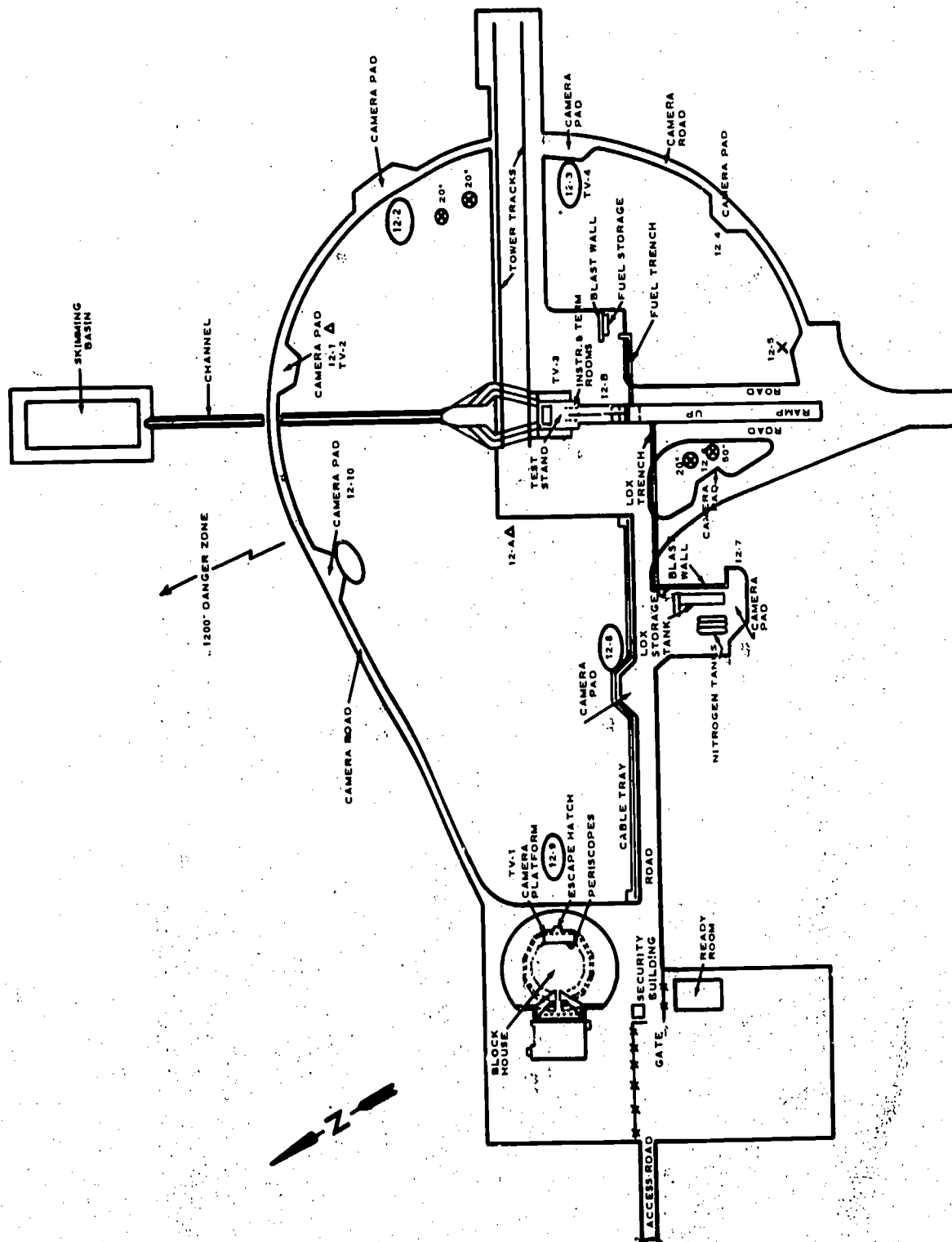
Figure 14-2. – Schematic drawing of typical launch complex (launch pad 12) at Cape Kennedy. Camera sites are indicated by complex number and camera locations clockwise around test stand. For example, 12-5 site is found at 5 o'clock from position North. Many of these sites have several cameras of various film sizes, frame rates, and focal length lenses. The actual camera installation depends upon particular vehicle requirements; 360°, or around-the-clock, coverage is necessary for evaluation of performance of any malfunction.
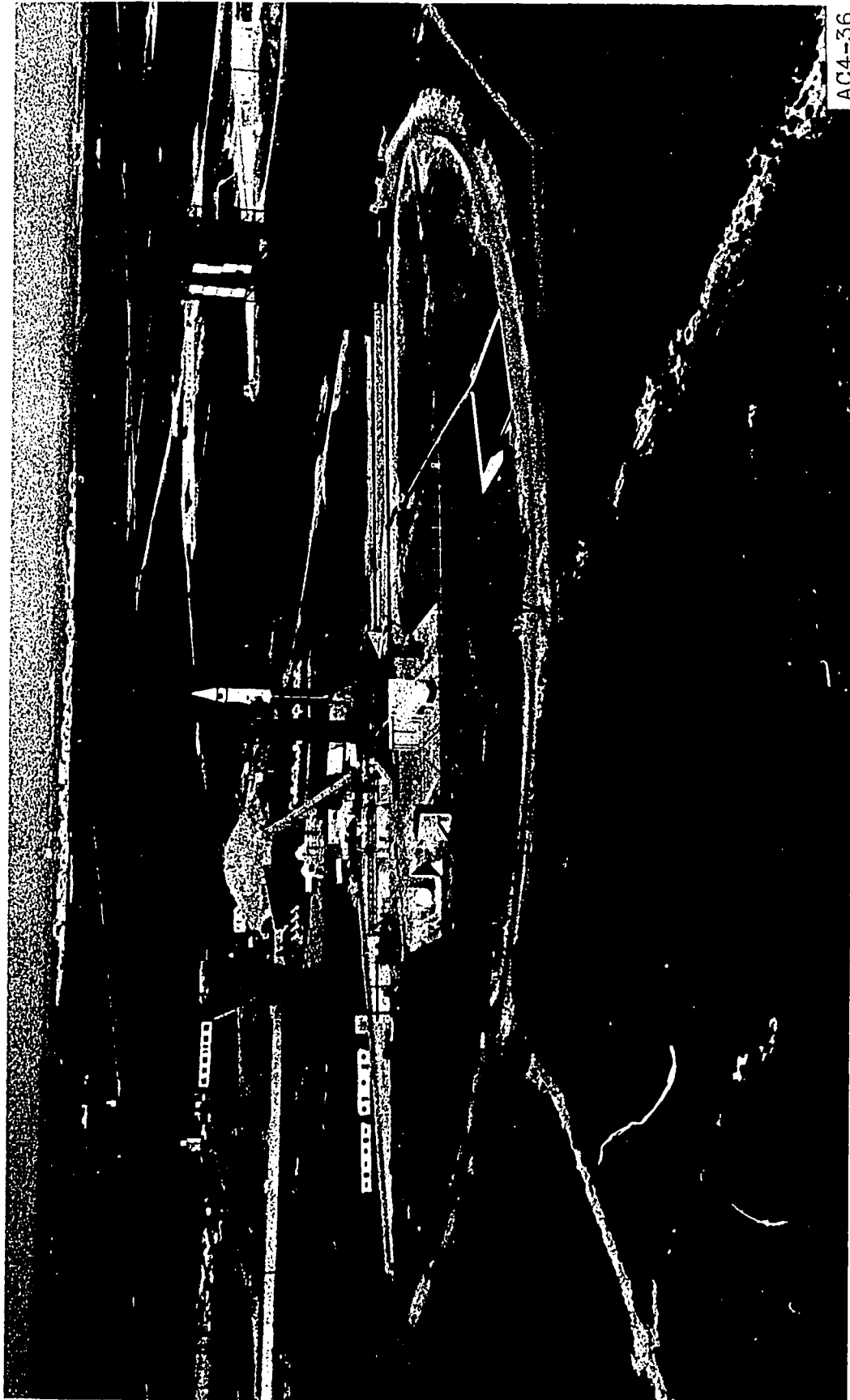
Figure 14-3. – Aerial view of Atlas-Centaur vehicle on launcher, with gantry, or service tower, rolled back.   Camera positions around perimeter road can be distinguished.

AC4-36
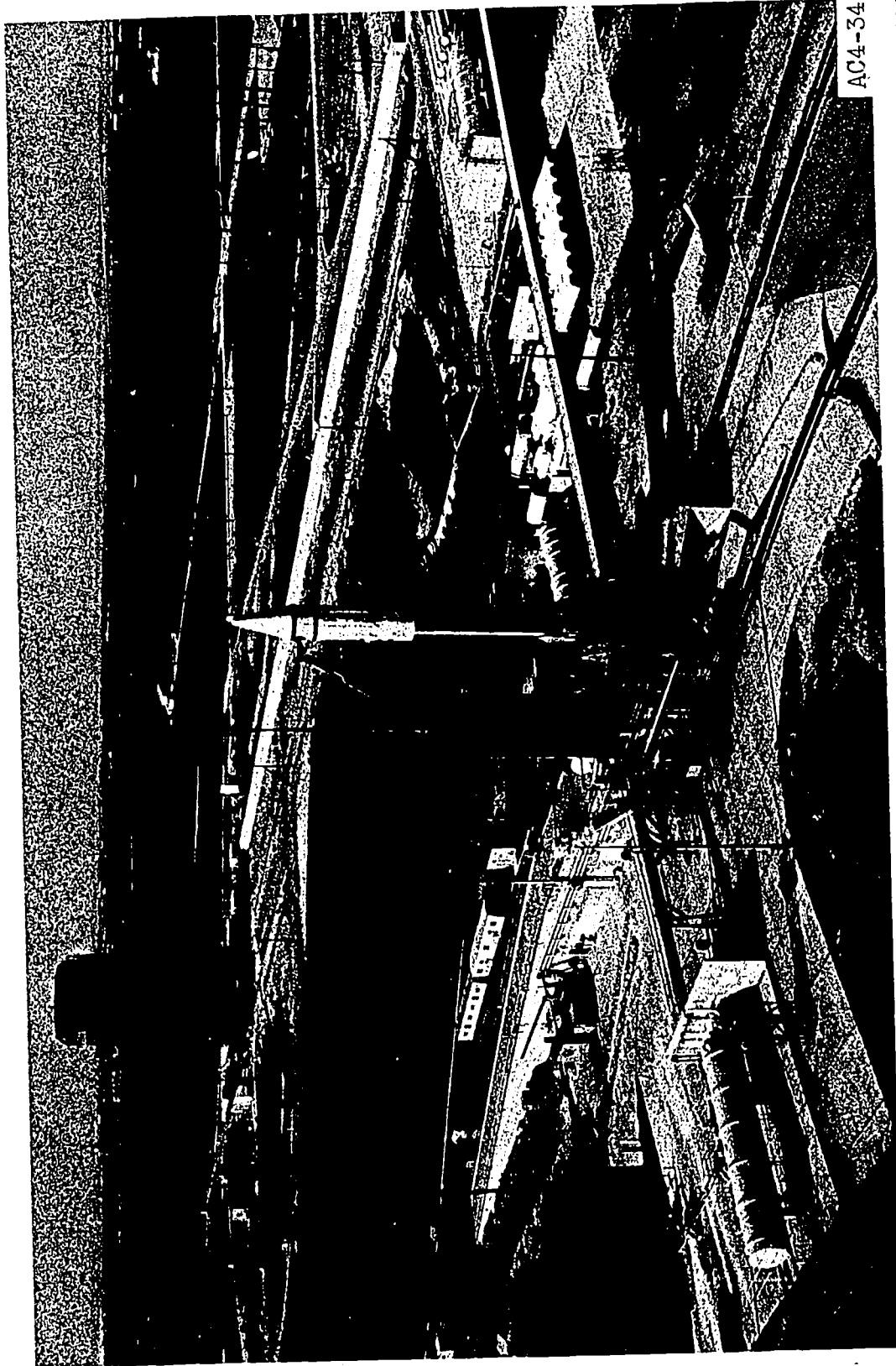
Figure 14-4. - Closeup aerial view of Atlas-Centaur vehicle and launch complex. Photographic instrumentation would provide data on launcher release action at base of vehicle, engine ignition, and umbilical-power disconnect action.
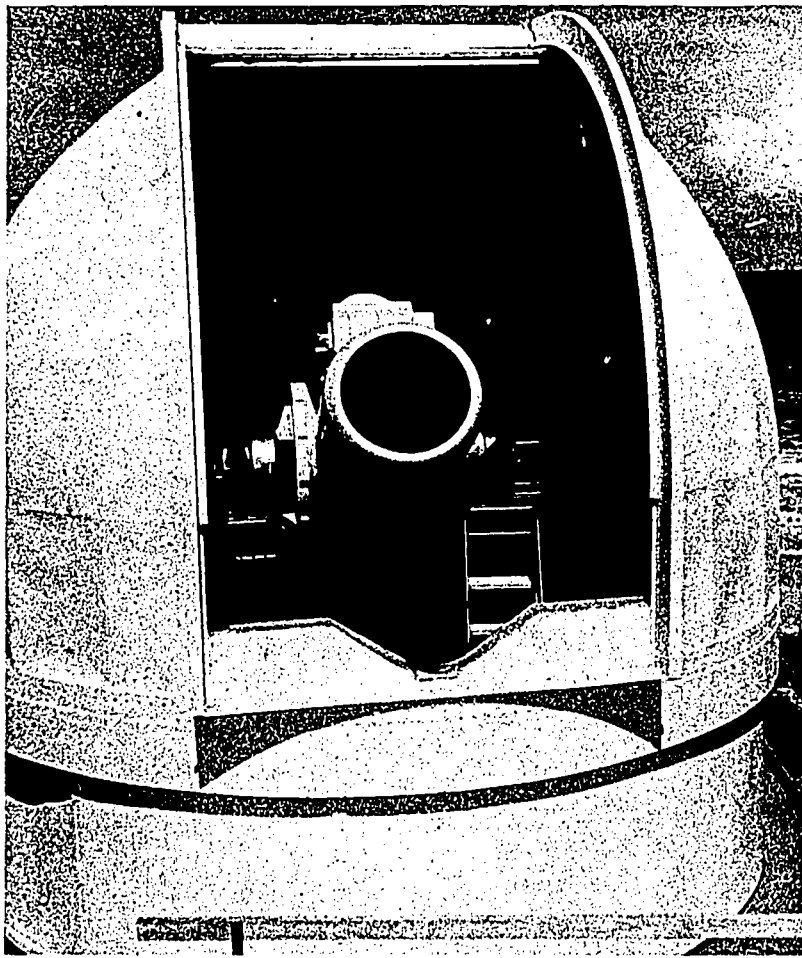
Figure 14-5. – Roti tracking camera with 500-inch lens. This camera is located at Melbourne Beach, over 20 miles from Cape Kennedy. Figure 14-7 was photographed by this camera when missile was at an altitude of 14 miles.
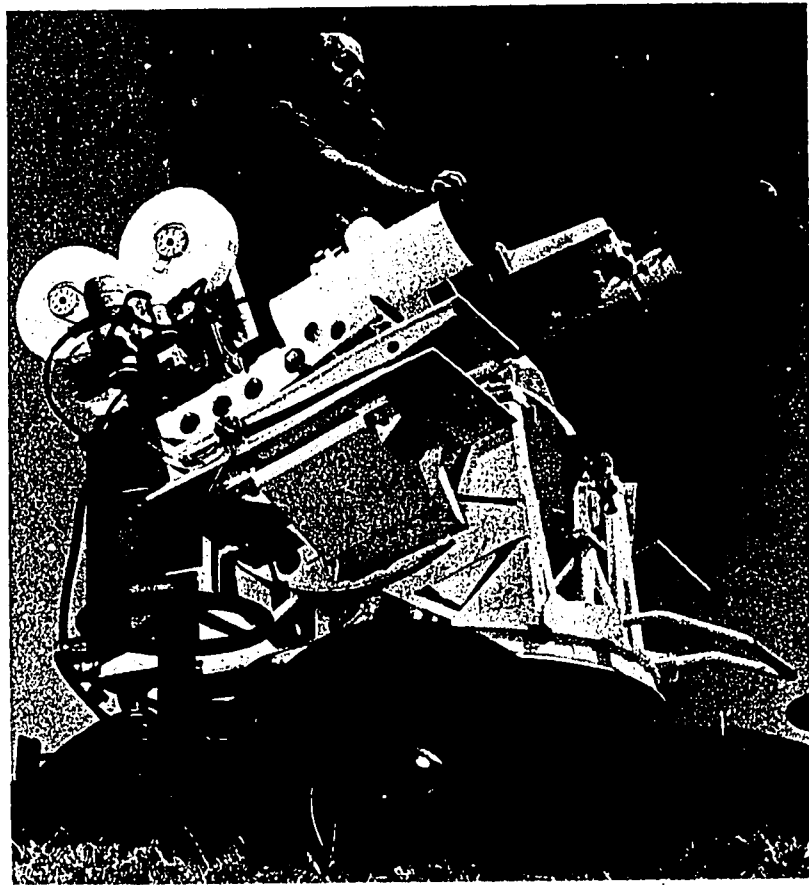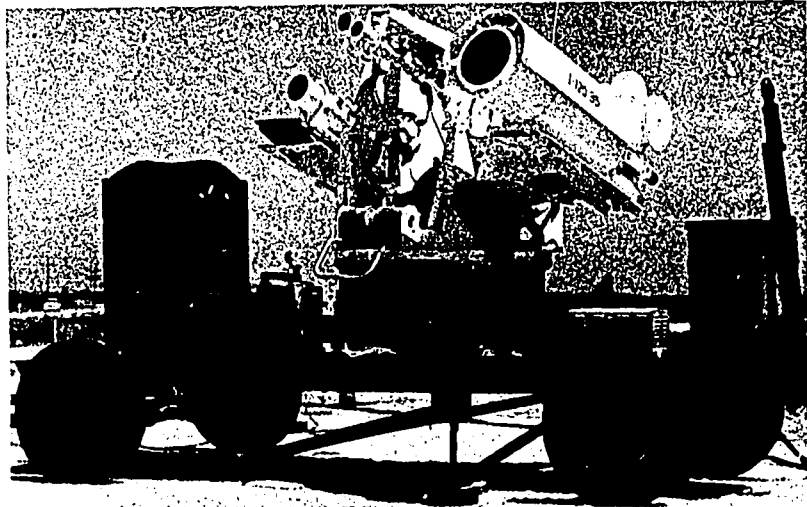
Figure 14-6. - Mobile optical trackers consisting of three to four cameras with lenses ranging in size from 20- to 120-inch focal length. These units are moved to suitable locations shown on Cape Kennedy map and operated by photographer seated on gimbal-mounted camera platform.

237

CS-37700
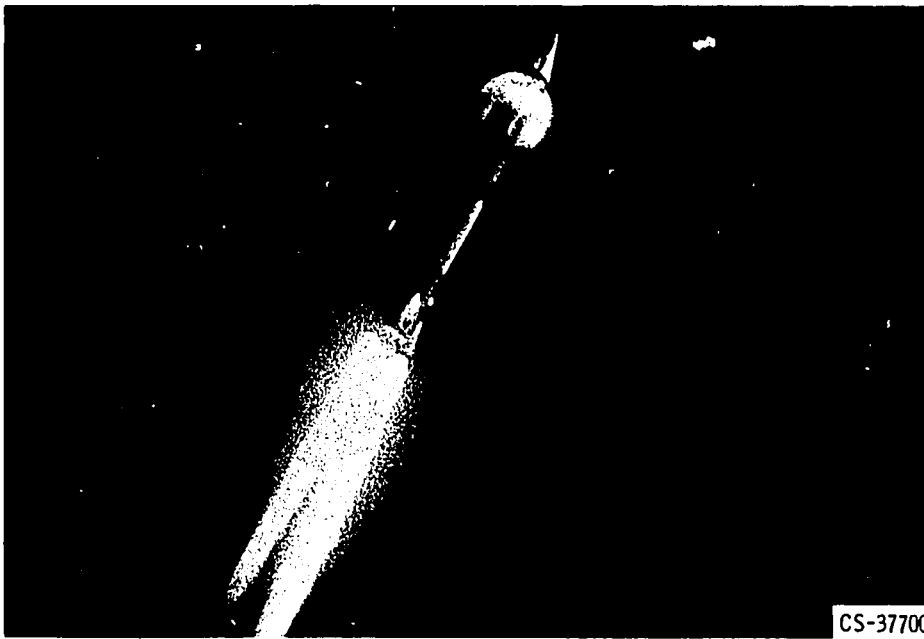
Figure 14-7. - Shock wave passing over nose cone of Atlas-Centaur vehicle. Photographed at altitude of 75 000 feet by Melbourne Beach Roti; lens, 500-inch focal length.
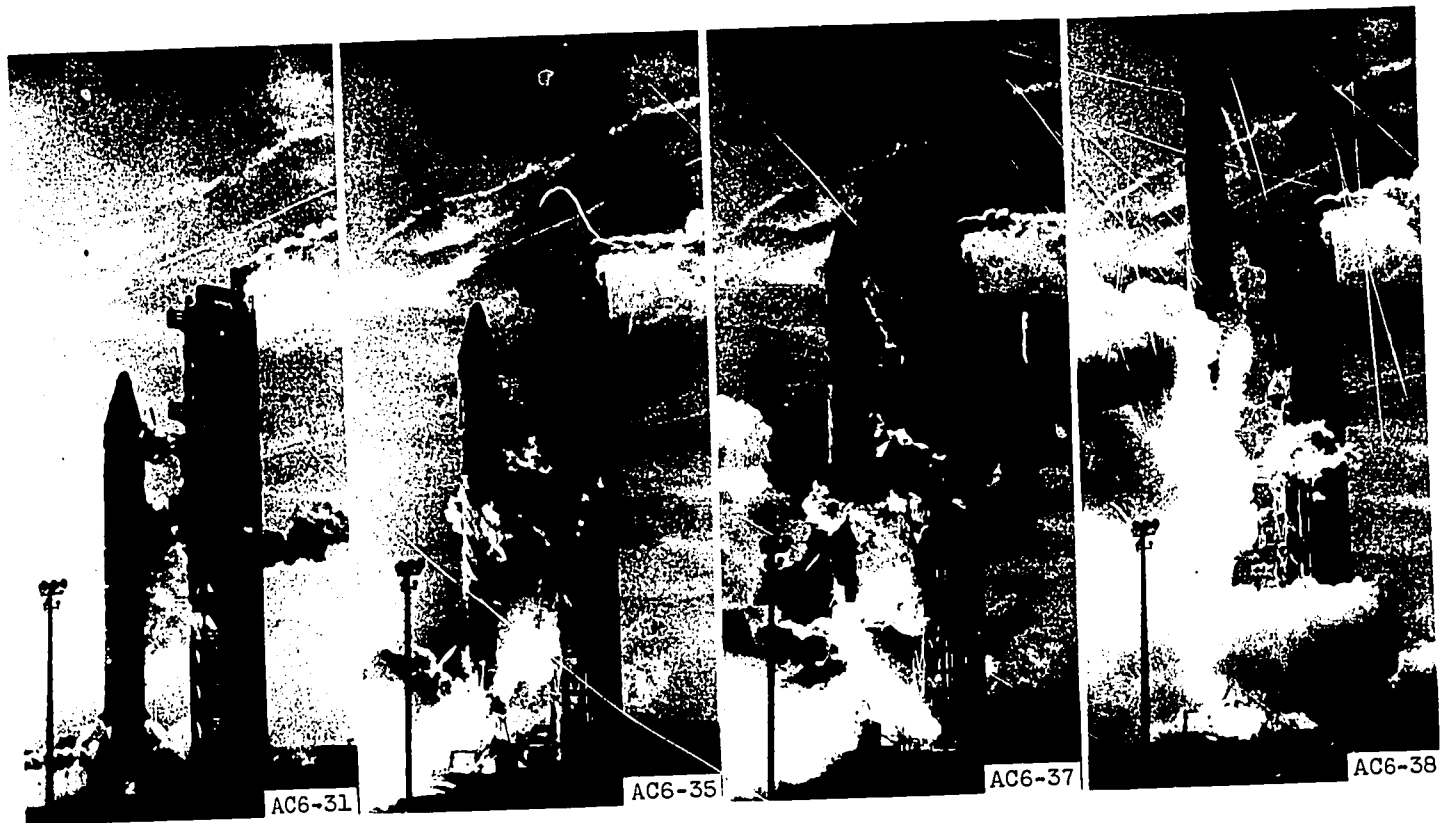
Figure 14-8. - Sequence of frames showing lift-off of Atlas-Centaur vehicle.
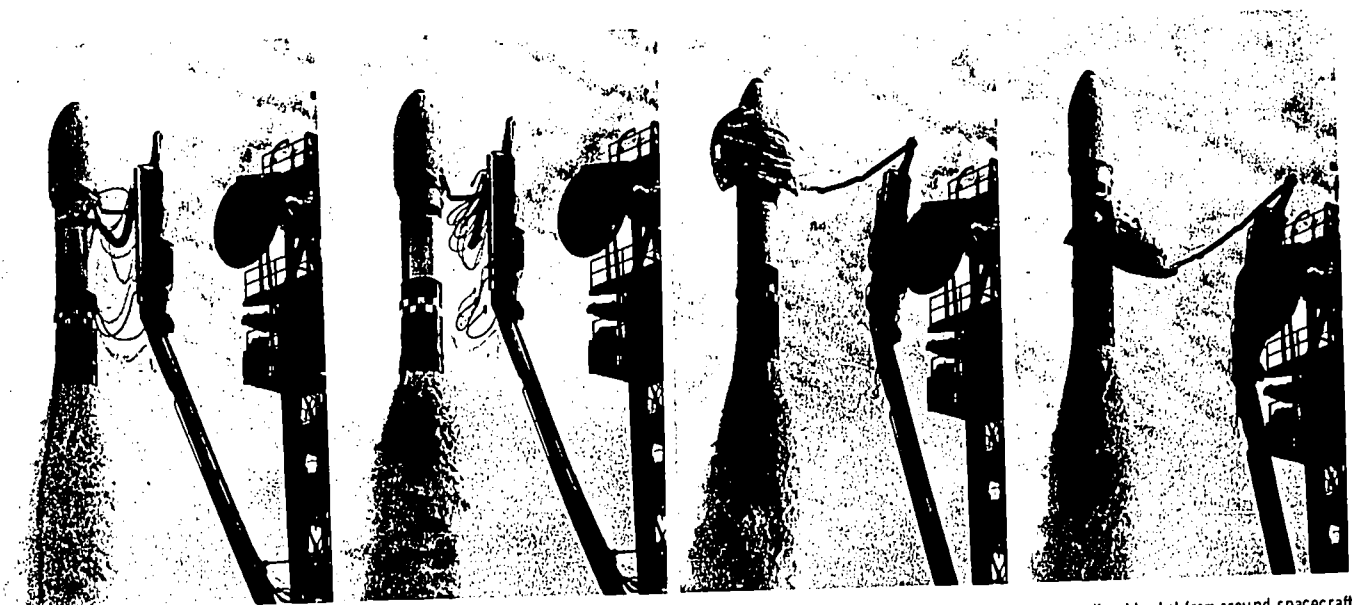
Figure 14-9. - Four frames from sequence showing general view of umbilical-cord and boom retraction. Notice removal of air-conditioning cooling blanket from around spacecraft. Installation of cameras is often required to study various small details included here. At times, camera concentration might be on one specific connector during release action.

239

AC/10-27

Figure 14-11. – Launch of Surveyor I as seen from top of service tower.

Agena Mariner-131

Figure 14-10. – Overall view of Atlas-Agena vehicle during
launch of Mariner spacecraft. This is same vehicle
shown in figure 14-9 after removal of cooling blanket.
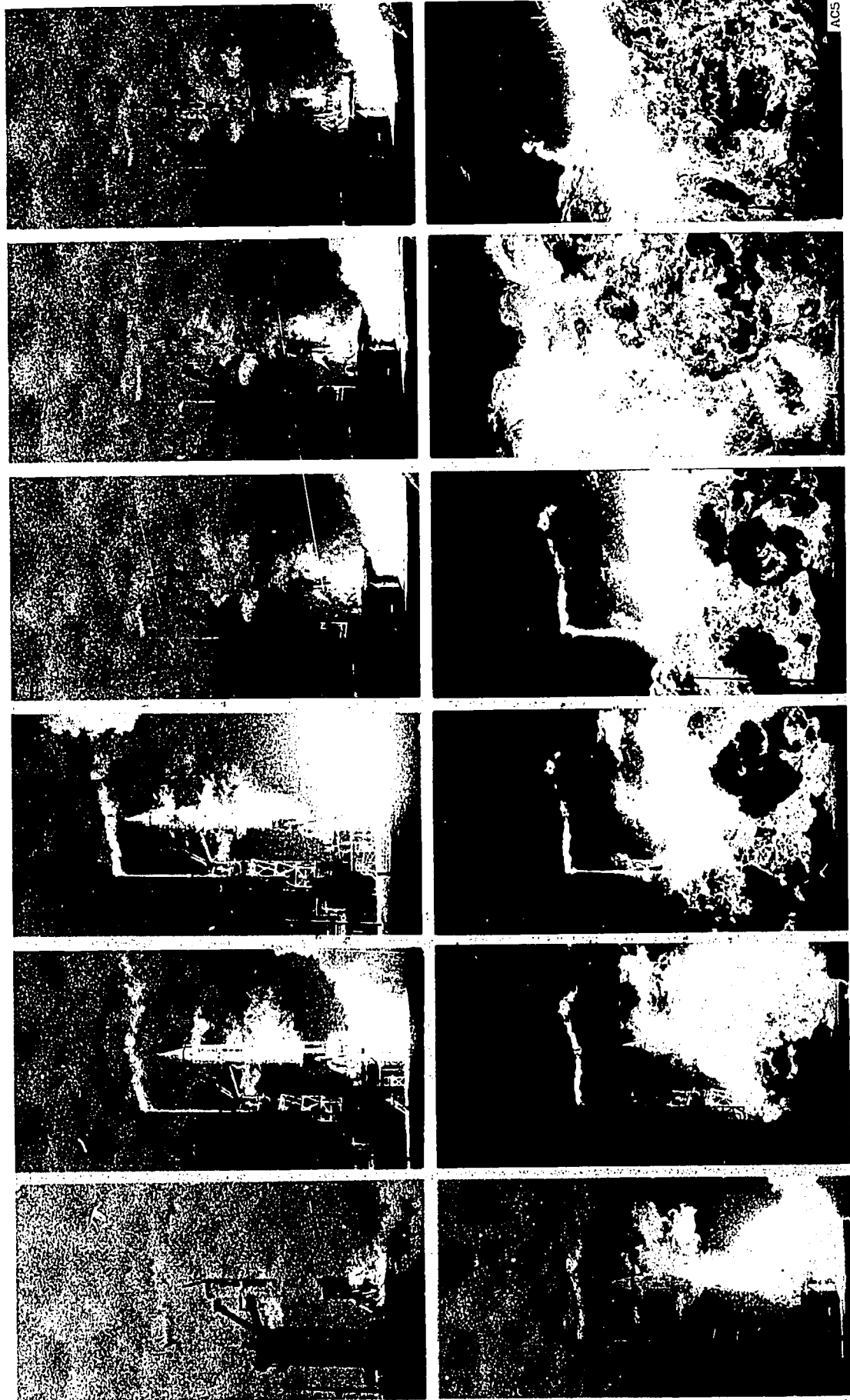
Figure 14-12. – Sequence showing explosion of vehicle on launch pad. In many instances, analysis of high-speed motion pictures is the only method of determining reasons for failure. Visual observations would not indicate that vehicle actually rose up 5 feet and then returned to launcher before explosion.

241

15. ROCKET MEASUREMENTS AND INSTRUMENTATION

Clarence C. Gettelman*

ROCKET ENGINE PERFORMANCE

Expressions which describe the performance of rocket engines involve many variables which cannot be measured directly. These expressions must be written in terms of variables that can be measured. Three equations from chapter 2 will be used to demonstrate how expressions are written in terms of measured quantities.

Total Impulse

When the thrust F is multiplied by the time t during which the engine operates, total impulse I_t is the result. The equation

$$I_t = Ft \tag{1}$$

is simple and meaningful, for from it the final velocity for any given payload can be calculated. The two variables F and t can both be measured directly - thrust with a load cell and time with a clock.

Specific Impulse

The specific impulse is more difficult to determine than total impulse. In the equation

$$I_{sp} = \frac{F}{\dot{W}} \tag{2}$$

the term $\dot{W}$ is the weight flow rate of propellant in pounds per second. This flow rate consists of the weight flow rates of both the fuel $\dot{W}_f$ and of the oxidizer $\dot{W}_o$. Therefore,

*Chief, Instrument Systems Research Branch.

I_{sp} can be written as

$$I_{sp} = \frac{F}{\dot{W}_f + \dot{W}_o} \tag{3}$$

Still, the weight flow rates of the fuel and the oxidizer are almost as difficult to measure separately as combined. However, since weight flow rate is the product of the density ρ and the volume flow rate $\dot{V}$ in gallons per second, the equation may now be shown as

$$I_{sp} = \frac{F}{\rho_f \dot{V}_f + \rho_o \dot{V}_o} \tag{4}$$

The volume flow rates can be measured. The densities, although constant at standard temperature and pressure, must be corrected for the temperature and pressure existing at the time of firing. Fortunately, both temperature and pressure can be measured easily. These two parameters, along with thrust and volume flow rate, enable the specific impulse equation to be reduced into measurable quantities.

Characteristic Gas Velocity

The equation which describes the characteristic gas velocity

$$c^* = \frac{gP_c A_t}{\dot{W}} \tag{5}$$

introduces two new variables for measurement: chamber pressure P_c and throat area A_t. Of the other two factors in the equation, g (the acceleration due to gravity) is a constant, and $\dot{W}$ has already been determined. Chamber pressure can be measured directly; so can throat area, although only when the throat is cold. Therefore, the measurement must be corrected for expansion caused by hot exhaust gases. Consequently, the temperature of the exhaust must also be determined. The equation for characteristic gas velocity modified to include these variables is

$$c^* = \frac{gP_c \left(\dfrac{\pi d^2}{4}\right)\Big/T}{\rho_f \dot{V}_f + \rho_o \dot{V}_o} \tag{6}$$

where $(\pi d^2/4)_T$ represents the throat area of the nozzle based on its diameter in feet and corrected for temperature.

Summary of Measurable Parameters

Once the equations defining typical characteristics of rocket performance have all been resolved into factors which are readily measurable (as in eqs. (1), (4), and (6)), instruments must be selected to measure thrust F, time t, volume flow rate V, pressure P, temperature T, and diameter d.

MEASUREMENTS

Force

Strain gage. - The sensing element of many thrust and pressure instruments, the strain gage, relies on the changing electrical properties of a thin wire for its operation. The resistance R of any particular wire is directly proportional to its length L and inversely proportional to its cross-sectional area A. The equation for this is

$$R \propto \frac{L}{A} \qquad (7)$$

If the wire is stretched, it becomes longer and its cross-sectional area becomes smaller; thus, the resistance increases. On the other hand, if the wire is compressed, its dimensions change in the opposite direction, and the resistance decreases. The change in
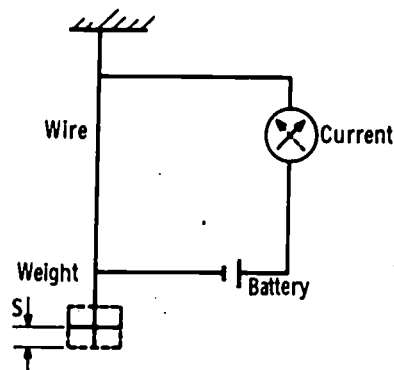
Figure 15-1. - Schematic of resistance change in a weighted hanging wire.

239

resistance, related to the force applied to the wire and measured with an ohmmeter, will indicate the magnitude of the force. Figure 15-1 shows this arrangement schematically.

Strain gages are not used singly but are arranged in a bridge circuit of four as shown in figure 15-2. This configuration allows the effect of the strain on the wires to be measured directly by a meter. In figure 15-2, the arrows indicate whether the forces are shortening or lengthening the wires. Note that when R1 and R2 get shorter, R3 and R4 get longer.
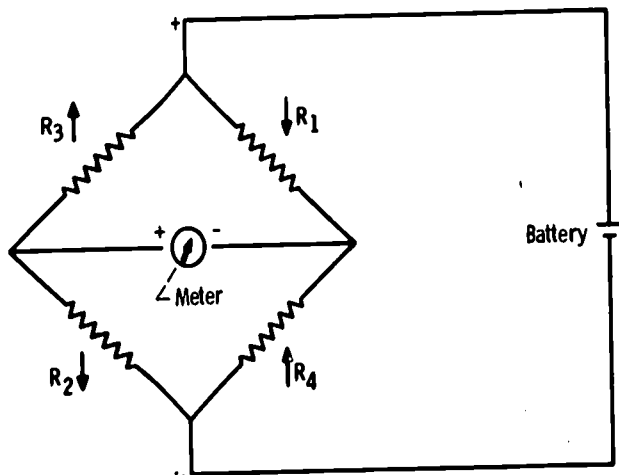
Figure 15-2. - Bridge arrangement of strain gages.
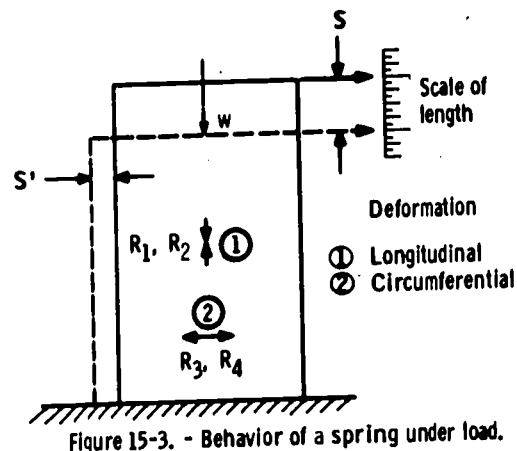
Figure 15-3. - Behavior of a spring under load.

Thrust. - Springs are important parts of both thrust and pressure transducers. A good spring is one that will deflect a given amount with a given load and reproduce the indication over a reasonable temperature range. Figure 15-3 shows the spring used in thrust transducers. The solid line shows the shape of the unloaded spring. When a load w is applied, compressing the spring, the length of the spring changes as indicated by the dotted line. The change of length S is determined largely by the spring material, and with a good spring this change is proportional to the load or force; that is, 1 pound produces 1 unit of deflection, 2 pounds 2 units of deflection, etc. As the sketch indicates, the compressed spring not only changes its length, but also changes its cross-sectional area. The amount of this lateral deformation S' is a material property related to S by Poisson's ratio

$$\mu = \frac{S'}{S} \tag{8}$$

whose value for metals is approximately 0.3; that is, S' = 0.3 S. The problem then is how to measure the deflections S or S', or both, of the spring.

240 245

The behavior of a strain gage under load is exactly like that of the spring; that is, the strain wire when loaded in tension increases its resistance because of both a change in length and a decrease in area. The strain gage can measure strains of about 0.0005 inch per inch. Consequently, strain gages are used. If a strain gage is installed on the spring in the orientation indicated in figure 15-3, then a compression of the spring will cause R1 and R2 of figure 15-2 to shorten, decreasing their resistance, and cause R3 and R4 to lengthen, increasing their resistance. The difference in resistances will then indicate the extent of deformation of the spring.

Thrust cells, springs with attached strain gages, are manufactured in many sizes to respond to a range of thrusts. Figure 15-4 shows some examples.

100 000 lb

5000 lb

10 lb

0.1 lb
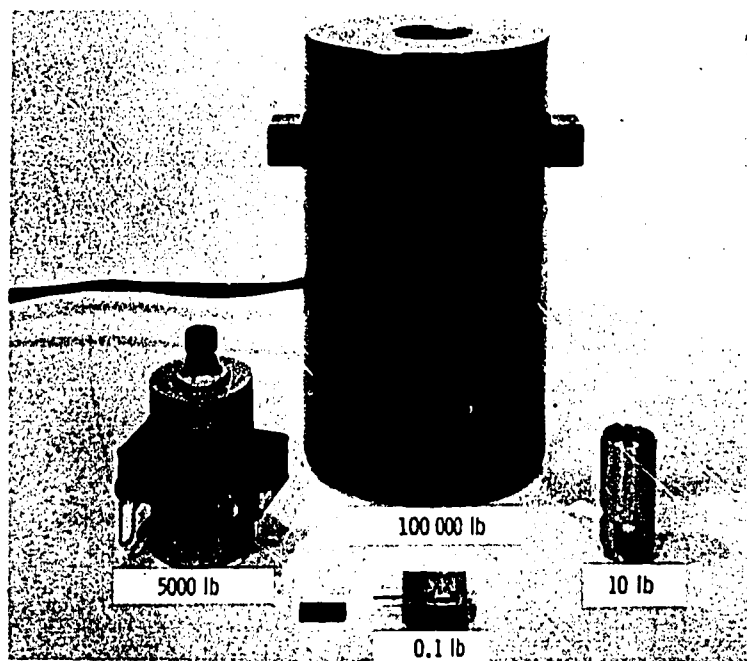
C-69844

Figure 15-4. - Thrust cells.

Pressure. - Pressures are also measured with strain gages, but, since pressures range from a fraction of a pound per square inch to thousands of pounds per square inch, extremes of spring sensitivity are required. The configuration shown in figure 15-5(a) has equal pressures ($P_1 = P_2$) on both sides of the spring element. When pressure P_2 is made greater than P_1 the spring deflects to the left as shown in figure 15-5(b). This deflection is a measure of the pressure and, in turn, determines the output of the strain gages bonded to the spring.

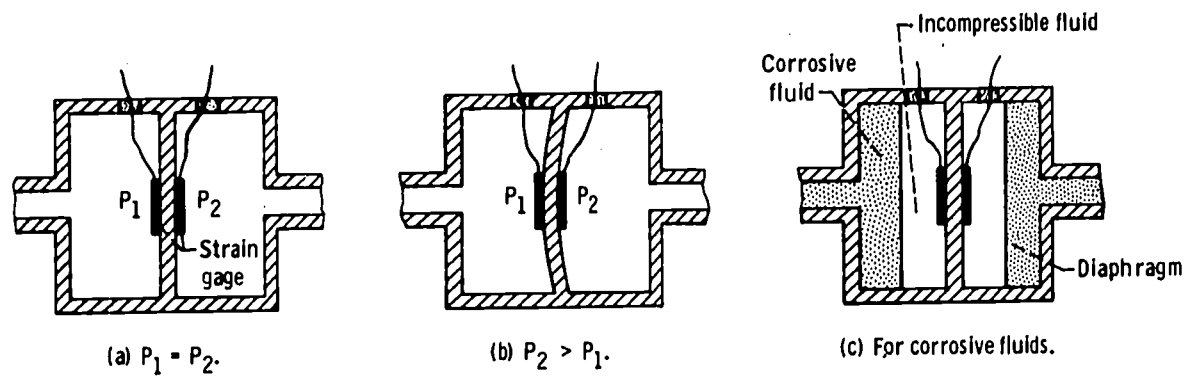The pressure gage illustrated in figure 15-5(a) is a differential gage and is of the

(a) $P_1 = P_2$.   (b) $P_2 > P_1$.   (c) For corrosive fluids.

Figure 15-5. – Schematic diagram of pressure transducers.

simple type in which the strain gages can be exposed to fluids whose pressure is being measured. In the case of corrosive propellants, such as fluorine, the strain gages must be put in suitable noncorrosive incompressible fluid and another diaphragm must be added as shown in figure 15-5(c). Absolute pressures can be measured by evacuating one side ($P_1 = 0$) and measuring the difference between it and another pressure (P_2). Figure 15-6 shows various types of strain gage pressure transducers.

Other spring configurations and deflection measuring schemes are used, and they vary in price from about \$1.00 to \$500.00, depending largely on the accuracy of the pressure gage.
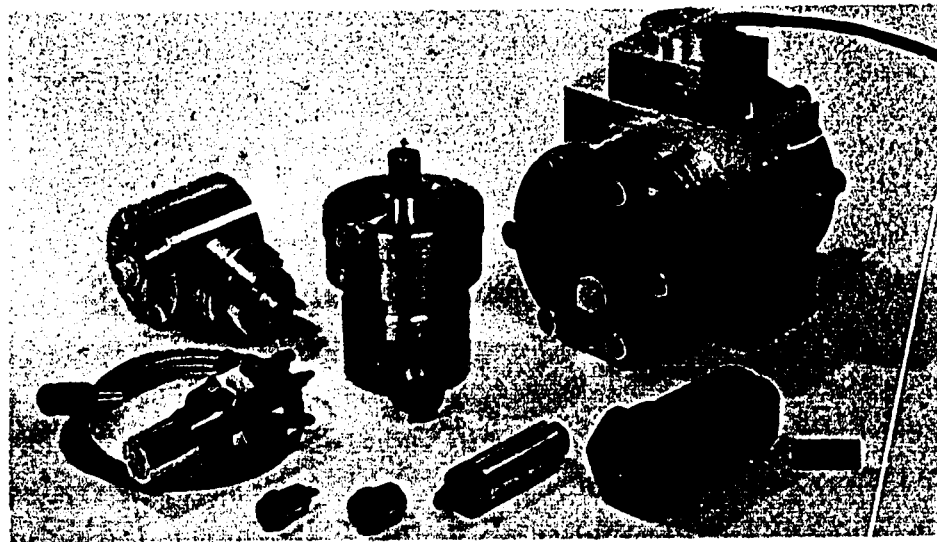
CS-32134

Figure 15-6. – Commercially available strain-gage pressure transducers.

Temperature

Two devices extensively used to measure temperature are the thermocouple, which is the least expensive and can be made small in size, and the resistance thermometer, which is more accurate, more complicated, and larger in size.

Thermocouple. - The thermocouple is a useful device used to measure temperature. When two thermocouple alloys are joined as shown in figure 15-7, a voltage is generated
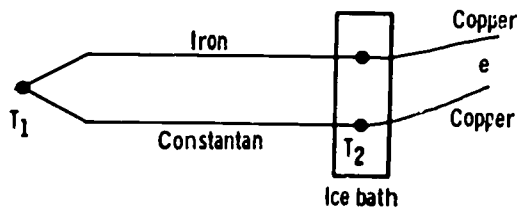

Figure 15-7. - Thermocouple.

which is a function of the difference between the temperatures T_1 and T_2. The temperature T_2 is usually controlled by placing that junction in an ice bath or other temperature controlled environment. The voltage e is then a function of the variable temperature T_1. National Bureau of Standards Circular 561 gives the temperature as a function of voltage for the following standard thermocouple alloys:

Chromel - Constantan
Copper - Constantan
Iron - Constantan
Chromel - Alumel
Platinum, 10 percent rhodium - platinum

The various alloys are used because of the characteristics such as voltage output, strength, stability, and cost, as functions of temperature level. The voltages generated are approximately 0.000020 volt per degree; hence, good voltage measuring equipment is required. Millions of feet of thermocouple wire are used in this country each year.

Resistance thermometer. - The resistance thermometer is based on the material property which relates temperature change with resistance change. Metals are used for temperatures above 20° K (the temperature of liquid hydrogen), and semiconductors, usually called insulators, are used at temperatures below 20° K. The best metal, because of the purity to which it can be made, is platinum, but where less accuracy is required, nickel may be used. These metals, in the form of wire, are wound so that there will be no strain produced which would also cause a change in resistance. The re-
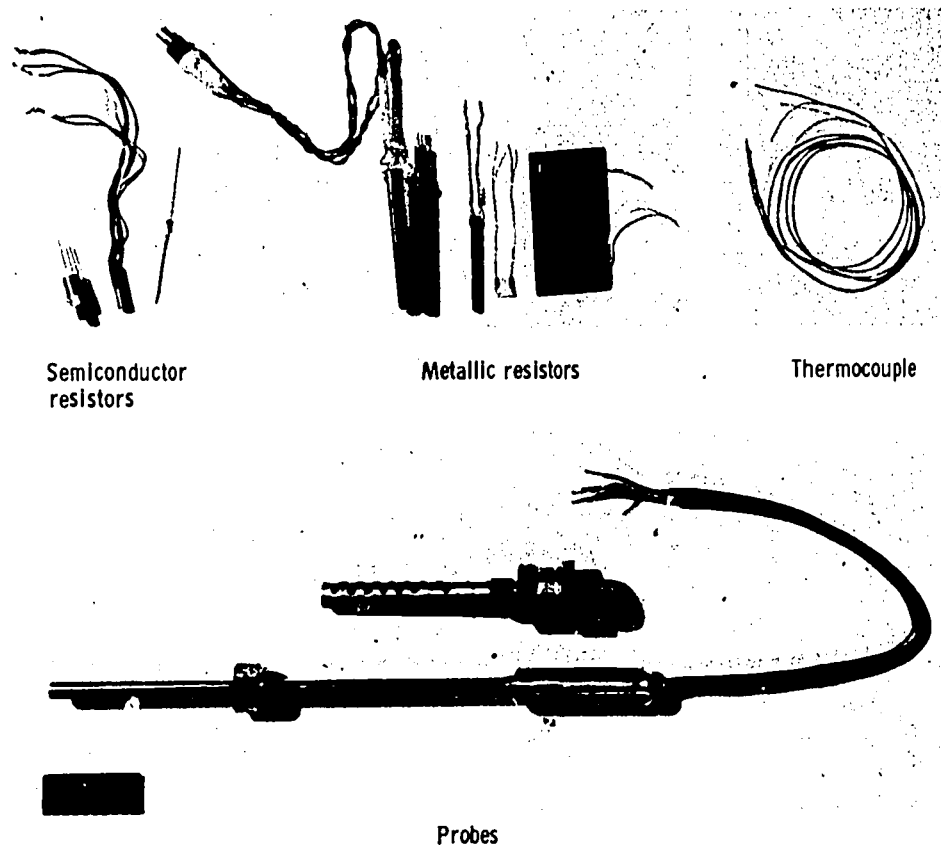
Semiconductor resistors   Metallic resistors   Thermocouple

Probes

Figure 15-8. – Temperature sensors.

sistance of metals increases as a function of temperature. The change of resistance (hence, change of temperature) is read with the same type of circuit used to measure strain (thrust, pressure) previously discussed and illustrated in figure 15-2, except that R_1, R_2, and R_3 are fixed resistors, and R_4 is the one whose resistance varies with temperature. Figure 15-8 shows platinum resistance thermometer elements along with probes suitable for insertion into a rocket-engine component. At temperatures near absolute zero, the change of resistance of metals becomes small and the thermometer looses its sensitivity. However, the resistance of semiconductors such as carbon and germanium increases with a decrease in temperature, and thus they function as resistance thermometers below the temperatures where metals loose their sensitivity.

Volume Flow Rate

Volume flow rate is most commonly measured by a volume displacement method. The gasoline we buy and the water we use are metered by this method. Another method of measuring volume flow rate utilizes the kinetic energy, or energy due to motion, of the fluid.

Volume displacement. - The simplest form of the volume displacement method is filling a known volume, emptying it, and counting the number of times this has been done.
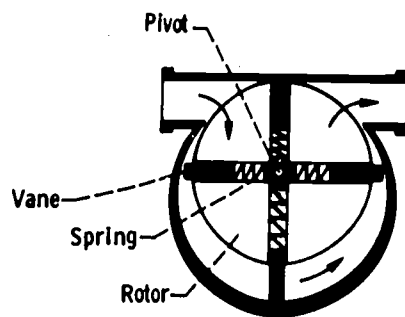
Figure 15-9. - Vane flowmeter.

More complex is the vane meter. This meter (fig. 15-9) has vanes which change length as a function of angle. Moved by the pressure of the fluid, the vanes rotate inside a casing, carrying between them a known quantity of fluid which discharges at the end of each revolution. The volume flow rate is proportional to the speed of rotation of the vanes. Many other devices operate in a similar way. These devices are usually inexpensive and accurate for a single fluid, but they do not work well with a variety of fluids.

Energy of flow. - When a fluid with a velocity v and a density ρ is stopped, it generates a pressure P greater than that which normally exists at that point in the fluid stream. This pressure due to the kinetic energy of the fluid is given by the equation

$$P = \frac{1}{2}\rho v^2 \tag{9}$$

The velocity v can be obtained in terms of the pressure P by rearranging the terms of equation (9)

$$v^2 = \frac{2P}{\rho} \tag{10}$$

or

$$v = \sqrt{\frac{2P}{\rho}} \tag{11}$$

Thus, as illustrated in figure 15-10, the velocity v in a pipe is determined by measuring the pressure generated by virtue of the kinetic energy of the fluid. Note that the velocity is not constant but goes to zero at the wall. The relations given hold only for incompressible fluids. Note that the pressure has to be measured across the diameter of the pipe. This is an accurate but time-consuming process.
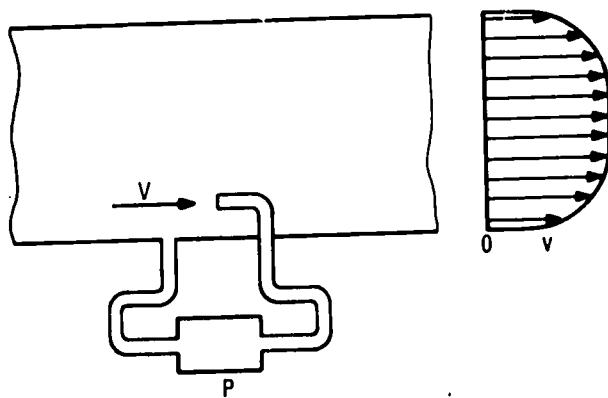
245

Figure 15-10. - Velocity flowmeter.

Nozzles and orifices utilize the same principle; flow of incompressible fluids of known density can be determined with one pressure measurement. This is made possible because a difference in pressure exists between the two sides of an orifice or nozzle which depends on the speed of flow through the constriction. This difference in pressure can be measured with a strain-gage differential pressure meter as shown in figure 15-11, and can be converted to volume flow.

The most useful device for measuring rocket propellant volume flow is the turbine meter. In this case the kinetic energy of the fluid causes a lightly loaded turbine to turn. The load on the turbine is bearing friction and a small amount of power required to measure the turbine speed. The turbine blade is made of magnetic material which, when it passes a coil-magnet combination, generates a pulse. The frequency of the pulses is a
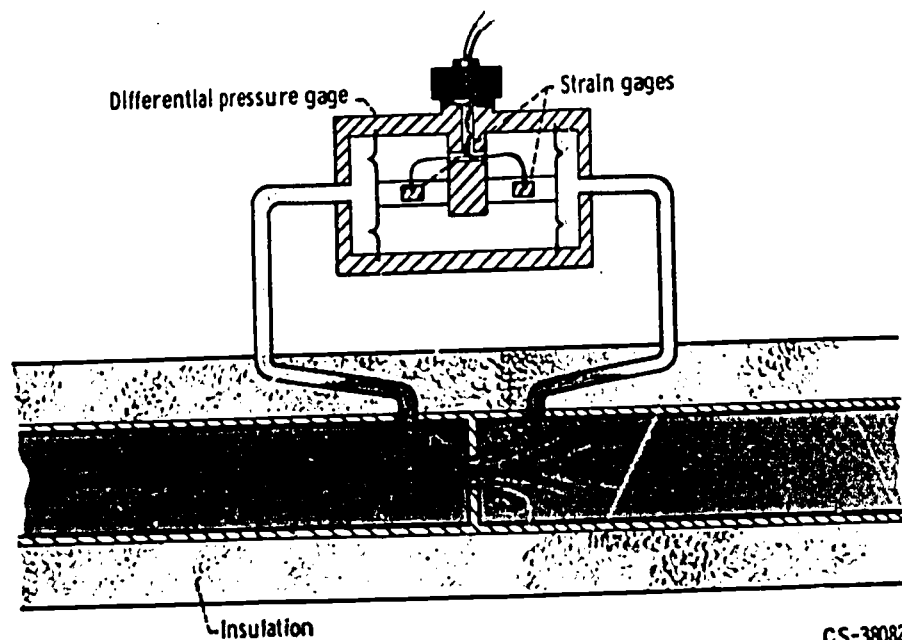
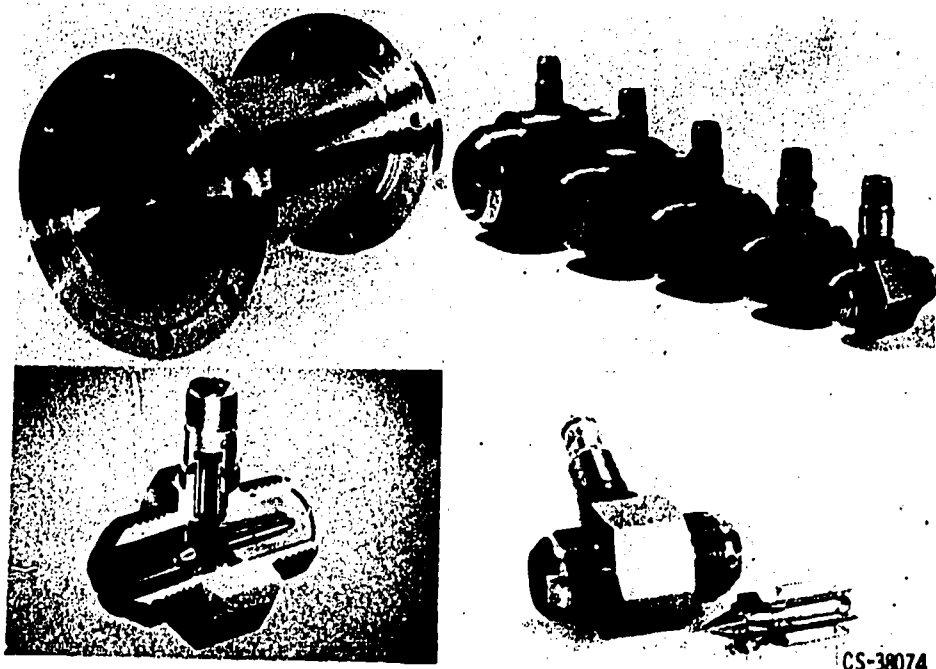Figure 15-11. - Head flowmeter installation.

251

Figure 15-12. - Turbine flowmeters.

measure of turbine speed. These devices are calibrated with water and the same cali-
bration can be used on most of the cryogenic and other fluids used in rocket testing. The
calibration is expressed as pulses per gallon. Figure 15-12 shows the parts of the tur-
bine meter, as well as a range of sizes.

The devices we have discussed to this point change some measured variable, such
as temperature, to an electrical voltage. With modern data systems this is an essential
requirement. Very little data is manually recorded; in fact, the data should be recorded
on a system which allows computer entry, such as a digital tape-recording system.

BIBLIOGRAPHY

Cook, Nathan H.; and Rabinowicz, Ernest: Physical Measurement and Analysis.
    Addison-Wesley Publishing Co., 1963.

Eckman, Donald P.: Industrial Instrumentation. John Wiley & Sons, Inc., 1950.

Stout, Melville B.: Basic Electrical Measurements. Prentice-Hall, Inc., 1950.

16. ELEMENTS OF COMPUTERS

Robert L. Miller*

Aids to computation are quite old, and evidence of them can be found in ancient history. The earliest aids were the fingers. Then groups of small objects such as pebbles were used loosely. Eventually, beads were strung on wires fixed in a frame; this became known as the abacus.

The abacus most likely originated in the Tigris-Euphrates valley and its use traveled both east and west along the routes of the caravans. Elaboration of the instrument and later development of the techniques of its manipulation made it applicable to multiplication, division, and even to the extraction of square and cube roots, as well as to addition and subtraction for which the instrument was probably originally intended. The abacus, despite its ancient origin, is still in use by the Oriental peoples.

After the invention of the abacus, 5000 years elapsed before the next computational aid was developed. During this time, gears and printers were used in the design of clocks. These machine elements paved the way for the development of calculating machinery.

Chapter 15 considered the techniques for measuring the physical quantities associated with testing rockets. Some of these physical quantities (thrust, pressure, and temperature) are converted to electrical signals by transducers such as strain gages and thermocouples. In order to solve equations with a computer whose inputs are introduced automatically, it is necessary to have each of the elements of the equation in the form required by the input to the computer, such as voltage. At this point, therefore, it becomes important to select the computer. This will be determined by the computations that need to be made, the accuracies required, and the form that the answers will take after the computations are made. An examination of the characteristics of the two basic types of computers, analog and digital, will reveal which would best fit the computing requirements of rocket testing.

ANALOG COMPUTER

In 1617, John Napier, following his invention of logarithms, published an account of his numbering rods, known as Napier's bones. Various forms of the bones appeared, some approaching the beginning of mechanical computation. Following the acceptance of

---

*Head, Digital Recording and Engineering Section.

logarithms, Oughtred (1630) developed the slide rule, and it received wide recognition by scientists before 1700. Everard (1755), Mannheim (1850), and others continued to improve it. Useful in solving simple problems which require an accuracy of only three or four significant figures, the slide rule is probably the ancestor of all those calculating devices whose operation is based on an analogy between numbers and physical magnitudes. Many such analogy devices, such as the planimeter, the integraph, and the differential analyzer have since been constructed. All analogy devices like the slide rule are limited to the accuracy of a physical measurement.

Many of the problems encountered in rocket testing are time dependent. Pressures and temperatures vary rapidly with time and so, therefore, does performance. This is particularly true in the startup and shutdown phases of operation. Any instabilities that occur are also time related. For computations that are performed on time-dependent measurements to be useful they must either be made at very short time intervals or must be continuous.

The analog computer can perform continuous calculations in either expanded, real, or compressed time.

Chapter 15 gave the method by which a typical rocket performance equation can be solved in terms of measured quantities:

$$I_{sp} = \frac{F}{\dot{W}} = \frac{F}{\rho_F \dot{V}_F + \rho_O \dot{V}_O} \tag{1}$$

where

I_{sp} specific impulse

F thrust, measured by a load cell

ρ_F fuel density

$\dot{V}_F$ volume flow rate of fuel (e.g., gal/min)

ρ_O oxidizer density

$\dot{V}_O$ volume flow rate of oxidizer

All of these variables can be measured directly during a test with the exception of the densities. The density of a liquid is essentially proportional to temperature and can be represented by

$$\rho = kT \tag{2}$$

where k is a constant, and T is the temperature of the liquid, which can be measured. Equation (1) now becomes

$$I_{sp} = \frac{F}{kT_F\dot{V}_F + kT_O\dot{V}_O} \tag{3}$$

Measuring the temperature and volume flow rate of both the fuel and oxidizer, along with the thrust, enables calculation of the specific impulse I_{sp}.

The analog computer is ideal for this problem because it can compute continuously in real time using several variables. The computer contains components which perform the basic arithmetic functions of addition, subtraction, multiplication, and division. The inputs and outputs of these components are voltages. A summing amplifier has two inputs and one output:
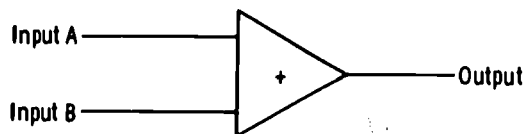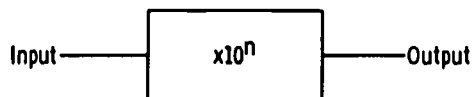

If a signal of 2 volts is received at input A and 3 volts at input B, the summing amplifier produces an output of 5 volts.

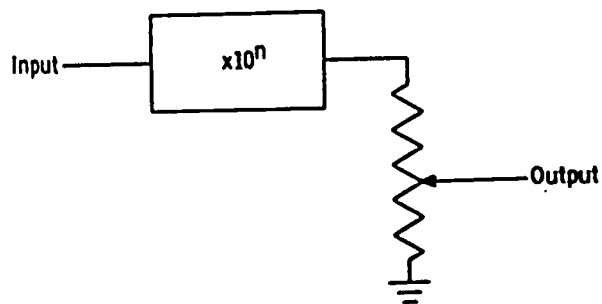Other components are multipliers and dividers:
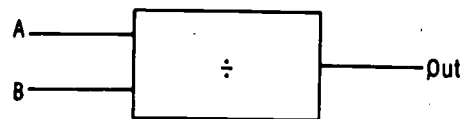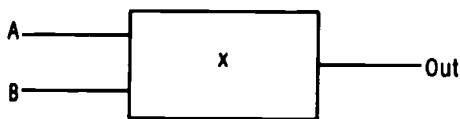
Another basic component is an amplifier which multiplies by a power of 10:

Multiplication by a constant other than a power of 10 can be accomplished by adding a potentiometer to the preceding component:

The effect of the potentiometer is to multiply by a number less than 1.

Equation (3) can be solved by interconnecting these basic components as instructed by the equation and introducing the signals directly from the transducers on the rocket. Note that all signals are multiplied by 1000 to make them large enough to be resolved by the computer (fig. 16-1).

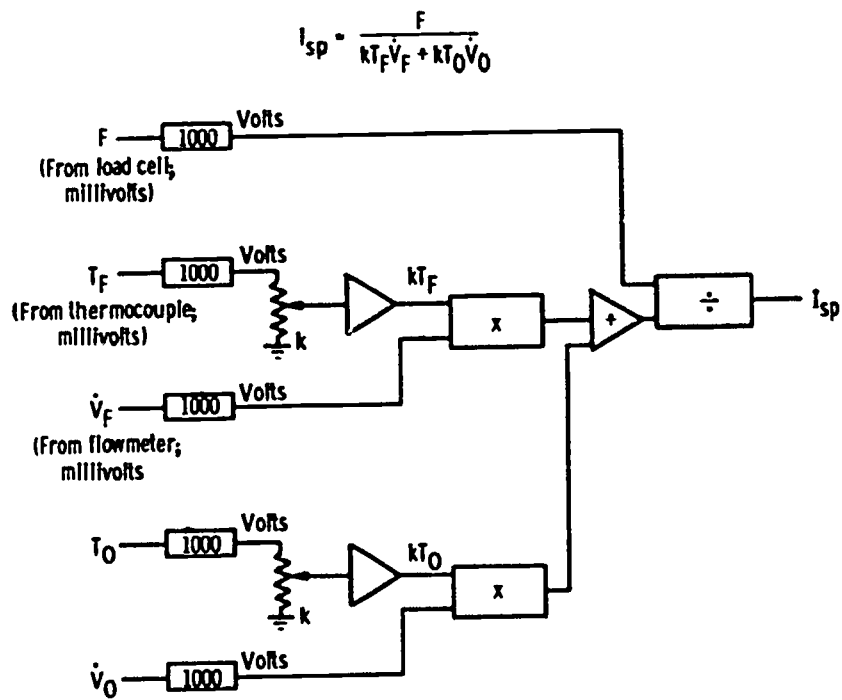$$I_{sp} = \frac{F}{kT_F \dot{V}_F + kT_0 \dot{V}_0}$$

Figure 16-1. - Analog setup for specific impulse calculation.

The answer to the computation is a voltage representing the specific impulse as a function of time. This could be read from a voltmeter, but the usual method of presentation is an oscilloscope or graphical plotter. If the plotter is adjusted to compensate for the electrical characteristics of the transducers, the amplification of the voltages through each stage of the computer, and the sensitivity of the plotter, specific impulse can be read directly in seconds.

The analog computer has many other components which perform mathematical functions more complex than generating voltage proportional to time. They are used in the

electrical simulation of physical problems; for example, they enable the engineer to investigate mechanical motion without having the mechanical device present.

DIGITAL COMPUTER

The digital computer differs from the analog in the fact that internally it operates with digits, rather than with voltages proportional to the numbers.

The electronic digital computer evolved from the mechanical adding machine and in many respects still maintains some of its basic characteristics. Like the adding machine, its input must be in the form of digits. Unfortunately, it cannot use the decimal digit system efficiently because of the many symbols used for each digit. The computer

TABLE 16-I. - BINARY NUMBERS AND THEIR DECIMAL

EQUIVALENTS UP TO 49

Decimal		Binary					Decimal		Binary					
		Decimal weight							Decimal weight					
10	1	16	8	4	2	1	10	1	32	16	8	4	2	1
	0					0	2	5		1	1	0	0	1
	1					1	2	6		1	1	0	1	0
	2				1	0	2	7		1	1	0	1	1
	3				1	1	2	8		1	1	1	0	0
	4			1	0	0	2	9		1	1	1	0	1
	5			1	0	1	3	0		1	1	1	1	0
	6			1	1	0	3	1		1	1	1	1	1
	7			1	1	1	3	2	1	0	0	0	0	0
	8		1	0	0	0	3	3	1	0	0	0	0	1
	9		1	0	0	1	3	4	1	0	0	0	1	0
1	0		1	0	1	0	3	5	1	0	0	0	1	1
1	1		1	0	1	1	3	6	1	0	0	1	0	0
1	2		1	1	0	0	3	7	1	0	0	1	0	1
1	3		1	1	0	1	3	8	1	0	0	1	1	0
1	4		1	1	1	0	3	9	1	0	0	1	1	1
1	5		1	1	1	1	4	0	1	0	1	0	0	0
1	6	1	0	0	0	0	4	1	1	0	1	0	0	1
1	7	1	0	0	0	1	4	2	1	0	1	0	1	0
1	8	1	0	0	1	0	4	3	1	0	1	0	1	1
1	9	1	0	0	1	1	4	4	1	0	1	1	0	0
2	0	1	0	1	0	0	4	5	1	0	1	1	0	1
2	1	1	0	1	0	1	4	6	1	0	1	1	1	0
2	2	1	0	1	1	0	4	7	1	0	1	1	1	1
2	3	1	0	1	1	1	4	8	1	1	0	0	0	0
2	4	1	1	0	0	0	4	9	1	1	0	0	0	1

works much better using the binary system in which only two different symbols are used for each digit. This corresponds to a circuit which is either conducting or not conducting, a relay that either is energized or is not energized, or a card with a hole punched or not punched. The binary digit is called a "bit," and the two possible states of this bit are represented by the symbols 0 and 1.

Since humans use the decimal system, it is necessary to convert from decimal to binary when using computers. Table 16-I shows the relation between binary numbers and their decimal equivalents up to 49.

The problem now arises of compatibility between the output of the measuring devices, or transducers, and the digital computer. The transducer output is continuous in millivolts, while the digital computer must have binary digits. To solve this problem an analog-to-digital (A-D) converter is used between the transducer and computer. This device, upon command, will convert a millivolt signal at its input into bits. The number of bits basically limits the resolution or accuracy of the measurement. Devices in use presently have 12 or 13 bits and attain a resolution of 1/4096. At each command, the millivolt input is converted into a 13-bit number.

Another problem arises because the digital computer can only accept one binary number or transducer output at a time; the problem is the need for sequentially connecting the transducer outputs to the A-D converter. A device known as a scanner, or multiplexer, is used for this sequencing. Shown in figure 16-2 are the components of a data system used to switch the analog signals from several transducers into an analog-to-digital converter for entry into a digital computer.
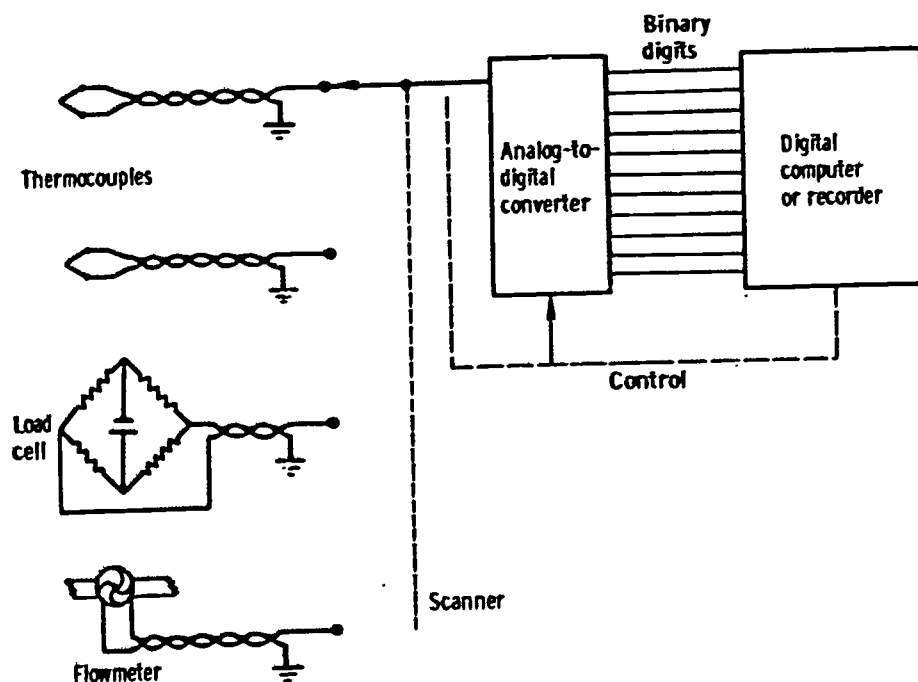

Figure 16-2. - Typical data system.

254

The scanner and analog-to-digital converter, along with the controls, are usually built into a data system which may or may not be connected directly to the computer. If it is not, the bits are recorded by the data system on either magnetic or paper tape for later entry into the computer.

Once the transducer signals have been sequentially converted to digital form, what happens inside a basic digital computer is block diagrammed in figure 16-3.
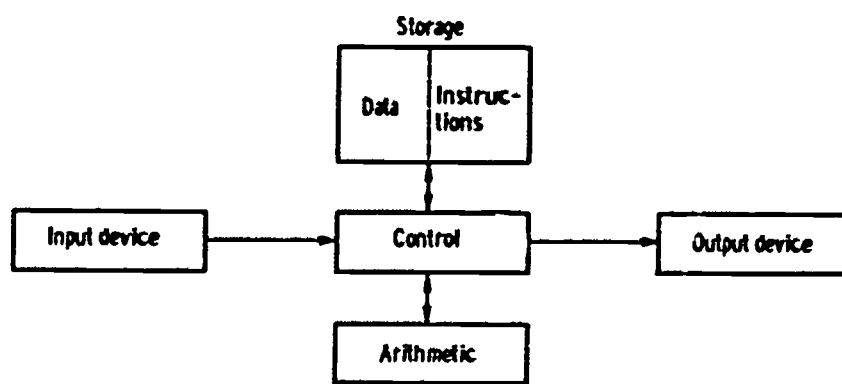

Figure 16-3. - Basic digital computer.

A simple computer, for which the input device is a punched card reader and the output device is an electric typewriter, must receive two kinds of information in order to carry out a computation. It must have numbers or <u>data</u> to use in the computation and <u>instructions</u> concerning what to do with the data. Much as the analog computer was programmed step by step to perform a complex computation, so is the digital machine instructed in simple, sequential steps. For example, if told to add A+B the computer will do so.

Rather than rely on the input device to supply each of the numbers and instructions as they are required, these are placed in the block marked Storage (fig. 16-3). All of the numbers and instructions necessary to solve a complex problem are held in Storage in a known, orderly manner. Control takes data and instruction numbers from the input device and places them in Storage. When all data and instruction are in Storage, the problem is started. Control sends data to Arithmetic and controls the operation to be performed there according to the basic instruction of add, subtract, multiply, and divide. The answer is held in Arithmetic for the next instruction. The instructions necessary to solve a problem are sequentially extracted from Storage by Control. Control executes the instructions by transferring data from Storage to Arithmetic and back. This continues until the problem is solved, at which time the final answers are sent to the output device for printing.

The series of instructions necessary to solve $X = \dfrac{B + C}{D}$ begins after the data B, C,

and D have been loaded in storage at locations much like slots in a file cabinet. Each slot, which can hold a number, has an address:

Address	Contents
1	B
2	C
3	D

The symbol 1 means the address 1, whereas the symbol (1) means the contents of address 1, or B. Similarly, A means the arithmetic section while (A) means the contents of that location.

The instructions necessary to solve for X would be as follows:

Instruction	Contents of A after operation
Send (1) to A	B
Add (2) to (A)	B + C
Divide (A) by (3)	$\dfrac{B + C}{D}$
Print (A)	Zero

Returning to the rocket problem, the equation for specific impulse is

$$I_{sp} = \frac{F}{k\dot{V}_F T_F + k\dot{V}_O T_O}$$

Assume that the data to solve this equation are loaded into the storage at the following locations:

Address	Contents
1	k
2	$\dot{V}_F$
3	T_F
4	$\dot{V}_O$
5	T_O
6	F
7	Empty

The instructions necessary to solve the equation would be as follows:

Instruction	Contents of A after operation
Send (1) to A	k
Multiply (2) by (A)	$k\dot{V}_F$
Multiply (3) by (A)	$k\dot{V}_F T_F$
Send (A) to 7	Zero
Send (1) to A	k
Multiply (4) by (A)	$k\dot{V}_O$
Multiply (5) by (A)	$k\dot{V}_O T_O$
Add (7) to (A)	$k\dot{V}_F T_F + k\dot{V}_O T_O$
Send (A) to 7	Zero
Send (6) to A	F
Divide (A) by (7)	$\dfrac{F}{k\dot{V}_F T_F + k\dot{V}_O T_O}$
Print (A)	Zero

In a typical situation the instructions necessary to carry out this computation would enter the computer on punched cards through a card reader similar to the one shown in figure 16-4. The data might come directly from an analog-to-digital converter in the

C-67-719

Figure 16-4. - Card reader-punch.

data system or from a magnetic tape recorded by the data system. Figure 16-5 shows magnetic tape units capable of reading or writing 80 000 bits per second.

The instructions, of course, are much more complex and there are many more measurements and computations than have been considered here. Together, the instructions are called the program for the test. Composing or writing the program for a test is a very complex job and is usually done by a mathematician.

Figure 16-5. - Magnetic tape units.

Output from the computer may be listed in decimal form by a high speed line printer (fig. 16-6). This printer can print up to 2500 decimal digits per second.

If graphical output is a more desirable presentation, the plotter shown in figure 16-7 may be used. Its input is from a magnetic tape prepared by the computer.

262

Figure 16-7. – Graph plotter and magnetic tape unit.

C-67-718

Figure 16-6. – High-speed line printer.

C-67-720

SELECTION OF COMPUTER

Either the analog or digital computer can be used to perform a typical computation in the study of rocket performance. Each machine has characteristics which either make it desirable or limit its capabilities for a particular job.

In summary, the analog computer can operate in real time and provide immediate continuous plots of computed results. Accuracy is about 99 percent on the average, and about 10 variables can be handled simultaneously.

The digital computer generally does not operate in real time, but it can perform much more complex calculations than the analog. It also has the advantage of a stored program giving increased flexibility in computations to be performed. And finally, the number of variables is unlimited, while their individual accuracies are limited only by the number of bits representing the variable.

17. ROCKET TESTING AND EVALUATION IN GROUND FACILITIES

John H. Povolny*

Rocket engines and vehicle stages must operate in a variety of environments. Some components need to perform well in space, others must be effective on the launch pad, still others must respond during atmospheric flight, but many need to function satisfactorily under all conditions from launch through orbit. Of these conditions, vibration, pressure, vacuum, temperature, humidity, mechanical stresses, and gravity forces are the most important ones affecting performance. Before NASA will commit any engine or other component to flight, they must be sure that it will perform perfectly. To achieve this, extensive testing is necessary. Ideally, test facilities for this purpose should be able to reproduce many of these environmental factors at the same time, but, practically, this is seldom possible, so the effects of environment are usually examined one or two at a time, and testing is often limited to those considered most significant.

Although the investigations usually range from tests of the smallest component to tests of the complete system in a simulated environment, this discussion ignores the smaller research setups and concentrates on the larger test facilities used by NASA at the Lewis Research Center.

AMBIENT FACILITIES

Back in the early 1940's, when rocketry became a serious study, engine research and development facilities consisted primarily of small (several hundred pounds thrust capacity), horizontal or vertical, sea-level test stands such as the one illustrated in figures 17-1 and 17-2. Then there was so much to learn about the fundamentals of rocket propulsion that these small-scale rigs were satisfactory. In fact, small test stands are still useful for basic research purposes. As the size of the engines increased, larger, vertical, sea-level test stands were built, such as the one illustrated in figure 17-3. This facility, located at the Lewis Research Center, will support experimental rockets having thrusts up to 50 000 pounds and using exotic propellants such as liquid hydrogen and liquid fluorine. The largest test stand built to date for liquid-propellant systems is for the M-1 engine and is located in Sacramento, California; the largest for solid-propulsion systems is for the 260-inch-diameter engine and is located near Homestead, Florida. The stand
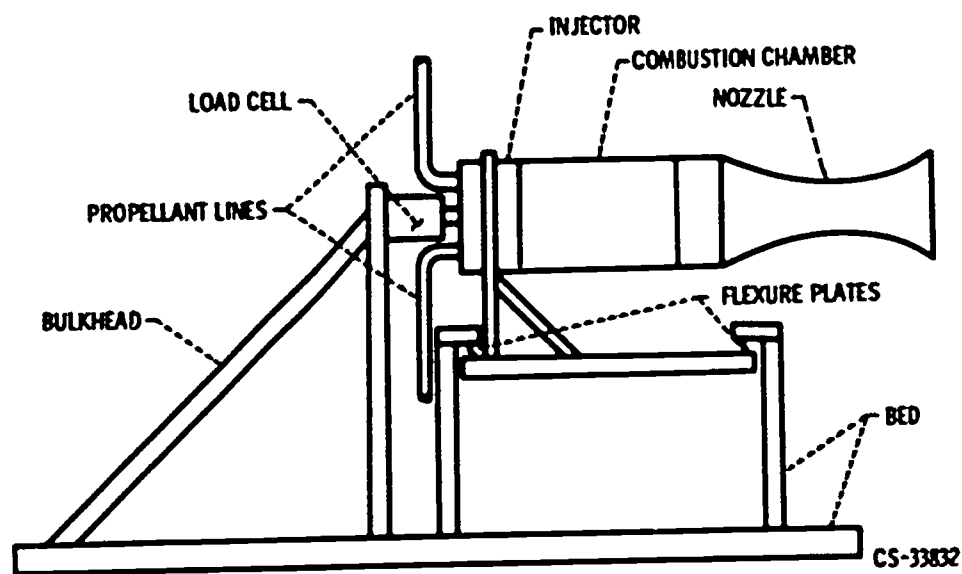
---

*Chief, Engine Research Branch.
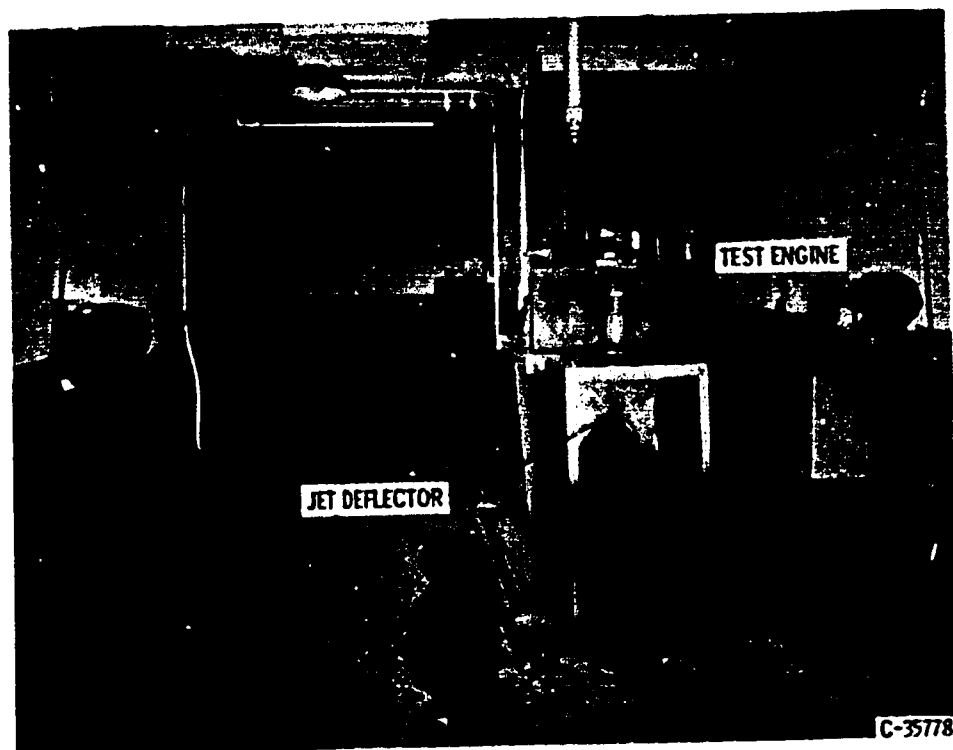
Figure 17-1. - Simple rocket thrust stand.

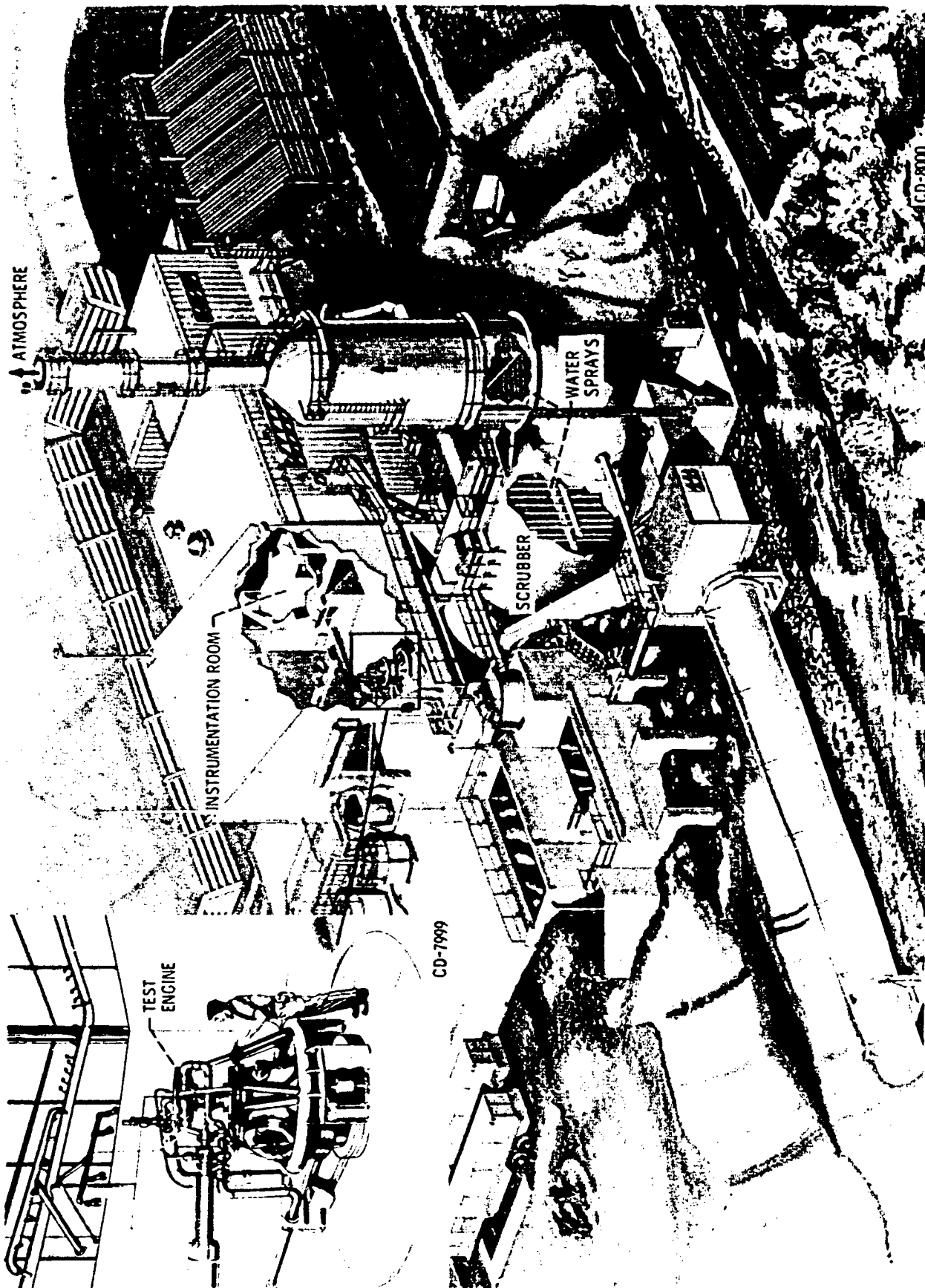Figure 17-2. - Small sea-level thrust stand.

267

ATMOSPHERE

WATER SPRAYS

SCRUBBER

CO-8000

CO-7999

INSTRUMENTATION ROOM

TEST ENGINE

Figure 17-3. - High-energy rocket test stand with closeup of engine installation.

263

Figure 17-4. – M-1 rocket test complex.

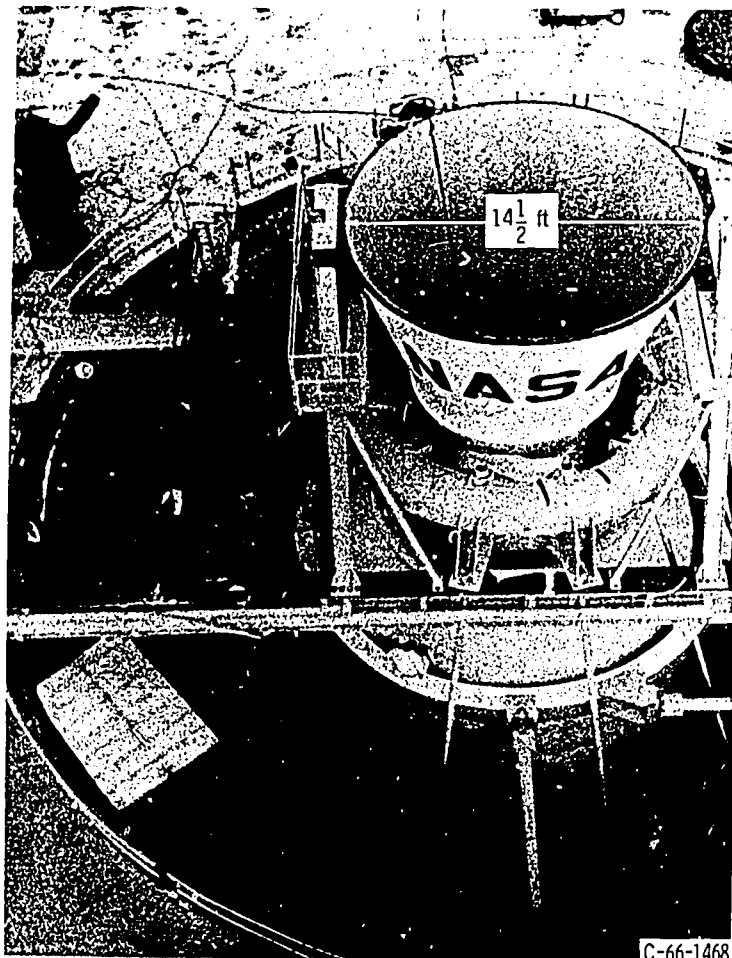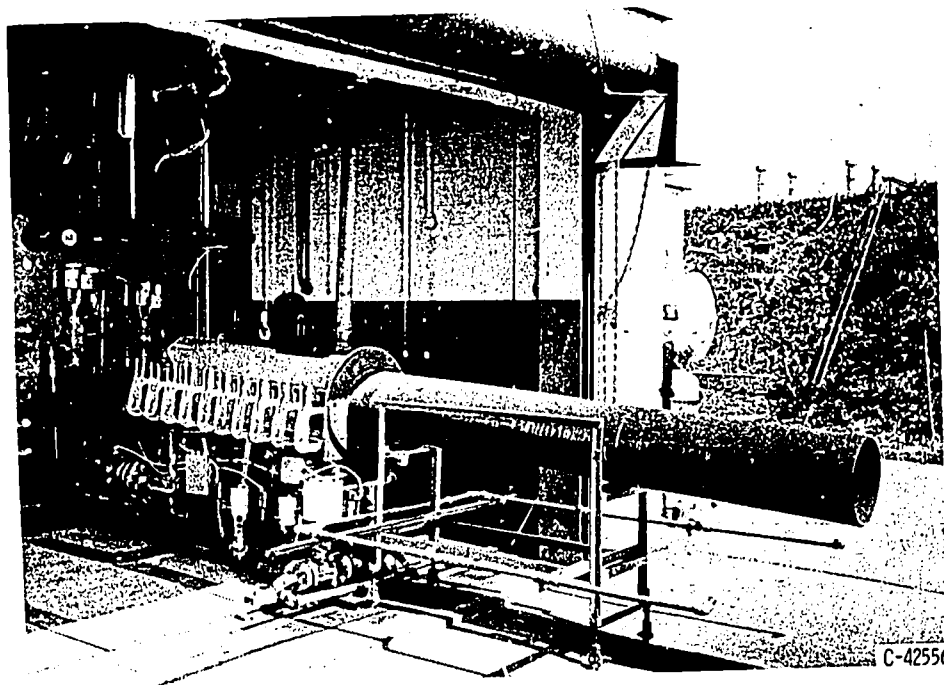Figure 17-5. – M-1 rocket test stand.

Figure 17-6. - 260-Inch-solid-rocket test stand.

and complex for the M-1 engine, which develops 1.5 million pounds of thrust, is illustrated in figures 17-4 and 17-5, and the stand for the 260-inch engine, which will develop 5.0 million pounds of thrust, in figure 17-6. The two stands are basically different in that the liquid-rocket stand consists of a tower from which the engines are fired downward, while the solid-rocket stand is a hole in the ground from which the engines are fired upward. The reason for this is that the solid engine performance is not influenced by gravity, and thus it can be fired in any attitude; furthermore, it is cheaper to dig a hole in the ground than to build a tower.

ALTITUDE FACILITIES

The facilities discussed so far are only useful for first-stage engines or engines which operate where altitude or space effects are not significant. Where this is not true, as in the case of upper-stage engines or engines with large-expansion-ratio exhaust nozzles, then high-altitude facilities are required. There are various ways of simulating

265

(a) Without flapper valve.
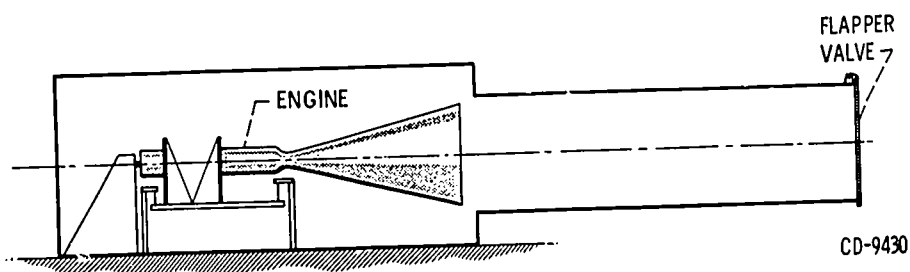
(b) With flapper valve.

Figure 17-7. – Rocket-exhaust ejector.

the desired altitudes; one of the simplest and least expensive is illustrated in figure 17-7. In this case, the entire test stand is enclosed in a tank which has one end left open so that the rocket exhaust can escape. The opening is fitted with a cylindrical tube called an ejector, which utilizes the energy of the exhausting gases to reduce the pressure in the tank. Pressures approaching 1 pound per square inch absolute, corresponding to an altitude slightly over 70 000 feet, have been obtained by this method. Although this technique provides altitude simulation once the engine is operating, it cannot simulate a high altitude for testing engine starting characteristics. This can easily be remedied, however, by adding a flapper valve to the exit end of the ejector tube and evacuating the system. When a high-altitude start is to be made, the vacuum pump is turned on and the pressure in the tank and ejector tube is thereby reduced, while the higher atmospheric pressure pushes on the outside of the flapper valve and gives a tight seal. When the desired pressure condition is achieved, the engine is ignited; exhaust from the engine

forces the flapper valve open and the operation is the same as before. If higher altitudes are required during engine operation, they are made possible by the addition of a steam ejector pump or by the installation of the entire engine and rocket exhaust ejector assembly inside a vacuum chamber.

The steam ejector pump is the method used at the B-1 facility located at the NASA Plum Brook Station (fig. 17-8). This installation has a vertical test stand, 135 feet high, currently capable of testing hydrogen-fluorine rockets with thrusts up to about 6000 pounds;

(a) Overall view of test facility.   (b) Test enclosure.   (c) Engine cross section.
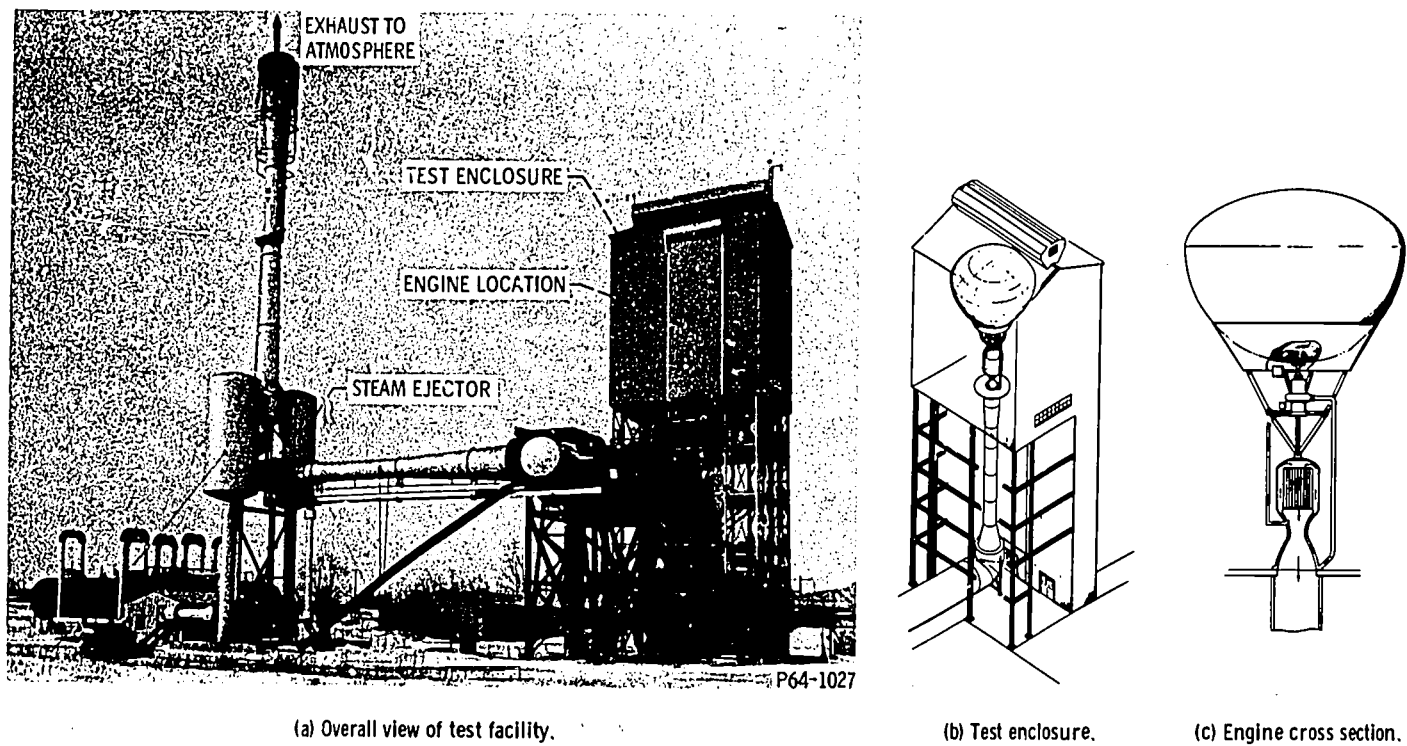
Figure 17-8. - B-1 test facility.

with some modification, it can accommodate engines with thrusts up to 75 000 pounds. The test engine is installed with the exhaust discharging down at about the 68-foot level, leaving a space above the engine for a 20 000-gallon propellant tank. This arrangement allows testing the propulsion system of a complete stage. Run time is limited to several minutes by the capacity of the propellant tanks or by the capacity of the storage system that supplies steam to the ejectors. The B-1 facility has no vacuum chamber for completely enclosing the rocket engine.
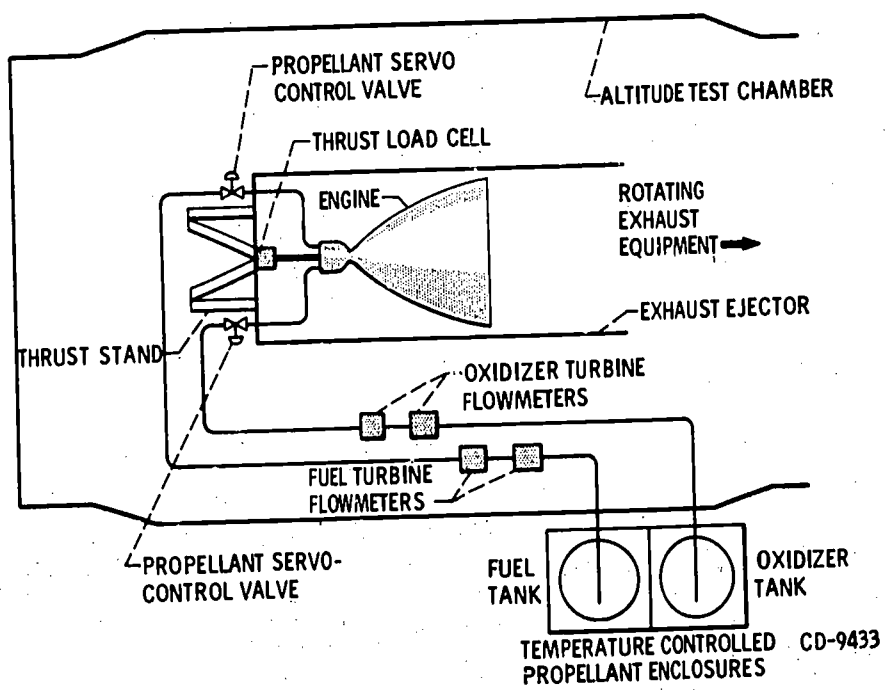
The vacuum chamber is used to simulate altitude at the Propulsion Systems Laboratory (PSL) at Lewis. Rocket engines installed in the PSL are illustrated in figures 17-9 to 17-11. The Centaur engine shown in figure 17-9 is using the PSL tank itself as the vacuum chamber and the flame tube as the exhaust ejector. The hot gases leaving the

FUEL TANK OXIDIZER TANK

AFTERBURNING
O_2 TANK FARM

VENTS
H_2 ↑ ↑ O_2

FUEL TURBINE
FLOWMETERS

OXIDIZER TURBINE
FLOWMETERS

FLAME TUBE

H_2 PUMP CHILL-DOWN VENT
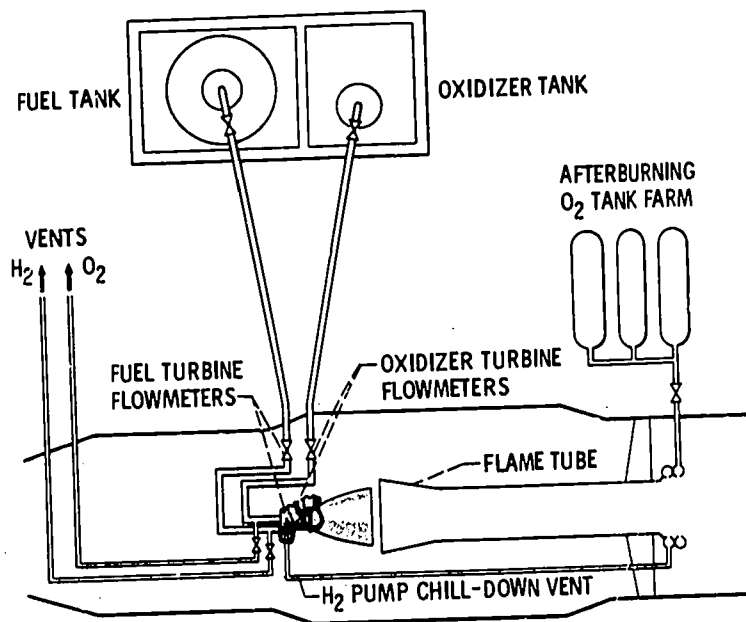
CD-9432

Figure 17-9. - Sketch of Centaur engine installed in Propulsion Systems Laboratory.

PROPELLANT SERVO
CONTROL VALVE

ALTITUDE TEST CHAMBER

THRUST LOAD CELL

ENGINE

ROTATING
EXHAUST
EQUIPMENT

EXHAUST EJECTOR

THRUST STAND

OXIDIZER TURBINE
FLOWMETERS

FUEL TURBINE
FLOWMETERS

PROPELLANT SERVO-
CONTROL VALVE

FUEL
TANK

OXIDIZER
TANK

TEMPERATURE CONTROLLED   CD-9433
PROPELLANT ENCLOSURES

Figure 17-10. - Sketch of engine with exhaust ejector.
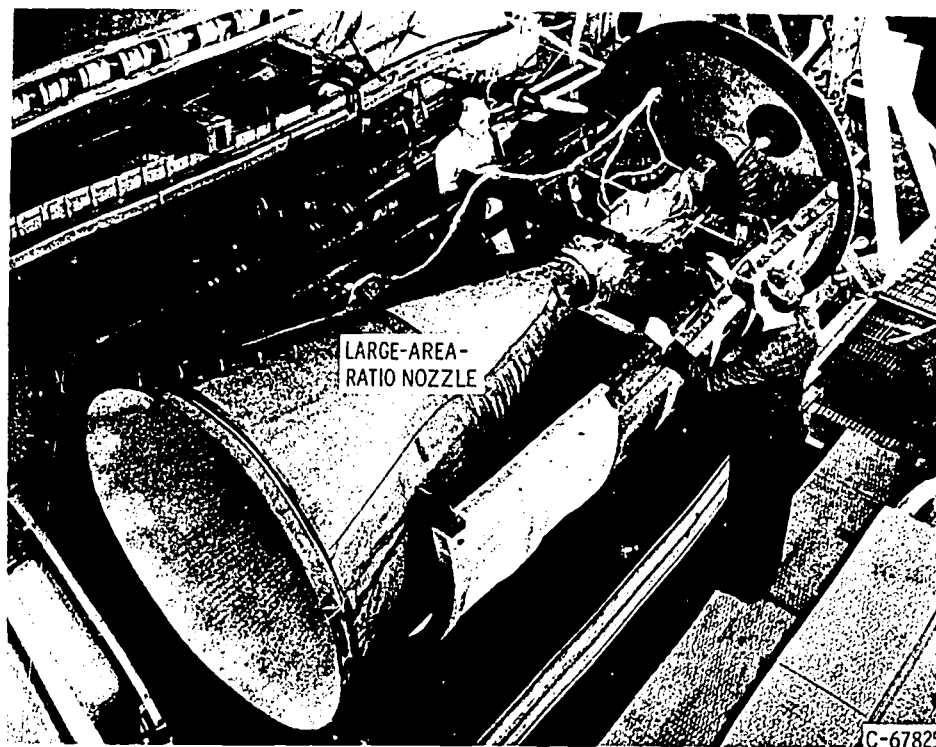
Figure 17-11. - Engine being installed in exhaust ejector in Propulsion Systems Laboratory.

flame tube are discharged into an evacuated system where they are first cooled and then removed by several banks of high-capacity pumps. Although satisfactory for many investigations, the vacuum obtainable by this method is limited by leakage through the PSL tank hatch. When the ultimate in vacuum is desired, as for a large-expansion-ratio rocket nozzle program, the engine is completely enclosed within an exhaust ejector as well (figs. 17-10 and 17-11). Engines having up to about 40 000 pounds thrust can be investigated in this facility.

COMBINED ENVIRONMENTS

Engine Testing

Testing rocket engines under a vacuum is significant because the thrust and efficiency of the rocket is determined as much by the pressure acting outside the engine as by what is going on inside. The latter, of course, is determined by how well the complete propulsion system (consisting of valves, meters, pumps, controls, tanks, etc.) functions, and this, in turn, is affected by other factors such as the thermal balance (and ultimately the temperature) of the various components and how long they have been in space. Obviously, this is of much greater concern for an upper stage that has to
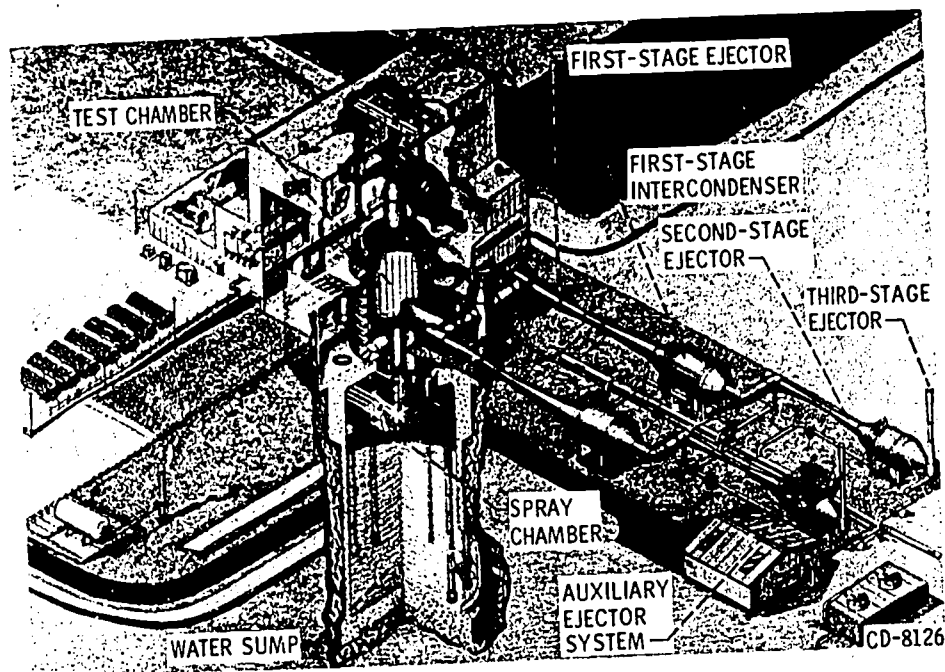
Figure 17-12. - Cross section of B-2 test facility.

function after being in space for some time than it is for the lower stages of a booster. With this in mind a new facility was designed with the capability of investigating the effects of thermal factors as well. This facility, which is approaching completion, is designated as the B-2 Spacecraft Propulsion Research Facility and is located at the NASA Plum Brook Station. Cutaway illustrations of this facility are presented in figures 17-12 and 17-13. Resembling the B-1 facility in that it is downward firing with the engine gases being pumped by both exhaust and steam ejector, the B-2 differs in having the exhaust ejector and cooling systems below ground; however the principal difference between the two facilities is that in the B-2, the complete stage, including the engines, can be exposed to a space environment for as long as desired before firing, whereas the B-1 installation can only produce a vacuum while the engine is running.

The space environment in the B-2 is simulated in a 38-foot-diameter chamber that surrounds the test vehicle. The inner wall of this chamber is lined with liquid-nitrogen panels (-320° F) that simulate the cold of space. Mounted near the inside wall is an array of quartz, infrared lamps that can be used to simulate solar heating. Proper coordination of these heaters with the liquid-nitrogen system will provide a satisfactory model of the space thermal environment. The space-vacuum environment that is required during testing is provided by a four-stage vacuum system that is connected to the chamber. This system will reduce the chamber pressure to 5×10^{-8} millimeter of mercury (equivalent to an altitude of about 200 miles) as long as the engines are not operating. Starting the engines destroys the vacuum and increases the pressure to an equiva-
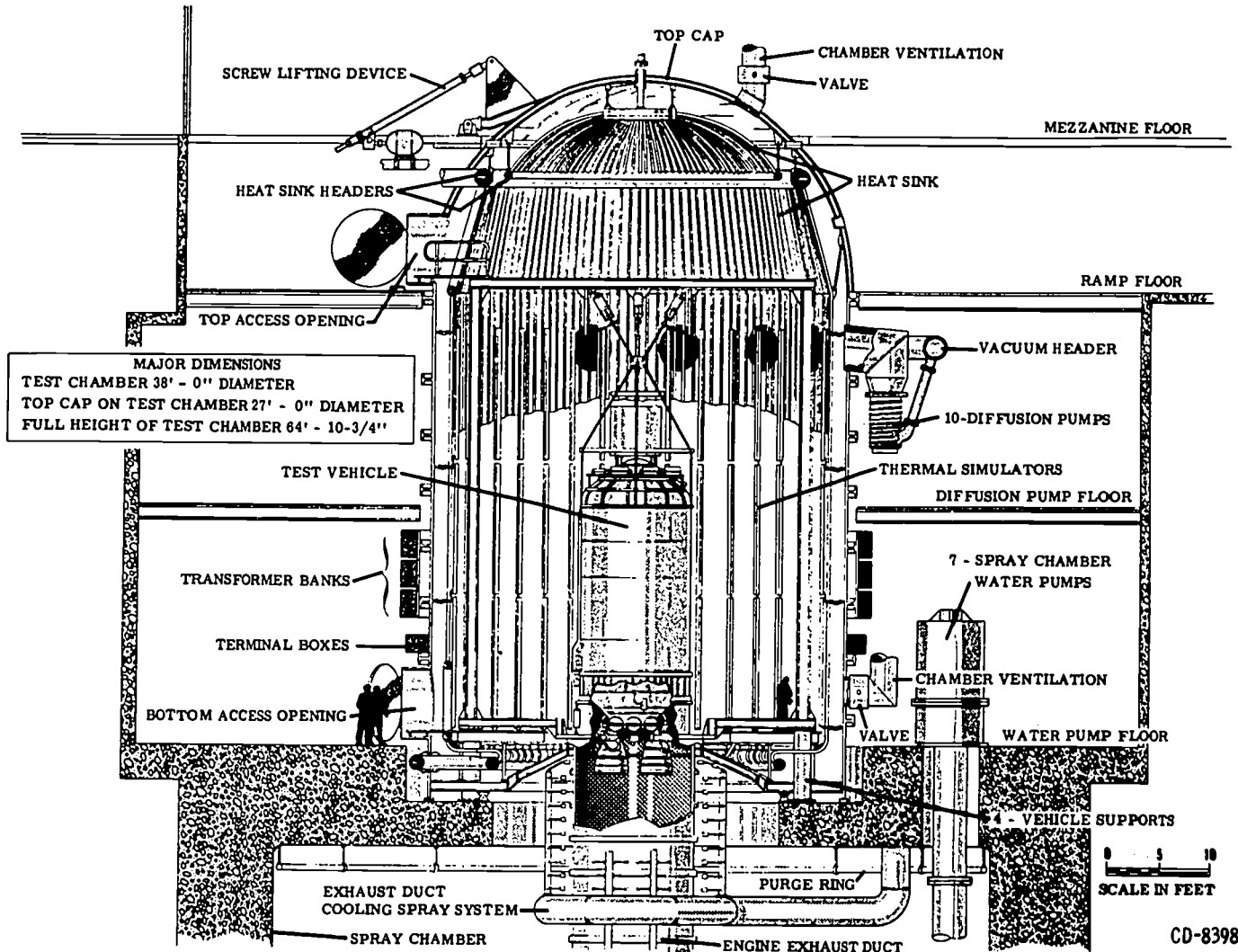
27 4

Figure 17-13. – Cross section of B-2 test chamber.

lent altitude of slightly less than 100 000 feet (about 20 miles); this is sufficient, however, for engine performance evaluation. The actual value of the equivalent altitude obtained during this phase is a function of engine size and becomes lower as the engines become bigger. The exhaust system is capable of handling total engine thrusts up to about 100 000 pounds for periods as long as 6 minutes.

Component Testing

In addition to rocket engine testing, space facilities in which the engines are not fired can be useful in many ways, such as determining the operating temperatures of
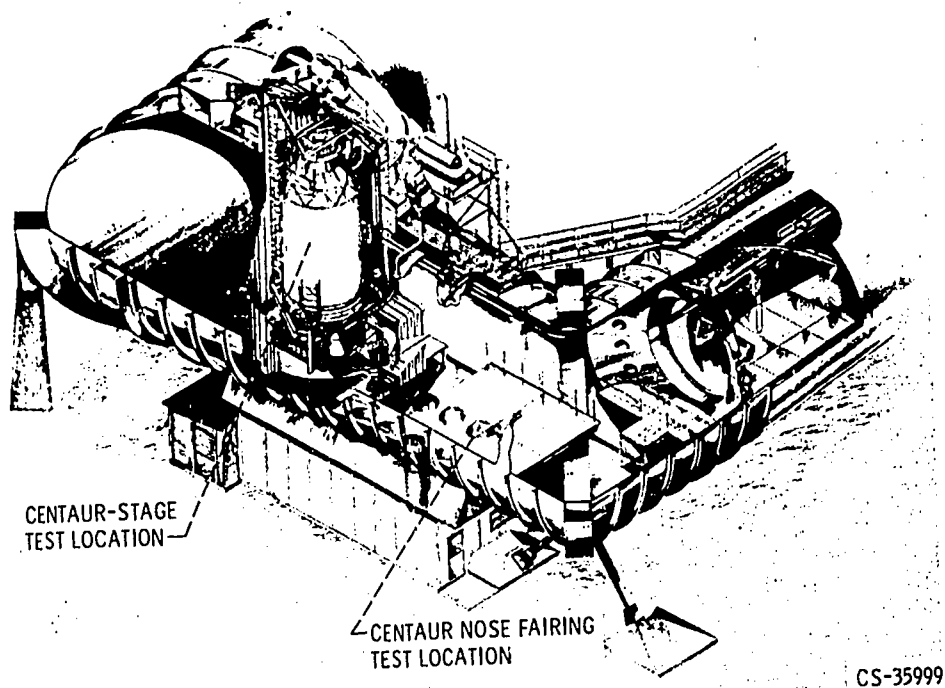
Figure 17-14. – Cross section of Space Power Chamber.

various components after a period of exposure or checking the function of electrical or mechanical components such as a power generating system, a guidance system, or the separation of a nose cone or insulation panels. One such facility that has been useful to the Centaur Project is known as the Space Power Chamber (SPC). This facility (fig. 17-14) was created by partitioning off and modifying a section of an old altitude wind tunnel and by installing liquid-nitrogen panels, solar heat simulators, and high-vacuum pumping equipment.

During space environment tests conducted on a complete Centaur stage in one end of this chamber, all the systems were actuated except for firing of the engines. Even the telemetry system was exercised, with data being transmitted to the Lewis telemetry station located in another building. A subsequent comparison of flight thermal data with that obtained in the test chamber showed excellent correspondence.

This chamber was also used for jettison tests of the Centaur nose fairing. In this case a real Centaur nose fairing with all its flight systems was installed in the opposite end of the chamber. During these tests an altitude of 100 miles was simulated, and although the nose cone had been successfully tested a number of times at sea-level pressure, it was not able to take the higher forces that were generated when the separation occurred in a vacuum. Needless to say, a redesign was required. When the redesigned nose cone was finally flown, a comparison of the flight data with that obtained in the vacuum chamber again showed good correspondence.
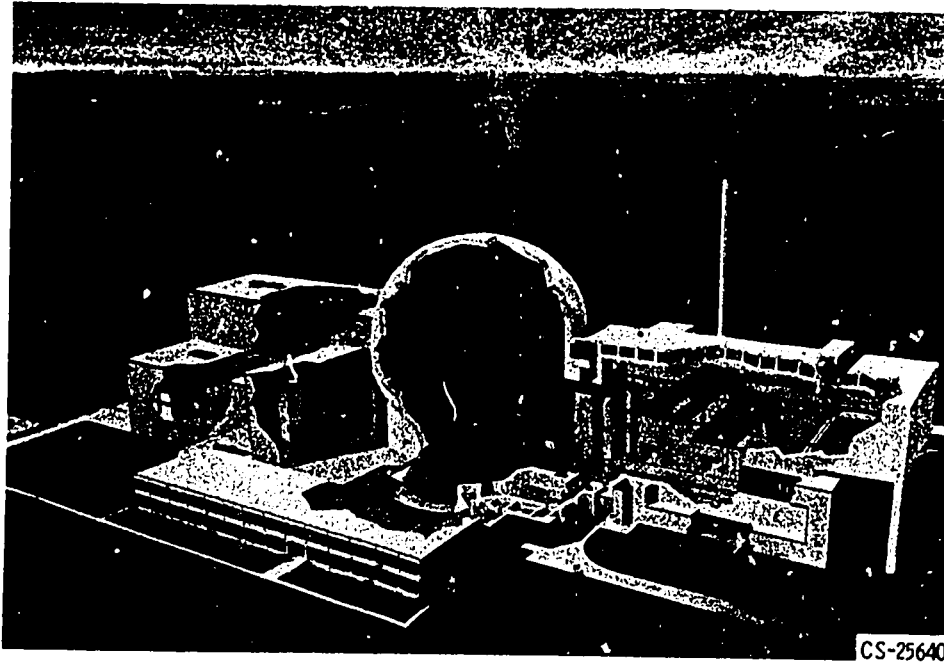
276

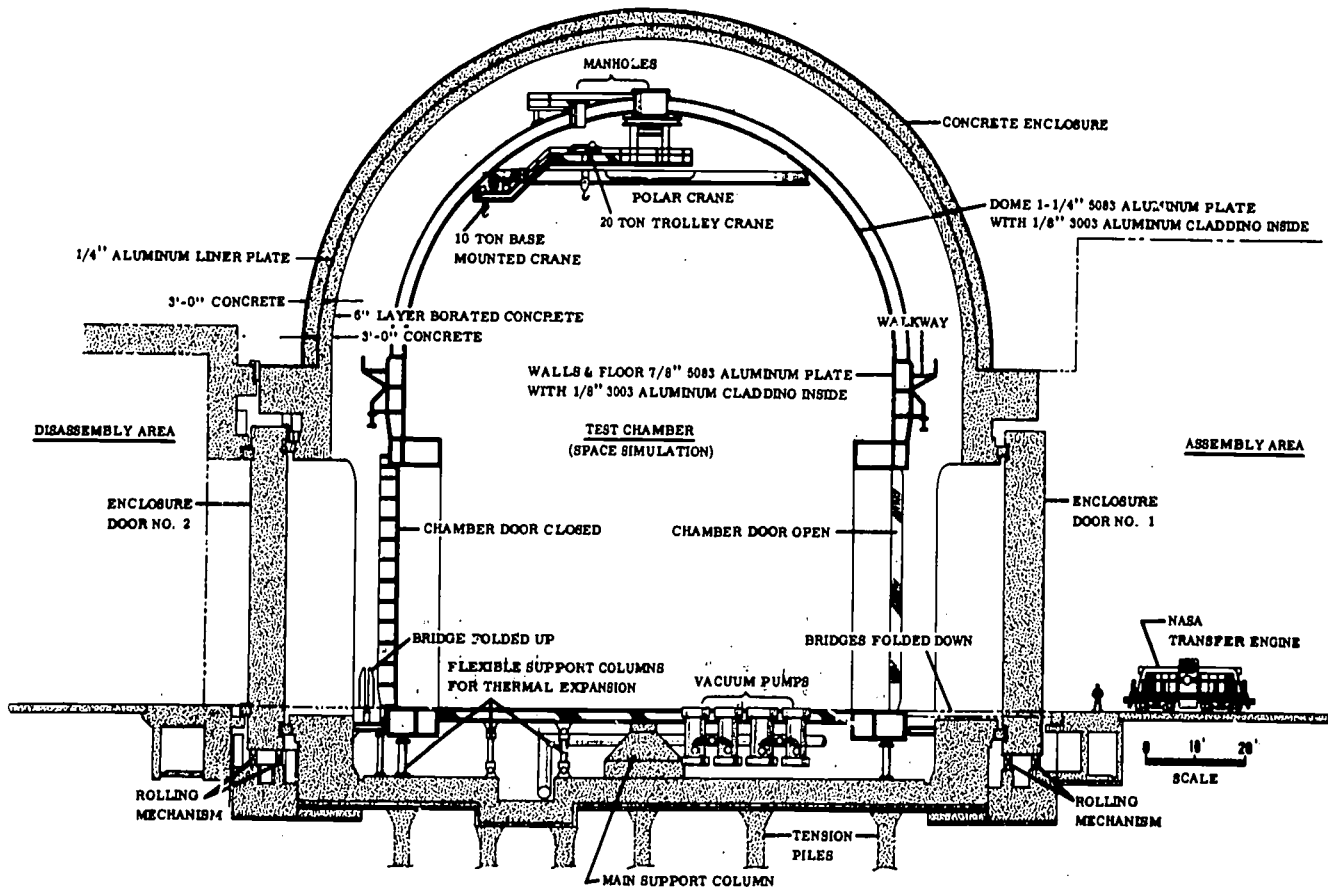Figure 17-15. - Cross section of Space Propulsion Facility.

Figure 17-16. - Cross section of Space Propulsion Facility test chamber.

273

Another Lewis space environmental facility of note is known as the Space Propulsion Facility (SPF), which is under construction at the Plum Brook Station and will be put into operation in early 1968. This facility, which is illustrated in figures 17-15 and 17-16, differs from the preceding one in that it will be used to test nuclear power generation and propulsion systems as well as larger, chemically propelled vehicles and spacecraft. The SPF will have an aluminum test chamber (fig. 17-16), 100 feet in diameter and $121\frac{1}{2}$ feet high, surrounded by a heavy concrete enclosure for nuclear shielding and containment. It will have facilities for assembly and disassembly of experiments and will be able to vibrate the system within a vacuum environment (ultimate capacity 6×10^{-8} mm Hg). It will also have experiment-control and data-acquisition systems. Rather than building in a thermal simulation system of heaters and cryogenic panels, these systems will be built for the particular experiment being conducted. The facility, of course, is designed to comply with all the AEC safety regulations applicable to reactors as large as 15 megawatts. The concrete shielding walls are approximately 6 feet thick so that the radiation levels experienced by people working nearby will be less than the levels specified by AEC. This is one of the most advanced space environmental chambers under construction and should be useful in future investigations.

STRUCTURAL DYNAMICS

In addition to the large facilities for evaluating the effects of the space environment on upper stage and propulsion system performance, large facilities are also necessary for determining the structural characteristics and capabilities of complete boosters. The reason for this is that, although it is generally possible to calculate the natural frequencies of the first and second bending modes of a complete launch vehicle as well as the dynamic loads that would be encountered at these frequencies, it is impossible to calculate these for the higher modes. Calculating the damping of the vehicle is also impossible. Further, there are additional factors such as the interplay between the propellant system and the structure which cannot be computed and which have a significant effect. Thus, the surest way to assess the structural capabilities of a vehicle is to test it on a dynamic test stand like that which has been successfully used for the Atlas-Centaur-Surveyor vehicle. This stand (fig. 17-17) is known as the E-stand and is located at the Plum Brook Station. As illustrated in figure 17-18, the method of installation is to suspend and position the complete vehicle by means of springs with natural frequencies (in combination with the masses involved) lower than those of the vehicle so that it can respond to the electrodynamic shaker without being influenced by the suspension and positioning systems. No environmental factor is simulated in these tests other than the dynamic force inputs.
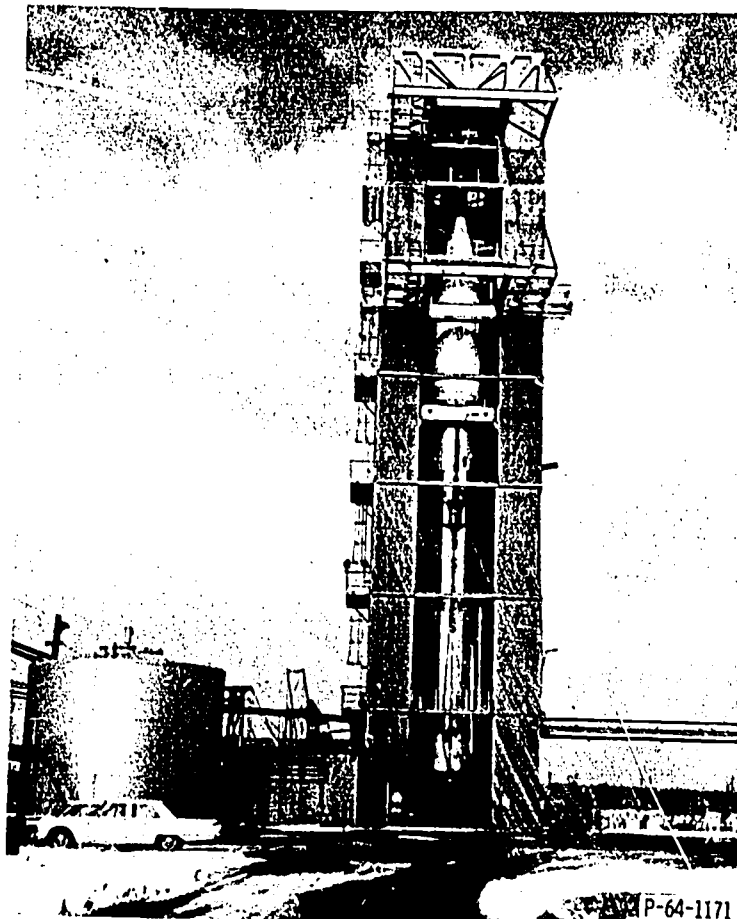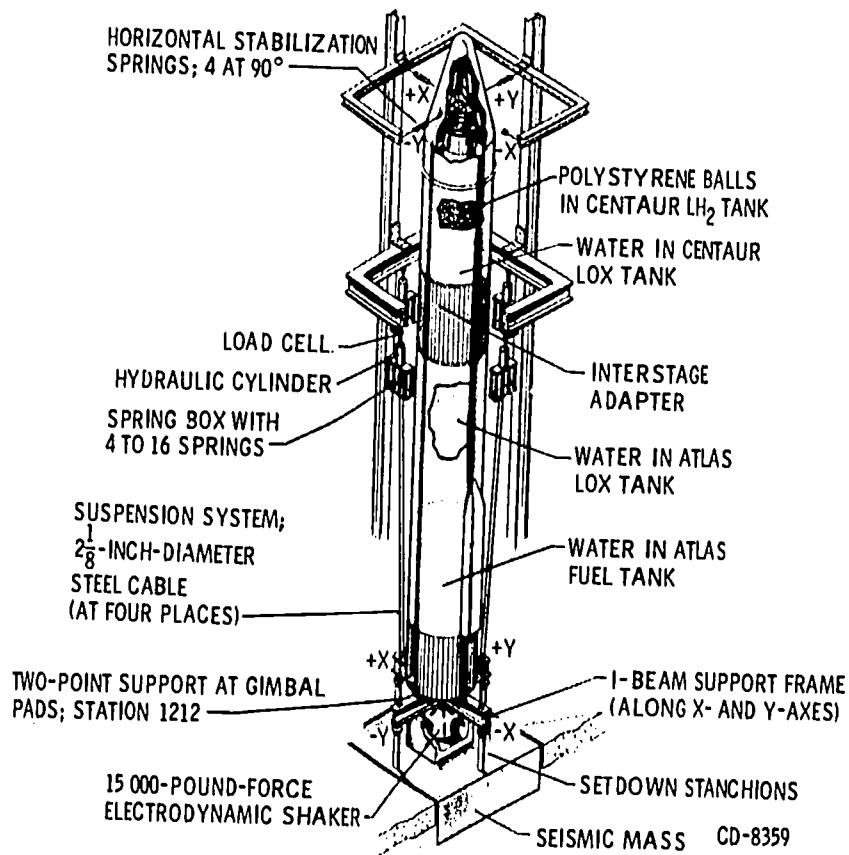
Figure 17-17. – E-stand.

HORIZONTAL STABILIZATION SPRINGS; 4 AT 90°

POLYSTYRENE BALLS IN CENTAUR LH$_2$ TANK

WATER IN CENTAUR LOX TANK

LOAD CELL

HYDRAULIC CYLINDER

SPRING BOX WITH 4 TO 16 SPRINGS

INTERSTAGE ADAPTER

WATER IN ATLAS LOX TANK

SUSPENSION SYSTEM; $2\frac{1}{8}$-INCH-DIAMETER STEEL CABLE (AT FOUR PLACES)

WATER IN ATLAS FUEL TANK

TWO-POINT SUPPORT AT GIMBAL PADS; STATION 1212

I-BEAM SUPPORT FRAME (ALONG X- AND Y-AXES)

15 000-POUND-FORCE ELECTRODYNAMIC SHAKER

SETDOWN STANCHIONS

SEISMIC MASS   CD-8359

Figure 17-18. – Atlas-Centaur Installed In E-stand.

Perhaps the following brief discussion will explain the nature of the problem better. Chapter 11 mentioned that the performance of a booster system is highly dependent on its weight, with the lighter systems having superior performance. Accordingly, structural weight is kept to a minimum and usually ranges between 6 and 10 percent of the total launch weight for the better systems. In addition, minimum drag requirements for the flight path through the atmosphere dictate a long slender vehicle. The result is a highly elastic vehicle with a continually changing natural frequency that is caused by the mass change due to propellant consumption and varying G-forces during flight. The problem is further complicated by the many different disturbances and forces that can be encountered:

(a) During engine ignition
(b) By the sudden launcher release at lift-off
(c) By the ground winds
(d) By the high altitude gusts (jetstream)
(e) By vectoring the engines
(f) As a result of coupling between the engine, propellant system, and structure
(g) By sloshing of the propellants
(h) During engine shutdown
(i) During separation of the stages
(j) During insulation-panel or nose-cone separation
(k) As a result of the aerodynamic and shock wave pressures generated during flight through the atmosphere
(l) By the firing of attitude control engines

These forces, acting singly or in combination, can produce one or more of the following types of deflection of the vehicle:

(a) Lateral - where the vehicle is deflecting normal to its centerline axis (bending)
(b) Longitudinal - where the vehicle is deflecting parallel to its centerline axis (becoming alternately shorter and longer); this can be either a nonreinforced or a reinforced oscillation which is augmented by the engine and propellant systems (called pogo) which results in much greater deflections
(c) Torsional - where the vehicle is rotating about its centerline axis in alternately opposite directions

Generally one or more modes of each type of deflection may develop during a flight, so the vehicle should be tested through at least the third mode, if possible. Inasmuch as a vehicle in flight is in free-free condition (no restraint at any point), the characteristic free-free deflection curves are used to define the modes of oscillation. Thus, a vehicle deflection curve that looks like ⌒ defines the first mode, one that looks like ⌒⌣ the second mode, and one like ⌣⌢⌣ the third.
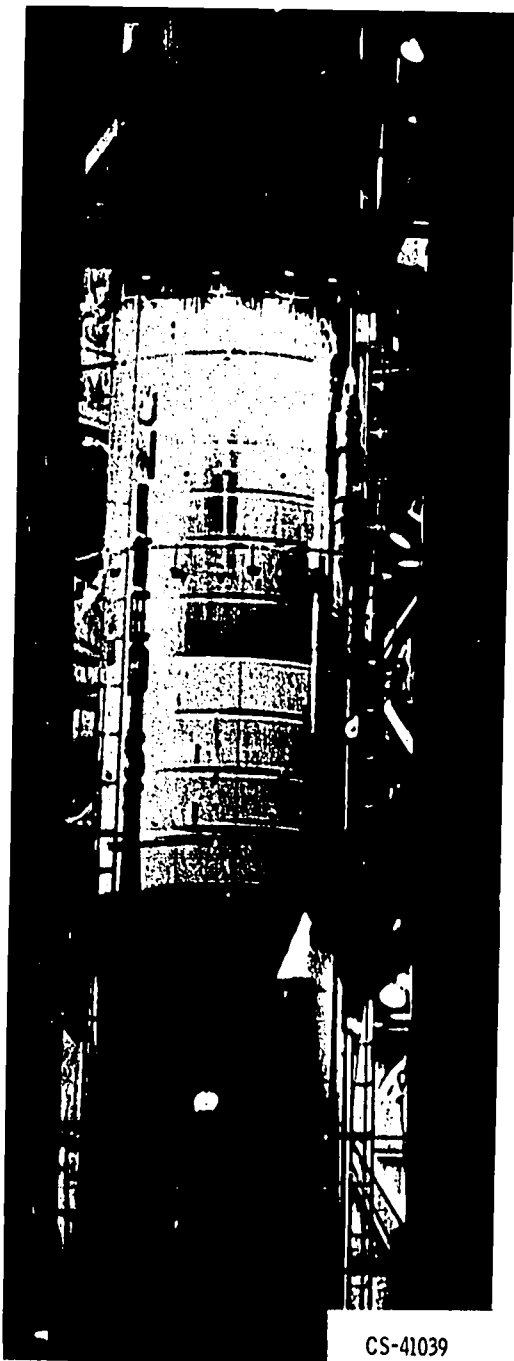
CS-41039

(a) Overall view following test.
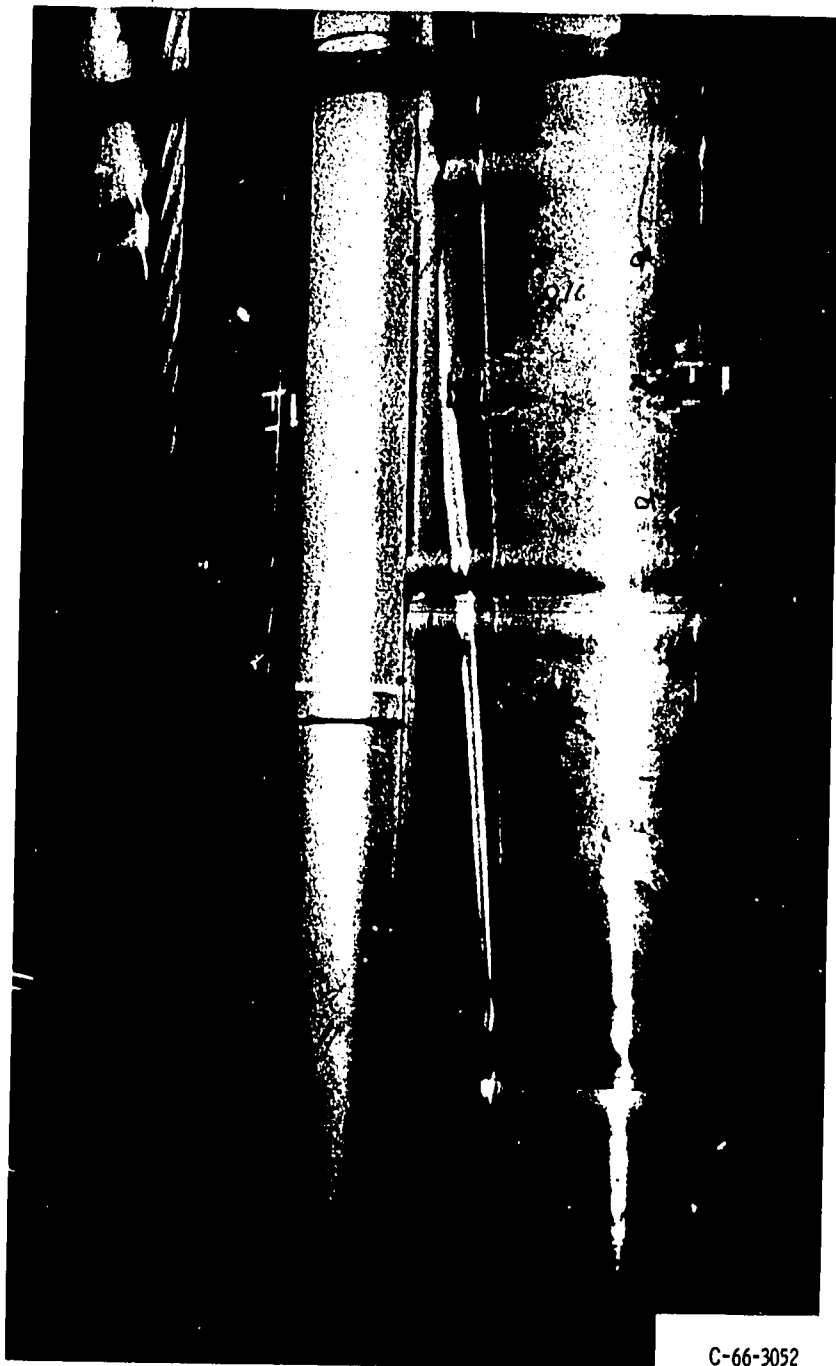
C-66-3052

(b) Closeup of wrinkle patterns.

Figure 17-19. - Atlas tested to ultimate load capacity.

In addition to the mode and type of deflection, another factor that must be considered is the amount of damping inherent in the vehicle. If it is equal to or greater than the critical damping, then a single, suddenly applied load will not make the vehicle oscillate at any of its natural frequencies. If it is less than critical, then the vehicle will oscillate at one of its natural frequencies but with a decreasing amplitude as follows: ⎰ⵠⵠⵠⵠ⎱ Vehicle damping is a difficult thing to predict and is best revealed by a full-scale experiment or by comparison with similar vehicles for which it is known.

A complete determination of the structural characteristics of a rocket booster in flight is a complex affair. The engineering approach that is generally employed is as follows: First, the structural equations defining the vehicle deflection modes at any point in time are derived (with the use of the spring-mass method), then the damping is estimated, and finally the effects of all the various disturbances are calculated. The vehicle is then tested in a stand similar to the E-Stand, and the experimental results are compared with those predicted. If they are the same, that is fine, but if not, then the equations must be modified until they represent the actual event. Once agreement is obtained, then flight performance can be reliably predicted.

In addition to dynamic response, the E-Stand is also valuable for determining the ultimate load capability of a launch vehicle. An experiment of this type was conducted on an Atlas booster (fig. 17-19) which revealed that the ultimate load capability of the Atlas was about 50 percent greater than had been previously assumed. This is a significant result because it means that the Atlas still has a substantial growth potential for future space missions.

RELIABILITY AND QUALITY ASSURANCE

All the foregoing discussion of facilities and environmental testing is concerned primarily with the performance evaluation of complete propulsion systems and stages. Every stage, of course, is made up of thousands of parts (over 300 000 in the Atlas), and it is difficult to ascertain that all these parts will satisfactorily function at one time, so that the intended mission will be successful. This was recognized as a problem area in the aerospace industry in the early 1950's, and it was then that reliability and quality assurance engineering, as known today, began. It combines the elements of engineering, statistics, and good sense for evaluating the probability that a given system, subsystem, or part will perform its intended function for a specified time under specified conditions.

The reliability field can be broken down into two basic areas: (1) design goal reliability and (2) use or operational reliability. During the design of a component an estimate can be made of its reliability if the reliabilities of the individual parts are known. This can be calculated from the mathematical expression for individual reliability,

$$R = e^{-t/MTBF}$$

where R is the reliability (or probability of success), e is a constant, t is the mission time, and $MTBF$ is the mean time between failures or operating hours divided by numbers of failures. For the more complex case where the failure of any one part will cause failure of the entire component, the total reliability equation is

$$R_{system} = R_1 \times R_2 \times R_3 \times \ldots R_N$$

It is thus evident that for high system reliability it is necessary to have extremely high part reliability.

Once the component has been built, it is still necessary to evaluate its reliability experimentally because manufacturing and assembly processes vary and also because the environment that the parts experience in this component may be somewhat different than that for which they were designed. This is usually done in a series of design evaluation and proof tests. If the failure rates from these tests are plotted against total operating time (for all components) a curve similar to the one in figure 17-20 is usually obtained.
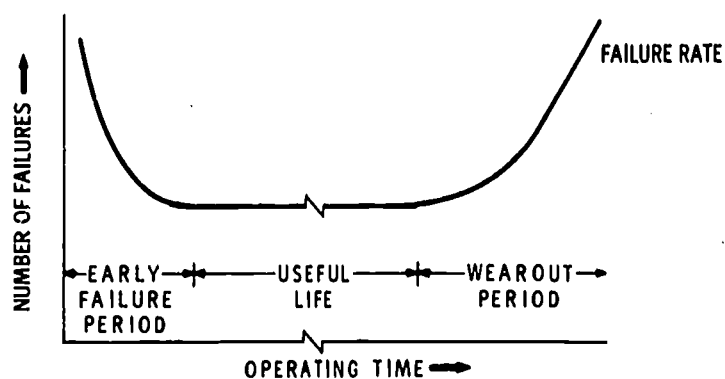

Figure 17-20. - Idealized failure rate curve.

The high failure rate that usually occurs in the early period is generally a result of initially poor parts, marginal design, or both. The high rate that is obtained in the later period is usually a result of wearing out. The fairly low, constant rate that falls between the two high rates is defined as the useful life. For a high reliability, the useful life should be long compared with the time a part has to operate, and the failure rate during the useful life should be as low as possible. Inasmuch as testing is the primary indicator of reliability, the more tests that are run and the more data that are obtained, the more confidence there will be in the results. Confidence can be reduced to a statistical value which reflects the degree of probability that a given statement of reliability is

correct. Of course, in order to achieve and maintain a given reliability, it is necessary to originate designs with sufficient operating margins, provide specifications for the processes as well as the finished parts, and enforce a comprehensive system of quality control or assurance. Constant vigilance and attention to detail is the price of high reliability.

18. LAUNCH OPERATIONS

Maynard I. Weston*

Launching and monitoring the flight of an unmanned scientific probe takes a good deal of money and the dedicated hard work of literally thousands of people. This effort can be clearly seen in the Atlas-Agena Lunar Orbiter B program. Although the vehicle has only a booster and an upper stage and involves fewer people and organizations than the more complicated Apollo launch vehicle, the types of activity needed to launch the Atlas-Agena are the same. The problems of the smaller vehicle illustrate those of the larger. For example, the same general type of documentation that is shown in table 18-I for the planning of an Atlas-Agena launch is required for all space launches regardless of vehicle size.

This discussion of the Atlas-Agena-Orbiter concentrates on the hardware, organization, testing, and support of a typical launch.

HARDWARE

Spacecraft

The Lunar Orbiter B spacecraft weighs 845 pounds and is covered by an aerodynamic shroud during atmospheric flight. In this configuration, with its solar panels and antennas folded, it is about 5 feet in diameter and almost 6 feet long. When the panels and antenna are unfolded in space, the maximum span increases to almost 19 feet. The spacecraft is carried into a translunar trajectory by a two-stage Atlas-Agena launch vehicle (fig. 18-1).

The main object of the Lunar Orbiter program is to learn as much as possible about the topography of the Moon. This information will be particularly useful during the Apollo manned lunar landings. The Orbiter spacecraft are equipped with cameras to give a detailed picture of the Moon's surface, and each Orbiter in the series travels a different path to photograph a different portion of the Moon.

---

*Chief, Operations Branch, Agena Project.

```
                              13.44 ft
        PAYLOAD
        SECTION

        AGENA D        12.63 ft

        BOOSTER
        ADAPTER        11.72 ft

104.48 ft

        ATLAS

                       66.69 ft
```
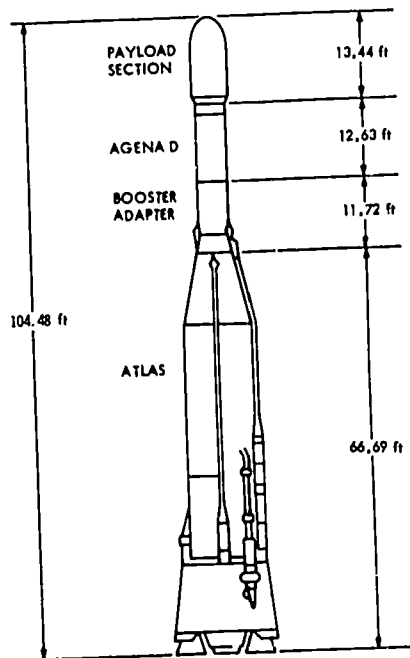
Figure 18-1. - Atlas-Agena launch vehicle.

Atlas Booster

The first stage of the launch vehicle, an Atlas booster (fig. 18-2), is built by General Dynamics/Convair and is about 70 feet long and 10 feet across, although it widens to 16 feet across the flared engine nacelles. The 388 340 pounds of thrust that propels the Atlas is generated by a booster system with two thrust chambers, a sustainer engine, and two vernier engines. All are single-start, fixed-thrust engines and operate on

CS-41446
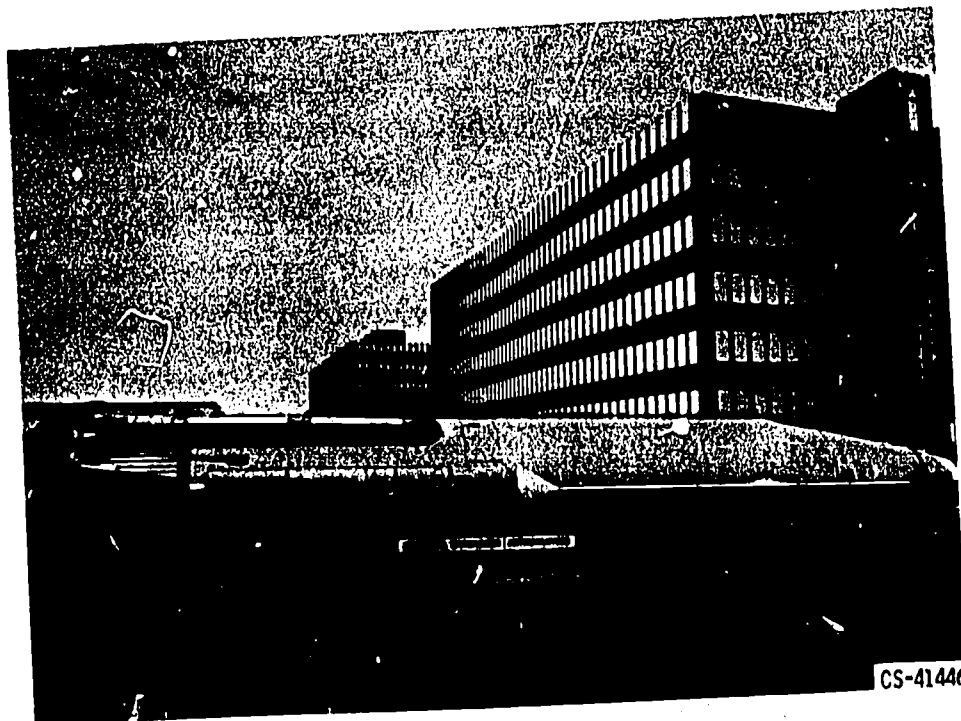
Figure 18-2. - Atlas booster.

liquid oxygen and kerosene. The Atlas is radio controlled by a computer-operated, ground-based system.

Agena Rocket

Lockheed Missiles and Space Company builds the second stage, an Agena rocket. It is about 23 feet long and 5 feet across. The liquid-propellant engine uses unsymmetrical dimethylhydrazine (UDMH) as fuel and inhibited, red, fuming, nitric acid (IRFNA) as oxidizer to generate 16 000 pounds of thrust for 240 seconds. This total thrust time can be divided into two separate burns. The Agena is guided by a preprogrammed autopilot system using horizon sensors and a velocity meter cutoff.

Launching Facilities

The Atlas-Agena-Orbiter is launched from Complex 13 at Cape Kennedy. All necessary facilities for conducting final tests, fueling, countdown, and launch, as well as installations for tracking, photographing, and monitoring significant events during the preparation, countdown, and launch, are available at Complex 13. These facilities and their relation to the remainder of Cape Kennedy are shown in figures 18-3 and 18-4. The launch complex has two major portions, the blockhouse and the test stand, and a variety of lesser supporting installations.
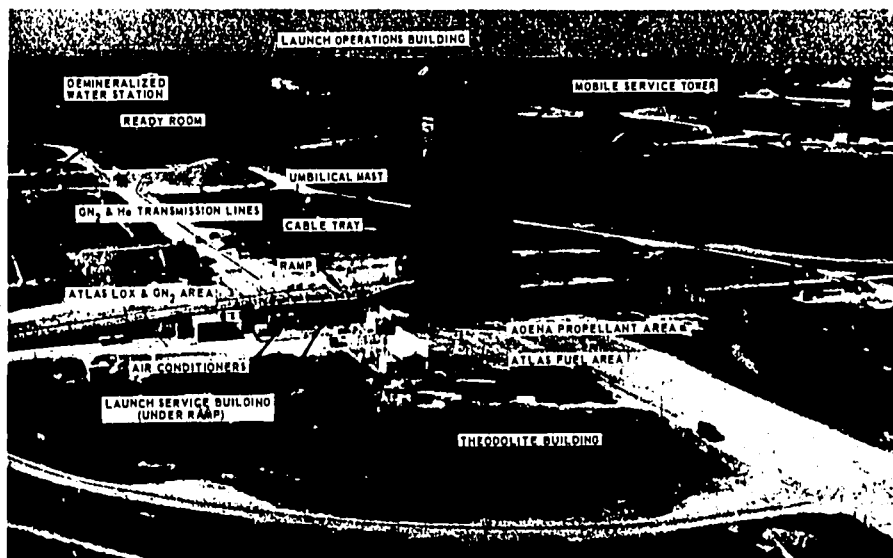

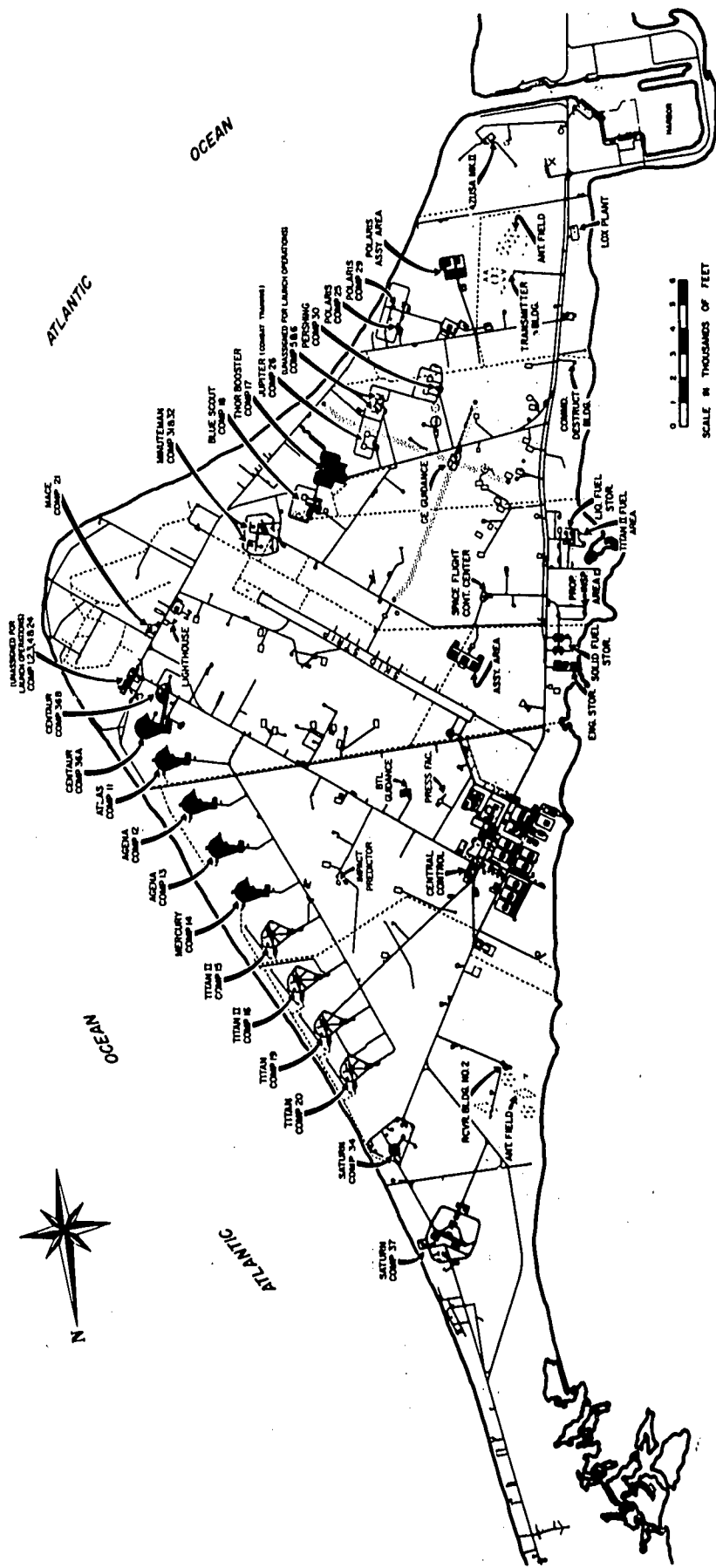Figure 18-3. - Launch Complex 13 at Cape Kennedy.

Figure 18-4. — Cape Kennedy facilities.

Blockhouse. - This structure is the control center for the entire launch operation. It is made of concrete, heavily reinforced with steel, has approximately 6400 square feet of floor space, and is about 800 feet from the test stand; a single, vault-type door is its only entrance, and this is sealed during launching. Inside are the consoles and equipment to control and monitor all systems of the launch vehicle, propellant loading and unloading, automatic sequencing, communications, launch pad, closed-circuit television, and land-line recording. The blockhouse is connected to the launch pad and propellant service area by weatherproof wiring tunnels.

Although the blockhouse has the facilities to monitor important spacecraft functions, as well as those of the vehicle, the primary center for this activity is the Deep Space Station at Cape Kennedy.

Test stand. - The major installations which comprise the test-stand area are the launch service building, the launcher mechanism, the service tower (gantry), the umbilical mast and boom, the propellant storage tanks and transfer equipment, various gas storage and loading facilities, general storage areas, and workshops.

The gantry is used for erecting the Atlas, the Agena, and the spacecraft, and for supporting the system during checkout and countdown. A launch mechanism is used for controlling the vehicle during the first moments of launch. The last function is effected by pneumatically operated holddown clamps, which restrain the vehicle until thrust is strong enough to ensure a stable flight.

Near the gantry is the spacecraft checkout van. It contains the facilities to test and monitor the operation of this system.

ORGANIZATION

A single agency is assigned complete responsibility for each NASA mission. Depending on the type of mission, this agency might be the Jet Propulsion Laboratory, the Goddard Space Flight Center, or one of the other NASA institutions. In the case of the Lunar Orbiter program, the operation is directed by the Langley Research Center (LRC), which coordinates the work of several different private, public, and military organizations. The Orbiter involves four major activities: The Lewis Research Center (LeRC) is responsible for the launch vehicle, the Eastern Test Range (ETR, an Air Force activity) for the launch and range support, the Jet Propulsion Laboratory (JPL) for coordinating and integrating tracking and data acquisition systems, and finally Langley's own development of the spacecraft. The overall organization of government and contractor elements responsible for the Lunar Orbiter prelaunch operations is shown in figure 18-5.
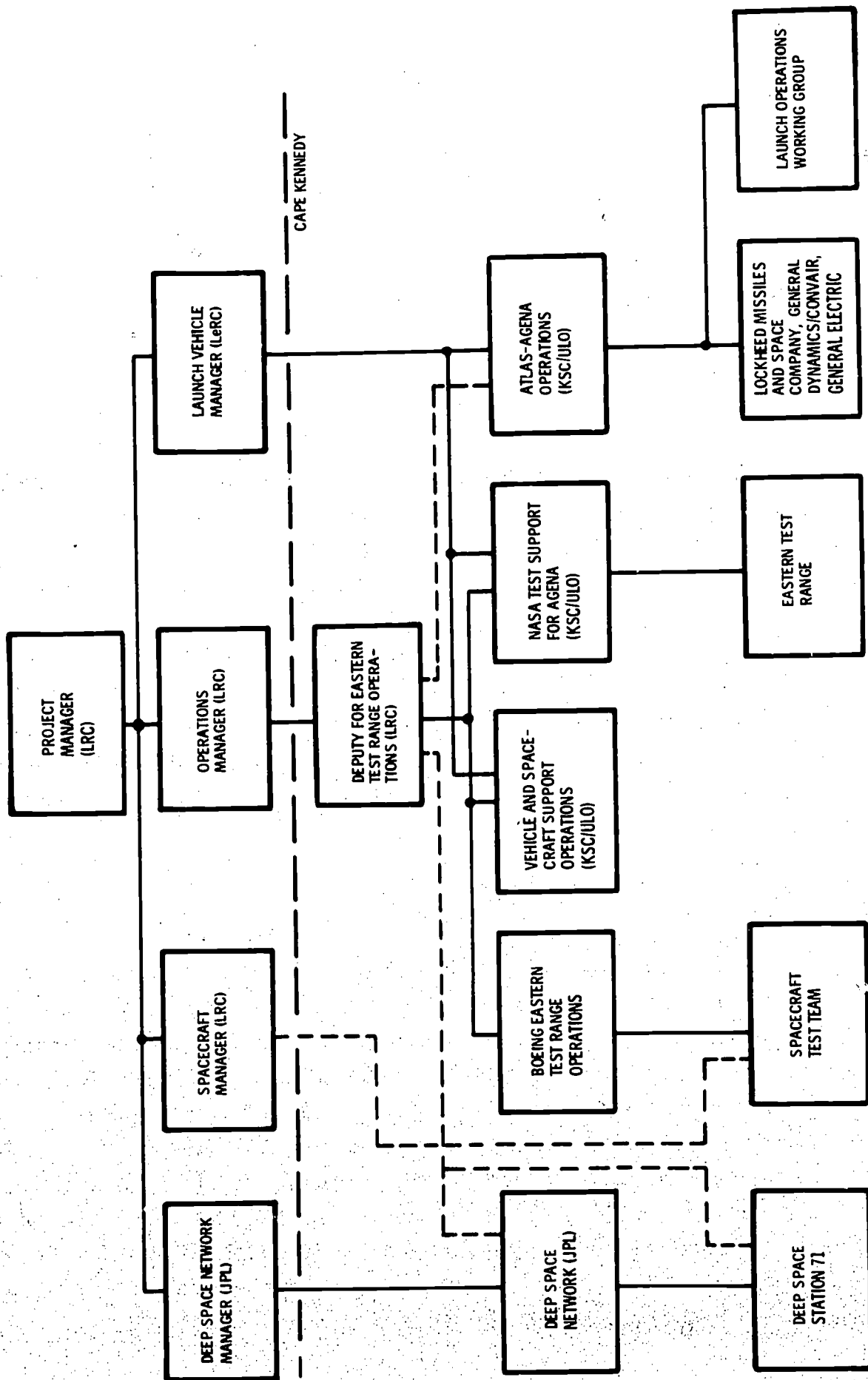
Figure 18-5. - Lunar Orbiter organization for Cape Kennedy prelaunch operations.

PROJECT MANAGER (LRC)

OPERATIONS MANAGER (LRC)

LAUNCH VEHICLE MANAGER (LeRC)

SPACECRAFT MANAGER (LRC)

DEEP SPACE NETWORK MANAGER (JPL)

DEPUTY FOR EASTERN TEST RANGE OPERATIONS (LRC)

CAPE KENNEDY

ATLAS-AGENA OPERATIONS (KSC/ULO)

NASA TEST SUPPORT FOR AGENA (KSC/ULO)

VEHICLE AND SPACE-CRAFT SUPPORT OPERATIONS (KSC/ULO)

BOEING EASTERN TEST RANGE OPERATIONS

DEEP SPACE NETWORK (JPL)

LAUNCH OPERATIONS WORKING GROUP

LOCKHEED MISSILES AND SPACE COMPANY, GENERAL DYNAMICS/CONVAIR, GENERAL ELECTRIC

EASTERN TEST RANGE

SPACECRAFT TEST TEAM

DEEP SPACE STATION 71

COORDINATION AND TEST SUPPORT

TECHNICAL DIRECTION

Launch Vehicle

Since the Atlas-Agena vehicle has two stages, the Lewis Research Center must coordinate the work of two contractors, General Dynamics/Convair (GD/C) and Lockheed Missiles and Space Company (LMSC). Each of these organizations is responsible for manufacturing, testing, and installing its section on the launch pad - GD/C the Atlas and LMSC the Agena. Lockheed, moreover, is responsible for integrating the two stages.

Spacecraft

Once the two stages are in place, the spacecraft must be installed. This is done by its contractor, The Boeing Company (TBC), under the direction of Langley Research Center.

Launch Facilities

The Eastern Test Range is operated by the Air Force to provide all the necessary supporting staff and installations required to launch and use space missions. The ETR coordinates the Atlas-Agena-Orbiter program with other launching activities, maintains the launching complex, and manages the lesser but important services such as housing, security, safety, and weather.

Tracking and Data

The tracking of the launch and the collection of the data that are the reason for the Orbiter are done by ETR in conjunction with the Deep Space Network, which is under the direction of the Jet Propulsion Laboratory.

PREPARATION AND LAUNCH

Preassembly Tests

Before the Atlas-Agena-Orbiter is launched, it must pass through several inspections and tests, both as individual components and as an assembled unit. Even before delivery to Cape Kennedy, each section must have passed a final quality test at the contractor's plant. Upon arrival at the Cape (figs. 18-6 and 18-7), each section is again tested by its contractor and then assembled. Figures 18-8, 18-9, and 18-10 show major assembly steps.
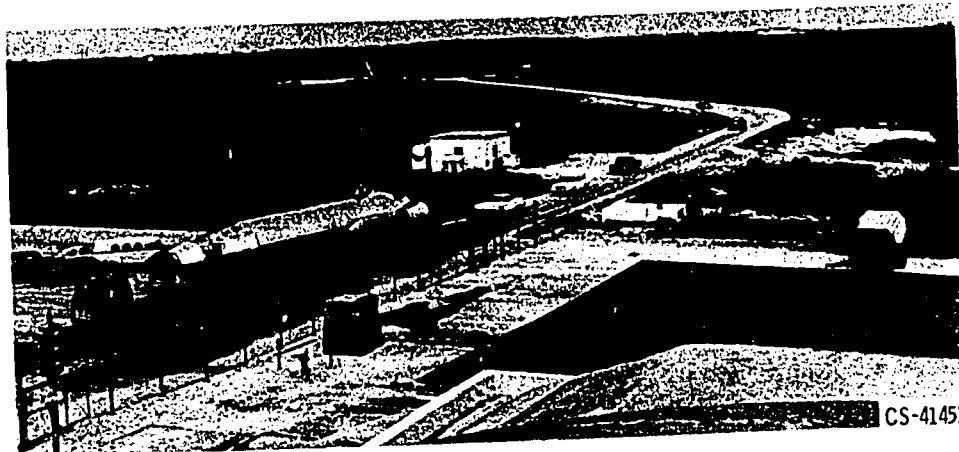

CS-41453

Figure 18-6. – Atlas transport to pad.
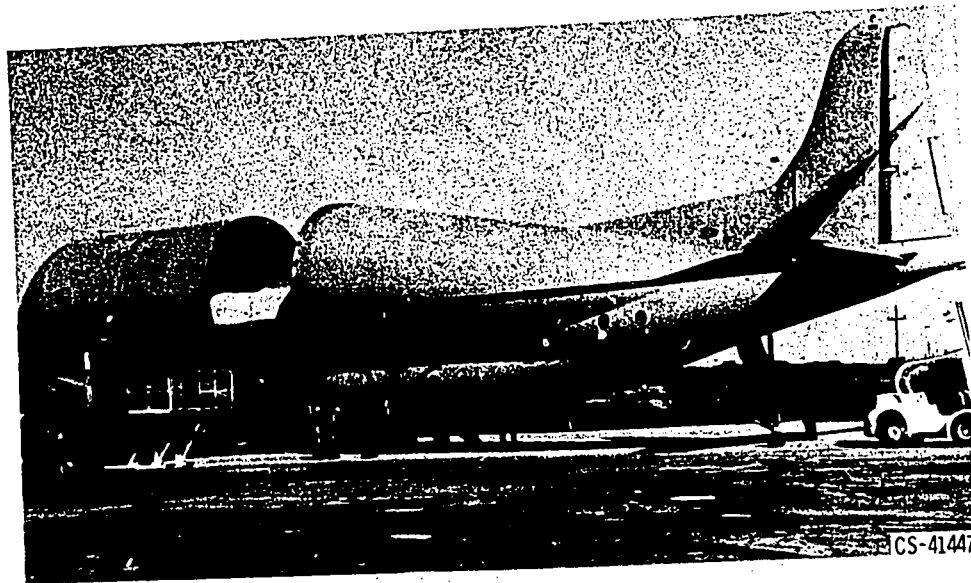
CS-41447

Figure 18-7. – Arrival of Agena stage.

292

Figure 18-8. – Atlas being erected on pad.
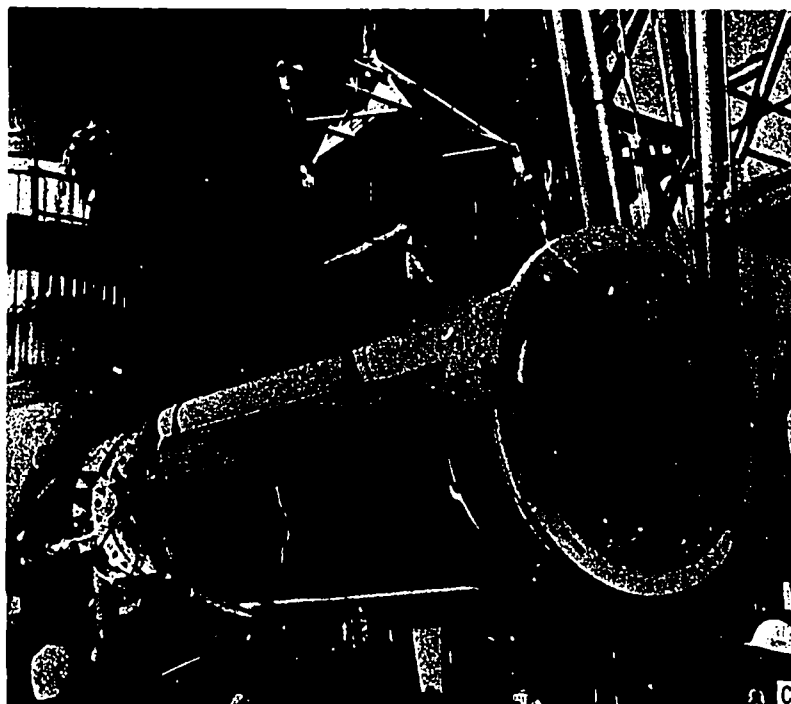
Figure 18-9. – Agena being raised to top of Atlas.
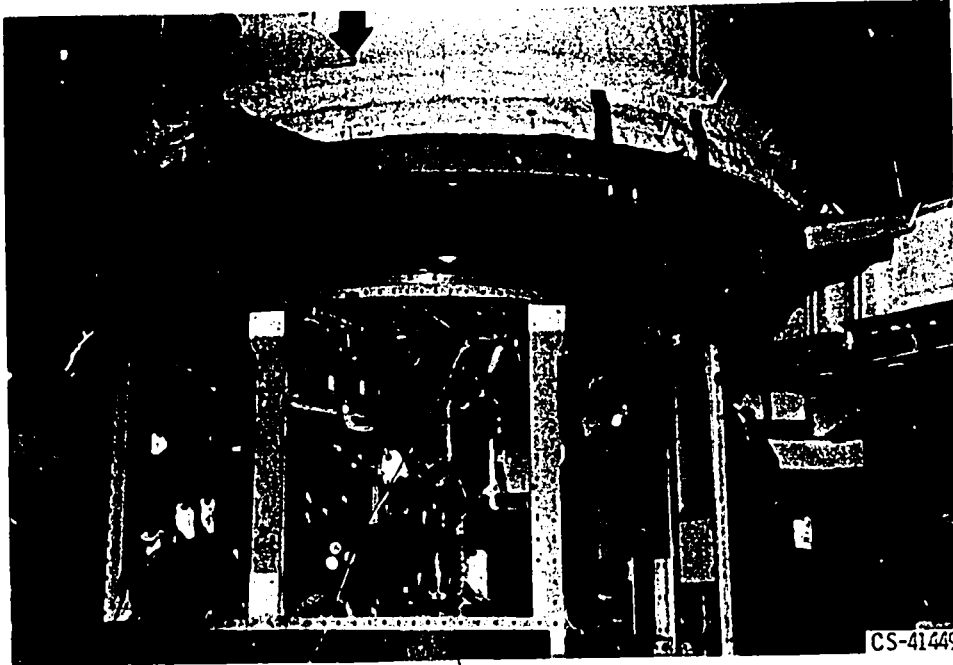
Figure 18-10. - Mating encapsulated Orbiter-B to Agena.

Assembly and Testing

The first stage, the Atlas vehicle, is the first section to be erected on the launch pad. As soon as it is in place, it is tested to ensure that all systems are still functioning properly and will respond only to the correct signals from the blockhouse. In addition, the Atlas fuel tanks are checked to make sure that they will withstand the temperatures and pressures imposed on them without leaking.

After the first stage is in place and has passed all the inspections, the Agena is installed. Testing now is conducted not only on the Agena but also on the electrical and mechanical connections between it, the Atlas, and the ground equipment.

The spacecraft is the last section to be installed on the vehicle. Again, the assembly tests are conducted to establish both the individual and combined reliability.

After it is determined that all systems of the Atlas-Agena-Orbiter and all systems on the ground are operating perfectly, a simulated launch is conducted. This operation gives the final assurance that all systems have been correctly integrated and that all supporting ground facilities are ready for the launch. This full dress rehearsal is as realistic as possible, even including fueling; only the last 19 seconds before the actual firing are omitted.

The prelaunch tests and operations outlined in figure 18-11 take place according to the schedule presented in figure 18-12.
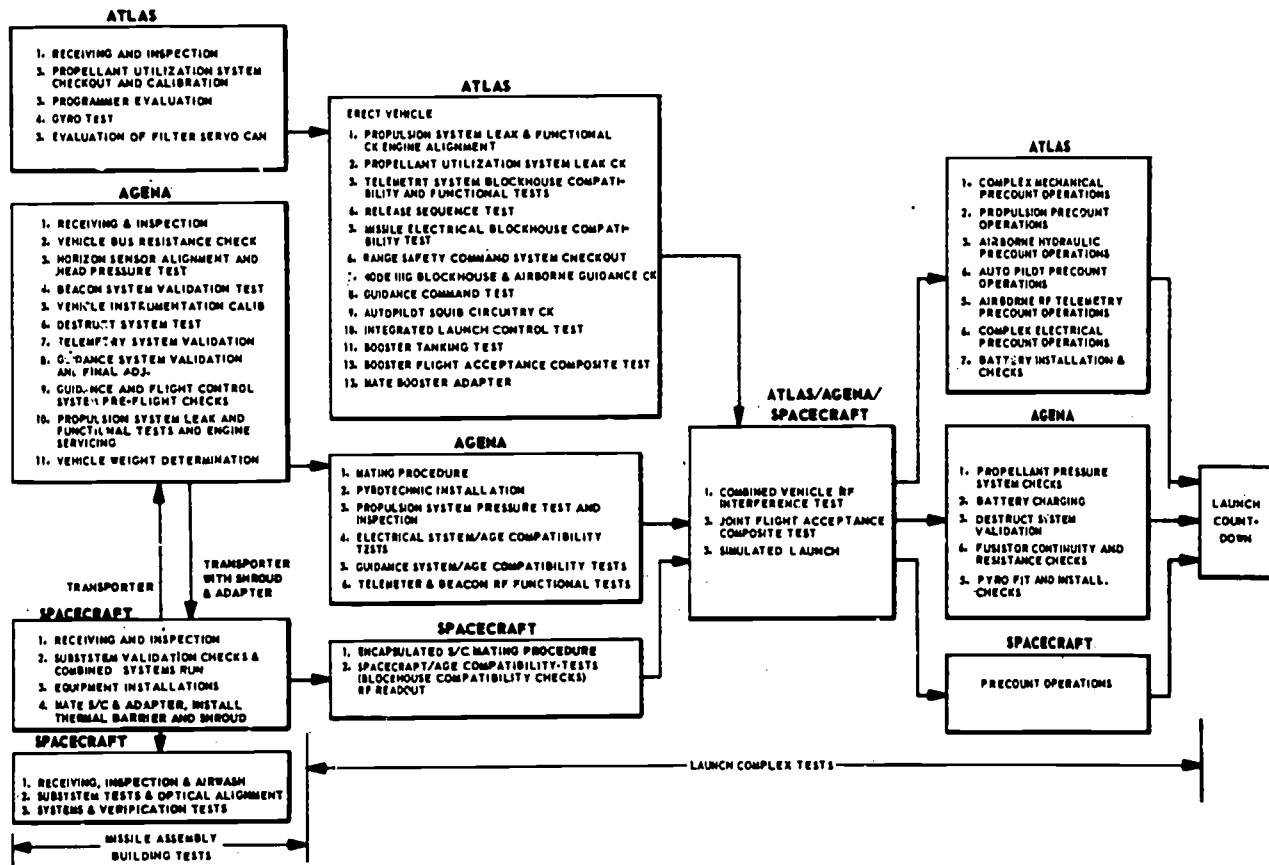
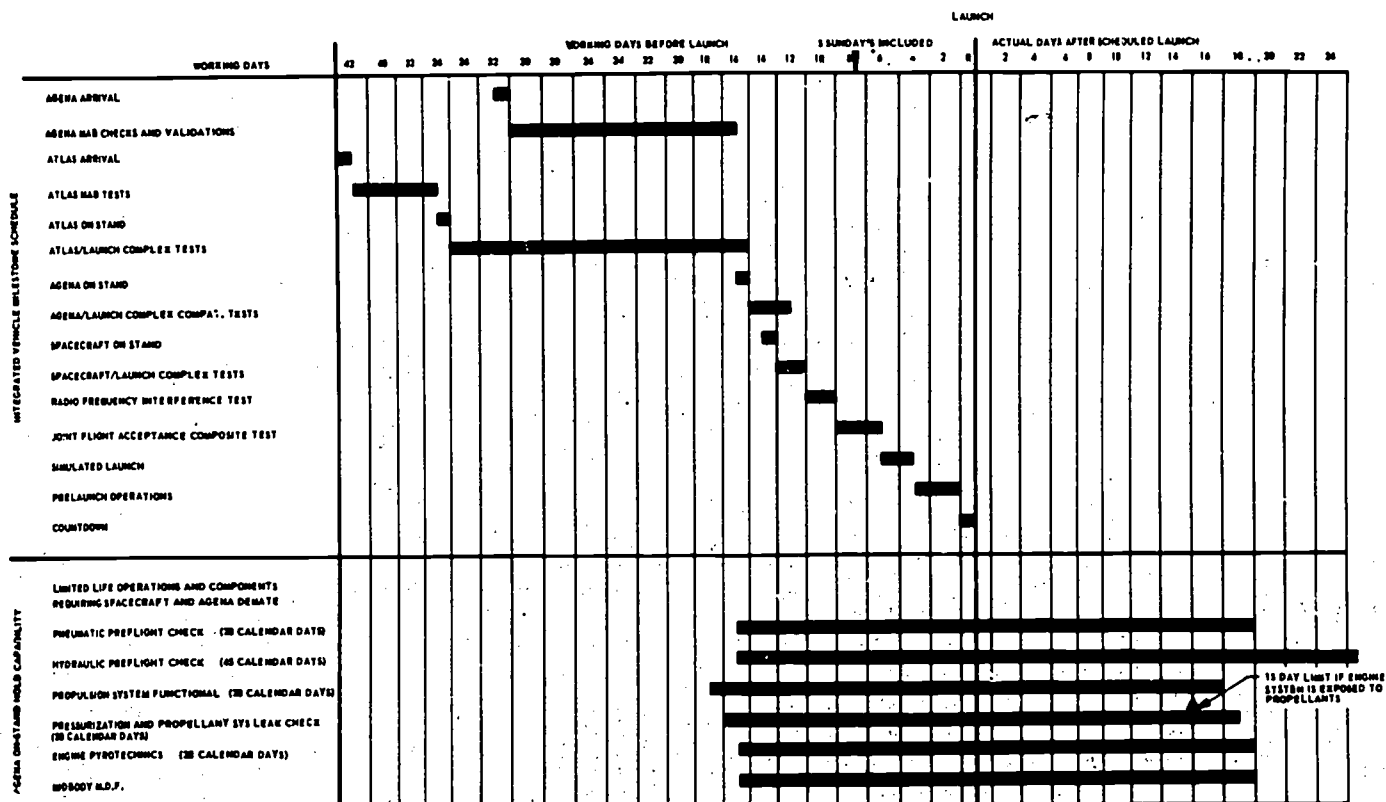Figure 18-11. - Prelaunch operations flow chart.

Figure 18-12. - Atlas-Agena-Orbiter integrated-vehicle milestones and Agena on-stand hold capability.
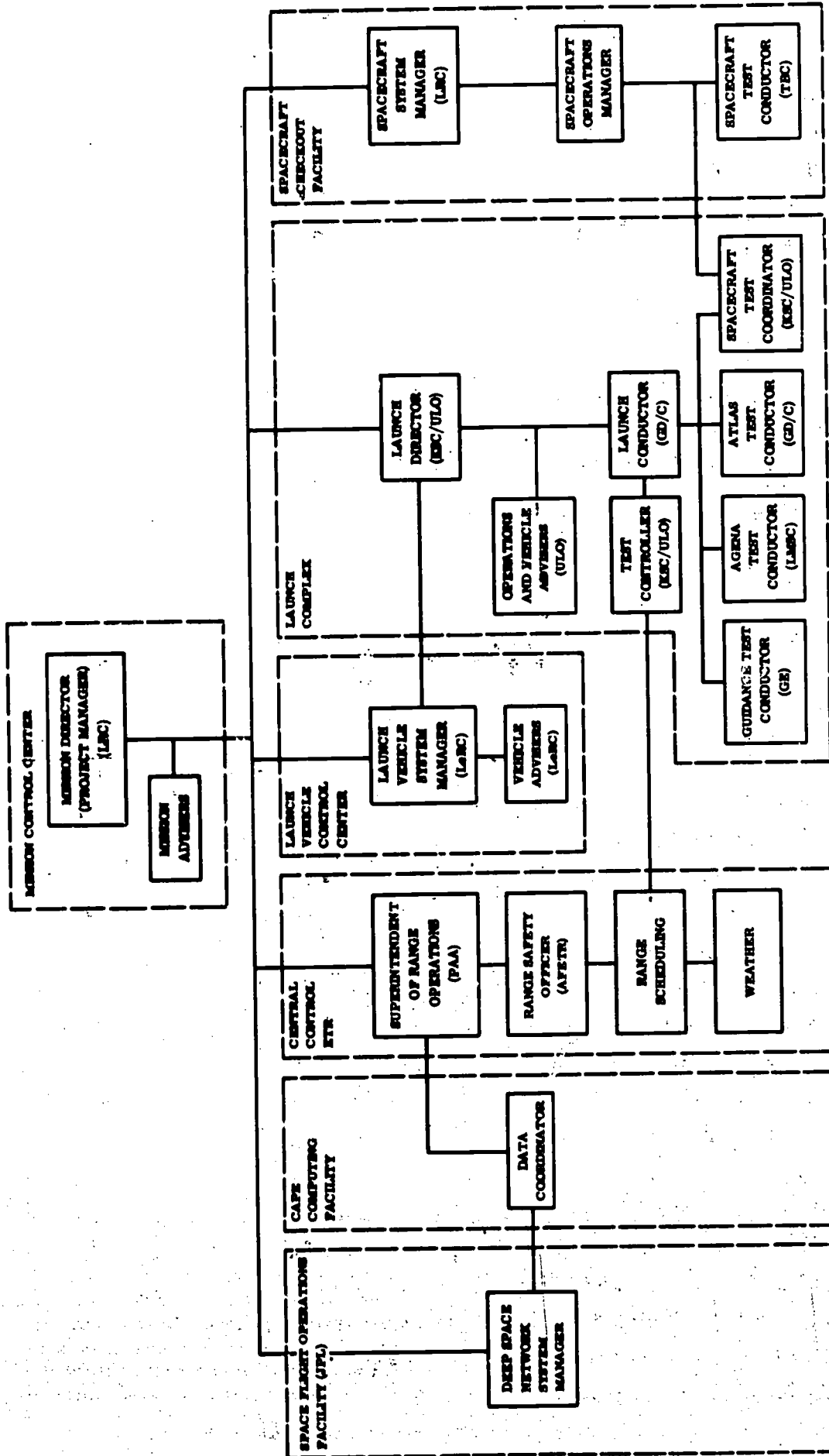
Figure 18-13. – Functional organization of space-flight operations.

Launch

The coordination of all the activities which must take place during a launch is handled by the Unmanned Launch Operation Directorate at the Kennedy Space Center (KSC/ULO). The relation of KSC/ULO to the other activities is shown in figure 18-13.

The operations and tasks that are performed during the countdown preceding the actual launch are carefully timed to ensure that nothing is overlooked and that everything is done in the correct order. Among the many tasks are fueling and checking all command and execution systems of the spacecraft, the vehicle, and the ground facilities. A summary of the countdown procedure is presented in table 18-II.

Although the launch is the most spectacular moment of the Atlas-Agena-Orbiter mission, it is probably the least demanding technically. Its success depends entirely on the thoroughness and accuracy of all the testing inspections and verifications that have gone on before. Design, manufacturing, and assembly play an important part as well. The launch is a conclusion, not a process.

WORLDWIDE SUPPORT

Flight Plan

To understand the support required from the tracking and telemetry stations around the world, a brief review of a typical Lunar Orbiter flight plan is in order. Precise timing, of course, varies with the launch day as well as with the launch time on a given day.

After launch, the vehicle rises vertically and turns a prescribed amount about its longitudinal (vertical) axis so that the desired azimuth is obtained when the pitch-over maneuver is started. After the Atlas booster engines are cut off and jettisoned, sustainer and vernier engines control vehicle position and velocity. Immediately following vernier engine cutoff, the nose fairing is jettisoned and Atlas-Agena separation occurs. After a pitch maneuver to the proper attitude, the Agena fires to inject the vehicle into a 100-mile parking orbit.

After coasting for a predetermined time in the Earth parking orbit, the Agena is fired a second time to place the vehicle in a translunar trajectory. This is followed by the separation of the spacecraft from the Agena and by an Agena retromaneuver to reduce the probability of its interfering with the spacecraft or hitting the Moon. A list of key events between launch and retromaneuver is given in table 18-III, and a schematic of the trajectory is shown in figure 18-14.
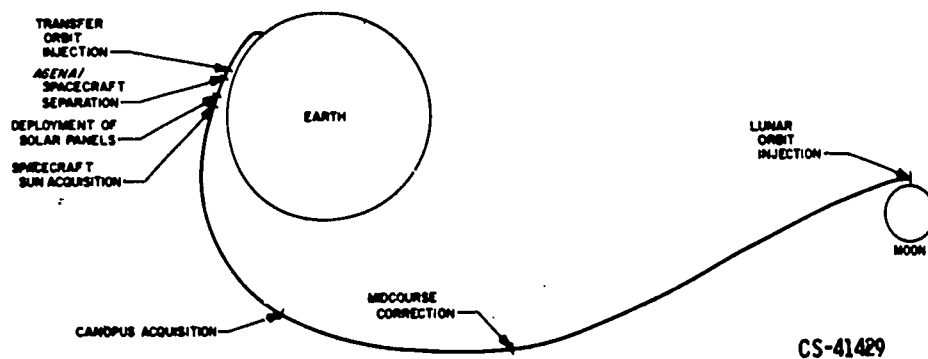
Figure 18-14. – Sequence of spacecraft flight events.

Ground Support

During the entire mission, the Atlas-Agena-Orbiter is in contact with the ground, both electronically and optically. Messages, consisting of commands to the vehicle and spacecraft and information to the ground, are constantly being exchanged. The facilities for this communication are distributed throughout the world; figure 18-15 shows the location primarily of the NASA ground-based communications activities, and table 18-IV lists the ETR facilities.

Telemetry. - Information generated or collected by the Orbiter or its vehicle is transmitted back to the ground stations near the ground track. At first, the information is received directly by Cape Kennedy, but later, other stations take over. The data are recorded on magnetic tape for immediate and later analysis.

Tracking. - Most of the installations that collect telemetry data are also involved in tracking; some stations are specifically designed for tracking only. Tracking can be either electronic or optical. Optical tracking is limited to the early stages of flight, so facilities for this are mostly near the launch area. Electronic tracking is not so limited and its distribution is world-wide.

Figure 18-15. — Geodetic positions of NASA tracking facilities.

CS-41436

TABLE 18-I. - FLIGHT PLANNING DOCUMENTS

Title	Publication date (a)	Description
Planning Estimate	L-24M	Describes general program and summarizes launch range support requirements. Must be approved before detailed range planning on program can be initiated.
Project Development Plan	L-24M	Describes the resources required for the Lunar Orbiter Program, including manpower estimates, program cost and funding, management organization. Delineates areas of responsibility among the NASA agencies and contractors.
Booster Requirements Document	L-18M	Combines into one document those launch vehicle system needs that are considered to be standard and not program-peculiar.
Program Requirements Document	L-12M	Defines those program needs that are levied on the launch support range by the user. Authorizes the range to take action to satisfy program needs.
Program Support Plan	L-10M[b]	Outlines the action to be taken by the launch range to satisfy program requirements and states whether the requirements can be met with existing resources or whether new facilities are needed.
Operations Requirement	(c)	Supplements the Program Requirements Document by describing in greater detail the final information, services, and related requirements for accomplishment of an individual test or test series within the overall program.
Operations Directive	(c)	Lists resources and methods to be used to support the test or test series.
Launch Operations Plan	L-9M, L-6M, L-3M, L-1M	Defines the flight objectives, system organization, space vehicle system configuration, operational range support facilities, data processing, launch constraints, and criteria requirements necessary to support program planning.
Flight Termination Systems Report	L-6M	Provides overall description of the space vehicle destruct system, including wiring diagrams and photographs, and a summary of test results showing system performance. This is the basic document for obtaining approval of the flight termination system for use on the range.

Range Safety Report	(d)	Provides trajectory data, dispersion data, and impact data resulting from malfunction or explosion during the ascent. Provides basic data for obtaining range approval for a flight on a particular launch azimuth.
Pad Safety Report	L-30D	Describes the space vehicle pyrotechnics, propellants, and pneumatics and defines the control of these items during testing and installation operations at the launch pad.
Countdown Manual	L-30D	Tabulates selected events from each individual contractor countdown and defines the combined operations necessary to verify space vehicle flight readiness.
Launch Information Package	L-10D, L-5D	Revises the Launch Operations Plan and lists the following final launch criteria: 1. Sequence of events 2. Telemetry system instrumentation and landline changes 3. Propellant loading information 4. Launch and hold limitations 5. Final velocity meter settings 6. Final weight statement 7. Launch window
Firing Tables and Supplementary Range Documentation	L-6W	Contains launch-to-lunar-encounter trajectories, launch plan, and launch window information - presented on a time-lapsed basis from launch.
Spacecraft Handling Plan	L-5M	Describes the hazardous spacecraft systems, their operation, and handling procedures.
Booster Guidance Equations	L-6W	These equations are used for the real-time control of the Atlas to increase the accuracy obtainable from the auto-pilot and flight control system.
Mission Operations Plan	L-3M	Presents the overall authority and control of launch and flight operations for the mission. The document defines agencies and agency relations, operations, resources required, documentation, and schedule of implementation and operations.

[a]Based on scheduled launch date where L-M, W, or D is launch date (L) minus x-number of months (M), weeks (W), or days (D).

[b]Document revised as required.

[c]Published 30 days before the particular test or test series.

[d]Final Trajectory Package portion of report published 6 weeks before scheduled launch date.

TABLE 18-II. - COUNTDOWN EVENTS

Time, EST	Count, min	Event
0941	T-460	Man countdown stations
0946	T-455	Start countdown
1009	T-432	Start preparations for spacecraft power turn-on
1011	T-430	Radiation clearance required
1041	T-400	Project Representative at Central Control console and check all communications lines with blockhouse
1046	T-395	Start spacecraft subsystem checks
		Agena ordnance delivered to pad
1056	T-385	Local radiofrequency silence until T-315 (spacecraft in low power mode)
		Start mechanical installation of vehicle pyrotechnics
1206	T-315	Range countdown starts
		Ordnance installation complete
		Radiofrequency silence released
1211	T-310	Start Agena telemetry and beacon checkout
1246	T-275	Range Safety Command Test
1306	T-255	Local radiofrequency silence until T-230 (spacecraft in low power mode)
		Start electrical hookup of pyrotechnics (Atlas and Agena)
1346	T-215	Spacecraft subsystems test complete
		Spacecraft programmer memory loading
1436	T-165	All personnel not involved in Agena tanking clear the pad area and retire to roadblock
1441	T-160	Pumphouse no. 4 manned and operational
1446	T-155	Start Agena fuel (UDMH) tanking
1451	T-150	Atlas telemetry warmup
1455	T-146	Guidance command test no. 1
1506	T-135	Agena fuel tanking complete
		Pad area clear for essential work
		Spacecraft programmer memory loading complete
1516	T-125	Remove service tower
1551	T-90	Start Agena oxidizer (IRFNA) tanking
		Agena beacon range calibration check
1616	T-65	Agena oxidizer tanking complete
1621	T-60	Built-in hold (50 min nominal)
		Clear all private vehicles and nonessential support vehicles from parking and pad areas
1711	T-60	Built-in hold ends
		Start spacecraft internal power checks
1720	T-51	Start guidance command test no. 2
1721	T-50	Spacecraft internal power checks complete
1736	T-35	Start liquid-oxygen tanking
1741	T-30	All systems verify that there are no outstanding problems
		Photo subsystem final preparations
1749	T-22	Start final Range Safety commitment
1804	T-7	Built-in 10-minute hold
1814	T-7	Built-in hold ends
		Agena switched to internal power
1816	T-5	Spacecraft switched to internal power
1818	T-3	Spacecraft programmer clock running
1819	T-2	Atlas switched to internal power
1821	T-0	Launch

TABLE 18-III. - SEQUENCE OF FLIGHT EVENTS

Event	Time	
	T+sec	min:sec
Liftoff	T+0	00:00
Start roll program	T+2	00:02
Start booster pitch program	T+15	00:15
Ground guidance commands to booster become effective	T+80	01:20
Booster engines cutoff	T+129.0	02:09.0
Jettison booster	T+132.1	02:12.1
Ground guidance commands to sustainer engine become effective	T+138.1	02:18.1
Start Agena restart timer[a]	T+250.7	04:10.7
Sustainer engine cutoff	T+287.2	04:47.2
Start Agena sequence timer[a]	T+290.6	04:50.6
Vernier engines cutoff	T+307.5	05:07.5
Jettison nose fairing	T+309.5	05:09.5
Atlas/Agena separation	T+311.5	05:11.5
Agena first-burn ignition[a]	T+364.5	06:04.5
Agena first-burn cutoff[a]	T+516.8	08:36.8
Agena second-burn ignition[a]	T+1315.0	21:55.0
Agena second-burn cutoff[a]	T+1401.5	23:21.5
Payload separation[a]	T+1567.7	26:07.7
Agena retromaneuver[a]	T+2167.7	36:07.7

[a]Time of occurrence is variable.

TABLE 18-IV. - EASTERN TEST RANGE INSTRUMENTATION

Station	Instrumentation	Use
Cape Kennedy (Station 1)	Ballistic cameras Cinetheodolites Radar Fixed camera systems Pad cameras Telemetry receiving station Command destruct Wire sky screen Television sky screen	Metric data Metric data Range safety Metric data Engineering sequential Vehicle/spacecraft data Range safety Range safety Range safety
Patrick AFB (Station 0)	Cinetheodolites Radar Cameras	Metric data Range safety Engineering sequential
Melbourne Beach	Cameras	Engineering sequential
Vero Beach	Cameras	Engineering sequential
Grand Bahama Island (Station 3)	Radar Ballistic cameras Telemetry receiving station Command destruct	Metric data Metric data Vehicle/spacecraft data Range safety
Merritt Island (Station 19)	Radar	Metric data
Grand Turk (Station 7)	Command destruct Radar	Range safety Metric data
Antigua (Station 91)	Radar Telemetry receiving station Command destruct	Metric data, range safety Vehicle/spacecraft data Range safety
Ascension (Station 12)	Radar Telemetry receiving station	Metric data Vehicle/spacecraft data
Bermuda	Radar	Metric data
Pretoria (Station 13)	Radar Telemetry receiving station	Metric data Vehicle/spacecraft data
Ship	Radar Telemetry receiving station	Metric data Vehicle/spacecraft data
Aircraft	Telemetry data receiving equipment	Return of data

305
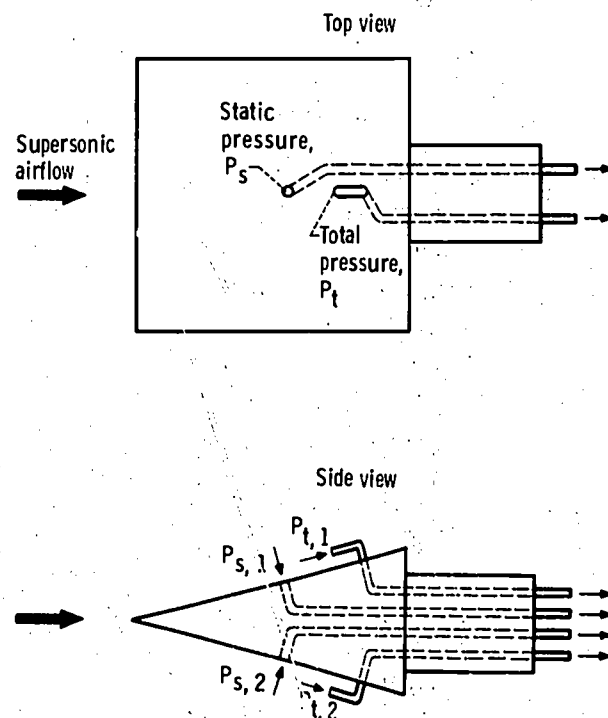
Figure 14-5. – Low-angle calibration wedge for measuring speed and angularity of airflow in supersonic wind tunnel.

bration wedge, shown in figure 14-5. Supersonic wind tunnels are normally calibrated with this type of instrument. The calibration wedge combines the functions of a pitot-static tube and a yawmeter. Measurements of static pressure P_s and total pressure P_t are used to calculate the speed of the airflow. Measurements of the static pressures P_{s_1} and P_{s_2} on opposite sides of the wedge are used to calculate the flow angularity.

The 10- by 10-Foot Supersonic Wind Tunnel was calibrated with a rake (fig. 14-6) consisting of 17 of these wedges. In this manner, a large portion of the cross-sectional area of the tunnel was calibrated at one time. Flow quality along the length of the test section was determined by translating the calibration rake. Flow angularity in perpendicular planes was determined by rotating the wedges 90°. Boundary-layer rakes were also installed at various locations on the tunnel walls to measure the thickness of the boundary layer. The measured boundary-layer thickness in the 10- by 10-Foot Supersonic Wind Tunnel varied from 9 to 12 inches.

At supersonic speeds, shock waves from the forward parts of the test model can reflect from the tunnel walls back onto the rear portions of the model. Calibration bodies, such as cone-cylinder models, can be tested over the complete range of Mach numbers to search for reflected shocks, which can be detected with static-pressure instrumentation. From these calibration results, reflection-free model lengths can be specified. Mach number ranges where reflections are a problem also can be noted and ignored for longer

Figure 14-6. - Calibration rake installed in the 10- by 10-Foot Supersonic Wind Tunnel.

models. Calibration bodies of various diameters can also be tested to determine the maximum test-model size that the tunnel can accommodate while still providing interference-free flow over the entire speed range. Limits are then placed on the ratio of model cross-sectional area to tunnel cross-sectional area (or blockage ratio) to obtain good test results. This blockage ratio varies with Mach number and can be as low as 3 percent at transonic speeds and as high as 15 percent at hypersonic speeds.

SUPPORT SYSTEMS

After the test-section flow conditions have been measured, installation of test hardware can begin. Methods of supporting the test article in the stream must be considered carefully, since support systems will interfere with the measurements, and corrections to the results must be kept to a minimum. Various ways are available to support the test models, depending to a great extent on the purpose of the test. A few of the techniques used at Lewis are illustrated in figure 14-7. Sting supports (fig. 14-7(a)) are useful when
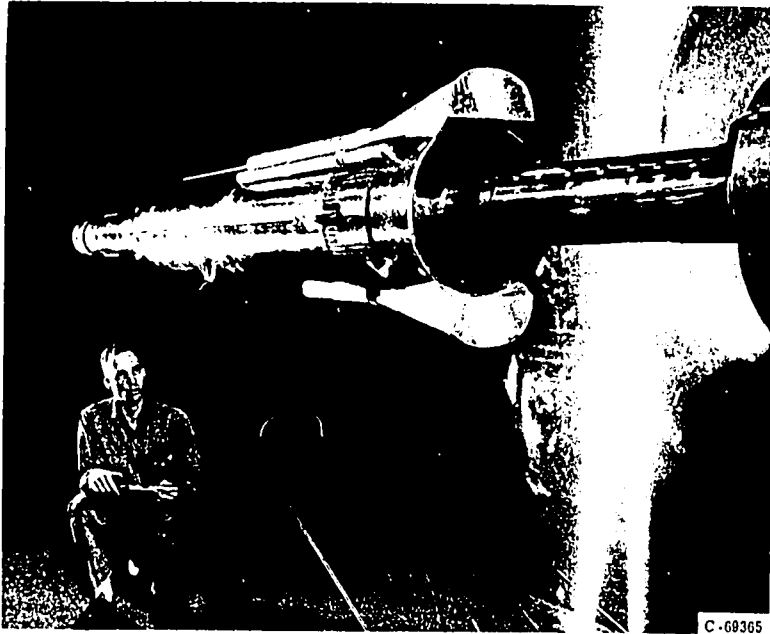
(a) Sting (Atlas/Agena).
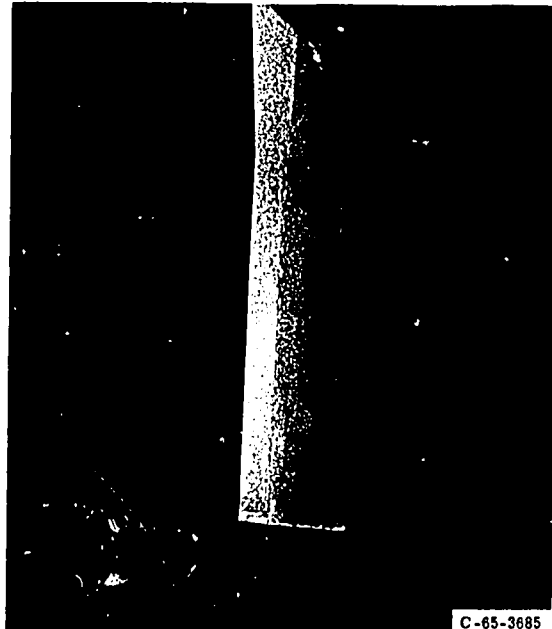
(b) Single strut (Saturn 5).
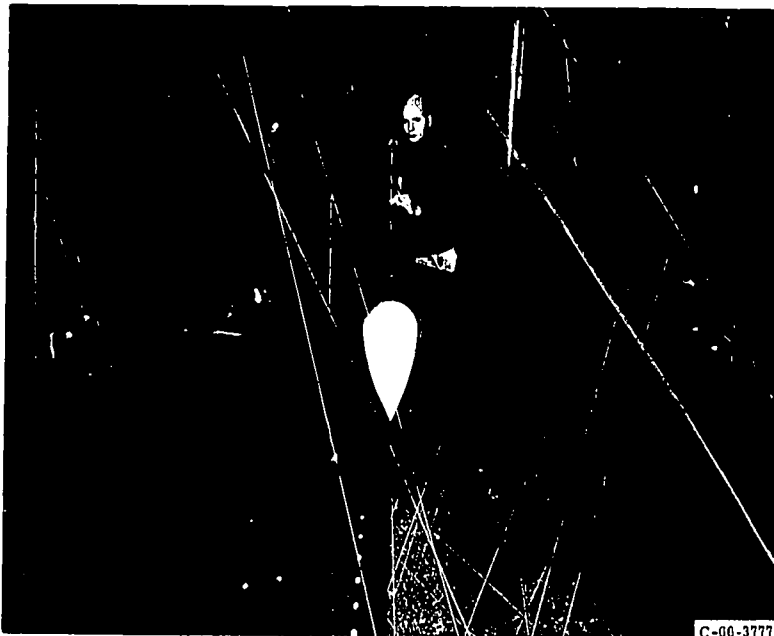
(c) Double strut (jet exit model).
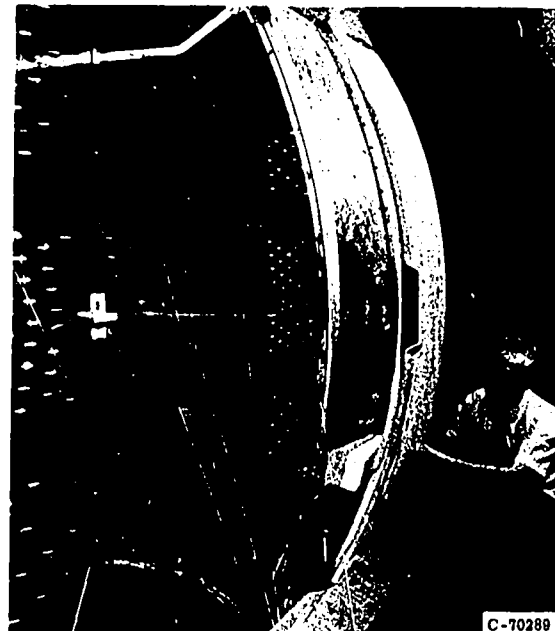
(d) Wall mount (Centaur weather shield).

Figure 14-7. – Typical methods of supporting test object in wind tunnel.

(e) Dynamic mount (Apollo launch escape vehicle).

(f) Wires (decelerator).

Figure 14-7. - Concluded.

external pressure distributions are being measured. Strut supports, either single (fig. 14-7(b)) or double (fig. 14-7(c)), are used when a high-pressure airflow through the test model is required, such as for nozzle tests. With struts, the area downstream of the model remains unobstructed, and the high-pressure airflow (higher pressure than the free-stream airflow) is brought into the model through an air line that can be housed in the normally hollow struts. The struts can also house instrumentation, electrical lines, and fuel lines. Sometimes, test models are mounted directly to the test-section walls (fig. 14-7(d)). Some special test programs require the use of unusual mounting techniques, such as those shown in figures 14-7(e) and (f). In some wind tunnels, unsupported, remotely controlled, powered models are tested. Magnetic suspension of test models has also been considered, but this technique presents a problem in obtaining information; telemetering may be one solution to this problem. It should be remembered that support interference effects are one of the main problems facing the wind-tunnel engineer.

TECHNIQUES OF VISUAL OBSERVATION OF FLOW

One of the simplest methods of obtaining information from a wind-tunnel test is by visual observation of the test model during and after the test. Most wind tunnels incorporate windows and appropriate illumination for this purpose. The airflow behavior can be made more clearly visible through the use of smoke, tufts, dye, china clay, etc. For thermal studies, temperature-sensitive paints that change color at various temperature

levels are used. Tests of structural integrity can be run with visual observation only, including a close inspection of the test model after shutdown to determine local damage.

Several optical systems have been developed for observing the flow around test models in supersonic wind tunnels. Two of these optical systems are the schlieren system and the shadowgraph system. Both systems are based on the principle that light rays are refracted (or bent) as they pass through regions of different density. Since strong density gradients (e.g., shock waves) occur in supersonic flow, the flow fields can be viewed by means of these optical systems.

Schlieren System

In the schlieren system (fig. 14-8), light from a point source on one side of the test section is bent by a lens into a beam of parallel rays. This beam is passed through the test section and is then collected by a second lens into an image of the point light source. If a knife edge is introduced at this image point, the intensity of the light being projected on the screen can be reduced. Thus, the image of the test section on the screen can be darkened uniformly to some shade of gray. Then, an object placed in the test section will appear on the screen as a black image (inverted) against a gray background.

When the wind tunnel is in operation, the interaction of the test model and the airflow creates regions of different densities (shock waves, flow separation, boundary layer) in the airflow. Light rays that pass through such regions of different densities are bent (refracted) so that they are no longer parallel to the average (unrefracted) rays in the beam. Therefore, these bent rays do not pass through the point image of the light source. As a result, these rays either completely miss the knife edge and create bright areas (brighter
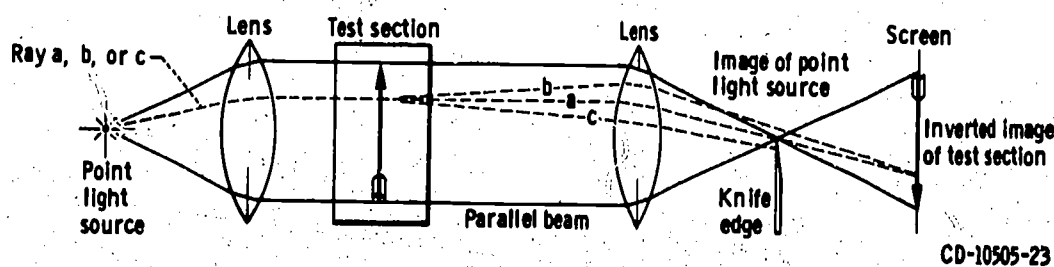

| Ray	History
a	Passes through point image of light source; intensity reduced by knife edge; resulting image on screen same shade of gray as background
b	Misses point image of light source; misses knife edge; intensity undiminished; resulting image on screen brighter than background
c	Misses point image of light source; blocked by knife edge; resulting image on screen darker than background

Figure 14-8. - Schematic diagram of schlieren system.

than the background) on the screen, or they are completely blocked by the knife edge and create dark areas (darker than the background) on the screen. Thus, the image on the screen (which can be photographed) shows the locations of regions of different densities around the test model and shows whether these regions have higher or lower than average densities.

Schlieren photographs of a model of a Mach 5.0 air inlet at several free-stream Mach numbers are shown in figure 14-9. These photos indicate the shock positions and how they change with free-stream velocity. The boundary layer along the spike is also visible, since it is a region of low density. Because of the orientation of the knife edge, high-density regions appear as dark areas on the top half of the inlet and as light areas on the bottom half. A schlieren photograph of the flow over a model of the Mariner payload shroud with the Agena second stage is shown in figure 14-10.
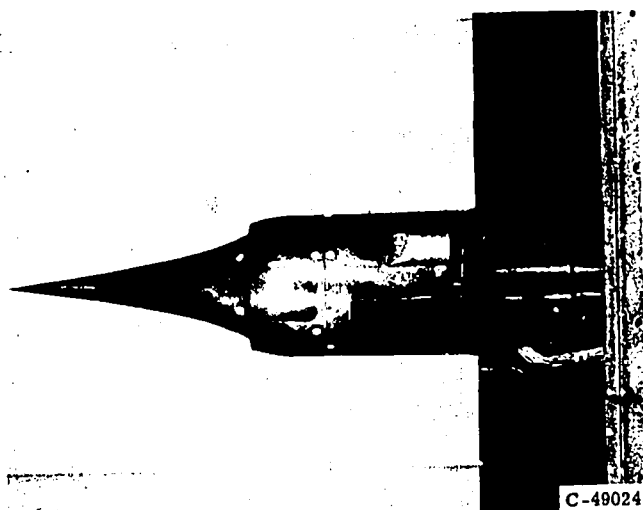
(a) Model of inlet.
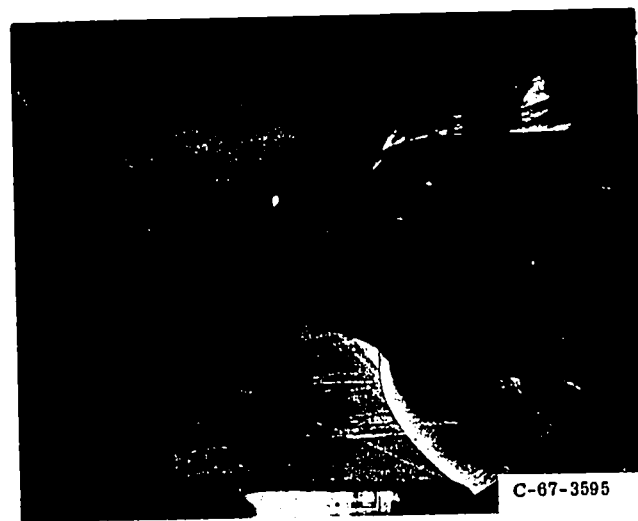
(b) Free-stream Mach number, 2.43.

(c) Free-stream Mach number, 3.43.
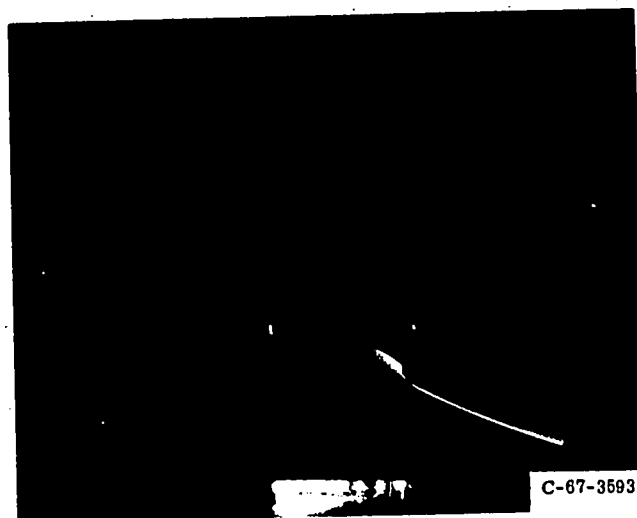
(d) Free-stream Mach number, 4.97.

Figure 14-9. - Schlieren photographs showing shock waves on model of Mach 5 air inlet operating at various free-stream Mach numbers. (Schlieren photographs taken in 1- by 1-Foot Variable Mach Number Wind Tunnel.)

(a) Test model.
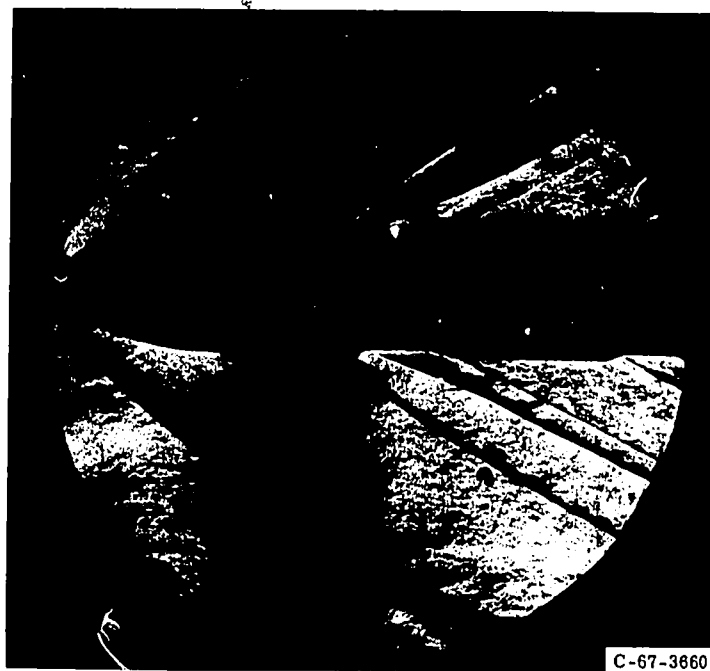
(b) Schlieren photograph (taken in 10- by 10-Foot Supersonic Wind Tunnel).

Figure 14-10. – Schlieren photograph showing shock structure on model of Mariner payload shroud with second-stage Agena. Free-stream Mach number, 2.0; angle of attack, -2°; altitude, 50 000 feet.

Shadowgraph System

In the shadowgraph system (fig. 14-11), light from a point source on one side of the test section is bent by a lens into a beam of parallel rays. As these parallel rays pass through the test section, they are bent by any density gradients that may be present. The light rays are then projected on a screen. The high-density regions of the test section
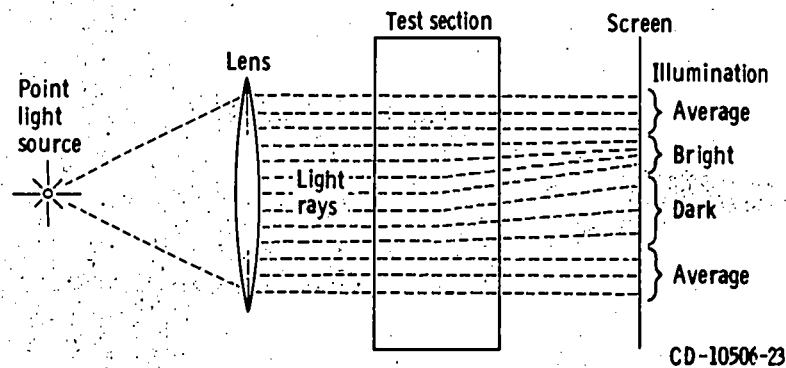
Figure 14-11. – Schematic diagram of shadowgraph system.

appear as dark areas on the screen. Figure 14-12 shows a shadowgraph of the Mach 5.0 isentropic spike air inlet (same inlet as in fig. 14-9) operating at a free-stream Mach number of 1.97. The shadowgraph shows shock waves and regions of local flow separation behind the strong shock wave on the inlet spike.

Schlieren photographs and shadowgraphs can provide both qualitative and quantitative results. For example, not only can the shock waves be observed, but their angles and locations can be accurately measured from the pictures. Usually, flow-field details such as boundary-layer thickness, local pressure variations, and flow velocities must be measured with other instrumentation.

INSTRUMENTATION

In addition to the optical systems described in the preceding section, the engineer can also use a variety of instrumentation to obtain information from wind-tunnel tests. Some of the basic instruments used for steady-state and transient measurements in wind tunnels are described briefly herein. A more thorough discussion of instrumentation is presented in chapter 13.
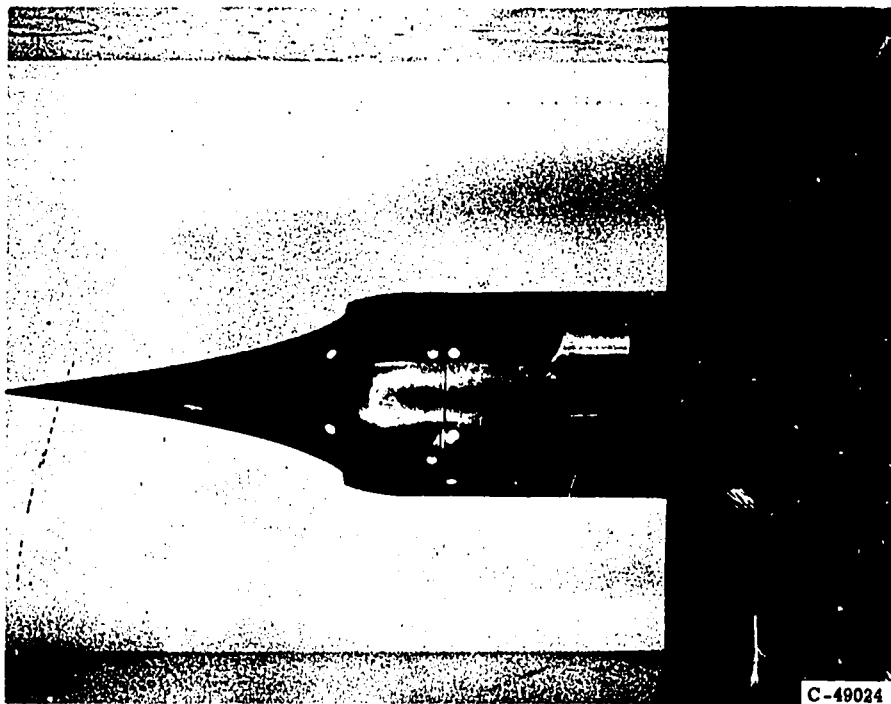
(a) Model inlet.
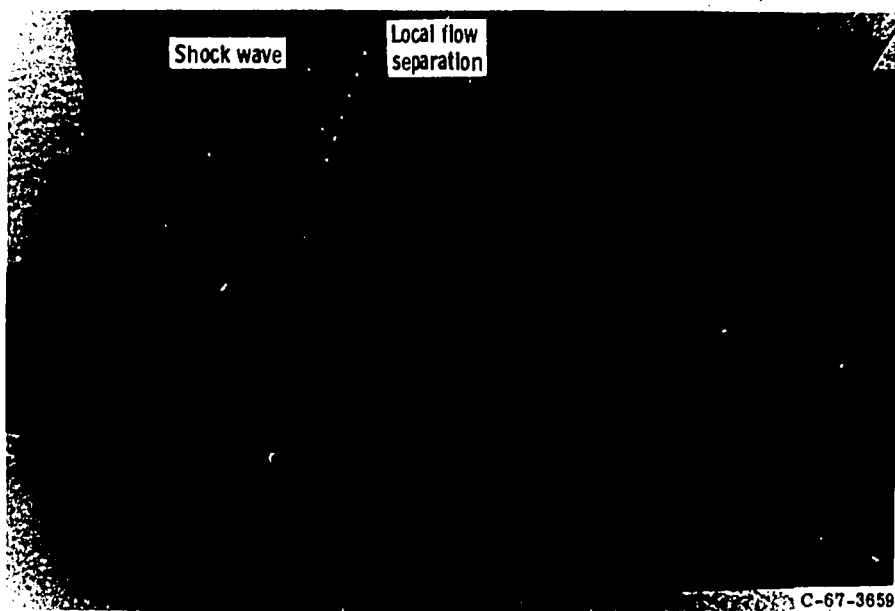
(b) Shadowgraph.

Figure 14-12. – Shadowgraph of model of Mach 5 air inlet operating at Mach 1.97 in the 18- by 18-Inch Supersonic Wind Tunnel.

Steady-State Measurements

Most wind-tunnel data are recorded at various steady-state conditions (i. e., condi
tions that are not varying with time) of the free-stream flow and test-model attitude.
Local flow conditions over the test model are measured with static-pressure orifices
and total-pressure, or pitot-pressure, rakes. Small wedges (fig. 14-5) can also be us
to provide local Mach number and flow angularity. Temperatures are measured with
thermocouples. Forces can be determined by integrating large numbers of static pres·
sures or by use of a force balance. Pressure integration is not as accurate as the dire
balance reading and requires a large amount of instrumentation. Normal procedure is
use a balance for a direct measurement of forces and to supplement these measuremen
with general information from static-pressure and pitot-pressure measurements.

Transient Measurements

Sometimes it is desirable or necessary to obtain data under transient conditions
(i. e., conditions that are changing with time). For example, it may be necessary to
measure the fluctuating pressures in the unsteady flow that exists in regions of flow se
aration or in regions where shock waves interact with the boundary layer. Transient
measurements are also required to obtain heat-transfer coefficients in thermal tests.
The use of an intermittent wind tunnel (blowdown or indraft) necessitates transient mea
urements, because the airflow in such a tunnel varies with time. Transient measureme
in wind-tunnel models can be made with transducers, calorimeters, and accelerometer

REFERENCE AXES

Force balances have been mentioned as one method of directly measuring the force
on a test model. The forces or moments acting on an object are measured along or
around three mutually perpendicular reference axes. These reference axes may be the
wind axes, the body axes, or the stability axes.

Wind-Axis System

Wind-tunnel tests of the external flow and forces on an aerodynamic shape are pri-
marily concerned with the wind-axis system (fig. 14-13(a)). Lift, drag, and yaw force
are always measured with respect to the direction of the relative wind. In a wind tunne.

(a) Wind-axis system.

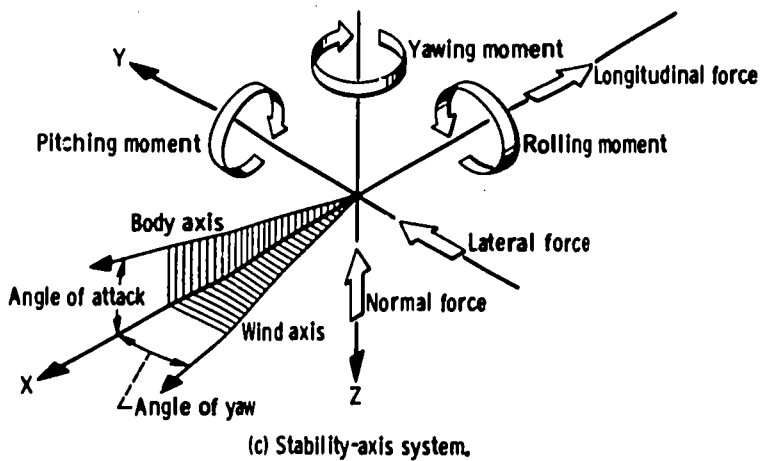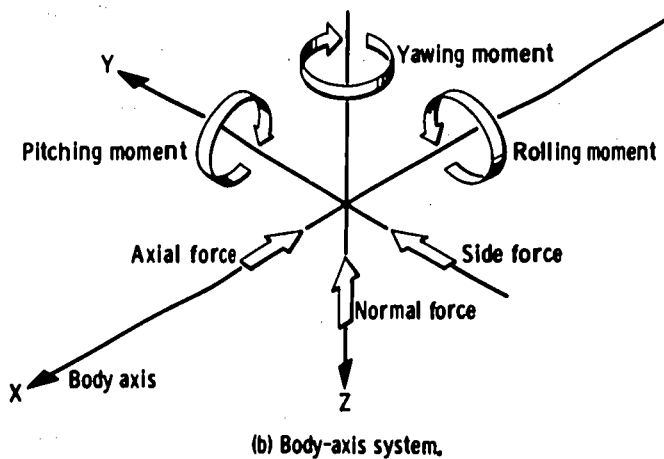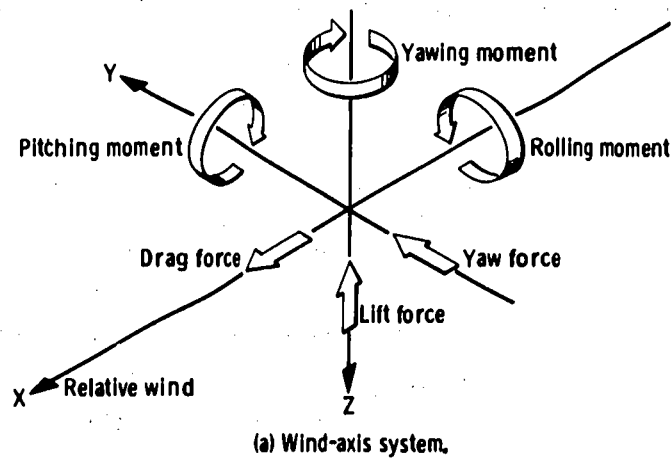(b) Body-axis system.

(c) Stability-axis system.

Figure 14-13. - Reference axes for force measurements in wind tunnels.
(Arrows indicate positive directions of axes, forces, moments and
displacements.)

the relative-wind direction (and the drag axis) is along the axis of the tunnel. The angle that the longitudinal body axis of the test model makes with the relative wind direction is referred to as the "angle of attack" in the pitch plane and the "angle of sideslip" in the yaw plane.

Body-Axis System

The body-axis system (fig. 14-13(b)) is one in which the axes move with the vehicle, and the resulting forces (axial, normal, and side) are measured relative to the longitudinal body axis of the test model. The forces and moments along and around these body axes are measured directly with an internal six-component balance. This axis system is normally used in propulsion tests, since the thrust of a vehicle or a nacelle is usually along the longitudinal body axis. In some propulsion tests, only one component of force is required. For example, for a nacelle mounted rigidly in the wind tunnel at zero angle of attack, the engineer is primarily interested in the single measurement of the resulting axial force (thrust or drag). This force can be measured with a single-component balance.

Stability-Axis System

The stability-axis system (fig. 14-13(c)) is a combination of the previous two systems. In the pitch plane (X - Z), the axes are alined with and perpendicular to the relative-wind direction. In the yaw plane (X - Y), the axes move with the body and are alined with and perpendicular to the longitudinal body axis. No matter which of the three sets of reference axes is used, the measured forces and moments can be easily converted from one system to the other by simple geometrical relations.

WIND-TUNNEL APPLICATIONS

Wind tunnels can be used for a wide variety of tests. The test models can be aircraft and missiles (scale models, full-scale vehicles, or full-scale components), boats, automobiles, bridges, buildings, propulsion systems (reciprocating engines with propellers, turbojets, ramjets, rockets), etc.

Most of the wind-tunnel testing here at the Lewis Research Center concerns the aerodynamics and thermodynamics of propulsion systems. The 8- by 6-foot and 10- by 10-foot wind tunnels were designed specifically for this purpose. These propulsion facilities can operate on two distinct cycles, propulsion or aerodynamic. For propulsion tests, when

316

(a) Air inlet (1/4-scale model of F-102 forebody).
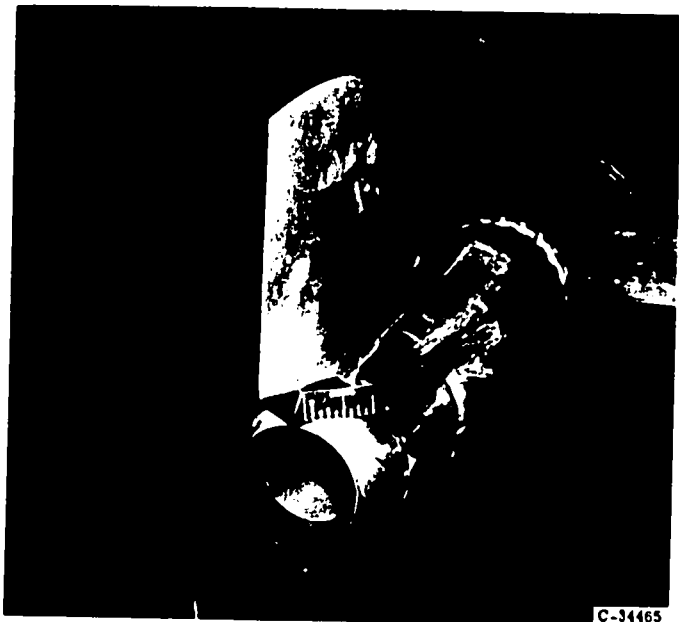
(b) Exhaust nozzle (model of F-104 afterbody).
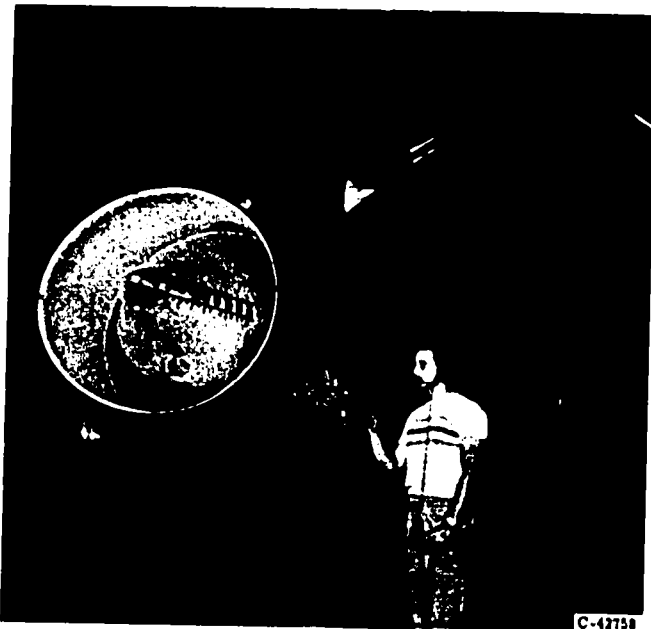
(c) Engine nacelle (full-scale B-58 nacelle, complete with
G.E. J79 turbojet engine).

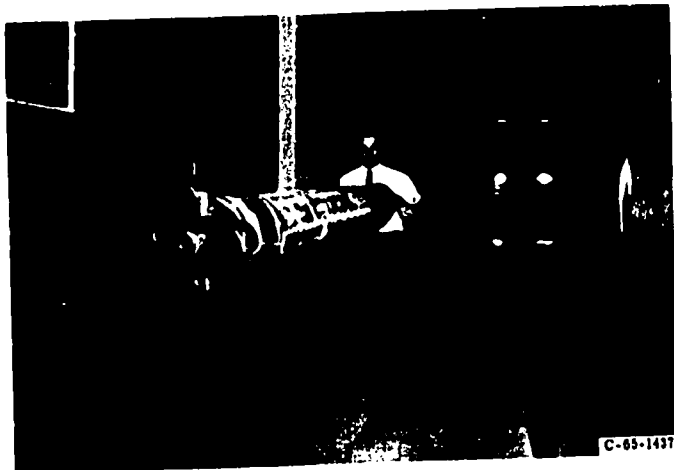(d) Nacelle - airframe configuration (supersonic airplane model).

Figure 14-14. - Wind-tunnel installations for testing propulsion systems and/or their components.

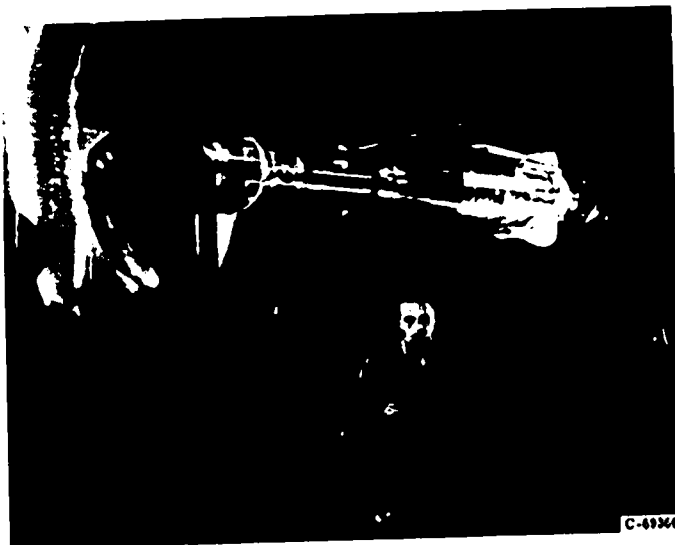(a) Saturn C-1, 1/27 scale. (Base-heating measurements.)

(b) Saturn S-1B, 1/20 scale. (Measurements of fin forces.)
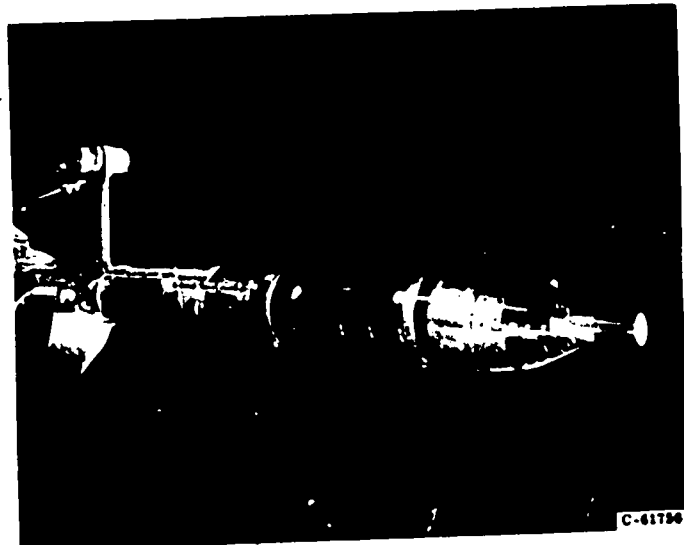
(c) Saturn 5, 1/45 scale. (Base-heating measurements.)

(d) Atlas/Centaur with Surveyor payload shroud, 1/10 scale. (Tests of hydrogen vent.)

(e) Atlas/Agena with Mariner payload shroud, 1/10 scale. (measurements of dynamic pressures.)

(f) Titan-Gemini, 6-percent scale. (Measurements of aerodynamic forces.)

Figure 14-15. - Wind-tunnel installations of boost vehicles.

operating engines are being studied, the air is brought through the test section once and is discharged back to the atmosphere (open circuit). For aerodynamic tests, the air is allowed to recirculate continuously (closed circuit). These facilities can be operated continuously on the propulsion cycle at supersonic speeds with the use of large air dryers. The expansion process by which supersonic velocities are achieved in the test section causes the air temperature to drop to sub-zero levels. Any moisture present in the airstream would condense in the nozzle and result in nonuniform flow conditions. It is therefore necessary to dry the air before it enters the tunnel, and this function is performed by the air dryer, where many tons of activated alumina act as a desiccant. Running time on the propulsion cycle is limited by the capacity of the dryer beds.

Some examples of the types of tests that have been performed in the Lewis propulsion wind tunnels in the past 15 years are illustrated in figures 14-14 and 14-15. Air-inlet tests have been conducted on most of the existing supersonic fighter planes and bombers, including the F-102 (fig. 14-14(a)), F-104, F-106, F-107, F-111, B-58, B-70, etc. Exhaust-nozzle tests have been conducted for the F-104 (fig. 14-14(b)), B-70, B-58, SST, etc. A complete nacelle for the B-58 bomber (fig. 14-14(c)) was tested at Mach 2.0 in the 10- by 10-Foot Supersonic Wind Tunnel prior to the first supersonic flight of that aircraft. This pod included both the full-scale inlet and the operating J79 turbojet engine. More recent tests have supported the development of the Saturn 1 (figs. 14-15(a) and (b)) and Saturn 5 (fig. 14-15(c)) boost vehicles and the development of the Atlas/Centaur (fig. 14-15(d)) and Atlas/Agena (fig. 14-15(e)) vehicles managed by the Lewis Research Center.

CONCLUDING REMARKS

This chapter has presented a brief discussion of items that should be considered in the design and operation of wind tunnels (e. g. , general wind tunnel types, power requirements, methods of supplying power, etc.). Some examples have been presented of typical calibration probes, support systems, visual flow-observation techniques, instrumentation, and models tested in the Lewis Research Center propulsion wind tunnels. It has been demonstrated over the years that wind tunnels can provide useful design information for a large variety of configurations for a modest expenditure of time, money, and manpower. Rigorous testing of subscale and full-scale models in wind tunnels prior to flight has proven to be a logical first step in the orderly development of flight systems.

REFERENCE

1. Goddard, Vincent P. : Development of Supersonic Streamline Visualization. University of Notre Dame, Mar. 1962 (NSF Grant 12488).

BIBLIOGRAPHY

Pope, Alan: Wind-Tunnel Testing. Second ed., John Wiley & Sons, Inc., 1954.

Pope, Alan; and Goin, Kennith L.: High-Speed Wind Tunnel Testing. John Wiley & Sons, Inc., 1965.

Pope, Alan; and Harper, John J.: Low-Speed Wind Tunnel Testing. John Wiley & Sons, Inc., 1966.

15. NAVIGATION

William H. Swann*

Because navigation is a broad and complex subject, a thorough explanation of it in a single chapter is impossible. Therefore, the discussion herein is limited to some of the fundamentals of air navigation. Celestial-navigation methods are not discussed at all.

For the purposes of navigation, the Earth can be considered to be a perfect sphere. This is not truly correct, but it is within the accuracy of the present methods of determining position, and the assumption greatly simplifies the calculations.

INTERSECTION OF A SPHERE WITH A PLANE

If any sphere is cut by a plane, the intersection of the two surfaces is a circle. At one extreme, where the plane is just tangent to the surface of the sphere, the intersection is only a point. As the cutting plane is moved deeper into the sphere, the circle of intersection grows larger. The largest circle is achieved when the cutting plane includes the point center of the sphere and the circle has the same radius as the sphere. Then, regardless of the direction in which the cutting plane is moved away from the center, the circle can only grow smaller. The largest circle that can be formed by this intersection, when the cutting plane contains the center of the sphere, is called a great circle. All the other circles are called small circles. A grid system, consisting of such circles, on the Earth's surface provides a universal method of identifying any point on Earth without reference to landmarks or place names.

Parallels of Latitude

A sphere is a continuous surface, without beginning or end. This is also true of the

*Chief, Aircraft Operations Branch.

Earth, whose only distinctive natural reference line is its axis of rotation, or polar axis. Thus, the poles are distinctive points on Earth, and the polar axis serves as the central axis for one set of reference circles (fig. 15-1). The most important circle of this set is the equator, a great circle halfway between the poles. The plane of the equator is perpendicular to the Earth's polar axis and divides the Earth into a northern and a southern hemisphere. Any small circle whose plane is parallel to the equator is called a parallel of latitude, or simply a parallel. Each parallel is everywhere equidistant from the poles, from the equator, and from every other parallel. Every point on the earth has a parallel passing through it which is designated by its angle to the north or south of the equator, measured from the center of the Earth.
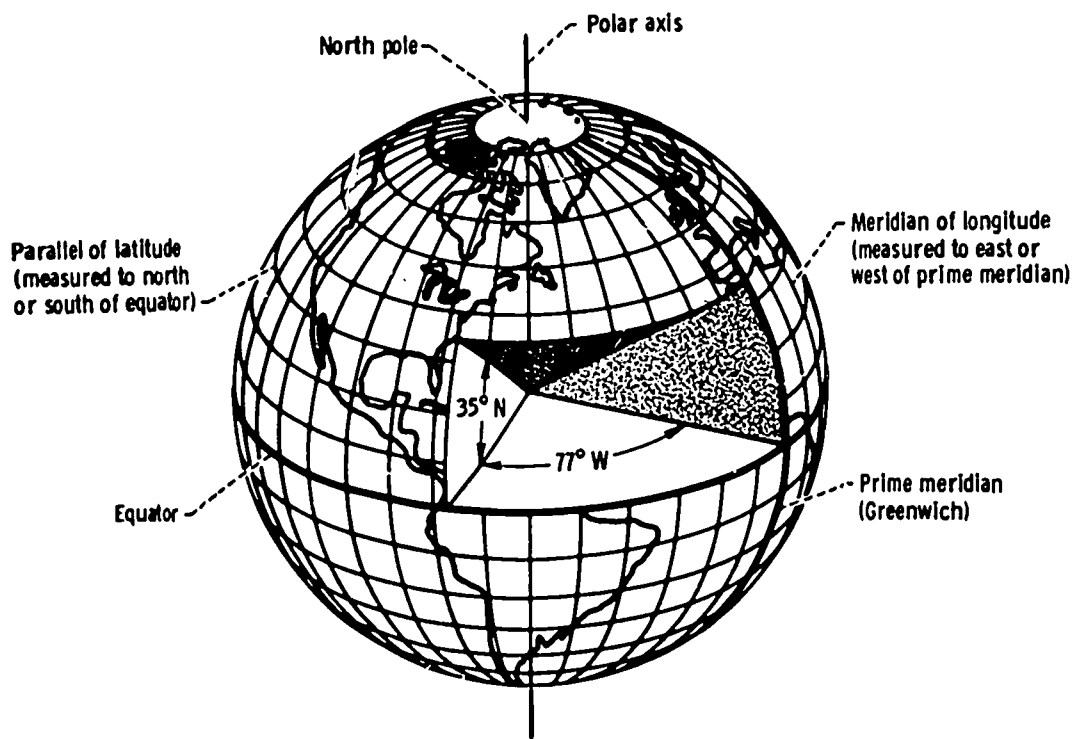

Figure 15-1. - Terrestrial grid system comprised of parallels of latitude and meridians of longitude.

Meridians of Longitude

A great circle passing through the poles is a meridian of longitude, or simply a meridian. Meridians correspond to the north - south streets of a city. Since all merid-

ians are great circles, none of them is distinctive, as is the equator among the parallels. Therefore, one meridian must be selected arbitrarily as a prime, or reference, meridian. In English-speaking countries and many others, the great circle passing through the observatory at Greenwich, England, is used as the prime meridian, and the other meridians are identified by their angular distance to the east or west of Greenwich.

GRID SYSTEM

The parallels and meridians intersect to form a grid system, as shown in figure 15-1. Any point on Earth can be identified by naming the parallel and meridian which pass through it. Thus, the 40° N. parallel and the 75° $10'$ W. meridian designate the location of Philadelphia. These coordinates are called latitude and longitude. The latitude of a point is its angular distance north or south of the equator and ranges from 0° at the equator to 90° N. and 90° S. at the poles. The longitude of a point is its angular distance east or west of the prime meridian (Greenwich) and ranges from 0° at the prime meridian to 180° E. or 180° W. of the prime meridian.

An important characteristic of a great circle (not necessarily a meridian) is that it marks the shortest distance between two points on the surface of the Earth. Actually, the shortest distance between any two points is along the straight line between them. However, if the two points are located on the surface of a sphere the straight line between them passes beneath the surface. Therefore, the shortest route along the surface of a sphere (e.g., the Earth) between two points is that route which most closely approximates a straight line. Any route between two points on the Earth's surface is curved. The least curved, and shortest route is the one whose radius of curvature is greatest. The maximum radius of curvature is the radius of the Earth (i.e., the radius of a great circle). Therefore, the shortest route between two points is an arc of the great circle that passes through the two points.

CHARTS (MAPS)

Now that we have described a grid system for naming positions on the Earth's surface, we must have some way of making this information available to the navigator. To do this we use a chart, or map. A chart is a diagrammatic representation on a flat surface of a portion of the curved surface of the Earth.

Desirable Characteristics

The Earth is a sphere and cannot be represented on a flat surface without some type of distortion. It can be truly represented only on a sphere, or globe. This is useful for some purposes. For navigation, however, it is inconvenient to carry and store a globe, even in sections. Therefore, navigational charts are always printed on flat sheets of paper. A chart should have the following desirable characteristics:

(1) The scale should be constant over the whole map.

(2) Angles should be accurately drawn.

(3) Great circles should be shown as straight lines.

(4) Rhumb lines (i.e., lines that cross successive meridians at a constant angle) should be shown as straight lines.

(5) Coordinates should be easy to find and easily plotted.

(6) Charts of adjacent areas of the same scale should be easily joined.

(7) Each cardinal direction (north, south, east, and west) should point the same way on every part of the chart.

(8) The chart should be simply and easily constructed.

(9) Equal areas should be shown equal.

Unfortunately, it is impossible to construct a chart which has all these features. In fact, some of them are mutually exclusive. Therefore, it is necessary to select the method of chart construction which fulfills the requirements of the particular mission. We draw our chart by locating the geographic features in a grid of meridians and parallels, known as a graticule. The construction of this grid is the critical part of the chart-making process, for this determines which of the characteristics the particular chart will have.

Projections

The two most common methods of chart construction are the Lambert projection and the Mercator projection.

Lambert projection. - The Lambert conformal conic projection is illustrated in figure 15-2. In this system, the surface features of the Earth are projected from the center point of the Earth onto the surface of a cone that intersects the Earth's surface along two parallels of latitude. The surface of the cone enters the Earth's surface at one parallel and emerges at another. These two parallels are called the standard parallels. The limits of the projection are parallels slightly beyond, or outside, the two standard
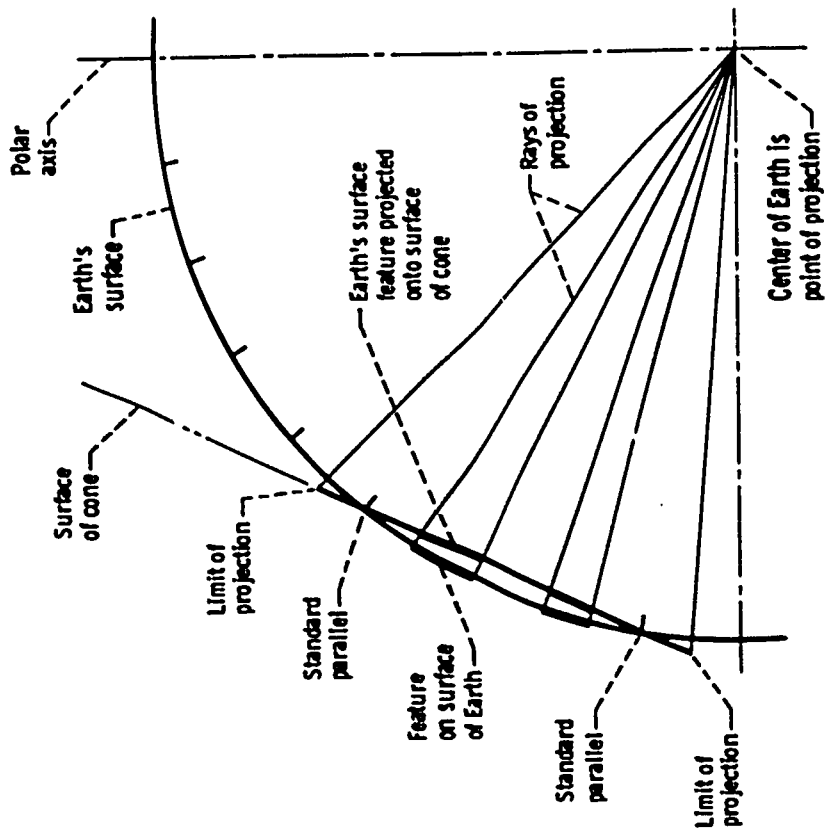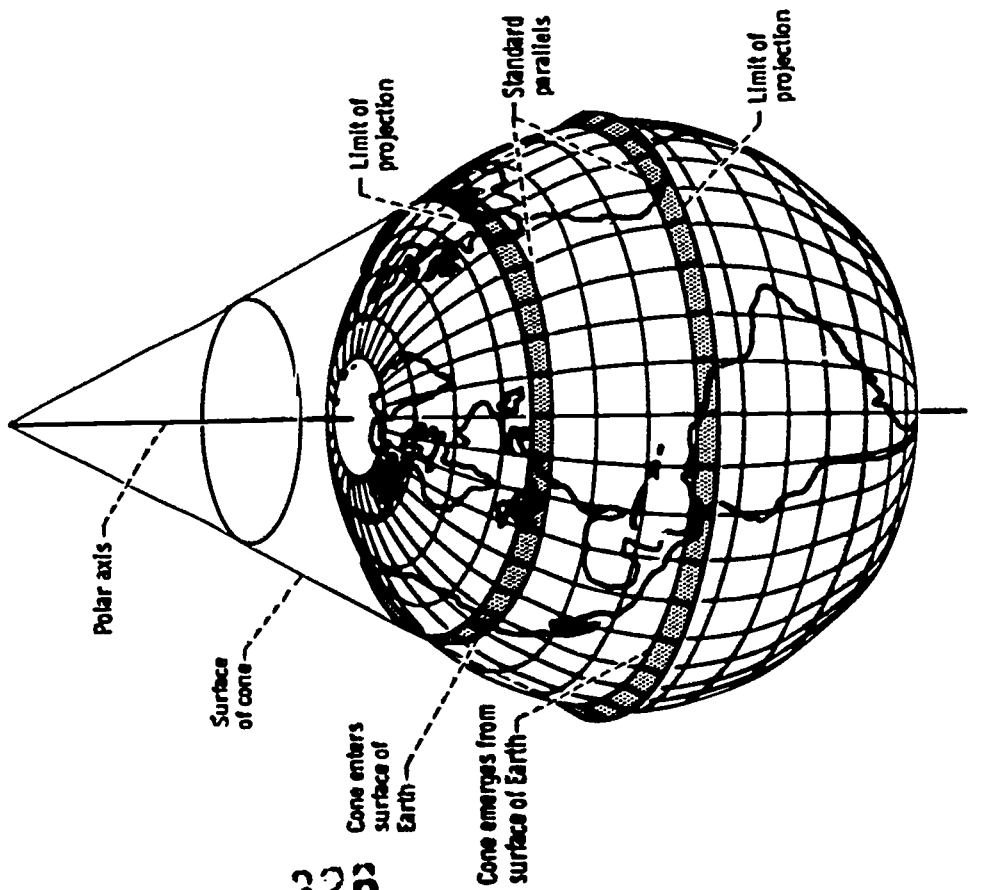
parallels. The apex, or tip, of the cone is outside the Earth and on the polar axis. The cone is coaxial with the Earth.

When the cone is unrolled on a plane surface, the resulting graticule shows parallels of latitude as concentric circles centered at the pole nearest the apex of the cone and shows meridians of longitude as straight lines converging on this pole. Thus, the meridians are normal to the parallels (i.e., the meridian is perpendicular to the line that is tangent to the parallel at the point of intersection).

With the Lambert projection, the angles formed at a given point of intersection of a meridian and a parallel are the same on the surface of the cone (or the chart) as on the surface of the Earth. Therefore, any other angles formed by the intersections of any other lines are also the same on both surfaces. Consequently, the Lambert projection is conformal. This means that the features of the Earth's surface retain their shapes on the chart.

The great advantage of a Lambert chart over other charts is that the scale of distance is practically constant over the entire chart (i.e., within the limits of the projection). Thus, the features of the Earth's surface retain their relative sizes on the chart. Actually, the scale is accurate along the standard parallels, is slightly reduced between the two standard parallels, and is slightly increased between the standard parallels and the limits of projection. For example, the standard parallels normally used for a Lambert projection of the United States are 33° and 45° North. Between parallels $30^\circ 30'$ and $47^\circ 30'$ North, the maximum error in the scale is only 1/2 percent. The maximum error for the entire chart of the United States is $2\frac{1}{2}$ percent in southern Florida.

Any straight line on a Lambert chart is very nearly a great circle. In the 2572 statute miles between New York City and San Francisco, the great circle and the straight line connecting them on a Lambert chart are only 9.5 miles apart at midcourse; for shorter lines the deviation is even less. Therefore, for practical purposes a straight line on the Lambert chart may be considered a great circle. A rhumb line (i.e., line of constant direction) is shown as a curved line. Between New York City and San Francisco, the rhumb line departs about 170 miles from the straight line.
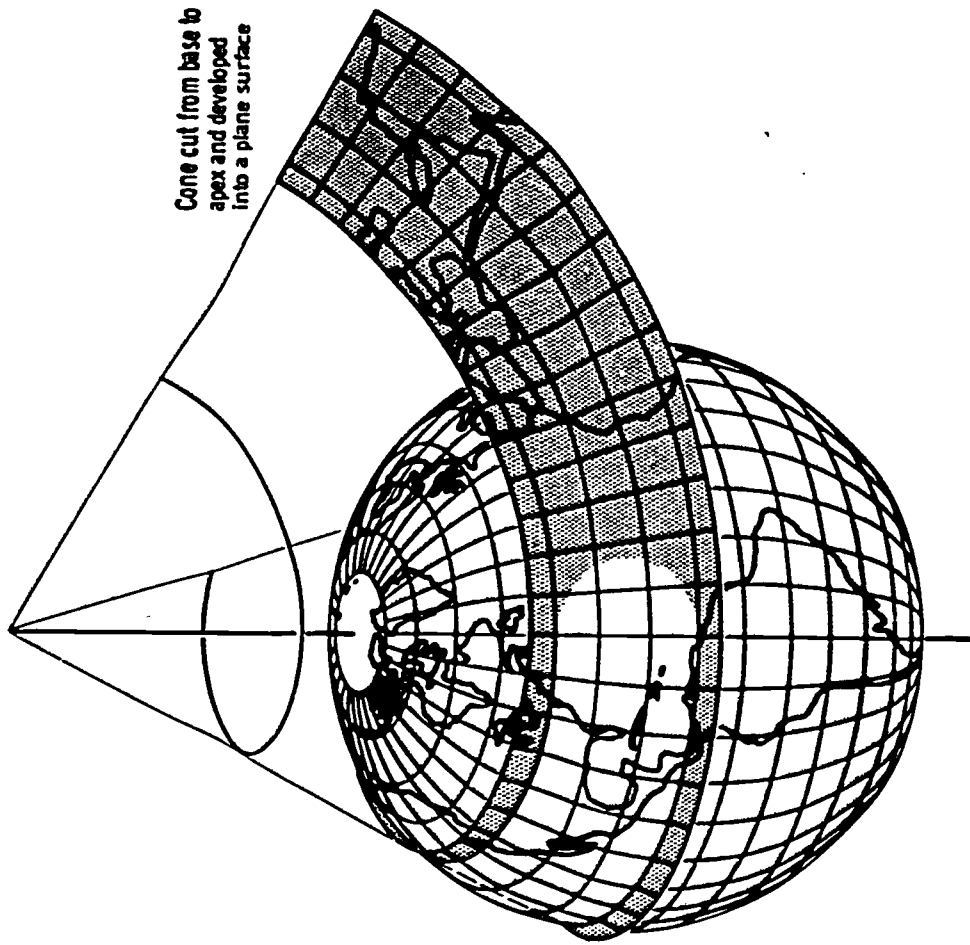
Diagram labels (top figure):

Polar axis

Earth's surface

Earth's surface feature projected onto surface of cone

Rays of projection

Center of Earth is point of projection

Surface of cone

Limit of projection

Standard parallel

Feature on surface of Earth

Standard parallel

Limit of projection

Diagram labels (bottom figure):

Limit of projection

Standard parallels

Limit of projection

Polar axis

Surface of cone

Cone enters surface of Earth

Cone emerges from surface of Earth

326

Cone cut from base to
apex and developed
into a plane surface

Figure 15-2. - Lambert conformal conic projection.

Mercator projection. - The Mercator conformal projection is basically a modified cylindrical projection. In a cylindrical projection (fig. 15-3), the surface features of the Earth are projected from the center point of the Earth onto the surface of a cylinder that is tangent to the Earth's surface along the equator. When the cylinder is unrolled on a plane surface, the resulting graticule consists of parallels of latitude and meridians of longitude that are straight and perpendicular to each other. The parallels of latitude are parallel and equal in length, and the spacing between them increases with increasing distance north or south of the equator. The meridians of longitude are parallel, equal in length, and equally spaced.

The increasing spacing between parallels of latitude to the north or south of the equator results in increasing distortion, or stretching, in the longitudinal (north-south) direction. With increasing distance to the north or south of the equator, there is also an increasing distortion in the latitudinal (east-west) direction. The reason for this is that in a cylindrical projection the parallels of latitude are equal in length, while on the surface of the Earth (a sphere) they become shorter with increasing distance from the equator. However, the longitudinal and latitudinal distortions are unequal. Therefore, a cylindrical projection changes the shapes, as well as the sizes, of the surface features of the Earth.

In a Mercator projection the graticule is modified (i.e., the spacing of the parallels of latitude is altered) so that at any point on the chart the scale is constant in all directions, and the longitudinal and latitudinal distortions are equal. Thus, small areas of the Earth's surface retain their correct shapes. However, the expanding scale does cause distortion in the shapes of large areas that extend for long distances to the north or south of the equator. The relative sizes of the Earth's surface features on the Mercator chart increase with increasing distance from the equator.

The principal feature of the Mercator chart is that a straight line connecting any two points gives the true direction between them and crosses all meridians at the same angle. Therefore, any such straight line on the map is a rhumb line. This feature is of great value in navigation because aircraft are commonly flown along rhumb lines. A rhumb line is not the shortest distance between two points, but for navigation purposes it represents the easiest and simplest course.
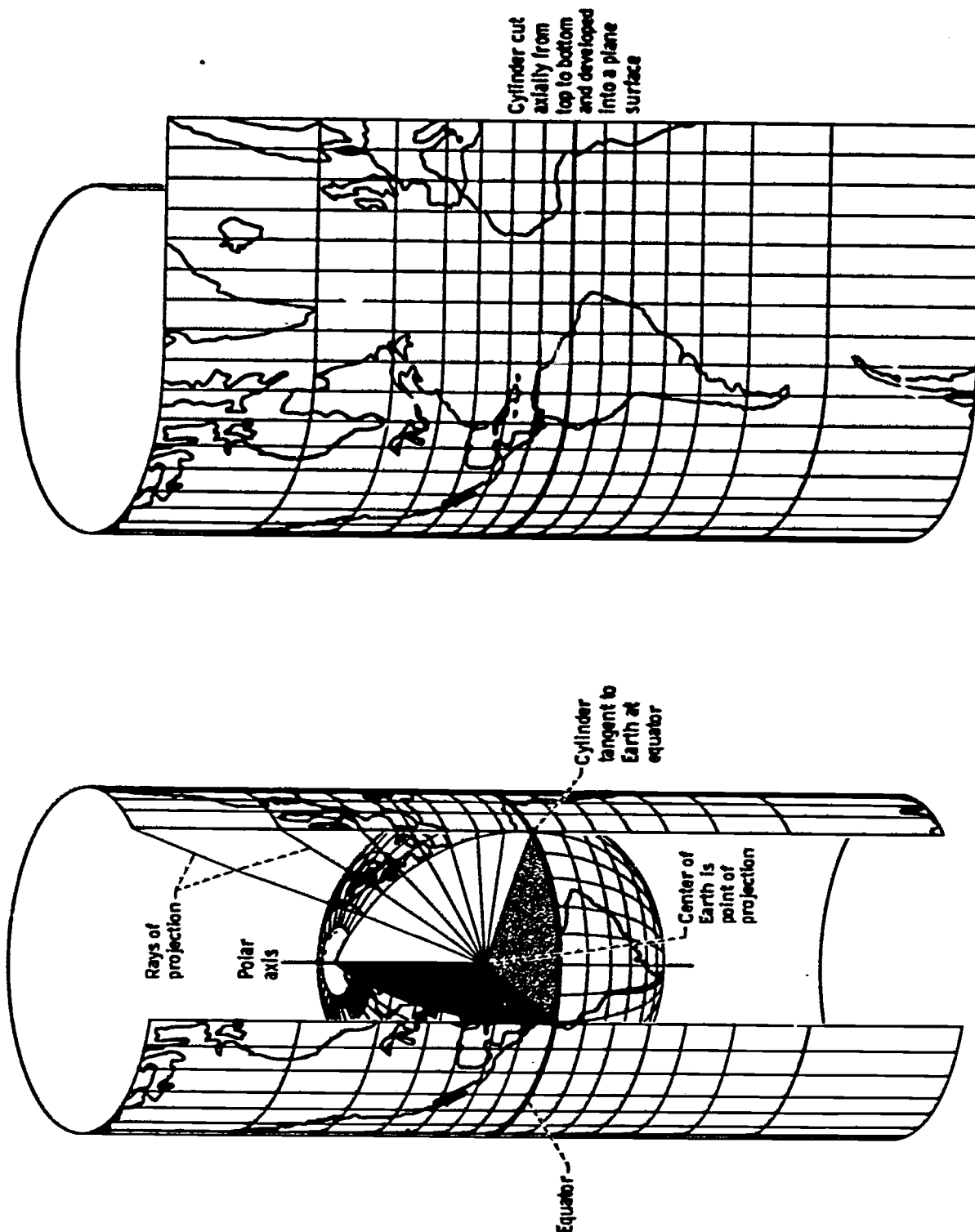
Cylinder cut axially from top to bottom and developed into a plane surface

Cylinder tangent to Earth at equator

Rays of projection

Polar axis

Center of Earth is point of projection

Equator

Figure 15-3. — Mercator cylindrical projection.

Scale

The scale of a chart is the ratio of a distance on the chart to the corresponding distance on the surface of the Earth. Charts are made to various scales for different purposes. If a chart is to show a large area of the Earth and not be too large, it must be drawn to a small scale. If it is to show much detail and not be cluttered, it must be drawn to a large scale. For the same size chart, a large-scale chart will show a much smaller area than a small-scale one.

The scale may be expressed by a simple statement, such as "1 inch equals 10 miles." It may be given as the representative fraction, such as "1:500 000" or "1/500 000." This means that 1 inch on the chart represents 500 000 inches (6.85 nautical miles) on the Earth's surface. Scale may be shown graphically on the chart by a graduated line labeled in terms of the distance it represents on the Earth's surface.

Features Shown on Aeronautical Charts

An aeronautical chart does not show all details of the Earth's surface. Instead, it shows and emphasizes those particular features which are useful to the airman. It shows those features which have the most distinctive appearance from the air. Some features are shown out of proportion to their true size for emphasis. For instance, the lines representing roads on sectional and regional charts may appear to be 1/4 mile wide if measured by the scale of the chart. Radio stations are prominently shown, although many are inconspicuous from the air. The following items are usually shown on aeronautical charts:

(1) Man-made features - cities, roads, railroads, etc.
(2) Water - oceans, lakes, rivers, streams, reservoirs, etc.
(3) Relief - difference in elevation of terrain
(4) Aeronautical features - airports, lights, radio facilities, airways, restricted areas, etc.

The symbols representing these various features are standard for any one series of charts but may differ between series.

PLOTTING AND MEASURING COURSES

We will discuss plotting and measuring only with reference to the Lambert chart, as it is the most used in general aviation. Most of the techniques also apply to the Mercator charts.

Distance

A straight line on a Lambert chart is approximately a segment of a great circle. Therefore, a line drawn on the chart between the points of departure and destination represents the shortest distance between them. This length of line can be transferred with a rule or with dividers to the scale on the edge of the chart to find the mileage. Many aeronautical plotters have several of the most common scales, so they may be used to measure distance directly on the chart.

Heading

Since the meridians converge at the poles on the Lambert chart, the angle between a straight line and the meridians varies as the aircraft flies along the route. To avoid the difficulty of flying a varying heading, the angle can be measured at the halfway point between the origin and the destination. This angle gives the constant heading, or rhumb line, which can be followed for the entire trip. For a long trip the rhumb-line course is considerably longer than the great-circle (shortest) course. Therefore, for a long trip the straight line between the origin and destination is divided into several segments. The angle of the rhumb line for each segment is measured at the halfway point of the segment. Thus, a great-circle course is approximated by a series of rhumb lines.

Magnetic Compass

The preceding discussion dealt with direction in terms of angles related to the geographic poles, or true directions. This creates a problem. There is no simple instrument that can be carried on the airplane and can measure angles relative to the geographic poles. The magnetic compass can measure angles and can be carried on an aircraft, but it has certain disadvantages. For example, the Earth's magnetic poles do not coincide with the geographic poles. Thus, even if the magnetic compass could be made to always point exactly at the magnetic pole, a variable correction would still be required. The correction required depends on the location of the compass relative to the magnetic and geographic poles, as shown in figure 15-4. The problem is further complicated by local variations in the Earth's magnetic field. However, for most areas of the Earth's surface these variations are well charted, and the combined effect of the magnetic pole and the local magnetic field is plotted on aeronautical charts as a series of isogonic lines, or lines of equal magnetic variation (fig. 15-5).

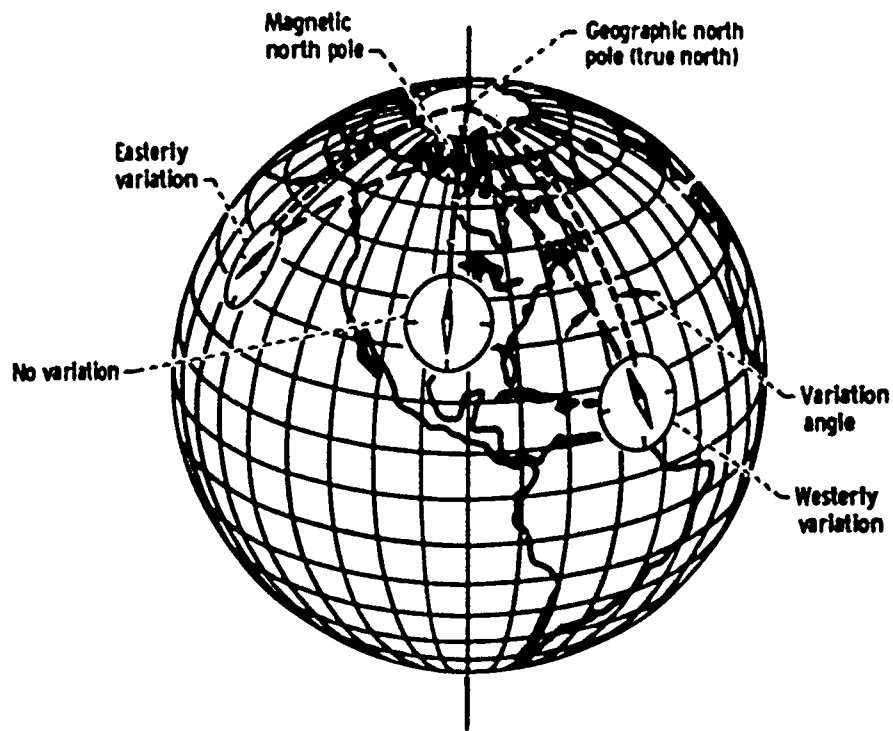Since a compass is affected by all magnetic fields, the aircraft itself also induces

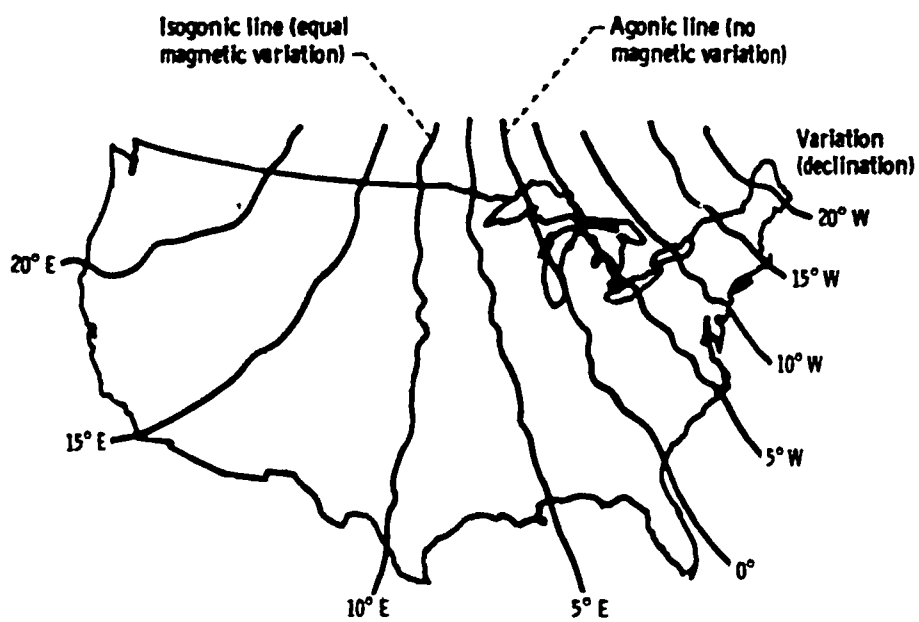Figure 15-4. - Magnetic variation (declination).

Figure 15-5. - Isogonic chart showing lines of equal magnetic variation (declination).

332

some error into the magnetic-compass system. The electrical systems of the aircraft create magnetic fields during operation. The ferrous parts of the aircraft also create magnetic fields that affect the compass. Hard landings, lightning strikes, and electrical storms can cause the local magnetic fields of the aircraft to change. Therefore, these magnetic fields must be checked periodically and recorded. The errors caused by local magnetic fields can be reduced by the use of compensating magnets located in or near the compass. But unless these errors are reduced to very small values of 1^0 or 2^0, they should be taken into account when flying. The error due to these local magnetic fields is called "deviation."

Effect of Wind on Flight Path of Aircraft

Any vehicle on the ground, such as an automobile, moves in the direction in which it is headed or steered and is affected very little by wind. An aircraft, however, seldom travels in the exact direction in which it is headed. This is due to the effect of wind on the aircraft.

Wind is the movement of an air mass relative to the Earth's surface. Wind direction is expressed as the direction from which the air mass is moving and is measured clockwise from true north. Wind speed is the rate of motion relative to the Earth's surface.

Consider the effect of the wind on a balloon, which has no motive power of its own. If the balloon is tied to the Earth with a string, the wind blows past it, just as it blows past any fixed object on the Earth. If the balloon is released, it moves with the air mass (wind), just as a bottle floating in a river moves downstream with the current. If the wind is blowing at 20 miles per hour from the west, in 1 hour the balloon will be 20 miles east of the point where it was released.

Any free object in the air moves downwind with the speed of the wind. This is just as true of an aircraft as it is of the balloon. However, the aircraft in flight is also moving forward through the air mass. Therefore, as shown in figure 15-6, the motion of the aircraft relative to the ground is governed by the motion of the aircraft through the air mass and by the motion of the air mass (i.e., the wind) relative to the Earth's surface. Each of these motions is defined by its direction and speed. Therefore, these motions are vectors. (Vector quantities and vector relations are discussed in chapter 4.)

The air vector is defined by the airplane's true heading (i.e., direction in which airplane is pointed) and by its true airspeed (i.e., speed of airplane relative to surrounding air), expressed in nautical miles per hour, or knots. The wind vector is defined by the direction from which it is blowing and by its speed, also expressed in knots. The aircraft's flight path relative to the ground (i.e., the track of the aircraft) and its speed relative to the ground (i.e., its ground speed) define the ground vector. The ground vector
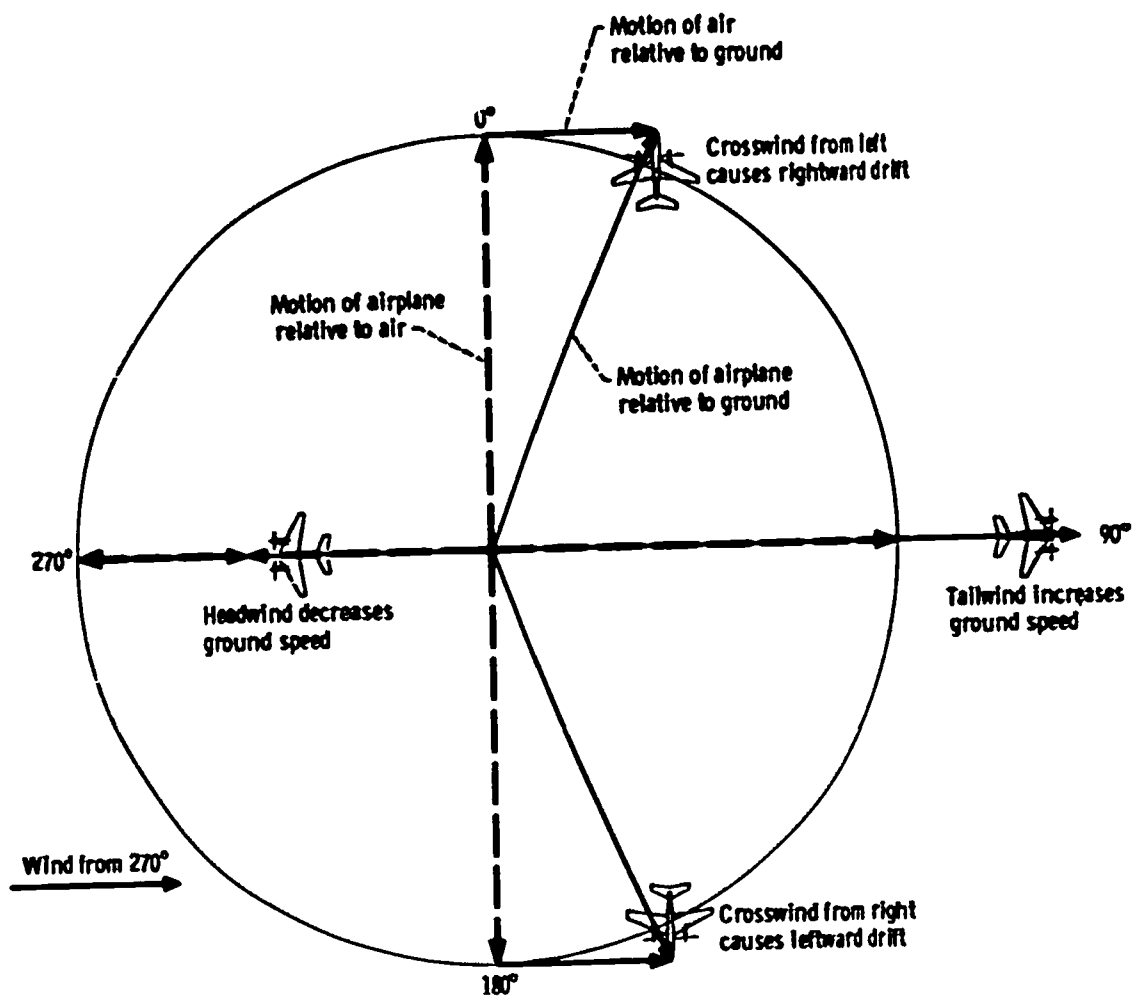
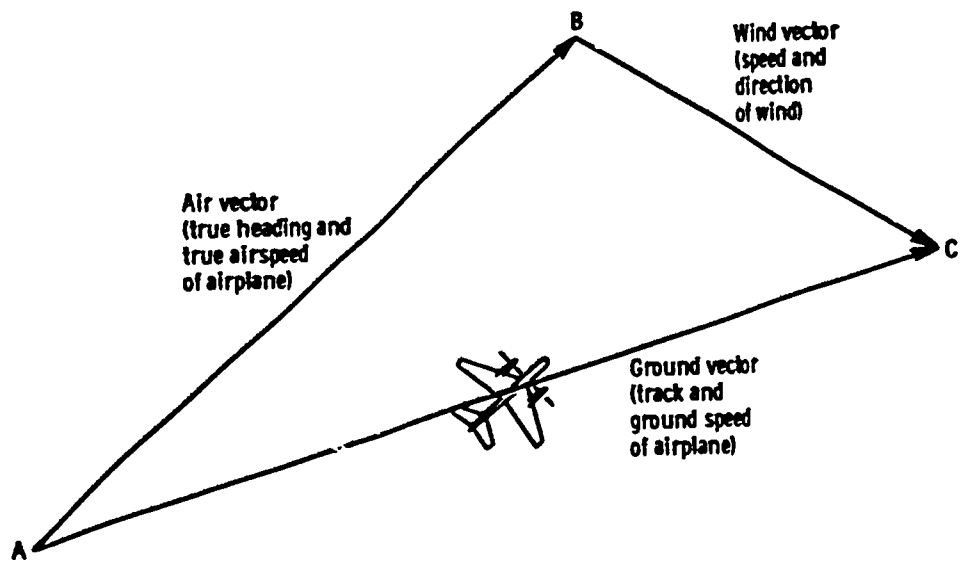Figure 15-6. - Effect of wind on flight path of aircraft.

Figure 15-7. - Vector diagram showing relation of air, wind, and ground vectors.

is the resultant of the air and wind vectors and can be determined by means of a vector diagram, as shown in figure 15-7. From a given point (A) a line is drawn in the direction of the true heading of the airplane. The length of this line is drawn proportional to the true airspeed of the airplane. This line (A-B) represents the air vector. From the head (B) of this air vector a line is drawn in the direction in which the air mass is moving. The length of this line is drawn proportional to the wind speed. This line (B-C) represents the wind vector. Finally, a line is drawn between the starting point (A), or tail, of the air vector and the end point (C), or head, of the wind vector. This line (A-C) represents the ground vector. The length of this vector represents the ground speed of the aircraft. The direction of this vector is the direction of the actual flightpath, or track, of the aircraft.

Obviously, a complete vector diagram represents six quantities (direction and speed for each of the three vectors). If any four of these six quantities are known, the remaining two can be determined by drawing a vector diagram. The vectors may be drawn in any sequence. However, the air and wind vectors (i.e., the component vectors) must be drawn head to tail, and the ground vector (i.e., the resultant vector) must be drawn tail
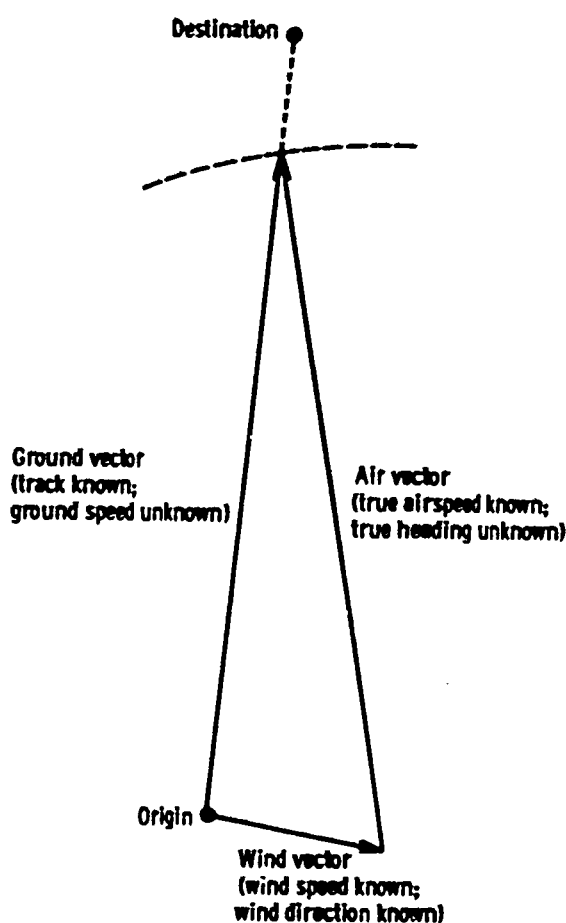
Figure 15-8. - Example vector diagram for common navigational problem of determining ground speed and true heading from known track, true airspeed, wind direction, and wind speed.

331

to tail with one of the components and head to head with the other.

A common navigational situation is one in which the track (course from origin to destination), the true airspeed, the wind direction, and the wind speed are known. The problem is tc determine the ground speed (a ground-vector element) and the true heading (an air-vector element). The following method is used to draw the vector diagram (fig. 15-8). From the origin a line is drawn in the direction of the track that is necessary to arrive at the destination. Also from the origin, the wind vector is drawn. Next, an arc of a circle whose radius is equivalent to the true airspeed and which is centered on the head of the wind vector is drawn to intersect the line representing the track. Finally, a line drawn from the head of the wind vector to this intersection completes the vector diagram. The direction of this line, relative to true North, is the true heading; this is the direction in which the aircraft must be pointed in order to fly the desired track over the ground. The ground speed of the aircraft is represented by the length of the line segment from the origin to the intersection of the track and the arc that marks the airspeed.

NAVIGATION SYSTEMS

The preceding discussion pertained to navigation by visual reference to the Earth's surface or by estimation of the effects of wind on the flight path, called dead reckoning. These methods work well when reference to visible landmarks can be maintained, at least at frequent intervals, but they cannot provide sufficient accuracy for safe operation under conditions of poor weather or for long flights over water. For this type of operation it is necessary to use some navigational aid, or system, that does not require visible landmarks. Some of the currently used navigation systems are discussed briefly in the following sections.

Radio Compass

The radio compass is an instrument that indicates the direction, or relative bearing, of any transmitting station within its frequency range of 100 to 1750 kilohertz (kHz).

The operation of the radio compass is dependent upon the characteristics of a loop antenna. A loop receiving antenna gives maximum reception when the plane of the loop is parallel to, or in line with, the direction of radio wave travel. As the loop is turned from this position, volume gradually decreases, and reaches a minimum when the plane of the loop is perpendicular to the direction of wave travel. The null position (i.e., the position of minimum or zero signal strength) is used for direction finding, as it can be more accurately determined. For a 25° rotation from the maximum signal position,

total signal strength changes less than 10 percent. For the same rotation from the null position, the signal strength changes by 50 percent.

When the loop is rotated to a null position, the radio station being received is located along a line that is perpendicular to the plane of the loop. However, the radio station may be located on either side of the plane of the loop, along this line. Therefore, the loop antenna has a 180° ambiguity. This ambiguity can be eliminated by turning the aircraft briefly to a course perpendicular to the radio beam. When the aircraft is first turned to this new course, the plane of the loop antenna in the null position is parallel to the course. As the aircraft flies along this straight-line course, the antenna must be rotated either clockwise or counterclockwise to maintain it in the null position. Clockwise rotation indicates that the station is to the right of the aircraft, and counterclockwise rotation indicates that it is to the left. Thus, the 180° ambiguity is eliminated, and the aircraft can then be turned back to its original course.

The 180° ambiguity of the loop antenna may also be avoided by connecting the receiver to an additional, omnidirectional antenna. This system (by a process of addition or subtraction of signal voltages from the two antennas) provides a single null, so that the direction to the station is known immediately. This arrangement also allows connection to an automatic servo system which will drive the loop to this single null position and indicate it to the pilot. The Automatic Direction Finder (ADF) is the configuration most used in today's aircraft.

Very-High-Frequency Omnidirectional Radio Range (VOR)

The Very-High-Frequency Omnidirectional Radio Range system, commonly called VHF omnirange, VOR, or omni, is the basic component of the navigation system of the airways in the United States and is coming more into use in other countries. It simplifies the task of navigation and eliminates most of the problems of static and interference found in the low-frequency navigation systems.

The operation of the VOR system is based on the creation of a phase difference between two transmitted signals. One of these signals, called the reference-phase signal, is radiated from the station in a circular, or omnidirectional, pattern. The other signal, called the variable-phase signal, is transmitted as a rotating field. This signal pattern rotates uniformly at 1800 revolutions per minute, which causes the phase of the signal to vary at a constant rate. Therefore, there is a different phase of this signal at each direction from the station. The difference in phase between the reference and variable signals is measured electronically by the aircraft receiver and indicates the direction from the transmitting station to the aircraft. This phase relationship between the two signals is illustrated in figure 15-9.
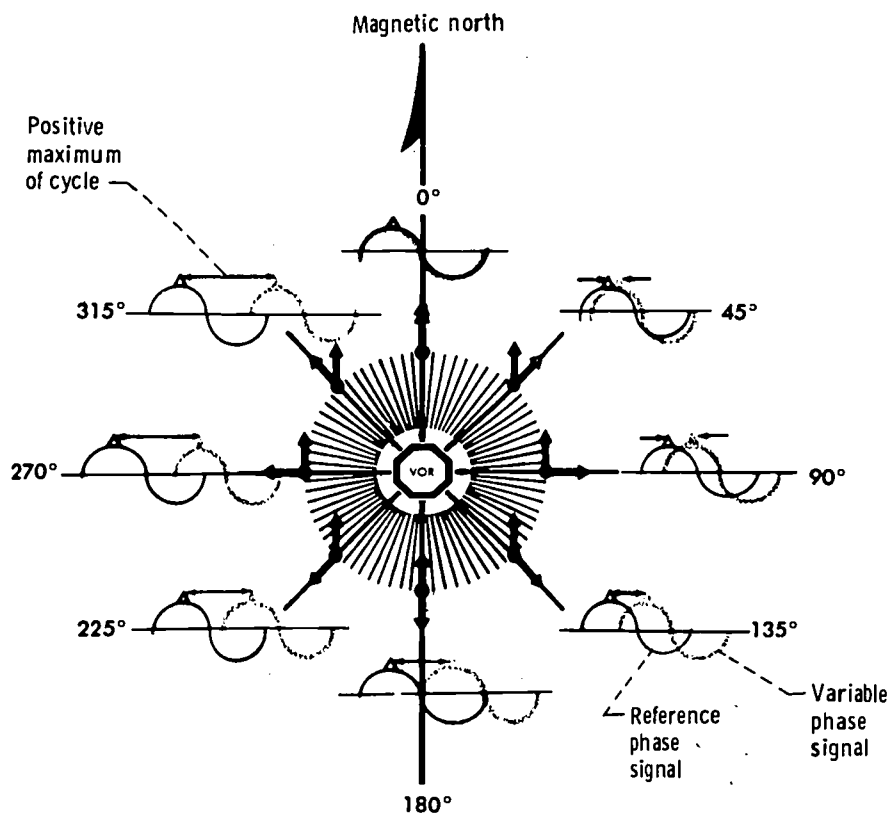
Figure 15-9. – Signal phase angle relation for VOR navigation system. (Signals from VOR station are in phase at magnetic north and vary elsewhere around the station.)
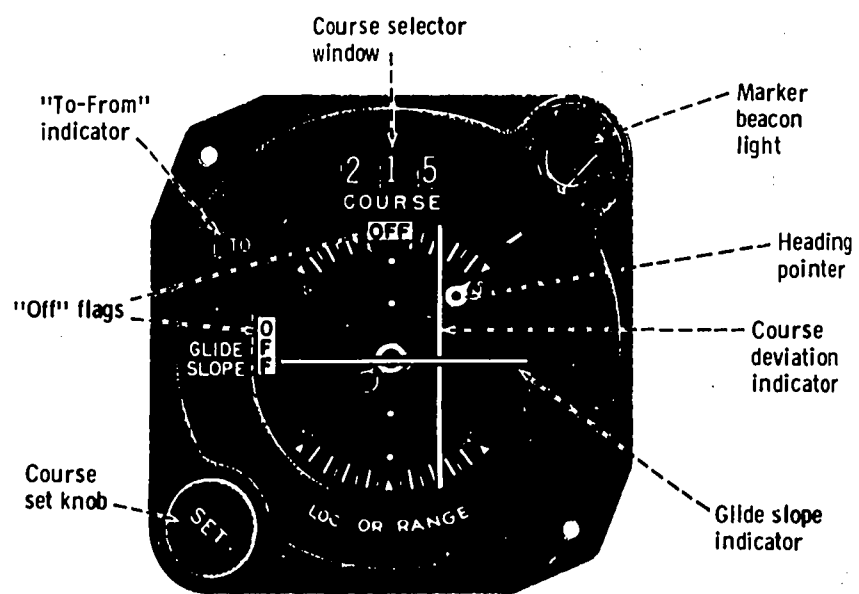

Figure 15-10. – Typical course indicator used with VOR navigation system.

338

The indicator shown in figure 15-10 is typical of the method of presentation of the VOR information to the pilot. The pilot selects the desired course. The "to-from" indicator shows whether the selected course, if intercepted and flown, will take him to or away from the station. The heading pointer shows the heading of the aircraft relative to the selected course. The deviation indicator (vertical needle) shows the position of the selected course in relation to the position of the aircraft. For simplification, the deviation indicator may be considered to be a portion of the selected course and the heading pointer to be the aircraft. Thus, in the illustration of figure 15-10, the aircraft is to the left of the desired track and is headed toward it at a 45^0 angle. The glide-slope indicator (horizontal needle) is used when the receiver is tuned to an instrument landing system and functions in the same way as the deviation indicator. When the glide-slope indicator is below the center of the instrument, the desired glide path is below the airplane.

Tactical Air Navigation (Tacan)

The Tactical Air Navigation (Tacan) system was developed in this country for military use. This system, which operates in the UHF range (1000 mHz), provides the pilot with direction information similar to that of the VOR system. In addition, the Tacan system provides the pilot with distance information, so that from a single ground station he can obtain a complete position fix. The primary advantage of this system over the VOR is ease of setting up the ground station. This makes the Tacan system valuable for military use. In the United States, most VOR stations also have Tacan facilities, so that military aircraft equipped only with Tacan may navigate over the civil airways system. Civil aircraft also make use of the distance information obtained from the Tacan signal.

A directional antenna system is rotated at 15 revolutions per second. The aircraft receives a signal that goes from maximum to minimum 15 times per second. As the maximum signal passes through North, a reference pulse is transmitted. The aircraft receiver measures the time between this reference pulse and the maximum signal strength. Secondary lobes on the antenna pattern and auxiliary pulses are superimposed on the basic pattern, as shown in figure 15-11, to provide a fine bearing reference and to give a system accuracy of $\pm1^0$. The bearing information is presented to the pilot on an instrument similar to that used in the VOR system.

Distance is determined with Tacan equipment by measuring the elapsed time between the sending of an interrogation pulse by the airborne set and the reception of a reply pulse from the ground unit. These pulses require about 12 microseconds round-trip travel time per nautical mile of distance from the ground station. Since a large number of aircraft may be interrogating the same ground beacon, the airborne set must be able to sort out for measurement only the pulses which are replies to its own interrogations. It does this
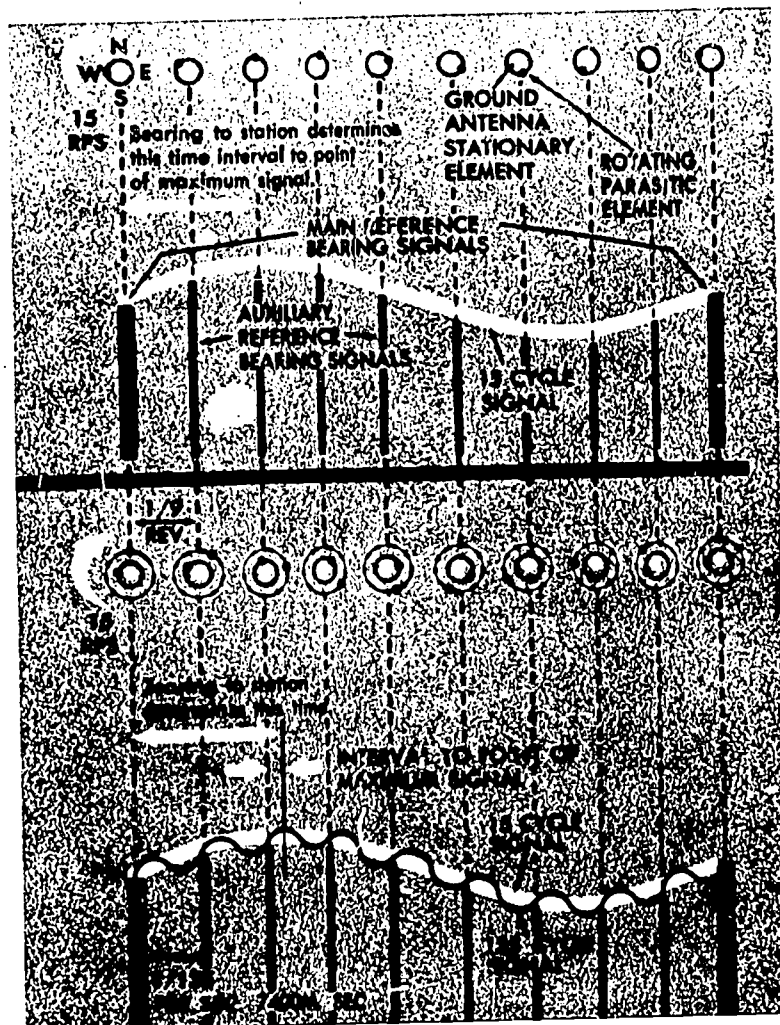
Figure 15-11. - Antenna and signal patterns for combined coarse and fine bearing signals of Tacan navigation system.

by sending its pulses on an irregular, random basis, then sorting out those replies whose pattern is synchronous with the pattern of the interrogations.

The distance measured by the Tacan equipment is the actual, slant range, not the horizontal range, between the aircraft and the ground station. The difference between the slant range and the horizontal range is negligible, except when the aircraft is very close to the station and at high altitude. Obviously, as the aircraft passes directly over the station, the distance indicated by the Tacan equipment is actually the altitude (in nautical miles) of the aircraft relative to the station.

Long-Range Navigation (Loran)

The radio systems previously discussed are basically short-range systems, good for ranges up to about 300 miles, and thus are not applicable to long-range or over-water

navigation. The radio-compass system might be considered an exception to this state-
ment, for it can be used for longer distances under ideal conditions. However, several
systems are available which provide equal or better accuracy and greater range. The
most popular of these ground-based systems is the Long Range Navigation (Loran) sys-
tem.

The ground equipment of the Loran system basically consists of pairs of transmitting
stations that broadcast pulsed signals. In each pair of stations, one is designated the
master station, the other, the slave. The two stations are a known distance apart. The
master station transmits a series of pulse signals which are received by both the aircraft
and the slave station. Some fixed delay time after it receives each master pulse signal,
the slave station transmits a matching pulse signal. The airborne receiver includes a
timing device which measures the difference between the arrival times of two matching
signals from the two stations. In this time-difference measurement, the time required

Line of position
determined from
signals of stations
M_1 and S_1

Fix

Line of position
determined from
signals of stations
M_2 and S_2

Slave
station
S_1

Common master
station $M_{1,2}$
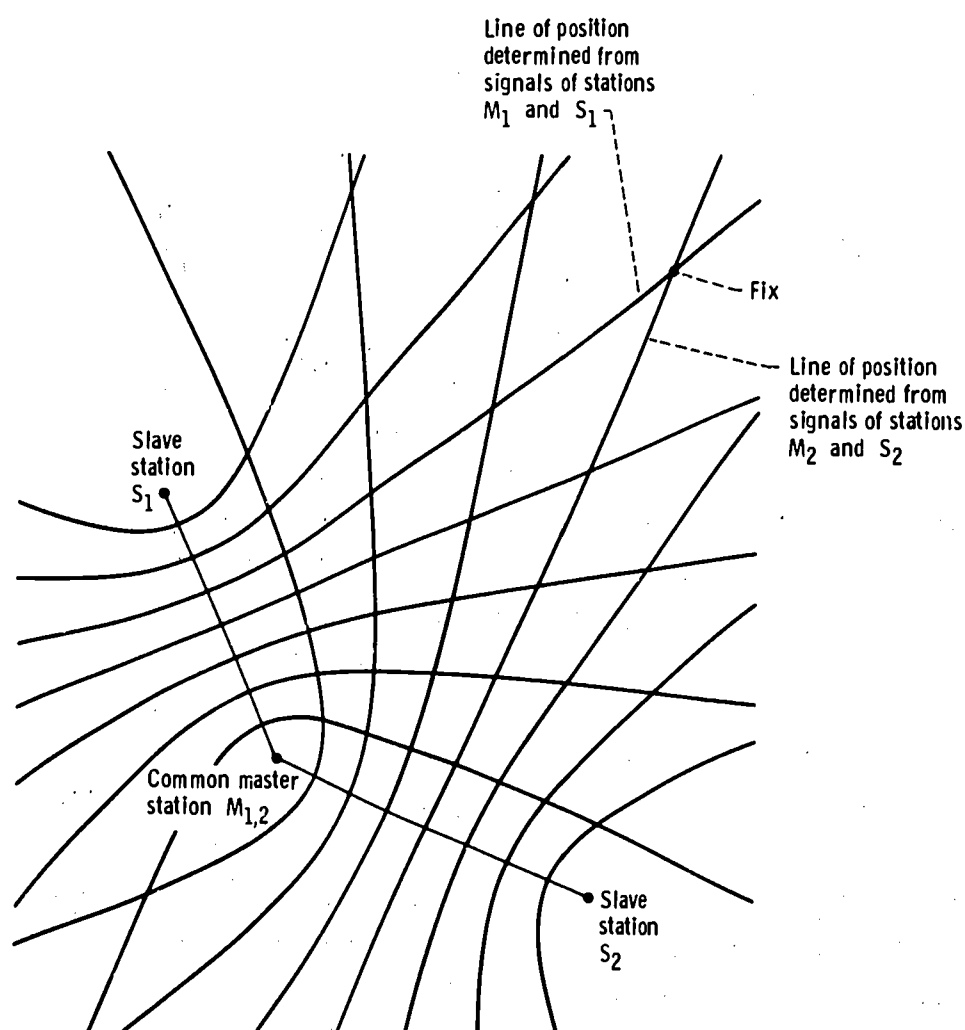
Slave
station
S_2

Figure 15-12. – Example Loran chart showing lines of constant time difference for pulsed signals
received from paired master and slave stations.

341

for a master signal to reach the slave station and the fixed time delay of the slave station are both taken into account. Thus, the remaining time difference represents the difference in the distances of the two stations from the aircraft. Special Loran charts, similar to figure 15-12, show series of lines of constant time difference for each pair of stations. Thus, the measured time difference for one pair of stations locates the aircraft along one of these lines. The time differences for two pairs of stations provide a fix (at intersection of lines) of the aircraft's position.

Doppler Navigation

Each of the previously described radio navigational aids or systems requires a source of information (e.g., transmitting stations) separate from the aircraft. Two navigation systems now coming into use on civil aircraft do not require any external information (such as radio signals) once they have been initially set. The two systems are known as Doppler navigation and inertial navigation. However, the Doppler system is not completely passive, as it requires a transmitter aboard the aircraft which sends out pulses to be reflected back from the surface of the Earth. Inertial systems are completely passive and require no signal or information to be radiated outside of the aircraft; therefore, they are of considerable interest for military applications, where detection is a consideration.

In the Doppler system, the normal navigational triangle of velocities is solved by high-accuracy, direct measurement of the aircraft's drift and ground speed. Determination of absolute direction is accomplished by adding heading from the aircraft's heading reference system to the Doppler drift. A suitable navigation computer which accepts the raw data on heading and Doppler drift can convert them to terms of aircraft present position and/or steering and distance information for a predetermined destination.

The Doppler effect works on the principle that a change of frequency occurs between received and transmitted signals when there is relative motion between receiver and transmitter. A simple analogy is that of a stationary observer listening to the whistle sound of a fast-moving express train. As the train approaches him the note of the whistle increases in frequency (and in pitch), reaches a maximum as the engine passes him, then decreases as the train speeds away from him. Similarly, if a moving airborne radar device transmits a beam of radio energy towards the ground, the echo signal received back from the point of reflection changes frequency by an amount proportional to the component of velocity along the beam.

A single-beam airborne antenna would have two disadvantages. First, it would not necessarily measure velocities along the aircraft's track, and second, it would include a vertical component in its measurements if the aircraft deviated at all from level flight.

To overcome the first of these disadvantages, two beams can be radiated, one to each side of the aircraft. Thus, a drift to left or to right during flight causes a greater Doppler shift in either the left or the right antenna, and suitable computation can resolve the difference into a measure of the drift angle. The difference in Doppler shifts can also be used as an error signal to drive the axis of the antenna array into coincidence with the airplane track. In this case, the drift angle is obtained by direct mechanical measurement.

Unwanted vertical components of velocity, the second disadvantage of a single-beam antenna, are eliminated by adding a rearward-directed beam to each forward-directed beam. This system has several advantages. First, the vertical component of velocity is virtually eliminated, since the amount present in the forward-directed beams is equal and opposite to that in the rearward-directed beams. Second, since the Doppler beat frequency is obtained by mixing signals from two beams rather than by single-beam measurement, greater precision of velocity determination is possible. Finally, the necessity for antenna stabilization in the pitching plane is largely eliminated. (Roll errors also affect the Doppler system; but except for special military applications, in which extreme accuracy is required, the expense of roll stabilization of the antenna is seldom justified.)

The Doppler system has certain operating limitations. Over smooth sea surfaces, the signals reflected back to the receiver are sometimes too weak to be usable, particularly if the aircraft is flying at great height. Also, the signal may be lost at certain critical altitudes.

Small residual errors are also present in the system. The principal sources of error in the Doppler radar system alone are antenna misalinement (perhaps 0.2^o on the average civil aircraft), variations in the absolute length of a nautical mile with latitude and altitude, and movement of the reflecting surface (e.g., movement of water surfaces due to winds and/or currents). With all these residual errors taken into account, the practical accuracy of most current Doppler radar systems is about 0.5 percent of distance flown along the track and about 0.5^o across the track. The above errors relate to only the Doppler radar and do not represent total system error.

Even though it is carefully fabricated, situated, calibrated, and compensated, the gyromagnetic compass is normally the largest single source of error in the complete Doppler system. The gyromagnetic compass can seldom provide an accuracy of better than 1.2^o across the track or 2.0 percent of distance flown along the track. Add in a little for computer error in resolution, and total error for the complete system becomes about 0.6 percent along and 2.6 percent across the track.

543

Inertial Navigation

The inertial navigation system is unique in that the entire system is carried on the aircraft, is completely self-contained, and requires no external information such as radio signals. Essentially, inertial navigation is the process of determining the speed and position of an aircraft from measurements of the accelerations of the aircraft.

Inertial navigation is based on Newton's laws of motion. According to the first law, a body in motion will continue to move at the same speed and in the same direction until it is acted upon by an external force. According to the second law, the force acting on a body is equal to the product of the mass of the body and its acceleration along the line of action of the force.

From these laws, the equations of motion for uniform conditions were developed:

$$s = ut \tag{1}$$

and

$$v = u^2 + 2as \tag{2}$$

where

s   distance

u   initial velocity

t   time

v   final velocity

a   acceleration

Where velocities and accelerations are constantly varying, these equations are expressed in calculus notation

$$v = a \, dt \tag{3}$$

and

$$s = v \, dt = a \, dt \times dt \tag{4}$$

According to equation (4), distance is equal to the integral of velocity with respect to time. Thus, a mechanized solution based on this equation can average and multiply velocities over infinitesimal periods of time to give an accurate value for distance traveled.

In mechanizing the solution, the first problem is to measure the vehicle accelerations. Thus, the basic components of an inertial navigation system are two accelerometers capable of sensing and measuring aircraft accelerations in the north-south and east-west directions. Several methods can be used for sensing accelerations. Perhaps the simplest is measuring the movement of a spring-restrained mass (Hooke's Law states that the extension of the spring is proportional to the force causing it). However, the basic sensitivity of such a system is not high. Greater sensitivity is usually achieved by using "force balance" instruments, in which the applied acceleration is measured by the force required to rebalance the system against the input acceleration. Such devices are remarkably accurate over a wide range of acceleration values. But if they are to perform their functions usefully and correctly, they must obviously be protected from the pitching, yawing, and rolling motions of the aircraft in which they are mounted. The accelerometers are therefore mounted on a gyro-stabilized, gimbaled platform, which maintains them in a horizontal position with respect to the local surface of the Earth, regardless of any changes in aircraft position and attitude. The gimbaled platform is stabilized by two or three gyroscopes. Such an acceleration-measuring system is capable of measuring the horizontal components of aircraft accelerations without being affected by unwanted vertical components of such accelerations.

But acceleration measurements alone are of little navigational use. The inertial navigation system therefore includes two sets of integrators. The first set integrates the accelerations with time to indicate velocities, and the second set integrates the velocities to indicate distances traveled in the north-south and east-west directions. These distances can then be fed to a navigational computer, tailored to the needs of the user, to produce an automatic, continuous, and accurate display of aircraft position, heading, and distance relative to a predetermined destination or track.

Nothing so useful could be quite that simple; the inertial navigation system is no exception. Gyroscopes need to be corrected for the effects of the Earth's rotation and the aircraft's motion, and this is normally accomplished by feedback from various stages of the inertial navigation system itself. Gyroscope biasing, to reduce errors resulting from mass unbalance and from other causes, is usually performed on the ground at set intervals.

The accelerometers are subject to errors caused by centrifugal forces (since the aircraft is moving around a curved path over the Earth's surface), coriolis forces (caused by the rotation of the Earth), polar compression (because the Earth is an oblate spheroid), and gravity magnitude variation. Therefore, correction terms must be continuously fed back to compensate for these errors.

In addition to all this, the stabilized platform, being a form of pendulum, must be maintained vertical despite horizontal accelerations which would tend to make it lag behind the local vertical by an angle dependent on the magnitude of the acceleration and the

length of the pendulum. This is accomplished by "Schuler tuning"; that is, the platform is made to simulate the behavior of a pendulum whose length is equal to the radius of the Earth. Such a pendulum (i.e., a Schuler pendulum) would always maintain its vertical orientation. The period of such a pendulum is given by

$$T = \frac{R}{g} \tag{5}$$

where

T period of pendulum, sec

R length of pendulum (radius of Earth), ft

g acceleration due to gravity, 32.17 ft/sec^2

If R were equal to the radius of the Earth, the period would be 84.4 minutes. The practical solution is to construct an electromechanical analogue having the same period as the Schuler pendulum. Such an analogue will maintain a vertical orientation relative to the surface of the Earth.

As an example of the sort of precision required, if one of the accelerometers is tilted from the horizontal by as little as $1/60^o$, the spurious gravity acceleration from this cause alone will introduce a system error of 12 nautical miles at the end of a 1-hour flight. The accelerometers themselves must be sufficiently sensitive and wide-ranging to cope with accelerations varying from perhaps 7 or 8 g to 0.000005 g. If the total navigation system is to be accurate to within 1 nautical mile for 1 hour of flight at 1000 miles per hour, an accelerometer in the system has to be accurate to within less than 0.0003 g.

As regards gyroscope accuracies, it does not seem so long ago that the old aircraft directional gyroscope, with a drift rate of perhaps 10° per hour, was still regarded as a marvelous instrument. Even now the gyroscopes in some gyromagnetic compasses in common use have a free-mode drift rate of more than 5° per hour. However, some currently used gyroscopes have drift rates of only 0.01^o per hour; and in the not-too-distant future, gyroscopes with drift rates as low as 0.001^o per hour will probably be used.

In spite of gyroscope inaccuracies, the inertial navigation system offers tremendous advantages for both civil and military aircraft. It eliminates the dependence upon the radio wave, transmitted or received, and on celestial and terrestrial references. Inertial navigation measurements (based on Newtonian laws of motion and gravitation) are carried out entirely within the aircraft. The system is therefore available at all times, in all places, regardless of weather, and (of particular importance to the military user) without making any tell-tale transmissions that could be intercepted and possibly jammed.

The accuracies provided by inertial navigation are high compared with the accuracies

of other navigation systems. For example, a maximum error of only 2 nautical miles per hour is well within the state of the art. This error is time dependent only; therefore, the faster the aircraft, the better the performance of the system in terms of accuracy per distance flown, a factor of particular importance for supersonic aircraft.

16. WEATHER SAFETY AND NAVIGATION IN SEVERE STORMS

I. Irving Pinkel*

STORM HAZARDS TO FLIGHT

Severe storms are the principal hazard to flight. The airplane is endangered by the strong, turbulent winds of the storm and by the hail and rain that often accompany it. Here we will describe the nature of these severe storms and some of the techniques for operating safely in storm areas.

An airplane can be lost in severe weather if buffeting from erratic winds places it in flight attitudes from which the pilot cannot recover. The airplane may fall out of control, or the pilot's attempt to restore correct airplane flight may result in a violent airplane maneuver that stresses the airframe to failure. Likewise, hail can damage the aerodynamic surfaces of the airplane sufficiently to require extreme skill to land the airplane safely. Aircraft flying at supersonic speeds (above 700 miles per hour) can receive similar damage from impacting rain droplets at these speeds. Figure 16-1 shows the damage to an airplane that flew through hail. The extensive damage to the leading edge of the wing raises the danger of airflow separation from the top surface of the wing as the aircraft slows for landing. Since the damage to each wing is somewhat different, each wing may generate a different lift, especially at low flight speeds, when the angle of attack is high. This difference in lift between the two sides of the wing may be too great for the pilot to compensate with ailerons and trim tabs, and the airplane may enter an uncontrollable roll on the landing approach. Fortunately, this did not happen to the airplane shown in the figure. It is clear from these considerations that flight through hail and heavy rain showers at high speed must be avoided. In order to do this, the pilot and those who direct his flight from the ground must understand the structure of the storm through which the airplane is flying so that the pilot may pick a safe path.

Severe thunderstorms present the most common flight weather problem. The U.S. Weather Bureau and its successor organization, the Environmental Science Services Administration, have a research center devoted solely to the study of severe storms. Through the work they have done by ground observations and flights through thunder-

---

*Director, NASA Aerospace Safety Research and Data Institute.
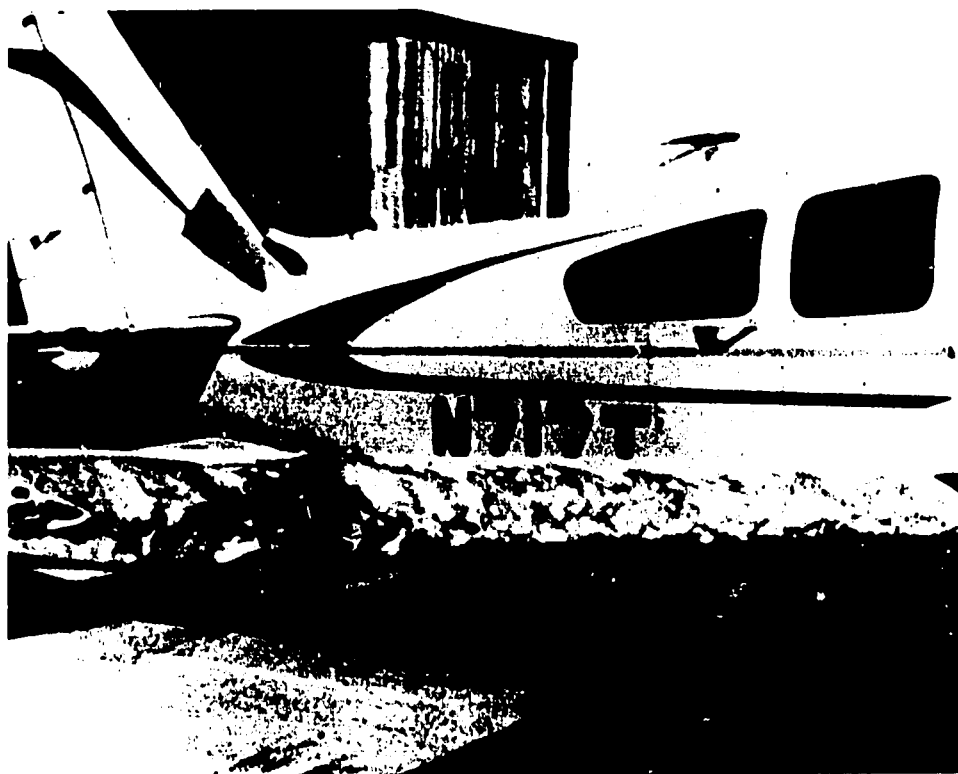
Figure 16-1. - Hail damage to airplane.

storms with instrumented airplanes, they have constructed the picture of the anatomy of the thunderstorm. This information has made it possible for aircraft to fly safely in storm areas.

CHARACTERISTICS OF A THUNDERSTORM

While no two thunderstorms are exactly alike, they all have certain features in common. They have similar modes of development to the violent condition we recognize as a severe storm and have common gross features by which the several stages of the storm's development and dissipation are identified.

The thunderstorm is made up of a series of thunder cells which are often between 5 and 10 miles in horizontal extension but in some instances may exceed 20 miles in horizontal extension. The pilot can recognize the thunderstorm that has reached a dangerous stage in development because its cells, from an airplane, have the appearance shown in figure 16-2. The base of the thunderstorm cloud is usually between 2000 and 10 000 feet from the surface. The tops can have far greater variation in height. They can extend from 15 000 to 60 000 feet. In some rare instances they have been reported at even higher levels. The pilot recognizes that the thunderstorm is fully developed and is, therefore, in a dangerous condition when he observes the prominent anvil cloud at the top

346
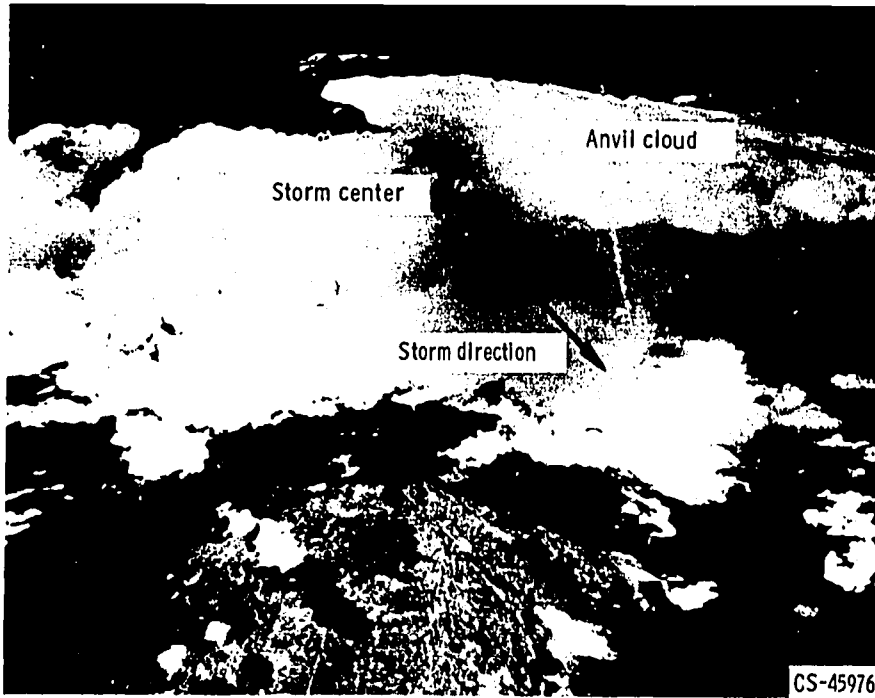
Figure 16-2. - Typical thunderstorm cell viewed from high altitude.

of the thunder cell (fig. 16-2).

By means of ground instrumentation and flights through thunderstorms, the dangerous zones have been mapped as shown in figure 16-3. Here we see a cloud which reaches from 5000 feet to 55 000 feet altitude. The zone of highest winds within the cloud appears as a curved column of air rising upward through the center of the cloud. Its location within the cloud can be roughly estimated from the fact that this rising column produces a bump in the upper perimeter of the cloud. In figure 16-3, this bump appears above
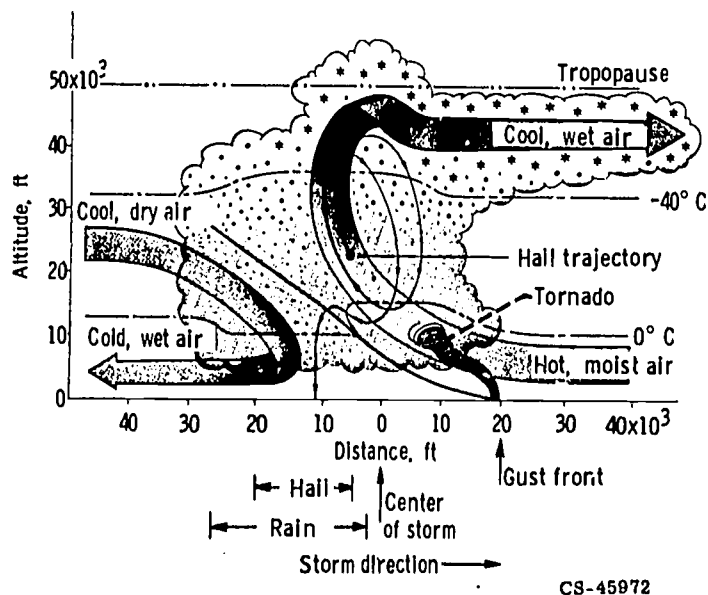
Figure 16-3. - Vertical section through thunderstorm cell showing air currents and areas of precipitation.

347

the 50 000 foot altitude level. This high-speed column of air originates close to ground level. At this low level, the air is moist and warm enough to have a density less than the cooler air which lies above it. Being less dense than the overlying air, this warm, moist air floats upward through the more dense overlayer. As the air rises, it cools, because it expands in the lower pressures of the higher altitudes. As the air cools, moisture is condensed and the heat of condensation from this moisture warms the air. The net effect is to give the rising air a temperature higher than it would have had if water condensation had not occurred. Because of this warming, the air retains a density less than that of the surrounding air, and so it continues to flow upward. As this air climbs through several thousand feet in this way, it acquires vertical speeds often in excess of 200 miles per hour. An aircraft that flies into such a jet of rising air could be tossed into flight attitudes that would require considerable skill on the part of the pilot to restore it to normal flight attitudes.

When a rising column of air achieves its highest level (immediately under the bump of the upper perimeter of the thunder cell), condensation is stopped. The moisture that condensed as water at lower levels has now frozen to hail in the intense cold of the higher altitudes. Since the velocity of the rising column of air which has blown the water and hail upward is dissipated in the upper altitudes of the thunder cell, the hail falls toward the ground and induces a downward draft of the local air. The falling column of air which moves with the hail is displaced horizontally from the rising vertical column. This displacement is in the direction of the movement of the entire thunder cell. Since the warm, moist air at ground level climbs slantwise through the base of the thunderstorm, the falling hail can drop into this rising column of warm, moist air and be carried aloft for another trip. The condensing moisture in this rising column of air which now carries hail can condense on the hail to add additional layers, and so the hailstone grows. This process of hailstone growth can be repeated as many as a dozen times to produce hailstones the size of golf balls, which eventually fall to the ground.

Clearly, the airplane should avoid the central part of the thunder cell which contains the high upward and downward winds laden with heavy rain and hail. Fortunately, airborne radar gets a very strong signal from rain drops and hail, so that these zones in the thunder cell are clearly visible to the pilot on his radar scope. Thus, an aircraft equipped with radar can fly through thunderstorms with reasonable security. An aircraft not equipped with radar can fly safely through storm areas if it is in radio communication with a ground radar station that can "see" the storm and guide the aircraft through it. An aircraft that is not equipped with radar and not in radio contact with a ground radar station depends on the pilot's judgment and what he can see of the structure of the thunderstorm. Therefore, without the aid of radar, an aircraft should not attempt to fly through thunderstorm areas at night, when the storm is not visible.

Tornadoes may form at the base of the thunder cloud, where some of the warm, moist air enters the cloud. Such a place is marked in figure 16-3. The tornado is visible as a

348

funnel shaped cloud attached to the cloud base and can, therefore, be avoided by the air-
craft during daylight. A tornado can also be detected by radar if the tornado contains de-
bris from the ground or if it contains precipitation.

An important, but less severe, zone of air currents within the thunder cell appears
at its trailing edge, where wind-borne, cool, dry air at high altitude enters the thunder
cloud and mixes with the cloud droplets. The droplets evaporate in this dry air. The
heat required for droplet evaporation is drawn from the air. This cooled air is now
more dense than the surrounding air of the cloud and sinks rapidly. This downward
stream of air can attain speeds which could upset the inexperienced pilot.

The zones on the ground, relative to the storm cloud, that are subject to precipitation
from the storm cloud are shown in figure 16-4. Information like this is useful to the air-
plane dispatcher, who can determine under what conditions he can dispatch an airplane
and the route it should take as it leaves the airport.
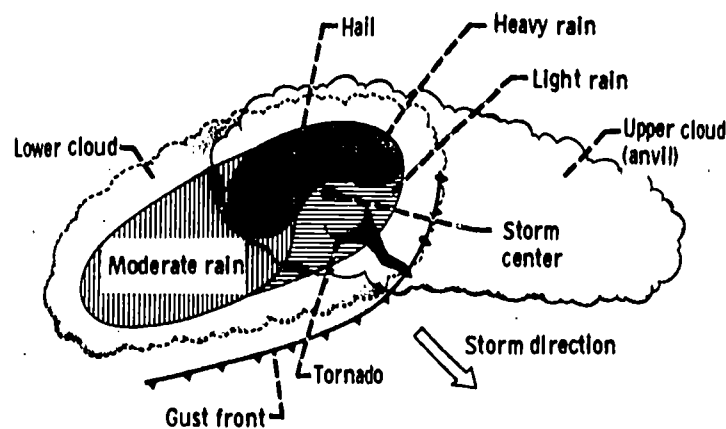
Figure 16-4. - Horizontal section through thunderstorm cell showing
areas of precipitation.

In addition to the vertically directed high winds mentioned previously, the thunder-
storm contains zones of highly turbulent air, which can buffet the airplane severely. Such
buffeting can cause failure of the main airplane structure and the loss of the airplane.
These turbulent zones, mapped in figure 16-5, lie adjacent to the strong vertical air cur-
rents.

The water droplets which make up many clouds, including those of the thunderstorm,
can exist at temperatures below the normal freezing point of water. The zones occupied
by these "supercooled" cloud droplets range from the freezing level, marked as 0° C in
figure 16-5, to altitudes where the temperature can drop to -20° C. In some rare in-
stances, water droplets are found in the cloud at -40° C.

As an aircraft flies through a cloud, the cloud droplets strike the leading surfaces.
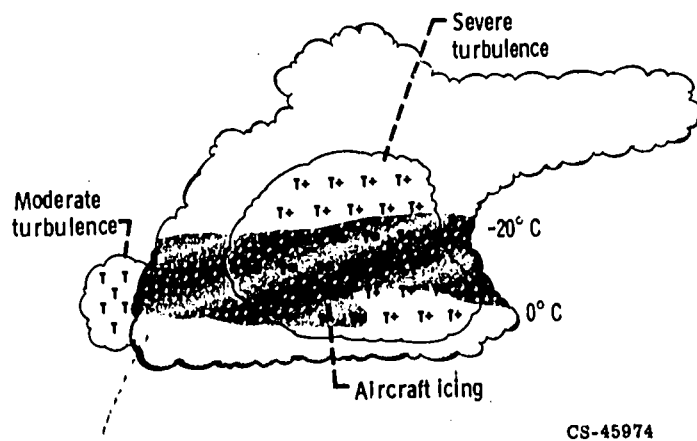
Figure 16-5. - Vertical section through thunderstorm cell showing areas of aircraft icing and turbulence.

When supercooled cloud droplets strike the airplane surface, they freeze. In a few minutes of flight, sizable ice accumulations may form on the aircraft. Such ice formation on the leading edges of wings and tail surfaces can so change the contour of these airplane members as to increase the airplane drag severely and reduce the effectiveness of wings and associated flight control surfaces. High drag slows the airplane and increases the fuel required to complete the flight. Deterioration of the aerodynamic quality of the wing and tail increases the pilot's problem of maintaining proper control. This decline in handling quality of the airplane becomes particularly important on landing, when the airplane moves slowly and is normally sluggish in its response to control movements. Ice accumulations on the aircraft increase the sluggishness to control and thereby increase the likelihood of a crash landing.

Ice is also collected on engine air intakes. The obstruction of the vital airflow to the engine is evident from the engine inlet icing shown in figure 16-6. Should chunks of such massive accumulations of ice break free and be ingested by the engine, the blading within the engine may be damaged.

Aircraft which are certified to fly through icing clouds are protected against ice accumulation by heating those surfaces on which water droplets of the cloud are likely to impinge. However, such icing protection is designed for moderate-to-severe icing conditions and may be inadequate for exceptionally severe icing. An understanding of the structure of the clouds that are most likely to produce severe icing allows the pilot to avoid icing conditions which are beyond the capability of the ice-prevention system of the aircraft. Many years of research flights through icing clouds and cloud-physics studies in NASA and other laboratories have given us a working understanding of this matter. Aircraft seldom get into difficulty now because of icing.

One remaining problem of the severe storm is the lightning hazard that accompanies

353
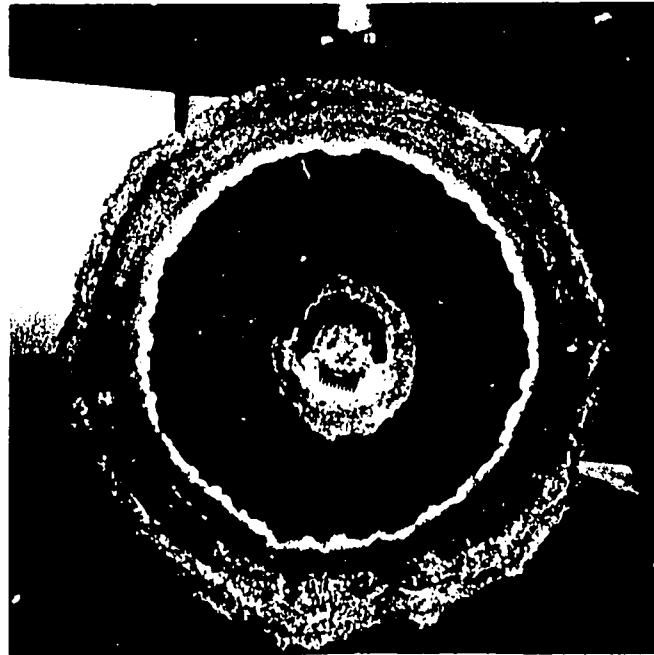
Figure 16-6. - Turbojet-engine inlet icing.

Negative **++++** Positive **++++** Ground
rain rain

CS-45975
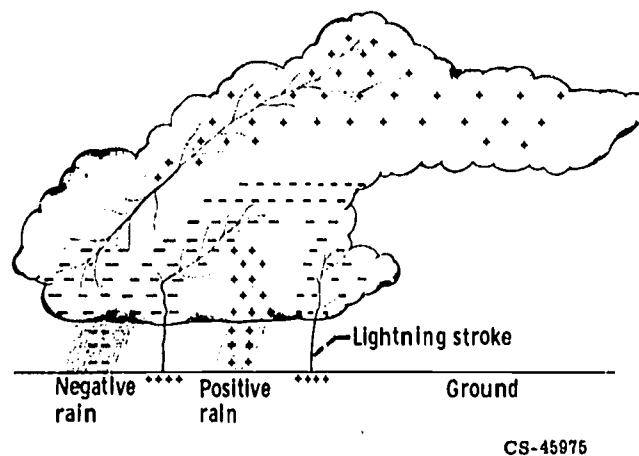
Figure 16-7. - Vertical section through thunderstorm cell
showing typical distribution of electrical charges.

it. Figure 16-7 shows a typical distribution of electrical charges within a thunder cell.
These charges reside on the rain drops, hail particles, and cloud droplets. In the cloud
illustrated in this figure, the positively charged droplets are mostly near the top of the
cloud and the negatively charged droplets are near the bottom. While this is generally
the case, the opposite often occurs. Lightning, which represents a discharge of elec-
tricity from the positive to the negative charges, occurs within the cloud as shown in the
figure. Also, the negative charges at the base of the cloud induce the Earth's surface im-
mediately below the cloud to acquire a positive charge. Lightning strikes between the
ground and the cloud occur when the potential difference is great enough to form a streak

of ionized air in the space between. The main lightning discharge follows this streak. Ionized air is a good conductor of electricity, whereas normal air is a poor conductor. Aircraft flying beneath the cloud may be struck by the lightning, but ordinarily the damage to the aircraft is modest. The all-metal construction of the aircraft makes it a good conductor of the electricity and it passes the lightning current harmlessly. At the points of the airplane where the strike enters and leaves, small pitting and local burning of the structure is often evident.

However, the lightning may strike the fuel system of the airplane at a location where a combustible atmosphere exists. The probability of ignition of the aircraft fuel is high enough to constitute real danger. Every effort is now being made to ensure that under no conditions will a lightning strike to the airplane ignite the aircraft's fuel, since such ignition is catastrophic.

NAVIGATION THROUGH STORM AREAS

In order to understand how a modern airplane navigates through an area of severe storms, it is useful to review one of the navigation systems most commonly used on commercial and military aircraft. This navigation system, called an omnidirectional radio range (omni), is based on a series of radio stations on the ground which represent the intersection of the airways flown by the aircraft. A flight plan between two airports can be designated by listing the radio stations over which the airplane will fly. Each radio station radiates a signal at a frequency which is distinct from all the others. The airplane tunes its receivers to this frequency. The receiver signal actuates a pointer on an instrument dial which shows the bearing of the radio station with respect to the aircraft. This situation is diagrammed in figure 16-8, which shows the ground-based radio station and five locations of the aircraft with respect to that radio station. The dial pointer in the figure, which corresponds to the dial on the instrument panel in the airplane, shows the compass bearing of the radio station relative to the location of the aircraft. It is obvious from the figure that if the aircraft passes directly over the omni station, the dial pointer reverses itself (i. e., rotates 180°). This reversal of the dial pointer provides the pilot with the exact fix of the aircraft with respect to the ground, because the exact location of the omni station is shown on his maps. When the aircraft is not directly above the omni station, the fix of the aircraft is determined from the bearing of the omni station in conjunction with data from distance-measuring equipment, or DME. (Omni navigation is discussed in more detail in chapter 15.)

A commercial pilot is required to fly along the airways for which he is cleared when he files his flight plan, prior to takeoff. Any deviation from this plan while he is enroute must be approved by the air-traffic controller who monitors his flight from the ground. Such request and approval is accomplished by radio communication.

355
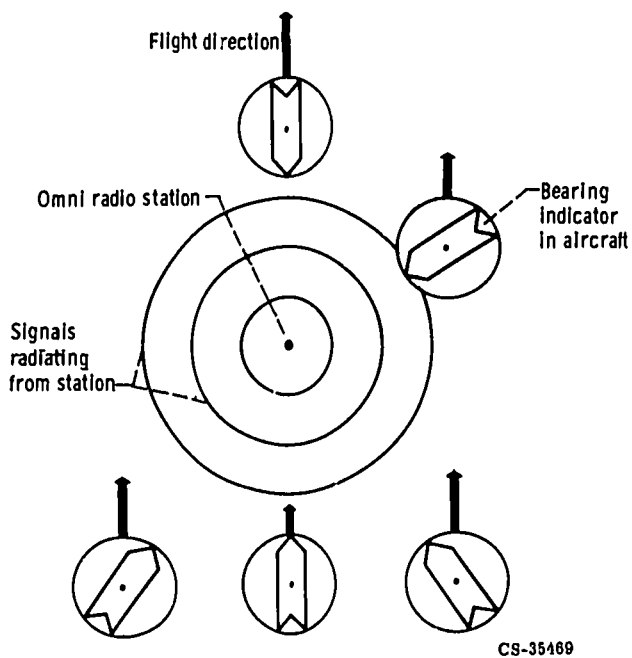
Figure 16-8. - Omnidirectional (omni) radio
navigation.
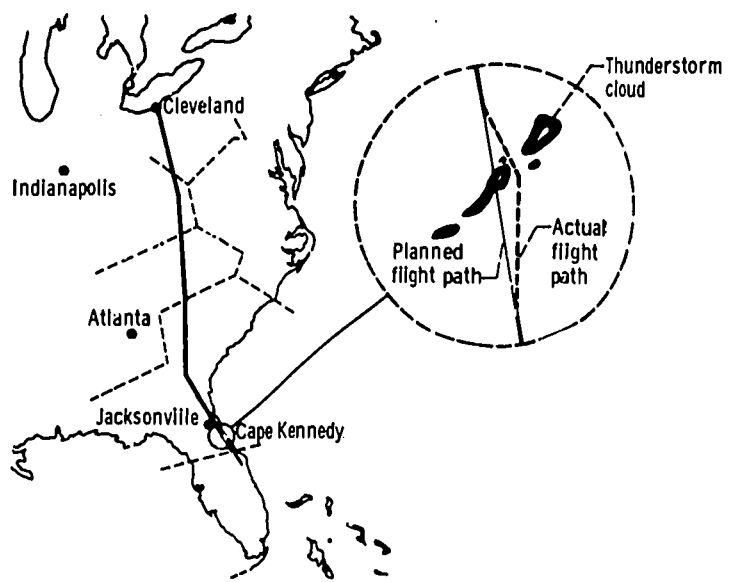
Figure 16-9. - Airway schematic with enroute storm.

Severe weather is one of the principal reasons for requesting deviation of the flight
from the prescribed plan. This situation is illustrated in figure 16-9, which shows a
typical flight route from Cleveland, Ohio, to Cape Kennedy, Florida. The diagram shows
that the aircraft encounters a thunderstorm in its path as it enters Florida. With the con-
sent of the Federal Aviation Administration controller, the aircraft is allowed to deviate
from its original plan, shown as a solid line in the figure, and to take the path shown by
the dashed line to avoid penetrating the thunderstorm cell in its path.

Most commercial airplanes are equipped with airborne radar systems which display
those portions of the clouds that contain rain, snow, or hail. The radar scope on the air-
plane shows the precipitation pattern within the clouds with respect to the direction of the
airplane flight path, as shown in figure 16-10(a), which is a photograph of such a radar
scope. The position of the airplane is indicated by the figure of the small airplane at the
center of the system of concentric circles marked on the screen. The concentric circles
represent fixed, known radial distances from the airplane. In a typical radar display,
the radial distance between circles is 10 miles. This radar presentation shows the pilot
how he can fly through the storm that lies in his path so as to avoid the precipitation
areas, which also mark the zones of high vertical winds and turbulence, as discussed
earlier. In the event that the thunderstorm appears as an unbroken line in his path, the
pilot can pick his way through the least hazardous portion of the storm by using a setting
on the radar which alters his radarscope presentation to show the zones of highest pre-
cipitation within the storm ahead. In the radarscope presentation shown in figure
16-10(b), the dark areas within the outlines of the zones of precipitation are the areas of
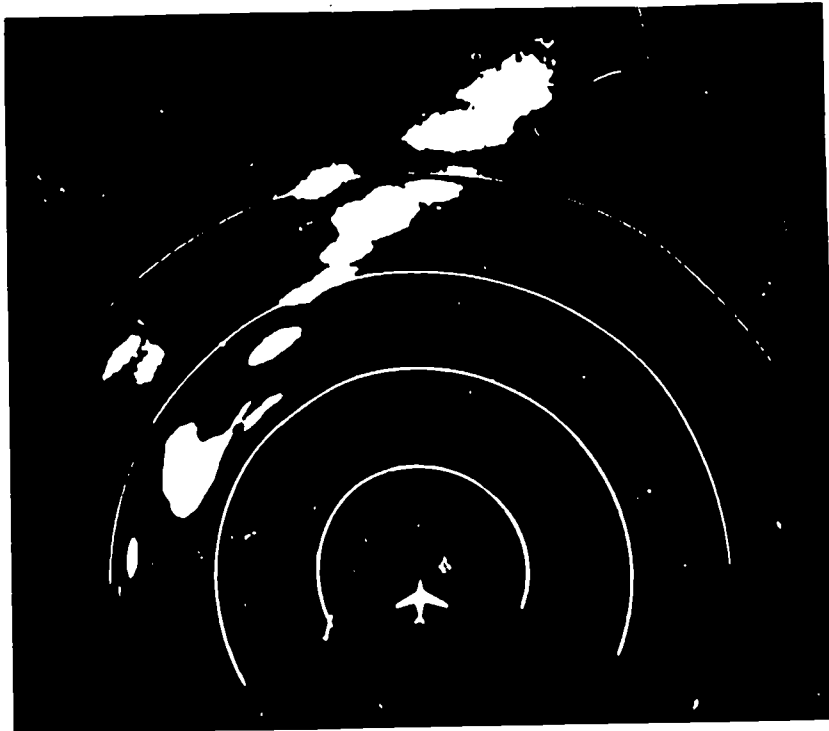
(a) Low-contrast image showing overall areas of precipitation.

CS-45197

(b) High-contrast image showing zones of most intense precipitation within overall areas of precipitation.

Figure 16-10. - Airborne radarscope presentations of precipitation pattern of storm.

most intense precipitation. The pilot picks his path to avoid these zones and accepts the buffeting he will receive by going through the milder portions of the storm.

CONCLUDING REMARKS

Our knowledge of the Earth's weather and how it influences aircraft flight is progressing rapidly. Instrumentation for navigation and control of aircraft is undergoing a major revolution at this time. Many of the limitations to aircraft flight imposed by the weather should be largely overcome in the next 10 years. After that time, aircraft will be instrumented for detecting turbulent air whether or not associated with storms. These aircraft will be equipped to fly through turbulent air smoothly and, in all probability, to land at airports under conditions of extremely poor to vanishing visibility. Those who have an interest in this subject should review its status periodically, because of the rapid changes which are in progress.

17. PROJECTS IN AERONAUTICS

James F. Connors*

Throughout the Lewis Explorer program in aeronautics, a concerted effort was made to generate a high level of interest and involvement among the participants. Whenever feasible, lectures were augmented by active demonstrations, visual aids, and supplementary films. On occasion, special tours to aeronautical points of interest were arranged. The participants became most directly involved in the program through research assignments, many of which were actual wind-tunnel experiments. The culmination of the program was a full-scale symposium on aeronautics - an excerise in communication - at which the young researchers reported the results of their projects.

DEMONSTRATIONS

The following is a sampling of demonstrations presented in conjunction with the various lectures. Most of these demonstrations can be easily duplicated or approximated by anyone interested in studying basic aerodynamic principles and flow phenomena.

Some demonstrations pertaining to the aerodynamics of an airfoil (chapter 4) are illustrated in figure 17-1. Basic aerodynamic phenomena were demonstrated by means of very simple equipment. For example, the Coanda effect was demonstrated by using a funnel to direct a stream of small, solid particles (shot) and a stream of fluid (water) against the side of a horizontally oriented cylinder (fig. 17-1(b)) and comparing the results. Also, the cylinder was rotated under the water stream to show increases and decreases in the Coanda effect.

For a demonstration of lift (fig. 17-1(c)), a vacuum sweeper was used to provide an airstream. Lift was produced by deflecting this airstream downward either through a bent cylindrical tube or by a curved vane. The lift was evidenced by an upward rotation of the supporting beam about its fulcrum. (Part of the equipment for this demonstration was assembled from a toy erector set.)

In another demonstration (fig. 17-1(d)), visual flow definition was achieved by suspending, or floating, lightweight particles (sawdust) on the surface of water and then

---

*Director of Technical Services.

moving a flat paddle through the water to show the turbulent wake pattern behind the paddle.

To demonstrate the vortex produced by a wing tip, a simulated wing (a flat board) was mounted on the side of an automobile (fig. 17-1(e)). When the auto was put into motion, the vortex from the simulated wing tip caused a rotation of a spinner that was mounted downstream of the tip.

In conjunction with the discussion of fluid flow through nozzles (chapter 11), a relatively simple water table (fig. 17-2) was used for flow visualization. The water table, based on the physical analogy between water flow and airflow, was used to study streamline patterns for convergent-divergent nozzle geometries under various operating modes. Streamlines can be made visible by placing dye crystals at regular intervals across the upstream end of the water table. Actual pressure distributions along a surface can be derived either from the variation in the distance between streamlines or from the variation in water height along the surface. Water-table studies are much like observing the flow patterns of the vortex that is set up when a bathtub is being drained or of the waves created when a rock is dropped into a calm pond.

EXPERIMENTS

Some basic aerodynamic principles were applied in simple, practical experiments that can be carried out by anyone studying aerodynamics. Many of these experiments were conducted in a moderately small, but fairly sophisticated, low-speed wind tunnel. Details of this particular tunnel, as well as plans and suggestions for constructing a simpler one, are presented in appendix A.

Aerodynamic drag values were obtained in the wind tunnel for a family of cylinders of varying size (1, 3, and 5 in. diam). Each cylinder spanned the tunnel test section. Results are shown in figures 17-3(a), (b), and (c). Flat-plate friction drag (fig. 17-3(d)) was determined as a function of Reynolds number (see definitions in chapter 2). Both laminar and turbulent boundary-layer profiles were obtained. Roughness (or grit) was added to the plate leading edge to ensure early transition to a turbulent layer. Small models of automobiles were used to determine the effect of styling, or configuration, on aerodynamic drag performance (figs. 17-3(e) and (f)). The advantages of streamlined automobile bodies were clearly demonstrated.

Aerodynamic lift was also studied in the wind tunnel for a wide range of airfoil shapes. Both infinite and finite wings were used. Infinite airfoils were those that completely spanned the tunnel and thus had no loss in lift at the ends. For each geometry, the variation in lift coefficient with angle of attack (fig. 17-4(a)) was determined beyond the maximum lift, or stall, point. Smoke (fig. 17-4(b)) and tufts (fig. 17-4(c)) were used

to illustrate the lifting- and stalled-wing conditions. Flaps were added to show that lift could be increased by increasing flap angle (fig. 17-4(d)). Decreasing the wing aspect ratio by shortening the span (fig. 17-4(e)) decreased the slope of the lift-versus-angle-of-attack curve (fig. 17-4(f)) and decreased the maximum attainable lift coefficient. The reason for this effect of the aspect ratio on the lift is that as the aspect ratio decreases, the local loss in lift at the ends becomes a progressively larger percentage of the total wing lift. The end lift loss, or tip effect, was demonstrated by visualization of the vortexes through the use of the tuft grid (fig. 17-4(g)). In effect, the high-pressure air under the wing leaks around to the low-pressure region on top of the wing. At the landing condition, where a specified lift coefficient is required (fig. 17-4(h)), the landing attitude of the aircraft (angle of attack) can be minimized by increasing wing aspect ratio and/or adding a flap.

In wind-tunnel experiments with an aircraft model having variable-sweep wings, the tip vortexes are very graphically illustrated by the tuft patterns at the rear of the test section. Figure 17-5 shows selected frames from a motion picture taken as the model angle of attack and the wing angle of sweep were systematically varied. The aforementioned leakage of air from the bottom to the top of the wing at angle of attack creates a trailing vortical flow behind the tip. It is an important aerodynamic effect in estimating aircraft performance.

An interesting project was called GARAGE, an acronym for Gravity Accelerated Rotational Aerodynamic Gaging Equipment. The project objective was to devise a simple, unique apparatus for effectively measuring lift of various airfoil models, without the obvious complexity and expense of using a wind tunnel.

The apparatus evolved from a rather complicated preliminary design (fig. 17-6(a)) to a relatively simple operational model (fig. 17-6(b)). An airfoil was attached to the extremity of a light, cantilever arm. This arm was connected to a vertical, freely-rotating shaft. A weight was suspended from a fishline that was run through a low-friction pulley and was carefully wound around the vertical shaft. When the weight was allowed to drop, its pull caused the fishline to unwind from the shaft, thereby causing the shaft, with the attached cantilever arm and airfoil, to rotate. The time required for the weight to drop through a measured distance was accurately recorded.

Attached to the outer end of the airfoil was a "whisker." Each time the airfoil made one revolution, the whisker struck a chalked piece of carbon paper mounted on a vertical meter stick. The vertical distance, of lift, of the airfoil was accurately measured at the completion of each run. This vertical rise of the airfoil could be statically calibrated to determine the corresponding lifting forces. The speed of the airfoil is directly proportional to the speed of the falling weight. The speed of the falling weight is a measure of the drag on the airfoil. A stroboscopic (or strobe) light could be used to stop motion and thereby obtain the frequency of rotation and a direct indication of the vertical displace-

ment of the airfoil at that rotational speed. The linear speed of the airfoil could be calculated from the frequency of rotation and the measured length of the cantilever arm supporting the airfoil (i.e., the radius of the circular path of the airfoil). Since drag varies (exponentially) with the square of the velocity, incremental differences in drag could thus be determined for the various airfoil shapes. Some experimentally obtained values of lift and drag with angle of attack are shown in figures 17-6(c) and (d).

Another research project was the design of a model airplane for maximum endurance. The specifications adopted for the project were based on the rules for an actual, worldwide, competitive endurance event, with a significant monetary prize. The specifications called for a wing area of 1800 square inches, a stabilizer area of 450 square inches, and a gross weight of 11 pounds. The initial concentration of effort was on the powerplant. To this end, a good-quality, 2-cycle, model-aircraft engine was selected. For this engine, a fuel system (fig. 17-7(a)) was designed, fabricated, and assembled for experimental evaluations and modifications. Objectives, of course, were to maximize the amount of fuel and engine performance and, at the same time, to minimize system weight. Engine performance (fig. 17-7(b)) was determined statically and then projected to estimate the performance at a flight speed of 30 feet per second. A 12-inch propeller was used to absorb the load and simulate installation performance. Aerodynamics were investigated to obtain a wing with a high lift-to-drag ratio (L/D). Techniques of lightweight construction were also investigated, and a wing section was fabricated. The resultant aircraft configuration after appropriate weight balancing is shown in figure 17-7(c). The analysis of the overall structure gave the weight distribution shown in table 17-I.

TABLE 17-I. - ESTIMATED
WEIGHT BREAKDOWN OF
MODEL AIRPLANE DE-
SIGNED FOR WORLD EN-
DURANCE FLIGHT RECORD

Component	Weight, lb
Wing structure	1.5
Fuselage structure	1.0
Tail structure	.3
Propulsion system	1.2
Control system	1.0
Fuel	6.0
Total aircraft	11.0

To study the aerodynamics of flight, experiments were conducted with small, hand-launched, indoor gliders. Construction details for the glider used and adjustments required for long-duration flight are discussed in appendix B. Two of the most important adjustments for stable flight are the correct location of the center of gravity and the proper "angular difference" between the wing and the horizontal tail. A detailed discussion of these parameters for a hand-launched glider is given in appendix C. (These are also discussed in detail in chapter 9, which deals with aircraft stability and control.)

The gliders were flown (fig. 17-8) to study stability and to determine lift-to-drag ratios and sink rates. The lift-to-drag ratio of an aircraft in steady, gliding flight was shown to be equal to the distance traveled horizontally divided by the attendant decrease in altitude, or, in other words, the glide ratio. This is an aerodynamic phenomenon unrelated to weight. To illustrate this, the weight of the glider was increased by adding clay at the center of gravity, and the experiment was repeated. Although the glide ratio did not change, the gliding speed and its vertical component, the sink rate, were noticeably increased. Also shown was the equality between the power required for level flight and the rate of change of potential energy noted during gliding flight.

TOURS

Tours of places of aeronautical interest constituted an important part of the Lewis Explorer program. The purpose of these tours was to relate the aeronautical studies to the real world of aviation.

During a tour of the hangar of the Lewis Research Center (fig. 17-9), aircraft and their components were described in detail to the group. Aircraft available for inspection were a Convair F-106, a Douglas C-47, a Convair T-29, and an Aerocommander.

A comprehensive tour of various aircraft was accomplished on a visit to the Air Force Museum in Dayton, Ohio. This museum has the world's largest military aeronautical exhibit. It contains over 100 aircraft and missiles, with numerous informative displays of hardware, documents, photographs, and personal memorabilia.

A tour was made of the Air Traffic Control Center at Oberlin, Ohio. This facility is under the jurisdiction of the Federal Aviation Agency (FAA), which, in turn, is under the Department of Transportation. The FAA is responsible for ensuring a safe and orderly flow of civil and military air traffic throughout the nation's airways. The heart of the operation of an Air Traffic Control Center is the radar room (fig. 17-10(a)), where the controller follows the flight of aircraft through his area and is in direct radio contact with the pilots. The controller assigns specific altitudes and clearances to the pilots and provides them with various weather advisories and flight directions. A computer room

(fig. 17-10(b)) provides the latest weather data and airline schedular data for the entire country.

Depending on weather conditions, all aircraft fly by one of two sets of FAA rules - either instrument flight rules (IFR), or visual flight rules (VFR). When the weather is clear, most pilots fly VFR; in bad weather, flights normally are conducted under IFR procedures.

Under VFR, the pilot flies by visual reference to the ground, and he is solely responsible for avoiding other aircraft. His obligation is more than "see and be seen" - it is to "see and avoid." But, when weather and visibility are poor and IFR weather conditions prevail, the responsibility for keeping aircraft separated rests with the air traffic controller. Even in good weather, many pilots, especially those flying high-speed aircraft, elect to fly under IFR in order to take advantage of the separation and the greater protection afforded by FAA's air traffic specialists. All major scheduled airline flights follow this procedure. To guard against possible conflicts in flight paths, all pilots flying under IFR must file flight plans with the FAA.

SYMPOSIUM ON AERONAUTICS

Any program should have a focal point toward which the overall effort is directed. For the Lewis Aerospace Explorer program, the focal point was a full-scale symposium on aeronautics (fig. 17-11). This was, of course, a valuable exercise in communication. Furthermore, it placed schedular deadlines on the various research projects and experiments undertaken by the youths and created a realistic sense of pressure to plan and conduct the experiments efficiently, to complete the projects on schedule, to analyze the results carefully, and to present the results in a professional manner. Except for brief welcoming statements by the Director of the Lewis Research Center and by the Post Adviser, the entire symposium was conducted by the Explorers and was highly successful.

APPENDIX A

WIND TUNNELS

The principal tool for any study of aerodynamics is a wind tunnel. The tunnel used in this Explorer program (fig. 17-12) was constructed by Lewis Technical Services personnel from a 19-horsepower motor, an axial-flow fan, wood, Lucite, and sheet-metal. The test section was 20 inches wide and 30 inches long. Windows were provided on both sides of the test section for viewing the models, and a 10-inch-diameter port was built into the top of the test section for lighting purposes.

Other details of the tunnel and its measuring capabilities are illustrated in figure 17-13. The tunnel flow calibration (fig. 17-13(a)) showed a flat, uniform profile at full power. Top speed was approximately 52 miles per hour. This flow survey was taken along the vertical centerline. Along the walls, the boundary-layer height appeared to be less than 1 inch. By decreasing fan speed and increasing the size of a bypass opening ahead of the motor, the tunnel flow velocity could be varied down to about 18 miles per hour. To ensure minimum disturbance from the fan, a 2-inch-thick honeycomb section was added downstream of the tunnel diffuser and just upstream of the fan.

For flow visualization, smoke was injected so as to follow streamlines in a filamentary fashion through the test section. The smoke generator (fig. 17-13(b)) consisted of a small, electrical strip heater, located within an inclined tube, upon which a light oil was allowed to drip. A small fan blew air across the heater inside the tube to carry the smoke upward through a coiled condenser section into a manifold from which it was injected into the tunnel inlet through a number of orifices. Several layers of fine-mesh screening and a high-contraction-ratio nozzle were used to ensure a low-turbulence inlet flow. Representative smoke pictures are shown in figure 17-13(c).

At the rear of the test section, a grid of nylon tufts (fig. 17-13(d)) was installed as an additional means of flow visualization. As indicated in the representative photos (fig. 17-13(e)), tufts, in this case attached directly to the test model, are light enough to lie back in the direction of the local streamline. Flow separation is evidenced by an obvious randomness in the observed direction of the tufts.

A simplified force-balance system (figs. 17-13(d) and (f)) was used to measure aerodynamic lifts and drags. First, without airflow in the tunnel, the system was balanced (by means of weights in the pans) so that the supporting shaft of the test model was centered in the hole in the test-section window. Then, with airflow in the tunnel, the system was rebalanced by means of additional weights. Since one end of the supporting shaft was held in a ball socket, the values of lift and drag were equivalent to double the weights that were added to rebalance the system.

A person, or group, studying aerodynamics may not have the ability or the means to

construct a sophisticated wind tunnel. However, a simple wind tunnel, powered by an ordinary electric fan, and suitable for elementary investigations and demonstrations of common aerodynamic problems and phenomena, can be constructed by almost anyone from readily available materials.

A typical tunnel of this type (fig. 17-14) consists of a Plexiglas enclosed test chamber of constant cross-sectional area, through which the air stream is drawn by a large, nonoscillating, electric fan. In the inlet of the test chamber, a simple flow straightener, similar in arrangement to the dividing partitions of an egg crate and constructed of heavy bond paper, provides a relatively constant flow distribution across the test section. A simple transition cone between the test section and the fan guard, made of either cloth or cardboard, serves as the diffuser section.

A tunnel with a test chamber 7 inches high and 10 inches wide, a size easily transportable, is capable of handling wing sections or complete models of 7 or 8 inches maximum span.

The tunnel frame should be constructed of an easily worked wood, with the floor and one side made of 1/4-inch-thick plywood. The inlet and outlet sections are of 3/4-inch-thick wood. All mating wood surfaces should be square and smooth to ensure rigidity and an airtight fit. Assembly is made with a waterproof wood glue and small brads and should generally follow the methods presented in figure 17-14.

The top and one side of the test chamber are of a transparent material, preferably Plexiglas, fitted into grooves in the plywood bottom and side panels. Rubber gaskets in the grooves, or small wood battens tacked along the edges of the Plexiglas panels, guard against air leaks.

Heavy bond paper should be used for construction of the flow straightener. Thirteen 1-inch strips, 10 inches long, and nineteen 1-inch strips, 7 inches long, are cut from the paper and are marked off lengthwise at 1/2-inch intervals. The paper strips are then slotted to the center line at 1/2-inch intervals. The 7-inch strips are then assembled on the 10-inch strips, slot into slot, in a manner similar to that used in constructing egg-crate partitions. Glue should be applied at each joint, and extreme care should be exercised to ensure good alinement. When the glue is dry, the structure should be sprayed or painted with thinned shellac or acetone dope for protection against curling of the paper sections. When the flow straightener is being glued into the tunnel inlet, extreme care should be taken to ensure that the eggcrate structure is perpendicular to the floor of the tunnel.

The transition cone, or diffuser, is made of either closely woven, medium-weight fabric or thin cardboard. The pattern to which the material is to be cut is shown in figure 17-14. In cutting the material, allowances should be made for the seam and, in the case of fabric, for a hem around the downstream end of the cone. The seam must be made tight. The upstream end of the cone is glued and tacked tightly around the outlet of

the test chamber. The downstream end of the cone is fastened securely to the fan guard. If the cone is made of fabric, the downstream end can be hemmed and can be secured by drawing it tightly over the fan guard by means of a drawstring in the hem.

Since an extension of the test chamber center line should correspond to the center line of the electric fan, a rigid base should be built up to support the tunnel. No exact dimensions can be given for the height of this base, as dimensions of the fan to be used may vary.

No attempt has been made to specify the methods of mounting models, as the tunnel itself is simple and straightforward and lends itself to a wide latitude of model-mounting systems, either of the rigid or of the "floating" type. A force-balance system, such as the one described earlier, may be used in this tunnel to measure aerodynamic forces on a model.

APPENDIX B

HAND-LAUNCHED, INDOOR GLIDER

Robert G. Spaulding[*]

The lectures, demonstrations, and experiments in aerodynamics were supplemented with a simple, yet challenging, glider building and flying project. Full-size plans for the small, hand-launched, indoor glider used in this activity are shown in figure 17-15. Details of con truction and adjustments are discussed herein.

Although several adjustments are particular to this model, generally speaking, the aerodynamic principles apply to all indoor gliders built for endurance flying. The term "launch phase" refers to the high-speed portion of flight, when the model is thrown vertically to its maximum altitude. "Glide phase" refers to the remainder of the flight. The goal is to make adjustments particular to each phase, thus producing the longest flight time.

This is a basic learning model. From here, follow-on projects employing sweptback or higher-aspect-ratio wings, longer tail moment arms, etc., can be developed, leading to original designs incorporating the best aerodynamic features.

Adjustments

Center of gravity. - The center of gravity (c.g.) is the balance point of the glider. It may be thought of as that point through which all the weight of the glider is acting. The location of the c.g. can be changed by adding or removing weight (clay) at the nose of the model (fig. 17-16). The farther back the c.g. is located, the tighter the circle of flight must be to keep the model from stalling. Therefore, if flying is to be done in a small room, the c.g. must be located relatively far back. For our glider, the c.g. should be located behind the leading edge of the wing by a distance equivalent to 70 to 80 percent of the wing chord.

Stabilizer tilt. - This adjustment (fig. 17-17) affects the diameter and direction of the turning circle during the gliding phase of the flight. Adjustment is made by twisting the tail boom.

A full-scale aircraft normally has its center of gravity located aft of the wing leading edge by a distance of 25 to 30 percent of the wing chord. To turn the aircraft in flight, one or more control surfaces must be deflected into the airstream. This method of turning the aircraft produces high drag.

---

[*]Experimental Wood Modelmaker.

For a hand-launched, indoor, endurance glider, the drag must be kept to a minimum. Therefore, the method used to turn a full-size aircraft should not be used to turn the glider. Instead, the glider can be caused to turn by tilting the stabilizer-and-fin assembly. Stabilizer tilt misalines the lift vectors on the wing and stabilizer and gives the glider a natural turn tendency. This is an aerodynamic function and results in a low drag factor. The effectiveness of stabilizer tilt can be increased by moving the center of gravity farther back to increase the load on the stabilizer. Moving the center of gravity rearward necessitates increasing the size of the stabilizer to keep the load factor of the stabilizer the same as that of the wing.

The stabilizer tilt shown in figure 17-17 will place the glider into a leftward gliding circle after a right-handed launch. For a left-handed launch and a rightward gliding circle, the stabilizer must be tilted in the opposite direction.

Angular difference. - Angular difference concerns the angular relation of the wing and the horizontal stabilizer (fig. 17-18). All aircraft must have an angular difference in order to maintain altitude. The amount required for our glider is so small that it should be built without any. Then, the necessary angular difference can be obtained by bending the tail boom.

Wing-tip weight. - Wing-tip weight is used to cause the glider to roll out of the launch phase and into the glide phase in a smooth, efficient manner. Adjustment is made (fig. 17-19) by adding weight (clay), as needed, to the under portion of the appropriate wing tip to cause the glider to roll to the right or left.

Weight on the left wing tip, as shown in figure 17-19, will cause the glider to roll out of the right-banked attitude of a right-handed launch and into a leftward gliding circle. For a left-handed launch and a rightward gliding circle, the weight must be placed on the right wing tip.

Rudder offset. - Rudder offset can be used to compensate for structural misalinement. Adjustment is accomplished by warping the trailing edge of the rudder (fig. 17-20).

Concluding Remarks

This small glider, if carefully constructed and properly adjusted, flies beautifully in small areas. It is hand launched, nearly vertically, in a steep, right bank. The launch adjustments assure proper and efficient flight during the high-speed launch phase. At the top of the climb, if adjustments are proper, the model will roll to the left, flatten out, and glide in tight, left circles. (As mentioned previously, for a left-handed launch and a rightward gliding circle, both the stabilizer-tilt and the wing-tip-weight adjustments must be reversed. That is, the stabilizer must be tilted to the left, and the weight must be placed on the right wing tip.)

Adjustments affect each other. After one adjustment has been successfully completed, other adjustments and readjustments will be necessary. Therefore, all adjustments must be integrated to bring out the best flying characteristics of the glider. Since adjustments create drag, they should be kept to a minimum.

APPENDIX C

EFFECTS OF CENTER-OF-GRAVITY LOCATION AND ANGULAR DIFFERENCE
ON FLIGHT CHARACTERISTICS OF HAND-LAUNCHED GLIDER

Fred W. Steffen[*]

Herein we will explain <u>why</u> the location of the center of gravity (c.g.) and the angular difference between the wing and the tail surfaces affects the flight characteristics of a hand-launched, endurance glider.

The following symbols are used in the discussion and the equations:

A.R.	aspect ratio, b^2/S
b	span
$\bar{c}$	mean chord, S/b
c.g.	center of gravity
d_t	moment arm of tail (measured from c.g. to point 1/4 of $\bar{c}$ aft of leading edge of tail surface)
d_w	moment arm of wing (measured from c.g. to point 1/4 of $\bar{c}$ aft of leading edge of wing)
d_1, d_2	lever arms of weights W_1 and W_2
L	lift force
S	surface area
S_t	tail surface area
S_w	wing surface area
V	velocity of glider relative to air
W_1, W_2	weights on opposite ends of balance beam
α	angle of attack (i.e., angle between surface and air-velocity direction)
α_t	tail angle of attack
α_w	wing angle of attack
$\Delta(\ )$	small increment in $(\ )$

---

[*]Aerospace Engineer, Propulsion Aerodynamics Branch.

369

The lift forces of the wing L_w and horizontal tail L_t acting through moment arms d_w and d_t about the center of gravity (fig. 17-21) create pitching moments (nose up or nose down). If the sum of the pitching moments about the center of gravity is zero, the glider is trimmed, and $L_w d_w = L_t d_t$. This condition is analogous to that of the balanced beam shown in figure 17-22(a), where $W_1 d_1 = W_2 d_2$. However, a trimmed glider may or may not be stable. A glider is statically stable if restoring pitching moments are created when the glider is rotated in the pitch plane. For example, the balanced beam (fig. 17-22(a)) is trimmed but not stable, because no restoring moments are created if the beam is tilted. In other words, if the beam is tilted, the moment $W_1 d_1$ is still equal to $W_2 d_2$. To make the beam stable, springs may be inserted under each end, as shown in figure 17-22(b). Then, as the beam is tilted, the springs create restoring moments, which tend to restore the beam to its original position.

Figure 17-23 shows a glider with a large amount of clay ballast in the nose, so that the center of gravity is ahead of the wing lift force. For the moment about the center of gravity to be zero, the force from the horizontal tail must be downward (i. e., the tail angle of attack α_t must be negative).

Endurance gliders, however, are usually trimmed with the center of gravity aft of the wing lift force, as shown in figure 17-24. This is done for two reasons: first, the weight of the required clay ballast is reduced, and a reduction in weight causes a reduction in sinking speed; second, both the wing and the tail contribute to the total lift force. Thus, a total lift force equal to the weight can be achieved at a lower gliding velocity V, which, in turn, results in a lower sinking speed. As before, for the glider to be in trim, $L_w d_w$ must be equal to $L_t d_t$ (i. e., the resultant pitching moment must be zero).

For any given location of the center of gravity, the glider can be trimmed at only one wing angle of attack $\alpha_{w,1}$ and one tail angle of attack $\alpha_{t,1}$. Individual adjustments in the wing and tail angles of attack are made by changing the angles of incidence of these surfaces. If the location of the center of gravity is such that the trim angle of incidence of the wing is greater than that of the tail (positive angular difference), the glider is statically stable in the pitch plane. This means that if the glider is pitched upward or downward from its trim attitude (i.e., if the angles of attack of the wing and tail are increased or decreased by some angle $\Delta\alpha$), restoring moments are developed which tend to return the glider to the trim attitude.

To simplify the explanation of how these restoring moments are developed, let us assume that the angles of attack of the wing and tail are equal to their angles of incidence. The lift force from a surface such as a wing or a horizontal tail is directly proportional to its angle of attack. The lift forces per unit area, L/S, for the wing and tail of a glider with positive angular difference are plotted against angle of attack α in figure 17-25(a). Since the angles of attack of the wing and tail are assumed to be equal to their angles of incidence, the trim angle of attack of the wing $\alpha_{w,1}$ is greater than that of the tail $\alpha_{t,1}$. (Although it is not essential to this discussion, the slopes of the two curves are shown to

370

be different. The slope of each curve is directly proportional to the aspect ratio of the surface. The aspect ratio A.R. is the square of the span b^2 divided by the surface area S. Since the wing usually has a greater aspect ratio than the tail, the curve for the wing has a greater slope than the curve for the tail.) Now if the trim angles of attack of the wing and tail, $\alpha_{w,1}$ and $\alpha_{t,1}$, are increased by $\Delta\alpha$ to $\alpha_{w,2}$ and $\alpha_{t,2}$, the lift per unit area of the tail $(L/S)_t$ is increased by a greater percentage than the lift per unit area of the wing $(L/S)_w$. In the example shown in figure 17-25(a), the tail force per unit area increases 100 percent, while the wing lift force increases by only 50 percent. This excess tail lift causes a nose-down moment which tends to restore the wing and tail angles of attack to their initial values. The glider, therefore, has static stability in pitch.

As the center of gravity is moved farther aft, a center-of-gravity location is reached, where, to achieve zero resultant pitching moment about the center of gravity, the angle of incidence of the tail must be equal to the angle of incidence of the wing (zero angular difference). This position of the center of gravity yields neutral static longitudinal stability and is called the neutral point. This situation is illustrated in figure 17-25(b), which again shows plots of the lift force per unit area L/S as a function of angle of attack α for the wing and tail surfaces. However, here the trim angle of attack of the wing $\alpha_{w,1}$ is equal to that of the tail $\alpha_{t,1}$. Therefore, increasing these angles of attack to $\alpha_{w,2}$ and $\alpha_{t,2}$ by some angle $\Delta\alpha$ produces the same percentage of change in the lift per unit area of the wing $(L/S)_w$ as in that of the tail $(L/S)_t$. Therefore, the resultant moment about the center of gravity remains zero regardless of the angle of attack, and no restoring moments are created. When a glider trimmed in this manner is flown, it often enters an accelerated dive (appears to "run downhill") and crash. For this reason, initial flights should be made with the center of gravity a comfortable distance ahead of the neutral point and with positive angular difference between the wing and the tail.

The location of the neutral point is also modified by the fact that the horizontal tail operates in the downwash of the wing. In other words, the wing acts as a flow straightener for the horizontal tail, so that when the glider is rotated from position 1 to position 2, the $\Delta\alpha_t$ is less than $\Delta\alpha_w$. Although this difference is small for model gliders, it does have the effect of moving the neutral point to a more forward position.

The neutral point for a hand-launched glider can be roughly calculated as follows. First, the percentages of increase in lift per unit area L/S with angle of attack α for both wing and tail are set equal (this is the situation with zero angular difference). In equation form, this can be written as

$$\frac{\Delta\left(\frac{L}{S}\right)_w}{\left(\frac{L}{S}\right)_{w,1}} = \frac{\Delta\left(\frac{L}{S}\right)_t}{\left(\frac{L}{S}\right)_{t,1}}$$

or

$$\frac{\left[\dfrac{\Delta\left(\dfrac{L}{S}\right)}{\Delta\alpha}\right]_w \Delta\alpha_w}{\left(\dfrac{L}{S}\right)_{w,1}} = \frac{\left[\dfrac{\Delta\left(\dfrac{L}{S}\right)}{\Delta\alpha}\right]_t \Delta\alpha_t}{\left(\dfrac{L}{S}\right)_{t,1}}$$

Since the wing and tail are both rigidly attached to the fuselage (and if downwash effects are disregarded),

$$\Delta\alpha_w = \Delta\alpha_t$$

Then,

$$\frac{\left(\dfrac{L}{S}\right)_{w,1}}{\left(\dfrac{L}{S}\right)_{t,1}} = \frac{\left[\dfrac{\Delta\left(\dfrac{L}{S}\right)}{\Delta\alpha}\right]_w}{\left[\dfrac{\Delta\left(\dfrac{L}{S}\right)}{\Delta\alpha}\right]_t}$$

For the resultant moment about the center of gravity to be zero,

$$\left(\frac{L}{S}\right)_{w,1} S_w d_w = \left(\frac{L}{S}\right)_{t,1} S_t d_t$$

Then

$$\frac{d_t}{d_w} = \frac{\left(\dfrac{L}{S}\right)_{w,1}}{\left(\dfrac{L}{S}\right)_{t,1}} \frac{S_w}{S_t} = \frac{\left[\dfrac{\Delta\left(\dfrac{L}{S}\right)}{\Delta\alpha}\right]_w S_w}{\left[\dfrac{\Delta\left(\dfrac{L}{S}\right)}{\Delta\alpha}\right]_t S_t}$$

Now

$$d_{total} = d_w + d_t$$

Therefore

$$d_t = \frac{d_{total}}{1 + \dfrac{d_w}{d_t}} = \frac{d_{total}}{1 + \dfrac{\left[\dfrac{\Delta\left(\dfrac{L}{S}\right)}{\Delta\alpha}\right]_t S_t}{\left[\dfrac{\Delta\left(\dfrac{L}{S}\right)}{\Delta\alpha}\right]_w S_w}}$$

If the aspect ratio of the wing is approximately equal to the aspect ratio of the tail, then

$$\left[\frac{\Delta\left(\dfrac{L}{S}\right)}{\Delta\alpha}\right]_w \approx \left[\frac{\Delta\left(\dfrac{L}{S}\right)}{\Delta\alpha}\right]_t$$

and

$$d_t \approx \frac{d_{total}}{1 + \dfrac{S_t}{S_w}}$$

(a) Meeting overview.

(b) Comparison of fluid flow and particle flow over a curved surface.

(c) Lift results from the bending of airflow either by passage through a bent tube or by deflection across an inclined surface.

(d) Fluid flow separates and produces a turbulent wake behind a moving blunt-based body.

(e) Tip of a finite airfoil produces vortex flow.

Figure 17-1. - Aerodynamics demonstrations.

375/375
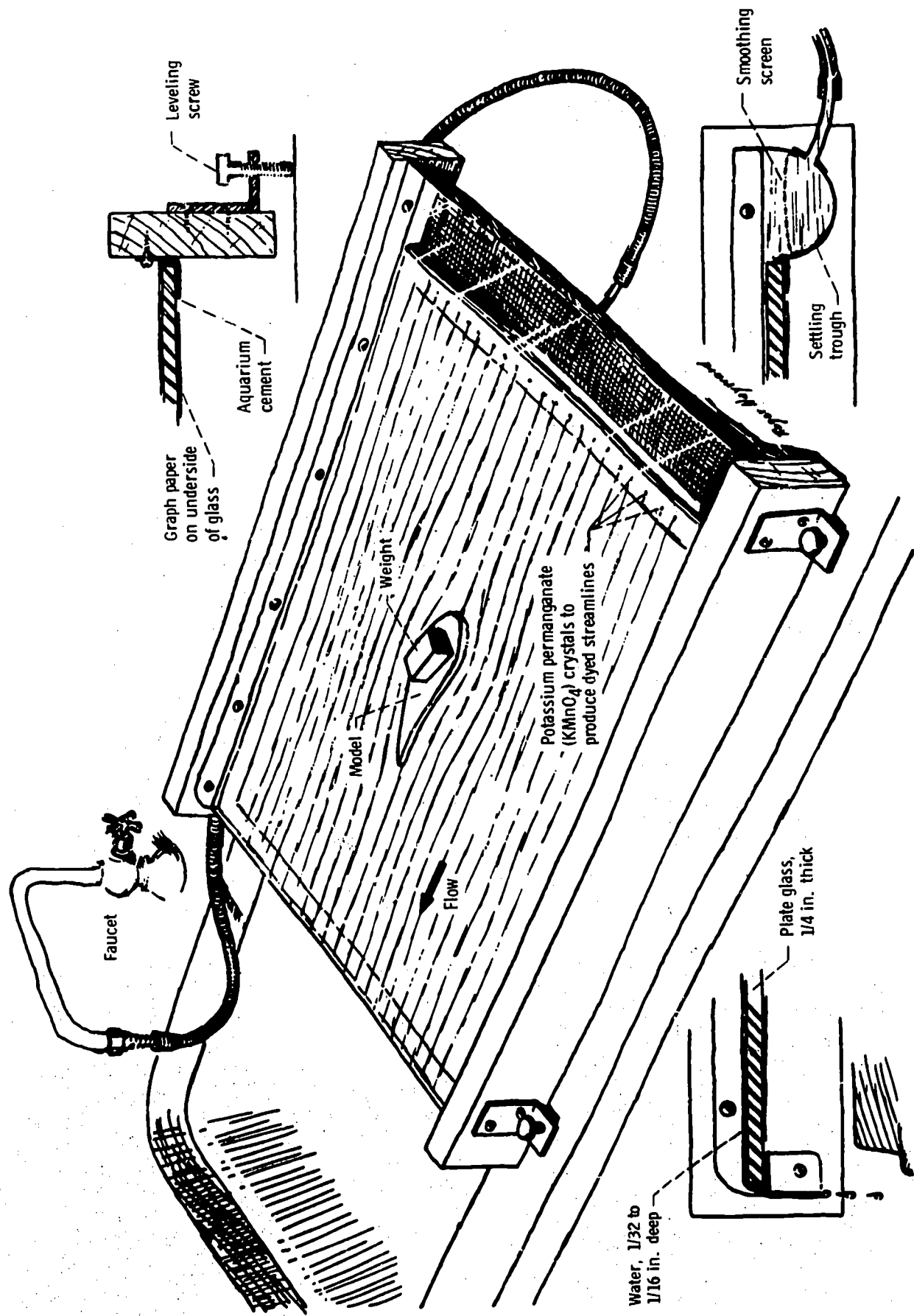
Figure 17-2. – Simple design for a water table.   (Courtesy of Scientific American.)

Leveling
screw

Aquarium
cement

Graph paper
on underside
of glass

Weight

Model

Potassium permanganate
(KMnO₄) crystals to
produce dyed streamlines

Flow

Faucet

Smoothing
screen

Settling
trough

Plate glass,
1/4 in. thick

Water, 1/32 to
1/16 in. deep
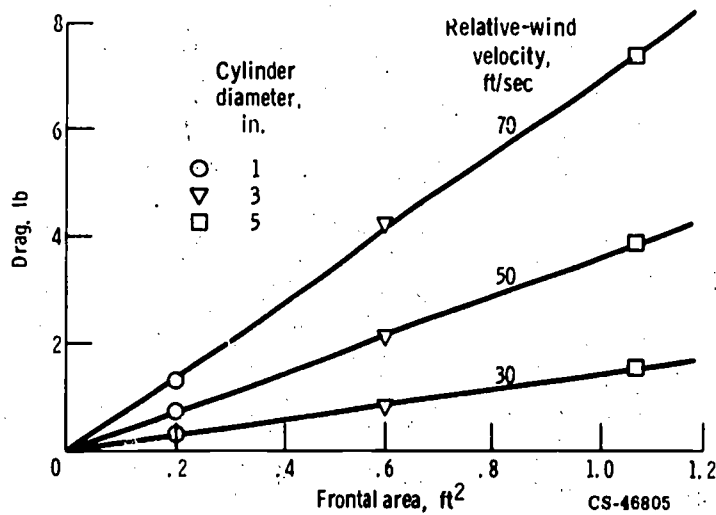
(a) Drag as a function of frontal area for circular cylinders.
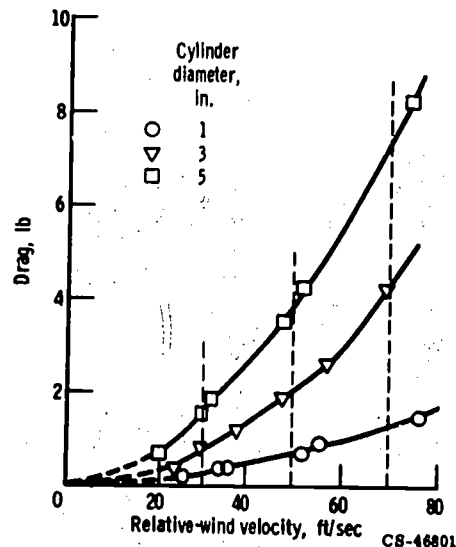
(b) Drag as a function of velocity for circular cylinders.
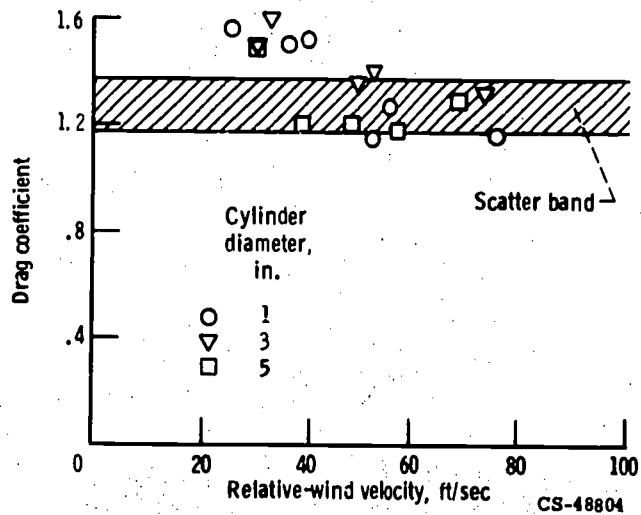
(c) Drag coefficient as a function of velocity for circular cylinders.
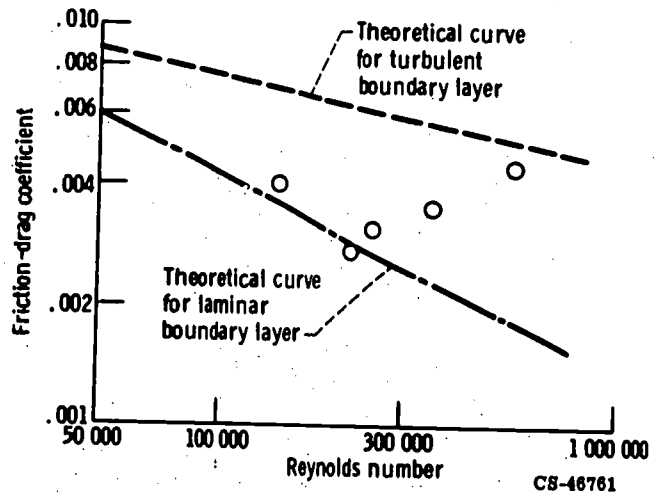
(d) Friction-drag coefficient as a function of Reynolds number for a flat plate.
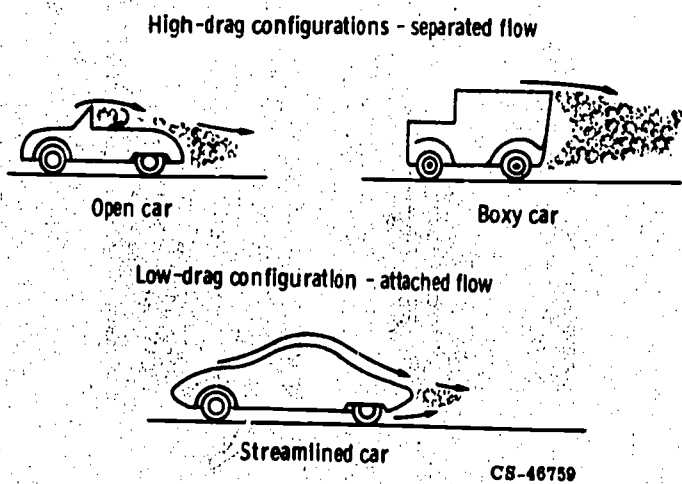
(e) Flow-separation patterns behind automobiles.
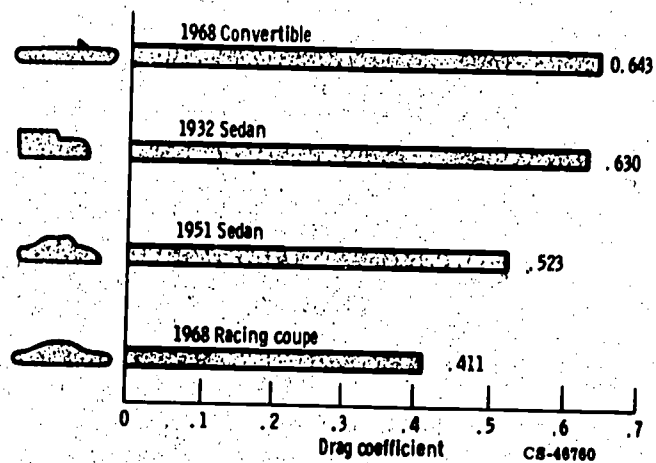
(f) Experimentally obtained drag results for automobiles traveling at 50 miles per hour.

Figure 17-3. - Wind-tunnel studies of drag.
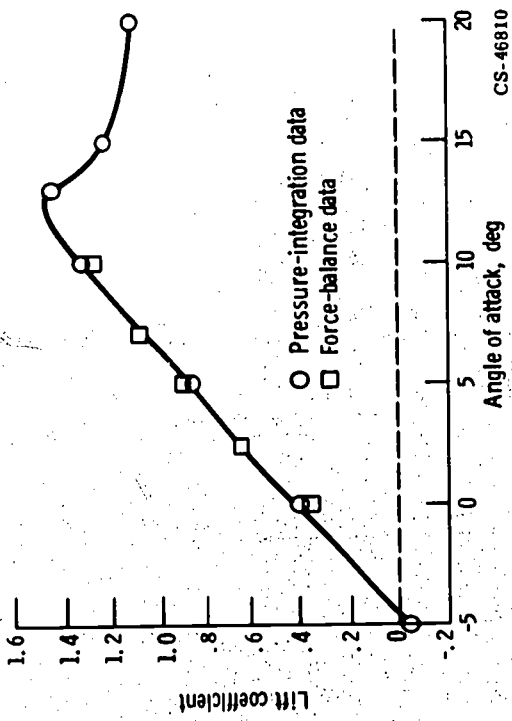
(a) Airfoil lift coefficient as a function of angle of attack.

CS-46810

O Pressure-integration data
□ Force-balance data

Lift coefficient

1.6, 1.4, 1.2, 1.0, .8, .6, .4, .2, 0, -.2

Angle of attack, deg: -5, 0, 5, 10, 15, 20

Moderate angle of attack

High angle of attack

CS-46812

(b) Use of smoke for visualization of airflow pattern over airfoil at moderate and high angles of attack.

Moderate angle of attack

High angle of attack

CS-46813

(c) Use of tufts for visualization of airflow pattern over airfoil at moderate and high angles of attack.
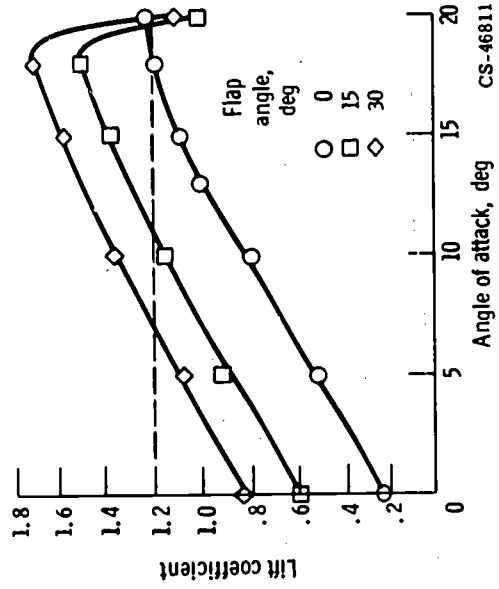
(d) Effect of flap on lift coefficient of airfoil.

CS-46811

Flap angle, deg
O 0
□ 15
◇ 30

Lift coefficient

1.8, 1.6, 1.4, 1.2, 1.0, .8, .6, .4, .2, 0

Angle of attack, deg: 5, 10, 15, 20

(f) Effect of aspect ratio on lift coefficient of airfoil.

Aspect ratio:
High (∞)
Medium (3, 2)
Low (1.6)

Angle of attack, deg

Lift coefficient

CS-46791

(h) Interrelation of the effects of wing angle of attack, aspect ratio, and flap on the lift coefficient of the wing.

Medium aspect ratio; with flap
Medium aspect ratio; without flap
Low aspect ratio; without flap
Required landing lift

Angle of attack, deg

Lift coefficient

CS-46790

(e) Finite wings with different aspect ratios (span/chord).

Aspect ratio:
High (∞)
Medium (3, 2)
Low (1.6)
Span
Chord
Relative wind

CS-46789

(g) Photograph of tuft pattern showing wing-tip vortexes.

Lift
Negative pressure
Positive pressure

CS-46788

Figure 17-4. - Wind-tunnel studies of lift.

379
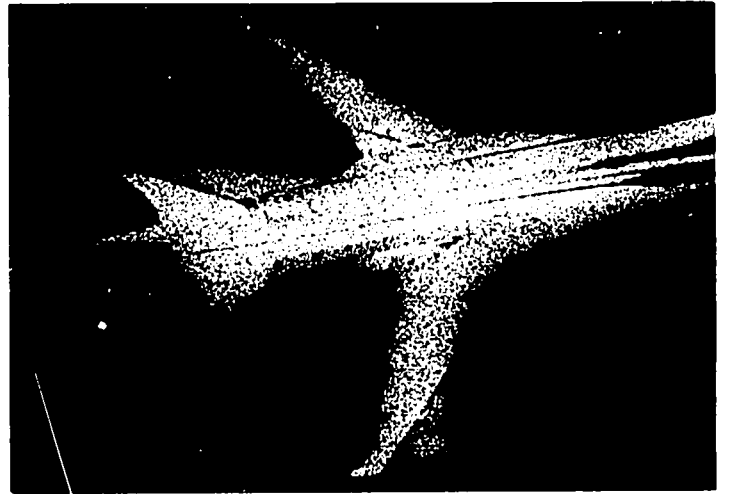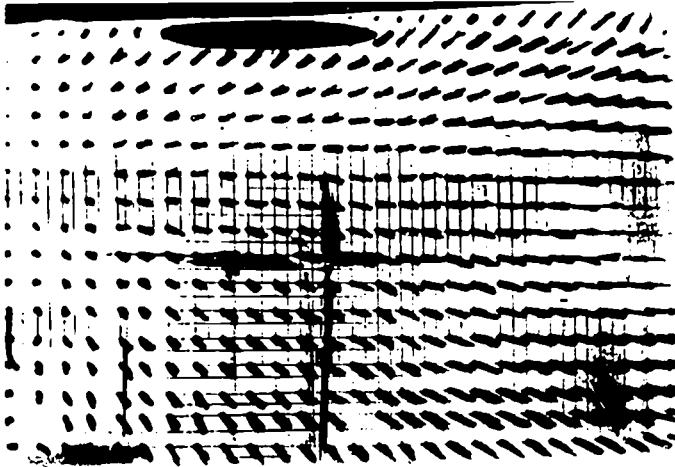
Zero angle of attack
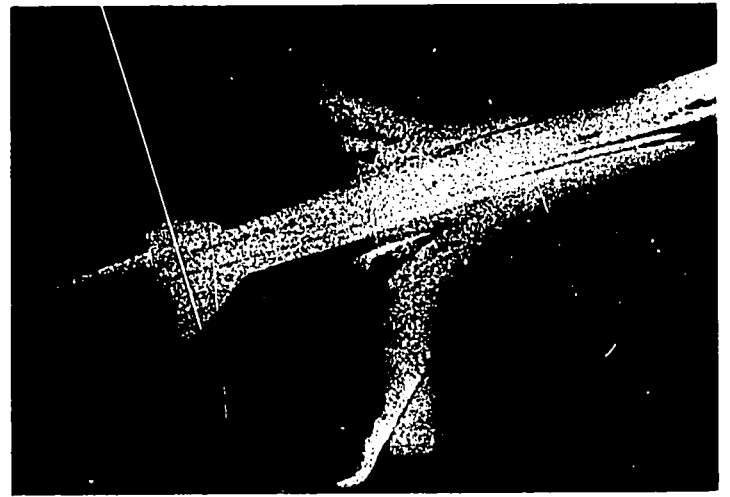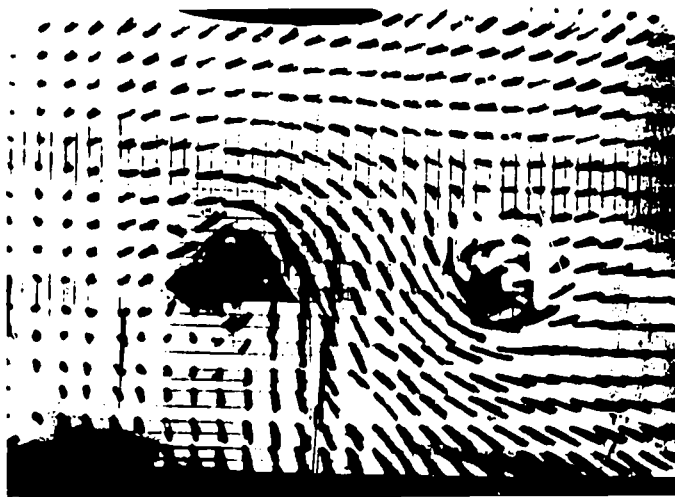
Moderate angle of attack
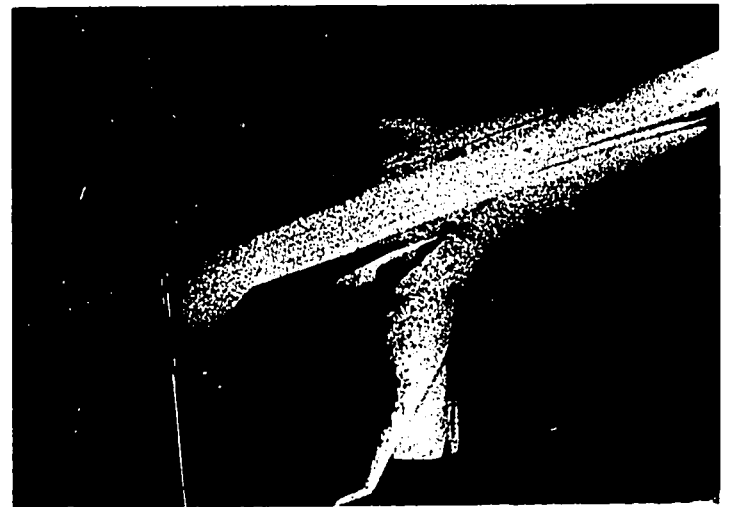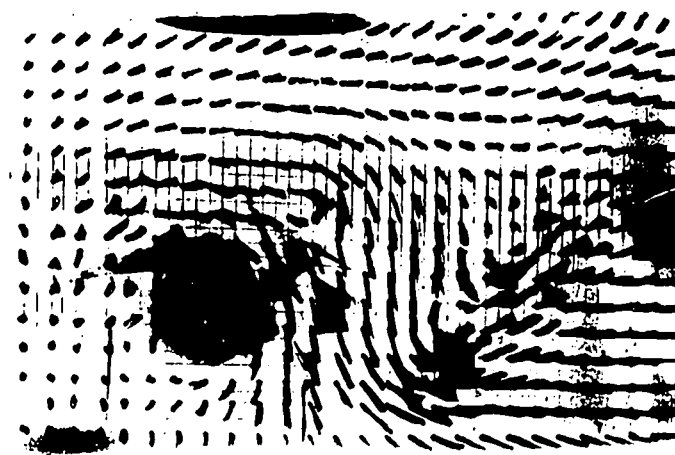
High angle of attack

(a) Wings unswept.

Figure 17-5. - Tuft patterns showing variation of downstream airflow with angle of attack for aircraft model with variable-sweep wing.
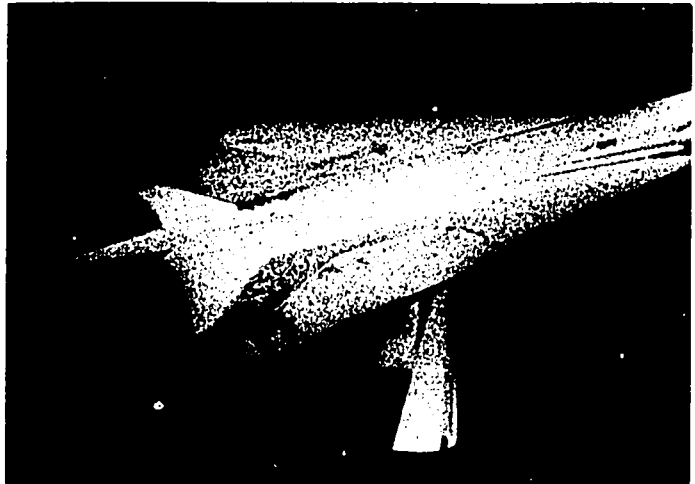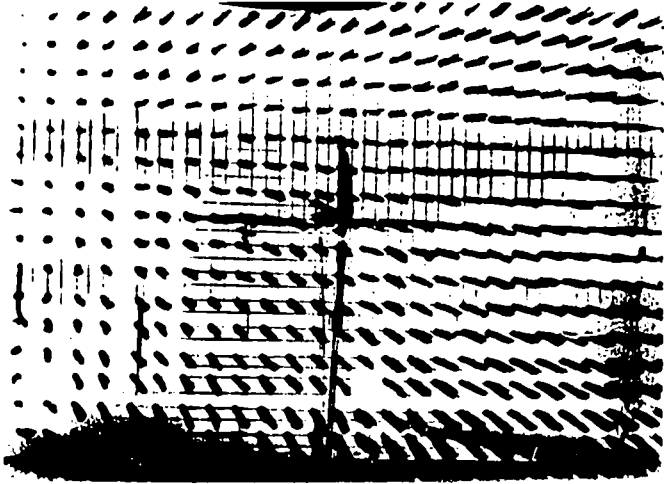
Zero angle of attack
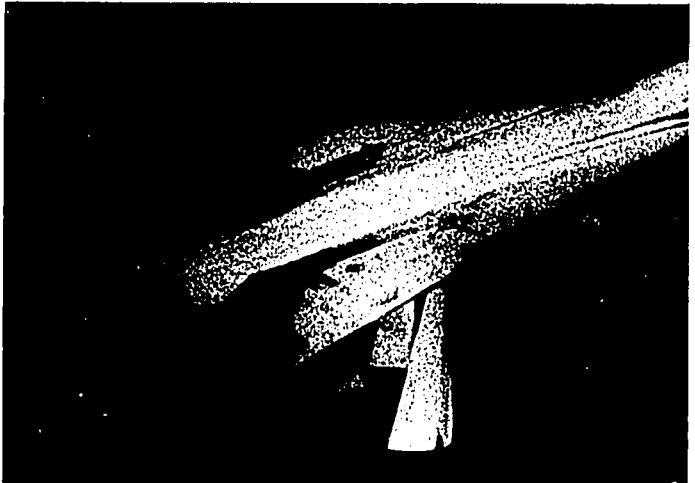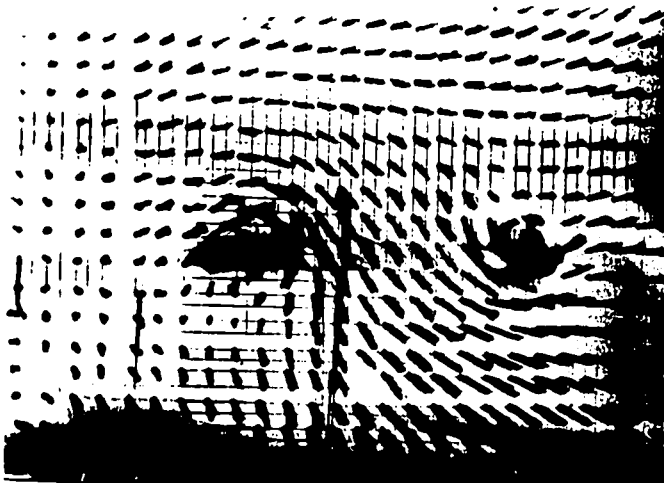
Moderate angle of attack
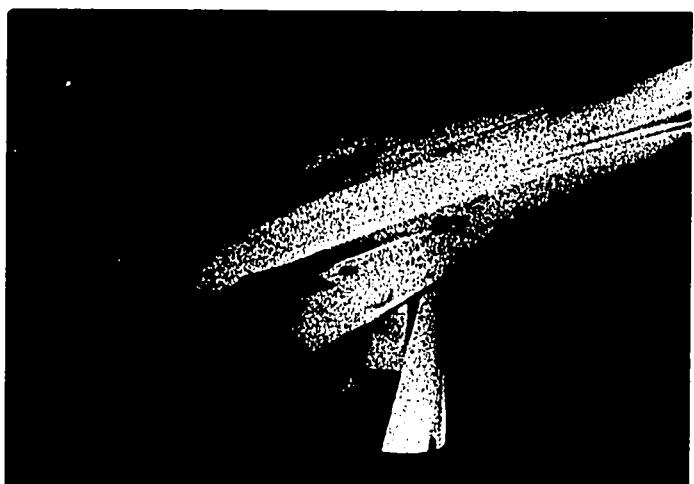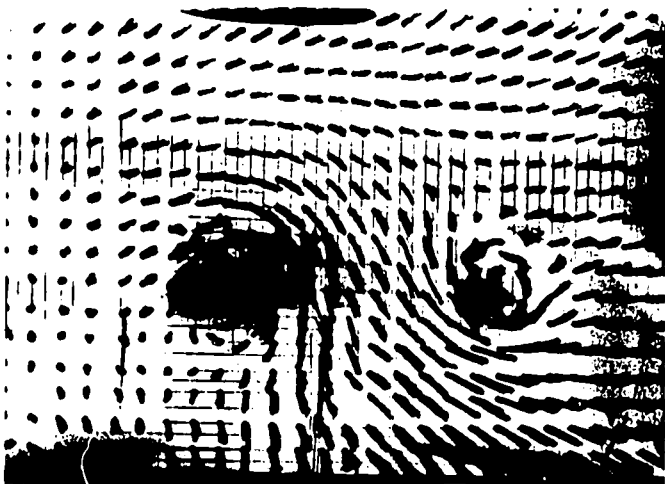
High angle of attack

(b) Wings fully swept.

Figure 17-5. - Concluded.
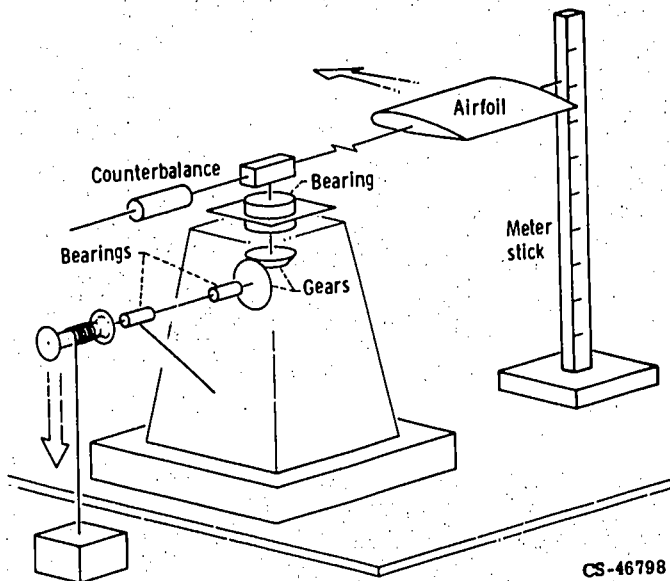
(a) Preliminary design of experimental apparatus.
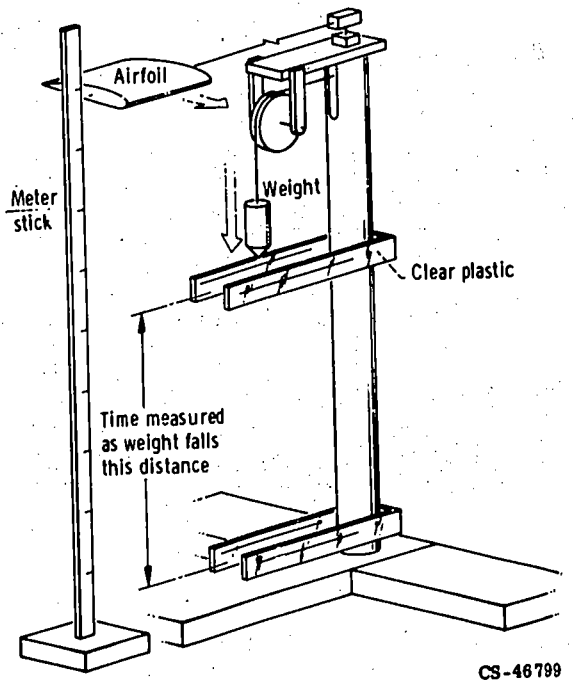
(b) Operational model of experimental apparatus.
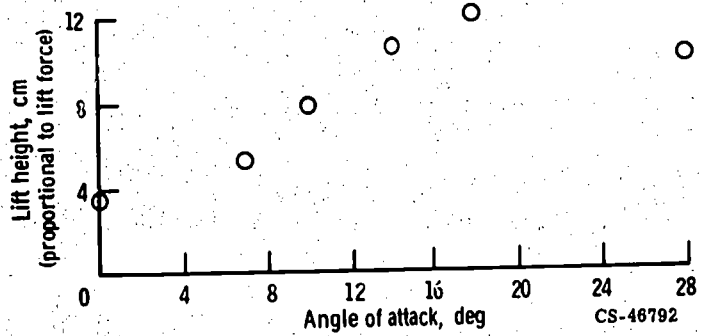
(c) Lift as a function of angle of attack for a plane wing. (Relative-wind velocity, ≈10 mph.)
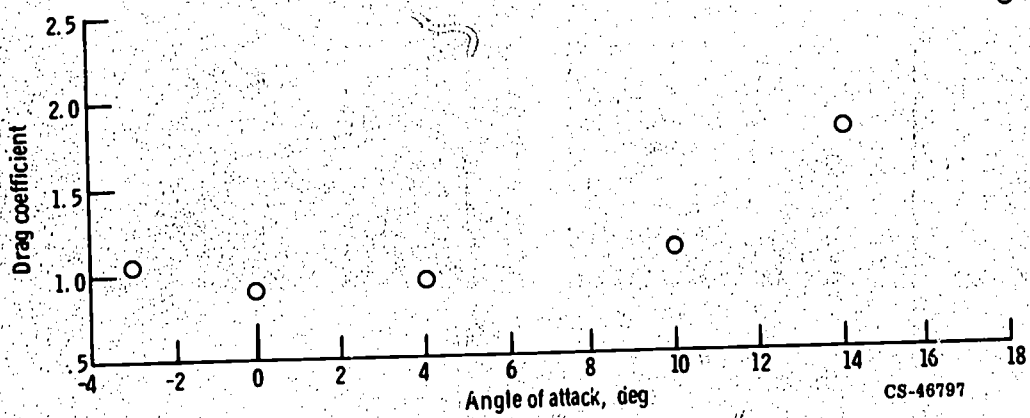
(d) Drag as a function of angle of attack for a plane wing.

Figure 17-6. - Project GARAGE (Gravity Accelerated Rotational Aerodynamic Gaging Equipment).
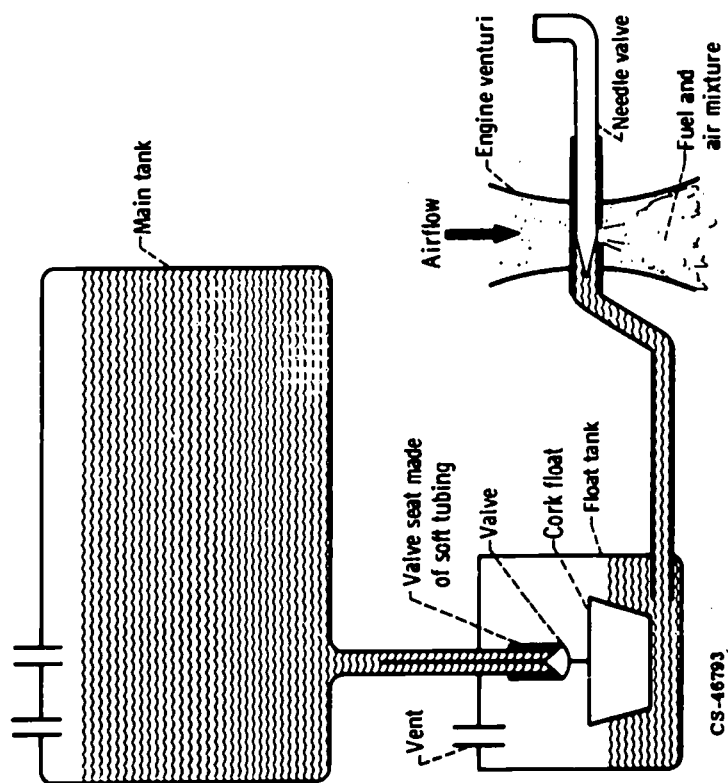
(a) Schematic diagram of fuel storage and metering system.

CS-46793
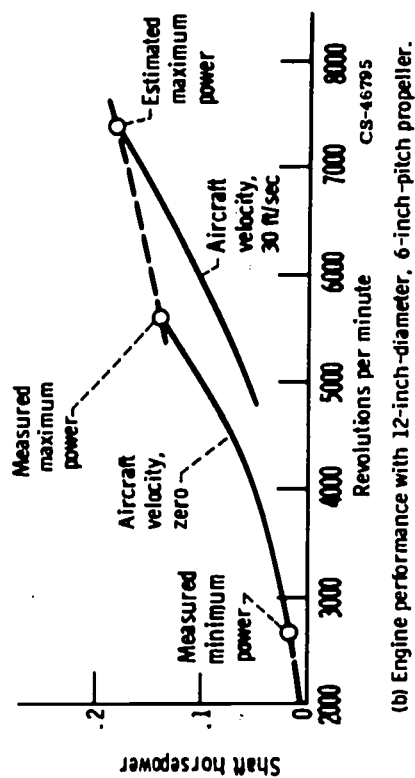
(b) Engine performance with 12-inch-diameter, 6-inch-pitch propeller.

CS-46795
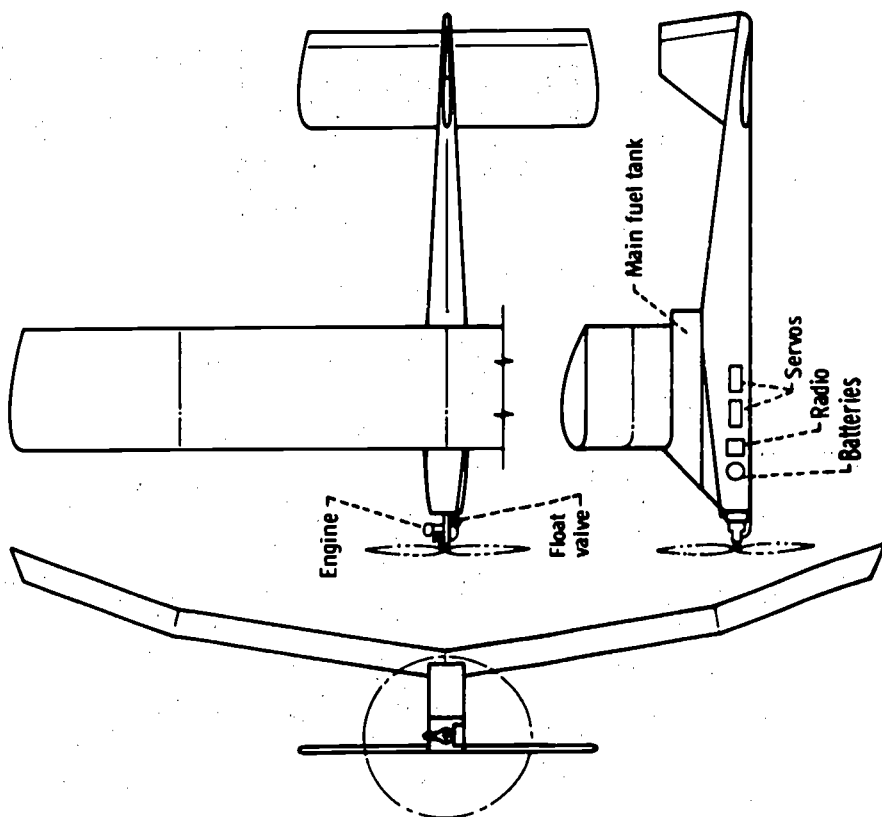
(c) Airplane configuration. (Wing area, 1800 in.^{2}; stabilizer area, 450 in.^{2}; gross weight, 11 lb.)

CS-46819

Figure 17-7. – Radio-controlled model airplane designed as a candidate for world endurance flight.

Figure 17-8. - Use of hand-launched, Indoor glider for aerodynamics study.

(a) Cockpit checkout.

(b) Landing-gear inspection.

(c) Discussion of engine and propeller.

(d) Pointing out control-surface details on the horizontal tail.

Figure 17-9. — Tour of hangar and aircraft.

(a) Air traffic control (or radar) room.
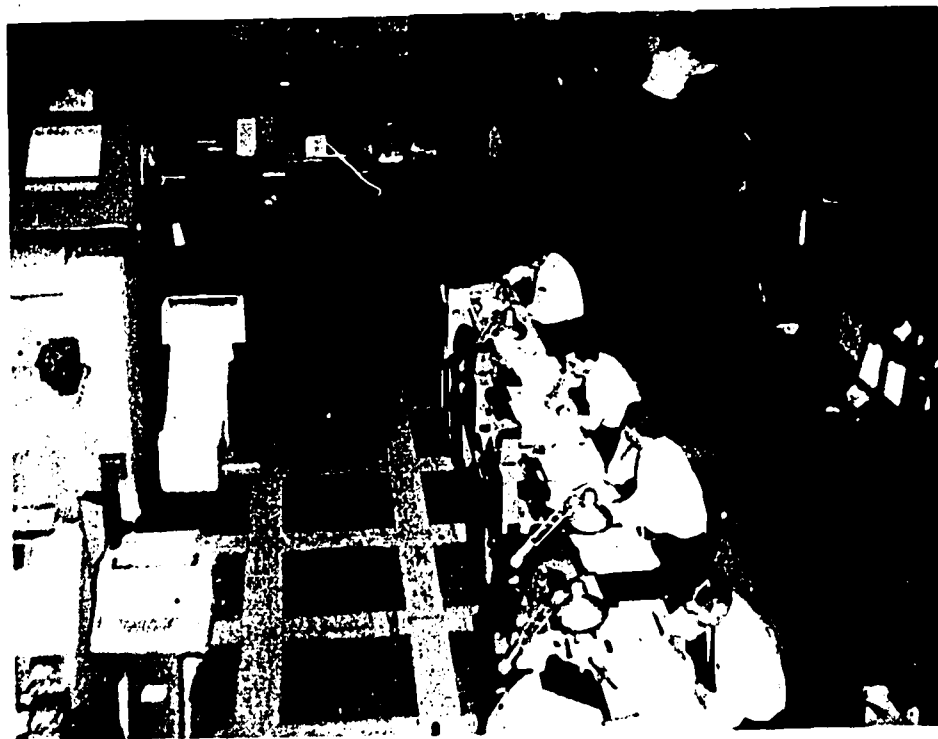
(b) Computer room (weather data and airline schedules).

Figure 17-10. – Tour of Air Traffic Control Center.

387
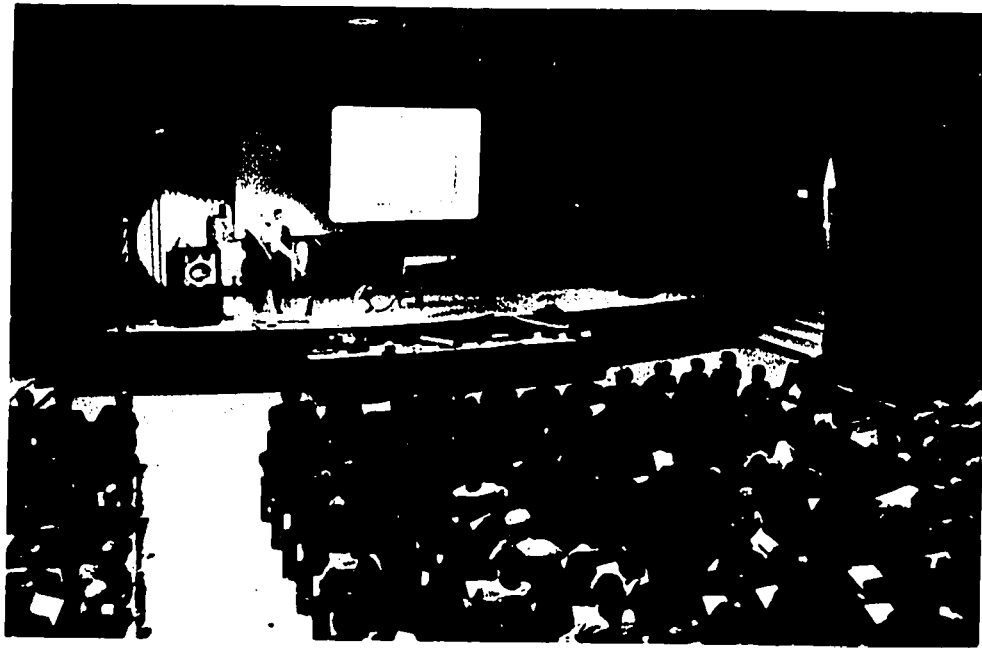
(a) Overview of auditorium.
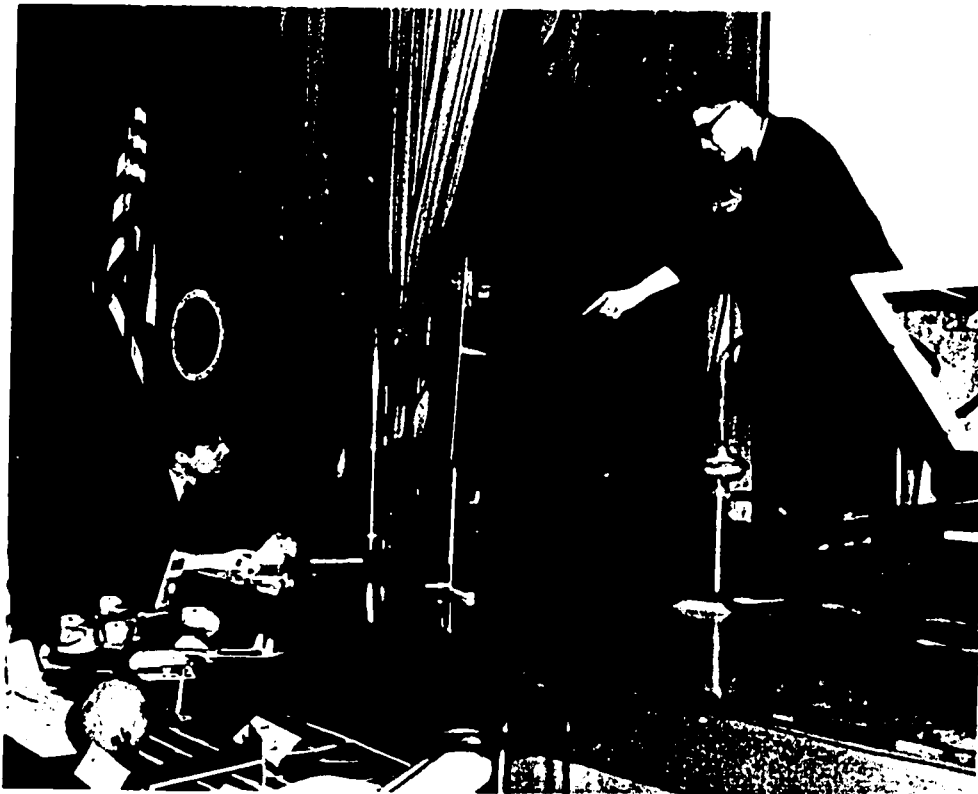
(b) Demonstration of Project GARAGE (aerodynamics experiment).

Figure 17-11. - Aeronautics symposium.
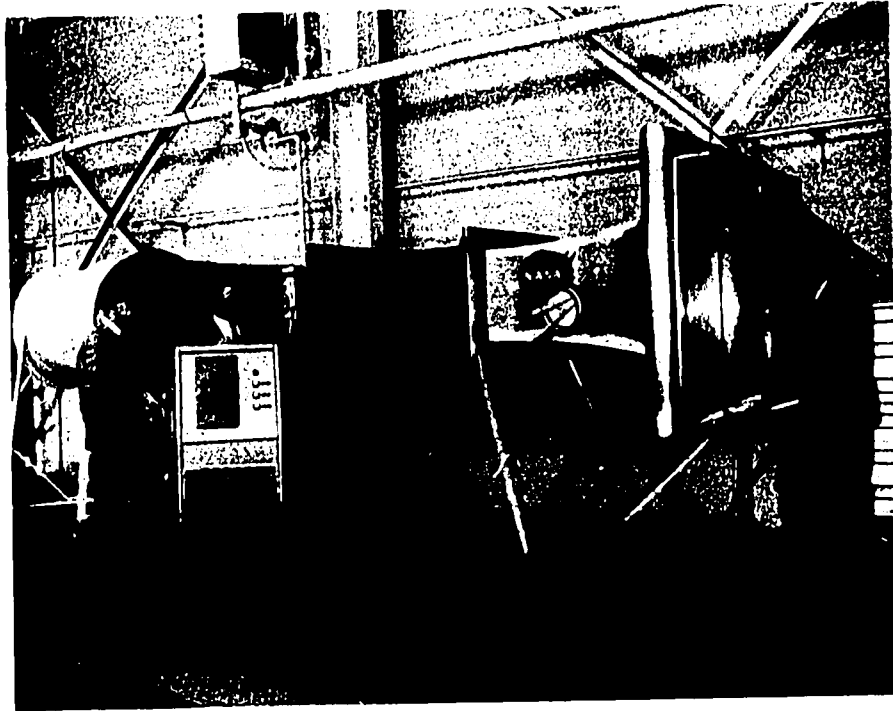
(a) Overall view of tunnel.
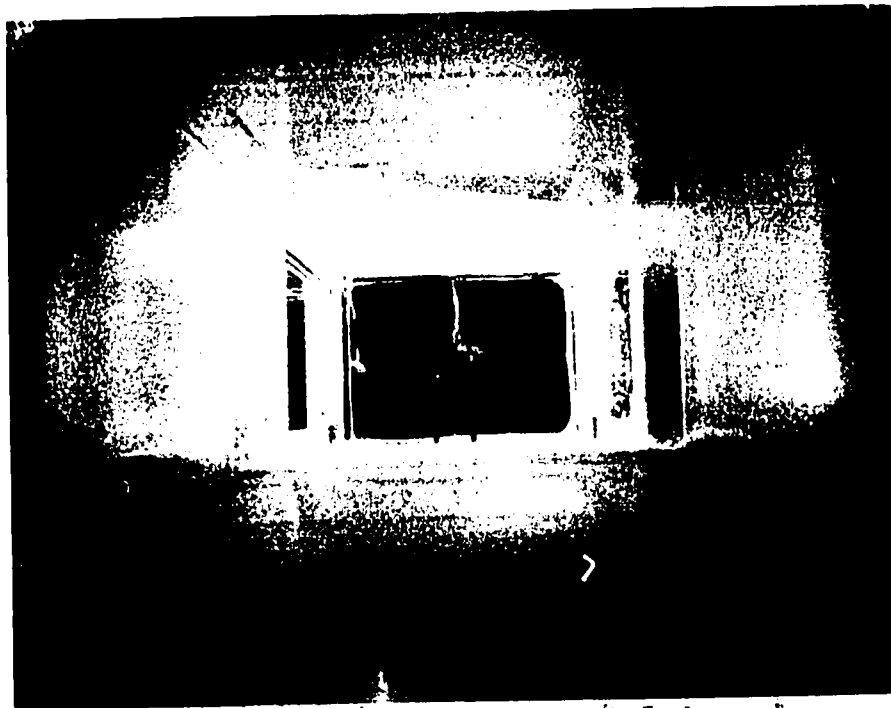
(b) View downstream through tunnel nozzle showing model installed in test section.

Figure 17-12. - Explorer wind tunnel.

389
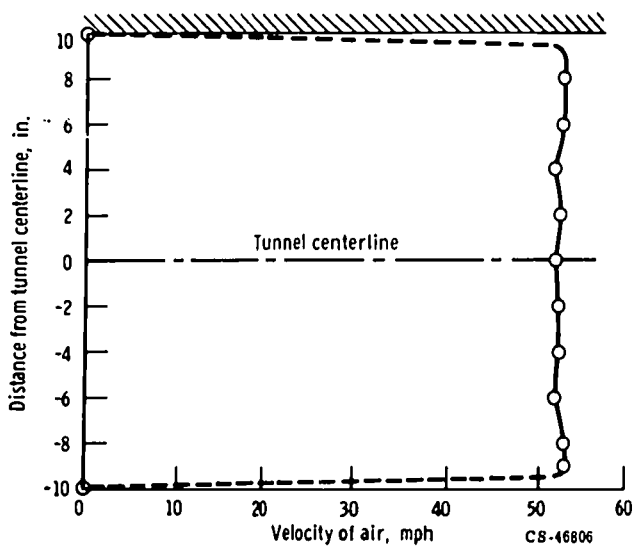
(a) Tunnel flow calibration at full power.
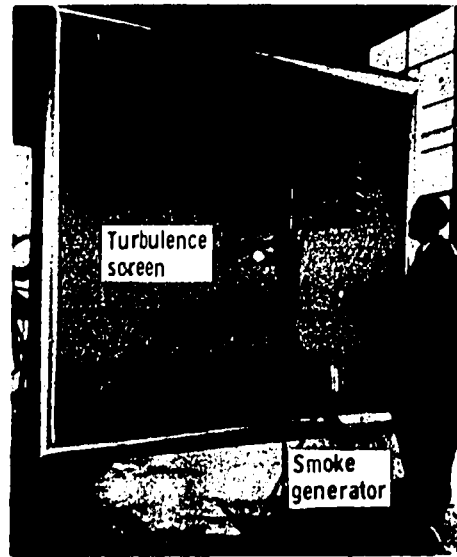
(b) Smoke generator and turbulence screen.

(c) Representative smoke pictures showing smooth and turbulent flow over airfoil.
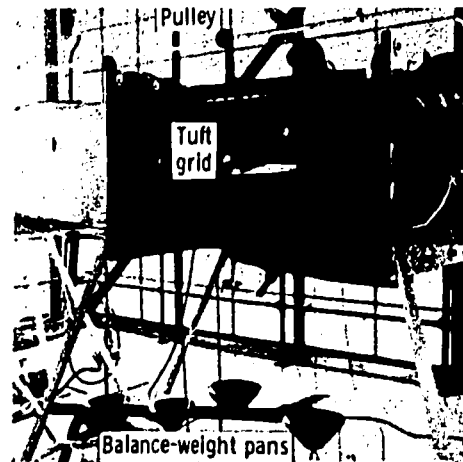
(d) Test section with balance-weight pans and tuft grid.
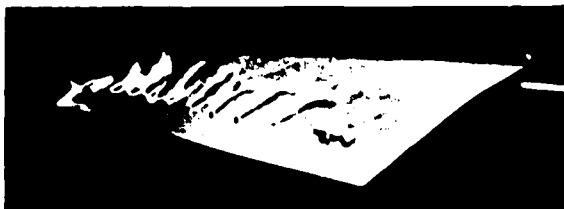
(e) Representative tuft pictures showing smooth and turbulent flow over airfoil.
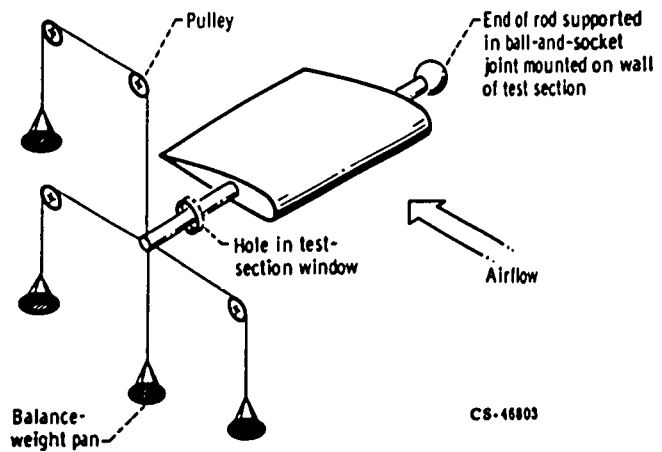
(f) Schematic of force-balance system for measuring lift and drag of airfoil.

Figure 17-13. - Explorer wind-tunnel details.

Stretchout line

$19\frac{13}{32}$

$19\frac{5}{64}$

Cut out as necessary for base of fan

90°

8

74°

$5\frac{1}{2}$

41°

74°

78°

78°

74°

41°

$5\frac{1}{2}$

Seam line

Electric fan

Fabric or cardboard

Plywood

18

34

3/4

3/4

Airflow

16

10

Glass or Plexiglas

3/4

1/4

10

18

3/4

3/4

Glass or Plexiglas

1/4

Plywood

Eggcrate flow straightener made of heavy bond paper

$8\frac{1}{2}$
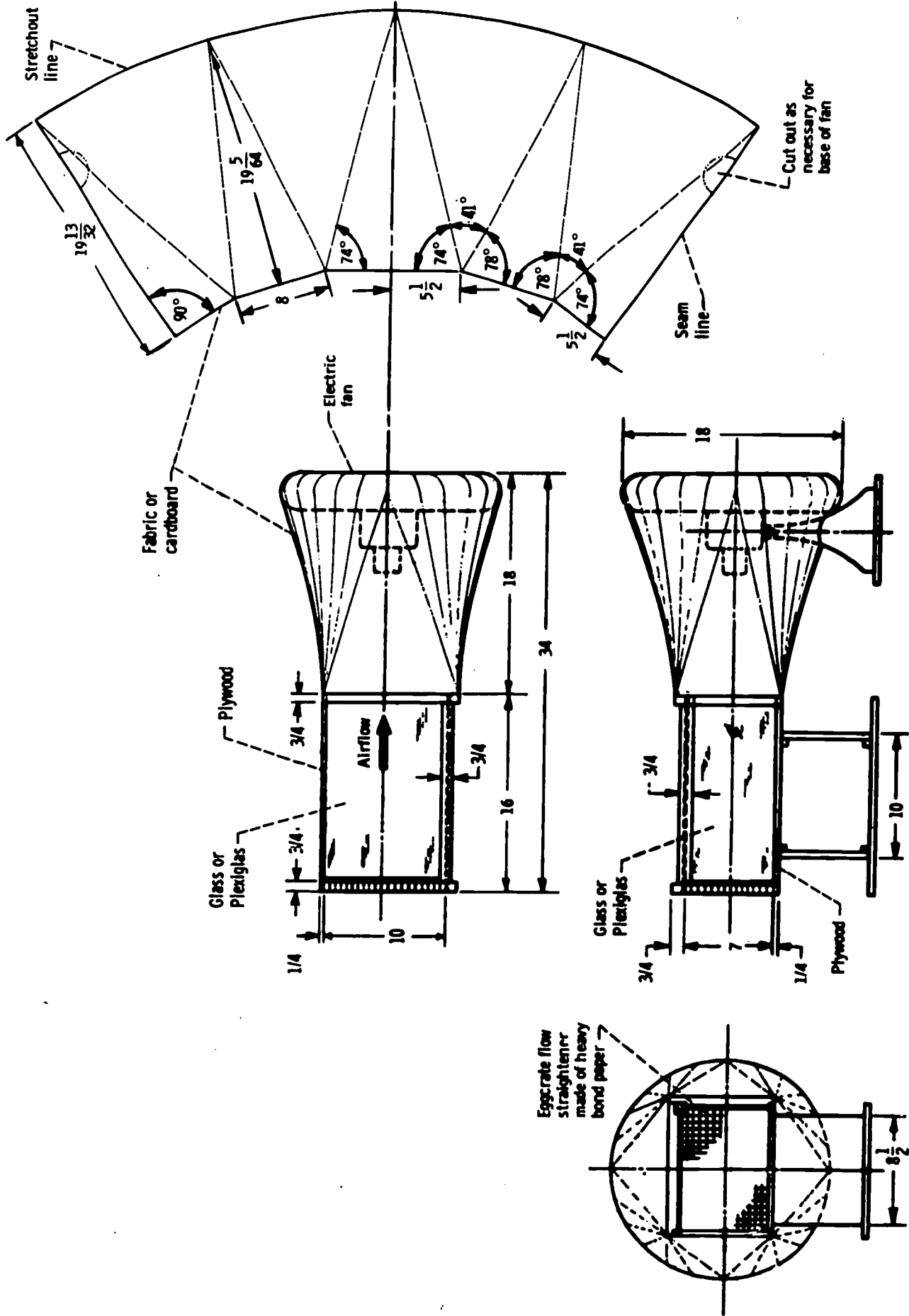
Figure 17-34. — Simple design for small, low-speed wind tunnel. (All linear dimensions in inches.)

Design Notes

Fuselage:
Made from 1/8-inch-thick hard balsa.
Sides tapered from wing leading edge forward and from wing trailing edge rearward.
All edges rounded except at wing and stabilizer mounting locations.

Wing:
Made from 1/16-inch-thick soft balsa.
Bottom surface flat.
Top surface tapered forward and rearward from high-point line.
Maximum thickness (1/16 in.) along high-point line.
Leading edge rounded.
Trailing edge tapered knife-edge thin.

Tail surfaces:
Made from 1/32-inch-thick medium hard balsa.
Leading edges rounded.
Trailing edges tapered knife-edge thin.

All parts of glider sanded for streamlining and lightening.
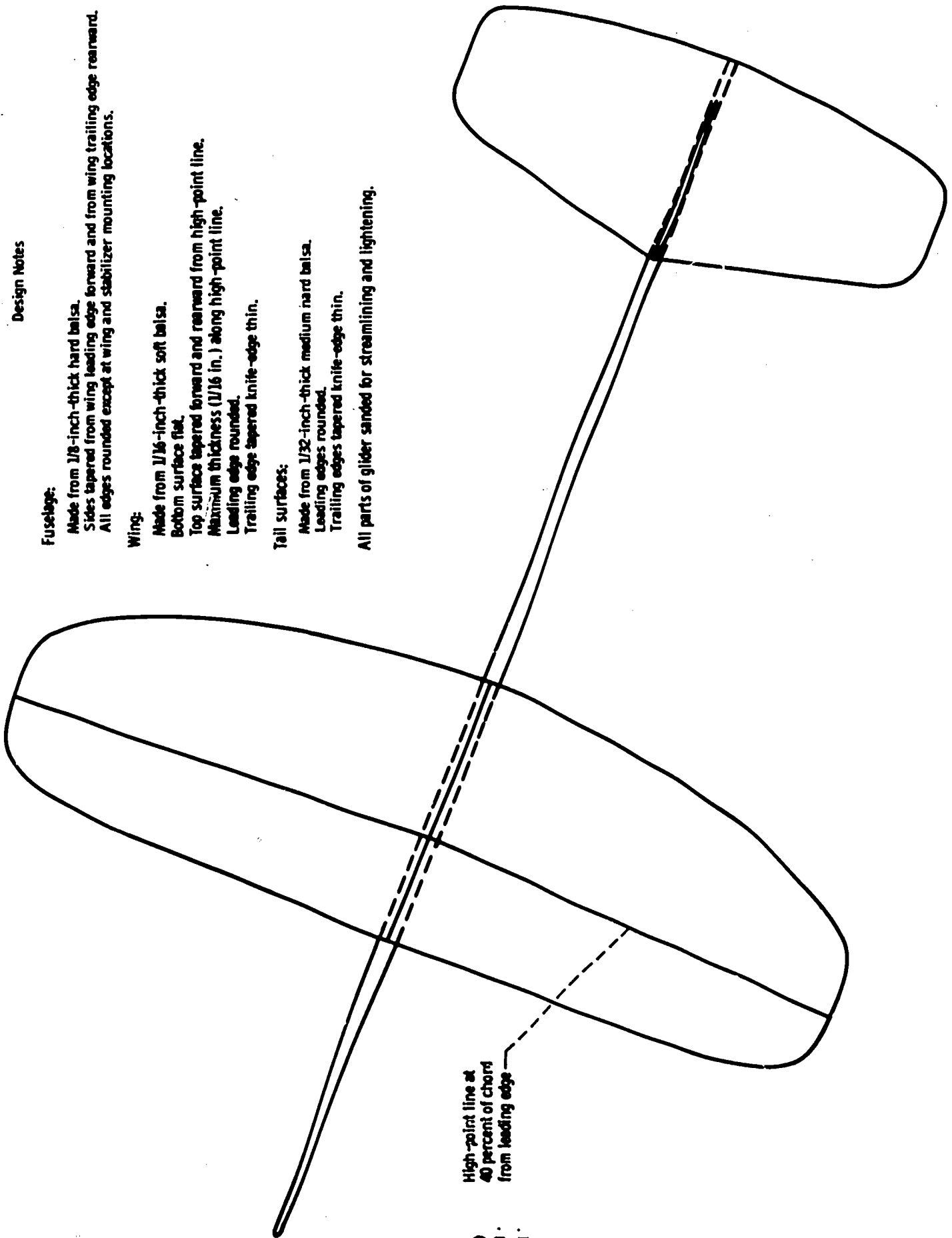
High-point line at
40 percent of chord
from leading edge

High point of wing section
(location of maximum
section thickness)

1/2-in. dihedral
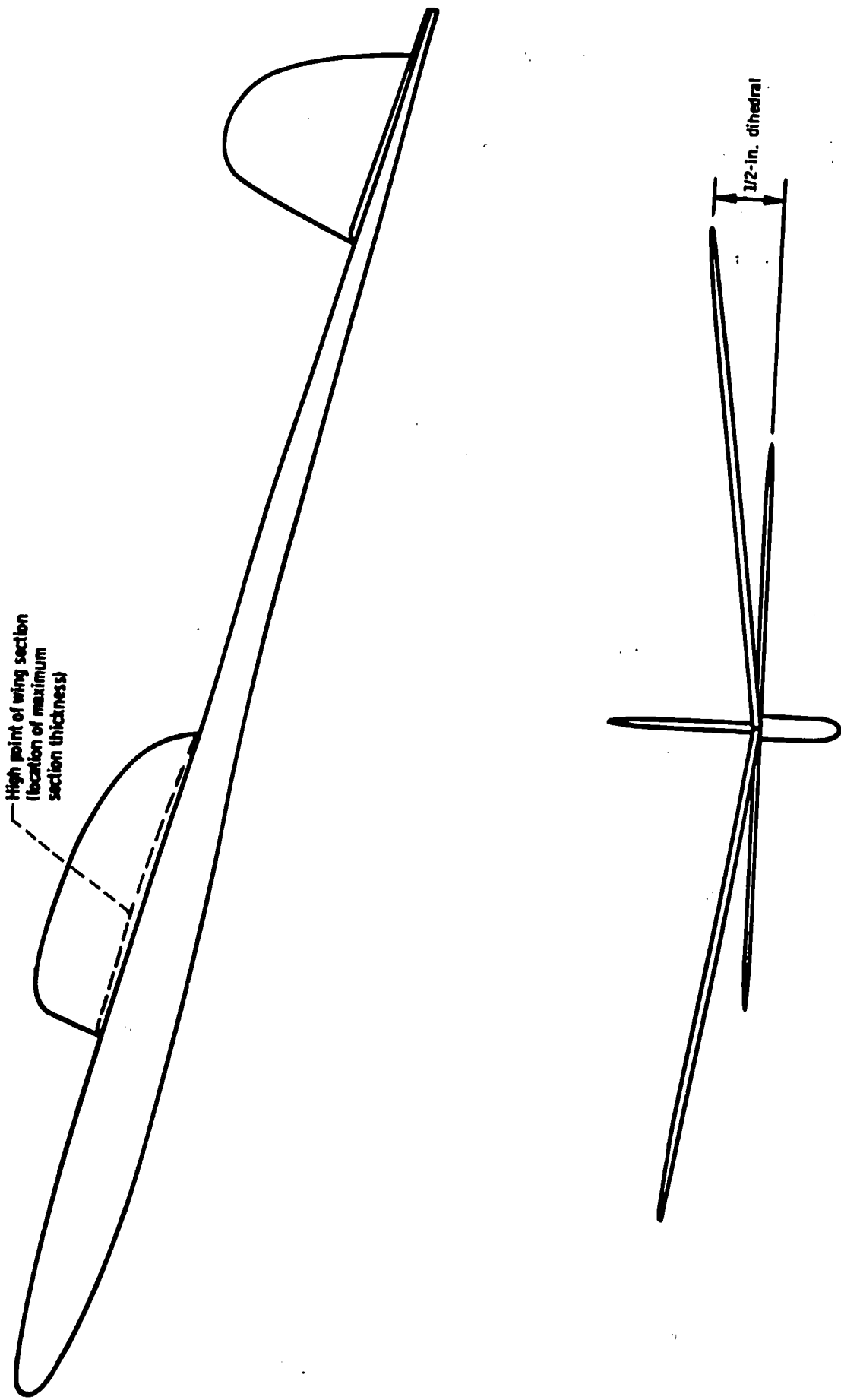
Figure 17-15. - Full-scale plans for small, hand-launched glider.

Wing
chord

Clay added or removed to
shift center of gravity
forward or rearward
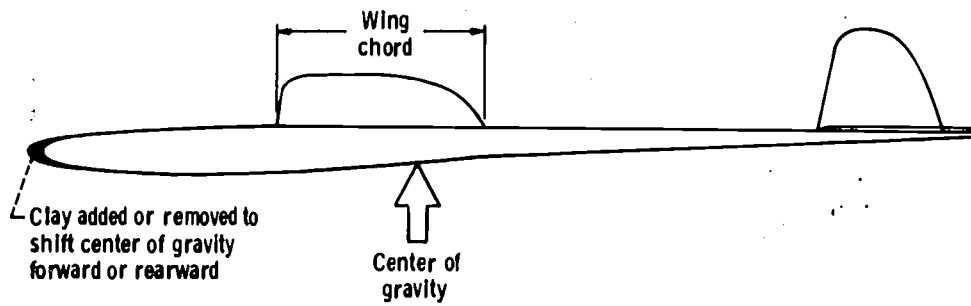
Center of
gravity

Figure 17-16. - Nose weight (clay) for adjustment of center of gravity.

Rear view

Stabilizer not tilted

Stabilizer tilted by twisting tail boom
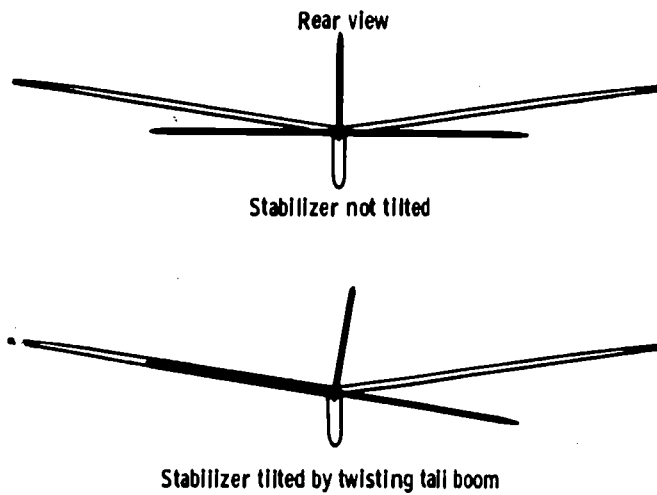
Figure 17-17. - Stabilizer tilt for adjustment of glide turning-circle di-
ameter. (Direction of turn is opposite to direction of tilt.)

Reference
line

Zero angular difference

Positive angular difference

Negative angular difference
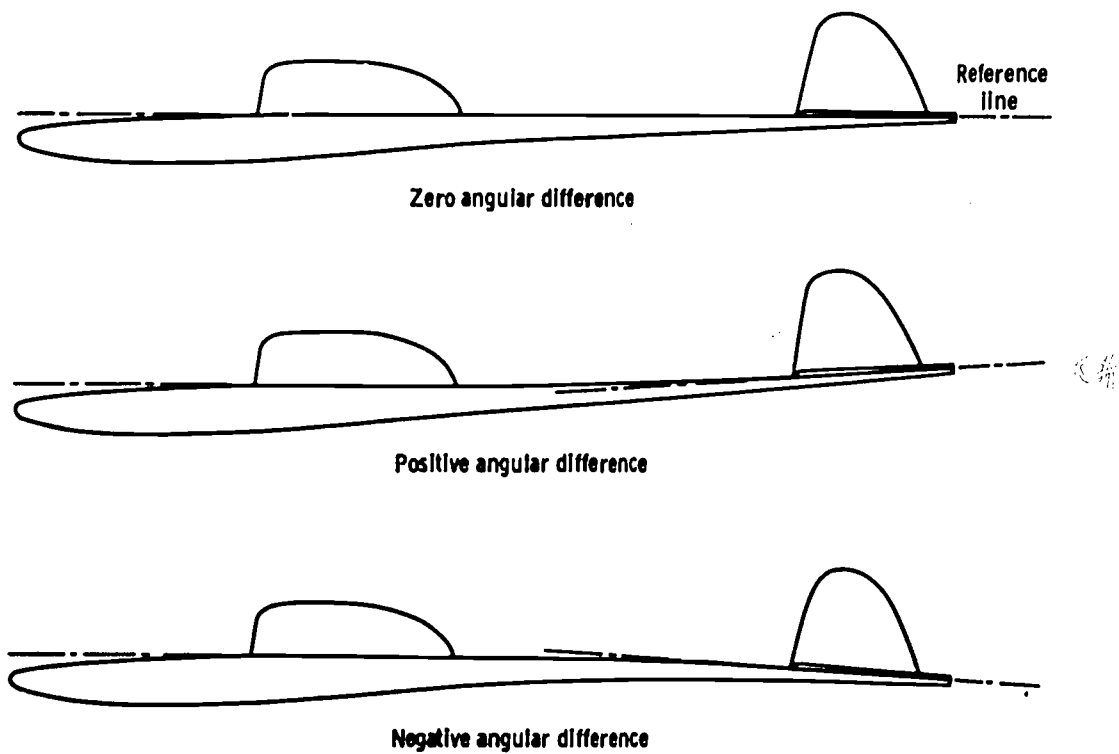
Figure 17-18. - Angular difference between wing and horizontal stabilizer.
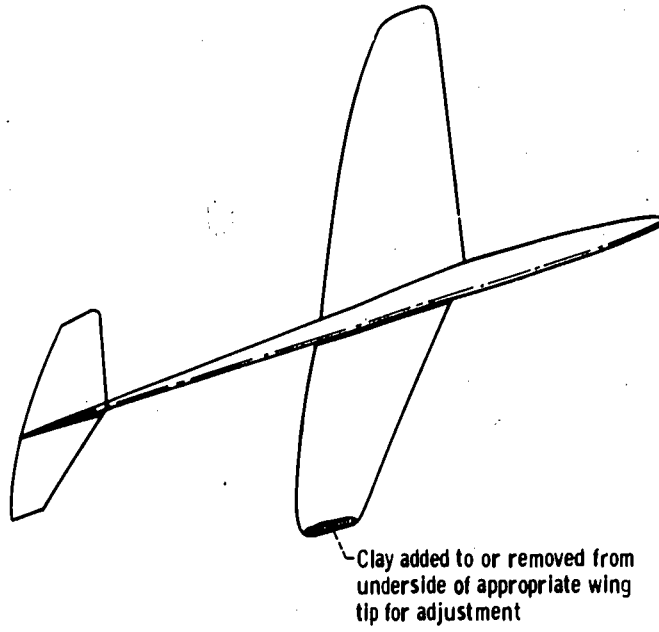
Clay added to or removed from
underside of appropriate wing
tip for adjustment

Figure 17-19. – Wing-tip weight (clay) for adjustment of glider roll
characteristics.
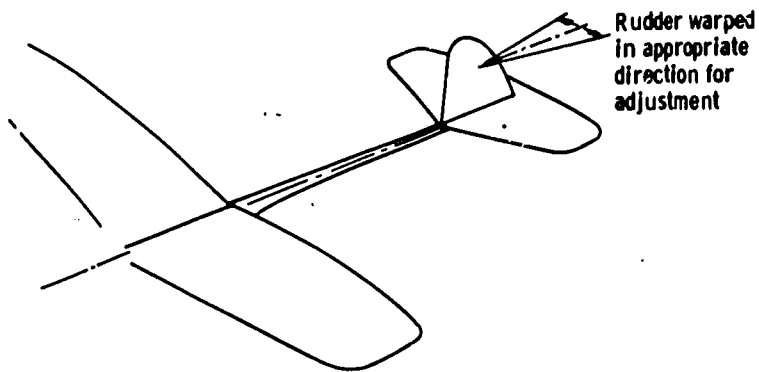
Rudder warped
in appropriate
direction for
adjustment

Figure 17-20. – Rudder offset for yaw adjustment to compensate for structural
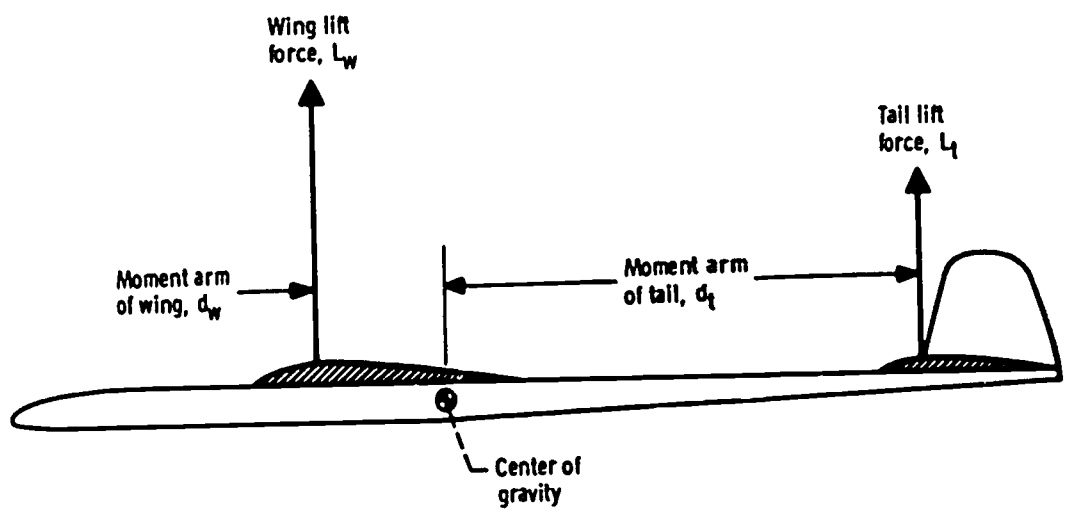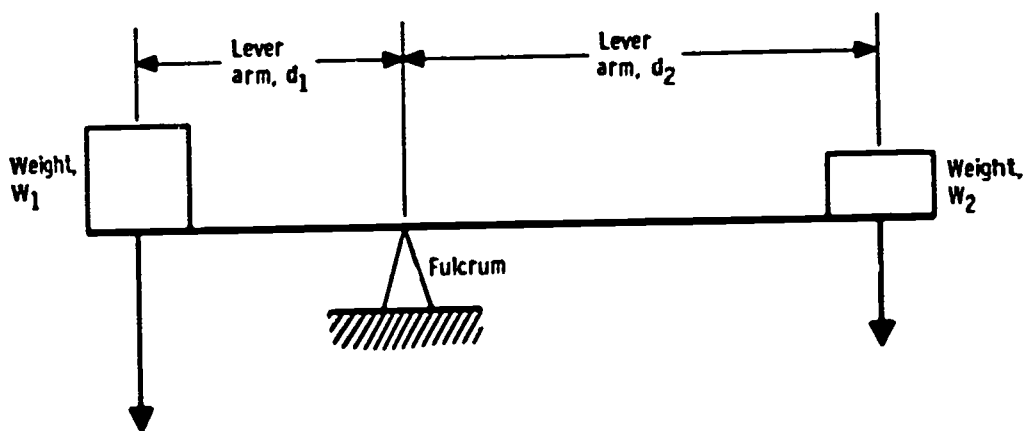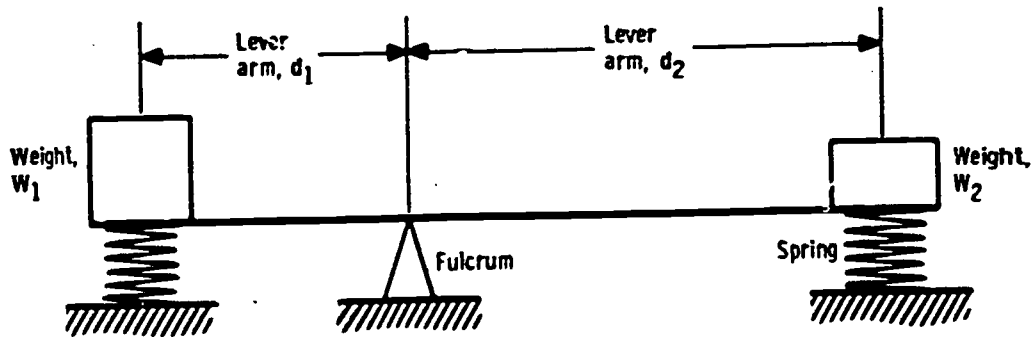misalinement.

Wing lift
force, L_w

Tail lift
force, L_t

Moment arm
of wing, d_w

Moment arm
of tail, d_t

Center of
gravity

Figure 17-21. - Forces and moments acting in the pitch plane on a hand-launched glider.

Lever
arm, d_1

Lever
arm, d_2

Weight,
W_1

Weight,
W_2

Fulcrum

(a) Beam balanced ($W_1 d_1 = W_2 d_2$) but unstable - no restoring moments.

Lever
arm, d_1

Lever
arm, d_2

Weight,
W_1

Weight,
W_2

Fulcrum

Spring

(b) Beam balanced ($W_1 d_1 = W_2 d_2$) and stable - restoring moments provided by springs.

Figure 17-22. - Unstable and stable balanced beams.
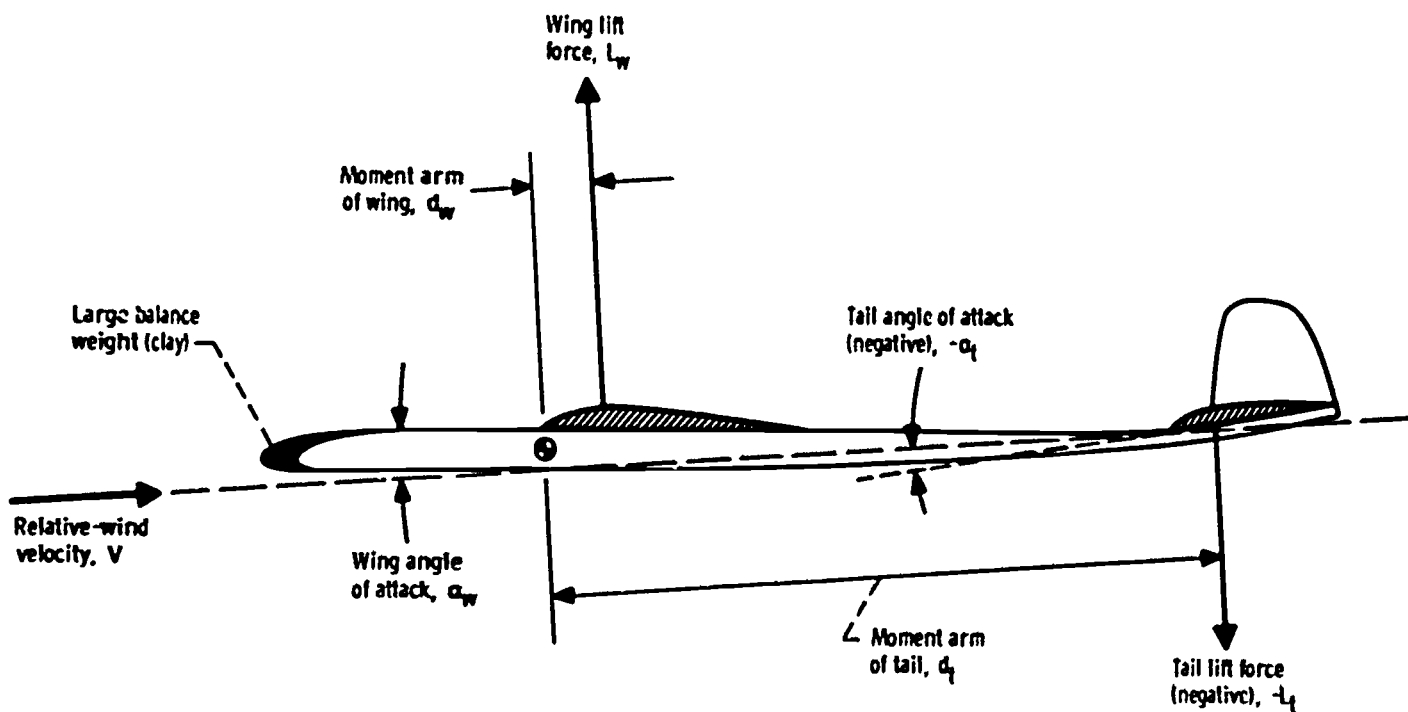
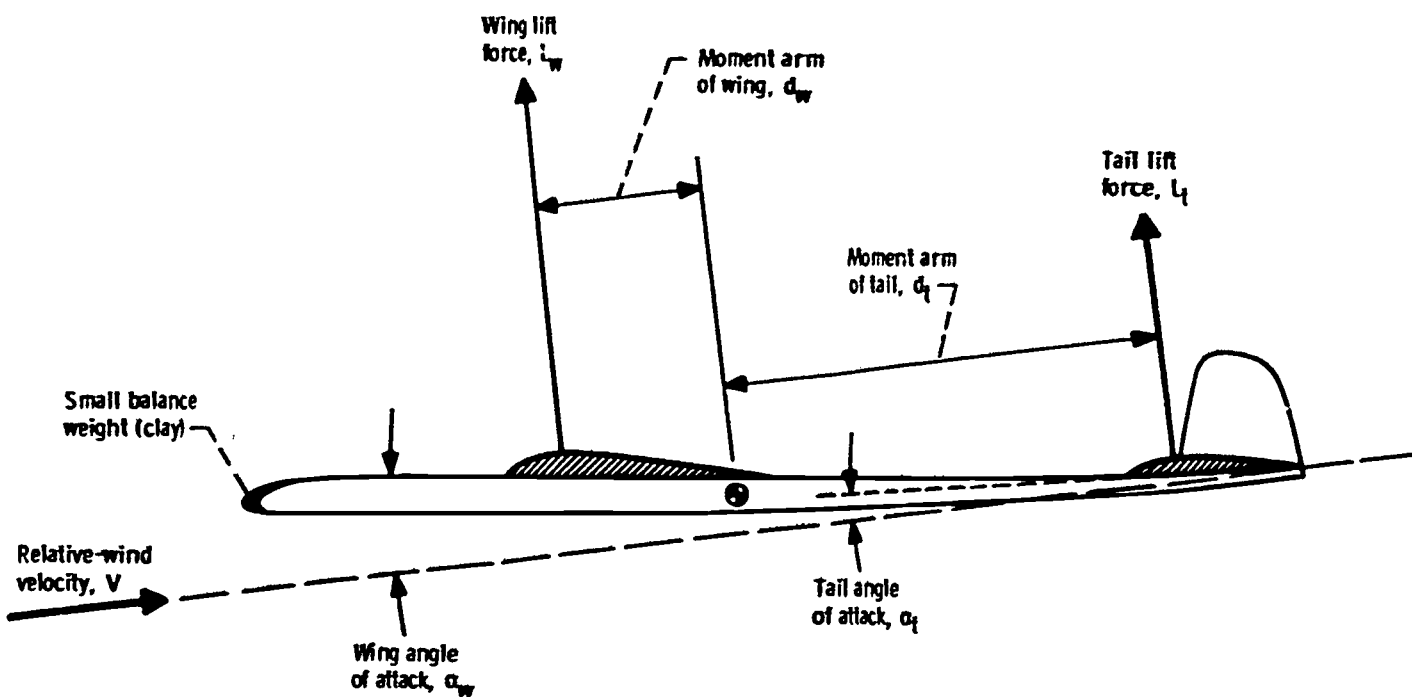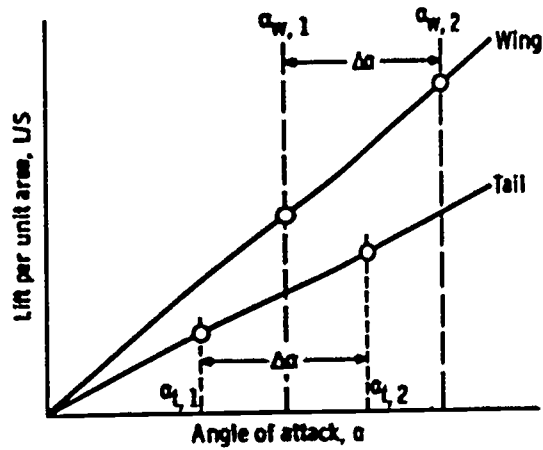Figure 17-23. – Glider trimmed with the center of gravity ahead of the wing lift force.
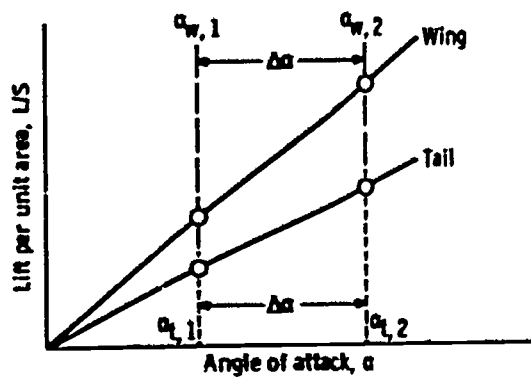

Figure 17-24. – Typical force and moment arrangement for an endurance glider.

397

(a) Positive angular difference between wing and tail $(\alpha_w > \alpha_t)$.

(b) Zero angular difference between wing and tail $(\alpha_w = \alpha_t)$.

Figure 17-25. – Variation of lift force per unit area with angle of attack for wing and tail surfaces.

398